

Central and Eastern United States Seismic Source Characterization for Nuclear Facilities

Volume 1: Chapters 1 to 4



U.S. Nuclear Regulatory Commission
Office of Nuclear Regulatory Research
Washington DC 20555
NUREG-2115



U.S. Department of Energy
1000 Independence Avenue SW
Washington, DC 20585
Report # DOE/NE-0140



Electric Power Research Institute
3420 Hillview Avenue
Palo Alto, CA 94304
Report # 1021097

AVAILABILITY OF REFERENCE MATERIALS IN NRC PUBLICATIONS

NRC Reference Material

As of November 1999, you may electronically access NUREG-series publications and other NRC records at NRC's Public Electronic Reading Room at <http://www.nrc.gov/reading-rm.html>.

Publicly released records include, to name a few, NUREG-series publications; *Federal Register* notices; applicant, licensee, and vendor documents and correspondence; NRC correspondence and internal memoranda; bulletins and information notices; inspection and investigative reports; licensee event reports; and Commission papers and their attachments.

NRC publications in the NUREG series, NRC regulations, and *Title 10, Energy*, in the Code of *Federal Regulations* may also be purchased from one of these two sources.

1. The Superintendent of Documents
U.S. Government Printing Office
Mail Stop SSOP
Washington, DC 20402-0001
Internet: bookstore.gpo.gov
Telephone: 202-512-1800
Fax: 202-512-2250
2. The National Technical Information Service
Springfield, VA 22161-0002
www.ntis.gov
1-800-553-6847 or, locally, 703-605-6000

A single copy of each NRC draft report for comment is available free, to the extent of supply, upon written request as follows:

Address: U.S. Nuclear Regulatory Commission
Office of Administration
Publications Branch
Washington, DC 20555-0001

E-mail: DISTRIBUTION.SERVICES@NRC.GOV

Facsimile: 301-415-2289

Some publications in the NUREG series that are posted at NRC's Web site address <http://www.nrc.gov/reading-rm/doc-collections/nuregs> are updated periodically and may differ from the last printed version. Although references to material found on a Web site bear the date the material was accessed, the material available on the date cited may subsequently be removed from the site.

Non-NRC Reference Material

Documents available from public and special technical libraries include all open literature items, such as books, journal articles, and transactions, *Federal Register* notices, Federal and State legislation, and congressional reports. Such documents as theses, dissertations, foreign reports and translations, and non-NRC conference proceedings may be purchased from their sponsoring organization.

Copies of industry codes and standards used in a substantive manner in the NRC regulatory process are maintained at—

The NRC Technical Library
Two White Flint North
11545 Rockville Pike
Rockville, MD 20852-2738

These standards are available in the library for reference use by the public. Codes and standards are usually copyrighted and may be purchased from the originating organization or, if they are American National Standards, from—

American National Standards Institute
11 West 42nd Street
New York, NY 10036-8002
www.ansi.org
212-642-4900

Legally binding regulatory requirements are stated only in laws; NRC regulations; licenses, including technical specifications; or orders, not in NUREG-series publications. The views expressed in contractor-prepared publications in this series are not necessarily those of the NRC.

The NUREG series comprises (1) technical and administrative reports and books prepared by the staff (NUREG-XXXX) or agency contractors (NUREG/CR-XXXX), (2) proceedings of conferences (NUREG/CP-XXXX), (3) reports resulting from international agreements (NUREG/IA-XXXX), (4) brochures (NUREG/BR-XXXX), and (5) compilations of legal decisions and orders of the Commission and Atomic and Safety Licensing Boards and of Directors' decisions under Section 2.206 of NRC's regulations (NUREG-0750).

Central and Eastern United States Seismic Source Characterization for Nuclear Facilities

Cosponsors

U.S. Department of Energy

1000 Independence Avenue SW
Washington, DC 20585

R. H. Lagdon, Jr.
Chief of Nuclear Safety
Office of the Under Secretary for Nuclear Security, S-5

M.E. Shields
Project Manager
Office of Nuclear Energy, NE-72

Electric Power Research Institute

3420 Hillview Avenue
Palo Alto, CA 94304

J. F. Hamel
Program Manager
Advanced Nuclear Technology

U.S. Nuclear Regulatory Commission

Office of Nuclear Regulatory Research
Washington DC 20555

R.G. Roche-Rivera
NRC Project Manager

*This document was **not** developed under a 10CFR50
Appendix B program.*

DISCLAIMER OF WARRANTIES AND LIMITATION OF LIABILITIES

EPRI DISCLAIMER

THIS DOCUMENT WAS PREPARED AS AN ACCOUNT OF WORK SPONSORED OR COSPONSORED BY THE ELECTRIC POWER RESEARCH INSTITUTE, INC. (EPRI). NEITHER EPRI, ANY MEMBER OF EPRI, ANY COSPONSOR BELOW, NOR ANY PERSON ACTING ON BEHALF OF ANY OF THEM:

(A) MAKES ANY WARRANTY OR REPRESENTATION WHATSOEVER, EXPRESS OR IMPLIED, (I) WITH RESPECT TO THE USE OF ANY INFORMATION, APPARATUS, METHOD, PROCESS, OR SIMILAR ITEM DISCLOSED IN THIS DOCUMENT, INCLUDING MERCHANTABILITY AND FITNESS FOR A PARTICULAR PURPOSE, OR (II) THAT SUCH USE DOES NOT INFRINGE ON OR INTERFERE WITH PRIVATELY OWNED RIGHTS, INCLUDING ANY PARTY'S INTELLECTUAL PROPERTY, OR (III) THAT THIS DOCUMENT IS SUITABLE TO ANY PARTICULAR USER'S CIRCUMSTANCE; OR

(B) ASSUMES RESPONSIBILITY FOR ANY DAMAGES OR OTHER LIABILITY WHATSOEVER (INCLUDING ANY CONSEQUENTIAL DAMAGES, EVEN IF EPRI OR ANY EPRI REPRESENTATIVE HAS BEEN ADVISED OF THE POSSIBILITY OF SUCH DAMAGES) RESULTING FROM YOUR SELECTION OR USE OF THIS DOCUMENT OR ANY INFORMATION, APPARATUS, METHOD, PROCESS, OR SIMILAR ITEM DISCLOSED IN THIS DOCUMENT.

DOE DISCLAIMER

THIS REPORT WAS PREPARED AS AN ACCOUNT OF WORK SPONSORED BY AN AGENCY OF THE UNITED STATES GOVERNMENT. NEITHER THE UNITED STATES GOVERNMENT NOR ANY AGENCY THEREOF, NOR ANY OF THEIR EMPLOYEES, MAKES ANY WARRANTY, EXPRESS OR IMPLIED, OR ASSUMES ANY LEGAL LIABILITY OR RESPONSIBILITY FOR THE ACCURACY, COMPLETENESS, OR USEFULNESS OF ANY INFORMATION, APPARATUS, PRODUCT, OR PROCESS DISCLOSED, OR REPRESENTS THAT ITS USE WOULD NOT INFRINGE PRIVATELY OWNED RIGHTS. REFERENCE HEREIN TO ANY SPECIFIC COMMERCIAL PRODUCT, PROCESS, OR SERVICE BY TRADE NAME, TRADEMARK, MANUFACTURER, OR OTHERWISE DOES NOT NECESSARILY CONSTITUTE OR IMPLY ITS ENDORSEMENT, RECOMMENDATION, OR FAVORING BY THE UNITED STATES GOVERNMENT OR ANY AGENCY THEREOF. THE VIEWS AND OPINIONS OF AUTHORS EXPRESSED HEREIN DO NOT NECESSARILY STATE OR REFLECT THOSE OF THE UNITED STATES GOVERNMENT OR ANY AGENCY THEREOF.

NRC DISCLAIMER

THIS REPORT WAS PREPARED AS AN ACCOUNT OF WORK SPONSORED BY AN AGENCY OF THE U.S. GOVERNMENT. NEITHER THE U.S. GOVERNMENT NOR ANY AGENCY THEREOF, NOR ANY EMPLOYEE, MAKES ANY WARRANTY, EXPRESSED OR IMPLIED, OR ASSUMES ANY LEGAL LIABILITY OR RESPONSIBILITY FOR ANY THIRD PARTY'S USE, OR THE RESULTS OF SUCH USE, OF ANY INFORMATION, APPARATUS, PRODUCT, OR PROCESS DISCLOSED IN THIS PUBLICATION, OR REPRESENTS THAT ITS USE BY SUCH THIRD PARTY WOULD NOT INFRINGE PRIVATELY OWNED RIGHTS. THE STATEMENTS, FINDINGS, CONCLUSIONS AND RECOMMENDATIONS ARE THOSE OF THE AUTHOR(S) AND DO NOT NECESSARILY REFLECT THE VIEW OF THE US NUCLEAR REGULATORY COMMISSION.

SPONSORS' ACKNOWLEDGMENTS

The project sponsors would like to acknowledge the following individuals for directing the project:

Coppersmith Consulting, Inc.
2121 N. California Blvd., #290
Walnut Creek, CA 94596

Technical Integration (TI) Lead
K.J. Coppersmith

Savannah River Nuclear Solutions, LLC
Savannah River Site
Building 730-4B, Room 313
Aiken, SC 29808

CEUS SSC Project Manager
L.A. Salomone

This document describes research sponsored by the Electric Power Research Institute (EPRI), U.S. Department of Energy (U.S. DOE) under Award Number DE-FG07-08ID14908, and the U.S. Nuclear Regulatory Commission (U.S. NRC) under Award Number NCR-04-09-144.

This publication is a corporate document that should be cited in the literature in the following manner:

Technical Report: Central and Eastern United States Seismic Source Characterization for Nuclear Facilities. EPRI, Palo Alto, CA, U.S. DOE, and U.S. NRC: 2012.

AUTHORS

This document was prepared by the following investigators:

Technical Integration Lead	Kevin J. Coppersmith
Project Manager	Lawrence A. Salomone
Technical Integration Team	Chris W. Fuller Laura L. Glaser Kathryn L. Hanson Ross D. Hartleb William R. Lettis Scott C. Lindvall Stephen M. McDuffie Robin K. McGuire Gerry L. Stirewalt Gabriel R. Toro Robert R. Youngs
Database Manager	David L. Slayter
Technical Support	Serkan B. Bozkurt Randolph J. Cumbest Valentina Montaldo Falero Roseanne C. Perman Allison M. Shumway Frank H. Syms Martitia (Tish) P. Tuttle, Paleoliquefaction Data Resource

**This document has been
reproduced from the best available copy.**

ABSTRACT

This report describes a new seismic source characterization (SSC) model for the Central and Eastern United States (CEUS). It will replace the *Seismic Hazard Methodology for the Central and Eastern United States*, EPRI Report NP-4726 (July 1986) and the *Seismic Hazard Characterization of 69 Nuclear Plant Sites East of the Rocky Mountains*, Lawrence Livermore National Laboratory Model, (Bernreuter et al., 1989). The objective of the CEUS SSC Project is to develop a new seismic source model for the CEUS using a Senior Seismic Hazard Analysis Committee (SSHAC) Level 3 assessment process. The goal of the SSHAC process is to represent the center, body, and range of technically defensible interpretations of the available data, models, and methods. Input to a probabilistic seismic hazard analysis (PSHA) consists of both seismic source characterization and ground motion characterization. These two components are used to calculate probabilistic hazard results (or seismic hazard curves) at a particular site. This report provides a new seismic source model.

Results and Findings

The product of this report is a regional CEUS SSC model. This model includes consideration of an updated database, full assessment and incorporation of uncertainties, and the range of diverse technical interpretations from the larger technical community. The SSC model will be widely applicable to the entire CEUS, so this project uses a ground motion model that includes generic variations to allow for a range of representative site conditions (deep soil, shallow soil, hard rock). Hazard and sensitivity calculations were conducted at seven test sites representative of different CEUS hazard environments.

Challenges and Objectives

The regional CEUS SSC model will be of value to readers who are involved in PSHA work, and who wish to use an updated SSC model. This model is based on a comprehensive and traceable process, in accordance with SSHAC guidelines in NUREG/CR-6372, *Recommendations for Probabilistic Seismic Hazard Analysis: Guidance on Uncertainty and Use of Experts*. The model will be used to assess the present-day composite distribution for seismic sources along with their characterization in the CEUS and uncertainty. In addition, this model is in a form suitable for use in PSHA evaluations for regulatory activities, such as Early Site Permit (ESPs) and Combined Operating License Applications (COLAs).

Applications, Values, and Use

Development of a regional CEUS seismic source model will provide value to those who (1) have submitted an ESP or COLA for Nuclear Regulatory Commission (NRC) review before 2011; (2) will submit an ESP or COLA for NRC review after 2011; (3) must respond to safety issues resulting from NRC Generic Issue 199 (GI-199) for existing plants and (4) will prepare PSHAs to meet design and periodic review requirements for current and future nuclear facilities. This work replaces a previous study performed approximately 25 years ago. Since that study was

completed, substantial work has been done to improve the understanding of seismic sources and their characterization in the CEUS. Thus, a new regional SSC model provides a consistent, stable basis for computing PSHA for a future time span. Use of a new SSC model reduces the risk of delays in new plant licensing due to more conservative interpretations in the existing and future literature.

Perspective

The purpose of this study, jointly sponsored by EPRI, the U.S. Department of Energy (DOE), and the NRC was to develop a new CEUS SSC model. The team assembled to accomplish this purpose was composed of distinguished subject matter experts from industry, government, and academia. The resulting model is unique, and because this project has solicited input from the present-day larger technical community, it is not likely that there will be a need for significant revision for a number of years. See also Sponsors' Perspective for more details.

Approach

The goal of this project was to implement the CEUS SSC work plan for developing a regional CEUS SSC model. The work plan, formulated by the project manager and a technical integration team, consists of a series of tasks designed to meet the project objectives. This report was reviewed by a participatory peer review panel (PPRP), sponsor reviewers, the NRC, the U.S. Geological Survey, and other stakeholders. Comments from the PPRP and other reviewers were considered when preparing the report. The SSC model was completed at the end of 2011.

Keywords

Probabilistic seismic hazard analysis (PSHA)
Seismic source characterization (SSC)
Seismic source characterization model
Central and Eastern United States (CEUS)

CONTENTS

Abstract.....	ix
Contents.....	xi
List of Figures	xxv
List of Tables.....	lxxvii
Executive Summary	lxxxv
Participatory Peer Review Panel Final Report Dated October 24, 2011	xcv
Project Acknowledgements.....	ciii
Sponsor’s Perspective	cv
Abbreviations	cix
1 INTRODUCTION	1-1
1.1 Background and History	1-1
1.1.1 EPRI-SOG and LLNL Projects	1-2
1.1.2 Development of the SSHAC Process	1-2
1.1.3 Implementation of the SSHAC Methodology	1-3
1.1.4 Regional SSC Model for Nuclear Facilities.....	1-3
1.1.5 Differences from USGS National Seismic Hazard Mapping Project.....	1-4
1.2 Purpose of the CEUS SSC Project	1-5
1.2.1 Implementation of SSHAC Level 3 Process	1-6
1.2.2 Goals: Stability and Longevity	1-8
1.2.3 Interface with Ground Motion Models	1-8
1.3 Study Region.....	1-10
1.4 Products of Project.....	1-10
1.4.1 Seismic Source Model for Study Region	1-10
1.4.2 Hazard Input Document.....	1-12
1.4.3 Documentation of Technical Bases for All Assessments	1-12
1.4.4 Other Key Products	1-13
1.4.4.1 Data Evaluation and Data Summary Tables.....	1-13

1.4.4.2 Database of Geologic, Geophysical, and Seismological Data.....	1-13
1.4.4.3 Earthquake Catalog with Uniform Moment Magnitudes.....	1-13
1.4.4.4 Updated Paleoseismicity Data and Guidance.....	1-14
1.4.4.5 Recommendations for Future Applications of SSC Model.....	1-14
2 SSHAC LEVEL 3 ASSESSMENT PROCESS AND IMPLEMENTATION	2-1
2.1 Goals and Activities of a SSHAC Assessment Process.....	2-2
2.1.1 Evaluation.....	2-4
2.1.2 Integration	2-4
2.2 Roles of CEUS SSC Project Participants.....	2-5
2.3 CEUS SSC Project Organization	2-7
2.4 Key Tasks and Activities	2-9
2.4.1 Database Development	2-9
2.4.2 Identification of Significant Issues	2-10
2.4.3 Workshop #1—Key Issues and Available Data	2-10
2.4.4 Workshop #2—Alternative Interpretations	2-12
2.4.5 Working Meetings.....	2-13
2.4.6 SSC Sensitivity Model Development	2-14
2.4.7 Workshop #3—Feedback	2-15
2.4.8 SSC Preliminary Model Development	2-16
2.4.9 Finalization and Review of SSC Draft and Final Model.....	2-17
2.4.10 Documentation	2-19
2.4.10.1 Development of the Hazard Input Document.....	2-19
2.4.10.2 Development of Earlier Draft Report.....	2-19
2.4.10.3 Draft Report Review.....	2-19
2.4.10.4 Final Report Development	2-20
2.5 Participatory Peer Review Panel.....	2-20
2.5.1 Roles and Responsibilities	2-20
2.5.2 Reviews and Feedback	2-20
2.5.3 Fulfillment of SSHAC-Prescribed Scope of Review of Both Technical and Process Issues	2-21
2.6 Consistency of CEUS SSC Assessment Process with SSHAC Guidelines	2-22
3 EARTHQUAKE CATALOG.....	3-1
3.1 Goals for the Earthquake Catalog Development.....	3-1
3.1.1 Completeness.....	3-1

3.1.2	Uniformity of Catalog Processing	3-2
3.1.3	Catalog Review	3-3
3.2	Catalog Compilation	3-4
3.2.1	Continental-Scale Catalogs	3-5
3.2.2	Regional Catalogs	3-7
3.2.3	Catalogs from Special Studies	3-7
3.2.4	Focal Depth Data.....	3-8
3.2.5	Nontectonic Events.....	3-9
3.2.6	Identification of Unique Earthquake Entries	3-9
3.3	Development of a Uniform Moment Magnitude Earthquake Catalog.....	3-11
3.3.1	Approach for Uniform Magnitude and Unbiased Recurrence Estimation	3-11
3.3.2	Estimation of E[M] for the CEUS SSC Project Catalog	3-19
3.3.2.1	Effect of Magnitude Rounding on Statistical Tests	3-19
3.3.2.2	Moment Magnitude Data.....	3-20
3.3.2.3	Estimation of E[M] from Body-Wave Magnitudes	3-22
3.3.2.4	Estimation of E[M] from M_L Magnitudes.....	3-28
3.3.2.5	Estimation of E[M] from M_S Magnitudes	3-29
3.3.2.6	Estimation of E[M] from M_C and M_D Magnitudes.....	3-30
3.3.2.7	Estimation of E[M] from the Logarithm of Felt Area	3-32
3.3.2.8	Estimation of E[M] from the Maximum Intensity, I_0	3-32
3.3.2.9	Uniform Moment Magnitude Catalog of E[M] and N^* Values.....	3-36
3.4	Identification of Independent Earthquakes	3-37
3.5	Catalog Completeness.....	3-39
4	CONCEPTUAL SEISMIC SOURCE CHARACTERIZATION FRAMEWORK.....	4-1
4.1	Needs for a Conceptual SSC Framework	4-2
4.1.1	Logic Tree Approach to Representing Alternatives and Assessing Uncertainties.....	4-2
4.1.1.1	Examples of Logic Trees	4-3
4.1.1.2	Assigning Weights to Logic Tree Branches	4-3
4.1.2	Data Identification and Evaluation	4-5
4.1.2.1	“Generic” Data Identification to Address Indicators of a Seismic Source	4-5
4.1.2.2	Data Evaluation for Particular Seismic Sources: Data Evaluation and Data Summary Tables	4-7
4.1.3	Methodology for Identifying Seismic Sources.....	4-9

4.1.3.1 Hazard-Informed Approach	4-11
4.1.3.2 Conclusions Regarding the Hazard Significance of Various SSC Issues.....	4-13
4.1.3.3 Criteria for Defining Seismic Sources	4-14
4.2 Master Logic Tree	4-18
4.2.1 Description of Logic Tree Elements.....	4-18
4.2.2 RLME Source Logic Tree	4-20
4.2.3 Mmax Zones Logic Tree.....	4-22
4.2.4 Seismotectonic Zones Branch.....	4-24
5 SSC MODEL: OVERVIEW AND METHODOLOGY.....	5-1
5.1 Overview of Spatial and Temporal Models.....	5-1
5.1.1 Spatial Model Considerations.....	5-1
5.1.2 Considerations Regarding Temporal Models	5-3
5.1.3 Perspective on CEUS SSC Models.....	5-4
5.2 Maximum Earthquake Magnitude Assessment.....	5-5
5.2.1 Approaches to Mmax Estimation in the CEUS	5-6
5.2.1.1 Bayesian Mmax Approach	5-8
5.2.1.2 Kijko Approach to Mmax Assessment	5-17
5.2.1.3 Weights for the Alternative Mmax Approaches.....	5-20
5.2.1.4 Example Mmax Distributions	5-20
5.2.2 Other Mmax Issues	5-21
5.3 Earthquake Recurrence Assessment.....	5-22
5.3.1 Smoothing to Represent Spatial Stationarity.....	5-22
5.3.2 Smoothing Approach	5-23
5.3.2.1 Development of Penalized-Likelihood Approach and Formulation	5-23
5.3.2.2 Application of the Model and Specification of Model Parameters.....	5-36
5.3.2.3 Exploration of Model Results in Parameter Space	5-40
5.3.2.4 Consideration of Constant b-Value Kernel Approaches	5-42
5.3.2.5 Comparison to EPRI-SOG Approach.....	5-45
5.3.2.6 Assessment of the Lombardi Study	5-46
5.3.3 Estimation of Recurrence for RLME Sources.....	5-47
5.3.3.1 Estimation of Occurrence Rates for the Poisson Model	5-48
5.3.3.2 Estimation of Occurrence Rates for a Renewal Model	5-51
5.3.3.3 Incorporating Uncertainty in the Input.....	5-52
5.3.3.4 RLME Magnitude Distribution	5-53

5.4 Assessment of Future Earthquake Characteristics	5-54
5.4.1 Tectonic Stress Regime	5-55
5.4.2 Sense of Slip/Style of Faulting.....	5-55
5.4.3 Strike and Dip of Ruptures	5-55
5.4.4 Seismogenic Crustal Thickness	5-56
5.4.5 Fault Rupture Area	5-57
5.4.6 Rupture Length-to-Width Aspect Ratio.....	5-57
5.4.7 Relationship of Rupture to Source Zone Boundaries	5-58
5.5 Predicted Seismic Moment Rate	5-58
6 SSC MODEL: RLME SOURCES AND MMAX ZONES BRANCH.....	6-1
6.1 RLME Sources	6-1
6.1.1 Charlevoix.....	6-3
6.1.1.1 Evidence for Temporal Clustering.....	6-4
6.1.1.2 Localizing Tectonic Features	6-4
6.1.1.3 Geometry and Style of Faulting	6-5
6.1.1.4 RLME Magnitude	6-7
6.1.1.5 RLME Recurrence	6-8
6.1.2 Charleston	6-10
6.1.2.1 Evidence for Temporal Clustering.....	6-11
6.1.2.2 Localizing Feature	6-12
6.1.2.3 Geometry and Style of Faulting	6-12
6.1.2.4 RLME Magnitude	6-15
6.1.2.5 RLME Recurrence	6-17
6.1.3 Cheraw Fault	6-22
6.1.3.1 Evidence for Temporal Clustering.....	6-23
6.1.3.2 Geometry and Style of Faulting	6-24
6.1.3.3 RLME Magnitude	6-25
6.1.3.4 RLME Recurrence	6-26
6.1.4 Meers Fault.....	6-28
6.1.4.1 Evidence for Temporal Clustering.....	6-29
6.1.4.2 Localizing Feature	6-29
6.1.4.3 Geometry and Style of Faulting	6-30
6.1.4.4 RLME Magnitude	6-31
6.1.4.5 RLME Recurrence	6-34

6.1.5 Reelfoot Rift–New Madrid Fault System	6-35
6.1.5.1 Evidence for Temporal Clustering.....	6-40
6.1.5.2 Geometry and Style of Faulting	6-42
6.1.5.3 RLME Magnitude	6-44
6.1.5.4 RLME Recurrence	6-47
6.1.6 Reelfoot Rift—Eastern Rift Margin Fault	6-50
6.1.6.1 Evidence for Temporal Clustering.....	6-53
6.1.6.2 Geometry and Style of Faulting	6-53
6.1.6.3 RLME Magnitude	6-54
6.1.6.4 RLME Recurrence	6-56
6.1.7 Reelfoot Rift—Marianna	6-57
6.1.7.1 Evidence for Temporal Clustering.....	6-58
6.1.7.2 Geometry and Style of Faulting	6-59
6.1.7.3 RLME Magnitude	6-60
6.1.7.4 RLME Recurrence	6-61
6.1.8 Reelfoot Rift—Commerce Fault Zone	6-62
6.1.8.1 Evidence for Temporal Clustering.....	6-63
6.1.8.2 Geometry and Style of Faulting	6-64
6.1.8.3 RLME Magnitude	6-65
6.1.8.4 RLME Recurrence	6-66
6.1.9 Wabash Valley	6-68
6.1.9.1 Evidence for Temporal Clustering.....	6-69
6.1.9.2 Geometry and Style of Faulting	6-69
6.1.9.3 RLME Magnitude	6-72
6.1.9.4 RLME Recurrence	6-73
6.2 Mmax Distributed Seismicity Source Zones.....	6-74
6.2.1 Definition of Mmax Zones	6-74
6.2.2 Criteria for Defining the MESE/NMESE Boundary	6-75
6.3 Maximum Magnitude Distributions for Mmax Distributed Seismicity Sources.....	6-76
6.3.1 Maximum Observed Earthquake Magnitude	6-76
6.3.2 Mmax Distributions	6-77
6.4 Recurrence Parameters	6-78
6.4.1 Rate and b-Value Maps for Single Zone and Two Zones.....	6-78
6.4.2 Comparison of Recurrence Parameters to Catalog.....	6-79

7 SSC MODEL: SEISMOTECTONIC ZONES BRANCH	7-1
7.1 Approaches and Data Used to Define Seismotectonic Zones	7-1
7.2 RLME Sources in the Seismotectonic Zones Branch.....	7-4
7.3 Seismotectonic Source Zones.....	7-4
7.3.1 St. Lawrence Rift Zone (SLR)	7-4
7.3.1.1 Background.....	7-5
7.3.1.2 Basis for Defining Seismotectonic Zone	7-11
7.3.1.3 Basis for Zone Geometry	7-12
7.3.1.4 Basis for Zone Mmax	7-12
7.3.1.5 Future Earthquake Characteristics	7-13
7.3.2 Great Meteor Hotspot Zone (GMH)	7-15
7.3.2.1 Background.....	7-16
7.3.2.2 Basis for Defining Seismotectonic Zone	7-18
7.3.2.3 Basis for Zone Geometry	7-19
7.3.2.4 Basis for Zone Mmax	7-19
7.3.2.5 Future Earthquake Characteristics	7-20
7.3.3 Northern Appalachian Zone (NAP)	7-21
7.3.3.1 Background.....	7-21
7.3.3.2 Basis for Defining Seismotectonic Zone	7-23
7.3.3.3 Basis for Zone Geometry	7-24
7.3.3.4 Basis for Zone Mmax	7-24
7.3.3.5 Future Earthquake Characteristics	7-25
7.3.4 Paleozoic Extended Crust (PEZ).....	7-25
7.3.4.1 Background.....	7-26
7.3.4.2 Basis for Defining Seismotectonic Zone	7-32
7.3.4.3 Basis for Zone Geometry	7-33
7.3.4.4 Basis for Zone Mmax	7-34
7.3.4.5 Future Earthquake Characteristics	7-36
7.3.5 Illinois Basin Extended Basement Zone (IBEB)	7-37
7.3.5.1 Background.....	7-38
7.3.5.2 Basis for Defining Seismotectonic Zone	7-38
7.3.5.3 Basis for Zone Geometry	7-40
7.3.5.4 Basis for Zone Mmax	7-41
7.3.5.5 Future Earthquake Characteristics	7-41
7.3.6 Reelfoot Rift Zone (RR)	7-42

7.3.6.1 Background.....	7-42
7.3.6.2 Basis for Defining Seismotectonic Zone	7-46
7.3.6.3 Basis for Zone Geometry	7-46
7.3.6.4 Basis for Zone Mmax.....	7-47
7.3.6.5 Future Earthquake Characteristics	7-48
7.3.7 Extended Continental Crust–Atlantic Margin Zone (ECC-AM)	7-48
7.3.7.1 Background.....	7-49
7.3.7.2 Basis for Defining Seismotectonic Zone	7-53
7.3.7.3 Basis for Geometry	7-54
7.3.7.4 Basis for Mmax	7-54
7.3.7.5 Future Earthquake Characteristics	7-55
7.3.8 Atlantic Highly Extended Crust Zone (AHEX).....	7-55
7.3.8.1 Basis for Defining Seismotectonic Zone	7-56
7.3.8.2 Basis for Geometry	7-57
7.3.8.3 Basis for Mmax	7-57
7.3.8.4 Future Earthquake Characteristics	7-57
7.3.9 Extended Continental Crust–Gulf Coast Zone (ECC-GC).....	7-58
7.3.9.1 Basis for Defining Seismotectonic Zone	7-58
7.3.9.2 Basis for Zone Geometry	7-59
7.3.9.3 Basis for Zone Mmax.....	7-62
7.3.9.4 Future Earthquake Characteristics	7-63
7.3.9.5 Possible Paleoliquefaction Features in Arkansas, Louisiana, and Mississippi	7-64
7.3.10 Gulf Coast Highly Extended Crust Zone (GHEX).....	7-65
7.3.10.1 Basis for Defining Seismotectonic Zone	7-66
7.3.10.2 Basis for Zone Geometry	7-66
7.3.10.3 Basis for Zone Mmax.....	7-66
7.3.10.4 Future Earthquake Characteristics	7-67
7.3.11 Oklahoma Aulacogen Zone (OKA).....	7-68
7.3.11.1 Basis for Defining Seismotectonic Zone	7-69
7.3.11.2 Basis for Zone Geometry	7-69
7.3.11.3 Basis for Zone Mmax.....	7-70
7.3.11.4 Future Earthquake Characteristics	7-70
7.3.12 Midcontinent-Craton Zone (MidC)	7-70
7.3.12.1 Background.....	7-71

7.3.12.2 Basis for Defining Seismotectonic Zone	7-76
7.3.12.3 Basis for Zone Geometry	7-77
7.3.12.4 Basis for Zone Mmax	7-77
7.3.12.5 Future Earthquake Characteristics	7-77
7.4 Maximum Magnitude Distributions for Seismotectonic Distributed Seismicity Sources	7-78
7.4.1 Maximum Observed Earthquake Magnitude	7-78
7.4.2 Mmax Distributions	7-79
7.5 Recurrence Parameters	7-80
7.5.1 Rate and b-Value Maps for Single Zone and Two Zones	7-80
7.5.2 Comparison of Recurrence Parameters to Catalog	7-80
8 DEMONSTRATION HAZARD CALCULATIONS	8-1
8.1 Background on Demonstration Hazard Calculations	8-1
8.2 Demonstration Hazard Calculations	8-2
8.2.1 Central Illinois Site	8-4
8.2.2 Chattanooga Site	8-5
8.2.3 Houston Site	8-6
8.2.4 Jackson Site	8-7
8.2.5 Manchester Site	8-9
8.2.6 Savannah Site	8-9
8.2.7 Topeka Site	8-10
9 USE OF THE CEUS SSC MODEL IN PSHA	9-1
9.1 Overview	9-1
9.2 Hazard Input Document (HID)	9-2
9.3 Implementation Instructions	9-2
9.3.1 Simplifications to Seismic Sources	9-2
9.3.1.1 Charleston RLME	9-3
9.3.1.2 Charlevoix RLME	9-3
9.3.1.3 Cheraw RLME	9-4
9.3.1.4 Commerce Fault Zone RLME	9-5
9.3.1.5 Eastern Rift Margin North RLME	9-5
9.3.1.6 Eastern Rift Margin South RLME	9-5
9.3.1.7 Marianna RLME	9-6
9.3.1.8 Meers RLME	9-6

9.3.1.9 New Madrid Fault System RLME.....	9-7
9.3.1.10 Wabash Valley RLME.....	9-7
9.3.1.11 Background Sources.....	9-8
9.3.2 Accessing the SSC Model and Components from the Website	9-8
9.3.3 Accessing Project Databases.....	9-9
9.3.4 Use of SSC Model with Site-Specific Refinements	9-10
9.4 Hazard Significance	9-10
9.4.1 Data Available to Evaluate the Precision of Seismic Hazard Estimates.....	9-10
9.4.2 Observed Imprecision in Seismic Hazard Estimates.....	9-11
9.4.2.1 Area Seismic Sources.....	9-11
9.4.2.2 RLME Seismic Sources	9-12
9.4.2.3 Ground Motion Equations	9-15
9.4.2.4 Site Response	9-19
9.4.3 Conclusions on the Precision in Seismic Hazard Estimates	9-19
10 REFERENCES	10-1
11 GLOSSARY OF KEY TERMS.....	11-1
A DESCRIPTION OF THE CEUS SSC PROJECT DATABASE	A-1
A.1 Data Sources	A-2
A.2 Project Database Design and Management.....	A-3
A.3 Workflow and Data Assessment.....	A-3
A.3.1 Workflow	A-3
A.3.2 Digital Data.....	A-4
A.3.3 Nondigital Data	A-4
A.4 Use of Project Database in Model Development	A-5
A.5 Metadata.....	A-5
A.6 Database Delivery Format	A-6
B EARTHQUAKE CATALOG DATABASE	B-1
B.1 CEUS SSC Uniform Moment Magnitude Earthquake Catalog	B-1
B.2 Moment Magnitude Data.....	B-2
B.3 Approximate Moment Magnitude Data	B-3
B.4 CEUS SSC Project Data.....	B-3

C DATA EVALUATION TABLES.....	C-1
Introduction	C-2
D DATA SUMMARY TABLES	D-1
Introduction	D-2
E CEUS PALEOLIQUEFACTION DATABASE, UNCERTAINTIES ASSOCIATED WITH PALEOLIQUEFACTION DATA, AND GUIDANCE FOR SEISMIC SOURCE CHARACTERIZATION.....	E-i
E.1 Development of the Paleoliquefaction Database	E-1
E.1.1 Database Structure	E-1
E.1.2 Regional Data Sets	E-4
E.2 Uncertainties Associated with Paleoliquefaction Data	E-24
E.2.1 Collection of Paleoliquefaction Data	E-24
E.2.2 Uncertainties Related to Interpretation of Paleoliquefaction Data.....	E-35
E.2.3 Recommendations for Future Research	E-43
E.3 Guidance for the Use of Paleoliquefaction Data in Seismic Source Characterization.....	E-44
E.4 Glossary.....	E-46
E.5 References	E-49
E.5.1 References Cited in Paleoliquefaction Database	E-49
E.5.2 References Cited in Appendix E	E-54
F WORKSHOP SUMMARIES	F-1
WORKSHOP 1: KEY ISSUES AND AVAILABLE DATA	
DAY 1–TUESDAY, JULY 22, 2008	F-1
DAY 2–WEDNESDAY, JULY 23, 2008	F-10
REFERENCES.....	F-17
WORKSHOP 2: ALTERNATIVE INTERPRETATIONS	
DAY 1–WEDNESDAY, FEBRUARY 18, 2009	F18
DAY 2–THURSDAY, FEBRUARY 19, 2009.....	F-24
DAY 3–FRIDAY, FEBRUARY 20, 2009	F-29
REFERENCES	F-34
WORKSHOP 3: FEEDBACK	
DAY 1–TUESDAY, AUGUST 25, 2009	F-42
DAY 2–WEDNESDAY, AUGUST 26, 2009.....	F-49

G BIOGRAPHIES OF PROJECT TEAM	G-1
EPRI MANAGEMENT	G-2
PROJECT MANAGER	G-2
TI TEAM	G-3
TECHNICAL SUPPORT.....	G-7
DATABASE MANAGER.....	G-9
PARTICIPATORY PEER REVIEW PANEL.....	G-9
SPONSOR REVIEWERS.....	G-14
H CEUS SSC MODEL HAZARD INPUT DOCUMENT (HID)	H-1
H.1 Introduction	H-1
H.2 Seismic Source Model Structure and Master Logic Tree	H-1
H.3 Mmax Zones Distributed Seismicity Sources	H-2
H.3.1 Division of Study Region	H-2
H.3.2 Location of Boundary of Mesozoic Extension	H-2
H.3.3 Magnitude Interval Weights for Fitting Earthquake Occurrence Parameters	H-2
H.3.4 Mmax Zones	H-2
H.3.5 Seismogenic Crustal Thickness	H-2
H.3.6 Future Earthquake Rupture Characteristics	H-3
H.3.7 Assessment of Seismicity Rates	H-3
H.3.8 Degree of Smoothing Applied in Defining Spatial Smoothing of Seismicity Rates	H-3
H.3.9 Uncertainty in Earthquake Recurrence Rates.....	H-3
H.3.10 Uncertainty in Maximum Magnitude.....	H-4
H.4 Seismotectonic Zones	H-4
H.4.1 Alternative Zonation Models	H-4
H.4.2 Magnitude Interval Weights for Fitting Earthquake Occurrence Parameters.....	H-4
H.4.3 Seismotectonic Zones.....	H-5
H.4.4 Seismogenic Crustal Thickness.....	H-5
H.4.5 Future Earthquake Rupture Characteristics	H-5
H.4.6 Assessment of Seismicity Rates	H-5
H.4.7 Degree of Smoothing Applied in Defining Spatial Smoothing of Seismicity Rates	H-5
H.4.8 Uncertainty in Earthquake Recurrence Rates	H-5
H.4.9 Uncertainty in Maximum Magnitude	H-6
H.5 RLME Sources	H-6

H.5.1 Charlevoix RLME Seismic Source Model	H-6
H.5.2 Charleston RLME Seismic Source Model.....	H-7
H.5.3 Cheraw RLME Seismic Source Model.....	H-9
H.5.4 Meers RLME Seismic Source Model	H-11
H.5.5 New Madrid Fault System RLME Seismic Source Model	H-12
H.5.6 Eastern Rift Margin Fault RLME Seismic Source Model	H-14
H.5.7 Marianna Zone RLME Seismic Source Model.....	H-15
H.5.8 Commerce Fault RLME Seismic Source Model.....	H-16
H.5.9 Wabash Valley RLME Seismic Source Model	H-18
/ PPRP REVIEW COMMENTS	I-1
CORRESPONDENCE—CONTENTS	I-3
Participatory Peer Review Panel (PPRP) Letters.....	I-3
Technical Integration (TI) Team and Project Manager (PM) Response to PPRP Letters.....	I-4
J MAGNITUDE-RECURRENCE MAPS FOR ALL REALIZATIONS AND ALL SOURCE-ZONE CONFIGURATIONS.....	J-1
K SCR DATABASE USED TO DEVELOP MMAX PRIOR DISTRIBUTIONS	K-1
K.1 SCR Earthquake Catalog.....	K-1
K.2 SCR Crustal Domains.....	K-3
L QUALITY ASSURANCE	L-1
L.1 BACKGROUND.....	L-1
L.2 CEUS SSC PROJECT	L-2
L.2.1 Introduction.....	L-2
L.3 BEST BUSINESS PRACTICES	L-3
L.3.1 General.....	L-3
L.4 CEUS SSC EARTHQUAKE CATALOG DEVELOPMENT	L-3
L.4.1 External Review of Earthquake Catalog.....	L-3
L.4.2 Simulation Testing.....	L-4
L.4.3 Checks for Consistency in Magnitude Conversion from Intensity	L-4
L.4.4 Use of Verified Computer Programs.....	L-4
L.5 RECURRENCE ANALYSIS AND SPATIAL SMOOTHING.....	L-4
L.5.1 Introduction.....	L-4
L.5.2 Recurrence Comparisons at the Source-Zone Level	L-5

L.5.3 Recurrence Comparisons for Portions of a Source Zone	L-5
L.5.4 Examination of Recurrence Maps	L-5
L.5.5 Test with a Synthetic Catalog Homogeneous Seismicity	L-5
L.5.6 Test for the Adequacy of Eight Maps to Represent Epistemic Uncertainty	L-6
L.6 HAZARD CALCULATION SOFTWARE	L-6
L.6.1 Introduction.....	L-6
L.6.2 Test for the Treatment of Variable b.....	L-6
L.6.3 Test for the Treatment of Dipping Ruptures Within a Source Zone.....	L-6
L.6.4 Tests for Treatment of Epistemic Uncertainty from Sources that Make Small Contribution to Hazard.....	L-6

LIST OF FIGURES

Figure 1.3-1 Map showing the study area and test sites for the CEUS SSC Project.....	1-15
Figure 2.3-1 CEUS SSC Project organization	2-33
Figure 2.3-2 Lines of communication among the participants of the CEUS SSC Project.....	2-34
Figure 2.4-1 Essential activities associated with a SSHAC Level 3 or 4 project (Coppersmith et al., 2010).....	2-35
Figure 3.2-1 Areal coverage of the primary earthquake catalog sources. Top: GSC catalog (Halchuk, 2009); bottom: USGS seismic hazard mapping catalog (Petersen et al., 2008). Red line denotes boundary of study region. Blue line denotes portion of each catalog used for development of project catalog.....	3-57
Figure 3.2-2 Histogram of M_L magnitudes from the GSC SHEEF catalog for the time period 1600-1899 and the region east of longitude -105° and south of latitude 53°	3-58
Figure 3.2-3 Histogram of M_L magnitudes from the GSC SHEEF catalog for the time period 1900-1929 and the region east of longitude -105° and south of latitude 53°	3-59
Figure 3.2-4 Histogram of M_L magnitudes from the GSC SHEEF catalog for the time period 1930-1979 and the region east of longitude -105° and south of latitude 53°	3-60
Figure 3.2-5 Histogram of M_L magnitudes from the GSC SHEEF catalog for the time period 1980-2007 and the region east of longitude -105° and south of latitude 53°	3-61
Figure 3.2-6 Histogram of M_L magnitudes from the revised catalog with GSC as the source for the time period 1928-1979	3-62
Figure 3.2-7 Map of the CEUS SSC Project catalog showing earthquakes of uniform moment magnitude $E[M]$ 2.9 and larger. Colored symbols denote earthquakes not contained in the USGS seismic hazard mapping catalog.	3-63
Figure 3.3-1 Illustration of equivalence of the M^* and γ^2 corrections to remove bias in earthquake recurrence relationships estimated from magnitudes with uncertainty	3-64
Figure 3.3-2 Approximate moment magnitudes from Atkinson (2004b) compared to values of M given in Table B-2 in Appendix B for earthquakes in common	3-65
Figure 3.3-3 Approximate moment magnitudes from Boatwright (1994) compared to values of M given in Table B-2 in Appendix B for earthquakes in common	3-66
Figure 3.3-4 Approximate moment magnitudes from Moulis (2002) compared to values of M given in Table B-2 in Appendix B for earthquakes in common.....	3-67
Figure 3.3-5 Difference between M_N reported by the GSC and M_N or $m_{Lg(f)}$ reported by the Weston Observatory catalog as a function of time.....	3-68
Figure 3.3-6 Spatial distribution of earthquakes with body-wave (m_b , m_{bLg} , M_N) and M magnitudes in the CEUS SSC Project catalog for the Midcontinent region. Color codes indicate the source of the body-wave magnitudes.....	3-69
Figure 3.3-7 m_b - M data for the earthquakes shown on Figure 3.3-6. Red curve shows the preferred offset fit $M = m_b - 0.28$	3-70

Figure 3.3-8 Residuals from offset fit shown on Figure 3.3-7 plotted against earthquake year	3-71
Figure 3.3-9 Spatial distribution of earthquakes with body wave (m_b , m_{bLg} , M_N) and M magnitudes in the CEUS SSC Project catalog for the northeastern portion of the study region. Color codes indicate the source of the body-wave magnitudes.	3-72
Figure 3.3-10 m_b -M data for the earthquakes shown on Figure 3.3-9. Red curve shows the preferred offset fit $M = m_b - 0.42$	3-73
Figure 3.3-11 Residuals from offset fit shown on Figure 3.3-10 plotted against earthquake year	3-74
Figure 3.3-12 Residuals for GSC data from offset fit shown on Figure 3.3-10 plotted against earthquake year.....	3-75
Figure 3.3-13 Residuals for WES data from offset fit shown on Figure 3.3-10 plotted against earthquake year.....	3-76
Figure 3.3-14 Residuals for data from sources other than GSC or WES from offset fit shown on Figure 3.3-10 plotted against earthquake year	3-77
Figure 3.3-15 Difference between body-wave magnitudes reported by LDO and those by other sources as a function of year	3-78
Figure 3.3-16 Spatial distribution of earthquakes with reported GSC body-wave magnitudes. Red and blue symbols indicate earthquakes with both m_b and M magnitudes for $m_b \geq 3.5$. Dashed line indicates the portion of the study region considered the “Northeast” for purposes of magnitude scaling.....	3-79
Figure 3.3-17 M - m_b as a function of time for m_b data from the GSC shown on Figure 3.3-16	3-80
Figure 3.3-18 Plot of magnitude differences $m_{bLg} - m(3 \text{ Hz})$ for the OKO catalog.....	3-81
Figure 3.3-19 Final m_b -M data set. Vertical dashed lines indicate the magnitude range used to develop the scaling relationship. Diagonal line indicates a one-to-one correlation.	3-82
Figure 3.3-20 Spatial distribution of earthquakes in the CEUS SSC Project catalog with instrumental M_L magnitudes.....	3-83
Figure 3.3-21 Spatial distribution of earthquakes in the CEUS SSC Project catalog with instrumental M_L magnitudes and M magnitudes	3-84
Figure 3.3-22 M_L -M data from the CEUS SSC Project catalog and robust regression fit to the data	3-85
Figure 3.3-23 Relationship between M_N and M_L for the GSC data	3-86
Figure 3.3-24 Data from the northeastern portion of the study region with M_L and M_C or M_D magnitude from catalog sources other than the GSC	3-87
Figure 3.3-25 Data from the northeastern portion of the study region with M_L and M magnitudes from sources other than the GSC.....	3-88
Figure 3.3-26 Spatial distribution of earthquakes in the CEUS SSC Project catalog with $M_S \geq 3$ magnitudes	3-89
Figure 3.3-27 M_S -M data from the CEUS SSC Project catalog and quadratic polynomial fit to the data	3-90
Figure 3.3-28 Spatial distribution of earthquakes in the CEUS SSC Project catalog with $M_C \geq 2.5$ magnitudes	3-91

Figure 3.3-29 Spatial distribution of earthquakes in the CEUS SSC Project catalog with $M_C \geq 2.5$ and M magnitudes	3-92
Figure 3.3-30 Spatial distribution of earthquakes in the CEUS SSC Project catalog with $M_D \geq 3$ magnitudes	3-93
Figure 3.3-31 Spatial distribution of earthquakes in the CEUS SSC Project catalog with both M_D and M magnitudes	3-94
Figure 3.3-32 M_C - M data from the CEUS SSC Project catalog and linear regression fit to the data	3-95
Figure 3.3-33 Spatial distribution of earthquakes with reported M_C and M_D magnitudes	3-96
Figure 3.3-34 Comparison of M_C and M_D magnitudes for the LDO and WES catalogs	3-97
Figure 3.3-35 Comparison of M_C with M_D for at least one of the two magnitude types reported in the OKO catalog	3-98
Figure 3.3-36 Comparison of M_C with M_D for at least one of the two magnitude types reported in the CERI catalog	3-99
Figure 3.3-37 Comparison of M_C with M_D for at least one of the two magnitude types reported in the SCSN catalog	3-100
Figure 3.3-38 Comparison of M_C with M_D for at least one of the two magnitude types reported in other catalogs for earthquakes in the Midcontinent portion of the study region	3-101
Figure 3.3-39 Relationship between M and M_C , M_D , or M_L for the Midcontinent portion of the study region.....	3-102
Figure 3.3-40 Comparison of M_C and M_D magnitudes with M_L magnitudes for the region between longitudes 105°W and 100°W	3-103
Figure 3.3-41 Comparison of m_b magnitudes with M_L magnitudes for the region between longitudes 105°W and 100°W	3-104
Figure 3.3-42 Comparison of m_b magnitudes with M_C and M_D magnitudes for the region between longitudes 105°W and 100°W	3-105
Figure 3.3-43 Spatial distribution of earthquake with $\ln(\text{FA})$ in the CEUS SSC Project catalog.....	3-106
Figure 3.3-44 Catalog $\ln(\text{FA})$ - M data and fitted model.....	3-107
Figure 3.3-45 Spatial distribution of earthquakes in the CEUS SSC Project catalog with reported values of I_0	3-108
Figure 3.3-46 I_0 and M data for earthquakes in the CEUS SSC Project catalog. Curves show locally weighted least-squares fit (Loess) to the data and the relationship published by Johnston (1996b).	3-109
Figure 3.3-47 I_0 and m_b data from the NCEER91 catalog. Plotted are the relationships between I_0 and m_b developed by EPRI (1988) (EPRI-SOG) and Sibol et al. (1987).....	3-110
Figure 3.3-48 Categorical model fits of I_0 as a function and M for earthquakes in the CEUS SSC Project catalog	3-111
Figure 3.3-49 Results from proportional odds logistic model showing the probability of individual intensity classes as a function of M	3-112
Figure 3.3-50 Comparison of I_0 and m_b data from the CEUS SSC Project catalog for those earthquakes with reported values of M (M set) and the full catalog (full set). Locally weighted least-squares fits to the two data sets are shown along with the	

relationship use to develop the EPRI (1988) catalog and the Sibol et al. (1987) relationship used in the NCEER91 catalog.....	3-113
Figure 3.3-51 Linear fits to the data from Figure 3.3-50 for $I_0 \geq V$	3-114
Figure 3.3-52 Comparison of I_0 and m_b data from the project, with m_b adjusted for the difference in m_b to M scaling	3-115
Figure 3.3-53 Linear fits to the data from Figure 3.3-52 for $I_0 \geq V$	3-116
Figure 3.3-54 Composite I_0 -M data set used for assessment of I_0 scaling relationship	3-117
Figure 3.3-55 Linear and inverse sigmoid models fit to the project data for $I_0 > IV$	3-118
Figure 3.4-1 Illustration of process used to identify clusters of earthquakes (from EPRI, 1988, Vol. 1): (a) local and extended time and distance windows, (b) buffer window, and (c) contracted window	3-119
Figure 3.4-2 Identification of secondary (dependent) earthquakes inside the cluster region through Poisson thinning (from EPRI, 1988, Vol. 1).....	3-120
Figure 3.4-3 Comparison of dependent event time and distance windows with results for individual clusters in the project catalog.....	3-121
Figure 3.5-1 Earthquake catalog and catalog completeness regions used in EPRI-SOG (EPRI, 1988)	3-122
Figure 3.5-2 CEUS SSC Project earthquake catalog and modified catalog completeness regions	3-123
Figure 3.5-3 Plot of year versus location for the CEUS SSC Project earthquake catalog. Red lines indicate the boundaries of the catalog completeness time periods.....	3-124
Figure 3.5-4 (1 of 7) “Stepp” plots of earthquake recurrence rate as a function of time for the individual catalog completeness regions shown on Figure 3.5-2	3-125
Figure 3.5-4 (2 of 7) “Stepp” plots of earthquake recurrence rate as a function of time for the individual catalog completeness regions shown on Figure 3.5-2	3-126
Figure 3.5-4 (3 of 7) “Stepp” plots of earthquake recurrence rate as a function of time for the individual catalog completeness regions shown on Figure 3.5-2	3-127
Figure 3.5-4 (4 of 7) “Stepp” plots of earthquake recurrence rate as a function of time for the individual catalog completeness regions shown on Figure 3.5-2	3-128
Figure 3.5-4 (5 of 7) “Stepp” plots of earthquake recurrence rate as a function of time for the individual catalog completeness regions shown on Figure 3.5-2	3-129
Figure 3.5-4 (6 of 7) “Stepp” plots of earthquake recurrence rate as a function of time for the individual catalog completeness regions shown on Figure 3.5-2	3-130
Figure 3.5-4 (7 of 7) “Stepp” plots of earthquake recurrence rate as a function of time for the individual catalog completeness regions shown on Figure 3.5-2	3-131
Figure 4.1.1-1 Example logic tree from the PEGASOS project (NAGRA, 2004) showing the assessment of alternative conceptual models on the logic tree. Each node of the logic tree represents an assessment that is uncertain. Alternative branches represent the alternative models or parameter values, and the weights associated with each branch reflect the TI Team’s relative degree of belief that each branch is the correct model or parameter value.	4-40
Figure 4.1.1-2 Example logic tree from the PVHA-U (SNL, 2008) project showing the treatment of alternative conceptual models in the logic tree	4-41

Figure 4.2.1-1 Master logic tree showing the Mmax zones and seismotectonic zones alternative conceptual models for assessing the spatial and temporal characteristics of future earthquake sources in the CEUS.....	4-42
Figure 4.2.2-1 Example of a logic tree for RLME sources. Shown is the tree for the Marianna RLME source.	4-43
Figure 4.2.2-2 Map showing RLME sources, some with alternative source geometries (discussed in Section 6.1).	4-44
Figure 4.2.3-1 Logic tree for the Mmax zones branch of the master logic tree.....	4-45
Figure 4.2.3-2 Subdivision used in the Mmax zones branch of the master logic tree. Either the region is considered one zone for purposes of Mmax or the region is divided into two zones as shown: a Mesozoic-and-younger extension (MESE) zone and a non-Mesozoic-and-younger zone (NMESE). In this figure the “narrow” MESE zone is shown	4-46
Figure 4.2.3-3 Subdivision used in the Mmax zones branch of the master logic tree. Either the region is considered one zone for purposes of Mmax or the region is divided into two zones as shown: a Mesozoic-and-younger extension (MESE) zone and a non-Mesozoic-and-younger zone (NMESE). In this figure the “wide” MESE zone is shown	4-47
Figure 4.2.4-1(a) Logic tree for the seismotectonic zones branch of the master logic tree	4-48
Figure 4.2.4-1(b) Logic tree for the seismotectonic zones branch of the master logic tree	4-49
Figure 4.2.4-2 Seismotectonic zones shown in the case where the Rough Creek Graben is not part of the Reelfoot Rift (RR), and the Paleozoic Extended Zone is narrow (PEZ-N)	4-50
Figure 4.2.4-3 Seismotectonic zones shown in the case where the Rough Creek Graben is part of the Reelfoot Rift (RR-RCG), and the Paleozoic Extended Zone is narrow (PEZ-N).....	4-51
Figure 4.2.4-4 Seismotectonic zones shown in the case where the Rough Creek Graben is not part of the Reelfoot Rift (RR), and the Paleozoic Extended Crust is wide (PEZ-W)	4-52
Figure 4.2.4-5 Seismotectonic zones shown in the case where the Rough Creek Graben is part of the Reelfoot Rift (RR-RCG), and the Paleozoic Extended Crust is wide (PEZ-W)	4-53
Figure 5.2.1-1 Diagrammatic illustration of the Bayesian Mmax approach showing (a) the prior distribution, (b) the likelihood function, and (c) the posterior distribution. The posterior distribution is represented by a discrete distribution (d) for implementation in hazard analysis.	5-72
Figure 5.2.1-2 Diagrammatic illustration of the Bayesian Mmax approach showing (a) the prior distribution, (b) the likelihood function, and (c) the posterior distribution. The posterior distribution is represented by a discrete distribution (d) for implementation in hazard analysis.	5-73
Figure 5.2.1-3 Median values of $m_{\max-obs}$ as a function of maximum magnitude, m^u , and sample size N , the number of earthquakes $\geq M$ 4.5.....	5-74
Figure 5.2.1-4 Histograms of $m_{\max-obs}$ for extended and non-extended superdomains	5-75

Figure 5.2.1-5 Histograms of $m_{\max-obs}$ for Mesozoic-and-younger extended (MESE) superdomains and for older extended and non-extended (NMESE) superdomains	5-76
Figure 5.2.1-6 Histograms of $m_{\max-obs}$ for Mesozoic-and-younger extended (MESE) superdomains and for older extended and non-extended (NMESE) superdomains using age of most recent extension for the age classification	5-77
Figure 5.2.1-7 Histograms of $m_{\max-obs}$ for Mesozoic-and-younger extended (MESE) superdomains and for older extended and non-extended (NMESE) superdomains using final sets indicated by asterisks in Tables 5.2.1-1 and 5.2.1-2	5-78
Figure 5.2.1-8 Histograms of $m_{\max-obs}$ for combined (COMB) superdomains using final sets indicated by asterisks in Table 5.2.1-3	5-79
Figure 5.2.1-9 Bias adjustments from $m_{\max-obs}$ to m^u for the three sets of superdomain analysis results presented in Table 5.2.1-4.....	5-80
Figure 5.2.1-10 Results of simulations of estimates of Mmax using the Bayesian approach for earthquake catalogs ranging in size from 1 to 1,000 earthquakes. True Mmax is set at the mean of the prior distribution.....	5-81
Figure 5.2.1-11 Comparison of the Kijko (2004) estimates of m^u for given values of $m_{\max-obs}$ and N , the number of earthquakes of magnitude ≥ 4.5 . Also shown is the median value of $m_{\max-obs}$ for given m^u obtained using Equation 5.2.1-2.....	5-82
Figure 5.2.1-12 Behavior of the cumulative probability function for m^u (Equation 5.2.1-9) for the K-S-B estimator and a value of $m_{\max-obs}$ equal to 6.....	5-83
Figure 5.2.1-13 Example Mmax distribution assessed for the Mesozoic-and-younger extended Mmax zone for the case where the zone is "narrow" (MESE-N). Distributions are shown for the Kijko approach and for the Bayesian approach using either the Mesozoic-and-younger extended prior distribution or the composite prior distribution. The final composite Mmax distribution, which incorporates the relative weights, is shown by the red probability distribution.	5-84
Figure 5.2.1-14 Example Mmax distribution assessed for the Northern Appalachian seismotectonic zone (NAP). Distributions are shown for the Kijko approach and for the Bayesian approach using either the Mesozoic-and-younger extended prior distribution or the composite prior distribution. Note that the Kijko results are shown in this example for illustration, even though they have zero weight. The final composite Mmax distribution, which incorporates the relative weights, is shown by the red probability distribution.	5-85
Figure 5.3.2-1 Likelihood function for rate per unit area in a Poisson process, for multiple values of the earthquake count N : (a) arithmetic scale, and (b) logarithmic scale used to illustrate decreasing COV as N increases	5-86
Figure 5.3.2-2 Likelihood function for b -value of an exponential magnitude distribution, for multiple values of the earthquake count N . The value of b is normalized by the maximum-likelihood estimate, which is derived from Equation 5.3.2-5.....	5-87
Figure 5.3.2-3 Histogram of magnitudes in the earthquake catalog used in this section. The minimum magnitude shown (M 2.9) is the lowest magnitude used in these recurrence calculations.	5-88

Figure 5.3.2-4 Objectively determined values of the penalty function for $\ln(\text{rate})$ for Case A magnitude weights. Source zones are sorted from smallest to largest. See list of abbreviations for full source-zone names.	5-89
Figure 5.3.2-5 Objectively determined values of the penalty function for beta for Case A magnitude weights	5-90
Figure 5.3.2-6 Objectively determined values of the penalty function for $\ln(\text{rate})$ for Case B magnitude weights	5-91
Figure 5.3.2-7 Objectively determined values of the penalty function for beta for Case B magnitude weights. Source zones are sorted from smallest to largest.	5-92
Figure 5.3.2-8 Objectively determined values of the penalty function for $\ln(\text{rate})$ for Case E magnitude weights	5-93
Figure 5.3.2-9 Objectively determined values of the penalty function for beta for Case E magnitude weights. Source zones are sorted from smallest to largest.	5-94
Figure 5.3.2-10 Mean map of rate and b -value for ECC-AM calculated using Case A magnitude weights	5-95
Figure 5.3.2-11 Mean map of rate and b -value for ECC-GC calculated using Case A magnitude weights	5-96
Figure 5.3.2-12 Mean map of rate and b -value for ECC-AM calculated using Case B magnitude weights	5-97
Figure 5.3.2-13 Mean map of rate and b -value for ECC-GC calculated using Case B magnitude weights	5-98
Figure 5.3.2-14 Mean map of rate and b -value for ECC-AM calculated using Case E magnitude weights	5-99
Figure 5.3.2-15 Mean map of rate and b -value for ECC-GC calculated using Case E magnitude weights	5-100
Figure 5.3.2-16 Sensitivity of seismic hazard at Manchester site to the strength of the prior on b	5-101
Figure 5.3.2-17 Sensitivity of seismic hazard at Topeka site to the strength of the prior on b	5-102
Figure 5.3.2-18 Sensitivity of seismic hazard at Manchester site to the choice of magnitude weights	5-103
Figure 5.3.2-19 Sensitivity of seismic hazard at Topeka site to the choice of magnitude weights	5-104
Figure 5.3.2-20 Sensitivity of seismic hazard from source NAP at Manchester site to the eight alternative recurrence maps for Case B magnitude weights	5-105
Figure 5.3.2-21 Sensitivity of seismic hazard from source MID-C–A at Topeka site to the eight alternative recurrence maps for Case B magnitude weights	5-106
Figure 5.3.2-22 Mean recurrence-parameter map for the study region under the highest weighted source-zone configuration in the master logic tree. See Sections 6.3 and 7.5 for all mean maps.	5-107
Figure 5.3.2-23 Map of the uncertainty in the estimated recurrence parameters, expressed as the coefficient of variation of the rate (left) and the standard deviation of the b -value (right) for the study region, under the highest weighted source-zone configuration in the master logic tree. See Appendix J for all maps of uncertainty.	5-108

Figure 5.3.2-24 First of eight equally likely realizations of the recurrence-parameter map for the study region under the highest weighted source-zone configuration in the master logic tree. See Appendix J for maps of all realizations for all source-zone configurations.....	5-109
Figure 5.3.2-25 Eighth of eight equally likely realizations of the recurrence-parameter map for the study region under the highest weighted source-zone configuration in the master logic tree. See Appendix J for maps of all realizations for all source-zone configurations.....	5-110
Figure 5.3.2-26 Map of geographic areas considered in the exploration of model results.....	5-111
Figure 5.3.2-27 Comparison of model-predicted earthquake counts for the USGS Eastern Tennessee area using Case A magnitude weights. The error bars represent the 16%–84% uncertainty associated with the data, computed using the Weichert (1980) procedure.	5-112
Figure 5.3.2-28 Comparison of model-predicted earthquake counts for the USGS Eastern Tennessee area using Case B magnitude weights.....	5-113
Figure 5.3.2-29 Comparison of model-predicted earthquake counts for the USGS Eastern Tennessee area using Case E magnitude weights.....	5-114
Figure 5.3.2-30 Comparison of model-predicted earthquake counts for the central New England area using Case A magnitude weights	5-115
Figure 5.3.2-31 Comparison of model-predicted earthquake counts for the central New England area using Case B magnitude weights	5-116
Figure 5.3.2-32 Comparison of model-predicted earthquake counts for the central New England area using Case E magnitude weights	5-117
Figure 5.3.2-33 Comparison of model-predicted earthquake counts for the Nemaha Ridge area using Case A magnitude weights	5-118
Figure 5.3.2-34 Comparison of model-predicted earthquake counts for the Nemaha Ridge area using Case B magnitude weights	5-119
Figure 5.3.2-35 Comparison of model-predicted earthquake counts for the Nemaha Ridge area using Case E magnitude weights	5-120
Figure 5.3.2-36 Comparison of model-predicted earthquake counts for the Miami, FL, area using Case A magnitude weights.....	5-121
Figure 5.3.2-37 Comparison of model-predicted earthquake counts for the Miami, FL, area using Case B magnitude weights.....	5-122
Figure 5.3.2-38 Comparison of model-predicted earthquake counts for the Miami, FL, area using Case E magnitude weights.....	5-123
Figure 5.3.2-39 Comparison of model-predicted earthquake counts for the St. Paul, MN, area using Case A magnitude weights.....	5-124
Figure 5.3.2-40 Comparison of model-predicted earthquake counts for the St. Paul, MN, area using Case B magnitude weights.....	5-125
Figure 5.3.2-41 Comparison of model-predicted earthquake counts for the St. Paul, MN, area using Case E magnitude weights.....	5-126
Figure 5.3.2-42 Recurrence parameters for the ECC-AM, MID-C–A, and NAP seismotectonic source zones and Case A magnitude weights computed using an objective adaptive kernel approach.....	5-127

Figure 5.3.3-1 Likelihood distribution for rate parameter λ derived using Equation 5.3.3-1 for $N = 2$ and $T = 2,000$ years. Top: normalized probability density function for λ . Bottom: resulting cumulative distribution function. Dashed lines show the cumulative probability levels for the Miller and Rice (1983) discrete approximation of a continuous probability distribution.	5-128
Figure 5.3.3-2 Uncertainty distributions for the age of Charleston RLMEs	5-129
Figure 5.4.4-1 Spatial distribution of earthquakes in the CEUS SSC Project catalog. Solid lines indicate the boundaries of the seismotectonic source zones (narrow interpretation)	5-130
Figure 5.4.4-2 Spatial distribution of earthquakes in the CEUS SSC Project catalog with good quality depth determinations used for assessing crustal thickness. Solid lines indicate the boundaries of the seismotectonic source zones (narrow interpretation).....	5-131
Figure 5.4.4-3 Distribution of better-quality focal depths in Mmax source zones.....	5-132
Figure 5.4.4-4 (1 of 3) Distribution of better-quality focal depths in seismotectonic source zones.....	5-133
Figure 5.4.4-4 (2 of 3) Distribution of better-quality focal depths in seismotectonic source zones.....	5-134
Figure 5.4.4-4 (3 of 3) Distribution of better-quality focal depths in seismotectonic source zones.....	5-135
Figure 6.1-1 Map showing the RLME sources characterized in the CEUS SSC model. Detailed alternatives to the source geometries are shown on figures associated with each RLME discussion.....	6-111
Figure 6.1-2a Map showing the RLME sources and seismicity from the CEUS SSC earthquake catalog. Some of the RLMEs occur in regions of elevated seismicity, but others do not.	6-112
Figure 6.1-2b Close-up of the Wabash Valley and New Madrid/Reelfoot Rift RLME sources and seismicity from the CEUS SSC earthquake catalog. Some of the RLMEs occur in regions of elevated seismicity, but others do not.	6-113
Figure 6.1.1-1 Logic tree for the Charlevoix RLME source	6-114
Figure 6.1.1-2 Seismicity and tectonic features of the Charlevoix RLME	6-115
Figure 6.1.1-3 Magnetic and gravity anomaly maps of the Charlevoix RLME	6-116
Figure 6.1.2-1a Logic tree for the Charleston RLME source	6-117
Figure 6.1.2-1b Logic tree for the Charleston RLME source	6-118
Figure 6.1.2-2 Charleston RLME source zones with (a) total magnetic anomaly and (b) residual isostatic gravity data	6-119
Figure 6.1.2-3 Postulated faults and tectonic features in the Charleston region	6-120
Figure 6.1.2-4 Postulated faults and tectonic features in the local Charleston area	6-121
Figure 6.1.2-5a Postulated faults and tectonic features in the Charleston region with Charleston RLME source zones	6-122
Figure 6.1.2-5b Postulated faults and tectonic features in the local Charleston area with Charleston RLME source zones	6-123
Figure 6.1.2-6 Schematic diagram showing contemporary, maximum, and minimum constraining age sample locations	6-124

Figure 6.1.2-7 Charleston space-time diagram of earthquakes interpreted from paleoliquefaction, contemporary-ages-only scenario	6-125
Figure 6.1.2-8 Charleston space-time diagram of earthquakes interpreted from paleoliquefaction, all-ages scenario	6-126
Figure 6.1.2-9 Distribution of liquefaction from earthquake A, contemporary-ages-only scenario	6-127
Figure 6.1.2-10 Distribution of liquefaction from earthquake B, contemporary-ages-only scenario	6-128
Figure 6.1.2-11 Distribution of liquefaction from earthquake C, contemporary-ages-only scenario	6-129
Figure 6.1.2-12 Distribution of liquefaction from earthquake D, contemporary-ages-only scenario	6-130
Figure 6.1.2-13 Distribution of liquefaction from earthquake E, contemporary-ages-only scenario	6-131
Figure 6.1.2-14 Distribution of liquefaction from earthquake A, all-ages scenario	6-132
Figure 6.1.2-15 Distribution of liquefaction from earthquake B, all-ages scenario	6-133
Figure 6.1.2-16 Distribution of liquefaction from earthquake C, all-ages scenario	6-134
Figure 6.1.2-17 Distribution of liquefaction from earthquake D, all-ages scenario	6-135
Figure 6.1.2-18 Distribution of liquefaction from earthquake E, all-ages scenario.....	6-136
Figure 6.1.2-19 Uncertainty distributions for the age of Charleston RLMEs.....	6-137
Figure 6.1.3-1 Logic tree for the Cheraw fault RLME source.....	6-138
Figure 6.1.3-2 Map (c) and hillshade relief images (a, b, and d) showing location of mapped Cheraw fault, possible northeast extension, and paleoseismic locality.....	6-139
Figure 6.1.3-3 Cheraw RLME source relative to (a) total magnetic anomaly and (b) residual isostatic gravity data	6-140
Figure 6.1.4-1 Meers fault location	6-141
Figure 6.1.4-2 Logic tree for the Meers fault source	6-142
Figure 6.1.5-1 Logic tree for the NMFS RLME source	6-143
Figure 6.1.5-2 Map showing seismicity and major subsurface structural features in the New Madrid region	6-144
Figure 6.1.5-3 Map showing geomorphic and near-surface tectonic features in the New Madrid region and locations of NMFS RLME fault sources	6-145
Figure 6.1.5-4 Rupture segments (a) and models (b) for the New Madrid faults from Johnston and Schweig (1996) and (c) the NMFS RLME fault sources	6-146
Figure 6.1.5-5 Map of NMSZ showing estimated ages and measured sizes of liquefaction features	6-147
Figure 6.1.5-6 Earthquake chronology for NMSZ from dating and correlation of liquefaction features at sites (listed at top) along N-S transect across region.....	6-148
Figure 6.1.5-7 Probability distributions for the age of the AD 900 and AD 1450 NMFS RLMEs	6-149
Figure 6.1.5-8 Liquefaction fields for the 1811-1812, AD 1450, and AD 900 earthquakes as interpreted from spatial distribution and stratigraphy of sand blows.....	6-150

Figure 6.1.6-1a Logic tree for the Reelfoot Rift–Eastern Rift Margin South RLME source. Two options for the southern extent of the ERM-S are considered: ERM-SCC includes the Crittenden County fault zone, and ERM-SRP includes the postulated zone of deformation based on fault picks identified in a high-resolution seismic profile along the Mississippi River.	6-151
Figure 6.1.6-1b Logic tree for the Reelfoot Rift–Eastern Rift Margin North RLME source.....	6-152
Figure 6.1.6-2 Map showing structural features and paleoseismic investigation sites along the eastern margin of the Reelfoot rift. The inset map shows the locations of inferred basement faults that border and cross the Reelfoot rift (Csontos et al., 2008) and the inferred Joiner Ridge–Meeman-Shelby fault (JR-MSF; Odum et al., 2010).	6-153
Figure 6.1.6-3 Maps showing surficial geology and locations of subsurface investigations at (a) Meeman-Shelby Forest State Park locality and (b) Union City site (MSF and UC on Figure 6.1.6-2). Modified from Cox et al. (2006) and Odum et al. (2010).	6-154
Figure 6.1.6-4 Figure showing the timing of events along the eastern Reelfoot rift margin. Modified from Cox (2009).....	6-155
Figure 6.1.7-1 Logic tree for the Reelfoot rift–Marianna RLME source	6-156
Figure 6.1.7-2 Map showing tectonic features and locations of paleoliquefaction sites in the vicinity of Marianna, Arkansas	6-157
Figure 6.1.7-3 Map showing liquefaction features near Daytona Beach lineament southwest of Marianna, Arkansas	6-158
Figure 6.1.8-1 Logic tree for the Commerce Fault Zone RLME source	6-159
Figure 6.1.8-2 Map showing tectonic features, seismicity, and paleoseismic localities along the Commerce Fault Zone RLME source	6-160
Figure 6.1.8-3 Location of the Commerce geophysical lineament and Commerce Fault Zone RLME source relative to the (a) regional magnetic anomaly map and (b) regional gravity anomaly map	6-161
Figure 6.1.8-4 Space-time diagram showing constraints on the location and timing of late Pleistocene and Holocene paleoearthquakes that may be associated with the Commerce Fault Zone RLME source.....	6-162
Figure 6.1.9-1 Logic tree for the Wabash Valley RLME source.....	6-163
Figure 6.1.9-2 Map showing seismicity, subsurface structural features, paleoearthquake energy centers, and postulated neotectonic deformation in the Wabash Valley region of southern Illinois and southern Indiana	6-164
Figure 6.1.9-3 Wabash Valley RLME source relative to (a) magnetic anomaly, and (b) residual isostatic gravity data	6-165
Figure 6.2-1 Map showing the two M _{max} zones for the “narrow” interpretation of the Mesozoic-and-younger extended zone	6-166
Figure 6.2-2 Map showing the two M _{max} zones for the “wide” interpretation of the Mesozoic-and-younger extended zone	6-167
Figure 6.3.1-1 Distributions for $m_{max-obs}$ for the M _{max} distributed seismicity source zones ..	6-168
Figure 6.3.2-1 M _{max} distributions for the study region treated as a single M _{max} zone	6-169
Figure 6.3.2-2 M _{max} distributions for the MESE-N M _{max} zone	6-170

Figure 6.3.2-3 Mmax distributions for the MESE-W Mmax zone	6-171
Figure 6.3.2-4 Mmax distributions for the NMESE-N Mmax zone	6-172
Figure 6.3.2-5 Mmax distributions for the NMESE-W Mmax zone	6-173
Figure 6.4.1-1 Mean map of rate and b-value for the study region under the source-zone configuration, with no separation of Mesozoic extended and non-extended; Case A magnitude weights	6-174
Figure 6.4.1-2 Mean map of rate and b-value for the study region under the source-zone configuration, with no separation of Mesozoic extended and non-extended; Case B magnitude weights	6-175
Figure 6.4.1-3 Mean map of rate and b-value for the study region under the source-zone configuration, with no separation of Mesozoic extended and non-extended; Case E magnitude weights	6-176
Figure 6.4.1-4 Mean map of rate and b-value for the study region under the source-zone configuration, with separation of Mesozoic extended and non-extended, narrow geometry for MESE; Case A magnitude weights	6-177
Figure 6.4.1-5 Mean map of rate and b-value for the study region under the source-zone configuration, with separation of Mesozoic extended and non-extended, narrow geometry for MESE; Case B magnitude weights	6-178
Figure 6.4.1-6 Mean map of rate and b-value for the study region under the source-zone configuration, with separation of Mesozoic extended and non-extended, narrow geometry for MESE; Case E magnitude weights	6-179
Figure 6.4.1-7 Mean map of rate and b-value for the study region under the source-zone configuration, with separation of Mesozoic extended and non-extended, wide geometry for MESE; Case A magnitude weights	6-180
Figure 6.4.1-8 Mean map of rate and b-value for the study region under the source-zone configuration, with separation of Mesozoic extended and non-extended, wide geometry for MESE; Case B magnitude weights	6-181
Figure 6.4.1-9 Mean map of rate and b-value for the study region under the source-zone configuration, with separation of Mesozoic extended and non-extended, wide geometry for MESE; Case E magnitude weights	6-182
Figure 6.4.2-1 Comparison of model-predicted earthquake counts for study region using Case A magnitude weights. The error bars represent the 16%–84% uncertainty associated with the data, computed using the Weichert (1980) procedure.....	6-183
Figure 6.4.2-2 Comparison of model-predicted earthquake counts for study region using Case B magnitude weights. The error bars represent the 16%–84% uncertainty associated with the data, computed using the Weichert (1980) procedure.....	6-184
Figure 6.4.2-3 Comparison of model-predicted earthquake counts for study region using Case E magnitude weights. The error bars represent the 16%–84% uncertainty associated with the data, computed using the Weichert (1980) procedure.....	6-185
Figure 6.4.2-4 Comparison of model-predicted earthquake counts for MESE-N using Case A magnitude weights. The error bars represent the 16%–84% uncertainty associated with the data, computed using the Weichert (1980) procedure.....	6-186
Figure 6.4.2-5 Comparison of model-predicted earthquake counts for MESE-N using Case B magnitude weights. The error bars represent the 16%–84% uncertainty associated with the data, computed using the Weichert (1980) procedure.....	6-187

Figure 6.4.2-6 Comparison of model-predicted earthquake counts for MESE-N using Case E magnitude weights. The error bars represent the 16%–84% uncertainty associated with the data, computed using the Weichert (1980) procedure.....	6-188
Figure 6.4.2-7 Comparison of model-predicted earthquake counts for MESE-W using Case A magnitude weights. The error bars represent the 16%–84% uncertainty associated with the data, computed using the Weichert (1980) procedure.....	6-189
Figure 6.4.2-8 Comparison of model-predicted earthquake counts for MESE-W using Case B magnitude weights. The error bars represent the 16%–84% uncertainty associated with the data, computed using the Weichert (1980) procedure.....	6-190
Figure 6.4.2-9 Comparison of model-predicted earthquake counts for MESE-W using Case E magnitude weights. The error bars represent the 16%–84% uncertainty associated with the data, computed using the Weichert (1980) procedure.....	6-191
Figure 6.4.2-10 Comparison of model-predicted earthquake counts for NMESE-N using Case A magnitude weights. The error bars represent the 16%–84% uncertainty associated with the data, computed using the Weichert (1980) procedure.....	6-192
Figure 6.4.2-11 Comparison of model-predicted earthquake counts for NMESE-N using Case B magnitude weights. The error bars represent the 16%–84% uncertainty associated with the data, computed using the Weichert (1980) procedure.....	6-193
Figure 6.4.2-12 Comparison of model-predicted earthquake counts for NMESE-N using Case E magnitude weights. The error bars represent the 16%–84% uncertainty associated with the data, computed using the Weichert (1980) procedure.....	6-194
Figure 6.4.2-13 Comparison of model-predicted earthquake counts for NMESE-W using Case A magnitude weights. The error bars represent the 16%–84% uncertainty associated with the data, computed using the Weichert (1980) procedure.....	6-195
Figure 6.4.2-14 Comparison of model-predicted earthquake counts for NMESE-W using Case B magnitude weights. The error bars represent the 16%–84% uncertainty associated with the data, computed using the Weichert (1980) procedure.....	6-196
Figure 6.4.2-15 Comparison of model-predicted earthquake counts for NMESE-W using Case E magnitude weights. The error bars represent the 16%–84% uncertainty associated with the data, computed using the Weichert (1980) procedure.....	6-197
Figure 7.1-1 Seismotectonic zones shown in the case where the Rough Creek graben is not part of the Reelfoot rift (RR) and the Paleozoic Extended Crust is narrow (PEZ-N)	7-83
Figure 7.1-2 Seismotectonic zones shown in the case where the Rough Creek graben is part of the Reelfoot rift (RR_RCG) and the Paleozoic Extended Crust is narrow (PEZ-N).....	7-84
Figure 7.1-3 Seismotectonic zones shown in the case where the Rough Creek graben is not part of the Reelfoot rift (RR) and the Paleozoic Extended Crust is wide (PEZ-W).....	7-85
Figure 7.1-4 Seismotectonic zones shown in the case where the Rough Creek graben is part of the Reelfoot rift (RR_RCG) and the Paleozoic Extended Crust is wide (PEZ-W).....	7-86
Figure 7.1-5 Example of comparing seismotectonic zones with magnetic map developed as part of the CEUS SSC Project.....	7-87
Figure 7.1-6 Example of comparing seismotectonic zones with isostatic gravity map developed as part of the CEUS SSC Project	7-88

Figure 7.1-7 Map of seismicity based on the earthquake catalog developed for the CEUS SSC Project.....	7-89
Figure 7.1-8 Map showing example comparison of seismotectonic zones with seismicity. Note the non-uniform spatial distribution of seismicity within the zones. Spatial smoothing of <i>a</i> - and <i>b</i> -values accounts for these spatial variations.....	7-90
Figure 7.3-1 Logic tree for the seismotectonic zones branch of the master logic tree.....	7-91
Figure 7.3.1-1 Significant earthquakes and paleoseismology of the SLR seismotectonic zone	7-92
Figure 7.3.1-2 Tectonic features of the SLR seismotectonic zone	7-93
Figure 7.3.1-3 Magnetic and gravity anomaly maps of the SLR seismotectonic zone	7-94
Figure 7.3.2-1 Significant earthquakes and paleoseismic study area in the region of the GMH seismotectonic zone	7-95
Figure 7.3.2-2 Igneous rocks attributed to the GMH seismotectonic zone	7-96
Figure 7.3.2-3 Relocated hypocentral depths and crustal depth of the GMH seismotectonic zone.....	7-97
Figure 7.3.2-4 Magnetic and gravity anomaly maps of the GMH seismotectonic zone	7-98
Figure 7.3.3-1 Seismicity of the NAP seismotectonic zone	7-99
Figure 7.3.3-2 Magnetic and gravity anomaly maps of the NAP seismotectonic zone	7-100
Figure 7.3.4-1 Seismicity and tectonic features of the PEZ seismotectonic zone.....	7-101
Figure 7.3.4-2 Magnetic and gravity anomaly maps of the PEZ seismotectonic zone	7-102
Figure 7.3.5-1 Map showing seismicity, subsurface Paleozoic and basement structures, and postulated energy centers for prehistoric earthquakes	7-103
Figure 7.3.5-2 Map showing alternative boundaries for Precambrian (proto-Illinois basin) rift basins.....	7-104
Figure 7.3.5-3 Maps showing the IBEB source zone boundaries, seismicity, and prehistoric earthquake centers relative to (a) regional magnetic anomalies and (b) regional gravity anomalies	7-105
Figure 7.3.6-1 Map of seismicity and geomorphic features and faults showing evidence for Quaternary neotectonic deformation and reactivation. Inset map shows basement structures associated with the Reelfoot rift.	7-106
Figure 7.3.6-2 Maps showing geophysical anomalies in the Reelfoot rift region	7-107
Figure 7.3.7-1 Mesozoic basins within the ECC-AM zone	7-108
Figure 7.3.7-2 Seismicity within the ECC-AM and AHEX zones.....	7-109
Figure 7.3.7-3 Magnetic and gravity data for ECC-AM and AHEX zones.....	7-110
Figure 7.3.7-4 Estimated locations of the 1755 M 6.1 Cape Ann earthquake	7-111
Figure 7.3.8-1 Correlation of interpreted transitional crust with the East Coast magnetic anomaly.....	7-112
Figure 7.3.9-1 The ECC-GC seismotectonic zone.....	7-113
Figure 7.3.10-1 The GHEX seismotectonic zone.....	7-114
Figure 7.3.11-1 The OKA seismotectonic zone and regional gravity and magnetic data	7-115
Figure 7.3.12-1 Simplified tectonic map showing the distribution of principal basement faults, rifts, and sutures in the Midcontinent.....	7-116

Figure 7.3.12-2 Maps showing major basement structural features relative to (a) regional magnetic anomalies and (b) regional gravity anomalies	7-117
Figure 7.3.12-3 Seismic zones and maximum observed earthquakes in the MidC zone	7-118
Figure 7.3.12-4 Alternative MidC source zone configurations	7-119
Figure 7.4.1-1 (1 of 3) Distributions for $m_{\max-obs}$ for the seismotectonic distributed seismicity source zones	7-120
Figure 7.4.1-1 (2 of 3) Distributions for $m_{\max-obs}$ for the seismotectonic distributed seismicity source zones	7-121
Figure 7.4.1-1 (3 of 3) Distributions for $m_{\max-obs}$ for the seismotectonic distributed seismicity source zones	7-122
Figure 7.4.2-1 Mmax distributions for the AHEX seismotectonic zone	7-123
Figure 7.4.2-2 Mmax distributions for the ECC_AM seismotectonic zone	7-124
Figure 7.4.2-3 Mmax distributions for the ECC_GC seismotectonic zone	7-125
Figure 7.4.2-4 Mmax distributions for the GHEX seismotectonic zone	7-126
Figure 7.4.2-5 Mmax distributions for the GMH seismotectonic zone	7-127
Figure 7.4.2-6 Mmax distributions for the IBEB seismotectonic zone	7-128
Figure 7.4.2-7 Mmax distributions for the MidC-A seismotectonic zone	7-129
Figure 7.4.2-8 Mmax distributions for the MidC-B seismotectonic zone	7-130
Figure 7.4.2-9 Mmax distributions for the MidC-C seismotectonic zone	7-131
Figure 7.4.2-10 Mmax distributions for the MidC-D seismotectonic zone	7-132
Figure 7.4.2-11 Mmax distributions for the NAP seismotectonic zone	7-133
Figure 7.4.2-12 Mmax distributions for the OKA seismotectonic zone	7-134
Figure 7.4.2-13 Mmax distributions for the PEZ_N seismotectonic zone	7-135
Figure 7.4.2-14 Mmax distributions for the PEZ_W seismotectonic zone	7-136
Figure 7.4.2-15 Mmax distributions for the RR seismotectonic zone	7-137
Figure 7.4.2-16 Mmax distributions for the RR_RCG seismotectonic zone	7-138
Figure 7.4.2-17 Mmax distributions for the SLR seismotectonic zone	7-139
Figure 7.5.1-1 Mean map of rate and b -value for the study region under the source-zone configuration with narrow interpretation of PEZ, Rough Creek graben associated with Midcontinent; Case A magnitude weights	7-140
Figure 7.5.1-2 Mean map of rate and b -value for the study region under the source-zone configuration with narrow interpretation of PEZ, Rough Creek graben associated with Midcontinent; Case B magnitude weights	7-141
Figure 7.5.1-3 Mean map of rate and b -value for the study region under the source-zone configuration with narrow interpretation of PEZ, Rough Creek graben associated with Midcontinent; Case E magnitude weights	7-142
Figure 7.5.1-4 Mean map of rate and b -value for the study region under the source-zone configuration with narrow interpretation of PEZ, Rough Creek graben associated with Reelfoot rift; Case A magnitude weights	7-143

Figure 7.5.1-5 Mean map of rate and b -value for the study region under the source-zone configuration with narrow interpretation of PEZ, Rough Creek graben associated with Reelfoot rift; Case B magnitude weights.....	7-144
Figure 7.5.1-6 Mean map of rate and b -value for the study region under the source-zone configuration with narrow interpretation of PEZ, Rough Creek graben associated with Reelfoot rift; Case E magnitude weights.....	7-145
Figure 7.5.1-7 Mean map of rate and b -value for the study region under the source-zone configuration with wide interpretation of PEZ, Rough Creek graben associated with Midcontinent; Case A magnitude weights	7-146
Figure 7.5.1-8 Mean map of rate and b -value for the study region under the source-zone configuration with wide interpretation of PEZ, Rough Creek graben associated with Midcontinent; Case B magnitude weights	7-147
Figure 7.5.1-9 Mean map of rate and b -value for the study region under the source-zone configuration with wide interpretation of PEZ, Rough Creek graben associated with Midcontinent; Case E magnitude weights	7-148
Figure 7.5.1-10 Mean map of rate and b -value for the study region under the source-zone configuration with wide interpretation of PEZ, Rough Creek graben associated with Reelfoot rift; Case A magnitude weights.....	7-149
Figure 7.5.1-11 Mean map of rate and b -value for the study region under the source-zone configuration with wide interpretation of PEZ, Rough Creek graben associated with Reelfoot rift; Case B magnitude weights.....	7-150
Figure 7.5.1-12 Mean map of rate and b -value for the study region under the source-zone configuration with wide interpretation of PEZ, Rough Creek graben associated with Reelfoot rift; Case E magnitude weights.....	7-151
Figure 7.5.2-1 Comparison of model-predicted earthquake counts for AHEx using Case A magnitude weights. No earthquake counts are shown because this source zone contains no seismicity.	7-152
Figure 7.5.2-2 Comparison of model-predicted earthquake counts for AHEx using Case B magnitude weights. No earthquake counts are shown because this source zone contains no seismicity.. . . .	7-153
Figure 7.5.2-3 Comparison of model-predicted earthquake counts for AHEx using Case E magnitude weights. No earthquake counts are shown because this source zone contains no seismicity.	7-154
Figure 7.5.2-4 Comparison of model-predicted earthquake counts for ECC_AM using Case A magnitude weights. The error bars represent the 16%–84% uncertainty associated with the data, computed using the Weichert (1980) procedure.	7-155
Figure 7.5.2-5 Comparison of model-predicted earthquake counts for ECC_AM using Case B magnitude weights. Error bars as in Figure 7.5.2-4.	7-156
Figure 7.5.2-6 Comparison of model-predicted earthquake counts for ECC_AM using Case E magnitude weights. Error bars as in Figure 7.5.2-4.	7-157
Figure 7.5.2-7 Comparison of model-predicted earthquake counts for ECC_GC using Case A magnitude weights. Error bars as in Figure 7.5.2-4.	7-158
Figure 7.5.2-8 Comparison of model-predicted earthquake counts for ECC_GC using Case B magnitude weights. Error bars as in Figure 7.5.2-4.	7-159
Figure 7.5.2-9 Comparison of model-predicted earthquake counts for ECC_GC using Case E magnitude weights. Error bars as in Figure 7.5.2-4.	7-160

Figure 7.5.2-10 Comparison of model-predicted earthquake counts for GHEX using Case A magnitude weights. Error bars as in Figure 7.5.2-4.	7-161
Figure 7.5.2-11 Comparison of model-predicted earthquake counts for GHEX using Case B magnitude weights. Error bars as in Figure 7.5.2-4.	7-162
Figure 7.5.2-12 Comparison of model-predicted earthquake counts for GHEX using Case E magnitude weights. Error bars as in Figure 7.5.2-4.	7-163
Figure 7.5.2-13 Comparison of model-predicted earthquake counts for GMH using Case A magnitude weights. Error bars as in Figure 7.5.2-4.	7-164
Figure 7.5.2-14 Comparison of model-predicted earthquake counts for GMH using Case B magnitude weights. Error bars as in Figure 7.5.2-4.	7-165
Figure 7.5.2-15 Comparison of model-predicted earthquake counts for GMH using Case E magnitude weights. Error bars as in Figure 7.5.2-4.	7-166
Figure 7.5.2-16 Comparison of model-predicted earthquake counts for IBEB using Case A magnitude weights. Error bars as in Figure 7.5.2-4.	7-167
Figure 7.5.2-17 Comparison of model-predicted earthquake counts for IBEB using Case B magnitude weights. Error bars as in Figure 7.5.2-4.	7-168
Figure 7.5.2-18 Comparison of model-predicted earthquake counts for IBEB using Case E magnitude weights. Error bars as in Figure 7.5.2-4.	7-169
Figure 7.5.2-19 Comparison of model-predicted earthquake counts for MidC-A using Case A magnitude weights. Error bars as in Figure 7.5.2-4.	7-170
Figure 7.5.2-20 Comparison of model-predicted earthquake counts for MidC-A using Case B magnitude weights. Error bars as in Figure 7.5.2-4.	7-171
Figure 7.5.2-21 Comparison of model-predicted earthquake counts for MidC-A using Case E magnitude weights. Error bars as in Figure 7.5.2-4.	7-172
Figure 7.5.2-22 Comparison of model-predicted earthquake counts for MidC-B using Case A magnitude weights. Error bars as in Figure 7.5.2-4.	7-173
Figure 7.5.2-23 Comparison of model-predicted earthquake counts for MidC-B using Case B magnitude weights. Error bars as in Figure 7.5.2-4.	7-174
Figure 7.5.2-24 Comparison of model-predicted earthquake counts for MidC-B using Case E magnitude weights. Error bars as in Figure 7.5.2-4.	7-175
Figure 7.5.2-25 Comparison of model-predicted earthquake counts for MidC-C using Case A magnitude weights. Error bars as in Figure 7.5.2-4.	7-176
Figure 7.5.2-26 Comparison of model-predicted earthquake counts for MidC-C using Case B magnitude weights. Error bars as in Figure 7.5.2-4.	7-177
Figure 7.5.2-27 Comparison of model-predicted earthquake counts for MidC-C using Case E magnitude weights. Error bars as in Figure 7.5.2-4.	7-178
Figure 7.5.2-28 Comparison of model-predicted earthquake counts for MidC-D using Case A magnitude weights. Error bars as in Figure 7.5.2-4.	7-179
Figure 7.5.2-29 Comparison of model-predicted earthquake counts for MidC-D using Case B magnitude weights. Error bars as in Figure 7.5.2-4.	7-180
Figure 7.5.2-30 Comparison of model-predicted earthquake counts for MidC-D using Case E magnitude weights. Error bars as in Figure 7.5.2-4.	7-181
Figure 7.5.2-31 Comparison of model-predicted earthquake counts for NAP using Case A magnitude weights. Error bars as in Figure 7.5.2-4.	7-182

Figure 7.5.2-32 Comparison of model-predicted earthquake counts for NAP using Case B magnitude weights. Error bars as in Figure 7.5.2-4.	7-183
Figure 7.5.2-33 Comparison of model-predicted earthquake counts for NAP using Case E magnitude weights. Error bars as in Figure 7.5.2-4.	7-184
Figure 7.5.2-34 Comparison of model-predicted earthquake counts for OKA using Case A magnitude weights. Error bars as in Figure 7.5.2-4.	7-185
Figure 7.5.2-35 Comparison of model-predicted earthquake counts for OKA using Case B magnitude weights. Error bars as in Figure 7.5.2-4.	7-186
Figure 7.5.2-36 Comparison of model-predicted earthquake counts for OKA using Case E magnitude weights. Error bars as in Figure 7.5.2-4.	7-187
Figure 7.5.2-37 Comparison of model-predicted earthquake counts for PEZ_N using Case A magnitude weights. Error bars as in Figure 7.5.2-4.	7-188
Figure 7.5.2-38 Comparison of model-predicted earthquake counts for PEZ_N using Case B magnitude weights. Error bars as in Figure 7.5.2-4.	7-189
Figure 7.5.2-39 Comparison of model-predicted earthquake counts for PEZ_N using Case E magnitude weights. Error bars as in Figure 7.5.2-4.	7-190
Figure 7.5.2-40 Comparison of model-predicted earthquake counts for PEZ_W using Case A magnitude weights. Error bars as in Figure 7.5.2-4.	7-191
Figure 7.5.2-41 Comparison of model-predicted earthquake counts for PEZ_W using Case B magnitude weights. Error bars as in Figure 7.5.2-4.	7-192
Figure 7.5.2-42 Comparison of model-predicted earthquake counts for PEZ_W using Case E magnitude weights. Error bars as in Figure 7.5.2-4.	7-193
Figure 7.5.2-43 Comparison of model-predicted earthquake counts for RR using Case A magnitude weights. Error bars as in Figure 7.5.2-4.	7-194
Figure 7.5.2-44 Comparison of model-predicted earthquake counts for RR using Case B magnitude weights. Error bars as in Figure 7.5.2-4.	7-195
Figure 7.5.2-45 Comparison of model-predicted earthquake counts for RR using Case E magnitude weights. Error bars as in Figure 7.5.2-4.	7-196
Figure 7.5.2-46 Comparison of model-predicted earthquake counts for RR_RCG using Case A magnitude weights. Error bars as in Figure 7.5.2-4.	7-197
Figure 7.5.2-47 Comparison of model-predicted earthquake counts for RR_RCG using Case B magnitude weights. Error bars as in Figure 7.5.2-4.	7-198
Figure 7.5.2-48 Comparison of model-predicted earthquake counts for RR_RCG using Case E magnitude weights. Error bars as in Figure 7.5.2-4.	7-199
Figure 7.5.2-49 Comparison of model-predicted earthquake counts for SLR using Case A magnitude weights. Error bars as in Figure 7.5.2-4.	7-200
Figure 7.5.2-50 Comparison of model-predicted earthquake counts for SLR using Case B magnitude weights. Error bars as in Figure 7.5.2-4.	7-201
Figure 7.5.2-51 Comparison of model-predicted earthquake counts for SLR using Case E magnitude weights. Error bars as in Figure 7.5.2-4.	7-202
Figure 8.1-1 Map showing the study area and seven test sites for the CEUS SSC Project	8-28
Figure 8.1-2 Mean VS profile for shallow soil site	8-29
Figure 8.1-3 Mean VS profile for deep soil site	8-30

Figure 8.1-4 Mean amplification factors for shallow soil site.....	8-31
Figure 8.1-5 Mean amplification factors for deep soil site.....	8-32
Figure 8.2-1a Central Illinois 10 Hz rock hazard: mean and fractile total hazard.....	8-33
Figure 8.2-1b Central Illinois 1 Hz rock hazard: mean and fractile total hazard.....	8-34
Figure 8.2-1c Central Illinois PGA rock hazard: mean and fractile total hazard.....	8-35
Figure 8.2-1d Central Illinois 10 Hz rock hazard: total and contribution by RLME and background	8-36
Figure 8.2-1e Central Illinois 1 Hz rock hazard: total and contribution by RLME and background	8-37
Figure 8.2-1f Central Illinois PGA rock hazard: total and contribution by RLME and background	8-38
Figure 8.2-1g Central Illinois 10 Hz rock hazard: contribution by background source	8-39
Figure 8.2-1h Central Illinois 1 Hz rock hazard: contribution by background source	8-40
Figure 8.2-1i Central Illinois PGA rock hazard: contribution by background source	8-41
Figure 8.2-1j Central Illinois 10 Hz rock hazard: comparison of three source models	8-42
Figure 8.2-1k Central Illinois 1 Hz rock hazard: comparison of three source models	8-43
Figure 8.2-1l Central Illinois PGA rock hazard: comparison of three source models.....	8-44
Figure 8.2-1m Central Illinois 10 Hz shallow soil hazard: total and total and contribution by RLME and background.....	8-45
Figure 8.2-1n Central Illinois 1 Hz shallow soil hazard: total and contribution by RLME and background	8-46
Figure 8.2-1o Central Illinois PGA shallow soil hazard: total and contribution by RLME and background	8-47
Figure 8.2-1p Central Illinois 10 Hz deep soil hazard: total and contribution by RLME and background	8-48
Figure 8.2-1q Central Illinois 1 Hz deep soil hazard: total and contribution by RLME and background	8-49
Figure 8.2-1r Central Illinois PGA deep soil hazard: total and contribution by RLME and background	8-50
Figure 8.2-1s Central Illinois 10 Hz hazard: comparison of three site conditions	8-51
Figure 8.2-1t Central Illinois 1 Hz hazard: comparison of three site conditions	8-52
Figure 8.2-1u Central Illinois PGA hazard: comparison of three site conditions.....	8-53
Figure 8.2-1v Central Illinois 10 Hz rock hazard: sensitivity to seismotectonic vs. Mmax zones.....	8-54
Figure 8.2-1w Central Illinois 1 Hz rock hazard: sensitivity to seismotectonic vs. Mmax zones.....	8-55
Figure 8.2-1x Central Illinois 10 Hz rock hazard: sensitivity to Mmax for source IBEB.....	8-56
Figure 8.2-1y Central Illinois 1 Hz rock hazard: sensitivity to Mmax for source IBEB.....	8-57
Figure 8.2-1z Central Illinois 10 Hz rock hazard: sensitivity to smoothing options	8-58
Figure 8.2-1aa Central Illinois 1 Hz rock hazard: sensitivity to smoothing options	8-59
Figure 8.2-1bb Central Illinois 10 Hz rock hazard: sensitivity to eight realizations for source IBEB, Case A	8-60

Figure 8.2-1cc Central Illinois 10 Hz rock hazard: sensitivity to eight realizations for source IBEB, Case B	8-61
Figure 8.2-1dd Central Illinois 10 Hz rock hazard: sensitivity to eight realizations for source IBEB, Case E	8-62
Figure 8.2-1ee Central Illinois 1 Hz rock hazard: sensitivity to eight realizations for source IBEB, Case A	8-63
Figure 8.2-1ff Central Illinois 1 Hz rock hazard: sensitivity to eight realizations for source IBEB, Case B	8-64
Figure 8.2-1gg Central Illinois 1 Hz rock hazard: sensitivity to eight realizations for source IBEB, Case E	8-65
Figure 8.2-2a Chattanooga 10 Hz rock hazard: mean and fractile total hazard	8-66
Figure 8.2-2b Chattanooga 1 Hz rock hazard: mean and fractile total hazard.....	8-67
Figure 8.2-2c Chattanooga PGA rock hazard: mean and fractile total hazard	8-68
Figure 8.2-2d Chattanooga 10 Hz rock hazard: total and contribution by RLME and background	8-69
Figure 8.2-2e Chattanooga 1 Hz rock hazard: total and contribution by RLME and background	8-70
Figure 8.2-2f Chattanooga PGA rock hazard: total and contribution by RLME and background	8-71
Figure 8.2-2g Chattanooga 10 Hz rock hazard: contribution by background source	8-72
Figure 8.2-2h Chattanooga 1 Hz rock hazard: contribution by background source	8-73
Figure 8.2-2i Chattanooga PGA rock hazard: contribution by background source	8-74
Figure 8.2-2j Chattanooga 10 Hz rock hazard: comparison of three source models	8-75
Figure 8.2-2k Chattanooga 1 Hz rock hazard: comparison of three source models	8-76
Figure 8.2-2l Chattanooga PGA rock hazard: comparison of three source models.....	8-77
Figure 8.2-2m Chattanooga 10 Hz shallow soil hazard: total and contribution by RLME and background	8-78
Figure 8.2-2n Chattanooga 1 Hz shallow soil hazard: total and contribution by RLME and background	8-79
Figure 8.2-2o Chattanooga PGA shallow soil hazard: total and contribution by RLME and background	8-80
Figure 8.2-2p Chattanooga 10 Hz deep soil hazard: total and contribution by RLME and background	8-81
Figure 8.2-2q Chattanooga 1 Hz deep soil hazard: total and contribution by RLME and background	8-82
Figure 8.2-2r Chattanooga PGA deep soil hazard: total and contribution by RLME and background	8-83
Figure 8.2-2s Chattanooga 10 Hz hazard: comparison of three site conditions	8-84
Figure 8.2-2t Chattanooga 1 Hz hazard: comparison of three site conditions	8-85
Figure 8.2-2u Chattanooga PGA hazard: comparison of three site conditions	8-86
Figure 8.2-2v Chattanooga 10 Hz rock hazard: sensitivity to seismotectonic vs. Mmax zones.....	8-87

Figure 8.2-2w Chattanooga 1 Hz rock hazard: sensitivity to seismotectonic vs. Mmax zones.....	8-88
Figure 8.2-2x Chattanooga 10 Hz rock hazard: sensitivity to Mmax for source PEZ-N.....	8-89
Figure 8.2-2y Chattanooga 1 Hz rock hazard: sensitivity to Mmax for source PEZ-N.....	8-90
Figure 8.2-2z Chattanooga 10 Hz rock hazard: sensitivity to smoothing options	8-91
Figure 8.2-2aa Chattanooga 1 Hz rock hazard: sensitivity to smoothing options	8-92
Figure 8.2-2bb Chattanooga 10 Hz rock hazard: sensitivity to eight realizations for source PEZ-N, Case A.....	8-93
Figure 8.2-2cc Chattanooga 10 Hz rock hazard: sensitivity to eight realizations for source PEZ-N, Case B.....	8-94
Figure 8.2-2dd Chattanooga 10 Hz rock hazard: sensitivity to eight realizations for source PEZ-N, Case E.....	8-95
Figure 8.2-2ee Chattanooga 1 Hz rock hazard: sensitivity to eight realizations for source PEZ-N, Case A.....	8-96
Figure 8.2-2ff Chattanooga 1 Hz rock hazard: sensitivity to eight realizations for source PEZ-N, Case B.....	8-97
Figure 8.2-2gg Chattanooga 1 Hz rock hazard: sensitivity to eight realizations for source PEZ-N, Case E.....	8-98
Figure 8.2-3a Houston 10 Hz rock hazard: mean and fractile total hazard.....	8-99
Figure 8.2-3b Houston 1 Hz rock hazard: mean and fractile total hazard.....	8-100
Figure 8.2-3c Houston PGA rock hazard: mean and fractile total hazard.....	8-101
Figure 8.2-3d Houston 10 Hz rock hazard: total and contribution by RLME and background	8-102
Figure 8.2-3e Houston 1 Hz rock hazard: total and contribution by RLME and background	8-103
Figure 8.2-3f Houston PGA rock hazard: total and contribution by RLME and background..	8-104
Figure 8.2-3g Houston 10 Hz rock hazard: contribution by background source	8-105
Figure 8.2-3h Houston 1 Hz rock hazard: contribution by background source	8-106
Figure 8.2-3i Houston PGA rock hazard: contribution by background source	8-107
Figure 8.2-3j Houston 10 Hz rock hazard: comparison of three source models	8-108
Figure 8.2-3k Houston is 1 Hz rock hazard: comparison of three source models.....	8-109
Figure 8.2-3l Houston PGA rock hazard: comparison of three source models.....	8-110
Figure 8.2-3m Houston 10 Hz shallow soil hazard: total and contribution by RLME and background	8-111
Figure 8.2-3n Houston 1 Hz shallow soil hazard: total and contribution by RLME and background	8-112
Figure 8.2-3o Houston PGA shallow soil hazard: total and contribution by RLME and background	8-113
Figure 8.2-3p Houston 10 Hz deep soil hazard: total and contribution by RLME and background	8-114
Figure 8.2-3q Houston 1 Hz deep soil hazard: total and contribution by RLME and background	8-115

Figure 8.2-3r Houston PGA deep soil hazard: total and contribution by RLME and background	8-116
Figure 8.2-3s Houston 10 Hz hazard: comparison of three site conditions.....	8-117
Figure 8.2-3t Houston 1 Hz hazard: comparison of three site conditions	8-118
Figure 8.2-3u Houston PGA hazard: comparison of three site conditions	8-119
Figure 8.2-3v Houston 10 Hz rock hazard: sensitivity to seismotectonic vs. Mmax zones	8-120
Figure 8.2-3w Houston 1 Hz rock hazard: sensitivity to seismotectonic vs. Mmax zones	8-121
Figure 8.2-3x Houston 10 Hz rock hazard: sensitivity to Mmax for source GHEX.....	8-122
Figure 8.2-3y Houston 1 Hz rock hazard: sensitivity to Mmax for source GHEX.....	8-123
Figure 8.2-3z Houston 10 Hz rock hazard: sensitivity to smoothing options.....	8-124
Figure 8.2-3aa Houston 1 Hz rock hazard: sensitivity to smoothing options	8-125
Figure 8.2-3bb Houston 10 Hz rock hazard: sensitivity to eight realizations for source GHEX, Case A	8-126
Figure 8.2-3cc Houston 10 Hz rock hazard: sensitivity to eight realizations for source GHEX, Case B	8-127
Figure 8.2-3dd Houston 10 Hz rock hazard: sensitivity to eight realizations for source GHEX, Case E	8-128
Figure 8.2-3ee Houston 1 Hz rock hazard: sensitivity to eight realizations for source GHEX, Case A	8-129
Figure 8.2-3ff Houston 1 Hz rock hazard: sensitivity to eight realizations for source GHEX, Case B	8-130
Figure 8.2-3gg Houston 1 Hz rock hazard: sensitivity to eight realizations for source GHEX, Case E	8-131
Figure 8.2-4a Jackson 10 Hz rock hazard: mean and fractile total hazard	8-132
Figure 8.2-4b Jackson 1 Hz rock hazard: mean and fractile total hazard	8-133
Figure 8.2-4c Jackson PGA rock hazard: mean and fractile total hazard	8-134
Figure 8.2-4d Jackson 10 Hz rock hazard: total and contribution by RLME and background	8-135
Figure 8.2-4e Jackson 1 Hz rock hazard: total and contribution by RLME and background	8-136
Figure 8.2-4f Jackson PGA rock hazard: total and contribution by RLME and background ..	8-137
Figure 8.2-4g Jackson 10 Hz rock hazard: contribution by background source	8-138
Figure 8.2-4h Jackson 1 Hz rock hazard: contribution by background source	8-139
Figure 8.2-4i Jackson PGA rock hazard: contribution by background source	8-140
Figure 8.2-4j Jackson 10 Hz rock hazard: comparison of three source models	8-141
Figure 8.2-4k Jackson is 1 Hz rock hazard: comparison of three source models.....	8-142
Figure 8.2-4l Jackson PGA rock hazard: comparison of three source models	8-143
Figure 8.2-4m Jackson 10 Hz shallow soil hazard: total and contribution by RLME and background	8-144
Figure 8.2-4n Jackson 1 Hz shallow soil hazard: total and contribution by RLME and background	8-145

Figure 8.2-4o Jackson PGA shallow soil hazard: total and contribution by RLME and background	8-146
Figure 8.2-4p Jackson 10 Hz deep soil hazard: total and contribution by RLME and background	8-147
Figure 8.2-4q Jackson 1 Hz deep soil hazard: total and contribution by RLME and background	8-148
Figure 8.2-4r Jackson PGA deep soil hazard: total and contribution by RLME and background	8-149
Figure 8.2-4s Jackson 10 Hz hazard: comparison of three site conditions	8-150
Figure 8.2-4t Jackson 1 Hz hazard: comparison of three site conditions	8-151
Figure 8.2-4u Jackson PGA hazard: comparison of three site conditions	8-152
Figure 8.2-4v Jackson 10 Hz rock hazard: sensitivity to seismotectonic vs. Mmax zones	8-153
Figure 8.2-4w Jackson 1 Hz rock hazard: sensitivity to seismotectonic vs. Mmax zones	8-154
Figure 8.2-4x Jackson 10 Hz rock hazard: sensitivity to Mmax for source ECC-GC	8-155
Figure 8.2-4y Jackson 1 Hz rock hazard: sensitivity to Mmax for source ECC-GC	8-156
Figure 8.2-4z Jackson 10 Hz rock hazard: sensitivity to smoothing options.....	8-157
Figure 8.2-4aa Jackson 1 Hz rock hazard: sensitivity to smoothing options.....	8-158
Figure 8.2-4bb Jackson 10 Hz rock hazard: sensitivity to eight realizations for source ECC-GC, Case A	8-159
Figure 8.2-4cc Jackson 10 Hz rock hazard: sensitivity to eight realizations for source ECC-GC, Case B	8-160
Figure 8.2-4dd Jackson 10 Hz rock hazard: sensitivity to eight realizations for source ECC-GC, Case E	8-161
Figure 8.2-4ee Jackson 1 Hz rock hazard: sensitivity to eight realizations for source ECC-GC, Case A	8-162
Figure 8.2-4ff Jackson 1 Hz rock hazard: sensitivity to eight realizations for source ECC-GC, Case B	8-163
Figure 8.2-4gg Jackson 1 Hz rock hazard: sensitivity to eight realizations for source ECC-GC, Case E	8-164
Figure 8.2-5a Manchester 10 Hz rock hazard: mean and fractile total hazard	8-165
Figure 8.2-5b Manchester 1 Hz rock hazard: mean and fractile total hazard	8-166
Figure 8.2-5c Manchester PGA rock hazard: mean and fractile total hazard	8-167
Figure 8.2-5d Manchester 10 Hz rock hazard: total and contribution by RLME and background	8-168
Figure 8.2-5e Manchester 1 Hz rock hazard: total and contribution by RLME and background	8-169
Figure 8.2-5f Manchester PGA rock hazard: total and contribution by RLME and background	8-170
Figure 8.2-5g Manchester 10 Hz rock hazard: contribution by background source.....	8-171
Figure 8.2-5h Manchester 1 Hz rock hazard: contribution by background source.....	8-172
Figure 8.2-5i Manchester PGA rock hazard: contribution by background source.....	8-173
Figure 8.2-5j Manchester 10 Hz rock hazard: comparison of three source models.....	8-174

Figure 8.2-5k Manchester 1 Hz rock hazard: comparison of three source models	8-175
Figure 8.2-5l Manchester PGA rock hazard: comparison of three source models.....	8-176
Figure 8.2-5m Manchester 10 Hz shallow soil hazard: total and contribution by RLME and background	8-177
Figure 8.2-5n Manchester 1 Hz shallow soil hazard: total and contribution by RLME and background	8-178
Figure 8.2-5o Manchester PGA shallow soil hazard: total and contribution by RLME and background	8-179
Figure 8.2-5p Manchester 10 Hz deep soil hazard: total and contribution by RLME and background	8-180
Figure 8.2-5q Manchester 1 Hz deep soil hazard: total and contribution by RLME and background	8-181
Figure 8.2-5r Manchester PGA deep soil hazard: total and contribution by RLME and background	8-182
Figure 8.2-5s Manchester 10 Hz hazard: comparison of three site conditions	8-183
Figure 8.2-5t Manchester 1 Hz hazard: comparison of three site conditions	8-184
Figure 8.2-5u Manchester PGA hazard: comparison of three site conditions.....	8-185
Figure 8.2-5v Manchester 10 Hz rock hazard: sensitivity to seismotectonic vs. Mmax zones.....	8-186
Figure 8.2-5w Manchester 1 Hz rock hazard: sensitivity to seismotectonic vs. Mmax zones.....	8-187
Figure 8.2-5x Manchester 10 Hz rock hazard: sensitivity to Mmax for source NAP	8-188
Figure 8.2-5y Manchester 1 Hz rock hazard: sensitivity to Mmax for source NAP	8-189
Figure 8.2-5z Manchester 10 Hz rock hazard: sensitivity to smoothing options	8-190
Figure 8.2-5aa Manchester 1 Hz rock hazard: sensitivity to smoothing options.....	8-191
Figure 8.2-5bb Manchester 10 Hz rock hazard: sensitivity to eight realizations for source NAP, Case A.....	8-192
Figure 8.2-5cc Manchester 10 Hz rock hazard: sensitivity to eight realizations for source NAP, Case B.....	8-193
Figure 8.2-5dd Manchester 10 Hz rock hazard: sensitivity to eight realizations for source NAP, Case E.....	8-194
Figure 8.2-5ee Manchester 1 Hz rock hazard: sensitivity to eight realizations for source NAP, Case A.....	8-195
Figure 8.2-5ff Manchester 1 Hz rock hazard: sensitivity to eight realizations for source NAP, Case B.....	8-196
Figure 8.2-5gg Manchester 1 Hz rock hazard: sensitivity to eight realizations for source NAP, Case E.....	8-197
Figure 8.2-6a Savannah 10 Hz rock hazard: mean and fractile total hazard.....	8-198
Figure 8.2-6b Savannah 1 Hz rock hazard: mean and fractile total hazard.....	8-199
Figure 8.2-6c Savannah PGA rock hazard: mean and fractile total hazard.....	8-200
Figure 8.2-6d Savannah 10 Hz rock hazard: total and contribution by RLME and background	8-201

Figure 8.2-6e Savannah 1 Hz rock hazard: total and contribution by RLME and background	8-202
Figure 8.2-6f Savannah PGA rock hazard: total and contribution by RLME and background	8-203
Figure 8.2-6g Savannah 10 Hz rock hazard: contribution by background source	8-204
Figure 8.2-6h Savannah 1 Hz rock hazard: contribution by background source	8-205
Figure 8.2-6i Savannah PGA rock hazard: contribution by background source	8-206
Figure 8.2-6j Savannah 10 Hz rock hazard: comparison of three source models	8-207
Figure 8.2-6k Savannah 1 Hz rock hazard: comparison of three source models.....	8-208
Figure 8.2-6l Savannah PGA rock hazard: comparison of three source models	8-209
Figure 8.2-6m Savannah 10 Hz shallow soil hazard: total and contribution by RLME and background	8-210
Figure 8.2-6n Savannah 1 Hz shallow soil hazard: total and contribution by RLME and background	8-211
Figure 8.2-6o Savannah PGA shallow soil hazard: total and contribution by RLME and background	8-212
Figure 8.2-6p Savannah 10 Hz deep soil hazard: total and contribution by RLME and background	8-213
Figure 8.2-6q Savannah 1 Hz deep soil hazard: total and contribution by RLME and background	8-214
Figure 8.2-6r Savannah PGA deep soil hazard: total and contribution by RLME and background	8-215
Figure 8.2-6s Savannah 10 Hz hazard: comparison of three site conditions.....	8-216
Figure 8.2-6t Savannah 1 Hz hazard: comparison of three site conditions.....	8-217
Figure 8.2-6u Savannah PGA hazard: comparison of three site conditions	8-218
Figure 8.2-6v Savannah 10 Hz rock hazard: sensitivity to seismotectonic vs. Mmax zones.....	8-219
Figure 8.2-6w Savannah 1 Hz rock hazard: sensitivity to seismotectonic vs. Mmax zones ..	8-220
Figure 8.2-6x Savannah 10 Hz rock hazard: sensitivity to Mmax for source ECC-AM.....	8-221
Figure 8.2-6y Savannah 1 Hz rock hazard: sensitivity to Mmax for source ECC-AM.....	8-222
Figure 8.2-6z Savannah 10 Hz rock hazard: sensitivity to smoothing options.....	8-223
Figure 8.2-6aa Savannah 1 Hz rock hazard: sensitivity to smoothing options	8-224
Figure 8.2-6bb Savannah 10 Hz rock hazard: sensitivity to eight realizations for source ECC-AM, Case A	8-225
Figure 8.2-6cc Savannah 10 Hz rock hazard: sensitivity to eight realizations for source ECC-AM, Case B	8-226
Figure 8.2-6dd Savannah 10 Hz rock hazard: sensitivity to eight realizations for source ECC-AM, Case E	8-227
Figure 8.2-6ee Savannah 1 Hz rock hazard: sensitivity to eight realizations for source ECC-AM, Case A	8-228
Figure 8.2-6ff Savannah 1 Hz rock hazard: sensitivity to eight realizations for source ECC-AM, Case B	8-229

Figure 8.2-6gg Savannah 1 Hz rock hazard: sensitivity to eight realizations for source ECC-AM, Case E	8-230
Figure 8.2-7a Topeka 10 Hz rock hazard: mean and fractile total hazard	8-231
Figure 8.2-7b Topeka 1 Hz rock hazard: mean and fractile total hazard	8-232
Figure 8.2-7c Topeka PGA rock hazard: mean and fractile total hazard	8-233
Figure 8.2-7d Topeka 10 Hz rock hazard: total and contribution by RLME and background	8-234
Figure 8.2-7e Topeka 1 Hz rock hazard: total and contribution by RLME and background...	8-235
Figure 8.2-7f Topeka PGA rock hazard: total and contribution by RLME and background ...	8-236
Figure 8.2-7g Topeka 10 Hz rock hazard: contribution by background source.....	8-237
Figure 8.2-7h Topeka 1 Hz rock hazard: contribution by background source.....	8-238
Figure 8.2-7i Topeka PGA rock hazard: contribution by background source	8-239
Figure 8.2-7j Topeka 10 Hz rock hazard: comparison of three source models.....	8-240
Figure 8.2-7k Topeka is 1 Hz rock hazard: comparison of three source models	8-241
Figure 8.2-7l Topeka PGA rock hazard: comparison of three source models	8-242
Figure 8.2-7m Topeka 10 Hz shallow soil hazard: total and contribution by RLME and background	8-243
Figure 8.2-7n Topeka 1 Hz shallow soil hazard: total and contribution by RLME and background	8-244
Figure 8.2-7o Topeka PGA shallow soil hazard: total and contribution by RLME and background	8-245
Figure 8.2-7p Topeka 10 Hz deep soil hazard: total and contribution by RLME and background	8-246
Figure 8.2-7q Topeka 1 Hz deep soil hazard: total and contribution by RLME and background	8-247
Figure 8.2-7r Topeka PGA deep soil hazard: total and contribution by RLME and background	8-248
Figure 8.2-7s Topeka 10 Hz hazard: comparison of three site conditions	8-249
Figure 8.2-7t Topeka 1 Hz hazard: comparison of three site conditions.....	8-250
Figure 8.2-7u Topeka PGA hazard: comparison of three site conditions	8-251
Figure 8.2-7v Topeka 10 Hz rock hazard: sensitivity to seismotectonic vs. Mmax zones	8-252
Figure 8.2-7w Topeka 1 Hz rock hazard: sensitivity to seismotectonic vs. Mmax zones.....	8-253
Figure 8.2-7x Topeka 10 Hz rock hazard: sensitivity to Mmax for source MidC-A	8-254
Figure 8.2-7y Topeka 1 Hz rock hazard: sensitivity to Mmax for source MidC-A	8-255
Figure 8.2-7z Topeka 10 Hz rock hazard: sensitivity to smoothing options.....	8-256
Figure 8.2-7aa Topeka 1 Hz rock hazard: sensitivity to smoothing options.....	8-257
Figure 8.2-7bb Topeka 10 Hz rock hazard: sensitivity to eight realizations for source MidC-A, Case A	8-258
Figure 8.2-7cc Topeka 10 Hz rock hazard: sensitivity to eight realizations for source MidC-A, Case B	8-259

Figure 8.2-7dd Topeka 10 Hz rock hazard: sensitivity to eight realizations for source MidC-A, Case E	8-260
Figure 8.2-7ee Topeka 1 Hz rock hazard: sensitivity to eight realizations for source MidC-A, Case A	8-261
Figure 8.2-7ff Topeka 1 Hz rock hazard: sensitivity to eight realizations for source MidC-A, Case B	8-262
Figure 8.2-7gg Topeka 1 Hz rock hazard: sensitivity to eight realizations for source MidC-A, Case E	8-263
Figure 9.3-1 1 Hz sensitivity to rupture orientation at Savannah for the Charleston regional source.....	9-24
Figure 9.3-2 10 Hz sensitivity to rupture orientation at Savannah for the Charleston regional source.....	9-25
Figure 9.3-3 1 Hz sensitivity to seismogenic thickness at Manchester for the Charlevoix area source	9-26
Figure 9.3-4 10 Hz sensitivity to seismogenic thickness at Manchester for the Charlevoix area source	9-27
Figure 9.3-5 1 Hz sensitivity to rupture orientation (dip) at Manchester for the Charlevoix area source	9-28
Figure 9.3-6 10 Hz sensitivity to rupture orientation (dip) at Manchester for the Charlevoix area source	9-29
Figure 9.3-7 1 Hz sensitivity to seismogenic thickness at Topeka for the Cheraw fault source	9-30
Figure 9.3-8 10 Hz sensitivity to seismogenic thickness at Topeka for the Cheraw fault source	9-31
Figure 9.3-9 1 Hz sensitivity to rupture orientation (dip) at Topeka for the Cheraw fault source	9-32
Figure 9.3-10 10 Hz sensitivity to rupture orientation at Topeka for the Cheraw fault source	9-33
Figure 9.3-11 1 Hz sensitivity to seismogenic thickness at Jackson for the Commerce area source	9-34
Figure 9.3-12 10 Hz sensitivity to seismogenic thickness at Jackson for the Commerce area source	9-35
Figure 9.3-13 1 Hz sensitivity to seismogenic thickness at Jackson for the ERM-N area source	9-36
Figure 9.3-14 10 Hz sensitivity to seismogenic thickness at Jackson for the ERM-N area source	9-37
Figure 9.3-15 1 Hz sensitivity to seismogenic thickness at Jackson for the ERM-S area source	9-38
Figure 9.3-16 10 Hz sensitivity to seismogenic thickness at Jackson for the ERM-S area source	9-39
Figure 9.3-17 1 Hz sensitivity to seismogenic thickness at Jackson for the Marianna area source	9-40
Figure 9.3-18 10 Hz sensitivity to seismogenic thickness at Jackson for the Marianna area source	9-41

Figure 9.3-19 1 Hz sensitivity to seismogenic thickness at Topeka for the Meers fault and OKA area sources.....	9-42
Figure 9.3-20 1 Hz sensitivity to seismogenic thickness at Houston for the Meers fault and OKA area sources.....	9-43
Figure 9.3-21 10 Hz sensitivity to seismogenic thickness at Topeka for the Meers fault and OKA area sources.....	9-44
Figure 9.3-22 10 Hz sensitivity to seismogenic thickness at Houston for the Meers fault and OKA area sources.....	9-45
Figure 9.3-23 1 Hz sensitivity to rupture orientation at Houston for the OKA area source	9-46
Figure 9.3-24 10 Hz sensitivity to rupture orientation at Houston for the OKA area source	9-47
Figure 9.3-25 1 Hz sensitivity to rupture orientation (dip) at Topeka for the OKA area source	9-48
Figure 9.3-26 1 Hz sensitivity to rupture orientation (dip) at Houston for the OKA area source	9-49
Figure 9.3-27 10 Hz sensitivity to rupture orientation (dip) at Topeka for the OKA area source	9-50
Figure 9.3-28 10 Hz sensitivity to rupture orientation (dip) at Houston for the OKA area source	9-51
Figure 9.3-29 1 Hz sensitivity to rupture orientation (dip) at Topeka for the Meers fault source	9-52
Figure 9.3-30 1 Hz sensitivity to rupture orientation (dip) at Houston for the Meers fault source	9-53
Figure 9.3-31 10 Hz sensitivity to rupture orientation (dip) at Topeka for the Meers fault source	9-54
Figure 9.3-32 10 Hz sensitivity to rupture orientation (dip) at Houston for the Meers fault source	9-55
Figure 9.3-33 1 Hz sensitivity to seismogenic thickness at Jackson for the NMFS fault sources.....	9-56
Figure 9.3-34 10 Hz sensitivity to seismogenic thickness at Jackson for the NMFS fault sources.....	9-57
Figure 9.3-35 1 Hz sensitivity to seismogenic thickness at Central Illinois for the Wabash Valley area source	9-58
Figure 9.3-36 10 Hz sensitivity to seismogenic thickness at Central Illinois for the Wabash Valley area source	9-59
Figure 9.3-37 1 Hz sensitivity to rupture orientation (dip) at Central Illinois for the Wabash Valley area source	9-60
Figure 9.3-38 10 Hz sensitivity to rupture orientation (dip) at Central Illinois for the Wabash Valley area source	9-61
Figure 9.3-39 1 Hz sensitivity to fault ruptures vs. point source for the Central Illinois site from the Mid C–A background source.....	9-62
Figure 9.3-40 10 Hz sensitivity to fault ruptures vs. point source for the Central Illinois site from the Mid C–A background source	9-63
Figure 9.4-1 COV_{MH} from EPRI (1989) team sources vs. ground motion amplitude for seven test sites: PGA (top), 10 Hz SA (middle), and 1 Hz SA (bottom).....	9-64

Figure 9.4-2 COV_{MH} from EPRI (1989) team sources vs. seismic hazard (i.e., annual frequency of exceedance) for seven test sites: PGA (top), 10 Hz SA (middle), and 1 9-Hz SA (bottom)	9-65
Figure 9.4-3 COV_{MH} from seismic source experts (PEGASOS project) vs. amplitude (top) and annual frequency (bottom)	9-66
Figure 9.4-4 COV_K and COV_{MH} from Charleston alternatives for PGA, plotted vs. PGA amplitude (top) and hazard (bottom). COV_{MH} is the total COV of mean hazard; see Table 9.4-2 for other labels for curves.	9-67
Figure 9.4-5 COV_K and COV_{MH} from Charleston alternatives for 10 Hz, plotted vs. 10 Hz amplitude (top) and hazard (bottom). COV_{MH} is the total COV of mean hazard; see Table 9.4-2 for other labels for curves.	9-68
Figure 9.4-6 COV_K and COV_{MH} from Charleston alternatives for 1 Hz, plotted vs. 1 Hz amplitude (top) and hazard (bottom). COV_{MH} is the total COV of mean hazard; see Table 9.4-2 for other labels for curves.	9-69
Figure 9.4-7 COV_K and COV_{MH} of total hazard from New Madrid for 1 Hz, plotted vs. 1 Hz amplitude (top) and hazard (bottom). COV_{MH} is the total COV; see the text for other labels for curves.	9-70
Figure 9.4-8 PGA hazard curves for Manchester test site	9-71
Figure 9.4-9 COV_{MH} of PGA hazard at Manchester site from ground motion equation vs. PGA	9-72
Figure 9.4-10 COV of PGA hazard at Manchester site from ground motion equation vs. hazard	9-73
Figure 9.4-11 COV of 10 Hz hazard at Manchester site from ground motion equations vs. hazard.....	9-74
Figure 9.4-12 COV of 1 Hz hazard at Manchester site from ground motion equations vs. hazard	9-75
Figure 9.4-13 1 Hz spectral acceleration hazard curves for Manchester test site	9-76
Figure 9.4-14 COV_{MH} of PGA hazard at Chattanooga from ground motion equation vs. hazard	9-77
Figure 9.4-15 COV_{MH} of 10 Hz hazard at Chattanooga from ground motion equation vs. hazard	9-78
Figure 9.4-16 COV_{MH} of 1 Hz hazard at Chattanooga site from ground motion equation vs. hazard.....	9-79
Figure 9.4-17 PGA hazard curves for Savannah test site.....	9-80
Figure 9.4-18 COV_{MH} of PGA hazard at Savannah site from ground motion equations vs. hazard	9-81
Figure 9.4-19 COV_{MH} of 10 Hz hazard at Savannah site from ground motion equations vs. hazard.....	9-82
Figure 9.4-20 COV_{MH} of 1 Hz hazard at Savannah site from ground motion equations vs. hazard	9-83
Figure 9.4-21 PGA hazard curves for Columbia site	9-84
Figure 9.4-22 COV_{MH} of PGA hazard at Columbia from ground motion equations vs. hazard	9-85

Figure 9.4-23 COV_{MH} of 10 Hz hazard at Columbia from ground motion equations vs. hazard	9-86
Figure 9.4-24 COV_{MH} of 1 Hz hazard at Columbia from ground motion equations vs. hazard	9-87
Figure 9.4-25 COV_{MH} of PGA hazard at Chattanooga (New Madrid only) vs. hazard	9-88
Figure 9.4-26 COV_{MH} of 10 Hz hazard at Chattanooga (New Madrid only) vs. hazard.....	9-89
Figure 9.4-27 COV_{MH} of 1 Hz hazard at Chattanooga (New Madrid only) vs. hazard.....	9-90
Figure 9.4-28 COV_{MH} for PGA and 1 Hz SA vs. ground motion amplitude resulting from alternative ground motion experts, PEGASOS project.....	9-91
Figure 9.4-29 COV_{MH} for PGA and 1 Hz SA vs. mean hazard from alternative ground motion experts, PEGASOS project	9-92
Figure 9.4-30 COV_{HAZ} from ground motion equations vs. mean hazard for Chattanooga	9-93
Figure 9.4-31 COV_{MH} from ground motion equations vs. mean hazard for Central Illinois	9-94
Figure 9.4-32 COV_{MH} from soil experts vs. PGA and 1 Hz SA, PEGASOS project	9-95
Figure 9.4-33 COV_{MH} from soil experts vs. mean hazard for PGA and 1 Hz SA, PEGASOS project.....	9-96
Figure 9.4-34 COV_{MH} resulting from site response models vs. mean hazard for four sites, 1 Hz (top) and 10 Hz (bottom).....	9-97
Figure 11-1 Geologic time scale (Walker and Geissman, 2009)	11-10
Figure A-1 GEBCO elevation data for the CEUS study area (BODC, 2009).	A-22
Figure A-2 CEUS SSC independent earthquake catalog	A-24
Figure A-3 Bedrock geology and extended crust after Kanter (1994).....	A-26
Figure A-4 Crustal provinces after Rohs and Van Schmus (2007)	A-28
Figure A-5 Geologic map of North America	A-31
Figure A-6 Locations of geologic cross sections in the CEUS	A-33
Figure A-7 Precambrian crustal boundary after Van Schmus et al. (1996)	A-35
Figure A-8a Precambrian geology and features after Reed (1993)	A-37
Figure A-8b Explanation of Precambrian geology and features after Reed (1993)	A-38
Figure A-9 Precambrian provinces after Van Schmus et al. (2007).....	A-40
Figure A-10 Precambrian units after Whitmeyer and Karlstrom (2007)	A-42
Figure A-11 Surficial materials in the conterminous United States after Soller et al. (2009).....	A-44
Figure A-12 Basement and sediment thickness in the USGS Crustal Database for North America. Symbol size represents overlying sediment thickness (km); symbol color represents basement thickness (km).	A-46
Figure A-13 Top of basement P-wave seismic velocity in the USGS Crustal Database for North America	A-47
Figure A-14 Sediment thickness for North America and neighboring regions	A-49
Figure A-15 Physiographic divisions of the conterminous United States after Fenneman and Johnson (1946)	A-51
Figure A-16 CEUS SSC free-air gravity anomaly grid. Shaded relief with 315-degree azimuth and 30-degree inclination applied.....	A-54

Figure A-17 CEUS SSC free-air gravity anomaly grid. Shaded relief with 180-degree azimuth and 30-degree inclination applied.....	A-55
Figure A-18 CEUS SSC complete Bouguer gravity anomaly grid with free-air gravity anomaly in marine areas. Shaded relief with 315-degree azimuth and 30-degree inclination applied.....	A-56
Figure A-19 CEUS SSC complete Bouguer gravity anomaly grid with free-air gravity anomaly in marine areas. Shaded relief with 180-degree azimuth and 30-degree inclination applied.....	A-57
Figure A-20 CEUS SSC residual isostatic gravity anomaly grid. Shaded relief with 315-degree azimuth and 30-degree inclination applied.	A-58
Figure A-21 CEUS SSC residual isostatic gravity anomaly grid Shaded relief with 180-degree azimuth and 30-degree inclination applied.	A-59
Figure A-22 CEUS SSC regional isostatic gravity anomaly grid.....	A-60
Figure A-23 CEUS SSC first vertical derivative of residual isostatic gravity anomaly grid.....	A-61
Figure A-24 CEUS SSC first vertical derivative of Bouguer gravity anomaly grid with free-air anomaly in marine areas	A-62
Figure A-25 CEUS SSC complete Bouguer (with marine free-air) gravity anomaly grid low pass filtered at 240 km.....	A-63
Figure A-26 CEUS SSC complete Bouguer (with marine free-air) gravity anomaly grid high pass filtered at 240 km. Shaded relief with 315-degree azimuth and 30-degree inclination applied.....	A-64
Figure A-27 CEUS SSC complete Bouguer (with marine free-air) gravity anomaly grid high pass filtered at 240 km. Shaded relief with 180-degree azimuth and 30-degree inclination applied.....	A-65
Figure A-28 CEUS SSC complete Bouguer (with marine free-air) gravity anomaly grid high pass filtered at 120 km. Shaded relief with 315-degree azimuth and 30-degree inclination applied.....	A-66
Figure A-29 CEUS SSC complete Bouguer (with marine free-air) gravity anomaly grid high pass filtered at 120 km. Shaded relief with 180-degree azimuth and 30-degree inclination applied.....	A-67
Figure A-30 CEUS SSC complete Bouguer (with marine free-air) gravity anomaly grid upward continued to 40 km	A-68
Figure A-31 CEUS SSC complete Bouguer (with marine free-air) gravity anomaly grid minus the complete Bouguer (with marine free-air) gravity anomaly upward continued to 40 km. Shaded relief with 315-degree azimuth and 30-degree inclination applied.....	A-69
Figure A-32 CEUS SSC complete Bouguer (with marine free-air) gravity anomaly grid minus the complete Bouguer (with marine free-air) gravity anomaly upward continued to 40 km. Shaded relief with 180-degree azimuth and 30-degree inclination applied.....	A-70
Figure A-33 CEUS SSC complete Bouguer (with marine free-air) gravity anomaly grid upward continued to 100 km	A-71
Figure A-34 CEUS SSC complete Bouguer (with marine free-air) gravity anomaly grid minus the complete Bouguer (with marine free-air) gravity anomaly anomaly	

upward continued to 100 km. Shaded relief with 315-degree azimuth and 30-degree inclination applied.....	A-72
Figure A-35 CEUS SSC complete Bouguer (with marine free-air) gravity anomaly grid minus the complete Bouguer (with marine free-air) gravity anomaly upward continued to 100 km. Shaded relief with 180-degree azimuth and 30-degree inclination applied.....	A-73
Figure A-36 CEUS SSC horizontal derivative of residual isostatic gravity anomaly grid	A-74
Figure A-37 CEUS SSC horizontal derivative of first vertical derivative of residual isostatic gravity anomaly grid	A-75
Figure A-38 Corrected heat flow values from the SMU Geothermal Laboratory Regional Heat Flow Database (2008)	A-77
Figure A-39 CEUS SSC total intensity magnetic anomaly grid (Ravat et al., 2009). Shaded relief with 315-degree azimuth and 30-degree inclination applied.....	A-80
Figure A-40 CEUS SSC total intensity magnetic anomaly grid (Ravat et al., 2009). Shaded relief with 180-degree azimuth and 30-degree inclination applied.....	A-81
Figure A-41 CEUS SSC differentially reduced to pole magnetic anomaly grid (Ravat, 2009). Shaded relief with 315-degree azimuth and 30-degree inclination applied.....	A-82
Figure A-42 CEUS SSC differentially reduced to pole magnetic anomaly grid (Ravat, 2009). Shaded relief with 180-degree azimuth and 30-degree inclination applied.....	A-83
Figure A-43 CEUS SSC tilt derivative of differentially reduced to pole magnetic anomaly grid (degrees) (Ravat, 2009)	A-84
Figure A-44 CEUS SSC horizontal derivative of tilt derivative of differentially reduced to pole magnetic anomaly grid (radians) (Ravat, 2009)	A-85
Figure A-45 CEUS SSC tilt derivative of differentially reduced to pole magnetic anomaly grid (Ravat, 2009)	A-86
Figure A-46 CEUS SSC amplitude of analytic signal magnetic anomaly grid (Ravat, 2009)	A-87
Figure A-47 CEUS SSC paleoliquefaction database	A-89
Figure A-48 CEUS SSC compilation of seismic reflection and seismic refraction lines.....	A-91
Figure A-49 USGS National Seismic Hazard Maps (Petersen et al., 2008)	A-93
Figure A-50 USGS NSHM ground motion hazard at spectral acceleration of 1 hz with 2% probability of exceedance in 50 years (Petersen et al., 2008)	A-94
Figure A-51 USGS NSHM ground motion hazard at spectral acceleration of 1 hz with 5% probability of exceedance in 50 years (Petersen et al., 2008)	A-95
Figure A-52 USGS NSHM ground motion hazard at spectral acceleration of 1 hz with 10% probability of exceedance in 50 years (Petersen et al., 2008)	A-96
Figure A-53 USGS NSHM ground motion hazard at spectral acceleration of 3 hz with 2% probability of exceedance in 50 years (Petersen et al., 2008)	A-97
Figure A-54 USGS NSHM ground motion hazard at spectral acceleration of 3 hz with 5% probability of exceedance in 50 years (Petersen et al., 2008)	A-98
Figure A-55 USGS NSHM ground motion hazard at spectral acceleration of 3 hz with 10% probability of exceedance in 50 years (Petersen et al., 2008)	A-99
Figure A-56 USGS NSHM ground motion hazard at spectral acceleration of 5 hz with 2% probability of exceedance in 50 years (Petersen et al., 2008)	A-100

Figure A-57 USGS NSHM ground motion hazard at spectral acceleration of 5 hz with 5% probability of exceedance in 50 years (Petersen et al., 2008)	A-101
Figure A-58 USGS NSHM ground motion hazard at spectral acceleration of 5 hz with 10% probability of exceedance in 50 years (Petersen et al., 2008)	A-102
Figure A-59 USGS NSHM peak ground acceleration with 2% probability of exceedance in 50 years (Petersen et al., 2008)	A-103
Figure A-60 USGS NSHM peak ground acceleration with 5% probability of exceedance in 50 years (Petersen et al., 2008)	A-104
Figure A-61 USGS NSHM peak ground acceleration with 10% probability of exceedance in 50 years (Petersen et al., 2008)	A-105
Figure A-62 Deformation of the North American Plate interior using GPS station data (Calais et al., 2006)	A-107
Figure A-63 Stress measurement update for the CEUS (Hurd, 2010).....	A-110
Figure A-64 CEUS SSC Project study area boundary	A-112
Figure A-65 USGS Quaternary fault and fold database (USGS, 2006)	A-114
Figure A-66 Quaternary features compilation for the CEUS (Crone and Wheeler, 2000; Wheeler, 2005; USGS, 2010)	A-116
Figure A-67 CEUS Mesozoic rift basins after Benson (1992).....	A-118
Figure A-68 CEUS Mesozoic rift basins after Dennis et al. (2004)	A-120
Figure A-69 CEUS Mesozoic rift basins after Schlische (1993).....	A-122
Figure A-70 CEUS Mesozoic rift basins after Withjack et al. (1998).....	A-124
Figure A-71 RLME zones for the CEUS	A-126
Figure A-72 Mesozoic and non-Mesozoic zones for the CEUS, wide interpretation.....	A-128
Figure A-73 Mesozoic and non-Mesozoic zones for the CEUS, narrow interpretation.....	A-129
Figure A-74 CEUS seismotectonic zones model A.....	A-130
Figure A-75 CEUS seismotectonic zones model B.....	A-131
Figure A-76 CEUS seismotectonic zones model C	A-132
Figure A-77 CEUS seismotectonic zones model D	A-133
Figure E-1 Map of CEUS showing locations of regional data sets included in the CEUS SSC Project paleoliquefaction database, including New Madrid seismic zone and surrounding region; Marianna, Arkansas, area; St. Louis region; Wabash Valley seismic zone and surrounding region; Arkansas-Louisiana-Mississippi region; Charleston seismic zone; Atlantic Coastal region and the Central Virginia seismic zone; Newburyport, Massachusetts, and surrounding region; and Charlevoix seismic zone and surrounding region.	E-68
Figure E-2 Diagram illustrating size parameters of liquefaction features, including sand blow thickness, width, and length; dike width; and sill thickness, as well as some of the diagnostic characteristics of these features.	E-69
Figure E-3 Diagram illustrating sampling strategy for dating of liquefaction features as well as age data, such as ¹⁴ C maximum and ¹⁴ C minimum, used to calculate preferred age estimates and related uncertainties of liquefaction features.....	E-70
Figure E-4 GIS map of New Madrid seismic zone and surrounding region showing portions of rivers searched for earthquake-induced liquefaction features by M.	

Tuttle, R. Van Arsdale, and J. Vaughn and collaborators (see explanation); information contributed for this report. Map projection is USA Contiguous Albers Equal Area Conic, North America Datum 1983.....	E-71
Figure E-5 GIS map of New Madrid seismic zone and surrounding region showing locations of liquefaction features for which there are and are not radiocarbon data. Map projection is USA Contiguous Albers Equal Area Conic, North America Datum 1983.	E-72
Figure E-6 GIS map of New Madrid seismic zone and surrounding region showing locations of liquefaction features that are thought to be historical or prehistoric in age or whose ages are poorly constrained. Map projection is USA Contiguous Albers Equal Area Conic, North America Datum 1983.	E-73
Figure E-7 GIS map of New Madrid seismic zone and surrounding region showing preferred age estimates of liquefaction features; features whose ages are poorly constrained are excluded. Map projection is USA Contiguous Albers Equal Area Conic, North America Datum 1983.	E-74
Figure E-8 GIS map of New Madrid seismic zone and surrounding region showing measured thicknesses of sand blows. Map projection is USA Contiguous Albers Equal Area Conic, North America Datum 1983.....	E-75
Figure E-9 GIS map of New Madrid seismic zone and surrounding region showing preferred age estimates and measured thicknesses of sand blows. Map projection is USA Contiguous Albers Equal Area Conic, North America Datum 1983.	E-76
Figure E-10 GIS map of New Madrid seismic zone and surrounding region showing measured widths of sand dikes. Map projection is USA Contiguous Albers Equal Area Conic, North America Datum 1983.....	E-77
Figure E-11 GIS map of New Madrid seismic zone and surrounding region showing preferred age estimates and measured widths of sand dikes. Map projection is USA Contiguous Albers Equal Area Conic, North America Datum 1983.	E-78
Figure E-12 GIS map of New Madrid seismic zone and surrounding region illustrating preferred age estimates and measured thicknesses of sand blows as well as preferred age estimates and measured widths of sand dikes for sites where sand blows do not occur. Map projection is USA Contiguous Albers Equal Area Conic, North America Datum 1983.....	E-79
Figure E-13 GIS map of Marianna, Arkansas, area showing seismicity and locations of paleoliquefaction features relative to mapped traces of Eastern Reelfoot rift margin fault, White River fault zone, Big Creek fault zone, Marianna escarpment, and Daytona Beach lineament. Map projection is USA Contiguous Albers Equal Area Conic, North America Datum 1983.	E-80
Figure E-14 (A) Trench log and (B) ground-penetrating radar profile, showing vertical sections of sand blows and sand dikes at Daytona Beach SE2 site along the Daytona Beach lineament southwest of Marianna, Arkansas. Vertical scale of GPR profile is exaggerated (modified from Al-Shukri et al., 2009).	E-81
Figure E-15 GIS map of Marianna, Arkansas, area showing locations of liquefaction features for which there are and are not radiocarbon data. Map projection is USA Contiguous Albers Equal Area Conic, North America Datum 1983.	E-82
Figure E-16 GIS map of Marianna, Arkansas, area showing locations of liquefaction features that are thought to be historical or prehistoric in age or whose ages are poorly constrained. To date, no liquefaction features thought to have formed during	

1811-1812 earthquakes have been found in area. Map projection is USA Contiguous Albers Equal Area Conic, North America Datum 1983.	E-83
Figure E-17 GIS map of Marianna, Arkansas, area showing preferred age estimates of liquefaction features; features whose ages are poorly constrained are excluded. Map projection is USA Contiguous Albers Equal Area Conic, North America Datum 1983.	E-84
Figure E-18 GIS map of Marianna, Arkansas, area showing measured thicknesses of sand blows. Map projection is USA Contiguous Albers Equal Area Conic, North America Datum 1983.	E-85
Figure E-19 GIS map of Marianna, Arkansas, area showing preferred age estimates and measured thicknesses of sand blows. Map projection is USA Contiguous Albers Equal Area Conic, North America Datum 1983.....	E-86
Figure E-20 GIS map of Marianna, Arkansas, area showing measured widths of sand dikes. Map projection is USA Contiguous Albers Equal Area Conic, North America Datum 1983.....	E-87
Figure E-21 GIS map of Marianna, Arkansas, area showing preferred age estimates and measured widths of sand dikes. Map projection is USA Contiguous Albers Equal Area Conic, North America Datum 1983.....	E-88
Figure E-22 GIS map of St. Louis, Missouri, region showing seismicity and portions of rivers searched for earthquake-induced liquefaction features by Tuttle and collaborators; information contributed for this report. Map projection is USA Contiguous Albers Equal Area Conic, North America Datum 1983.	E-89
Figure E-23 GIS map of St. Louis, Missouri, region showing locations of liquefaction features, including several soft-sediment deformation structures, for which there are and are not radiocarbon data. Map projection is USA Contiguous Albers Equal Area Conic, North America Datum 1983.	E-90
Figure E-24 GIS map of St. Louis, Missouri, region showing locations of liquefaction features that are thought to be historical or prehistoric in age or whose ages are poorly constrained. Map projection is USA Contiguous Albers Equal Area Conic, North America Datum 1983.....	E-91
Figure E-25 GIS map of St. Louis, Missouri, region showing preferred age estimates of liquefaction features; features whose ages are poorly constrained, including several that are prehistoric in age, are not shown. Map projection is USA Contiguous Albers Equal Area Conic, North America Datum 1983.....	E-92
Figure E-26 GIS map of St. Louis, Missouri, region showing measured thicknesses of sand blows at similar scale as used in Figure E-8 of sand blows in New Madrid seismic zone. Note that few sand blows have been found in St. Louis region. Map projection is USA Contiguous Albers Equal Area Conic, North America Datum 1983.	E-93
Figure E-27 GIS map of St. Louis, Missouri, region showing preferred age estimates and measured thicknesses of sand blows. Map projection is USA Contiguous Albers Equal Area Conic, North America Datum 1983.....	E-94
Figure E-28 GIS map of St. Louis, Missouri, region showing measured widths of sand dikes at similar scale as that used in Figure E-10 for sand dikes in New Madrid seismic zone. Map projection is USA Contiguous Albers Equal Area Conic, North America Datum 1983.	E-95

Figure E-29 GIS map of St. Louis, Missouri, region showing measured widths of sand dikes at similar scale as that used in Figures E-42 and E-48 for sand dikes in the Newburyport and Charlevoix regions, respectively. Map projection is USA Contiguous Albers Equal Area Conic, North America Datum 1983.	E-96
Figure E-30 GIS map of St. Louis, Missouri, region showing preferred age estimates and measured widths of sand dikes. Map projection is USA Contiguous Albers Equal Area Conic, North America Datum 1983.	E-97
Figure E-31 GIS map of Wabash Valley seismic zone and surrounding region showing portions of rivers searched for earthquake-induced liquefaction features (digitized from McNulty and Obermeier, 1999). Map projection is USA Contiguous Albers Equal Area Conic, North America Datum 1983.	E-98
Figure E-32 GIS map of Wabash Valley seismic zone and surrounding region showing measured widths of sand dikes at similar scale as that used in Figures E-10 and E-11 for sand dikes in New Madrid seismic zone. Map projection is USA Contiguous Albers Equal Area Conic, North America Datum 1983.	E-99
Figure E-33 GIS map of Wabash Valley region of Indiana and Illinois showing preferred age estimates and paleoearthquake interpretation. Map projection is USA Contiguous Albers Equal Area Conic, North America Datum 1983.	E-100
Figure E-34 GIS map of Arkansas-Louisiana-Mississippi (ALM) region showing paleoliquefaction study locations. Map projection is USA Contiguous Albers Equal Area Conic, North America Datum 1983.	E-101
Figure E-35 GIS map of Charleston, South Carolina, region showing locations of paleoliquefaction features for which there are and are not radiocarbon dates. Map projection is USA Contiguous Albers Equal Area Conic, North America Datum 1983.	E-102
Figure E-36 GIS map of Charleston, South Carolina, region showing locations of historical and prehistoric liquefaction features. Map projection is USA Contiguous Albers Equal Area Conic, North America Datum 1983.	E-103
Figure E-37 Map of Atlantic coast region showing areas searched for paleoliquefaction features by Gelinis et al. (1998) and Amick, Gelinis, et al. (1990). Rectangles indicate 7.5-minute quadrangles in which sites were investigated for presence of paleoliquefaction features. The number of sites investigated is shown within that quadrangle, if known. Orange and yellow indicate quadrangles in which paleoliquefaction features were recognized.	E-104
Figure E-38 Map of Central Virginia seismic zone region showing portions of rivers searched for earthquake-induced liquefaction features by Obermeier and McNulty (1998).	E-105
Figure E-39 GIS map of Newburyport, Massachusetts, and surrounding region showing seismicity and portions of rivers searched for earthquake-induced liquefaction features (Gelinis et al., 1998; Tuttle, 2007, 2009). Solid black line crossing map represents Massachusetts–New Hampshire border. Map projection is USA Contiguous Albers Equal Area Conic, North America Datum 1983.	E-106
Figure E-40 GIS map of Newburyport, Massachusetts, and surrounding region showing locations of liquefaction features for which there are and are not radiocarbon dates. Map projection is USA Contiguous Albers Equal Area Conic, North America Datum 1983.	E-107

Figure E-41 GIS map of Newburyport, Massachusetts, and surrounding region showing locations of liquefaction features that are thought to be historical or prehistoric in age or whose ages are poorly constrained. Map projection is USA Contiguous Albers Equal Area Conic, North America Datum 1983.	E-108
Figure E-42 GIS map of Newburyport, Massachusetts, and surrounding region showing measured widths of sand dikes. Map projection is USA Contiguous Albers Equal Area Conic, North America Datum 1983.	E-109
Figure E-43 GIS map of Newburyport, Massachusetts, and surrounding region showing preferred age estimates and measured widths of sand dikes. Map projection is USA Contiguous Albers Equal Area Conic, North America Datum 1983.	E-110
Figure E-44 Map of Charlevoix seismic zone and adjacent St. Lawrence Lowlands showing mapped faults and portions of rivers along which reconnaissance and searches for earthquake-induced liquefaction features were performed. Charlevoix seismic zone is defined by concentration of earthquakes and locations of historical earthquakes northeast of Quebec City. Devonian impact structure in vicinity of Charlevoix seismic zone is outlined by black dashed line. Taconic thrust faults are indicated by solid black lines with sawteeth on upper plate; lapetan rift faults are shown by solid black lines with hachure marks on downthrown side (modified from Tuttle and Atkinson, 2010).	E-111
Figure E-45 GIS map of Charlevoix seismic zone and surrounding region showing locations of liquefaction features, including several soft-sediment deformation structures, for which there are and are not radiocarbon data. Note the location of 1988 M 5.9 Saguenay earthquake northwest of the Charlevoix seismic zone. Map projection is USA Contiguous Albers Equal Area Conic, North America Datum 1983.	E-112
Figure E-46 GIS map of Charlevoix seismic zone and surrounding region showing locations of liquefaction features that are modern, historical, or prehistoric in age, or whose ages are poorly constrained. Map projection is USA Contiguous Albers Equal Area Conic, North America Datum 1983.	E-113
Figure E-47 GIS map of Charlevoix seismic zone and surrounding region showing preferred age estimates of liquefaction features; features whose ages are poorly constrained are excluded. Map projection is USA Contiguous Albers Equal Area Conic, North America Datum 1983.	E-114
Figure E-48 GIS map of Charlevoix seismic zone and surrounding region showing measured widths of sand dikes. Map projection is USA Contiguous Albers Equal Area Conic, North America Datum 1983.	E-115
Figure E-49 GIS map of Charlevoix seismic zone and surrounding region showing preferred age estimates and measured widths of sand dikes. Map projection is USA Contiguous Albers Equal Area Conic, North America Datum 1983.	E-116
Figure E-50 Photograph of moderate-sized sand blow (12 m long, 7 m wide, and 14 cm thick) that formed about 40 km from epicenter of 2001 M 7.7 Bhuj, India, earthquake (from Tuttle, Hengesh, et al., 2002), combined with schematic vertical section illustrating structural and stratigraphic relations of sand blow, sand dike, and source layer (modified from Sims and Garvin, 1995).	E-117
Figure E-51 Tree trunks buried and killed by sand blows, vented during 1811-1812 New Madrid earthquakes (from Fuller, 1912).	E-118

Figure E-52 Large sand-blow crater that formed during 2002 M 7.7 Bhuj, India, earthquake. Backpack for scale. Photograph: M. Tuttle (2001).	E-119
Figure E-53 Sand-blow crater that formed during 1886 Charleston, South Carolina, earthquake. Photograph: J.K. Hillers (from USGS Photograph Library).	E-120
Figure E-54 Photograph of sand blow and related sand dikes exposed in trench wall and floor in New Madrid seismic zone. Buried soil horizon is displaced downward approximately 1 m across two dikes. Clasts of soil horizon occur within dikes and overlying sand blow. Degree of soil development above and within sand blow suggests that it is at least several hundred years old and formed prior to 1811-1812 New Madrid earthquakes. Organic sample (location marked by red flag) from crater fill will provide close minimum age constraint for formation of sand blow. For scale, each colored intervals on shovel handle represents 10 cm. Photograph: M. Tuttle.....	E-121
Figure E-55 Sand dikes, ranging up to 35 cm wide, originate in pebbly sand layer and intrude overlying diamicton, These features were exposed in cutbank along Cahokia Creek about 25 km northeast of downtown St. Louis (from Tuttle, 2000).	E-122
Figure E-56 Photograph of small diapirs of medium sand intruding base of overlying deposit of interbedded clayey silt and very fine sand, and clasts of clayey silt in underlying medium sand, observed along Ouelle River in Charlevoix seismic zone. Sand diapirs and clasts probably formed during basal erosion and foundering of clayey silt due to liquefaction of the underlying sandy deposit. Red portion of shovel handle represents 10 cm (modified from Tuttle and Atkinson, 2010).....	E-123
Figures E-57 (A) Load cast formed in laminated sediments of Van Norman Lake during 1952 Kern County, California, earthquake. Photograph: J. Sims (from Sims, 1975). (B) Load cast, pseudonodules, and related folds formed in laminated sediment exposed along Malbaie River in Charlevoix seismic zone. Sand dikes crosscutting these same laminated sediments occur at a nearby site. For scale, each painted interval of the shovel handle represents 10 cm (modified from Tuttle and Atkinson, 2010).	E-124
Figure E-58 Log of sand blow and uppermost portions of related sand dikes exposed in trench wall at Dodd site in New Madrid seismic zone. Sand dikes were also observed in opposite wall and trench floor. Sand blow buries pre-event A horizon, and a subsequent A horizon has developed in top of sand blow. Radiocarbon dating of samples collected above and below sand blow brackets its age between 490 and 660 yr BP. Artifact assemblage indicates that sand blow formed during late Mississippian (300–550 yr BP or AD 1400–1670) (modified from Tuttle, Collier, et al., 1999).	E-125
Figures E-59 (A) Photograph of earthquake-induced liquefaction features found in association with cultural horizon and pit exposed in trench wall near Blytheville, Arkansas, in New Madrid seismic zone. Photograph: M. Tuttle. (B) Trench log of features shown in (A). Sand dike formed in thick Native American occupation horizon containing artifacts of early Mississippian cultural period (950–1,150 yr BP). Cultural pit dug into top of sand dike contains artifacts and charcoal used to constrain minimum age of liquefaction features (modified from Tuttle and Schweig, 1995).	E-126
Figure E-60 In situ tree trunks such as this one buried and killed by sand blow in New Madrid seismic zone offer opportunity to date paleoearthquakes to the year and season of occurrence. Photograph: M. Tuttle.	E-127

Figure E-61 Portion of dendrocalibration curve illustrating conversion of radiocarbon age to calibrated date in calendar years. In example, 2-sigma radiocarbon age of 2,280–2,520 BP is converted to calibrated date of 770–380 BC (from Tuttle, 1999).	E-128
Figure E-62 Empirical relation developed between A horizon thickness of sand blows and years of soil development in New Madrid region. Horizontal bars reflect uncertainties in age estimates of liquefaction features; diamonds mark midpoints of possible age ranges (from Tuttle et al., 2000).	E-129
Figure E-63 Diagram illustrating earthquake chronology for New Madrid seismic zone for past 5,500 years based on dating and correlation of liquefaction features at sites (listed at top) across region from north to south. Vertical bars represent age estimates of individual sand blows, and horizontal bars represent event times of 138 yr BP (AD 1811-1812); 500 yr BP \pm 150 yr; 1,050 yr BP \pm 100 yr; and 4,300 yr BP \pm 200 yr (modified from Tuttle, Schweig, et al., 2002; Tuttle et al., 2005).	E-130
Figure E-64 Diagram illustrating earthquake chronology for New Madrid seismic zone for past 2,000 years, similar to upper portion of diagram shown in Figure E-63. As in Figure E-63, vertical bars represent age estimates of individual sand blows, and horizontal bars represent event times. Analysis performed during CEUS SSC Project derived two possible uncertainty ranges for timing of paleoearthquakes, illustrated by the darker and lighter portions of the colored horizontal bars, respectively: 503 yr BP \pm 8 yr or 465 yr BP \pm 65 yr, and 1,110 yr BP \pm 40 yr or 1055 \pm 95 yr (modified from Tuttle, Schweig, et al., 2002).	E-131
Figure E-65 Maps showing spatial distributions and sizes of sand blows and sand dikes attributed to 500 and 1,050 yr BP events. Locations and sizes of liquefaction features that formed during AD 1811-1812 (138 yr BP) New Madrid earthquake sequence shown for comparison (modified from Tuttle, Schweig, et al., 2002).	E-132
Figure E-66 Liquefaction fields for 138 yr BP (AD 1811-1812); 500 yr BP (AD 1450); and 1,050 yr BP (AD 900) events as interpreted from spatial distribution and stratigraphy of sand blows (modified from Tuttle, Schweig, et al., 2002). Ellipses define areas where similar-age sand blows have been mapped. Overlapping ellipses indicate areas where sand blows are composed of multiple units that formed during sequence of earthquakes. Dashed ellipse outlines area where historical sand blows are composed of four depositional units. Magnitudes of earthquakes in 500 yr BP and 1,050 yr BP are inferred from comparison with 1811-1812 liquefaction fields. Magnitude estimates of December (D), January (J), and February (F) main shocks and large aftershocks taken from several sources; rupture scenario from Johnston and Schweig (1996; modified from Tuttle, Schweig, et al., 2002).	E-133
Figure E-67 Empirical relation between earthquake magnitude and epicentral distance to farthest known sand blows induced by instrumentally recorded earthquakes (modified from Castilla and Audemard, 2007).	E-134
Figure E-68 Distances to farthest known liquefaction features indicate that 500 and 1,050 yr BP New Madrid events were at least of M 6.7 and 6.9, respectively, when plotted on Ambraseys (1988) relation between earthquake magnitude and epicentral distance to farthest surface expression of liquefaction. Similarity in size distribution of historical and prehistoric sand blows, however, suggests that paleoearthquakes were comparable in magnitude to 1811-1812 events or M \sim 7.6 (modified from Tuttle, 2001).	E-135
Figure H-1-1 Region covered by the CEUS SSC model.	H-44

Figure H-2-1 Master logic tree for the CEUS SSC model.....	H-45
Figure H-3-1 Logic tree for the Mmax zones branch of the master logic tree.....	H-46
Figure H-3-2 Mesozoic extended (MESE-W) and non-extended (NMESE-W) Mmax zones for the “wide” interpretation.....	H-47
Figure H-3-3 Mesozoic extended (MESE-N) and non-extended (NMESE-N) Mmax zones for the “narrow” interpretation.....	H-48
Figure H-4-1(a) Logic tree for the seismotectonic zones branch of the master logic tree.....	H-49
Figure H-4-1(b) Logic tree for the seismotectonic zones branch of the master logic tree.....	H-50
Figure H-4-2 Seismotectonic zones shown in the case where the Rough Creek Graben is not part of the Reelfoot Rift (RR) and the Paleozoic Extended zone is narrow (PEZ-N).....	H-51
Figure H-4-3 Seismotectonic zones shown in the case where the Rough Creek Graben is part of the Reelfoot Rift (RR-RCG) and the Paleozoic Extended zone is narrow (PEZ-N).....	H-52
Figure H-4-4 Seismotectonic zones shown in the case where the Rough Creek Graben is not part of the Reelfoot Rift (RR) and the Paleozoic Extended zone is wide (PEZ-W).....	H-53
Figure H-4-5 Seismotectonic zones shown in the case where the Rough Creek Graben is part of the Reelfoot Rift (RR-RCG) and the Paleozoic Extended zone is wide (PEZ-W).....	H-54
Figure H-5-1 Logic tree for the RLME source branch of the master logic tree.....	H-55
Figure H-5-2 Location of RLME sources in the CEUS SSC model.....	H-56
Figure H-5.1-1 Logic tree for Charlevoix RLME source.....	H-57
Figure H-5.1-2 Charlevoix RLME source geometry.....	H-58
Figure H-5.2-1(a) Logic tree for Charleston RLME source.....	H-59
Figure H-5.2-1(b) Logic tree for Charleston RLME source.....	H-60
Figure H-5.2-2 Charleston RLME alternative source geometries.....	H-61
Figure H-5.3-1 Logic tree for Cheraw RLME source.....	H-62
Figure H-5.3-2 Cheraw RLME source geometry.....	H-63
Figure H-5.4-1 Logic tree for Meers RLME source.....	H-64
Figure H-5.4-2 Meers RLME source geometries.....	H-65
Figure H-5.5-1 Logic tree for NMFS RLME source.....	H-66
Figure H-5.5-2 New Madrid South (NMS) fault alternative RMLE source geometries: Blytheville Arch-Bootheel Lineament (BA-BL) and Blytheville Arch-Blytheville fault zone (BA-BFZ).....	H-67
Figure H-5.5-3 New Madrid North (NMN) fault alternative RMLE source geometries: New Madrid North (NMN_S) and New Madrid North plus extension (NMN_L).....	H-68
Figure H-5.5-4 Reelfoot Thrust (RFT) fault alternative RMLE source geometries: Reelfoot thrust (RFT_S) and Reelfoot thrust plus extensions (RFT_L).....	H-69
Figure H-5.6-1 Logic tree for ERM-S RLME source.....	H-70
Figure H-5.6-2 Logic tree for ERM-N RLME source.....	H-71
Figure H-5.6-3 ERM-S RLME source geometries.....	H-72

Figure H-5.6-4 ERM-N RLME source geometry	H-73
Figure H-5.7-1 Logic tree for Marianna RLME source	H-74
Figure H-5.7-2 Marianna RLME source geometry	H-75
Figure H-5.8-1 Logic tree for Commerce Fault Zone RLME source	H-76
Figure H-5.8-2 Commerce RLME source geometry	H-77
Figure H-5.9-1 Logic tree for Wabash Valley RLME source	H-78
Figure H-5.9-2 Wabash Valley RLME source geometry	H-79
Figure J-1 Map of the rate and b -value for the study region under the Mmax zonation, with no separation of Mesozoic extended and non-extended; Case A magnitude weights: Realization 1	J-2
Figure J-2 Map of the rate and b -value for the study region under the Mmax zonation, with no separation of Mesozoic extended and non-extended; Case A magnitude weights: Realization 2	J-3
Figure J-3 Map of the rate and b -value for the study region under the Mmax zonation, with no separation of Mesozoic extended and non-extended; Case A magnitude weights: Realization 3	J-4
Figure J-4 Map of the rate and b -value for the study region under the Mmax zonation, with no separation of Mesozoic extended and non-extended; Case A magnitude weights: Realization 4	J-5
Figure J-5 Map of the rate and b -value for the study region under the Mmax zonation, with no separation of Mesozoic extended and non-extended; Case A magnitude weights: Realization 5	J-6
Figure J-6 Map of the rate and b -value for the study region under the Mmax zonation, with no separation of Mesozoic extended and non-extended; Case A magnitude weights: Realization 6	J-7
Figure J-7 Map of the rate and b -value for the study region under the Mmax zonation, with no separation of Mesozoic extended and non-extended; Case A magnitude weights: Realization 7	J-8
Figure J-8 Map of the rate and b -value for the study region under the Mmax zonation, with no separation of Mesozoic extended and non-extended; Case A magnitude weights: Realization 8	J-9
Figure J-9 Map of the coefficient of variation of the rate and the standard deviation of the b -value for the study region under the Mmax zonation, with no separation of Mesozoic extended and non-extended; Case A magnitude weights.....	J-10
Figure J-10 Map of the rate and b -value for the study region under the Mmax zonation, with no separation of Mesozoic extended and non-extended; Case B magnitude weights: Realization 1	J-11
Figure J-11 Map of the rate and b -value for the study region under the Mmax zonation, with no separation of Mesozoic extended and non-extended; Case B magnitude weights: Realization 2	J-12
Figure J-12 Map of the rate and b -value for the study region under the Mmax zonation, with no separation of Mesozoic extended and non-extended; Case B magnitude weights: Realization 3	J-13

Figure J-13 Map of the rate and b -value for the study region under the Mmax zonation, with no separation of Mesozoic extended and non-extended; Case B magnitude weights: Realization 4	J-14
Figure J-14 Map of the rate and b -value for the study region under the Mmax zonation, with no separation of Mesozoic extended and non-extended; Case B magnitude weights: Realization 5	J-15
Figure J-15 Map of the rate and b -value for the study region under the Mmax zonation, with no separation of Mesozoic extended and non-extended; Case B magnitude weights: Realization 6	J-16
Figure J-16 Map of the rate and b -value for the study region under the Mmax zonation, with no separation of Mesozoic extended and non-extended; Case B magnitude weights: Realization 7	J-17
Figure J-17 Map of the rate and b -value for the study region under the Mmax zonation, with no separation of Mesozoic extended and non-extended; Case B magnitude weights: Realization 8	J-18
Figure J-18 Map of the coefficient of variation of the rate and the standard deviation of the b -value for the study region under the Mmax zonation, with no separation of Mesozoic extended and non-extended; Case B magnitude weights.....	J-19
Figure J-19 Map of the rate and b -value for the study region under the Mmax zonation, with no separation of Mesozoic extended and non-extended; Case E magnitude weights: Realization 1	J-20
Figure J-20 Map of the rate and b -value for the study region under the Mmax zonation, with no separation of Mesozoic extended and non-extended; Case E magnitude weights: Realization 2	J-21
Figure J-21 Map of the rate and b -value for the study region under the Mmax zonation, with no separation of Mesozoic extended and non-extended; Case E magnitude weights: Realization 3	J-22
Figure J-22 Map of the rate and b -value for the study region under the Mmax zonation, with no separation of Mesozoic extended and non-extended; Case E magnitude weights: Realization 4	J-23
Figure J-23 Map of the rate and b -value for the study region under the Mmax zonation, with no separation of Mesozoic extended and non-extended; Case E magnitude weights: Realization 5	J-24
Figure J-24 Map of the rate and b -value for the study region under the Mmax zonation, with no separation of Mesozoic extended and non-extended; Case E magnitude weights: Realization 6	J-25
Figure J-25 Map of the rate and b -value for the study region under the Mmax zonation, with no separation of Mesozoic extended and non-extended; Case E magnitude weights: Realization 7	J-26
Figure J-26 Map of the rate and b -value for the study region under the Mmax zonation, with no separation of Mesozoic extended and non-extended; Case E magnitude weights: Realization 8	J-27
Figure J-27 Map of the coefficient of variation of the rate and the standard deviation of the b -value for the study region under the Mmax zonation, with no separation of Mesozoic extended and non-extended; Case E magnitude weights.....	J-28

Figure J-28 Map of the rate and b -value for the study region under the M_{max} zonation, with separation of Mesozoic extended and non-extended; Case A magnitude weights: Realization 1	J-29
Figure J-29 Map of the rate and b -value for the study region under the M_{max} zonation, with separation of Mesozoic extended and non-extended; Case A magnitude weights: Realization 2	J-30
Figure J-30 Map of the rate and b -value for the study region under the M_{max} zonation, with separation of Mesozoic extended and non-extended; Case A magnitude weights: Realization 3	J-31
Figure J-31 Map of the rate and b -value for the study region under the M_{max} zonation, with separation of Mesozoic extended and non-extended; Case A magnitude weights: Realization 4	J-32
Figure J-32 Map of the rate and b -value for the study region under the M_{max} zonation, with separation of Mesozoic extended and non-extended; Case A magnitude weights: Realization 5	J-33
Figure J-33 Map of the rate and b -value for the study region under the M_{max} zonation, with separation of Mesozoic extended and non-extended; Case A magnitude weights: Realization 6	J-34
Figure J-34 Map of the rate and b -value for the study region under the M_{max} zonation, with separation of Mesozoic extended and non-extended; Case A magnitude weights: Realization 7	J-35
Figure J-35 Map of the rate and b -value for the study region under the M_{max} zonation, with separation of Mesozoic extended and non-extended; Case A magnitude weights: Realization 8	J-36
Figure J-36 Map of the coefficient of variation of the rate and the standard deviation of the b -value for the study region under the M_{max} zonation, with separation of Mesozoic extended and non-extended; Case A magnitude weights.....	J-37
Figure J-37 Map of the rate and b -value for the study region under the M_{max} zonation, with separation of Mesozoic extended and non-extended; Case B magnitude weights: Realization 1	J-38
Figure J-38 Map of the rate and b -value for the study region under the M_{max} zonation, with separation of Mesozoic extended and non-extended; Case B magnitude weights: Realization 2	J-39
Figure J-39 Map of the rate and b -value for the study region under the M_{max} zonation, with separation of Mesozoic extended and non-extended; Case B magnitude weights: Realization 3	J-40
Figure J-40 Map of the rate and b -value for the study region under the M_{max} zonation, with separation of Mesozoic extended and non-extended; Case B magnitude weights: Realization 4	J-41
Figure J-41 Map of the rate and b -value for the study region under the M_{max} zonation, with separation of Mesozoic extended and non-extended; Case B magnitude weights: Realization 5	J-42
Figure J-42 Map of the rate and b -value for the study region under the M_{max} zonation, with separation of Mesozoic extended and non-extended; Case B magnitude weights: Realization 6	J-43

Figure J-43 Map of the rate and b -value for the study region under the M_{max} zonation, with separation of Mesozoic extended and non-extended; Case B magnitude weights: Realization 7	J-44
Figure J-44 Map of the rate and b -value for the study region under the M_{max} zonation, with separation of Mesozoic extended and non-extended; Case B magnitude weights: Realization 8	J-45
Figure J-45 Map of the coefficient of variation of the rate and the standard deviation of the b -value for the study region under the M_{max} zonation, with separation of Mesozoic extended and non-extended; Case B magnitude weights.....	J-46
Figure J-46 Map of the rate and b -value for the study region under the M_{max} zonation, with separation of Mesozoic extended and non-extended; Case E magnitude weights: Realization 1	J-47
Figure J-47 Map of the rate and b -value for the study region under the M_{max} zonation, with separation of Mesozoic extended and non-extended; Case E magnitude weights: Realization 2	J-48
Figure J-48 Map of the rate and b -value for the study region under the M_{max} zonation, with separation of Mesozoic extended and non-extended; Case E magnitude weights: Realization 3	J-49
Figure J-49 Map of the rate and b -value for the study region under the M_{max} zonation, with separation of Mesozoic extended and non-extended; Case E magnitude weights: Realization 4	J-50
Figure J-50 Map of the rate and b -value for the study region under the M_{max} zonation, with separation of Mesozoic extended and non-extended; Case E magnitude weights: Realization 5	J-51
Figure J-51 Map of the rate and b -value for the study region under the M_{max} zonation, with separation of Mesozoic extended and non-extended; Case E magnitude weights: Realization 6	J-52
Figure J-52 Map of the rate and b -value for the study region under the M_{max} zonation, with separation of Mesozoic extended and non-extended; Case E magnitude weights: Realization 7	J-53
Figure J-53 Map of the rate and b -value for the study region under the M_{max} zonation, with separation of Mesozoic extended and non-extended; Case E magnitude weights: Realization 8	J-54
Figure J-54 Map of the coefficient of variation of the rate and the standard deviation of the b -value for the study region under the M_{max} zonation, with separation of Mesozoic extended and non-extended; Case E magnitude weights.....	J-55
Figure J-55 Map of the rate and b -value for the study region under the M_{max} zonation, with separation of Mesozoic extended and non-extended; Case A magnitude weights: Realization 1	J-56
Figure J-56 Map of the rate and b -value for the study region under the M_{max} zonation, with separation of Mesozoic extended and non-extended; Case A magnitude weights: Realization 2	J-57
Figure J-57 Map of the rate and b -value for the study region under the M_{max} zonation, with separation of Mesozoic extended and non-extended; Case A magnitude weights: Realization 3	J-58

Figure J-58 Map of the rate and b -value for the study region under the Mmax zonation, with separation of Mesozoic extended and non-extended; Case A magnitude weights: Realization 4	J-59
Figure J-59 Map of the rate and b -value for the study region under the Mmax zonation, with separation of Mesozoic extended and non-extended; Case A magnitude weights: Realization 5	J-60
Figure J-60 Map of the rate and b -value for the study region under the Mmax zonation, with separation of Mesozoic extended and non-extended; Case A magnitude weights: Realization 6	J-61
Figure J-61 Map of the rate and b -value for the study region under the Mmax zonation, with separation of Mesozoic extended and non-extended; Case A magnitude weights: Realization 7	J-62
Figure J-62 Map of the rate and b -value for the study region under the Mmax zonation, with separation of Mesozoic extended and non-extended; Case A magnitude weights: Realization 8	J-63
Figure J-63 Map of the coefficient of variation of the rate and the standard deviation of the b -value for the study region under the Mmax zonation, with separation of Mesozoic extended and non-extended; Case A magnitude weights.....	J-64
Figure J-64 Map of the rate and b -value for the study region under the Mmax zonation, with separation of Mesozoic extended and non-extended; Case B magnitude weights: Realization 1	J-65
Figure J-65 Map of the rate and b -value for the study region under the Mmax zonation, with separation of Mesozoic extended and non-extended; Case B magnitude weights: Realization 2	J-66
Figure J-66 Map of the rate and b -value for the study region under the Mmax zonation, with separation of Mesozoic extended and non-extended; Case B magnitude weights: Realization 3	J-67
Figure J-67 Map of the rate and b -value for the study region under the Mmax zonation, with separation of Mesozoic extended and non-extended; Case B magnitude weights: Realization 4	J-68
Figure J-68 Map of the rate and b -value for the study region under the Mmax zonation, with separation of Mesozoic extended and non-extended; Case B magnitude weights: Realization 5	J-69
Figure J-69 Map of the rate and b -value for the study region under the Mmax zonation, with separation of Mesozoic extended and non-extended; Case B magnitude weights: Realization 6	J-70
Figure J-70 Map of the rate and b -value for the study region under the Mmax zonation, with separation of Mesozoic extended and non-extended; Case B magnitude weights: Realization 7	J-71
Figure J-71 Map of the rate and b -value for the study region under the Mmax zonation, with separation of Mesozoic extended and non-extended; Case B magnitude weights: Realization 8	J-72
Figure J-72 Map of the coefficient of variation of the rate and the standard deviation of the b -value for the study region under the Mmax zonation, with separation of Mesozoic extended and non-extended; Case B magnitude weights.....	J-73

Figure J-73 Map of the rate and b -value for the study region under the Mmax zonation, with separation of Mesozoic extended and non-extended; Case E magnitude weights: Realization 1	J-74
Figure J-74 Map of the rate and b -value for the study region under the Mmax zonation, with separation of Mesozoic extended and non-extended; Case E magnitude weights: Realization 2	J-75
Figure J-75 Map of the rate and b -value for the study region under the Mmax zonation, with separation of Mesozoic extended and non-extended; Case E magnitude weights: Realization 3	J-76
Figure J-76 Map of the rate and b -value for the study region under the Mmax zonation, with separation of Mesozoic extended and non-extended; Case E magnitude weights: Realization 4	J-77
Figure J-77 Map of the rate and b -value for the study region under the Mmax zonation, with separation of Mesozoic extended and non-extended; Case E magnitude weights: Realization 5	J-78
Figure J-78 Map of the rate and b -value for the study region under the Mmax zonation, with separation of Mesozoic extended and non-extended; Case E magnitude weights: Realization 6	J-79
Figure J-79 Map of the rate and b -value for the study region under the Mmax zonation, with separation of Mesozoic extended and non-extended; Case E magnitude weights: Realization 7	J-80
Figure J-80 Map of the rate and b -value for the study region under the Mmax zonation, with separation of Mesozoic extended and non-extended; Case E magnitude weights: Realization 8	J-81
Figure J-81 Map of the coefficient of variation of the rate and the standard deviation of the b -value for the study region under the Mmax zonation, with separation of Mesozoic extended and non-extended; Case E magnitude weights.....	J-82
Figure J-82 Map of the rate and b -value for the study region under the seismotectonic zonation, with narrow interpretation of PEZ; Case A magnitude weights: Realization 1	J-83
Figure J-83 Map of the rate and b -value for the study region under the seismotectonic zonation, with narrow interpretation of PEZ; Case A magnitude weights: Realization 2	J-84
Figure J-84 Map of the rate and b -value for the study region under the seismotectonic zonation, with narrow interpretation of PEZ; Case A magnitude weights: Realization 3	J-85
Figure J-85 Map of the rate and b -value for the study region under the seismotectonic zonation, with narrow interpretation of PEZ; Case A magnitude weights: Realization 4	J-86
Figure J-86 Map of the rate and b -value for the study region under the seismotectonic zonation, with narrow interpretation of PEZ; Case A magnitude weights: Realization 5	J-87
Figure J-87 Map of the rate and b -value for the study region under the seismotectonic zonation, with narrow interpretation of PEZ; Case A magnitude weights: Realization 6	J-88

Figure J-88 Map of the rate and b -value for the study region under the seismotectonic zonation, with narrow interpretation of PEZ; Case A magnitude weights: Realization 7	J-89
Figure J-89 Map of the rate and b -value for the study region under the seismotectonic zonation, with narrow interpretation of PEZ; Case A magnitude weights: Realization 8	J-90
Figure J-90 Map of the coefficient of variation of the rate and the standard deviation of the b -value for the study region under the seismotectonic zonation, with narrow interpretation of PEZ; Case A magnitude weights	J-91
Figure J-91 Map of the rate and b -value for the study region under the seismotectonic zonation, with narrow interpretation of PEZ; Case B magnitude weights: Realization 1	J-92
Figure J-92 Map of the rate and b -value for the study region under the seismotectonic zonation, with narrow interpretation of PEZ; Case B magnitude weights: Realization 2	J-93
Figure J-93 Map of the rate and b -value for the study region under the seismotectonic zonation, with narrow interpretation of PEZ; Case B magnitude weights: Realization 3	J-94
Figure J-94 Map of the rate and b -value for the study region under the seismotectonic zonation, with narrow interpretation of PEZ; Case B magnitude weights: Realization 4	J-95
Figure J-95 Map of the rate and b -value for the study region under the seismotectonic zonation, with narrow interpretation of PEZ; Case B magnitude weights: Realization 5	J-96
Figure J-96 Map of the rate and b -value for the study region under the seismotectonic zonation, with narrow interpretation of PEZ; Case B magnitude weights: Realization 6	J-97
Figure J-97 Map of the rate and b -value for the study region under the seismotectonic zonation, with narrow interpretation of PEZ; Case B magnitude weights: Realization 7	J-98
Figure J-98 Map of the rate and b -value for the study region under the seismotectonic zonation, with narrow interpretation of PEZ; Case B magnitude weights: Realization 8	J-99
Figure J-99 Map of the coefficient of variation of the rate and the standard deviation of the b -value for the study region under the seismotectonic zonation, with narrow interpretation of PEZ; Case B magnitude weights	J-100
Figure J-100 Map of the rate and b -value for the study region under the seismotectonic zonation, with narrow interpretation of PEZ; Case E magnitude weights: Realization 1	J-101
Figure J-101 Map of the rate and b -value for the study region under the seismotectonic zonation, with narrow interpretation of PEZ; Case E magnitude weights: Realization 2	J-102
Figure J-102 Map of the rate and b -value for the study region under the seismotectonic zonation, with narrow interpretation of PEZ; Case E magnitude weights: Realization 3	J-103

Figure J-103 Map of the rate and b -value for the study region under the seismotectonic zonation, with narrow interpretation of PEZ; Case E magnitude weights: Realization	
4	J-104
Figure J-104 Map of the rate and b -value for the study region under the seismotectonic zonation, with narrow interpretation of PEZ; Case E magnitude weights: Realization	
5	J-105
Figure J-105 Map of the rate and b -value for the study region under the seismotectonic zonation, with narrow interpretation of PEZ; Case E magnitude weights: Realization	
6	J-106
Figure J-106 Map of the rate and b -value for the study region under the seismotectonic zonation, with narrow interpretation of PEZ; Case E magnitude weights: Realization	
7	J-107
Figure J-107 Map of the rate and b -value for the study region under the seismotectonic zonation, with narrow interpretation of PEZ; Case E magnitude weights: Realization	
8	J-108
Figure J-108 Map of the coefficient of variation of the rate and the standard deviation of the b -value for the study region under the seismotectonic zonation, with narrow interpretation of PEZ; Case E magnitude weights	
.....	J-109
Figure J-109 Map of the rate and b -value for the study region under the seismotectonic zonation, with narrow interpretation of PEZ; Case A magnitude weights: Realization	
1	J-110
Figure J-110 Map of the rate and b -value for the study region under the seismotectonic zonation, with narrow interpretation of PEZ; Case A magnitude weights: Realization	
2	J-111
Figure J-111 Map of the rate and b -value for the study region under the seismotectonic zonation, with narrow interpretation of PEZ; Case A magnitude weights: Realization	
3	J-112
Figure J-112 Map of the rate and b -value for the study region under the seismotectonic zonation, with narrow interpretation of PEZ; Case A magnitude weights: Realization	
4	J-113
Figure J-113 Map of the rate and b -value for the study region under the seismotectonic zonation, with narrow interpretation of PEZ; Case A magnitude weights: Realization	
5	J-114
Figure J-114 Map of the rate and b -value for the study region under the seismotectonic zonation, with narrow interpretation of PEZ; Case A magnitude weights: Realization	
6	J-115
Figure J-115 Map of the rate and b -value for the study region under the seismotectonic zonation, with narrow interpretation of PEZ; Case A magnitude weights: Realization	
7	J-116
Figure J-116 Map of the rate and b -value for the study region under the seismotectonic zonation, with narrow interpretation of PEZ; Case A magnitude weights: Realization	
8	J-117
Figure J-117 Map of the coefficient of variation of the rate and the standard deviation of the b -value for the study region under the seismotectonic zonation, with narrow interpretation of PEZ; Case A magnitude weights	
.....	J-118

Figure J-118 Map of the rate and b -value for the study region under the seismotectonic zonation, with narrow interpretation of PEZ; Case B magnitude weights: Realization 1	J-119
Figure J-119 Map of the rate and b -value for the study region under the seismotectonic zonation, with narrow interpretation of PEZ; Case B magnitude weights: Realization 2	J-120
Figure J-120 Map of the rate and b -value for the study region under the seismotectonic zonation, with narrow interpretation of PEZ; Case B magnitude weights: Realization 3	J-121
Figure J-121 Map of the rate and b -value for the study region under the seismotectonic zonation, with narrow interpretation of PEZ; Case B magnitude weights: Realization 4	J-122
Figure J-122 Map of the rate and b -value for the study region under the seismotectonic zonation, with narrow interpretation of PEZ; Case B magnitude weights: Realization 5	J-123
Figure J-123 Map of the rate and b -value for the study region under the seismotectonic zonation, with narrow interpretation of PEZ; Case B magnitude weights: Realization 6	J-124
Figure J-124 Map of the rate and b -value for the study region under the seismotectonic zonation, with narrow interpretation of PEZ; Case B magnitude weights: Realization 7	J-125
Figure J-125 Map of the rate and b -value for the study region under the seismotectonic zonation, with narrow interpretation of PEZ; Case B magnitude weights: Realization 8	J-126
Figure J-126 Map of the coefficient of variation of the rate and the standard deviation of the b -value for the study region under the seismotectonic zonation, with narrow interpretation of PEZ; Case B magnitude weights	J-127
Figure J-127 Map of the rate and b -value for the study region under the seismotectonic zonation, with narrow interpretation of PEZ; Case E magnitude weights: Realization 1	J-128
Figure J-128 Map of the rate and b -value for the study region under the seismotectonic zonation, with narrow interpretation of PEZ; Case E magnitude weights: Realization 2	J-129
Figure J-129 Map of the rate and b -value for the study region under the seismotectonic zonation, with narrow interpretation of PEZ; Case E magnitude weights: Realization 3	J-130
Figure J-130 Map of the rate and b -value for the study region under the seismotectonic zonation, with narrow interpretation of PEZ; Case E magnitude weights: Realization 4	J-131
Figure J-131 Map of the rate and b -value for the study region under the seismotectonic zonation, with narrow interpretation of PEZ; Case E magnitude weights: Realization 5	J-132
Figure J-132 Map of the rate and b -value for the study region under the seismotectonic zonation, with narrow interpretation of PEZ; Case E magnitude weights: Realization 6	J-133

Figure J-133 Map of the rate and b -value for the study region under the seismotectonic zonation, with narrow interpretation of PEZ; Case E magnitude weights: Realization 7	J-134
Figure J-134 Map of the rate and b -value for the study region under the seismotectonic zonation, with narrow interpretation of PEZ; Case E magnitude weights: Realization 8	J-135
Figure J-135 Map of the coefficient of variation of the rate and the standard deviation of the b -value for the study region under the seismotectonic zonation, with narrow interpretation of PEZ; Case E magnitude weights	J-136
Figure J-136 Map of the rate and b -value for the study region under the seismotectonic zonation, with wide interpretation of PEZ; Case A magnitude weights: Realization 1 ...	J-137
Figure J-137 Map of the rate and b -value for the study region under the seismotectonic zonation, with wide interpretation of PEZ; Case A magnitude weights: Realization 2 ...	J-138
Figure J-138 Map of the rate and b -value for the study region under the seismotectonic zonation, with wide interpretation of PEZ; Case A magnitude weights: Realization 3 ...	J-139
Figure J-139 Map of the rate and b -value for the study region under the seismotectonic zonation, with wide interpretation of PEZ; Case A magnitude weights: Realization 4 ...	J-140
Figure J-140 Map of the rate and b -value for the study region under the seismotectonic zonation, with wide interpretation of PEZ; Case A magnitude weights: Realization 5 ...	J-141
Figure J-141 Map of the rate and b -value for the study region under the seismotectonic zonation, with wide interpretation of PEZ; Case A magnitude weights: Realization 6 ...	J-142
Figure J-142 Map of the rate and b -value for the study region under the seismotectonic zonation, with wide interpretation of PEZ; Case A magnitude weights: Realization 7 ...	J-143
Figure J-143 Map of the rate and b -value for the study region under the seismotectonic zonation, with wide interpretation of PEZ; Case A magnitude weights: Realization 8 ...	J-144
Figure J-144 Map of the coefficient of variation of the rate and the standard deviation of the b -value for the study region under the seismotectonic zonation, with wide interpretation of PEZ; Case A magnitude weights	J-145
Figure J-145 Map of the rate and b -value for the study region under the seismotectonic zonation, with wide interpretation of PEZ; Case B magnitude weights: Realization 1 ...	J-146
Figure J-146 Map of the rate and b -value for the study region under the seismotectonic zonation, with wide interpretation of PEZ; Case B magnitude weights: Realization 2 ...	J-147
Figure J-147 Map of the rate and b -value for the study region under the seismotectonic zonation, with wide interpretation of PEZ; Case B magnitude weights: Realization 3 ...	J-148
Figure J-148 Map of the rate and b -value for the study region under the seismotectonic zonation, with wide interpretation of PEZ; Case B magnitude weights: Realization 4 ...	J-149
Figure J-149 Map of the rate and b -value for the study region under the seismotectonic zonation, with wide interpretation of PEZ; Case B magnitude weights: Realization 5 ...	J-150
Figure J-150 Map of the rate and b -value for the study region under the seismotectonic zonation, with wide interpretation of PEZ; Case B magnitude weights: Realization 6 ...	J-151
Figure J-151 Map of the rate and b -value for the study region under the seismotectonic zonation, with wide interpretation of PEZ; Case B magnitude weights: Realization 7 ...	J-152
Figure J-152 Map of the rate and b -value for the study region under the seismotectonic zonation, with wide interpretation of PEZ; Case B magnitude weights: Realization 8 ...	J-153

Figure J-153 Map of the coefficient of variation of the rate and the standard deviation of the b -value for the study region under the seismotectonic zonation, with wide interpretation of PEZ; Case B magnitude weights	J-154
Figure J-154 Map of the rate and b -value for the study region under the seismotectonic zonation, with wide interpretation of PEZ; Case E magnitude weights: Realization 1 ...	J-155
Figure J-155 Map of the rate and b -value for the study region under the seismotectonic zonation, with wide interpretation of PEZ; Case E magnitude weights: Realization 2 ...	J-156
Figure J-156 Map of the rate and b -value for the study region under the seismotectonic zonation, with wide interpretation of PEZ; Case E magnitude weights: Realization 3 ...	J-157
Figure J-157 Map of the rate and b -value for the study region under the seismotectonic zonation, with wide interpretation of PEZ; Case E magnitude weights: Realization 4 ...	J-158
Figure J-158 Map of the rate and b -value for the study region under the seismotectonic zonation, with wide interpretation of PEZ; Case E magnitude weights: Realization 5 ...	J-159
Figure J-159 Map of the rate and b -value for the study region under the seismotectonic zonation, with wide interpretation of PEZ; Case E magnitude weights: Realization 6 ...	J-160
Figure J-160 Map of the rate and b -value for the study region under the seismotectonic zonation, with wide interpretation of PEZ; Case E magnitude weights: Realization 7 ...	J-161
Figure J-161 Map of the rate and b -value for the study region under the seismotectonic zonation, with wide interpretation of PEZ; Case E magnitude weights: Realization 8 ...	J-162
Figure J-162 Map of the coefficient of variation of the rate and the standard deviation of the b -value for the study region under the seismotectonic zonation, with wide interpretation of PEZ; Case E magnitude weights	J-163
Figure J-163 Map of the rate and b -value for the study region under the seismotectonic zonation, with wide interpretation of PEZ; Case A magnitude weights: Realization 1 ...	J-164
Figure J-164 Map of the rate and b -value for the study region under the seismotectonic zonation, with wide interpretation of PEZ; Case A magnitude weights: Realization 2 ...	J-165
Figure J-165 Map of the rate and b -value for the study region under the seismotectonic zonation, with wide interpretation of PEZ; Case A magnitude weights: Realization 3 ...	J-166
Figure J-166 Map of the rate and b -value for the study region under the seismotectonic zonation, with wide interpretation of PEZ; Case A magnitude weights: Realization 4 ...	J-167
Figure J-167 Map of the rate and b -value for the study region under the seismotectonic zonation, with wide interpretation of PEZ; Case A magnitude weights: Realization 5 ...	J-168
Figure J-168 Map of the rate and b -value for the study region under the seismotectonic zonation, with wide interpretation of PEZ; Case A magnitude weights: Realization 6 ...	J-169
Figure J-169 Map of the rate and b -value for the study region under the seismotectonic zonation, with wide interpretation of PEZ; Case A magnitude weights: Realization 7 ...	J-170
Figure J-170 Map of the rate and b -value for the study region under the seismotectonic zonation, with wide interpretation of PEZ; Case A magnitude weights: Realization 8 ...	J-171
Figure J-171 Map of the coefficient of variation of the rate and the standard deviation of the b -value for the study region under the seismotectonic zonation, with wide interpretation of PEZ; Case A magnitude weights	J-172
Figure J-172 Map of the rate and b -value for the study region under the seismotectonic zonation, with wide interpretation of PEZ; Case B magnitude weights: Realization 1 ...	J-173

Figure J-173 Map of the rate and b -value for the study region under the seismotectonic zonation, with wide interpretation of PEZ; Case B magnitude weights: Realization 2 ...	J-174
Figure J-174 Map of the rate and b -value for the study region under the seismotectonic zonation, with wide interpretation of PEZ; Case B magnitude weights: Realization 3 ...	J-175
Figure J-175 Map of the rate and b -value for the study region under the seismotectonic zonation, with wide interpretation of PEZ; Case B magnitude weights: Realization 4 ...	J-176
Figure J-176 Map of the rate and b -value for the study region under the seismotectonic zonation, with wide interpretation of PEZ; Case B magnitude weights: Realization 5 ...	J-177
Figure J-177 Map of the rate and b -value for the study region under the seismotectonic zonation, with wide interpretation of PEZ; Case B magnitude weights: Realization 6 ...	J-178
Figure J-178 Map of the rate and b -value for the study region under the seismotectonic zonation, with wide interpretation of PEZ; Case B magnitude weights: Realization 7 ...	J-179
Figure J-179 Map of the rate and b -value for the study region under the seismotectonic zonation, with wide interpretation of PEZ; Case B magnitude weights: Realization 8 ...	J-180
Figure J-180 Map of the coefficient of variation of the rate and the standard deviation of the b -value for the study region under the seismotectonic zonation, with wide interpretation of PEZ; Case B magnitude weights	J-181
Figure J-181 Map of the rate and b -value for the study region under the seismotectonic zonation, with wide interpretation of PEZ; Case E magnitude weights: Realization 1 ...	J-182
Figure J-182 Map of the rate and b -value for the study region under the seismotectonic zonation, with wide interpretation of PEZ; Case E magnitude weights: Realization 2 ...	J-183
Figure J-183 Map of the rate and b -value for the study region under the seismotectonic zonation, with wide interpretation of PEZ; Case E magnitude weights: Realization 3 ...	J-184
Figure J-184 Map of the rate and b -value for the study region under the seismotectonic zonation, with wide interpretation of PEZ; Case E magnitude weights: Realization 4 ...	J-185
Figure J-185 Map of the rate and b -value for the study region under the seismotectonic zonation, with wide interpretation of PEZ; Case E magnitude weights: Realization 5 ...	J-186
Figure J-186 Map of the rate and b -value for the study region under the seismotectonic zonation, with wide interpretation of PEZ; Case E magnitude weights: Realization 6 ...	J-187
Figure J-187 Map of the rate and b -value for the study region under the seismotectonic zonation, with wide interpretation of PEZ; Case E magnitude weights: Realization 7 ...	J-188
Figure J-188 Map of the rate and b -value for the study region under the seismotectonic zonation, with wide interpretation of PEZ; Case E magnitude weights: Realization 8 ...	J-189
Figure J-189 Map of the coefficient of variation of the rate and the standard deviation of the b -value for the study region under the seismotectonic zonation, with wide interpretation of PEZ; Case E magnitude weights	J-190
Figure K-1 Comparison of relationships between number of reporting stations and moment magnitude presented in Johnston et al. (1994) and Johnston (1996b).	K-41
Figure K-2 Comparison of relationships between isoseismal areas and moment magnitude presented in Johnston et al. (1994) and Johnston (1996b).	K-42

LIST OF TABLES

Table 2.2-1 Technical Meetings Conducted as Part of the CEUS SSC Project.....	2-29
Table 2.2-2 Contributors to the CEUS SSC Project.....	2-30
Table 3.2-1 Summary of Earthquakes Added–USGS Earthquake Catalog by Time Period.....	3-44
Table 3.2-2 Summary of Earthquakes Added–USGS Earthquake Catalog by Source.....	3-45
Table 3.3-1 Conversion Relationships Used–Develop Uniform Moment Magnitudes E[M].....	3-46
Table 3.4-1 Comparison of CEUS SSC Catalog Declustering Results Obtained Using the EPRI (1988) Approach with the Gardner Knopoff (1974) Approach	3-47
Table 3.5-1 Probability of Detection and Equivalent Periods of Completeness for the CEUS for Magnitude Weighting Case A	3-48
Table 3.5-2 Probability of Detection and Equivalent Periods of Completeness for the CEUS for Magnitude Weighting Case B	3-51
Table 3.5-3 Probability of Detection and Equivalent Periods of Completeness for the CEUS for Magnitude Weighting Case E	3-54
Table 4.1.2-1 Sample table indicating particular types of data that can be considered in the identification and characterization of seismic sources (Table 2, ANSI/ANS-2.27- 2008).....	4-26
Table 4.1.2-2 Sample table identifying the types of data that can be considered for characterizing different types of seismic sources, and an evaluation of the relative usefulness or credibility of the various data types (Budnitz et al., 1997).....	4-27
Table 4.1.2-3 Table showing the “generic” (not source-specific) evaluation of data to address indicators of a unique seismic source. The table indicates the TI Team’s assessment of the types of data that can be used to address the indicators and their relative usefulness.	4-28
Table 4.1.2-4 Example of Data Evaluation Table for the Illinois Basin–Extended Basement Zone (IBEB)	4-34
Table 4.1.2-5 Example of Data Summary Table for the Extended Continental Crust– Atlantic Margin (ECC-AM) and Atlantic Highly Extended Crust (AHEX) Zones	4-35
Table 4.1.3-1 Criteria Used to Define the Seismotectonic Zones and Mmax Zones	4-37
Table 4.2.2-1 RLME Sources.....	4-38
Table 4.2.4-1 Seismotectonic Zones	4-39
Table 5.2.1-1 Mesozoic-and-Younger Extended Superdomains (MESE).....	5-60
Table 5.2.1-2 Older Extended and Non-Extended Superdomains (NMESE)	5-61
Table 5.2.1-3 Composite SCR Superdomains (COMP).....	5-62
Table 5.2.1-4 Results of Analyses of Updated SCR Superdomains	5-63

Table 5.2.1-5 Source Zones, $P(m^u > 8\frac{1}{4})$ Values, and Weights on Kijko (2004) K-S-B Estimates	5-64
Table 5.2.1-6 Mmax Distributions for the Two Example Seismic Sources.....	5-65
Table 5.3.2-1 Alternative Cases Considered for the Magnitude-Dependent Weights.....	5-65
Table 5.3.3-1 Miller and Rice (1983) Discrete 5-Point Approximation to a Continuous Probability Distribution and the Modified Form Used in This Study	5-65
Table 5.4-1 Assessment of Default Characteristics of Future Earthquakes in the CEUS.....	5-66
Table 5.4-2 Characteristics of Future Earthquakes for Individual Seismic Sources	5-68
Table 5.4-3 Estimates of D_{90} for Individual Seismic Source Zones.....	5-71
Table 6.1-1 Summary of Data Used to Assess RLME Recurrence Frequencies.....	6-80
Table 6.1.1-1 Charlevoix RLME Recurrence Frequency	6-83
Table 6.1.2-1 Summary of Interpreted Charleston Earthquake Ages and Sizes from “Contemporary Ages Only” Scenario	6-84
Table 6.1.2-2 Summary of Interpreted Charleston Earthquake Ages and Sizes from “All Ages” Scenario.....	6-84
Table 6.1.2-3 Charleston Liquefaction Feature Ages Used to Assess Ages of Prehistoric Earthquakes	6-85
Table 6.1.2-4 Charleston RLME Recurrence Frequency for Poisson Model	6-86
Table 6.1.2-5 Charleston RLME Recurrence Frequency for Renewal Model	6-87
Table 6.1.3-1 Range of Cheraw Fault Estimated Magnitudes (M).....	6-88
Table 6.1.3-2 Cheraw RLME In-Cluster Recurrence Frequency	6-89
Table 6.1.3-3 Cheraw RLME In-Cluster Slip Rates	6-89
Table 6.1.3-4 Cheraw RLME Out-of-Cluster Recurrence Frequency	6-90
Table 6.1.3-5 Cheraw RLME Out-of-Cluster Slip Rates	6-90
Table 6.1.4-1 Range of Estimated Meers Fault Earthquake Magnitudes (M).....	6-91
Table 6.1.4-2 Meers RLME In-Cluster Recurrence Frequency.....	6-91
Table 6.1.4-3 Meers RLME Out-of-Cluster Recurrence Frequency.....	6-91
Table 6.1.5-1 Preferred Ages for Paleoearthquakes in the New Madrid Region ¹	6-92
Table 6.1.5-2 Magnitude Comparisons for New Madrid 1811-1812 Earthquake Sequence	6-93
Table 6.1.5-3 Liquefaction Constraints on Age of AD 1450 NMFS RLME.....	6-94
Table 6.1.5-4 Liquefaction Constraints on Age of AD 900 NMFS RLME.....	6-95
Table 6.1.5-5 NMFS In-Cluster RLME Recurrence Frequency—Poisson Model	6-96
Table 6.1.5-6 NMFS In-Cluster RLME Recurrence Frequency—Renewal Model	6-96
Table 6.1.5-7 NMFS Out-of-Cluster RLME Recurrence Frequency—Poisson Model	6-96
Table 6.1.6-1 Range of ERM-S Estimated Magnitudes (M).....	6-97
Table 6.1.6-2 Range of ERM-N Estimated Magnitudes (M)	6-98
Table 6.1.6-3 ERM-S RLME Recurrence Frequency.....	6-98
Table 6.1.6-4 ERM-N RLME Recurrence Frequency	6-99
Table 6.1.7-1 Marianna RLME Recurrence Frequency	6-99

Table 6.1.8-1 Range of Commerce Fault Zone RLME Estimated Magnitudes (M).....	6-100
Table 6.1.8-2 Commerce Fault Zone RLME Recurrence Frequency.....	6-101
Table 6.1.9-1 Liquefaction Evidence for Prehistoric Earthquakes in the Southern Illinois Basin	6-102
Table 6.1.9-2 Wabash RLME Recurrence Frequency	6-109
Table 6.2-1 Alternative Mmax Zonation Models	6-109
Table 6.3.2-1 Maximum Magnitude Distributions for Mmax Distributed Seismicity Sources	6-110
Table 7.1-1 Data Summary and Data Evaluation Tables for Seismotectonic Zones in Appendices C and D	7-81
Table 7.4.2-1 Maximum Magnitude Distributions for Seismotectonic Distributed Seismicity Sources.....	7-82
Table 8.1-1 Description of Seven Test Sites.....	8-13
Table 8.2.1-1 Mean and Select Fractiles for Rock Hazard at Central Illinois: Digital Data for Figures 8.2-1a through 8.2-1c.....	8-14
Table 8.2.2-1 Mean and Select Fractiles for Rock Hazard at Chattanooga: Digital Data for Figures 8.2-2a through 8.2-2c.....	8-16
Table 8.2.3-1 Mean and Select Fractiles for Rock Hazard at Houston: Digital Data for Figures 8.2-3a through 8.2-3c.....	8-18
Table 8.2.4-1 Mean and Select Fractiles for Rock Hazard at Jackson: Digital Data for Figures 8.2-4a through 8.2-4c.....	8-20
Table 8.2.5-1 Mean and Select Fractiles for Rock Hazard at Manchester: Digital Data for Figures 8.2-5a through 8.2-5c.....	8-22
Table 8.2.6-1 Mean and Select Fractiles for Rock Hazard at Savannah: Digital Data for Figures 8.2-6a through 8.2-6c.....	8-24
Table 8.2.7-1 Mean and Select Fractiles for Rock Hazard at Topeka: Digital Data for Figures 8.2-7a through 8.2-7c.....	8-26
Table 9.4-1 Available Information for Determining the Precision of Mean Hazard	9-21
Table 9.4-2 Summary of an Example Logic Tree Representing Uncertainties for the Charleston Seismic Zone	9-21
Table 9.4-3 Basic Weights Given in EPRI (2004) for Ground Motion Equations	9-22
Table 9.4-4 Ground Motion Equations and Weights Used in USGS 2008 National Hazard Map for CEUS	9-23
Table 9.4-5 Minimum COV _{MH} Values Observed in Seismic Hazard	9-23
Table A-1 CEUS SSC GIS Database	A-7
Table B-1 Earthquake Catalog.....	B-6
Table B-2 Moment Magnitude Data	B-312
Table B-3 Approximate Moment Magnitude Data	B-324
Table C-5.4 Data Evaluation Future Earthquake Characteristics	C-3
Table C-6.1.1 Data Evaluation Charlevoix RLME	C-9
Table C-6.1.2 Data Evaluation Charleston RLME	C-14
Table C-6.1.3 Data Evaluation Cheraw Fault RLME	C-30

Table C-6.1.4 Data Evaluation Oklahoma Aulacogen RLME	C-36
Table C-6.1.5 Data Evaluation Reelfoot Rift–New Madrid Fault System RLMEs	C-42
Table C-6.1.6 Data Evaluation Reelfoot Rift–Eastern Margin Fault(s) RLMEs.....	C-51
Table C-6.1.7 Data Evaluation Reelfoot Rift–Marianna RLME	C-62
Table C-6.1.8 Data Evaluation Reelfoot Rift–Commerce Fault Zone RLME	C-67
Table C-6.1.9 Data Evaluation Wabash Valley RLME	C-75
Table C-7.3.1 Data Evaluation St. Lawrence Rift Zone	C-83
Table C-7.3.2 Data Evaluation Great Meteor Hotspot Zone	C-92
Table C-7.3.3 Data Evaluation Northern Appalachian Zone.....	C-99
Table C-7.3.4 Data Evaluation Paleozoic Extended Crust Zone	C-105
Table C-7.3.5 Data Evaluation Illinois Basin-Extended Basement Zone	C-112
Table C-7.3.6 Data Evaluation Reelfoot Rift Zone.....	C-124
Tables C-7.3.7/7.3.8 Data Evaluation Extended Continental Crust—Atlantic.....	C-131
Tables C-7.3.9/7.3.10 Data Evaluation Extended Continental Crust–Gulf Coast	C-138
Table C-7.3.12 Data Evaluation Midcontinent-Craton Zone	C-146
Table D-5.4 Data Summary Future Earthquake Characteristics.....	D-3
Table D-6.1.1 Data Summary Charlevoix RLME	D-10
Table D-6.1.2 Data Summary Charleston RLME.....	D-17
Table D-6.1.3 Data Summary Cheraw Fault RLME	D-35
Table D-6.1.4 Data Summary Oklahoma Aulacogen RLME.....	D-38
Table D-6.1.5 Data Summary Reelfoot Rift–New Madrid Seismic Zone (NMSZ) Region.....	D-44
Table D-6.1.9 Data Summary Wabash Valley RLME	D-92
Table D-7.3.1 Data Summary St. Lawrence Rift Zone (SLR)	D-121
Table D-7.3.2 Data Summary Great Meteor Hotspot Zone (GMH).....	D-141
Table D-7.3.3 Data Summary Northern Appalachian Zone (NAP)	D-151
Table D-7.3.4 Data Summary Paleozoic Extended Crust Zone.....	D-163
Table D-7.3.7 Data Summary Extended Continental Crust Zone–Atlantic Margin (ECC-AM).....	D-191
Table D-7.3.9 Data Summary Extended Continental Crust Zone–Gulf Coast (ECC-GC).....	D-225
Table D-7.3.12 Data Summary Midcontinent-Craton Zone (MidC)	D-240
Table E-1.2-1. Summary of Information on Liquefaction Features in Regional Data Sets.....	E-5
Table E-1.2-2 Summary of Type and Prevalence of Paleoliquefaction Features	E-7
Table E-2.1.3. Summary of Dating Techniques Used in Paleoliquefaction Studies.....	E-30
Table E-2.2. Uncertainties Related to Interpretation of Paleoearthquake Parameters	E-36
Table 1: Key Questions and Topics That Workshop 2 Presenters Were Asked to Address	F-35
Table H-3-1 Weighted Alternative Seismogenic Crustal Thickness Values for Mmax Zones	H-20
Table H-3-2 Aleatory Distributions for Characterization of Future Earthquake Ruptures for Mmax Zones	H-20

Table H-3-3 Maximum Magnitude Distributions for Mmax Distributed Seismicity Sources	H-20
Table H-4-1 Seismotectonic Source Zones	H-21
Table H-4-2 Weighted Alternative Seismogenic Crustal Thickness Values for Seismotectonic Zones.....	H-21
Table H-4-3 Aleatory Distributions for Characterization of Future Earthquake Ruptures for Seismotectonic Zones.....	H-22
Table H-4-4 Maximum Magnitude Distributions for Seismotectonic Distributed Seismicity Sources	H-24
Table H-5.1-1 Charlevoix RLME Magnitude Distribution	H-25
Table H-5.1-2 Annual Frequencies for Charlevoix RLME Events Data Set 1: 1870 and 1663	H-25
Table H-5.1-3 Annual Frequencies for Charlevoix RLME Events Data Set 2: 3 Earthquakes in 6–7 kyr BP.....	H-25
Table H-5.1-4 Annual Frequencies for Charlevoix RLME Events Data Set 3: 4 Earthquakes in 9.5–10.2 kyr BP.....	H-26
Table H-5.2-1 Charleston RLME Magnitude Distribution.....	H-26
Table H-5.2-2 Annual Frequencies for Charleston RLME Events Poisson Model, 2,000- Year Time Period Earthquakes 1886, A, B, and C.....	H-26
Table H-5.2-3 Annual Frequencies for Charleston RLME Events Poisson Model, 5,500- Year Time Period Earthquakes 1886, A, B, and C.....	H-27
Table H-5.2-4 Annual Frequencies for Charleston RLME Events Poisson Model, 5,500- Year Time Period Earthquakes 1886, A, B, C, and D	H-27
Table H-5.2-5 Annual Frequencies for Charleston RLME Events Poisson Model, 5,500- Year Time Period Earthquakes 1886, A, B, C, and E	H-27
Table H-5.2-6 Annual Frequencies for Charleston RLME Events Poisson Model, 5,500- Year Time Period Earthquakes 1886, A, B, C, D, and E.....	H-28
Table H-5.2-7 Annual Frequencies for Charleston RLME Events BPT Renewal Model, α = 0.3, 2,000-Year Time Period Earthquakes 1886, A, B, and C	H-28
Table H-5.2-8 Annual Frequencies for Charleston RLME Events BPT Renewal Model, α = 0.5, 2,000-Year Time Period Earthquakes 1886, A, B, and C	H-28
Table H-5.2-9 Annual Frequencies for Charleston RLME Events BPT Renewal Model, α = 0.7, 2,000-Year Time Period Earthquakes 1886, A, B, and C	H-29
Table H-5.2-10 Annual Frequencies for Charleston RLME Events BPT Renewal Model, α = 0.3, 5,500-Year Time Period Earthquakes 1886, A, B, and C	H-29
Table H-5.2-11 Annual Frequencies for Charleston RLME Events BPT Renewal Model, α = 0.5, 5,500-Year Time Period Earthquakes 1886, A, B, and C	H-29
Table H-5.2-12 Annual Frequencies for Charleston RLME Events BPT Renewal Model, α = 0.7, 5,500-Year Time Period Earthquakes 1886, A, B, and C	H-30
Table H-5.2-13 Annual Frequencies for Charleston RLME Events BPT Renewal Model, α = 0.3, 5,500-Year Time Period Earthquakes 1886, A, B, C, and D.....	H-30
Table H-5.2-14 Annual Frequencies for Charleston RLME Events BPT Renewal Model, α = 0.5, 5,500-Year Time Period Earthquakes 1886, A, B, C, and D.....	H-30

Table H-5.2-15 Annual Frequencies for Charleston RLME Events BPT Renewal Model, α = 0.7, 5,500-Year Time Period Earthquakes 1886, A, B, C, and D	H-31
Table H-5.2-16 Annual Frequencies for Charleston RLME Events BPT Renewal Model, α = 0.3, 5,500-Year Time Period Earthquakes 1886, A, B, C, and E	H-31
Table H-5.2-17 Annual Frequencies for Charleston RLME Events BPT Renewal Model, α = 0.5, 5,500-Year Time Period Earthquakes 1886, A, B, C, and E	H-31
Table H-5.2-18 Annual Frequencies for Charleston RLME Events BPT Renewal Model, α = 0.7, 5,500-Year Time Period Earthquakes 1886, A, B, C, and E	H-32
Table H-5.2-19 Annual Frequencies for Charleston RLME Events BPT Renewal Model, α = 0.3, 5,500-Year Time Period Earthquakes 1886, A, B, C, D, and E	H-32
Table H-5.2-20 Annual Frequencies for Charleston RLME Events BPT Renewal Model, α = 0.5, 5,500-Year Time Period Earthquakes 1886, A, B, C, D, and E	H-32
Table H-5.2-21 Annual Frequencies for Charleston RLME Events BPT Renewal Model, α = 0.7, 5,500-Year Time Period Earthquakes 1886, A, B, C, D, and E	H-33
Table H-5.3-1 Cheraw RLME Magnitude Distribution	H-33
Table H-5.3-2 Annual Frequencies for Cheraw RLME Events In-Cluster Case, Data Set: 2 Earthquakes in 20–25 kyr	H-33
Table H-5.3-3 Annual Frequencies for Cheraw RLME Events In-Cluster Case, Data Set: 3 Earthquakes in 20–25 kyr	H-34
Table H-5.3-4 Slip Rates for Cheraw Fault In-Cluster Case, Data Set: 3.2–4.1 m in 20–25 kyr	H-34
Table H-5.3-5 Annual Frequencies for Cheraw RLME Events Out-of-Cluster Case, Time Between Clusters	H-34
Table H-5.3-6 Slip Rates for Cheraw Fault Out-of-Cluster Case, Data Set: 7–8 m in 0.4–2.0 myr	H-35
Table H-5.4-1 Meers RLME Magnitude Distribution	H-35
Table H-5.4-2 Annual Frequencies for Meers RLME Events In-Cluster Case	H-35
Table H-5.4-3 Annual Frequencies for Meers RLME Events Out-of-Cluster Case	H-36
Table H-5.5-1 NMFS RLME Magnitude Distribution	H-36
Table H-5.5-2 Annual Frequencies for NMFS RLME Events In-Cluster Case, Poisson Model	H-36
Table H-5.5-3 Annual Frequencies for NMFS RLME Events In-Cluster Case, BPT Model, α = 0.3	H-37
Table H-5.5-4 Annual Frequencies for NMFS RLME Events In-Cluster Case, BPT Model, α = 0.5	H-37
Table H-5.5-5 Annual Frequencies for NMFS RLME Events In-Cluster Case, BPT Model, α = 0.7	H-37
Table H-5.5-6 Annual Frequencies for NMFS RLME Events Out-of-Cluster Case, Poisson Model	H-38
Table H-5.6-1 ERM-S RLME Magnitude Distribution	H-38
Table H-5.6-2 ERM-N RLME Magnitude Distribution	H-38
Table H-5.6-3 Annual Frequencies for ERM-S RLME Events Data Set: 2 Earthquakes in 17.7–21.7 kyr	H-39

Table H-5.6-4 Annual Frequencies for ERM-S RLME Events Data Set: 3 Earthquakes in 17.7–21.7 kyr	H-39
Table H-5.6-5 Annual Frequencies for ERM-S RLME Events Data Set: 4 Earthquakes in 17.7–21.7 kyr	H-39
Table H-5.6-6 Annual Frequencies for ERM-N RLME Events Data Set: 1 Earthquake in 12–35 kyr	H-40
Table H-5.6-7 Annual Frequencies for ERM-N RLME Events Data Set: 2 Earthquakes in 12–35 kyr	H-40
Table H-5.7-1 Marianna RLME Magnitude Distribution	H-40
Table H-5.7-2 Annual Frequencies for Marianna RLME Events Data Set: 3 Earthquakes in 9.6–10.2 kyr.....	H-41
Table H-5.7-3 Annual Frequencies for Marianna RLME Events Data Set: 4 Earthquakes in 9.6–10.2 kyr.....	H-41
Table H-5.8-1 Commerce RLME Magnitude Distribution.....	H-41
Table H-5.8-2 Annual Frequencies for Commerce RLME Events Data Set: 2 Earthquakes in 18.9–23.6 kyr	H-42
Table H-5.8-3 Annual Frequencies for Commerce RLME Events Data Set: 3 Earthquakes in 18.9–23.6 kyr	H-42
Table H-5.9-1 Wabash RLME Magnitude Distribution	H-42
Table H-5.9-2 Annual Frequencies for Wabash RLME Events Data Set: 2 Earthquakes in 11–13 kyr.....	H-43
PPRP Comment Response Table	(Appendix I)
Table K-1 SCR Earthquake Catalog	K-5
Table K-2 SCR Domains Updated from Johnston et al. (1994)	K-34

EXECUTIVE SUMMARY

The Central and Eastern United States Seismic Source Characterization for Nuclear Facilities (CEUS SSC) Project was conducted over the period from April 2008 to December 2011 to provide a regional seismic source model for use in probabilistic seismic hazard analyses (PSHAs) for nuclear facilities. The study replaces previous regional seismic source models conducted for this purpose, including the Electric Power Research Institute–Seismicity Owners Group (EPRI-SOG) model (EPRI, 1988, 1989) and the Lawrence Livermore National Laboratory model (Bernreuter et al., 1989). Unlike the previous studies, the CEUS SSC Project was sponsored by multiple stakeholders—namely, the EPRI Advanced Nuclear Technology Program, the Office of Nuclear Energy and the Office of the Chief of Nuclear Safety of the U.S. Department of Energy (DOE), and the Office of Nuclear Regulatory Research of the Nuclear Regulatory Commission (NRC). The study was conducted using Senior Seismic Hazard Analysis Committee (SSHAC) Study Level 3 methodology to provide high levels of confidence that the data, models, and methods of the larger technical community have been considered and the center, body, and range of technically defensible interpretations have been included.

The regional seismic source characterization (SSC) model defined by this study can be used for site-specific PSHAs, provided that appropriate site-specific assessments are conducted as required by current regulations and regulatory guidance for the nuclear facility of interest. This model has been designed to be compatible with current and anticipated ground-motion characterization (GMC) models. The current recommended ground-motion models for use at nuclear facilities are those developed by EPRI (2004, 2006a, 2006b). The ongoing Next Generation Attenuation–East (NGA-East) project being supported by the NRC, DOE, and EPRI will provide ground-motion models that are appropriate for use with the CEUS SSC model. The methodology for a SSHAC Level 3 project as applied to the CEUS SSC Project is explained in the SSHAC report (Budnitz et al., 1997), which was written to discuss the evolution of expert assessment methodologies conducted during the previous three decades for purposes of probabilistic risk analyses. The methodological guidance provided in the SSHAC report was intended to build on the lessons learned from those previous studies and, specifically, to arrive at processes that would make it possible to avoid the issues encountered by the previous studies (NRC, 2011).

The SSHAC assessment process, which differs only slightly for Level 3 and 4 studies, is a technical process accepted in the NRC’s seismic regulatory guidance (Regulatory Guide 1.208) for ensuring that uncertainties in data and scientific knowledge have been properly represented in seismic design ground motions consistent with the requirements of the seismic regulation 10 CFR Part 100.23 (“Geologic and Seismic Siting Criteria”). Therefore, the goal of the SSHAC assessment process is the proper and complete representation of knowledge and uncertainties in the SSC and GMC inputs to the PSHA (or similar hazard analysis). As discussed extensively in

the SSHAC report (Budnitz et al., 1997) and affirmed in NRC (2011), a SSHAC assessment process consists of two important sequential activities, *evaluation* and *integration*. For a Level 3 assessment, these activities are conducted by the Technical Integration (TI) Team under the leadership of the TI Lead. As described in NRC (2011),

The fundamental goal of a SSHAC process is to carry out properly and document completely the activities of evaluation and integration, defined as:

Evaluation: The consideration of the complete set of data, models, and methods proposed by the larger technical community that are relevant to the hazard analysis.

Integration: Representing the center, body, and range of technically defensible interpretations in light of the evaluation process (i.e., informed by the assessment of existing data, models, and methods).

Each of the assessment and model-building activities of the CEUS SSC Project is associated with the evaluation and integration steps in a SSHAC Level 3 process. Consistent with the requirements of a SSHAC process, the specific roles and responsibilities of all project participants were defined in the Project Plan, and adherence to those roles was the responsibility of the TI Lead and the Project Manager. The technical assessments are made by the TI Team, who carry the principal responsibility of evaluation and integration, under the technical leadership of the TI Lead. The Database Manager and other technical support individuals assist in the development of work products. Resource and proponent experts participate by presenting their data, models, and interpretations at workshops and through technical interchange with the TI Team throughout the project. The Participatory Peer Review Panel (PPRP) is responsible for a continuous review of both the SSHAC process being followed and the technical assessments being made. The project management structure is headed by the Project Manager, who serves as the liaison with the sponsors and the PPRP and manages the activities of all participants. The SSHAC Level 3 assessment process and implementation is discussed in depth in Chapter 2 of this report.

Each of the methodology steps in the SSHAC guidelines (Budnitz, 1997) was addressed adequately during the CEUS SSC Project. Furthermore, the project developed a number of enhancements to the process steps for conducting a SSHAC Study Level 3 project. For example, the SSHAC guidelines call for process steps that include developing a preliminary assessment model, calculating hazard using that model in order to identify the key issues, and finalizing the model in light of the feedback provided from the hazard calculations and sensitivity analyses. Because of the regional nature of the project and the multitude of assessments required, four rounds of model-building and three rounds of feedback were conducted. These activities ensured that all significant issues and uncertainties were identified and that the appropriate effort was devoted to the issues of most significance to the hazard results. A comparison of the activities conducted during the CEUS SSC Project with those recommended in the SSHAC guidelines themselves (Section 2.6) led to the conclusion that the current standards of practice have been met for a SSHAC Study Level 3 process—both those that are documented in the SSHAC report and those that resulted from precedents set by projects conducted since the SSHAC report was issued.

The catalog of past earthquakes that have occurred in a region is an important source of information for the quantification of future seismic hazards. This is particularly true in stable continental regions (SCRs) such as the CEUS where the causative mechanisms and structures for the occurrence of damaging earthquakes are generally poorly understood, and the rates of crustal deformation are low such that surface and near-surface indications of stresses in the crust and the buildup and release of crustal strains are difficult to quantify. Because the earthquake catalog is used in the characterization of the occurrence of future earthquakes in the CEUS, developing an updated earthquake catalog for the study region was an important focus of the CEUS SSC Project. The specific goals for earthquake catalog development and methods used to attain those goals are given in Chapter 3.

The earthquake catalog development consists of four main steps: catalog compilation, assessment of a uniform size measure to apply to each earthquake, identification of dependent earthquakes (catalog declustering), and assessment of the completeness of the catalog as a function of location, time, and earthquake size. An important part of the catalog development process was review by seismologists with extensive knowledge and experience in catalog compilation. The result is an earthquake catalog covering the entire study region for the period from 1568 through the end of 2008. Earthquake size is defined in terms of the moment magnitude scale (Hanks and Kanamori, 1979), consistent with the magnitude scale used in modern ground-motion prediction equations (GMPEs) for CEUS earthquakes. A significant contribution of the CEUS SSC Project is the work conducted to develop an updated and consistent set of conversion relationships between various earthquake size measures (instrumental magnitudes and intensity) and moment magnitude.

The conceptual SSC framework described in Chapter 4 was developed early in the CEUS SSC Project in order to provide a consistent approach and philosophy to SSC by the TI Team. This framework provides the basic underpinnings of the SSC model developed for the project, and it led to the basic structure and elements of the master logic tree developed for the SSC model. In considering the purpose of the CEUS SSC Project, the TI Team identified three attributes that are needed for a conceptual SSC framework:

1. A systematic, documented approach to treating alternatives using logic trees, including alternative conceptual models for future spatial distributions of seismicity (e.g., stationarity); alternative methods for expressing the future temporal distribution of seismicity (e.g., renewal models, Poisson models); and alternative data sets for characterizing seismic sources (e.g., paleoseismic data, historical seismicity data).
2. A systematic approach to identifying applicable data for the source characterization, evaluating the usefulness of the data, and documenting the consideration given to the data by the TI Team.
3. A methodology for identifying seismic sources based on defensible criteria for defining a seismic source, incorporating the lessons learned in SSC over the past two decades, and identifying the range of approaches and models that can be shown to be significant to hazard.

Each of these needs was addressed by the methodology used in the project. For example, the need for a systematic approach to identifying and evaluating the data and information that underlie the source characterization assessments was met by the development of Data Summary

and Data Evaluation tables. These tables were developed for each seismic source to document the information available at the time of the CEUS SSC assessments (the Data Summary tables) and the way those data were used in the characterization process (the Data Evaluation tables). Given the evolution of approaches to identifying seismic sources, it is appropriate to provide a set of criteria and the logic for their application in the CEUS SSC Project. In the project, unique seismic sources are defined to account for distinct differences in the following criteria:

- Earthquake recurrence rate
- Maximum earthquake magnitude (M_{max})
- Expected future earthquake characteristics (e.g., style of faulting, rupture orientation, depth distribution)
- Probability of activity of tectonic feature(s)

Rather than treat these criteria as operating simultaneously or without priority, the CEUS SSC methodology works through them sequentially. Further, because each criterion adds complexity to the seismic source model, it is applied only if its application would lead to hazard-significant changes in the model. In this way, the model becomes only as complex as required by the available data and information.

The CEUS SSC master logic tree is tied to the conceptual SSC framework that establishes the context for the entire seismic source model. The master logic tree depicts the alternative interpretations and conceptual models that represent the range of defensible interpretations, and the relative weights assessed for the alternatives. By laying out the alternatives initially, the subsequent detailed source evaluations were conducted within a framework that ensures consistency across the sources. Important elements of the master logic tree are as follows:

- Representation of the sources defined based on paleoseismic evidence for the occurrence of repeated large-magnitude earthquakes (RLMEs, defined as two or more earthquakes with $M \geq 6.5$).
- Alternatives to the spatial distribution of earthquakes based on differences in maximum magnitudes (M_{max} zones approach).
- Representation of uncertainty in spatial stationarity of observed seismicity based on smoothing of recurrence parameters.
- Representation of possible differences in future earthquake characteristics (e.g., style, seismogenic thickness, and orientation of ruptures), which lead to definition of seismotectonic zones in the logic tree (seismotectonic zones approach).

The methodologies used by the project to make the SSC assessments are discussed in Chapter 5. The heart of any SSC model for PSHA is a description of the future spatial and temporal distribution of earthquakes. Continued analysis of the historical seismicity record and network monitoring by regional and local seismic networks has led to acceptance within the community that the general spatial patterns of observed small- to moderate-magnitude earthquakes provide predictive information about the spatial distribution of future large-magnitude earthquakes. The analyses leading to this conclusion have focused on whether the observed patterns of earthquakes

have varied through time; therefore, in effect, this is an assessment of uncertainty in whether small- to moderate-magnitude earthquakes have been relatively stationary through time. However, the available data on larger-magnitude earthquakes and their relationship to the spatial distribution of smaller earthquakes based on the observed record are quite limited. These data are not sufficient to allow confidence in the predictions generated by empirical spatial models. For this reason, geologic and geophysical data are needed to specify the locations of future earthquakes in addition to the observed patterns of seismicity.

Detailed studies in the vicinity of large historical and instrumental earthquakes, and liquefaction phenomena associated with them, coupled with field and laboratory studies of geotechnical properties, are leading to a stronger technical basis for (1) placing limits on the locations of paleoearthquakes interpreted by the distribution of liquefaction phenomena and (2) defining their magnitudes. In some cases, the paleoseismic evidence for RLMEs is compelling, and the TI Team has included the RLME source in the SSC model. The locations of RLME sources notwithstanding, the spatial distribution of distributed seismicity sources has advanced in PSHA largely because of the assumption of spatial stationarity, and the SSC and hazard community uses approaches to “smooth” observed seismicity to provide a map that expresses the future spatial pattern of recurrence rates. The CEUS SSC model is based largely on the assumption, typical in PSHA studies, that spatial stationarity of seismicity is expected to persist for a period of approximately 50 years.

Estimating M_{max} in SCRs such as the CEUS is highly uncertain despite considerable interest and effort by the scientific community over the past few decades. M_{max} is defined as the upper truncation point of the earthquake recurrence curve for individual seismic sources, and the typically broad distribution of M_{max} for any given source reflects considerable epistemic uncertainty. Because the maximum magnitude for any given seismic source in the CEUS occurs rarely relative to the period of observation, the use of the historical seismicity record provides important but limited constraints on the magnitude of the maximum event. Because of the independent constraints on earthquake size, those limited constraints are used to estimate the magnitudes of RLME. For distributed seismicity source zones, two approaches are used to assess M_{max} : the Bayesian approach and the Kijko approach. In the Bayesian procedure (Johnston et al., 1994), the prior distribution is based on the magnitudes of earthquakes that occurred worldwide within tectonically analogous regions. As part of the CEUS SSC Project, the TI Team pursued the refinement and application of the Bayesian M_{max} approach because it provides a quantitative and repeatable process for assessing M_{max} .

The TI Team also explored alternative approaches for the assessment of M_{max} that provide quantitative and repeatable results, and the team identified the approach developed by Kijko (2004) as a viable alternative. While the Kijko approach requires fewer assumptions than the Bayesian approach in that it uses only the observed earthquake statistics for the source, this is offset by the need for a relatively larger data sample in order to get meaningful results. Both approaches have the positive attribute that they are repeatable given the same data and they can be readily updated given new information. The relative weighting of the two approaches for inclusion in the logic tree is source-specific, a function of the numbers of earthquakes that are present within the source upon which to base the M_{max} assessment: sources with fewer earthquakes are assessed to have little or no weight for the Kijko approach, while those with

larger numbers of events are assessed higher weight for the Kijko approach. In all cases, because of the stability of the Bayesian approach and the preference for “analogue” approaches within the larger technical community, the Bayesian approach is assessed higher weight than the Kijko approach for all sources.

A major effort was devoted to updating the global set of SCR earthquakes and to assessing statistically significant attributes of those earthquakes following the approach given in Johnston et al. (1994). In doing so, it was found that the only significant attribute defining the prior distribution is the presence or absence of Mesozoic-or-younger extension. The uncertainty in this assessment is reflected in the use of two alternative priors: one that takes into account the presence or absence of crustal domains having this attribute, and another that combines the entire CEUS region as a single SCR crustal domain with a single prior distribution. The use of the Bayesian—and Kijko—approach requires a definition of the largest observed magnitude within each source, and this assessment, along with the associated uncertainty, was incorporated into the Mmax distributions for each seismic source. Consideration of global analogues led to the assessment of an upper truncation to all Mmax distributions at $8\frac{1}{4}$ and a lower truncation at $5\frac{1}{2}$. The broad distributions of Mmax for the various seismic source zones reflect the current epistemic uncertainty in the largest earthquake magnitude within each seismic source.

The CEUS SSC model is based to a large extent on an assessment that spatial stationarity of seismicity will persist for time periods of interest for PSHA (approximately the next 50 years). Stationarity in this sense does not mean that future locations and magnitudes of earthquakes will occur exactly where they have occurred in the historical and instrumental record. Rather, the degree of spatial stationarity varies as a function of the type of data available to define the seismic source. RLME sources are based largely on paleoseismic evidence for repeated large-magnitude ($M \geq 6.5$) earthquakes that occur in approximately the same location over periods of a few thousand years. On the other hand, patterns of seismicity away from the RLME sources within the Mmax and seismotectonic zones are defined from generally small- to moderate-magnitude earthquakes that have occurred during a relatively short (i.e., relative to the repeat times of large events) historical and instrumental record. Thus, the locations of future events are not as tightly constrained by the locations of past events as for RLME sources. The spatial smoothing operation is based on calculations of earthquake recurrence within one-quarter-degree or half-degree cells, with allowance for “communication” between the cells. Both *a*- and *b*-values are allowed to vary, but the degree of variation has been optimized such that *b*-values vary little across the study region.

The approach used to smooth recurrence parameters is a refinement of the penalized-likelihood approach used in EPRI-SOG (EPRI, 1988), but it is designed to include a number of elements that make the formulation more robust, realistic, and flexible. These elements include the reformulation in terms of magnitude bins, the introduction of magnitude-dependent weights, catalog incompleteness, the effect of Mmax, spatial variation of parameters within the source zone, and the prior distributions of *b*. A key assessment made by the TI Team was the weight assigned to various magnitude bins in the assessment of smoothing parameters (Cases A, B, and E). This assessment represents the uncertainty in the interpretation that smaller magnitudes define the future locations and variation in recurrence parameters. Appropriately, the penalized-likelihood approach results in higher spatial variation (less smoothing) when the low-magnitude

bins are included with high weight, and much less variation (higher smoothing) in the case where the lower-magnitude bins are given low or zero weight. The variation resulting from the final set of weights reflects the TI Team's assessment of the epistemic uncertainty in the spatial variation of recurrence parameters throughout the SSC model.

The earthquake recurrence models for the RLME sources are somewhat simpler than those for distributed seismicity sources because the magnitude range for individual RLMEs is relatively narrow and their spatial distribution is limited geographically such that spatial variability is not a concern. This limits the problem to one of estimating the occurrence rate in time of a point process. The data that are used to assess the occurrence rates are derived primarily from paleoseismic studies and consist of two types: data that provide estimated ages of the paleoearthquakes such that the times between earthquakes can be estimated, and data that provide an estimate of the number of earthquakes that have occurred after the age of a particular stratigraphic horizon. These data are used to derive estimates of the RLME occurrence rates and their uncertainty.

The estimation of the RLME occurrence rates is dependent on the probability model assumed for the temporal occurrence of these earthquakes. The standard model applied for most RLME sources in this study is the Poisson model, in which the probability of occurrence of an RLME in a specified time period is completely characterized by a single parameter, λ , the rate of RLME occurrence. The Poisson process is “memoryless”—that is, the probability of occurrence in the next time interval is independent of when the most recent earthquake occurred, and the time between earthquakes is exponentially distributed with a standard deviation equal to the mean time between earthquakes. For two RLME sources (Reelfoot Rift–New Madrid fault system and the Charleston source), the data are sufficient to suggest that the occurrence of RLMEs is more periodic in nature (the standard deviation is less than the mean time between earthquakes). For these RLME sources a simple renewal model can also be used to assess the probability of earthquake occurrence. In making an estimate of the probability of occurrence in the future, this model takes into account the time that has elapsed since the most recent RLME occurrence.

The CEUS SSC model has been developed for use in future PSHAs. To make this future use possible, the SSC model must be combined with a GMC model. At present, the GMPEs in use for SCRs such as the CEUS include limited information regarding the characteristics of future earthquakes. In anticipation of the possible future development of GMPEs for the CEUS that will make it possible to incorporate similar types of information, a number of characteristics of future earthquakes in the CEUS are assessed. In addition to characteristics that might be important for ground motion assessments, there are also assessed characteristics that are potentially important to the modeling conducted for hazard analysis. Future earthquake characteristics assessed include the tectonic stress regime, sense of slip/style of faulting, strike and dip of ruptures, seismogenic crustal thickness, fault rupture area versus magnitude relationship, rupture length-to-width aspect ratio, and relationship of ruptures to source boundaries.

Chapters 6 and 7 include discussions of the seismic sources that are defined by the Mmax zones and the seismotectonic zones branches of the master logic tree. Because of convincing evidence for their existence, both approaches include RLME sources. The rarity of repeated earthquakes relative to the period of historical observation means that evidence for repeated events comes

largely from the paleoseismic record. By identifying the RLMEs and including them in the SSC model, there is no implication that the set of RLMEs included is in fact the total set of RLMEs that might exist throughout the study region. This is because the presently available studies that locate and characterize the RLMEs have been concentrated in certain locations and are not systematic across the entire study region. Therefore, the evidence for the existence of the RLMEs is included in the model where it exists, but the remaining parts of the study region are also assessed to have significant earthquake potential, which is evidenced by the inclusion of moderate-to-large magnitudes in the Mmax distributions for every Mmax zone or seismotectonic zone.

In Chapter 6, each RLME source is described in detail by the following factors: (1) evidence for temporal clustering, (2) geometry and style of faulting, (3) RLME magnitude, and (4) RLME recurrence. The descriptions document how the data have been evaluated and assessed to arrive at the various elements of the final SSC model, including all expressions of uncertainty. The Data Summary and Data Evaluation tables (Appendices C and D) complement the discussions in the text, documenting all the data that were considered in the course of data evaluation and integration process for each particular seismic source.

Alternative models for the distributed seismicity zones that serve as background zones to the RLME sources are either Mmax zones or seismotectonic zones. The Mmax zones are described in Chapter 6 and are defined according to constraints on the prior distributions for the Bayesian approach to estimating Mmax. The seismotectonic zones are described in Chapter 7 and are identified based on potential differences in Mmax as well as future earthquake characteristics. Each seismotectonic zone in the CEUS SSC model is described according to the following attributes: (1) background information from various data sets; (2) bases for defining the seismotectonic zone; (3) basis for the source geometry; (4) basis for the zone Mmax (e.g., largest observed earthquake); and (5) future earthquake characteristics. Uncertainties in the seismotectonic zone characteristics are described and are represented in the logic trees developed for each source.

For purposes of demonstrating the CEUS SSC model, seismic hazard calculations were conducted at seven demonstration sites throughout the study region, as described in Chapter 8. The site locations were selected to span a range of seismic source types and levels of seismicity. The results from the seismic hazard calculations are intended for scientific use to demonstrate the model, and they should not be used for engineering design. Mean hazard results are given for a range of spectral frequencies (PGA, 10 Hz, and 1 Hz) and for a range of site conditions. All calculations were made using the EPRI (2004, 2006) ground-motion models such that results could be compared to understand the SSC effects alone. Sensitivity analyses were conducted to provide insight into the dominant seismic sources and the important characteristics of the dominant seismic source at each site. The calculated mean hazard results are compared with the results using the SSC model from the 2008 U.S. Geological Survey national seismic hazard maps and the SSC model from the Combined Operating License applications for new nuclear power reactors. The hazard results using the CEUS SSC model given in Chapter 8 are reasonable and readily understood relative to the results from other studies, and sensitivities of the calculated hazard results can be readily explained by different aspects of the new model. The TI Team concludes that the SSC model provides reasonable and explainable calculated seismic hazard

results, and the most important aspects of the SSC model to the calculated hazard (e.g., recurrence rates of RLME sources, recurrence parameters for distributed seismicity sources, M_{max}) and their uncertainties have all been appropriately addressed.

Presumably, the GMC model input to the PSHA calculations will be replaced in the future by the results of the ongoing NGA-East project. The calculated hazard at the demonstration sites in Chapter 8 comes from the regional CEUS SSC model and does not include any local refinements that might be necessary to account for local seismic sources. Depending on the regulatory guidance that is applicable for the facility of interest, additional site-specific studies may be required to provide local refinements to the model.

To assist future users of the CEUS SSC model, Chapter 9 presents a discussion on the use of the model for PSHA. The basic elements of the model necessary for hazard calculations are given in the Hazard Input Document (HID). This document provides all necessary parameter values and probability distributions for use in a modern PSHA computer code. The HID does not, however, provide any justification for the values, since that information is given in the text of this report.

Chapter 9 also describes several simplifications to seismic sources that can be made to increase efficiency in seismic hazard calculations. These simplifications are recommended on the basis of sensitivity studies of alternative hazard curves that represent a range of assumptions on a parameter's value. Sensitivities are presented using the test sites in this study. For applications of the seismic sources from this study, similar sensitivity studies should be conducted for the particular site of interest to confirm these results and to identify additional simplifications that might be appropriate. For the seismic sources presented, only those parameters that can be simplified are discussed and presented graphically. The sensitivity studies consisted of determining the sensitivity of hazard to logic tree branches for each node of the logic tree describing that source. The purpose was to determine which nodes of the logic tree could be collapsed to a single branch in order to achieve more efficient hazard calculations without compromising the accuracy of overall hazard results.

Finally, this report provides a discussion of the level of precision that is associated with seismic hazard estimates in the CEUS. This discussion addresses how seismic hazard estimates might change if the analysis were repeated by independent experts having access to the same basic information (geology, tectonics, seismicity, ground-motion equations, site characterization). It also addresses how to determine whether the difference in hazard would be significant if this basic information were to change and that change resulted in a difference in the assessed seismic hazard. This analysis was performed knowing that future data and models will continue to be developed and that a mechanism for evaluating the significance of that information is needed. Based on the precision model evaluated, if an alternative assumption or parameter is used in a seismic hazard study, and it potentially changes the calculated hazard (annual frequency of exceedence) by less than 25 percent for ground motions with hazards in the range 10^{-4} to 10^{-6} , that potential change is within the level of precision at which one can calculate seismic hazard. It should be noted, however, that a certain level of precision does not relieve users from performing site-specific studies to identify potential capable seismic sources within the site region and vicinity as well as to identify newer models and data. Also, this level of precision does not relieve users from fixing any errors that are discovered in the CEUS SSC model as it is

Executive Summary

implemented for siting critical facilities. In addition, NRC has not defined a set value for requiring or not requiring siting applicants to revise or update PSHAs.

Included in the report are appendices that summarize key data sets and analyses: the earthquake catalog, the Data Summary and Data Evaluation tables, the paleoliquefaction database, the HID, and documentation important to the SSHAC process. These data and analyses will assist future users of the CEUS SSC model in the implementation of the model for purposes of PSHA. The entire report and database will be provided on a website after the Final Project Report is issued.

The TI Team, Project Manager, and Sponsors determined the approach for quality assurance on the CEUS SSC Project in 2008, taking into account the SSHAC assessment process and national standards. The approach was documented in the CEUS SSC Project Plan dated June 2008 and discussed in more detail in the CEUS SSC Report (Appendix L). Beyond the assurance of quality arising from the external scientific review process, it is the collective, informed judgment of the TI Team (via the process of evaluation and integration) and the concurrence of the PPRP (via the participatory peer review process), as well as adherence to the national standard referred to in Appendix L, that ultimately lead to the assurance of quality in the process followed and in the products that resulted from the SSHAC hazard assessment framework.

October 24, 2011

Cliff Munson
Senior Technical Advisor
Office of New Reactors
U.S. Nuclear Regulatory Commission
Washington, DC 20555

Robert Roche
Project Manager
Office of Nuclear Regulatory Research
U.S. Nuclear Regulatory Commission
Washington, DC 20555

Richard H. Lagdon, Jr.
Chief of Nuclear Safety
Office of the Under Secretary for Nuclear
Security, S-5
U.S. Department of Energy
1000 Independence Avenue SW
Washington, DC 20585

Thomas P. Miller
Senior Technical Advisor
Office of Nuclear Energy, NE-72/GTN
U.S. Department of Energy
1000 Independence Avenue SW
Washington, DC 20585

Jeffrey F. Hamel
Advanced Nuclear Technology Program
Manager
Electric Power Research Institute
3420 Hillview Avenue
Palo Alto, CA 94304

Gentlemen:

Reference: *Central and Eastern United States Seismic Source Characterization for Nuclear Facilities Project: Participatory Peer Review Panel Final Report*

Introduction

This letter constitutes the final report of the PPRP¹ (“the Panel”) for the *Central and Eastern United States Seismic Source Characterization for Nuclear Facilities Project* (the “CEUS SSC Project” or “the Project”). The eight Panel members (Jon P. Ake, Walter J. Arabasz, William J. Hinze, Annie M. Kammerer, Jeffrey K. Kimball, Donald P. Moore, Mark D. Petersen, J. Carl Stepp) participated in the Project in a manner fully consistent with the SSHAC Guidance.² The Panel was actively engaged in all phases and activities of the Project’s implementation, including final development of the Project Plan and planning of the evaluation and integration activities, which are the core of the SSHAC assessment process.

¹ Participatory Peer Review Panel

² Budnitz, R. J., G. Apostolakis, D. M. Boore, L. S. Cluff, K. L. Coppersmith, C. A. Cornell, and P. A. Morris, 1997. *Recommendations for Probabilistic Seismic Hazard Analysis: Guidance on Uncertainty and the Use of Experts* (known as the “Senior Seismic Hazard Analysis Committee Report,” or the “SSHAC Guidance”). NUREG/CR-6372, U. S. Nuclear Regulatory Commission. TIC; 235076. Washington, DC.

The Panel's involvement, described more fully later in this letter, also included review of analyses performed by the Project to support the evaluation and integration processes, review of interim evaluation and integration products, and review of the interim draft project report and the final project report. Additionally, panel members participated in specific analyses as resource experts, and panel members were observers in or participated as resource experts in eight of the eleven Technical Integrator Team (TI Team) working meetings held to implement the integration phase of the assessment process. We want to express our appreciation for the opportunity to participate in the CEUS SSC Project in this way.

In the remainder of this letter we provide our observations and conclusions on key elements of the project implementation process, and we summarize our reviews of the draft and final project reports. As we explain in our comments, assurance that the center, body, and range of the technically-defensible interpretations ("CBR of the TDI")³ have been properly represented in the CEUS SSC Model fundamentally comes from implementing the structure and rigor of the SSHAC Guidance itself. We are aware that the SSHAC Guidance is accepted by the Nuclear Regulatory Commission and the Department of Energy for developing seismic hazard models that provide reasonable assurance, consistent with the seismic safety decision-making practices of these agencies, of compliance with their seismic safety policies and regulatory requirements. For these reasons, we describe aspects of the SSHAC Guidance to provide context for our observations and conclusions.

Project Plan: Conformity to the SSHAC Assessment Process

The SSHAC Guidance recognizes that observed data, available methods, models, and interpretations all contain uncertainties. These uncertainties lead to alternative scientific analyses and interpretations. In other words, experts in the broad technical community do not hold a single interpretation. Accepting this scientific situation, the SSHAC assessment process is designed to engage the scientific community in an orderly assessment of relevant data, methods, models, and interpretations that constitute current scientific knowledge as the basis for development of a seismic hazard model that represents the CBR of the TDI.

The assessment process is carried out by means of two main activities: *evaluation* and *integration*.⁴ In implementation, the evaluation activities are structured to inform the integration activities. The evaluations are carried out by means of workshops in which the TI Team engages proponents of alternative interpretations that represent the range of relevant current community knowledge. Resource experts in the various relevant data sets are also engaged. The workshops have the dual purposes of, first, evaluating the degree to which alternative interpretations are supported by observed data and, second, defining uncertainties in the degree to which the interpretations are defensible, given the observed data. Integration is carried out by individual evaluator experts or evaluator expert teams (Level 4 process) or by a Technical Integrator (TI) Team (Level 3 process) who, informed by the evaluation activities, characterize the range of

³ See Section 2.1 in the CEUS SSC Final Report for discussion of concepts relating to the center, body, and range of the "technically-defensible interpretations" vs. the center, body, and range of the "informed technical community."

⁴ For an excellent discussion of this two-stage process, see *Practical Implementation Guidelines for SSHAC Level 3 and 4 Hazard Studies*, USNRC NUREG-XXXX, Draft for Review, Office of Nuclear Regulatory Research, May 2011.

defensible alternative interpretations in an integrated hazard model and assess the scientific uncertainty distribution. Based on our review of the Project Plan and our subsequent discussions with the Project Team, we concurred that the Plan conformed with the SSHAC Guidance, incorporating lessons learned from fourteen years experience using the Guidance, and that the planned implementation was structured to properly carry out the SSHAC assessment process for development of the CEUS SSC Model.

SSHAC Level 3 Assessment Process

The SSHAC Guidance describes implementation processes for four levels of assessment depending on the scientific complexity of the assessment and the intended use of the assessed hazard model. For an assessment such as the regional SSC model for the Central and Eastern United States, which will be used at many sites for making safety and licensing decisions for nuclear facilities, the SSHAC Guidance recommends using an assessment Level 3 or Level 4.

There are process differences between a Level 3 and Level 4 implementation, but the objective is the same: to obtain from multiple proponent experts information that supports an informed assessment of the range of existent relevant interpretations and associated uncertainties that together represent current community knowledge and to perform an informed assessment of the CBR of the TDI. We understand that within the SSHAC assessment process “technically defensible” means that observed data are sufficient to support evaluation of the interpretation and the corresponding uncertainty.

In a Level 4 assessment process a TI Team facilitates the assessment, identifying and engaging proponent and resource experts, performing supporting analyses, and conducting knowledge evaluation workshops and assessment integration working meetings. Multiple experts or teams of experts perform as evaluators of the range of existent interpretations and as integrators of the hazard model. The individual evaluator experts or evaluator expert teams take ownership of their individual or team assessments. In a Level 3 assessment all of these activities are consolidated under a single TI Team consisting of a TI Lead, multiple evaluator experts representing the scope of required scientific expertise, and experienced data and hazard analysts.

As we noted earlier in this report, assurance that the CBR of the TDI is properly represented in a hazard model comes from rigorously implementing the SSHAC assessment process itself. We note that an important lesson learned from multiple implementations of the SSHAC Guidance over the past fourteen years is that the Level 3 and Level 4 assessment processes provide comparably high assurance that the relevant scientific knowledge and the community uncertainty distribution are properly assessed and represented in the hazard model. The Level 3 assessment is significantly more integrated and cohesive and is more efficient to implement. These considerations led us to endorse use of the Level 3 assessment for implementation of the CEUS SSC Project in our Workshop No. 1 review letter. During the course of the Project we observed that the higher level of cohesiveness inherent in the Level 3 assessment process leads to significantly improved communication, facilitating the experts’ performance of their technical work.

Overall Project Organization

A complex project with multiple sponsors such as the CEUS SSC Project cannot be successful unless it is well organized and energetically managed so that the various participants understand the interconnectedness of their activities and perform their technical work as a cohesive group. In this regard the adopted project management structure allowed the Project Manager to provide integrated overall project leadership, manage the database development activities, and effectively maintain communication with the PPRP and project sponsors while allowing TI Team lead to concentrate on the structural and technical activities of the assessment as the Project unfolded. We conclude that the project organization was effective overall and particularly so with regard to facilitating the TI Team's implementation of the assessment process.

Implementing the SSHAC Level 3 Assessment Process

Irrespective of the level of implementation, evaluation and integration are the main activities of a SSHAC assessment. The evaluation activities aim to identify and evaluate all relevant available data, models, methods, and scientific interpretations as well as uncertainties associated with each of them. The integration activities, informed by the evaluations, aim to represent the CBR of the TDI in a fully integrated SSC model.

Evaluation

Consistent with the SSHAC Guidance the evaluation phase of the CEUS SSC project accomplished a comprehensive evaluation of the data, models, methods, and scientific interpretations existent in the larger technical community that are relevant to the SSC model. In significant part the process was carried out in three structured workshops, each focusing on accomplishing a specific step in the evaluation process.

The first workshop (WS-1) focused on evaluations of relevant geological, geophysical, and seismological datasets (including data quality and uncertainties) and on identification of hazard-significant data and hazard-significant SSC assessment issues. It became clear that a number of issues relating to the earthquake catalog, the paleoliquefaction data set, the potential-field geophysical data, updating procedures for assessing maximum earthquake magnitude, and development of procedures for assessing earthquake recurrence would require focused analyses. These analyses were appropriately carried out within the TI Team working interactively with appropriate resource experts recognized by the larger scientific and technical community.

WS-2 focused on evaluations of the range of alternative scientific interpretations, methods, and models within the larger scientific community and on corresponding uncertainties. WS-3 focused on evaluations of hazard feedback derived at seven representative test locations using a preliminary CEUS SSC model. Specifically, the workshop focused on the identification of the key issues of most significance to completing the SSC model assessment.

Experience has shown that evaluations to gain understanding of the quality of various data sets and uncertainties associated with them are essential for fully informing an SSC assessment. We observed that in WS-1 resource experts for the various data sets did a high-quality job of describing the data sets and giving their perspective about the data quality and associated uncertainties. We conclude that the understanding of data quality and uncertainties gained in WS-1 together with continued interactions between the TI Team and data resource experts

significantly informed the TI Team's evaluations. The TI Team's evaluations of the data quality and uncertainties are well documented in the innovative "Data Summary Tables" and "Data Evaluation Tables" included in the Project Report. Importantly, the TI Team continued to effectively engage data resource experts in productive analyses of potential-field geophysical data, the earthquake catalog, development of the paleoearthquake data set (including an integrated assessment of the paleoliquefaction data in order to extend the earthquake catalog), the development of methods for assessing maximum earthquakes, and the development of earthquake recurrence analyses. All of these focused analyses strongly informed the assessment process. Moreover, documentation of the analyses resulted in stand-alone products of the Project that will serve future users of the CEUS SSC Model.

The compilation and evaluation of potentially relevant methods, models, and alternative scientific interpretations representing the community knowledge and corresponding uncertainties must be considered the core process activity of any SSHAC assessment. This step was largely carried out in WS-2. Success in defining the community knowledge depends on fully engaging proponent experts representing the range of methods, models, and interpretations existent at the time. Full engagement means that the proponent experts completely and clearly describe their interpretations and the data that support them and provide their individual evaluations of corresponding uncertainties. We observed that the actions taken by the Project and TI Team to explain the workshop goals and to guide participants toward meeting those goals was very productive. We conclude that the workshop was highly successful in meeting the stated goals and that it fully met the expectation of the SSHAC Guidance with respect to evaluating the range of alternative scientific interpretations. The discussions during the workshop and between the TI Team and Panel following the workshop evolved the "SSC Framework" concept, which provided transparent criteria that framed the TI Team's systematic identification and assessment of seismic sources throughout the CEUS.

Feedback from hazard calculations and sensitivity analyses is an important step in a SSHAC assessment to understand the importance of elements of the model and inform the final assessments. For development of a regional SSC model to be used for site-specific probabilistic seismic hazard analyses (PSHAs) at many geographically distributed sites, feedback based on the preliminary model is particularly important. Following WS-2 a preliminary SSC model termed "the SSC sensitivity model," was developed and used for hazard sensitivity calculations that were evaluated in WS-3. While the SSC sensitivity model was clearly preliminary, the evaluation of sensitivity results that took place in WS-3 provided important feedback for completing analyses and for supporting the TI Team's development of the preliminary CEUS SSC model. The Panel was able to review the preliminary model and provide feedback in a subsequent project briefing meeting on March 24, 2010.

Together the three workshops provided the TI Team interactions with the appropriate range of resource and proponent experts. These experts were carefully identified to present, discuss, and debate the data, models, and methods that together form the basis for assuring that the CBR of the TDI have been properly represented in the hazard model. Experts representing academia, government, and private industry participated. The TI Team also reached out to a wide range of experts as they developed the database and performed the integration activities to develop the SSC model. The Panel participated throughout this process, and is satisfied that the TI Team fully engaged appropriate experts to accomplish the goals of a SSHAC Guidance.

Integration

Consistent with the SSHAC Guidance, integration is the process of assessing the CBR of the TDI and representing the assessment in the SSC model. Informed by the evaluation process, the integration process includes representation of the range of defensible methods, models, and interpretations of the larger technical community together with new models and methods developed by analyses during the evaluation and integration process.

For the CEUS SSC Project, development of the earthquake catalog, methods for assessing and representing maximum earthquake magnitudes, and methods for earthquake recurrence assessment continued during the integration process. The Panel reviewed all the analyses at various stages of development and provided comments and recommendations. The TI Team performed the integration process by means of eleven working meetings. Members of the Panel participated in most of these working meetings as observers or resource experts. The full Panel participated in the discussions during both feedback meetings and provided formal comments and recommendations following the meetings. We observed that the integration process was thorough and that it acceptably complied with the SSHAC Guidance. Based on our participation and observations we conclude that the integrated CEUS SSC Model appropriately represents the center, body, and range of current methods, models and technically defensible interpretations.

PPRP Engagement

Consistent with the SSHAC Guidance, the Panel was fully engaged in peer-review interactions with the TI Team and the Project Manager of the CEUS SSC Project throughout the entire project period—from development of the Project Plan in early to mid 2008 through production of the Final Project Report in mid to late 2011.⁵ The Panel provided both written and oral peer-review comments on both technical and process aspects at many stages of the Project's evolution. Key PPRP activities, leading up to this final report, have included:

- Review of the Project Plan.
- Formulation of a PPRP implementation plan, specifically for the CEUS SSC Project, to ensure adherence to the general guidance provided by SSHAC and NUREG-1563 for the scope and goals of a PPRP review.
- Involvement in *each* of the three Project workshops, including advising in the planning stage; participating collectively as a review panel during the workshop (and individually as resource experts when requested by the TI Team), providing timely comments on technical and process issues; and submitting a written report of the Panel's observations and recommendations following each workshop.
- Development and implementation of a process, together with the TI Team, to document the resolution of recommendations made in PPRP formal communications.
- Participation as observers (and occasionally as resource experts when requested by the TI Team) in eight of the TI Team's 11 working meetings.
- Peer-review and written comments, including several informal reports, on the TI Team's intermediate work products, particularly early versions of the CEUS SSC Model.

⁵ See CEUS SSC Final Report: Section 2.5, Table 2.2-1, and Appendix I

- Direct interaction with the TI Team and Project Manager in more than 20 teleconferences and four face-to-face briefings—in addition to the three workshops and eight working meetings of the TI Team noted above.
- Extensive, critical peer-review of the Project’s 2010 Draft Report and 2011 Final Report.

The Panel, collectively and individually, fully understood the SSHAC Guidance for a structured participatory peer review and the requirements for a Level 3 assessment process; had full and frequent access to information and interacted extensively with the TI Team and Project Manager throughout the entire project; provided peer-review comments at numerous stages; and, as documented within the Final Project Report, was fully engaged to meet its peer-review obligations in an effective way.

Project Report

The SSHAC Guidance makes clear that adequate documentation of process and results is crucial for their understanding and use by others in the technical community, by later analysis teams, and by the project sponsors. The Panel understood what was needed to conform to the SSHAC requirements, and it was committed to ensuring that the documentation of technical details associated with the CEUS SSC Model in the Project Report was clear and complete. The Panel was equally committed to ensuring the transparency of process aspects of the project, both in implementation and in description in the Project Report.

The Panel provided lengthy compilations of review comments (see Appendix I of the Project Report) for both the 2010 Draft Report and the 2011 Final Report. These included hundreds of comments, categorized as general, specific, relating to clarity and completeness, or editorial. The massive amount of detail provided by the TI Team in the Project Report and the intensiveness of the Panel’s review comments both reflect great diligence and a mutual understanding by the TI Team and the PPRP of the thoroughness and high quality of documentation expected in the Project Report.

The Project Manager and the TI Lead provided review criteria to the Panel for both the draft and final versions of the Project Report. The criteria for reviewing the Draft Report⁶ covered the range of technical and process issues consistent with requirements of the SSHAC Guidance, including draft implementation guidance (see footnote #4). Key criteria, among others, include sufficiency of explanatory detail; adequate consideration of the full range of data, models, and methods—and the views of the larger technical community; adequate justification of the data evaluation process, logic-tree weights, and other technical decisions; proper treatment of uncertainties; and conformance to a SSHAC Level 3 assessment process. To be clear, the PPRP is charged with judging the adequacy of the documented *justification* for the CEUS SSC Model and its associated logic-tree weights. The TI Team “owns” the Model and logic-tree weights.

Criteria for reviewing the Final Report focused on reaching closure to comments made on the Draft Report and ensuring that no substantive issues remained unresolved. To that end, among its many review comments on the Final Report the Panel identified “mandatory” comments, which the TI Team was required to address in the final version of the Project Report.

⁶ See PPRP report dated October 4, 2010, in Appendix I of CEUS SSC Final Report

The Panel made thorough, extensive efforts in its documented reviews of the 2010 Draft Report and the 2011 Final Report (as well as in many related interactions with the TI Team) to ensure a high-quality Project Report that fully meets SSHAC requirements for clear, complete, and transparent documentation of all aspects of the CEUS SSC Project. We are pleased to confirm that implementation of the CEUS SSC Project fully conformed with the SSHAC Guidance and that the resulting CEUS SSC Model properly meets the SSHAC goal of representing the center, body, and range of technically-defensible interpretations.

This concludes our PPRP Final Report for the CEUS SSC Project.




Jon P. Ake



Walter J. Arabasz



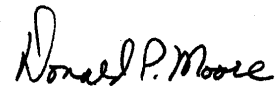
William J. Hinze



Annie M. Kammerer



Jeffrey K. Kimball



Donald P. Moore



Mark D. Petersen



J. Carl Stepp

Copy:

Lawrence A. Salomone

Kevin J. Coppersmith

Brent Gutierrez

PROJECT ACKNOWLEDGMENTS

This study was sponsored by the Electric Power Research Institute (EPRI) Advanced Nuclear Technology Action Plan Committee, the U.S. Department of Energy (DOE) Office of Nuclear Energy and Office of the Chief of Nuclear Safety, and the U.S. Nuclear Regulatory Commission (NRC) Office of Nuclear Regulatory Research. Technical experts from the DOE, NRC, U.S. Geological Survey, Defense Nuclear Facility Safety Board, industry, and academia participated in the study as part of the Technical Integration (TI) Team or as members of the Participatory Peer Review Panel (PPRP). Any statements, opinions, findings, conclusions, or recommendations expressed in this material are those of the authors and do not necessarily reflect those of the participating or sponsoring agencies.

Jeffrey F. Hamel was the EPRI Advanced Nuclear Technology Program Manager. Lawrence A. Salomone of Savannah River Nuclear Solutions, LLC, served as the Project Manager for the study. Kevin J. Coppersmith of Coppersmith Consulting Inc., served as the lead for the TI Team. J. Carl Stepp of Earthquake Hazards Solutions, and Walter J. Arabasz, Research Professor Emeritus of Geology and Geophysics at the University of Utah, served as Co-chairmen for the PPRP. The entire Central and Eastern United States Seismic Source Characterization Project Team and their roles are discussed in Section 2 and are shown on the project organization chart (Figure 2.3-1) of the report.

The authors of the report wish to acknowledge the contributions of the following people: the resource experts who participated in Workshop 1, the proponent experts who participated in Workshop 2, and the technical experts who provided valuable insights, perspective, and references throughout the study. The names of all these contributors are listed in Table 2.2-2.

In addition, the authors of the report appreciate the support of Geraldine Moore-Butler as administrative assistant and Nancy L. Sutherland as technical editor for the project. This report was assembled at AMEC.

Page intentionally left blank

SPONSORS' PERSPECTIVE

This report describes a new seismic source characterization model for the Central and Eastern United States (CEUS) for use in probabilistic seismic hazard analysis (PSHA) for nuclear facilities. PSHA has become a generally accepted procedure for supporting seismic design, seismic safety and decision making for both industry and government. Input to a PSHA consists of seismic source characterization (SSC) and ground motion characterization (GMC); these two components are necessary to calculate probabilistic hazard results (or seismic hazard curves) at a particular geographic location.

The 1986 Electric Power Research Institute and Seismicity Owners Group (EPRI-SOG) study included both an SSC and GMC component. Recent applications for new commercial reactors have followed U.S. Nuclear Regulatory Commission (NRC) regulatory guidance (RG 1.208) by using the EPRI-SOG source model as a starting point and updating it as appropriate on a site-specific basis. This CEUS SSC Project has developed a new SSC model for the CEUS to replace the SSC component of the EPRI-SOG study.

The CEUS SSC Project was conducted using a Senior Seismic Hazard Analysis Committee (SSHAC) Level 3 process, as described in the NRC publication, *Recommendations for Probabilistic Seismic Hazard Analysis: Guidance on Uncertainty and Use of Experts* (NUREG/CR-6372). The goal of the SSHAC process is to represent the center, body, and range of technically defensible interpretations of the available data, models, and methods. The CEUS SSC model is applicable to any site within the CEUS and can be used with the EPRI 2004/2006 GMC model to calculate seismic hazard at any site of interest. Long-term efforts to replace the EPRI 2004/2006 GMC model with the Next Generation Attenuation Relationships for Central and Eastern North America obtained from the NGA-East Project is scheduled for completion in 2014.

The updated CEUS SSC model provides industry and government with the following: a new model for the commercial nuclear industry to perform PSHAs for future reactor license applications; the NRC to support its review of early site permit (ESP) and construction and operating license (COL) applications; and the U.S. Department of Energy (DOE) to support modern PSHAs to meet design and periodic review requirements for its current and future nuclear facilities. Specific benefits of the model are as follows:

- **Consistency:** For many sites, seismic sources at distances up to 300 km (186 mi.) or more significantly contribute to hazard at some spectral frequencies. Consequently, seismic hazard models for many sites have significant geologic overlap. If done separately, there is a likelihood of conflicting assessments for the same regions. A regional source model allows for consistent input into a PSHA. An updated conceptual SSC framework that provides a

consistent basis for identifying and characterizing seismic sources in the CEUS has been developed. The NRC will no longer need to review each time each applicant's regional SSC model when the accepted CEUS SSC model is used. This will avoid lengthy review of the regional SSC model in ESP and COL applications for sites within the CEUS that use the accepted regional CEUS SSC model to develop its site-specific SSC model.

- **Stability:** This CEUS SSC model was developed using the accepted state-of-practice SSHAC methodology that involved the following tasks:
 - Development of a comprehensive database and new tools for documenting the data consideration process.
 - Multiple workshops to identify applicable data, debate alternative hypotheses, and discuss feedback.
 - Multiple working meetings by the Technical Integration (TI) Team to develop the SSC model and fully incorporate uncertainties.
 - Technical advancements in a number of areas, such as developing a uniform earthquake catalog, developing an updated approach for assessing maximum magnitude, compiling data evaluation tables, incorporating paleoseismic data, and using spatial smoothing tools.
 - Participatory peer review, including four panel briefings, multiple interactions, and periodic formal feedback.
 - Proper documentation of all process and technical aspects of the project.

Experience has shown that stability is best achieved through proper and thorough characterization of our knowledge and uncertainties, coupled with the involvement of the technical community, regulators, and oversight groups.

- **Greater Longevity:** An explicit goal of the SSHAC methodology is to represent the center, body, and range of the technically defensible interpretations of the available data, models, and methods. Using the SSHAC process provides reasonable assurance that this goal has been achieved. Representing the center, body, and range of interpretations at the time of the study means that as new information is acquired and various interpretations evolve as a result, the current thinking at any point is more likely to be addressed in the study. As new information becomes available, an existing SSC will require periodic reviews to evaluate the implications of the new findings. The need for updates to a particular study is now better understood as a result of findings of the CEUS SSC Project sensitivity studies to determine the significance of source characteristics.
- **Cost and Schedule Savings:** The CEUS SSC model can be used to perform a PSHA at any geographic location within the CEUS. It is applicable at any point within the CEUS, subject to site-specific refinements required by facility-specific regulations or regulatory guidance. Having stable, consistent input into a regional PSHA will reduce the time and cost required to complete a commercial nuclear site's ESP or COL licensing application, prepare a DOE site's PSHA, and develop design input for new commercial and DOE mission-critical nuclear facilities.

- **Advancement of Science:** The CEUS SSC Project provides new data, models, and methods. This information was shared at three workshops with international observers as a means to provide technology transfer for application in other regions. The CEUS SSC earthquake catalog, which merges and reconciles several catalogs and provides a uniform moment magnitude for all events, and the CEUS SSC paleoliquefaction database provide a new baseline for future research and updates. New approaches used in this project for spatial smoothing of recurrence parameters, assessment of maximum magnitude, and systematical documentation of all data considered and evaluated also benefit future research and PSHA updates.

The sponsors of the CEUS SSC Project are utilities and vendors on the EPRI Advanced Nuclear Technology Action Plan Committee, the DOE Office of Nuclear Energy, the DOE Office of the Chief of Nuclear Safety, and the NRC Office of Nuclear Regulatory Research. Technical experts from the DOE, NRC, U.S. Geological Survey (USGS), and Defense Nuclear Facility Safety Board (DNFSB) participated in the study as part of the TI Team or as members of the Participatory Peer Review Panel (PPRP).

The product of the CEUS SSC Project is a robust peer-reviewed regional CEUS SSC model for use in PSHAs. This model will be applicable to the entire CEUS, providing an important baseline for future research and updates. The CEUS SSC Project demonstrates that a SSHAC Level 3 approach can achieve the goals of considering the knowledge and uncertainties of the larger technical community within a robust and transparent framework. The value of the new CEUS SSC model has been enhanced by the participation of key stakeholders from industry, government, and academia who were part of the CEUS SSC Project Team.

Looking forward, the NRC will publish NUREG-2117 (2012), *Practical Implementation Guidelines for SSHAC Level 3 and 4 Hazard Studies* that provides SSHAC guidance on the need to update a regional model. The guidance covers updating both regional and site-specific assessments. It addresses the “refinement” process of starting with a regional model and refining it for site-specific applications.

Page intentionally left blank

ABBREVIATIONS

AD	anno domini (in the year of the Lord)
AFE	annual frequency of exceedance
AIC	Akaike information criterion
ALM	Alabama-Louisiana-Mississippi (zone of possible paleoseismic features)
AM	Atlantic Margin (seismotectonic zone)
AHEX	Atlantic Highly Extended Crust (seismotectonic zone)
ANSS	U.S. Advanced National Seismic System
ANT	Advanced Nuclear Technology
APC	Action Plan Committee
BA	Blytheville arch
BC	before Christ
BCFZ	Big Creek fault zone
BFZ	Blytheville fault zone
BL	Bootheel lineament
BMA	Brunswick magnetic anomaly
BP	before present
BPT	Brownian passage time
BTP	Branch Technical Position
CAD	computer-aided design

Abbreviations

CBR	center, body, and range
CCFZ	Crittenden County fault zone
CDZ	Commerce deformation zone
CENA	Central and Eastern North America
CERI	Center for Earthquake Research and Information
CEUS	Central and Eastern United States
CFZ	Commerce fault zone
CFR	Code of Federal Regulations
CGL	Commerce geophysical lineament
CGRGC	Cottonwood Grove–Rough Creek graben
CI	confidence interval
CNWRA	Center for Nuclear Waste Regulatory Analysis
COCORP	Consortium for Continental Reflection Profiling
COCRUST	Consortium for Crustal Reconnaissance Using Seismic Techniques
COL	combined construction and operating license
COLA	combined operating license application
COMP	composite prior, composite superdomain
CON	contemporary (with earthquake occurrence)
COV	coefficient of variation
CPT	cone penetration test
CVSZ	Central Virginia seismic zone
D&G	Dewey and Gordon (1984 catalog)
DEM	digital elevation model

DNFSB	Defense Nuclear Facilities Safety Board
DOE	U.S. Department of Energy
DWM	Division of Waste Management
ECC	Extended Continental Crust
ECC-AM	Extended Continental Crust–Atlantic Margin (seismotectonic zone)
ECC-GC	Extended Continental Crust–Gulf Coast (seismotectonic zone)
ECFS	East Coast fault system
ECFS-C	East Coast fault system—central segment
ECFS-N	East Coast fault system—northern segment
ECFS-S	East Coast fault system—southern segment
EC-SFS	East Coast–Stafford fault system
ECMA	East Coast magnetic anomaly
ECRB	East Continent rift basin
ECTM	Eastern Canada Telemetered Network
E[M]	expected moment magnitude listed in the CEUS SSC catalog for an earthquake
ENA	eastern North America
EP	Eau Plain shear zone
EPRI	Electric Power Research Institute
EPRI-SOG	Electric Power Research Institute–Seismicity Owners Group
ERM	Eastern rift margin
ERM-N	Eastern rift margin—north
ERM-RP	Eastern rift margin—river (fault) picks
ERM-S	Eastern rift margin—south

Abbreviations

ERM-SCC	Eastern rift margin—south/Crittenden County
ERM-SRP	Eastern rift margin—south/river (fault) picks
ERRM	Eastern Reelfoot Rift Margin
ESP	early site permit
ESRI	Environmental Systems Research Institute
ETSZ	Eastern Tennessee seismic zone
EUS	Eastern United States
FAFC	Fluorspar Area fault complex
FGDC	Federal Geographic Data Committee
ft	foot or feet
FTP	file transfer protocol
ft/s	feet per second
ft/yr	feet per year
FWLA	Fugro William Lettis & Associates
FWR	Fort Wayne rift
Ga	billion years ago
GC	Gulf Coast
GCVSZ	Giles County, Virginia, seismic zone
GHEX	Gulf Coast Highly Extended Crust (seismotectonic zone)
GIS	geographic information system
GLTZ	Great Lakes tectonic zone
GMC	ground-motion characterization (model)
GMH	Great Meteor Hotspot (seismotectonic zone)

GMPE	ground-motion prediction equation
GMRS	ground-motion response spectra
GPR	ground-penetrating radar
GPS	global positioning system
GSC	Geological Survey of Canada
Gyr	gigayears (10^9 years)
HF	Humboldt fault
HID	hazard input document
I_0	maximum intensity
IAEA	International Atomic Energy Agency
IBEB	Illinois Basin Extended Basement (seismotectonic zone)
IPEEE	Individual Plant Examination for External Events
IRM	Iapetan rifted margin
ISC	International Seismological Centre
ITC	informed technical community
ka	thousand years ago
K-Ar	potassium-argon
km	kilometer(s)
km ²	square kilometer(s)
km/sec	kilometers per second
K-S	Kijko-Sellevoll
K-S-B	Kijko-Sellevoll-Bayes
kyr	thousand years

Abbreviations

LDO	Lamont-Doherty Earth Observatory (catalog)
LHS	Latin hypercube sampling
LLNL	Lawrence Livermore National Laboratory
ln(FA)	logarithm of felt area (with felt area measured in km ²)
LS	least squares
LSA	La Salle anticlinal belt
LWLS	locally weighted least squares
m	meter(s)
M	magnitude
M, M _w	moment magnitudes
Ma	million years ago
MAR	Marianna (RLME source)
m _b	body-wave magnitude (short period)
m _{bLg}	body-wave magnitude determined from higher-mode (L _g) surface waves
M _C	coda magnitude
MCMC	Markov Chain Monte Carlo
M _D	duration magnitude
MESE	Mesozoic and younger extended crust
MESE-N	Mesozoic-and-younger extended crust or Mmax zone that is “narrow”
MESE-W	Mesozoic-and-younger extended crust or Mmax zone that is “wide”
mi.	mile(s)
mi. ²	square mile(s)
MIDC	midcontinent

MidC	Midcontinent-Craton (seismotectonic zone)
Mfa	felt-area magnitude
M _L	local magnitude
M _{max} , Mmax	maximum magnitude
MMI	modified Mercalli intensity
mm/yr	millimeters per year
M _N	Nuttli magnitude
M ₀	Scalar seismic moment
MRS	Midcontinent rift system
m/s	meters per second
M _S	surface-wave magnitude
MSF	Meeman-Shelby fault
M _w	
Myr	million years
NAD83	North American Datum of 1983
NAP	Northern Appalachian (seismotectonic zone)
Nd	neodymium
NEDB	National Earthquake Database
NEI	Nuclear Energy Institute
NEIC	National Earthquake Information Center
NF	Niagara fault zone
NMESE	Non-Mesozoic and younger extended crust
NMESE-N	Mesozoic-and-younger extended crust or Mmax zone that is “narrow”

Abbreviations

NMESE-W	Mesozoic-and-younger extended crust or Mmax zone that is “wide”
NMFS	New Madrid fault system
NMN	New Madrid North fault
NMS	New Madrid South fault
NMSZ	New Madrid seismic zone
NN	New Madrid north (fault segment as designated by Johnston and Schweig, 1996)
NOAA	National Oceanic and Atmospheric Administration
NPP	nuclear power plant(s)
NR	Nemaha Ridge
NRC	U.S. Nuclear Regulatory Commission
NRHF	Nemaha Ridge–Humboldt fault
NSHMP	National Seismic Hazard Mapping Project
NW	New Madrid west (fault segment as designated by Johnston and Schweig, 1996)
OKA	Oklahoma aulacogen (seismotectonic zone)
OKO	Oklahoma Geological Survey Leonard Geophysical Observatory (catalog)
OSL	optically stimulated luminescence
P_a	probability of activity (of being seismogenic)
PEZ	Paleozoic Extended Crust (seismotectonic zone)
PGA	peak ground acceleration
PM	Project Manager
PPRP	Participatory Peer Review Panel
PSHA	probabilistic seismic hazard analysis
PVHA	probabilistic volcanic hazard analysis

RCG	Rough Creek graben
RF	Reelfoot fault
RFT	Reelfoot thrust (fault)
RLME	repeated large-magnitude earthquake (source)
RR	Reelfoot rift zone
RS	Reelfoot South (fault segment)
SA	spectral acceleration
SCL	St. Charles lineament
SCML	south-central magnetic lineament
SCR	stable continental region
SCSN	South Carolina Seismic Network
SEUS	Southeastern United States (catalog)
SEUSSN	Southeastern United States Seismic Network
SGFZ	Ste. Genevieve fault zone
SHmax	maximum horizontal stress, compression, or principal stress
SLR	St. Lawrence rift (seismotectonic zone)
SLTZ	Spirit Lake tectonic zone
SLU	Saint Louis University (catalog)
SNM	Sanford et al. (2002 catalog)
SOG	Seismicity Owners Group
SPT	standard penetration test
SRA	Stover, Reagor, and Algermissen (1984 catalog)
SRTM	Shuttle Radar Topography Mission

Abbreviations

SSC	seismic source characterization
SSE	safe shutdown earthquake
SSHAC	Senior Seismic Hazard Analysis Committee
Str&Tur	Street and Turcotte (1977 catalog)
SUSN	Southeastern United States Network
TC	technical community
TFI	technical facilitator/integrator
TI	technical integration
USGS	U.S. Geological Survey
USNSN	U.S. National Seismograph Network
UTC	Coordinated Universal Time
V_P/V_S	ratio of P-wave velocity to S-wave velocity
WES	Weston Observatory (catalog)
WIPP	Waste Isolation Pilot Project
WQSZ	Western Quebec seismic zone
WRFZ	White River fault zone
WUS	Western United States
WVFS	Wabash Valley fault system
WVSZ	Wabash Valley seismic zone
WWSSN	World-Wide Standardized Seismograph Network

1

CHAPTER 1

INTRODUCTION

1.1 Background and History

The Central and Eastern United States Seismic Source Characterization for Nuclear Facilities (CEUS SSC) Project was conducted over the period from April 2008 to December 2011 to provide a regional seismic source model for use in probabilistic seismic hazard analyses (PSHAs) for nuclear facilities. As such, the CEUS SSC model replaces regional seismic source models for this region that are currently accepted by the Nuclear Regulatory Commission (NRC) for assessing seismic design bases and their associated uncertainties satisfying the requirements of the seismic regulation, 10 CFR Part 100.23. The models being replaced are the Electric Power Research Institute–Seismicity Owners Group (EPRI-SOG) SSC model (EPRI, 1988) and the Lawrence Livermore National Laboratory (LLNL) SSC model (Bernreuter et al., 1989) sponsored by the NRC.

Unlike the pioneering EPRI and LLNL projects, which were conducted independently, the CEUS SSC Project had multiple stakeholders who joined to sponsor it. They include the EPRI Advanced Nuclear Technology Program, the U.S. Department of Energy (DOE) Office of Nuclear Energy and Office of the Chief of Nuclear Safety, and the NRC Office of Nuclear Regulatory Research. Importantly, in the time since these early regional seismic source models were developed, the methodology for developing PSHA models has benefited from extensive application and regulatory review. As will be described in Section 1.1.2, following review of the EPRI and LLNL SSC models, which were developed using somewhat different process methodologies to evaluate and quantify uncertainties, the NRC, DOE, and EPRI jointly sponsored development of a standard methodology called the SSHAC methodology. This project used a SSHAC Level 3 assessment process in order to adequately ensure compliance with the requirement of the seismic regulations to properly quantify uncertainties in seismic design basis for nuclear facilities.

The regional SSC model developed by this project can be used for site-specific PSHAs with appropriate site-specific refinements as required by current regulatory guidance. For example, NRC Regulatory Guide 1.208 requires the development of an up-to-date, site-specific earth science database to support every nuclear facility license application. In the course of developing the database, local refinements to the CEUS SSC model may be necessary to accommodate local information.

The SSC model has incorporated earthquake source parameters in order to be compatible with current and anticipated ground-motion characterization (GMC) models. The current accepted

ground-motion models for use at nuclear facilities are those developed by EPRI (2004, 2006). The ongoing Next Generation Attenuation–East Project will provide ground motion models that are appropriate for use with the CEUS SSC model; these models are expected to be adopted as part of the seismic safety regulatory guidance, replacing the EPRI (2004, 2006) models.

The remainder of this chapter provides a summary of the historical context for the CEUS SSC Project and a description of how the project meets the needs of the seismic hazard community.

1.1.1 EPRI-SOG and LLNL Projects

The CEUS SSC Project replaces the SSC components of the landmark seismic hazard projects conducted in the 1980s by EPRI-SOG (EPRI, 1988) and LLNL (Bernreuter et al., 1989). Both of these projects developed PSHA models for application in the broad region of the United States to the east of the Rocky Mountains. Recent licensing applications for nuclear facilities submitted to the NRC have followed regulatory guidance by using the EPRI-SOG SSC model as a starting point, with updates as appropriate on a site-specific basis for site-specific PSHAs. However, while the regional SSC model has been updated for specific sites, it has not been systematically updated to account for the significant new data in the CEUS. The CEUS SSC Project takes full advantage of the following historical and new sources: data used to develop the two previous CEUS models; new data and information developed over the past 20 years, including that developed for the U.S. Geological Survey (USGS) seismic hazard mapping program (Petersen et al., 2008); and other information and hazard analyses that were developed as part of licensing actions for proposed and existing nuclear power facilities. In addition to the new data, updated methods for evaluating the data and quantifying uncertainties have been implemented in the CEUS SSC Project.

1.1.2 Development of the SSHAC Process

Methodological guidance on how to perform a PSHA properly representing uncertainty was developed by the Senior Seismic Hazard Analysis Committee (SSHAC) in 1997 in a study jointly sponsored by the NRC, DOE, and EPRI (Budnitz et al., 1997). Both technical and procedural guidance was developed by SSHAC based on its evaluations of past PSHAs, which included the EPRI-SOG and LLNL models. Although both of those large projects relied on evaluations and assessments by multiple experts, there were significant technical and procedural differences between the two. There were also significant differences between the hazard results obtained at many of the same sites. The formation of SSHAC was motivated by the need to (1) understand these differences and (2) develop guidelines for evaluating and quantifying uncertainty in seismic hazard models—specifically, guidelines that would ensure that future PSHAs would satisfy the requirements for seismic safety regulation of nuclear facilities. The final guidelines resulting from the study were published in 1997 in NUREG/CR-6372 (Budnitz et al., 1997) and, following review by a committee of the National Academy of Sciences, were incorporated into the NRC’s seismic regulatory procedures guidance.

The SSHAC guidelines provide a structured procedure for systematically compiling applicable data sets, evaluating those data relative to their application for SSC, assembling representatives

of alternative hypotheses and interpretations within the technical community for discussion of their hypotheses and associated uncertainties, and performing integration of a SSC model that represents the center, body, and range of technically defensible interpretations in light of the views of the larger technical community. The formalism imposed by the SSHAC process was not available at the time the EPRI-SOG and LLNL projects were conducted two decades ago, so it is timely that a new SSC model was developed that takes advantage of the technical and procedural knowledge gained since those studies were carried out. As will be discussed in Section 2.1, the CEUS SSC Project is only the latest in a number of PSHA model development projects conducted using the SSHAC guidelines since the time of their issuance.

Under NRC sponsorship, the USGS completed an assessment of the lessons learned from the application of the SSHAC process in various projects since the SSHAC guidelines were issued. The results of that evaluation are given in Hanks et al. (2009). In light of the experience gained in actual SSHAC projects, the NRC (2011) has developed a NUREG document that provides detailed implementation guidance for conducting SSHAC Level 3 and 4 projects. That document will be issued later this year.

1.1.3 Implementation of the SSHAC Methodology

SSHAC concluded that *how* a seismic hazard project is carried out can be just as important as *what* is being assessed technically. This emphasizes that process methodology is important, and experience implementing the methodology is equally important. The project team assembled for the CEUS SSC Project is composed of distinguished experts from industry, government, and academia. These experts have extensive experience in developing PSHAs for sites both throughout the United States and worldwide. In addition, most of these experts have developed key data sets used for SSC in the CEUS and have participated in important studies that form the basis for conducting PSHAs. Most of the participants have considerable experience with implementing SSHAC processes as either expert evaluators or peer reviewers. The roles and responsibilities of participants in the CEUS SSC Project were explicitly defined, following SSHAC guidelines, for a successful Level 3 assessment project (see Section 2.2), and were diligently followed. Because many of the project participants have significant experience on recent and ongoing SSHAC projects, they knew these roles and appreciated their importance from the outset. All participants were reminded of their roles throughout the project. This experience makes the project team exceptionally qualified to develop the CEUS SSC model.

1.1.4 Regional SSC Model for Nuclear Facilities

The CEUS SSC Project is a user-community-based project for developing a regional SSC model in that it has the sponsorship of multiple user stakeholders. Site-specific seismic hazard assessments will be required as part of licensing proposed sites for next-generation nuclear power plants in the CEUS. Likewise, sites in the DOE nuclear facility complex require updated seismic hazard assessments. Conducting these assessments and updates independently is a time-consuming, overlapping, and costly process; therefore, developing a regional seismic source model that can be applied to all sites in the CEUS is highly stabilizing and cost-beneficial. Furthermore, developing the CEUS SSC model using the SSHAC Level 3 process, which has

been developed and endorsed by nuclear utilities, the NRC, and the DOE, provides a stable basis for future site-specific PSHAs for any nuclear facility. Standardization at a regional level will provide a consistent basis for computing seismic hazard, which will assist regulators such as the NRC and the Defense Nuclear Facilities Safety Board (DNFSB) in their safety review and oversight of nuclear facilities.

The CEUS SSC model was developed by a comprehensive implementation of a transparent, and traceable process, as described in this report. The model will be used by the following groups:

- Utilities that have submitted or will submit an Early Site Permit (ESP) application or a Combined Construction and Operating License (COL) application for NRC review.
- The NRC, DNFSB, and other regulatory and review groups that are responsible for ensuring the seismic safety of existing and new nuclear facilities.
- The DOE, which is responsible for conducting seismic design studies and seismic safety evaluations of new and existing nuclear facilities.
- The NRC and utilities that must respond to generic seismic safety issues for existing plants.

1.1.5 Differences from USGS National Seismic Hazard Mapping Project

In 2008, as part of the USGS National Seismic Hazard Mapping Project, national seismic hazard maps were released (Petersen et al., 2008) that are updates of previous seismic hazard maps developed by the USGS (e.g., Frankel et al., 1996, 2002). The national seismic hazard maps display the ground-motion hazard component of the seismic provisions of national building codes and support earthquake insurance rate structures and public policy decisions related to the national infrastructure. Earthquake strong ground motions for varying probability levels across the United States are displayed on these maps consistent with the seismic design basis requirements of national building codes. The maps are not intended to serve as seismic design bases for nuclear power plants, however.

Although many of the same types of data underpin the development of both the USGS seismic hazard mapping project and the CEUS SSC model, the products have different uses and different demands. For example, the CEUS SSC model is used to obtain seismic hazard at lower annual frequencies of exceedance (AFEs) than those required for the USGS seismic hazard maps. This is because the CEUS SSC Project is focused on the needs of nuclear facilities, whose seismic design requirements are more stringent than those of conventional infrastructure facilities, and whose safety analyses depend on occurrence of rare ground motions because of the critical safety requirements of these facilities. Thus, while the national seismic hazard maps are focused on AFEs in the range of 10^{-2} to 4×10^{-4} , the CEUS SSC model must support PSHAs focusing on AFEs in the range of 10^{-3} to 10^{-7} for design and safety evaluations for nuclear facilities. The properly complete representation of uncertainty at very low AFEs that must meet the requirements of the seismic regulations for nuclear facilities demands a focused effort to assess and represent low-probability hypotheses and parameter values, and also careful evaluation and characterization of large, rare earthquakes, such as those interpreted from the paleoseismic record, and maximum earthquake magnitudes for all seismic sources.

As part of the effort to ensure that these critical demands have been satisfied, the evaluation processes of the CEUS SSC Project involved the active participation of scientists who have contributed to the development of the national seismic hazard maps. Their participation was a major factor in ensuring that the CEUS SSC model properly represents the center, body, and range of current technical community knowledge.

1.2 Purpose of the CEUS SSC Project

The objective of this project is to develop a regional SSC model for the CEUS that can be used to obtain site-specific PSHAs for nuclear facilities and that includes the following:

- A comprehensive project database as the basis for the evaluation and integration processes underpinning the development of the CEUS SSC model.
- Assessment and incorporation of uncertainties in data and in the range of technical interpretations of earthquake processes that constitute current scientific community knowledge.
- Detailed and traceable documentation of the evaluation and integration processes that support the SSC model.
- A comprehensive participatory peer review of both the technical and process aspects of the project.

The achievement of this objective provides reasonable assurance of stability and longevity for the SSC model.

Experience has shown that stability and longevity are achieved through comprehensive characterization of current scientific knowledge and associated uncertainties. Assurance that this has been achieved is enhanced by the participatory involvement of the technical community, regulators, and oversight groups. The process guidance developed by SSHAC sets the goal of *all* probabilistic hazard analyses, namely, to “represent the center, the body, and the range of the technical interpretations that the larger informed technical community would have if they were to conduct the study” (Budnitz et al., 1997). As documented in Section 2.1, there is assurance that the SSHAC goal has been met by the CEUS SSC Project’s implementation of the SSHAC Level 3 process.

In using the CEUS SSC model for site-specific PSHAs in accordance with current regulations and regulatory guidance (e.g., NRC Regulatory Guide 1.208), site-specific studies will be required to identify any potential refinements needed for the regional seismic sources and any potential capable seismic sources within the site region and vicinity. The findings of these site-specific studies could indicate possible local sources of seismicity (e.g., local faults with evidence of Quaternary activity, or nearby tectonic features with a significant probability of being seismogenic).

1.2.1 Implementation of SSHAC Level 3 Process

SSHAC defines four “study levels” representing increasing process implementation complexity that can be used to evaluate and assess the knowledge and uncertainties in the important components of a PSHA. While the SSHAC labeled these “study levels,” they are described as levels of increasing complexity of process implementation. The SSHAC guidance emphasizes that independent of the process implementation complexity, the goal is to represent the center, body, and range of technically defensible interpretations in light of an evaluation of the available data, models, and methods in the larger technical community.

According to the current SSHAC guidance (NRC, 2011), the two higher levels of process implementation complexity (Levels 3 and 4) should be used to develop regional PSHA models for sites requiring high levels of regulatory assurance—including nuclear facilities—to remain stable over an extended period of time, and for regions of complex seismotectonics where there are contentious alternative scientific interpretations. Lower SSHAC levels are recommended for non-nuclear facilities or for sites that have existing and viable Level 3 or 4 assessments. The higher assessment levels provide the degree of assurance required by the regulators for seismic safety decision-making.

Both SSHAC Levels 3 and 4 implementation processes formalize interactions with the technical community through a series of workshops in which the peer reviewers fully participate and sponsors and other oversight groups may attend and offer observations. The key difference between Level 3 and Level 4 is that the former entails evaluations and integration of the SSC model by a Technical Integration (TI) team of evaluators, while the latter uses individual (or small teams) of evaluators. For both levels, the expert evaluators are charged with evaluating the current scientific community knowledge and performing as integrators in their characterization and assessment of current knowledge and uncertainty in the SSC model. These broad interactions lead to higher assurance that alternative interpretations of complex scientific/technical issues representing the range of knowledge of the scientific community have been completely evaluated and properly characterized and that the associated uncertainties are understood and properly assessed.

Selection of a SSHAC level depends primarily on the amount and nature of uncertainty, controversy, and complexity involved, but also on regulatory concerns and public perceptions. The time and resources that the sponsor can commit to a proposed project may also be determinants of the level. As the SSHAC level increases, project costs and the number of participants involved increase; the broad acceptance of the final product, however, is also expected to increase. The lessons learned from conducting PSHAs at SSHAC Levels 3 and 4 were compiled and evaluated in a joint USGS and NRC study that began in 2007 and was reported in USGS Open-File Report 2009-1093 (Hanks et al., 2009). These lessons learned were then used to develop more specific recommendations for the selection of SSHAC levels given in NRC (2011).

From a review of Level 4 projects completed since the SSHAC guidance was written, the three or four years required to complete these projects and the high associated costs were cited as posing significant barriers for project sponsors (Hanks et al., 2009, p. 44). The additional time

and costs associated with Level 4 projects can be attributed to the need to train the experts in the evaluation process, conduct individual working meetings with each expert, and prepare individual documentation of the evaluations and assessments made by each expert. In contrast, the TI team on a Level 3 project is trained as a team in the evaluation process, works together in workshops and working meetings, and develops a single comprehensive report of its evaluation of the state of scientific knowledge and integration to characterize and represent the center, body, and range of technically defensible interpretations. Now that the SSHAC methodology has been in use for a number of years, a Level 3 process has been established as suitable for developing regionally applicable seismic hazard models intended for computing PSHAs at multiple sites over an extended time.

The use of a Level 3 process is also consistent with the needs of the sponsors, who are responsible for safe design and operation of nuclear facilities. The CEUS SSC Project was conducted during a period when it could take full advantage of the experience gained from recent and ongoing SSHAC Level 3 projects, the lessons learned from a systematic review of past SSHAC projects (Hanks et al., 2009), and the NRC's detailed implementation guidance for Level 3 and 4 projects (NRC, 2011).

The selection of the SSHAC Level 3 methodology for the CEUS SSC Project was made during the planning stages and is summarized in the Project Plan. The decision was made by the Project Manager in consultation with the Project Sponsors and the TI Lead. The detailed recommendations for the selection of SSHAC levels given in Chapter 6 of more recent guidance (NRC, 2011) were not available at that time, but the decision criteria given in the original SSHAC guidelines (Table 3-1 in Budnitz, 1997) were used. The SSHAC guidelines do not define an explicit "prescription" for the appropriate SSHAC study level for a given set of conditions, but they indicate that the decision should be based on a consideration of the "issue degree" and various "decision factors."

The issue degree includes consideration of whether the technical issue of interest (seismic source characterization in the CEUS, in this case) is uncertain, controversial, subject to diverse interpretations, complex, and significant to hazard. Clearly, all of these factors apply. The decision factors include regulatory concern, available resources, and public perception. Given the significant issue degree and in light of the decision factors, it was decided that the project should be conducted at a high SSHAC level (i.e., Level 3 or 4). A SSHAC Level 3 methodology was selected over a Level 4 because of the advantages in maintaining a reasonable cost and schedule for completion of the study.

Comparison of the decision to use the SSHAC Level 3 methodology with the recommendations given in the current regulatory guidance (NRC, 2011, Ch. 6) supports the decision. For example, Chapter 6 in that document describes the decision criteria to be used in the selection of the SSHAC level as a function of the "viability" of the preexisting hazard study. The position taken in the guidance is that there is no significant difference in the degree of regulatory assurance provided by the SSHAC Level 3 or Level 4 methodology. As discussed in Section 6.3 and Table 6.1 of the NRC guidance (2011), SSHAC Level 3 or 4 methodologies are appropriate for nuclear facilities when the previous hazard study was either not conducted using the SSHAC methodology or was conducted using a Level 2 or lower SSHAC level, or where the existing

study is not viable. Viable is defined as (1) based on a consideration of data, models, and methods in the larger technical community; and (2) representative of the center, body, and range of technically defensible interpretations.

Given these criteria, the existing regional seismic hazard studies in the CEUS would not be considered viable and, given the explicit application of the CEUS SSC Project for nuclear facilities, a SSHAC Level 3 or 4 would be consistent with the current regulatory guidance. Because of the equivalent levels of regulatory assurance for Level 3 and 4 studies, coupled with the cost and schedule advantages of Level 3, the selection of a Level 3 methodology for the CEUS SSC Project is reasonable and defensible.

1.2.2 Goals: Stability and Longevity

Stability and longevity are important goals of the SSHAC assessment methodology, and these goals are highly important to the CEUS SSC Project. Stability means that the integrated assessments that result from a SSHAC assessment process should generally not be subject to significant change without new hazard-critical scientific findings. This is because the knowledge of the affected scientific community has been systematically compiled and evaluated throughout the project, and uncertainties in the community knowledge have been appropriately characterized and represented in the CEUS SSC model.

Longevity means that the model will last for a number of years before requiring a significant revision or update. New scientific findings will continue to be promulgated after the project is completed, along with new models and methods for interpreting data. Although evaluations of evolving scientific knowledge may potentially lead to the need to update elements of the model during site-specific use, it is likely that the regional model will remain viable, avoiding the need for an extensive revision for a number of years. Experience shows that community knowledge will not change in a systematic and significant way in a short time. The process of gathering scientific data, developing interpretations and hypotheses regarding those data, and vetting those hypotheses within the technical community takes time. With periodic updates, as necessary to reflect advances in the field as well as new data sources, the CEUS SSC model is expected to last several years before a significant revision is needed.

1.2.3 Interface with Ground Motion Models

After the EPRI-SOG project was completed, EPRI performed a major CEUS ground-motion project targeted on developing an understanding of ground motion variability. The project resulted in the EPRI ground-motion model for the CEUS (EPRI, 1993), which included an assessment of epistemic uncertainty in the median motions and an assessment of aleatory variability. The project involved nearly all of the then-active ground-motion modeling experts. Consequently, it stimulated follow-on research by a number of the participants who produced an equal number of ground motion models in the years following. The EPRI (1993) model, together with models developed by individual researchers, formed the body of knowledge for development of the EPRI (2004) GMC model for the CEUS, which updated the assessment of epistemic uncertainty in the median models and aleatory variability.

The EPRI (2004) ground-motion project was the first avowed application of a SSHAC Level 3 process. The development of a composite understanding of ground motion attenuation is a contentious, complex issue, and uncertainty in ground motion contributes significantly to the uncertainty in PSHA. A SSHAC-defined Level 3 process was implemented, in which a TI team was responsible for conducting workshops involving the community of ground-motion-modeling scientists to compile and evaluate current knowledge. The TI team was additionally responsible for integrating the knowledge base and characterizing the range of knowledge and assessing the composite distribution of ground motion based on evaluations of available information, including interactions with ground motion experts.

The TI team for the EPRI (2004) ground motion project brought together, in a series of three workshops, a panel of ground motion experts comprising proponents of the range of available models. The workshops were structured to gain a common understanding of the uncertainties in the modeling approaches and to develop the evaluation and assessment process for representing the uncertainty distribution of the technical community. The final product of the project was a ground-motion attenuation model defined by a set of equations and coefficients for estimating ground motion measures and their aleatory variability (standard deviation) as a function of earthquake magnitude and source-to-site distance. The model includes the epistemic uncertainty in the median estimate of ground motions and in the aleatory variability. The model is applicable to two general regions in the CEUS: the Midcontinent (CEUS excluding the Gulf Coast) and the Gulf Coast. The model is applicable to three classes of seismic sources: general conditions involving area sources; distant, large-magnitude sources; and nearby large-magnitude seismic sources.

Shortly after completion of the EPRI (2004) project, another project (EPRI, 2006) was conducted at a SSHAC Level 2 to further examine the value of the standard deviation for the ground motion variability for the CEUS. The value of the standard deviation in the models developed in the EPRI (2004) ground-motion project was much larger than recent studies of large data sets of ground motions applicable to the Western United States (WUS) had shown. An evaluation of differences in the standard deviation in the CEUS and WUS, based on the variability of the source, path, and site terms, indicated that the WUS intra-event standard deviations are generally applicable to the CEUS, with some epistemic uncertainty about the effect of focal depth at short distances. The evaluation also indicated that the inter-event standard deviations may be larger in the CEUS than in the WUS, based on larger variability in the stress drops. Alternative models for the total standard deviation (combined intra-event and inter-event) were developed that can be applied to the CEUS. Overall, these new models show a significant reduction in the total standard deviation, particularly at short distances. Compared to the EPRI (2004) models, this lower value of the standard deviation tends to reduce the computed hazard.

The EPRI (2004) GMC model and an updated assessment of aleatory variability (EPRI, 2006) together are the most current and applicable ground-motion model for the CEUS and are currently in use in ground motion analyses for COL applications. The ongoing Next Generation Attenuation–East project is aimed at replacing the GMC model developed by EPRI (2004, 2006). That effort has just begun and is not scheduled for completion until 2014. In anticipation of the types of ground motion models that will result from that project, the CEUS SSC Project provides outputs that are judged to be compatible with the needs of future ground-motion models. For

example, seismic sources are each characterized according to the characteristics of future earthquakes (see Section 5.4), such as the style of faulting, seismogenic crustal thickness, depth distributions, and orientation of ruptures.

1.3 Study Region

The project study region (Figure 1.3-1) is the region within which the CEUS SSC model has been developed. The SSC model is applicable to all sites within the project study region; however, for application at particular sites, such as those near the study region boundaries, additional seismic sources may need to be defined depending on the applicable regulations or guidance. The western boundary is located approximately along the foothills of the Rocky Mountains at longitude 105° W. On the north, the study region extends a minimum of 322 km (200 mi.) from the U.S.-Canadian border. On the south and east, the study region includes the offshore area a minimum of 322 km (200 mi.) from the coastline. Only seismic sources that lie within continental crust are included. The earthquake catalog developed for the CEUS SSC Project includes coverage of the entire area within the study region boundaries.

Seismic sources that are *not* considered in this project are those in areas outside the study region boundaries; this applies to sources in the WUS, Mexico, Canada, and the Caribbean Plate boundary area.

1.4 Products of Project

The CEUS SSC Project resulted in a series of products that document the bases for the technical assessments made and that provide the inputs to probabilistic seismic hazard analyses at locations in the CEUS. These products are discussed below.

1.4.1 Seismic Source Model for Study Region

A seismic source model has been developed for the CEUS that contains descriptions of parameters that define the frequency of occurrence, spatial distribution, and rupture characteristics of potential future earthquakes. A conceptual SSC model was developed for use on the project, which is hazard-informed and takes advantage of knowledge gained from SSC projects conducted over the past several years. The framework includes a hierarchical approach to the identification and characterization of seismic sources that considers the importance of seismic source characteristics to the hazard results. The hierarchy calls for identifying seismic sources—and quantifying their characteristics—according to their importance to earthquake recurrence, maximum magnitudes, future earthquake rupture characteristics, and the activity of tectonic features. Following directly from this framework, sources of repeated large-magnitude earthquakes (RLMEs; magnitude [**M**] greater than 6.5) are identified where recurrence is defined primarily from the paleoseismic record.

The choice of **M** 6.5 is simply because this is a magnitude earthquake that can usually be confidently identified within the paleoseismic record. Two alternative approaches to defining the spatial distribution of earthquakes outside of the RLME sources were (1) to define source

boundaries only on the basis of maximum magnitude differences, and (2) to define zones by their different seismotectonic characteristics. (Note that for simplicity in this section and later in the report, the term *RLME* is used to refer to the actual past earthquakes and the forecast of future occurrences; the term *RLME source* is used to refer to the seismic source used to model the spatial and temporal distribution of the RLMEs.)

The spatial distribution of future earthquakes is defined by the geometry of the RLME sources, the maximum-earthquake source zones, and the seismotectonic zones. In all cases, uncertainties in these boundaries are captured by alternatives in the logic tree. In addition, the spatial distribution of the recurrence rate within the zones is defined using a spatial smoothing process that allows for spatial variation in *a*- and *b*-values. The temporal distribution of earthquakes that occur within RLME sources is defined by alternative temporal models that provide for the occurrence of temporally clustered behavior and, if the data suggest it, a temporal renewal process. The CEUS SSC model placed heavy emphasis on the compilation and analysis of paleoseismic data, reflecting the focus on these types of data by the larger technical community in recent years.

The upper truncation of the earthquake recurrence relationships occurs at the maximum magnitude (*M*_{max}), and these are estimated for all seismic sources. The assessment of *M*_{max} for sources in stable continental regions (SCRs) such as the CEUS is subject to considerable uncertainty. The CEUS SSC Project employed two methods for assessing *M*_{max}: a Bayesian methodology using an updated SCR database of earthquake magnitudes and related information, and a well-founded mathematical procedure that estimates *M*_{max} based on seismic data (where sufficient) only for the source being considered. Many of the *M*_{max} distributions are quite broad and reflect the uncertainties that currently attend the conceptual models and parameter uncertainties regarding constraints on *M*_{max}.

The identification and quantification of uncertainties associated with seismic source characteristics is an important component of a PSHA. As recognized by SSHAC (Budnitz et al., 1997), a PSHA incorporates both aleatory variability and epistemic uncertainty. Aleatory variability is the natural randomness in a process that is known and understood. Examples of aleatory variabilities include an assessment of the size and location of the next earthquake, and the relative frequency of earthquakes having different rupture orientations. Epistemic uncertainty is the scientific uncertainty in a process that is due to limited data and knowledge. Examples include alternative recurrence models to describe future earthquakes, and the probability distribution describing the maximum magnitude of a particular seismic source. Epistemic uncertainties in the CEUS SSC model are captured in the master logic tree and the logic trees for each seismic source.

Epistemic uncertainty is the result of limited data (often, very limited). In seismic hazard analyses, evaluating alternative models involves considering alternative simplified physical models, data from analogous regions, and empirical observations. These are subjective. In some cases, uncertainties are developed from formal statistical assessment of fitting models to data (e.g., recurrence rate and *b*-value parameters obtained from fitting the truncated exponential recurrence model to recorded seismicity).

The CEUS SSC model was developed in four stages. After the second workshop, a “sensitivity SSC model” was developed that was designed to incorporate all potentially important source characteristics. This model was used in hazard calculations and sensitivity analyses discussed at the third workshop as feedback. With that feedback, a “preliminary SSC model” was developed that focused more specifically on the quantification of uncertainties. After review of another round of hazard calculations and sensitivity analyses, a “Draft SSC model” was developed, which was described in the Draft Project Report. The TI Team and the PPRP reviewed the associated hazard calculations and sensitivity analyses for that model and made refinements that are now part of the “Final SSC model” described in this report. These refinements included additional work in the magnitude conversions for the CEUS SSC Project earthquake catalog and the inclusion of a range of smoothing parameters to express the epistemic uncertainty in the spatial variation of recurrence parameters.

1.4.2 Hazard Input Document

A hazard input document (HID; see Appendix H) was prepared to provide the documentation necessary for users to implement the CEUS SSC model in PSHA calculations for future applications. The HID contains all of the information required for a future user to exercise the model within a PSHA, but it does not include the technical basis or justification for the elements of the model. Included are the logic tree structure, all branches and weights, and tabulations of the outputs from all calculations conducted within the context of the source characterization effort. Such outputs include the Mmax distributions for all sources, recurrence calculations using paleoseismic data for the RLME sources, and spatially defined *a*- and *b*-values resulting from the smoothing algorithm. The purpose of the HID is to ensure that the expert assessments made by the TI Team are captured faithfully and accurately and delivered for use by the hazard analyst for a PSHA at a specific site. For the CEUS SSC Project, the final HID was used by the hazard analyst to carry out hazard calculations at seven demonstration sites (Figure 1.3-1), as summarized in Chapter 8.

1.4.3 Documentation of Technical Bases for All Assessments

The results of a PSHA serve a range of users with different needs, from earth scientists to engineers and regulators. The SSHAC process requires complete documentation of every step of the methodology used and the results obtained, thereby allowing all users to understand the technical justification for all parts of the assessment. This report documents the process and methodology followed for the project and the technical bases for the models, parameter values, and weights included in the source model. For example, Section 5.2 provides a detailed description of the methodology that was used to develop assessments of maximum magnitude (Mmax) for individual seismic sources, including the epistemic uncertainties that result from alternative conceptual models and from the range of parameter uncertainties. The Mmax methodology is then applied to each seismic source using the source-specific information related to the largest observed earthquakes within the zone, the numbers of earthquakes of various magnitudes, and the tectonic characteristics of the zone. The source-specific characteristics and resulting Mmax distributions are provided in the applicable sections of Chapters 6 and 7.

The documentation for the CEUS SSC Project describes the process used to compile and evaluate the data, models, and methods, and to integrate current knowledge and uncertainties in a logic tree format depicting alternatives that represent the center, body, and range of technically defensible interpretation. The goal of the project documentation is to provide an adequate basis for future users of the project to fully understand the process that was implemented, data that were used, evaluations that were performed, and the technical bases for the characterization and uncertainty assessments represented in the models.

1.4.4 Other Key Products

In addition to the key products identified above, which have direct application to future seismic hazard studies, the CEUS SSC Project also resulted in a number of other products that have value for future users. These products are described below.

1.4.4.1 Data Evaluation and Data Summary Tables

The CEUS SSC model development entailed the consideration of an extensive amount of data. Part of the responsibility of the TI team is to document the data that were used in the assessment. To supplement this documentation, the TI Team developed a series of tables that specifically identify all of the data that were considered by the team (Data Summary tables) and that indicate the team's views of the quality of the data and the degree of reliance placed on any given data set (Data Evaluation tables). These tables provide a clear picture to future users of the data that were available at the time the project was conducted and how those data were used. The data tables are discussed in Section 4.1.2 and are given in Appendices C and D.

1.4.4.2 Database of Geologic, Geophysical, and Seismological Data

Because more than two decades have passed since the large regional seismic hazard studies (EPRI-SOG and LLNL) were conducted, the CEUS SSC Project entailed the compilation of a large amount of potentially applicable data. While no new data were gathered for the CEUS SSC Project (e.g., geologic mapping, paleoseismic investigations), a new regional database was developed for the project for use in SSC. The comprehensive database was formatted in a manner that allowed for dissemination of the data to all TI Team members during the course of the project. Where applicable, GIS data layers were developed that included new geophysical data compilations developed specifically for the project. A list of the available data sets included in the project database is provided in Appendix A. The project database, which includes an extensive bibliography of literature compiled for the project, was designed to be publically available following the completion of the project. In addition, a project website was developed for public use and can be found at www.ceus-ssc.com.

1.4.4.3 Earthquake Catalog with Uniform Moment Magnitudes

The CEUS SSC Project devoted a major effort to developing a comprehensive and uniform earthquake catalog for use on the project. Starting with the USGS national catalog and a number of regional catalogs, the various catalogs were updated to include all earthquakes through 2008. For modern PSHAs, moment magnitude is required for ground-motion prediction equations and

must be assessed for all earthquakes in the catalog. Accordingly, magnitude conversions between various instrumental magnitudes and moment magnitude were reassessed. Likewise, existing special studies of a number of historical earthquakes were reviewed in order to develop reliable moment magnitudes for these shocks. Uncertainties in the magnitude of all instrumental and historical earthquakes are included in the catalog. The CEUS SSC Project earthquake catalog is discussed in Chapter 3 and was used in defining and characterizing seismic sources as well as characterizing recurrence and Mmax parameters in the SSC model.

1.4.4.4 Updated Paleoseismicity Data and Guidance

Because of the significance of paleoliquefaction data in the CEUS, part of the scope of the project was to compile that data and develop written guidance for representing uncertainty in evaluations and interpretations of that data to estimate the locations, occurrence times, and magnitudes of causative earthquakes. The purpose of this study is to provide a basis for seismic source characterizers in the future to evaluate paleoseismic data relative to their quality and associated uncertainties. The results of the paleoseismicity study are given in Appendix E.

1.4.4.5 Recommendations for Future Applications of SSC Model

The CEUS SSC Project provides one of two models that are needed for PSHA calculations. Still, during the course of the project, hazard calculations were conducted for purposes of evaluating the significance of various SSC issues and providing that information as feedback to the TI Team. These calculations were carried out using the EPRI (2004, 2006) ground-motion models at seven demonstration sites for purposes of illustration. The area covered by this model is shown on Figure 1.3-1, along with the locations of the test sites used for hazard sensitivity calculations. In addition, as documented in this report, hazard was calculated for purposes of comparison with other hazard studies.

This report contains an evaluation of the “precision” of the hazard estimates for use in evaluating whether changes to the seismic hazard are significant. This provides a basis for evaluating the significance of new findings and associated hazard changes in the future. And finally, the report includes a discussion of how the results of this project should be applied in the future. This discussion is given in Chapter 9.

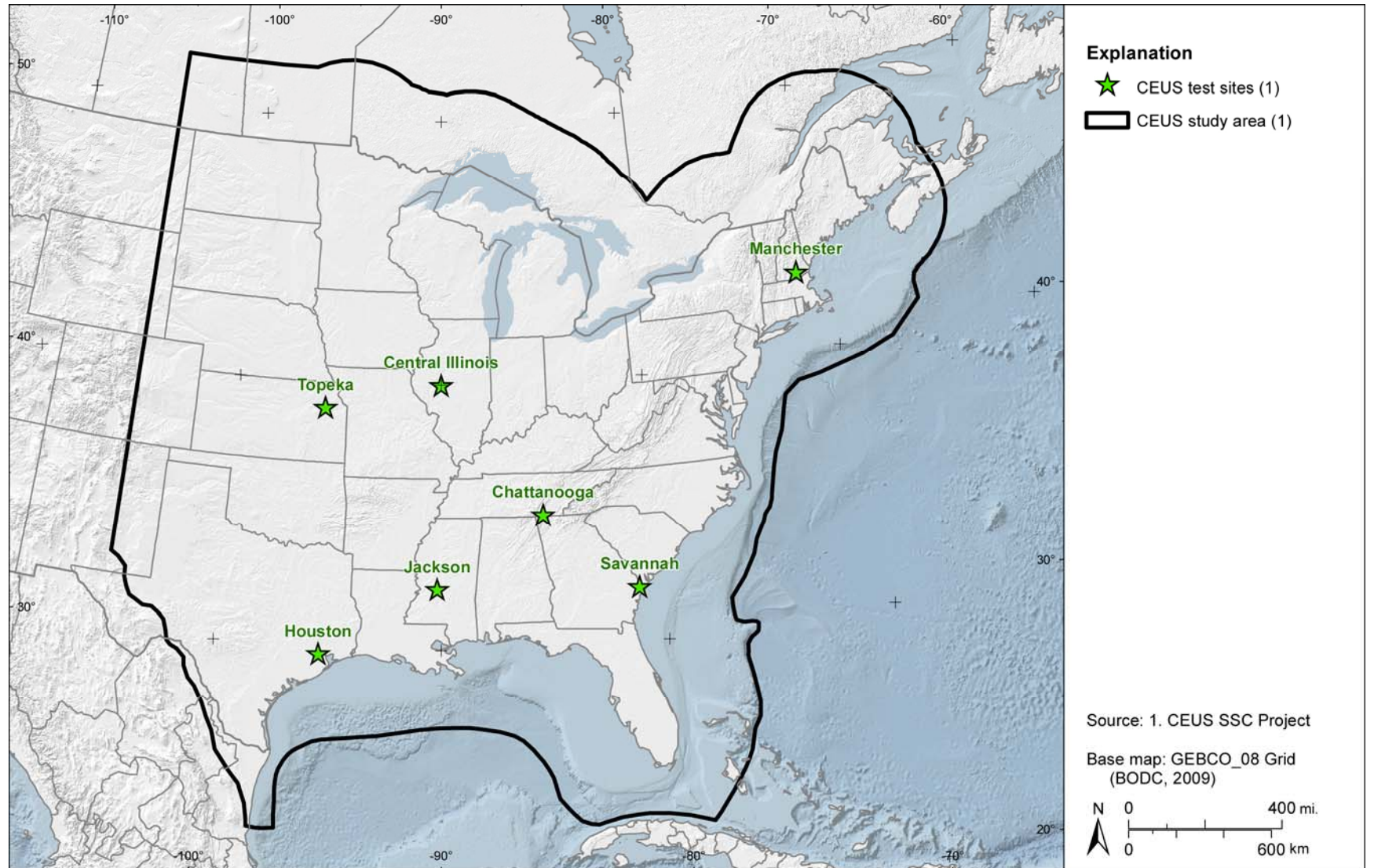


Figure 1.3-1
Map showing the study area and test sites for the CEUS SSC Project

2

CHAPTER 2 SSHAC LEVEL 3 ASSESSMENT PROCESS AND IMPLEMENTATION

This chapter describes the SSHAC Level 3 assessment process, how it was implemented to assess the CEUS SSC model, and how that implementation was accomplished in compliance with the SSHAC guidance.

The “SSHAC assessment process,” which differs only slightly for Level 3 and 4 studies, is a technical process accepted in the NRC’s seismic regulatory guidance (Regulatory Guide 1.208) for reasonably ensuring that uncertainties in data and scientific knowledge have been properly represented in seismic design ground motions consistent with the requirements of the seismic regulation 10 CFR Part 100.23. Therefore, the goal of the SSHAC assessment process is the proper and complete representation of knowledge and uncertainties in the SSC and GMC inputs to the PSHA (or similar hazard analysis). This reasonable representation of knowledge and uncertainties is referred to in the SSHAC guidance as “the center, the body, and the range of the informed technical community.” The SSHAC assessment process, if properly implemented, provides high levels of confidence that the SSHAC goal has been met. Therefore, the way it is conducted is important and subject to “process” as well as “technical” peer view. A key responsibility of the Participatory Peer Review Panel (PPRP) is to ensure that the SSHAC assessment process has been properly implemented.

SSHAC developed guidance for four “study levels” of implementing an assessment that depend on the degree of uncertainty and contention involved and on the intended use of the seismic hazard model. SSHAC recommended that a Level 3 or Level 4 assessment process be used for complex assessments, the products of which have high public importance and attract public scrutiny, such as regional seismic hazard models intended to be used over a sustained time period as base-case models for site-specific PSHAs. Such models require the highest level of assurance that the community uncertainty distribution has been properly represented. For the CEUS SSC Project, the decision to use a SSHAC Level 3 assessment process was based on experience with implementing the SSHAC guidance, which has shown that a properly executed Level 3 assessment process can provide a level of assurance of meeting the SSHAC goals comparable to that of Level 4, which is more costly and time-consuming to implement (selection discussed in the Project Plan and Section 1.2.1).

Discussion of the SSHAC process in this chapter comes from four sources:

1. The SSHAC document itself (Budnitz et al., 1997).
2. A summary of workshops conducted to identify lessons learned from the implementation of SSHAC in actual projects (Hanks et al., 2009).

3. A summary of the ongoing efforts of the NRC to develop more specific SSHAC guidelines (Coppersmith et al., 2010).
4. Draft NRC guidance for the implementation of SSHAC Level 3 and 4 projects (NRC, 2011).

This chapter begins with a discussion of the fundamental SSHAC goals and activities that make up a SSHAC assessment process. This is followed by a discussion of the SSHAC Level 3 assessment process implemented by the CEUS SSC Project, including the roles of key participants, project organization, key activities, and the PPRP. The final section summarizes how the CEUS SSC assessment process compares with the process prescribed in the SSHAC guidelines.

2.1 Goals and Activities of a SSHAC Assessment Process

Any PSHA requires that both knowledge and uncertainties be assessed and incorporated into the analysis. The SSHAC guidance expresses that fundamental goal in this way:

Regardless of the scale of the PSHA study, the goal remains the same: to represent the center, the body, and the range of technical interpretations that the larger informed technical community would have if they were to conduct the study. (Budnitz et al., 1997, p. 21)

An important part of the definition is the term “informed,” which is defined by SSHAC:

Regardless of the level of the study, the goal in the various approaches is the same: to provide a representation of the informed scientific community’s view of the important components and issues and, finally, the seismic hazard. (“Informed” in this sense assumes, hypothetically perhaps, that the community of experts were provided with the same data and level of interaction as that of the evaluators). (Budnitz et al., 1997, p. 26)

Thus there are two aspects of what constitutes an “informed” member of the technical community; the individual (1) is assumed to have knowledge of the project-specific and other relevant data, and (2) is assumed to have gone through the same interactive process that the evaluator experts have gone through in the project. Such an interactive process involves multiple workshops, structured interactions with proponents of alternative viewpoints to reveal the technical basis for various hypotheses, and feedback cycles to understand the implications of all technical assessments and associated uncertainties. The Technical Integration (TI) Team carries the responsibility of representing the center, body, and range of the views of the informed technical community.

“The center, the body, and the range” is taken to mean an appropriate representation of knowledge and uncertainty in the important components to a hazard assessment and is referred to by the SSHAC as “the community distribution.” A proper representation of the community distribution as defined in SSHAC appropriately meets the requirements of the NRC’s seismic regulation, 10 CFR 100.23.

After a review of multiple SSHAC projects and lessons learned, the NRC (2011) revisited the terminology associated with the SSHAC goals and proposed alternative wording:

The key statement in the SSHAC guidelines, that encapsulates the ethos of the SSHAC approach, is as follows: “Regardless of the scale of the PSHA, study the goal remains the same: to represent the center, the body, and the range that the larger informed technical

community would have if they were to conduct the study” (NUREG/CR-6372). For brevity, the “center, body, and range of the informed technical community” is denoted CBR of the ITC. A key word in the concept is “informed,” which is specifically defined in the SSHAC guidelines to mean an expert who has full access to the complete database developed for a project, and has fully participated in the interactive SSHAC process. In other words, the selected experts who participate in the PSHA study must endeavor to represent “*the larger informed technical community*” by assuming the hypothetical case where the others in the larger technical community become “informed” through participation in the same process. The SSHAC guidelines recognize that this is a hypothetical exercise, but the goal would be to ensure that a broad range of views are considered. In practice, however, the term “informed” is often either ignored or misinterpreted as simply meaning expert in the field of interest. Thus, the process of capturing or representing the CBR of the ITC has been viewed by some as a process of somehow conducting a poll or surveying the larger community for their opinions.

In the spirit of maintaining the fundamental SSHAC objective and clarifying the concept with terms that reflect actual practice, an alternative statement of the fundamental objective of the SSHAC process is presented in this report. This alternate description explains that the objective of the SSHAC guidance is actually achieved through a two-stage process of *evaluation* followed by *integration*. Therefore, consistent with the original intent of the SSHAC guidance, we recast the goals of the SSHAC process in terms of the two main activities (i.e., evaluation and integration) by the following statement:

The fundamental goal of a SSHAC process is to carry out properly and document completely the activities of evaluation and integration, defined as:

Evaluation: The consideration of the complete set of data, models, and methods proposed by the larger technical community that are relevant to the hazard analysis.

Integration: Representing the center, body, and range of technically defensible interpretations in light of the evaluation process (i.e., informed by the assessment of existing data, models, and methods).

In light of these definitions, we propose that it is clearer to refer to the CBR of the “technically defensible interpretations” (TDI), instead of CBR of the ITC. However, it is important to emphasize that the careful evaluation of the larger technical community’s viewpoints remains a vital part of the SSHAC process. We simply have removed the term “informed” because of its specialized definition in the original SSHAC guidelines. Similarly, we propose to replace the term “community distribution” that is used frequently in the original SSHAC guidelines to describe the outcome from a SSHAC assessment process with the term “integrated distribution.” This is to remove any perception that the final assessments and models were arrived at through a mere poll of the community.” (NRC, 2011)

As discussed extensively in the SSHAC report (Budnitz et al., 1997) and affirmed in NRC (2011), a SSHAC assessment process consists of two important sequential activities, which, for a Level 3 assessment, are conducted by the TI Team under the leadership of the TI Lead: *evaluation* and *integration*. Each activity is discussed below related to the particular CEUS SSC model-development activities that are entailed.

2.1.1 Evaluation

The TI Team evaluates relevant data, models, and methods that pertain to SSC inputs to a hazard analysis. The activities associated with evaluation are as follows:

- *Identify hazard-significant issues.* Hazard calculations and sensitivity analyses are performed at the beginning of the project to help steer the data compilation toward hazard-significant issues. After a preliminary model is developed, hazard calculations are done again to evaluate hazard sensitivity for feedback.
- *Identify and compile project-specific data in a database.* The project database is a fundamental tool with which the TI Team makes its evaluations. Workshop #1 helps in the data identification process as resource experts are assembled, and contacts with the larger technical community are made outside the workshop throughout the evaluation process.
- *Collect new data.* If resources allow, new data may be gathered that address particular SSC issues.
- *Conduct and document the data evaluation process.* A comprehensive review of pertinent data is conducted to identify their relevance to SSC (Data Summary tables) and to evaluate the data relative to their use in the SSC model (Data Evaluation tables). The data evaluation process continues throughout the integration process.
- *Evaluate alternative data, models, and methods that exist within the technical community.* The purpose of this evaluation is to gain a clear understanding of the data, models, and methods that have been proposed in the community, including their technical bases, strengths, weaknesses, and uncertainties. Facilitated discussions among proponent and resource experts can help with this in Workshop #2 and other communications outside the workshop. It is important to focus the discussions on the specific issues of importance to SSC.

2.1.2 Integration

Integration is model-building by the TI Team to arrive at a defensible expression of knowledge and uncertainty in inputs to SSC. This includes the full expression of the model elements (logic tree branches), their relative weights, and the range of credible uncertainties. The activities associated with integration are as follows:

- *Understand expert assessment issues:* The TI Team must understand the tools and issues associated with quantifying epistemic uncertainty and aleatory variability. It must also understand—and counter—common expert assessment issues (anchoring, availability, and other cognitive biases).
- *Develop SSC models:* The TI Team must identify technically defensible conceptual models and parameter values and include them in the SSC logic tree. Weights are assigned that reflect the degree of support for the models and parameter values in the available data and current technical understanding. The TI Team can develop new and innovative models to explain the available data, and it can develop new methods for analyzing the data and building the models, as long as the methods are consistent with the goal of expressing knowledge and uncertainties about the key issues. This activity is done at least twice: once

for a preliminary SSC model and again for the final SSC model. For the CEUS SSC Project, model-building occurred four times: for the SSC Sensitivity model, SSC Preliminary model, Draft SSC model, and Final SSC model.

- *Perform hazard sensitivity calculations and collect feedback:* These are run based on the preliminary SSC model developed by the TI Team in order to identify the most significant model elements and the importance of the uncertainties to the hazard results. These are provided as feedback and were discussed at Workshop #3. Hazard calculations and sensitivity analyses are also conducted, based on the final SSC model, to provide additional understanding of the model components and associated uncertainties.
- *Document the bases for the assessments:* The TI Team is responsible for documenting activities so that the reader can understand the basis for the model elements and the expressions of uncertainty made (weights on tree branches, parameter distributions, etc.). New data gathered for the project, along with new models and methods developed by the TI Team, impose the burden of high levels of documentation in order for reviewers of the report to understand their technical basis and application.

As noted previously, the evaluation and integration process is sequential during the SSHAC assessment process. During the *evaluation* phase, the applicable data are compiled and evaluated and the views of the technical community—expressed by proponent and resource experts—are duly considered. During the *integration* phase, models are developed by the TI Team as part of the evaluation process. Integration does not entail a poll or vote of the views of the larger technical community. It is model-building by the TI Team that is informed by its careful evaluation of all applicable data, its knowledge of the views of the community on certain issues, its discussions in workshops, and its direct communication with members of the community. The TI Team constructs an integrated model, usually expressed as a logic tree, which reflects knowledge and uncertainties in models and parameter values.

2.2 Roles of CEUS SSC Project Participants

The roles that various participants play in a SSHAC assessment process are important and are defined specifically in the SSHAC guidelines (Budnitz et al., 1997). The CEUS SSC Project was conducted in accordance with SSHAC guidelines for Level 3 projects, which explicitly define the roles of project participants who contribute to a PSHA project. Beginning with the review of the Project Plan at the Kick-Off Meeting on May 8, 2008, all project participants were informed of their expected roles before their participation, and they were reminded of their roles at the beginning of each workshop, at working meetings, and at other opportunities throughout the project. Table 2.2-1 identifies the meetings that were conducted during the course of the project, including the participants and meeting dates. SSHAC descriptions of the Project Sponsor; Project Manager; Technical Integrator; resource, proponent, and evaluator experts; and participatory peer reviewers are described below. NRC (2011, Section 3.6) provides additional discussion of these roles and responsibilities in a review of projects conducted using the SSHAC guidelines. Organization for the CEUS SSC Project, including its structure and lines of communication within that structure, is explained in Section 2.3.

The *Project Sponsor* is the entity that provides financial support for a project and “owns” the results of the study in the sense of property ownership. The CEUS SSC Project has three

sponsors: the NRC, DOE, and EPRI. The *Project Manager* is defined as the individual responsible for maintaining project scope, budgets, and schedules and coordinating communications among the project participants and the Project Sponsor(s). The *Technical Integrator* is defined as a single entity—e.g., an individual or team—that is responsible for conducting the evaluation and integration processes. As discussed in Section 2.1, a Level 3 assessment includes evaluation and integration by a TI Team under the technical leadership of the *TI Lead*.

Three types of experts having distinctive roles are identified in a SSHAC assessment process: resource experts, proponent experts, and evaluator experts. A *resource expert* is a technical expert with specialized knowledge of a particular data set, model, or method of importance to the hazard analysis. The expertise may be in the form of site-specific experience, or knowledge of particular methodologies or procedures. A number of resource experts participated in Workshop #1 and summarized their data sets. In addition, a number of resource experts were contacted outside the workshop environment to provide their data and expertise (Table 2.2-2). A *proponent expert* is an expert who advocates a particular hypothesis or technical position. At Workshop #2, several proponent experts presented their tectonic hypotheses to the TI Team and debated the merits of their models. The workshop also provided the opportunity for the TI Team to question the proponent experts regarding the technical support and uncertainties associated with their models. An *evaluator expert* is an expert who can evaluate the relative credibility of multiple alternative hypotheses to explain a given set of observations. Each evaluator expert uses professional judgment to quantify uncertainties, based on review and evaluation of all potential hypotheses and available data. An evaluator may challenge a proponent's position and question the technical basis for conclusions as a means of gaining insight into the uncertainties.

The members of the CEUS SSC TI Team were charged with fulfilling the roles of evaluator experts. At the outset of their participation on the project, the Team members were instructed in working meetings, and later reminded at workshops, that their role as evaluator experts would entail an objective evaluation and integration process, as described in Section 2.1 of this report. The need for removal of a member who would not assume the proper evaluator expert role was described, as was the process that would be followed by the TI Lead to carry out the removal, should it be necessary. The TI Lead is responsible for ensuring that all TI Team members know their roles as evaluators and that they maintain those roles throughout the course of the project.

Peer review is considered a key aspect of the Level 3 assessment process. This is to ensure that the process followed is adequate, uncertainties are properly considered and incorporated into the analysis, and the results provide a reasonable representation of the diversity of views of the technical community. *Technical peer review* is the review of the earth sciences aspects of a study, including a review to ensure that all applicable technical hypotheses have been considered. A review of how the study is structured and executed is referred to as a *process peer review*. Two different methods for peer review are described in SSHAC. *Participatory peer review* is defined as an ongoing or continuous process that provides the peer reviewers with full and frequent access throughout the entire project, in contrast to a late-stage peer review that occurs when a project has almost been completed. The principal benefit of a participatory peer review is that if problems are discovered, the opportunity exists for a mid-course correction without the need for work to be substantially redone at the end. SSHAC strongly recommends the use of a participatory peer review for both technical and process reviews for projects in

which a Level 3 approach is used. Accordingly, a participatory peer review process was used on the CEUS SSC Project.

2.3 CEUS SSC Project Organization

The project organization is shown on Figure 2.3-1, and the functions are summarized below.

Project Sponsors: The CEUS SSC Project was jointly sponsored by the DOE, NRC, and utilities and vendors under the auspices of the EPRI Advanced Nuclear Technology (ANT) program, Action Plan Committee (APC). The joint sponsorship of the study by both public and private sector representatives is unique for regional seismic hazard assessments in the United States. It signifies the recognition by the multiple parties that they have common needs—a fully defensible seismic source model that can be used for nuclear facility sites throughout the CEUS—and common goals of seismic hazard inputs that are stable and long-lived. Sponsor representatives were present at all workshops and key project meetings.

Project Management: Project management responsibilities were divided between those related to contract management; technical communication with sponsors, the TI Lead, and the PPRP; and those related to scope, budget, and schedule. EPRI assumed responsibility for contract management and provided the fundamental interface for contracts. These responsibilities included contracting with sponsors and CEUS SSC Project participants, providing support for workshops, and establishing requirements for the project report and website. The Project Manager was responsible for developing the project plan; communicating with the sponsors, TI Lead, and the PPRP; and developing project tools for maintaining project scope, budgets, and schedules. The lines of communication for the project are shown on Figure 2.3-2. Jeffrey F. Hamel, EPRI ANT Program, communicated directly with the CEUS SSC Project Manager, Lawrence A. Salomone. Mr. Salomone, who established the industry-government partnership for the CEUS SSC study, was the principal interface with the TI Lead, the PPRP, and the project sponsor representatives (Figure 2.3-2). He assisted EPRI management in establishing and maintaining project budgets and schedules and preparing status reports, and he had primary responsibility for the delivery of all technical products. He was the principal spokesperson to the outside community, which included the DOE, NRC, USGS, and industry.

Participatory Peer Review Panel (PPRP): Members of the PPRP were responsible for reviewing both the technical and process aspects of the CEUS SSC Project. They were observers at the majority of the technical meetings held during the course of the project (see Table 2.2-1). They attended all project workshops and provided feedback and written comments after each workshop. They attended 8 of the 11 TI Team working meetings to observe the process and progress of the project. They also attended three PPRP briefings to review in depth the technical assessments being made by the TI Team at key points during the study. A fourth PPRP briefing, the closure briefing, was held to bring closure to the entire project review process. Throughout the project, the PPRP provided verbal and written comments that assisted the TI Team in carrying out its assessments. PPRP responsibilities included reviewing and providing written comments on the Project Plan and reviewing both the Draft Project Report and the Final Project Report developed by the TI Team.

Technical Integration (TI) Team: The TI Team, led by Kevin J. Coppersmith, had primary responsibility for developing and documenting the technical basis for all project assessments and

products, as described in Section 2.4. The 12-member TI Team was responsible for implementing the SSHAC Level 3 methodology throughout the project, including all key assessment steps of evaluation and integration. Such steps include working with the Project Manager to develop the Project Plan, developing the project database, conducting three workshops, facilitating the requisite expert interactions, conducting 11 working meetings, communicating with the PPRP, and documenting all process and technical aspects of the study in a project report. Members of the TI Team and the Project Manager wrote the project report.

Database Manager: The Database Manager was responsible for retrieving and compiling applicable data for use in developing the SSC model. These data sets were provided in the formats appropriate for use in the TI Team’s deliberations. The Database Manager provided support for resolving copyright issues, working meetings, workshops, and PPRP briefings, as needed.

Technical Support: The TI Team was assisted in a number of areas by several individuals. The technical support team provided support to the hazard calculations, interpretations of the paleoliquefaction database, compilation of the geophysical databases, assistance with graphics and GIS, and development of workshop summaries and the project report.

Resource Experts, Proponent Experts, Specialty Contractors, and Other Project

Participants: A large number of representatives of the larger technical community participated in the project as resource experts, proponent experts, and specialty contractors. Steps were taken by the TI Team, as supported by the PPRP, to ensure that the participation of resource experts and proponent experts in Workshops #1 and #2 was appropriate and complete in order to be representative of the range of current scientific community interpretations, for which awareness and knowledge were required. The PPRP reviewed the list of resource experts and proponents selected for Workshop 1 and Workshop 2, respectively. *Specialty contractors* were engaged on the project to provide certain technical products, including geophysical maps, stress interpretations, and guidance for the assessment of paleoliquefaction. Personnel from the USGS played an extended role in this project to ensure that all supportable interpretations of the scientific community were fully identified, evaluated, and represented in the SSC model. Several USGS personnel provided detailed review and feedback on specific issues (e.g., the earthquake catalog, Mmax, and methods), which were considered in the assessment of the SSC model by the TI Team.

Technical knowledge and experience on specific topics of discussion were provided at the workshops by resource experts and proponent experts. The workshops provided an important opportunity for the TI Team evaluators to gain knowledge regarding specific databases in Workshop #1 and to question and challenge the findings of the proponent experts in Workshop #2. Table 2.2-2 provides a list of the resource experts who gave presentations at Workshop #1 and the proponent experts who participated in Workshop #2. Throughout the project, a number of technical experts provided their insights, data, and viewpoints at the request of members of the TI Team. These individuals are listed in Table 2.2-2. Their participation was invaluable in keeping the TI Team abreast of current data, models, and methods and for providing a basis for assessing the technical bases and uncertainties associated with recent and ongoing studies in the technical community.

2.4 Key Tasks and Activities

As outlined at the beginning of the project in the Project Plan, the CEUS SSC Project was structured around a set of tasks and activities that would fulfill the requirements of a SSHAC Level 3 project (Coppersmith et al., 2010). The key tasks and activities that define the CEUS SSC Project are described in this section. The components of a typical SSHAC Level 3 or 4 project and their interactions are illustrated on Figure 2.4-1.

2.4.1 Database Development

A fundamental resource developed as part of the CEUS SSC Project is the project database. The database mainly provides information for the use of the TI Team in its evaluation and integration processes. Most of the database consists of publications from the professional literature, maps, and similar documents. To respond to project needs, many of the maps in the database were entered into a GIS format. All documents were entered in a format that allowed them to be displayed, geo-registered, and superposed for the consideration of the TI Team in working meetings. A summary of the project database is given in Appendix A, and a description of the data is provided in the metadata files, which provide a means of searching by data type.

Although the major data compilation effort occurred early in the project, the project database continued to be developed throughout the course of the project. Identification of the data sets that populate the database began at project initiation, based on the SSC experience of the TI Team members. More data sets were identified in Workshop #1 (Significant Issues and Data). Resource experts who participated in the workshop presented their own specific data and, after the workshop, they provided lists of recommended references for consideration by the project. Throughout the course of the project, members of the TI Team communicated with a large number of researchers in the technical community and continued to identify data that were in the process of being developed and could be included in the project database. To supplement the existing data, certain new data were compiled for use by the project, including gravity maps, magnetic anomaly maps, an update to the U.S. stress map, and a compilation of paleoliquefaction data. In addition, a new earthquake catalog was developed using existing catalogs and new magnitude conversions and other updates (see Chapter 3). No new data were collected (e.g., field geologic investigations, geophysical surveys) as part of the CEUS SSC Project.

The database is considered a deliverable of the project, and it has been placed in a format that will allow it to be used by researchers in the future via a dedicated website www.ceus-ssc.com.

An allied activity to the development of the database development was the development of a conceptual SSC framework, which is documented in Chapter 4. The framework was developed in light of the knowledge and understanding of earthquake processes in the technical community, the experiences of the TI Team in characterizing seismic sources in the CEUS and other stable continental regions (SCRs), and suggestions and feedback from members of the PPRP. Among other things, the conceptual SSC framework provides a documented approach to identifying relevant data, evaluating those data for their specific use in the SSC model, and defining seismic sources according to a prioritized set of criteria that are hazard-informed. The conceptual SSC framework, which was developed early in the project and reviewed by the PPRP and during Workshops #1 and #2, provided a basis for all the evaluation and integration activities conducted by the TI Team.

2.4.2 Identification of Significant Issues

SSC for purposes of a PSHA is a specialized activity, and the technical issues within SSC that are important to seismic hazard are a subset of the larger range of issues that define seismologic, geologic, and tectonic interpretations. To provide a focus on the data, models, and methods of greatest importance to the hazard, sensitivity calculations were conducted. The experience by the TI Team gained from past seismic hazard analyses was also considered in the identification of hazard-significant issues. Workshop #1 was partially devoted to the identification and discussion of the technical SSC issues of greatest significance to a PSHA conducted for purposes of the design and review of nuclear facilities. The goal in that discussion was to focus on the data that would be most useful in defining the SSC model at the annual frequencies of interest (e.g., 10^{-3} to 10^{-7} /yr) for nuclear facilities. For example, data were identified that would be important to constraining maximum magnitudes, paleoseismic recurrence estimates, and the recurrence rate of larger-magnitude earthquakes. Likewise, information was identified that could be used to quantify the uncertainties in these assessments, such as the characteristics of global SCR earthquakes, age estimates of paleoseismic earthquakes, and uncertainties in earthquake catalog completeness as a function of location, time, and magnitude.

Also, as discussed in Chapter 4, throughout the project an effort was made to keep the project “hazard-informed” in the sense that highest priority would be given to the issues having the most significance to the hazard results. The goal was not to eliminate issues but to ensure that those issues of highest significance were adequately addressed. This is especially important in a regional study of this kind that includes extensive earth sciences data sets developed for a variety of purposes by numerous researchers.

2.4.3 Workshop #1—Key Issues and Available Data

The goals of Workshop #1 were as follows:

- Introduce the participants in the project to the goals, expectations, and schedule for the project.
- Identify the key issues that would need to be addressed in the course of the SSC.
- Review the available data, including data quality.
- Identify the path forward for the project.

The workshop began with a description of the importance of the CEUS SSC Project to groups involved with the nuclear industry, including utilities, regulators, and oversight groups. By assembling a single team of experts to develop a new and stable CEUS SSC, the science for seismic hazard assessment would be advanced, plus there would be cost and schedule-related benefits for existing and planned nuclear facilities. An explanation of SSHAC assessment process goals, study levels, and responsibilities was provided. This included a discussion of the roles of the TI Team members as evaluator experts. The Team was reminded, as they were in all subsequent workshops and working meetings, that they were expected to be objective evaluators of the available data, models, and methods. They were also reminded that the SSHAC assessment process would entail both evaluation and integration, as defined in the SSHAC guidelines.

Three questions are involved in defining SSC: Where will future earthquakes occur? How large will they be? and How frequently will they happen? The scientific assessments needed for SSC were described, including quantification of uncertainties, and examples from projects conducted in the United States and other countries.

The first session of the workshop focused on a review of the technical issues of importance to the CEUS SSC Project in the context of preparing a PSHA. The sensitivity of seismic hazard results to input parameter choices and associated uncertainties was discussed for several localities, including the New Madrid and Charleston regions. Defining and properly considering sensitivities is an important goal of the project. It was noted that for seismic sources having potentially large earthquake magnitudes (e.g., New Madrid and Charleston regions), assessments of parameters such as characteristic magnitude distributions and source zone locations are particularly important because these sources could potentially affect local and distant sites.

The next session of the workshop focused on data that are available and that may be useful in addressing the key issues discussed in the previous session. The structure of the database being developed for the project was described. Additional analysis was planned for some data sets to make them more useful for the project. After hearing a review of the data documentation process and a brief description of the data sets that had been compiled, workshop participants considered possible gaps in the available data sets.

The bulk of the workshop focused on data and information that could potentially be used for SSC in the CEUS. Data presentations were made by resource experts who had been involved in the development of pertinent databases. Before the workshop, the TI Team reviewed the data being compiled in the database and identified resource experts to participate in the workshop (Table 2.2-2). The list of resource experts was reviewed by the PPRP to ensure that a broad spectrum of experts from the scientific community were identified. Although it is not possible to allow the participation of all resource experts in the technical community, the TI Team identified a representative group of participants from the spectrum of disciplines that are important to seismic source characterization. Those resource experts who were not already participants in the workshop were contacted by TI Team members to discuss their data and gain access to it. Members of the community who provided their data and interpretations are listed in Table 2.2-2.

At the workshop, the resource experts had been asked to focus on data accessibility, formats, and applicability. While first-order interpretations of data were provided, discussions of alternative interpretations and models of the data were kept to a minimum for this workshop. First, presentations were given on gravity data, magnetic data, and a global seismic refraction catalog. Next, the complexities of the origins of earthquakes within stable continental regions were described, as were tectonic features of the Precambrian basement in the Midcontinent, in situ stress and earthquake focal mechanisms, strain fields in the Eastern United States, and paleoliquefaction at localities within the CEUS. The final session of the workshop was focused on the seismicity catalog to be compiled, including the primary sources of earthquake data and the plans to identify dependent events and to assess catalog completeness. Presentations were also made on the approaches used to develop the USGS catalog and selected regional catalogs, including work to identify historical earthquakes.

Workshop #1 was documented on a CD. The CD, which contained the agenda, presentations, a workshop summary, a list of participants, the PPRP letter report, and a photo album of

participants, was distributed to all participants; the contents are posted on the EPRI website. The TI Lead and Project Manager hosted a half-day briefing for international observers and young professionals prior to the workshop to improve their understanding of the context of the workshop and its role in the SSHAC assessment process.

2.4.4 Workshop #2—Alternative Interpretations

The goals of Workshop 2 were as follows:

- Review the project SSHAC Level 3 methodology, ground rules, expert roles, and peer review processes.
- Provide an opportunity for the project (TI) team to understand proponent views on important technical issues.
- Discuss the range of alternative views and uncertainties within the larger technical community.
- Discuss the path forward for the project.

The goals of the workshop were accomplished by a series of presentations and discussions designed to provide the TI Team with information it would need to develop a preliminary SSC model. In the development of this model, the knowledge and uncertainties in available data, models, and methods must be taken into consideration. A series of workshop presentations were made by proponent experts who had been asked to provide their views on key technical issues posed in written questions from the TI Team that were provided to each proponent before the workshop. The proponents were also asked to include discussions of the uncertainties associated with their views. The workshop provided an important opportunity for the TI Team to gain a better understanding of the community's views, to directly question the experts regarding the technical bases for their interpretations, and to debate alternative viewpoints regarding key SSC issues. In several cases, the proponent experts were encouraged to debate the pros and cons of their hypotheses among themselves in a facilitated format, thus allowing the TI Team to understand the key technical bases and uncertainties associated with the alternative models.

Before the workshop, the TI Team reviewed those data, models, and methods being proposed by the technical community having relevance to SSC in the CEUS. The team then identified members of the community who would provide a summary of their viewpoints during the course of the workshop. The list of proponent experts was reviewed by the PPRP to ensure that a broad spectrum of views in the scientific community were represented. Representatives from the USGS were also asked to provide their views on whether there were additional models or methods that should be represented. Those proponent experts are identified in Table 2.2-2. Although it is not possible to allow the participation of all proponent experts in the technical community, the TI Team identified a representative group of participants from across the spectrum of applicable data, models, and methods of importance to the CEUS seismic source characterization. Those proponent experts who were not already participants in the workshop were contacted by members of the TI Team to gain access to their published and unpublished interpretations, and an understanding of their viewpoints and the uncertainties in their interpretations. Members of the community who participated in providing their interpretations are identified in Table 2.2-2.

After the introductory session of the workshop, presentations were made on the following topics:

- Seismicity and seismic parameters, including maximum magnitudes, in selected areas of the CEUS (e.g., the Charlevoix and lower St. Lawrence Seaway regions).
- Tectonic features throughout the CEUS, including neotectonic features in the Appalachian Piedmont, Ouachita sub-detachment structures, rifts in the Midcontinent, faults and folds in the Illinois Basin, and Quaternary deformation features in the New Madrid region.
- Paleoliquefaction evidence throughout the CEUS, including in the Mississippi Valley and the Wabash Valley, and methods for quantifying uncertainties in paleoliquefaction studies.
- Alternative interpretations of the state of stress, strain, and earthquake hazards in the regions surrounding the epicenters of the large-magnitude New Madrid and Charleston earthquakes.
- Seismic sources in the Gulf of Mexico.
- Source model features of the 2008 USGS national hazard maps for the CEUS, focused on source characterization in the New Madrid and Charleston.

During the course of these presentations, facilitated discussions occurred, focused on implications to SSC for hazard analysis, including the conceptual models that would represent the range of interpretations and the degree of support of the models based on available data. Proponents provided all references related to their work after the workshop.

Workshop #2 was documented on a CD. The CD, which contained the agenda, presentations, a workshop summary, a list of participants, the PPRP letter report, and a photo album of participants, was distributed to all participants; the contents are posted on the EPRI website. The TI Lead and Project Manager hosted a half-day briefing for international observers and young professionals prior to the workshop to improve their understanding of the context of the workshop and its role in the SSHAC assessment process.

2.4.5 Working Meetings

Although the workshops provided an opportunity for the TI Team to consider and discuss a variety of topics, much of the actual SSHAC assessment processes of evaluation and integration occurred at the working meetings that took place between and after the workshops. Eleven working meetings were held with the entire TI Team (Table 2.2-1), most meetings typically lasting two to three days, and many other subgroup meetings, webinars, and conference calls were held to discuss and resolve the numerous technical issues associated with the project assessments. Each working meeting was focused on one or more agenda items that required attention by the TI Team, including the following:

- Identification of potential participants at workshops, including resource experts at Workshop #1 to discuss their data sets, and proponent experts at Workshop #2 to discuss their alternative models and methods.
- Development of a conceptual SSC framework and the associated master logic tree.
- Approaches to developing the Data Summary and Data Evaluation tables.
- Issues associated with the new earthquake catalog.

- Alternative approaches to Mmax assessment and updates to the Bayesian approach and their implications.
- Approaches to spatial smoothing.
- Defining and characterizing repeated large-magnitude earthquake (RLME) sources.
- Use of the paleoseismic data to define the size and recurrence of RLME sources.
- Renewal vs. Poisson recurrence models.
- Alternatives to seismotectonic zones.
- Structure of logic trees, alternatives to include as logic tree branches, and weights on branches.
- Hazard feedback and recurrence sensitivity analyses.

Much of the planning for the workshops in terms of developing the agendas and identifying participants was conducted in the working meetings. This allowed the entire TI Team to consider the larger technical community and ensure that a representative cross section of experts was asked to participate in the workshops. Although the workshops provided a forum for interaction among the large number of resource and proponent experts who participated, additional contacts were made with members of the larger technical community outside the workshops (see Table 2.2-2); the working meetings provided the opportunity for all TI Team members to discuss the results of those additional communications. At the same time, the TI Team members devoted considerable effort to completing their Data Evaluation and Data Summary tables that document the data, models, and methods that were considered. These are provided in Appendices C and D.

The working meetings were typically held in a conference room environment, with the project database available at all times for projection and discussion. Working Meetings #10 and 11 were held using a conference-call/webinar format. One to three representatives from the PPRP attended 8 of the 11 working meetings in order to observe the deliberation and technical assessment processes (Table 2.2-1). Each working meeting ended with a set of actions for various members of the TI Team to pursue and to bring back to the entire team at the next meeting.

2.4.6 SSC Sensitivity Model Development

As discussed in Section 2.1, a SSHAC assessment process begins with *evaluation* of available data, models, and methods, followed by the *integration* process of model-building to incorporate knowledge and uncertainty. The integration process on the CEUS SSC Project occurred in four stages beginning with development of the “SSC Sensitivity model” and associated hazard calculations, development of the “SSC Preliminary model” and associated hazard calculations, development of the “Draft SSC model” and associated hazard calculations, and development of the “Final SSC model” and associated hazard calculations. As a tool to assist the TI Team in the development of its SSC model, a “conceptual SSC framework” was developed (Chapter 4) that provided a basis for documenting the data consideration and evaluation process, defining the key criteria for identifying seismic sources, and structuring the SSC model around a master logic tree. As the integration process ran through the four stages of SSC model development, the conceptual SSC framework provided a common structure for the TI Team.

A key part of a SSHAC Level 3 assessment process is the opportunity to receive and consider feedback about the implications of preliminary assessments. To do so, the SSC Sensitivity model was developed, which included a wide range of conceptual models and parameter values. Based on the conceptual SSC framework, a master logic tree was developed that describes the basic approaches and conceptual models for characterizing the spatial and temporal distribution of future seismicity. For example, the master logic tree for the SSC Sensitivity model included alternative approaches to the spatial characterization of seismicity, ranging from the smoothing of all past earthquakes to the identification of seismotectonic source zones. Paleoseismic data were included in the definition and characterization of RLME sources, and the background zones were defined based on observed seismicity. A key aspect of the SSC Sensitivity model was including models and parameter values that describe a wide range of uncertainty so that the feedback calculations could be carried out to show the relative importance of these assessments. The focus of the SSC Sensitivity model was not on the weights on the logic tree, but the range of branches on the logic tree in order to show their effect on the calculated hazard results and their potential contributions to uncertainty. These hazard calculations and sensitivity analyses were the subject of Workshop #3 Feedback.

2.4.7 Workshop #3—Feedback

The goals of Workshop 3 were as follows:

- Review the progress of the project in terms of meeting key milestones, such as development of the database and earthquake catalog.
- Review the SSHAC assessment process being followed.
- Discuss the seismicity catalog developed for the CEUS SSC Project.
- Discuss the seismic source characteristics of the SSC Sensitivity model.
- Present feedback to the TI Team and staff in the form of SSC sensitivity analyses and hazard sensitivity analyses.
- Identify the key issues of most significance to the SSC models.
- Discuss the analyses being conducted related to hazard significance.
- Discuss the path forward for the CEUS SSC Project.

These goals were accomplished by a series of presentations and discussions. Basic principles of the SSHAC assessment process and their implementation in the CEUS SSC Project were described. A discussion was presented on the TI Team's role in the *evaluation* process of evaluating the data, models, and methods of the larger technical community, and in the *integration* process of building models that represent current knowledge and uncertainties. Discussion was presented regarding the need to document the data, models, and methods that have been considered during the evaluation phase of the project. A case history was described that traced the CEUS SSC Project documentation of an alternative model that postulates that the New Madrid seismic zone will not be seismically active in the future. Proponents for these models participated in Workshop #2, they were contacted and responded to requests for their current relevant data and interpretations, Data Summary and Data Evaluation tables documented that the TI Team has considered the data and proponent views, a representation of the model

could be found in the SSC logic tree, and discussion of the proposed model would be documented in the project report in the description of seismic sources associated with the New Madrid seismic zone. It was concluded that there is clear documented evidence that the data and interpretations provided by the proponent experts were evaluated and documented appropriately by the TI Team.

Development of the CEUS SSC earthquake catalog was described next, including compilation and merging existing catalogs, magnitude conversions to define all earthquakes by moment magnitude, declustering, and assessment of catalog completeness. A preliminary earthquake catalog was completed for use in preparing the hazard sensitivity analyses to be discussed in the workshop. Representatives from the USGS were present at the workshop and were specifically asked to provide their views on the various aspects of the earthquake catalog. Maximum magnitude distributions under development for the CEUS SSC Project source zones were described. Representatives from the USGS also provided their views on the the maximum magnitude methodologies being used.

Hazard results for seven demonstration site locations were presented. The seismic sources contributing to the hazard, the various parameter estimation approaches used, and model sensitivity were discussed for each of the demonstration sites. Both RLME and regional source zones were described and the sensitivity results were compared. Based on these calculations and sensitivity analyses, a set of conclusions was drawn regarding the most important SSC issues that either contribute most to mean hazard or are important contributors to the uncertainty in the hazard. In addition to hazard sensitivity, calculated results were discussed pertaining to the SSC issues that contribute most to Mmax and earthquake recurrence. The outcome of these feedback studies was that the TI Team could set priorities for focusing on the SSC issues and uncertainties of most significance in developing the SSC Preliminary model.

Quantifying the precision of seismic hazard results in the CEUS was discussed in the next presentation. The purpose of the analysis described was to derive quantitative estimates of how seismic hazard results might change if studies were repeated by different researchers using the same basic information. This type of quantification gives an indication of how well the hazard is understood and how precise our calculated hazard values are. This can also provide information in the future on whether changes in hazard due to new findings should be considered significant. (A discussion of the hazard precision results and conclusions is given in Section 9.4.) The final workshop presentations focused on the path forward for the project, including how the project results will be used.

Workshop #3 was documented on a CD. The CD, which contained the agenda, presentations, a workshop summary, a list of participants, the PPRP letter report, and a photo album of participants, was distributed to each participant; the contents are posted on the EPRI website. The TI Lead and Project Manager hosted a half-day briefing for international observers and young professionals before the workshop to improve their understanding of the context of the workshop and its role in the SSHAC assessment process.

2.4.8 SSC Preliminary Model Development

After Workshop #3 and armed with the feedback information, the TI Team proceeded to develop the SSC Preliminary model. Unlike the SSC Sensitivity model, which contained a number of

elements strictly for purposes of sensitivity analysis, the SSC Preliminary model included a logic tree that was intended to represent knowledge and uncertainties, or the center, body, and range of technically defensible interpretations (NRC, 2011). The ranges of branches on the SSC logic tree and their relative weights assigned to the branches were developed by the TI Team through extensive discussions of the available data, models, and methods. The integration process requires that the Team members objectively evaluate the available information and define the center, body, and range of technically defensible interpretations. To do so, the Team was encouraged to consider all methods for uncertainty treatment (e.g., logic trees, continuous probability distributions) and, if desired, build new models to capture current knowledge and uncertainty. For example, strong belief that the available paleoseismic data related to the existence and location of RLMs are compelling led to spatial models that include these sources and that define the uncertainties in their geometry.

Alternative models regarding the spatial variations in M_{max} and future earthquake characteristics led to alternative models of seismic sources (e.g., M_{max} zones versus seismotectonic zones). Consideration of spatial variation of recurrence parameters led to the refinement of approaches to expressing spatial stationarity and the aleatory variability of future recurrence parameters through smoothing. The degree of support in the available data that the model elements hold were expressed as weights on alternative branches of the logic tree. Uncertainties in parameter values were expressed as probability distributions. The sequence of nodes within the logic tree expresses the dependencies of assessments from general conceptual models on the left to parameter distributions that define the models on the right.

2.4.9 Finalization and Review of SSC Draft and Final Model

After the SSC Preliminary model was developed, a second round of hazard calculations and sensitivity analyses was conducted to provide feedback to the TI Team. These analyses focused on the remaining issues of most importance to the model. The elements of the SSC Preliminary model were presented to the PPRP in a briefing as a means of keeping the PPRP informed of the TI Team's deliberations. During the briefing, the PPRP provided its comments on the key elements of the SSC model and identified key issues that required resolution as the model-development process continued. Another version of the earthquake catalog was developed, after incorporating comments provided by the USGS and other outside experts, and working meetings were held to finalize the SSC Draft model. Discussions focused on the most important technical issues, the weights on alternative elements of the logic tree, and the final quantification of uncertainties. For example, the issue of alternative approaches to maximum magnitude assessments was debated and a series of meetings and conference calls were conducted in order to consider the implications and relative defensibility of alternative conceptual models governing the M_{max} estimates. Consideration and discussion also centered on the most appropriate approaches to smoothing of recurrence parameters. The approach used (discussed in Section 5.3.2) allows for a number of assessments to be made (e.g., strength of the prior distribution on the a -, and b -values) and a number of sensitivity analyses were conducted in order to understand the implications of different aspects of the model, and to compare it to other smoothing approaches.

The SSC Draft model was completed and, as defined in the SSHAC guidelines, it is based on a systematic evaluation of the data, models, and methods proposed by the larger technical

community and an integration process that provides the TI Team's representation of the center, body, and range of technically defensible interpretations. The model was documented in a Hazard Input Document (HID) and Draft Project Report, which were issued to the PPRP and other groups for review (see Section 2.4.10).

In anticipation of detailed reviews, the TI Team continued its refinement of the SSC Draft model after submittal of the Draft Report and while it was being reviewed. A key issue concerned the assessments of earthquake recurrence, which showed for many sources that the "predicted" recurrence rate averaged over the source based on the smoothing approach adopted was overpredicting the rates of "observed" larger-magnitude earthquakes in the catalog. A number of exploratory analyses were conducted to shed light on the reason for this mismatch. Issues related to the earthquake catalog were considered, including the merging of multiple catalog sources, spatial variations in completeness, conversions of various magnitudes and intensity to moment magnitude, and declustering. At the same time, issues related to recurrence estimation were evaluated, including the use of various magnitudes in constraining the exponential recurrence distributions, the influence of the strength of the prior distribution on b -values, and the degree of spatial stationarity between the locations of large-magnitude earthquakes and future large-magnitude events.

As discussed in Section 2.5.2, the PPRP issued a comprehensive set of comments on the Draft SSC model and identified key issues that would require resolution in the development of the Final SSC model. Working Meeting #9 on February 7 and 8, 2011, was later conducted with observation by the full PPRP to review these last key issues associated with the earthquake catalog and the recurrence assessments. Working Meetings #10 and 11 were conducted using a webinar format to review the results of ongoing and exploratory work. A few remaining issues, many identified in the comments from the PPRP on the Draft Report, were also dealt with at this time, such as the bases for the weights given in the master logic tree and methods for assessing seismic crustal thickness.

The SSC Final model includes refinements that deal with the outstanding issues identified. For example, the refined model shows reasonable agreement between the recurrence rates for various seismic sources and the observed frequency of earthquakes. Likewise, the review of the catalog led to refinements of the spatial and temporal distribution of catalog completeness estimates. Also, conversions were refined to provide consistent estimates of intensity-to- m_b -to- M and intensity-to- M . Accordingly, the refined conversions could be used for moment magnitude estimates for the entire catalog and, in turn, the observed frequency of observed earthquakes was recalculated for all seismic sources. Hazard calculations were conducted using the refined SSC Final model and associated sensitivity analyses were carried out. These hazard results and sensitivity analyses are included in this report.

The refinements to the SSC model, associated hazard results, and revisions made to the project report were reviewed and discussed with the PPRP in a briefing held on June 21 and 22, 2011. The briefing provided an opportunity for the PPRP members to gain a full and complete understanding of the process and technical aspects of the project and to provide oral comments on the SSC Final model.

2.4.10 Documentation

The SSC Final model was documented in an HID (as was done earlier for the Draft SSC model and the Draft Project Report) to provide a basis for hazard calculations, and the Final Project Report was developed. The steps involved in this documentation are summarized below.

2.4.10.1 Development of the Hazard Input Document

Upon completion of the SSC Final model, the essential elements of the model were documented in the HID for the project (Appendix H). The HID is the key deliverable of the project that can be used for hazard calculations in the future. Specifically, this document is meant for the hazard analyst—providing clarity about the model to be implemented and obviating the need to distill the model from the full report. The HID helps ensure that implementation of the model, which can be challenging due to its size and complexity, is as intended. The technical assessments that constitute the SSC Final model are not justified or discussed in the HID. Rather, the HID includes the logic tree structure for all assessments, the associated branches and weights, and the output recurrence and Mmax distributions that are required for the PSHA. The technical justifications for the assessments in the HID are given in this project report.

2.4.10.2 Development of Earlier Draft Report

The Draft Project Report documented all the assessments made by the TI Team in 2010 and summarizes the methodology that was used to make the assessments. The Draft Report was developed by all members of the TI Team and the Project Manager. It summarized all the key process steps, discussed their consistency with a SSHAC Level 3 assessment process, provided a description of all key project deliverables, and provided a technical discussion and explanation for all elements of the SSC Final model. The appendices to the report provided project-specific documentation of key products such as the final HID, Data Evaluation and Data Summary tables, the project database including the earthquake catalog, and summaries of the workshops and project written communications. The goal of both the Draft and Final Project reports is to provide a self-contained complete description of all aspects of the project such that future readers of the report will understand the methodology, the technical elements of the SSC model, and the technical bases for all assessments.

2.4.10.3 Draft Report Review

Review of the Draft Report was conducted by the PPRP, sponsors, USGS, and other groups, and written review comments were provided to the TI Team for its consideration. The TI Team was instructed to give highest priority to the PPRP comments, but to consider all the reviewer comments in making revisions to the project report. All reviewer comments were considered by the TI Team, and the responses to reviewer comments were summarized in comment response tables. The goal of the report review process was to provide the PPRP and other stakeholders an opportunity to comment on the completeness, clarity, and consistency of the documentation of the SSC model. Consistent with its role within a SSHAC process, the PPRP provided its comments pertaining to both the documentation of the process followed in the project as well as the technical assessments included in the SSC model.

Review of the Draft Report by the sponsors was facilitated by briefings held with members of the TI Team and the NRC (on August 10, 2010); with the utilities (on November 4, 2010); and with the utilities, NRC, and DOE (held February 9–10, 2011). A Final Report was developed that reflects revisions made in light of reviewer comments as well as a description of all refinements made to the model by the TI Team after issuance of the Draft Report (described above in Section 2.4.9). The Final Report was issued to the PPRP and Sponsor reviewers in two installments, on June 16 and August 5, 2011, for their review and concurrence. To assist the review, a briefing was held with the PPRP to review all aspects of the SSC model and the report documentation (June 21–22, 2011).

2.4.10.4 Final Report Development

The fundamental bases for revisions to the Draft Report were the written comments provided by the PPRP and other reviewers. In addition, the TI Team recognized the need to refine certain elements of the SSC Draft model and improve the documentation of the process aspects and technical assessments made for the project. A systematic process was followed for responding to each of the reviewer comments to ensure that all comments were addressed. The Final Report was issued to the PPRP for its final review and concurrence, and a final PPRP closure briefing was held September 7–8, 2011.

2.5 Participatory Peer Review Panel

2.5.1 Roles and Responsibilities

SSHAC guidance specifies that if a PSHA project is to be successful, the crucial need for a strong peer review process cannot be overemphasized. The members of the PPRP met the SSHAC criteria that peer reviewers “must be ‘peers’ in the true sense: recognized experts on the subject matter under review” (Budnitz et al., 1997, p. 48). The purpose of peer review is to provide assurance of the following:

- A proper SSHAC Level 3 process has been followed.
- The diversity of views prevailing within the technical community has been considered.
- Knowledge and uncertainties have been properly quantified and incorporated into the analysis.
- Documentation is clear and complete.

The CEUS SSC Project used a *participatory* peer review process, which involved continuous review throughout all phases of the project. As recommended by the SSHAC guidelines, the PPRP was responsible for reviewing both the technical and process aspects of the project. The peer reviewers interacted frequently with the TI Team, provided formal written comments at regular intervals, and reviewed and approved the project report.

2.5.2 Reviews and Feedback

The purpose of a participatory peer review process, as opposed to a “late-stage” process, is to provide advice and recommendations during the course of the study and not just near the end. Such feedback is valuable to the TI Team and improves the focus and quality of the evaluation

and integration processes. For example, early in the project, the PPRP reviewed the Project Plan and provided its views on the planned work activities. Also, members of the PPRP identified data sets that could be considered by the TI Team. PPRP review comments were instrumental in the TI Team's developing a data documentation process—including Data Evaluation and Data Summary tables—that would benefit future users of the study. As another example, the PPRP provided its views on how feedback calculations should be considered by the TI Team and cautioned that the calculations should not limit the team's approach to representing the full range of legitimate views within the technical community. These reviews and recommendations were invaluable in assisting the TI Team in enhancing the assessment process being followed. The technical reviews also greatly assisted the team in focusing on key technical issues and ensuring a complete evaluation of all applicable data, models, and methods.

To assist in the PPRP's monitoring and review of the project, PPRP briefings were held with the TI Team on May 13, 2009; March 24, 2010; and June 21–22, 2011; as well as the final closure briefing September 7–8, 2011 (Table 2.2-1). These briefings served as opportunities for the PPRP to ask questions and gain clarification about the SSC Sensitivity model, SSC Preliminary model, SSC Draft model, and SSC Final model. They also provided the TI Team with feedback on the models and alerted the Team to the need to provide technical bases and documentation on the key technical assessments. In addition to the briefings, representatives from the PPRP were present as observers at 8 of the 11 working meetings of the TI Team. This provided the PPRP with additional perspective on the technical assessments being made by the TI Team.

In terms of written review of the project report, the PPRP provided an extensive set of comments on the Draft Report that addressed both technical issues and process issues. The TI Team members responded to all the comments and summarized their responses in Comment Reponse tables, which are included in Appendix I. After revision of the Draft Report in light of comments from the PPRP, as well as comments from the sponsors and other groups (i.e., Defense Nuclear Facilities Safety Board, USGS), a draft Final Report was issued. The PPRP then provided a detailed review of that document (see comments in Appendix I). The PPRP comments on the draft Final Report were defined as either “mandatory,” meaning that the review comments must be addressed by the TI Team in its final documentation of the project report, or “non-mandatory,” meaning that the comments are intended solely to help improve the Final Report.

2.5.3 Fulfillment of SSHAC-Prescribed Scope of Review of Both Technical and Process Issues

The SSHAC guidelines highly recommend that a participatory peer review process be followed and that the peer review process for a Level 3 project be directed at both the technical and process aspects of the study (Budnitz et al., 1997, p. 50). The “technical” aspects include the TI Team's evaluation process for considering the applicable data, models, and methods that exist within the larger technical community, and the integration process that represents the center, body, and range of technically defensible interpretations. The technical aspects require a high level of technical expertise on the part of the PPRP, while the process aspects require a knowledge and experience in the application of SSHAC assessment processes. “Process” aspects include carrying out all methodological steps, such as developing a project database, conducting workshops, developing feedback, encouraging technical interaction and debate, and documentation. The PPRP for the CEUS SSC Project included the requisite expertise and

experience to fulfill both aspects of its charge. Individual members of the panel are acknowledged experts in the technical fields related to SSC, and most members have had considerable project experience related to SSHAC studies or studies using similar methodologies (see Appendix G).

The final product of the SSHAC peer review process is a final closure letter from the PPRP providing its views on whether the TI Team has successfully implemented a SSHAC Level 3 process and whether, as a result, the technical assessments included in the SSC model are technically defensible and adequately documented. The PPRP was presented with the Final Report of the project as well as written comment response forms that documented the manner in which all written comments provided by the PPRP, sponsors, USGS, and other reviewers were addressed. To support its final review, a closure briefing was held with the PPRP on September 7 and 8, 2011. The final activity conducted by the PPRP was the development of its closure letter, which is included in this report.

2.6 Consistency of CEUS SSC Assessment Process with SSHAC Guidelines

The SSHAC Level 3 assessment process is a structured technical assessment process accepted in the NRC's seismic regulatory guidance for ensuring that uncertainties in data and scientific knowledge have been properly represented in seismic design ground motions. The TI Team is responsible for meeting and documenting these goals, and peer reviewers are responsible for evaluating whether these goals have been met. As an accepted expert assessment process that includes participatory peer review of both the process and technical aspects, the SSHAC Level 3 assessment process, if conducted properly, provides confidence that the data, models, and methods of the larger technical community have been considered and that the center, body, and range of technically defensible interpretations have been represented.

This section compares the process followed in the CEUS SSC Project with that prescribed in the SSHAC guidelines in order to draw conclusions about whether the SSHAC assessment process has been adequately followed. Chapter 4, *Methodology for Characterizing Seismic Sources*, of the SSHAC report (Budnitz et al., 1997) is the applicable section for evaluating the CEUS SSC assessment process. The SSHAC report devotes most of the methodology discussion to attributes of a Level 4 assessment process, with only minor attention given to the attributes of a Level 3 assessment process. Nevertheless, experience on projects conducted over the past 15 years has shown that the differences in the implementation of Levels 3 and 4 are small (mainly related to the assessment by individual evaluator experts rather than an evaluator team). Therefore, the methodology steps specified in the SSHAC guidelines for a Level 4 assessment for SSC (Budnitz et al., 1997, p. 70) can serve as the basis for comparison with the CEUS SSC assessment process.

The following discussion will first present the methodology steps exactly as given in the SSHAC guidelines, and then provide a summary of how each step was addressed in the CEUS SSC Project. Aspects of the steps that pertain to Level 4 projects are adjusted, as appropriate, to pertain to a Level 3 project.

The basic steps in the recommended methodology for SSC are given below in terms of the specific application to SSC.

1. Conduct careful expert selection. The process of expert selection should be based on a clear set of criteria aimed at capturing a full range of diversity of expert interpretations.

The members of the CEUS SSC TI Team were selected based on their experience and technical expertise. As a group, the Team's expertise spanned the wide range needed to conduct SSC, including the disciplines of geology, geophysics, tectonics, seismology, and hazard analysis. The team members are acknowledged experts in their respective fields and are thoroughly acquainted with the active researchers in those fields, as well as in the areas of important ongoing research. In addition to having disciplinary expertise, the TI Team had considerable experience in conducting an SSC for a PSHA. As a result, the team members understood the important issues for such an analysis as well as the current tools for uncertainty treatment.

In addition to the TI Team, a large number of representatives of the larger technical community participated in the project as resource experts, proponent experts, and specialty contractors. Steps were taken by the TI Team, as supported by the PPRP, to ensure that the participation of Resource Experts and Proponent Experts in Workshops #1 and #2 was appropriate and complete in order to be representative of the range of current scientific community interpretations. Specialty contractors were engaged on the project to provide certain technical products, such as geophysical maps, stress interpretations, and guidance for the assessment of paleoliquefaction. Personnel from the USGS played an extended role in this project to ensure that all supportable interpretations of the scientific community were fully identified, evaluated, and represented in the SSC model. Several USGS personnel provided detailed review and feedback on specific issues (e.g., the earthquake catalog, Mmax, and methods), which were considered in the assessment of the SSC model by the TI Team.

2. TFI role. The technical facilitator/integrator should play a strong role, running workshops and expert interactions, monitoring the behavior and participation of the experts, conducting calculations and sensitivity analyses, documenting the final results, and taking intellectual responsibility for the results of the project.

The SSHAC Level 3 equivalent of the TFI is the TI Lead, who has technical responsibility for the assessment, leads the TI Team, and works with the specialty contractors charged with certain activities (e.g., hazard calculations, database management, report production). For the CEUS SSC Project, the TI Lead was responsible for organizing all workshops, working meetings, and PPRP briefings. The TI Lead also was responsible for establishing the SSHAC ground rules for all these interactions and for ensuring that all project participants understood and abided by their particular SSHAC-prescribed roles. Throughout the assessment process it was emphasized to all TI Team members that they would be required to assume intellectual ownership of all aspects of the SSC model. The TI Lead was responsible for organizing the report preparation process and for ensuring completeness and consistency in the contributions from the various team members.

3. Provide a uniform data base to all experts. SSC-related data sets, as defined by the experts themselves, should be provided to all of the experts in formats most useful to the experts.

From the outset of the CEUS SSC Project, database development was a strong focus. An earthquake catalog was developed from a variety of sources, and considerable effort was associated with providing an estimate of moment magnitude for all earthquakes in the catalog. An accessible database was developed for use by the TI Team that was derived from both existing information and newly compiled data sets, including GIS-based components such as

magnetic anomaly, gravity, and stress data. *Workshop #1—Significant Issues and Available Data* was devoted to the identification of available data that would be specifically applicable to addressing the key SSC issues. A number of resource experts with knowledge of applicable data sets made presentations on their data sets and provided a basis for the project data development process. The resource experts provided information related to the quality of the data, their formats, and the history of data development in key regions throughout the CEUS. In addition to the geophysical data sets, the project also sponsored the compilation and evaluation of paleoseismic data because of the importance of that data to the identification and characterization of seismic sources in the region.

As part of the Conceptual SSC Framework for the project (see Chapter 4), a process was instituted for documenting the data that were considered by the TI Team in its evaluations. First, in a “generic” table that is generally applicable to the entire study region, the applicable types of data were identified that have potential use in SSC. Then all data that were considered for particular subregions or source zones were identified in Data Summary tables, which include a description of each data source’s relevance to SSC. Then, for those data that are used in the source characterization process, Data Evaluation tables for each seismic source were developed that provide an evaluation of the quality of the data and degree of reliance given to each data source in the source characterization process. The goal of these tables is to provide clear documentation of the data sets that were available to the TI Team at the time of its evaluations; the tables also provide an evaluation of the data relative to their specific use on the CEUS SSC Project.

The Data Summary and Evaluation tables are viewed by both the TI Team and the PPRP as critical to the success of the project. This is the first project to rigorously and systematically document this information, and it is viewed by the PPRP as essential information to support the descriptions and discussion found in Chapters 6 and 7. Early in the project, the PPRP encouraged the TI Team to create a system that would more effectively document the data identification and data evaluation processes, and the TI Team developed the format for the Data Summary and Data Evaluation tables. It is expected that the structure of these tables will provide a valuable methodology step for future SSHAC Level 3 projects.

4. Conduct multiple expert interactions. Interaction among SSC experts is strongly recommended, through such vehicles as workshops, small working meetings, etc.

The heart of the SSHAC assessment process is technical expert interaction. These interactions allow the TI Team members to carry out their evaluation and integration processes, including identifying and evaluating data; witnessing the debate of alternative hypotheses by members of the technical community; challenging the views of proponent experts in order to understand the uncertainties; developing models that portray the knowledge and uncertainties in SSC model components; considering feedback related to preliminary assessments; and arriving at an integrated model that represents current knowledge and uncertainties. Considerable learning and reexamination of held views occurs and is encouraged during the course of these interactions. The CEUS SSC Project took full advantage of this notion in conducting three topical workshops, 11 working meetings, four PPRP briefings, and three meetings to brief the international observers and young professionals attending the workshops. In addition, numerous subgroup meetings, conference calls, and webinars were held among the TI Team members during the course of the development of the SSC Sensitivity model, the SSC Preliminary model, the SSC

Draft model, and the Final SSC model. Each interaction was structured and facilitated to focus on the goals of the SSHAC assessment process, and participants were reminded of their roles and responsibilities within that context.

In addition to the interactions among the TI Team members, all members interacted extensively with members of the technical community through personal visits, e-mails, telephone calls, and attendance at professional society meetings. Such communication allowed team members to be apprised of current research and to gain an understanding of the uncertainties associated with available data, models, and methods. Team members were also participants in pertinent professional meetings, such as the NRC-sponsored workshop on methods for assessing maximum magnitudes held at the USGS in Golden, Colorado (Wheeler, 2009), the USGS workshop on the CEUS Earthquake Hazards Program held in Memphis, Tennessee, October 28–29, 2009, and the Seismological Society of America meeting in Memphis, Tennessee, April 13–15, 2011. The goal in these interactions was to gain an understanding of the current knowledge and uncertainties regarding the technical issues of significance to seismic sources in the CEUS.

5. Elicit SSC judgments from experts. Individual expert elicitations should be conducted through person-to-person interviews. Elicitations of expert teams are also acceptable.

The notion of individual expert elicitations is specific to a Level 4 assessment process and thus not directly applicable. However, the assessment and evaluation process that occurs within such expert interviews was carried out by the TI Team. Nine of the 11 working meetings (see Section 2.4.5) were multi-day meetings of the TI Team to review data and develop the SSC assessments. Each working meeting was structured around particular aspects of the ongoing evaluation and integration process.

One or more members of the PPRP participated as observers in 6 of the 9 multi-day working meetings and in 8 of the 11 total working meetings. Between working meetings, subgroups developed their interpretations of specific aspects of the model (e.g., geometries of particular zones, paleoseismic recurrence parameters) and their findings were brought to the entire TI Team for evaluation at the working meetings. It was emphasized throughout the assessment that all members of the TI Team would be expected to claim intellectual ownership of the integrated SSC model.

6. Conduct sensitivity analyses and submit feedback to experts. Following the elicitations, extensive sensitivity analyses should be conducted by the TFI and provided to the experts. They then should interact again as a group to review their interpretations.

A hallmark of a SSHAC Level 3 or 4 assessment process is the consideration of feedback by the expert evaluators and the use of that information to gain additional insights into the importance of various aspects of the models. Feedback is provided in terms of both implications to calculated seismic hazard results and implications to various components of the SSC model itself (e.g., earthquake recurrence rates). Three complete feedback cycles were conducted in the CEUS SSC Project. In the first, an SSC Sensitivity model was developed that provided a complete expression of the knowledge and uncertainties regarding seismic source characteristics in the study area. The elements of the model and their uncertainties were quantified using a logic tree approach, thus allowing for hazard calculation and sensitivity studies that isolated the relative

significance of various assessments in the model. The SSC Sensitivity model included some elements that were designed to illustrate the significance of various technical issues and their uncertainties. The feedback results from the SSC Sensitivity model were presented at *Workshop #3—Feedback*, where conclusions were drawn regarding the most important contributors to the mean hazard at seven demonstration sites throughout the study region. This information provided a basis for focusing the subsequent effort on the significant issues. For example, the magnitude and recurrence rate of RLME sources were shown to be quite important, particularly those like the Meers and Cheraw faults whose recurrence rates based on paleoseismic evidence is higher than rates based solely on observed historical seismicity.

After the first round of feedback, the SSC Preliminary model was developed. This model defined the source characteristics and their uncertainties, as expressed in the logic tree branches and associated weights. All the data evaluations and information gained from expert interactions were brought to bear in the development of this model. A second round of feedback was collected to help focus the effort further. This feedback was discussed in a briefing with the PPRP, and the key technical issues were identified. The discussion centered on the range of views on these issues that had been considered during the evaluation process and the way knowledge and uncertainties had been represented in the SSC Preliminary model. The feedback discussions led to a number of focused activities, including additional work in developing a uniform earthquake catalog, consistent and statistically appropriate treatment of the paleoseismic data, refinement of the approach to spatial smoothing of seismicity to allow for variable *a*- and *b*-values, new approaches to reanalyzing the available worldwide database of earthquakes within stable continental regions for purposes of estimating maximum earthquakes, and approaches to incorporating paleoearthquakes into the assessment of the largest observed events for purposes of Mmax assessment. The calculated feedback coming from exercising the SSC Preliminary model was indispensable, and the comments and insights provided by members of the PPRP were valuable as well. The feedback was used to develop the Draft SSC model, which was included in the Draft Project Report along with hazard calculations and sensitivity analyses designed to provide insight into the relative importance of various aspects of the model. The Draft SSC model was reviewed in the Draft Project Report by the PPRP, and a briefing was held to review all of its components. In light of this feedback, the Final SSC model was developed; the model is described in detail in this Final Project Report.

7. Finalize SSC interpretations and combine at hazard level. Integration/aggregation of SSC interpretations usually occurs at the hazard level. The TFI should create the proper conditions, through the application of 1 through 6 above, to combine the expert judgments using equal weights. Allowance should be made for cases where unequal weights are appropriate.

As discussed in Section 2.1, the SSHAC assessment process calls for two important activities: evaluation and integration. This methodology step is integration and, although the specific issues related to combining multiple-expert assessments are not applicable to a Level 3 process, the need for an integration step is applicable and vital. Integration is model-building and the proper representation of current knowledge and uncertainties. Throughout the project, the TI Team members fulfilled their roles as *evaluators* of available data, models, and methods by representing their knowledge and uncertainties in the SSC assessments. They further fulfilled their *integrator* roles by defining branches and weights on the logic tree that they believed would

best represent the views of the larger technical community if it had a similar knowledge of the project databases and if it had gone through the same interactive process.

Speaking to a Level 4 assessment process, the SSHAC guidelines allow for the TFI to consider combining expert assessments using unequal weights. This allowance (which has never been applied in an actual SSHAC project) is provided in case the experts do not fulfill their roles as evaluators and integrators. In that case, the TFI is given the authority to adjust the weights on the component expert models in order to provide—in aggregate—an integrated model that properly represents the center, body, and range of technically defensible interpretations. It is likewise possible to imagine a similar situation within a Level 3 TI Team, whereby a team member does not play the role of an evaluator and integrator. In such a situation, the TI Lead would be responsible for reminding the person of his or her proper role and, if necessary, removing the person from the team. Because all team members are responsible for all aspects of the model, however, it is unlikely that any individual team member would have a significant effect on the integration process. In fact, no such problems presented themselves on the CEUS SSC Project.

8. Peer review. An active or “participatory” peer review should be conducted throughout the study with the particular focus of the process that was followed in conducting the SSC assessment.

A participatory peer review process is essential for a SSHAC Level 3 project, and the SSHAC guidelines call for review of both the technical and process aspects of the project. The technical part of the review entails identifying any data, models, or methods that exist within the technical community that the TI Team may not be aware of, reviewing the evaluation process in workshops and working meetings to offer advice regarding hypotheses and views of members of the community, and reviewing the technical bases provided by the TI Team regarding their integration process to represent the center, body, and range of technically defensible interpretations in light of the data, models, and methods available in the larger technical community. The advantage of a participatory peer review process over a late-stage review process is that the review comments and advice of the PPRP can be used to make mid-course corrections. There were several such comments that led to improvements in the CEUS SSC Project, as follows:

- Numerous data sets were identified by PPRP members for inclusion in the project database.
- New data compilations developed for the project (e.g., aeromagnetic anomaly, gravity, stress, and paleoliquefaction) were suggested and assisted by the PPRP.
- The structure of the database and associated metadata benefited from PPRP advice.
- The concept of more explicit data documentation led to the development of the Data Summary and Data Evaluation tables.
- Written comments after each workshop provided suggestions for process and technical aspects of the project.
- Detailed feedback and questioning at three PPRP briefings offered perspectives on the sensitivity and preliminary SSC models and on their success at representing current knowledge and uncertainties.

- Ongoing comments and suggestions led to improvement in addressing several key SSC issues, including approaches to Mmax assessment, magnitude conversions for the earthquake catalog, recurrence smoothing approaches, consistency of recurrence rates with observed frequencies, and application of criteria for identification of seismic sources.

The PPRP provided a review of the Draft Report and commented on its clarity and completeness in documenting the technical and process aspects of the project.

In addition to the PPRP, other groups provided review comments on the Draft Report. These included the sponsors, USGS, and others. The USGS provided a review of two important aspects of the project: advice regarding any data, models, or methods that should be considered by the TI Team, and review of the project earthquake catalog. Likewise, the sponsors of the CEUS SSC Project provided their review comments in the spirit of ensuring a clear and complete documentation of the project and its technical assessments.

As summarized above, each of the methodology steps in the SSHAC guidelines for SSC was followed in the CEUS SSC Project. In some cases, additional steps were added to ensure that the intent of the SSHAC assessment process was fulfilled.

**Table 2.2-1
Technical Meetings Conducted as Part of the CEUS SSC Project**

Meeting Title	Date	Participants	Observers
Kick-Off Meeting	May 8, 2008	TI Lead, Project Manager (PM), PPRP	
International (Int'l) Observers Briefing	July 21, 2008	TI Lead, PM, Int'l Observers	
Workshop #1	July 22–23, 2008	TI Team, PM	PPRP, Sponsors, USGS, International Observers
Working Meeting #1	Sept. 12–13, 2008	TI Team, PM	
Working Meeting #2	Nov. 3–4, 2008	TI Team, PM	PPRP
Working Meeting #3	Jan. 5–6, 2009	TI Team, PM	PPRP
Int'l Observers Briefing	Feb. 17, 2009	TI Lead, PM, Int'l Observers	
Workshop #2	Feb. 18–20, 2009	TI Team, PM	PPRP, Sponsors, USGS, Int'l Observers
Working Meeting #4	March 3–4, 2009	TI Team, PM	
Working Meeting #5	April 21–22, 2009	TI Team, PM	
PPRP Briefing	May 13, 2009	TI Team, PM, PPRP	
Int'l Observers Briefing	Aug. 24, 2009	TI Lead, PM, Int'l Observers	
Workshop #3	Aug. 25–26, 2009	TI Team, PM	PPRP, Sponsors, USGS, Int'l Observers
Working Meeting #6	Oct. 20–21, 2009	TI Team, PM	PPRP
Working Meeting #7	Jan. 12–13, 2010	TI Team, PM	PPRP
PPRP Briefing	March 24, 2010	TI Team, PM, PPRP	
Working Meeting #8	April 13–14, 2010	TI Team, PM	PPRP
NRC Briefing	Aug. 10, 2010	TI Lead and Team Reps, PM, NRC	
Utilities Briefing	Nov. 4, 2010	TI Lead and Team Reps, PM, Utilities/EPRI	
Working Meeting #9	Feb. 7–8, 2011	TI Team, PM	PPRP
Sponsors Briefing	Feb. 9–10, 2011	TI Team, PM, Sponsors	
Working Meeting #10 (webinar)	April 1, 2011	TI Team, PM	PPRP
Working Meeting #11 (webinar)	May 12, 2011	TI Team, PM	PPRP
PPRP Briefing	June 21–22, 2011	TI Team, PM, PPRP	
Sponsors Briefing (webinar)	July 21, 2011	TI Team, PM, Sponsors	
PPRP Closure Briefing	Sept. 7–8, 2011	TI Team, PM, PPRP, Sponsors	

**Table 2.2-2
Contributors to the CEUS SSC Project**

Resource Experts at Workshop #1	
Ebel, John	Boston College
Hatcher, Robert	University of Tennessee, Knoxville
Keller, Randy	University of Oklahoma
Mooney, Walter	USGS
Mueller, Charles	USGS
Munsey, Jeffrey	Tennessee Valley Authority
Newman, Andrew	Georgia Tech
Obermeier, Steve	USGS, retired
Ravat, Dhananjay	University of Kentucky
Tuttle, Martitia (Tish)	M. Tuttle & Associates
Van Schmus, Randy	University of Kansas
Zoback, Mark	Stanford University
Proponent Experts at Workshop #2	
Adams, John	Natural Resources Canada
Angell, Michael	Fugro William Lettis & Associates
Calais, Eric	Purdue University
Chapman, Martin	Virginia Tech
Cox, Randy	University of Memphis
Drahovzal, James	University of Kentucky
Ebel, John	Boston College
Forte, Alessandro	University of Quebec
Givler, Robert	Fugro William Lettis & Associates
Green, Russell	Virginia Tech
Kafka, Alan	Boston College
Kenner, Shelley	Consultant
Mazzotti, Stephane	Geological Survey of Canada
McBride, John	Brigham Young University
Mueller, Charles	USGS
Olson, Scott	University of Illinois
Pazzaglia, Frank	Lehigh University
Petersen, Mark	USGS
Smalley, Bob	University of Memphis

Stein, Seth	Northwestern University
Talwani, Pradeep	University of South Carolina
Thomas, William	University of Kentucky
Tuttle, Martitia (Tish)	M. Tuttle & Associates
Van Arsdale, Roy	University of Memphis
Zoback, Mark	Stanford University
Technical Experts Who Contributed During Course of CEUS SSC Project	
Adams, John	Geological Survey of Canada
Atkinson, Gail	University of Western Ontario
Bakun, Bill	USGS
Baldwin, John	Fugro William Lettis & Associates
Baranoski, Mark	Ohio Division of Geology
Berry, Henry	Maine Geological Survey
Boyd, Oliver	USGS
Brown, Larry	Cornell University
Calais, Eric	Purdue University
Chapman, Martin	Virginia Tech
Clowes, Ron	University of British Columbia
Counts, Ron	University of Kentucky
Cox, Randy	University of Memphis
Crain, Kevin	AREVA, University of Oklahoma
Crone, Anthony	USGS
Dhananjay, Ravat	University of Kentucky
Dineva, Savka	University of Western Ontario
Dyer-Williams, Kathleen	Consultant
Ebel, John	Boston College
Esch, John	Michigan Department of Environmental Quality
Frankel, Arthur	USGS
Givler, Robert	Fugro William Lettis & Associates
Green, Russell	Virginia Tech
Halchuck, Stephen	Geological Survey of Canada
Hansen, Mike	Ohio Department of Natural Resources
Harrison, Rich	USGS
Hatcher, Robert	University of Tennessee, Knoxville
Hough, Susan	USGS

Chapter 2
SSHAC Level 3 Assessment Process and Implementation

Hurd, Owen	Stanford University
Johnston, Arch	CERI
Keller, Randy	University of Oklahoma
Luza, Ken	Oklahoma Geological Survey
Magnani, Beatrice	University of Memphis
Mahan, Shannon	USGS
Mahdi, Hanan	University of Arkansas at Little Rock
Maybee, Steve	Office of Massachusetts State Geologist
McCollough, Jane	West Virginia Geological Survey
Mitchell, Frances	Queen's University
Mueller, Charles	USGS
Munsey, Jeffrey	Tennessee Valley Authority
Niemi, Tina	University of Missouri–Kansas City
Olson, Scott	University of Illinois at Urbana-Champaign
Pratt, Tom	USGS
Reger, Jim	Maryland Geological Survey
Ruff, Larry	University of Michigan, Ann Arbor
Ruffman, Alan	Geomarine Associates, Ltd.
Rupp, John	Indiana Geological Survey
Sharnburger, Charles	Millersville University, Pennsylvania
Al-Shukri, Haydar	University of Arkansas at Little Rock
Tinsley, John	USGS
Van Arsdale, Roy	University of Memphis
Vaughn, James	Consultant
Wang, Zhenming	Kentucky Geological Survey
Wheeler, Russell	USGS
Williams, Robert	USGS
Withers, Mitch	University of Memphis
Woolery, Ed	University of Kentucky

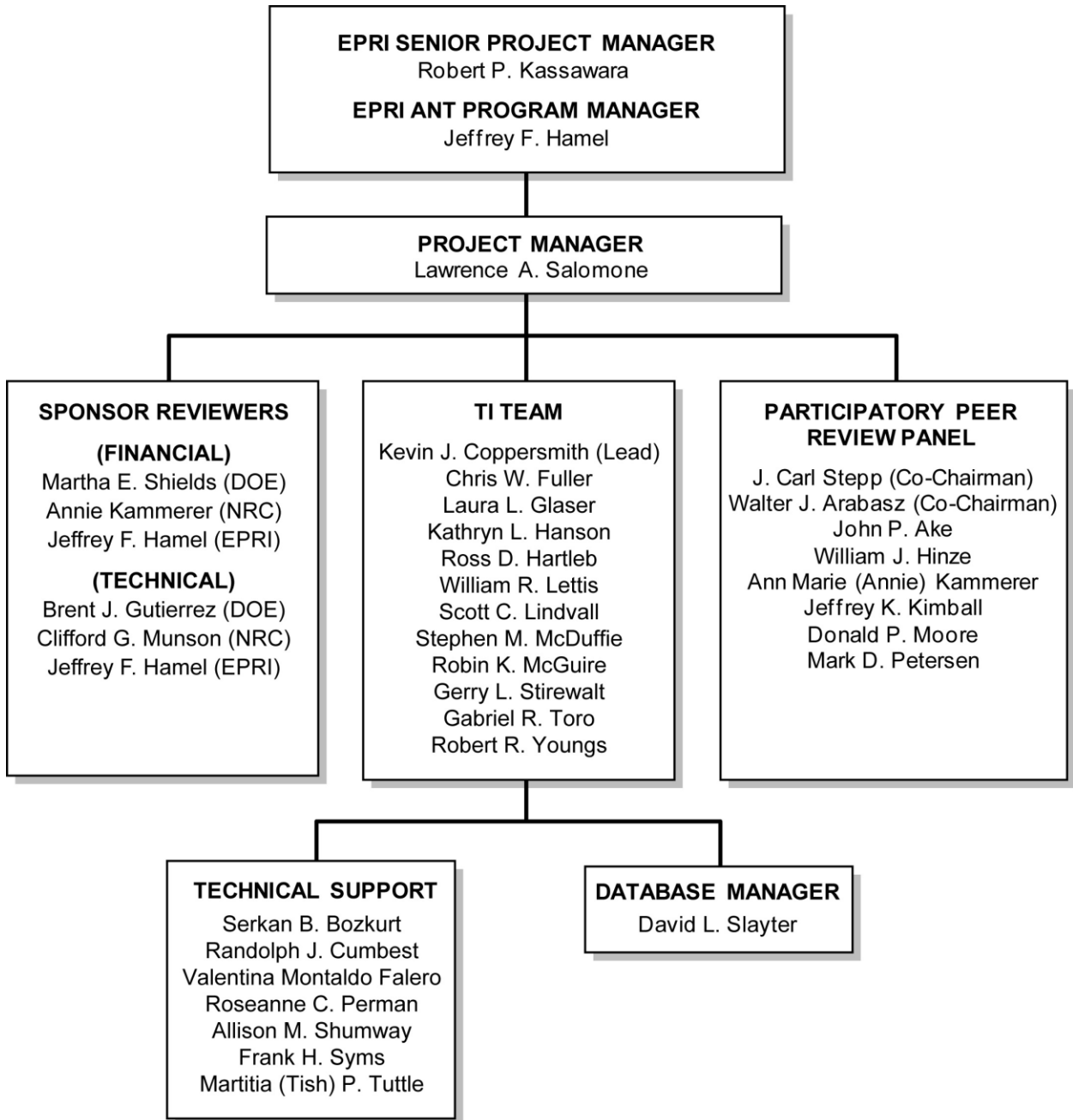


Figure 2.3-1
CEUS SSC Project organization

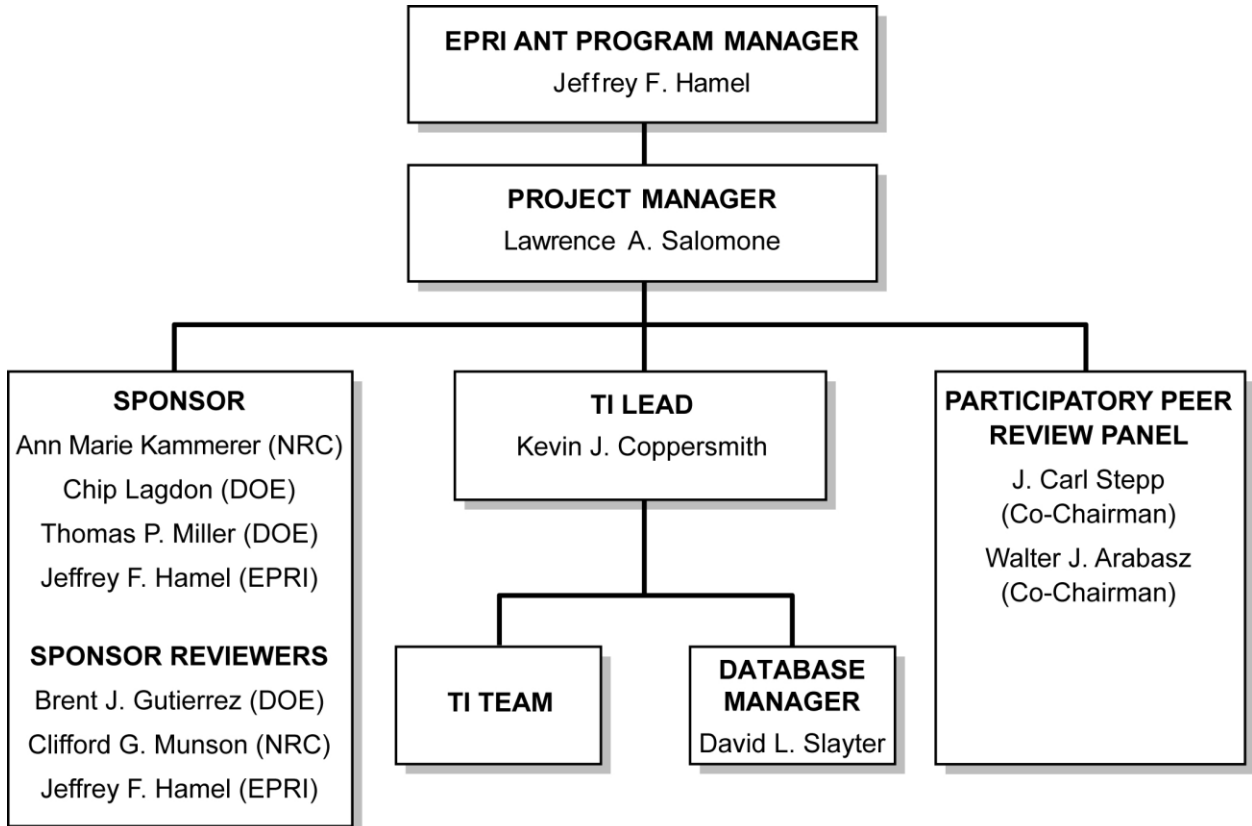


Figure 2.3-2
Lines of communication among the participants of the CEUS SSC Project

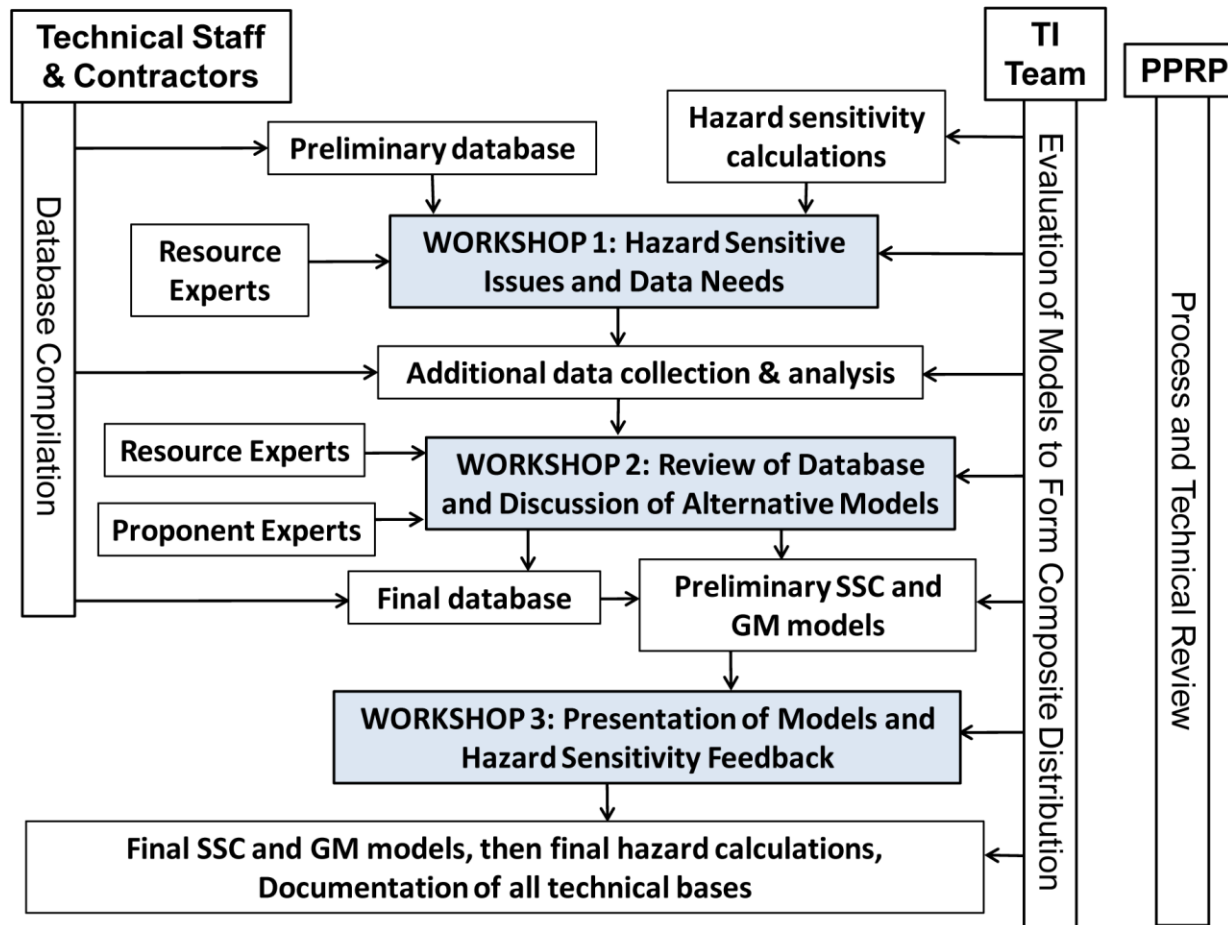


Figure 2.4-1
Essential activities associated with a SSHAC Level 3 or 4 project (Coppersmith et al., 2010)

3

CHAPTER 3 EARTHQUAKE CATALOG

This chapter describes the development of the earthquake catalog for the CEUS SSC Project. The catalog development consists of four major steps: catalog compilation, assessment of a uniform size measure to apply to each earthquake, identification of dependent earthquakes (catalog declustering), and an assessment of the completeness of the catalog as a function of location, time, and earthquake size. Each of these steps is described in detail in the chapter. The result is an earthquake catalog covering the entire study region defined in Chapter 1 for the time period of 1568 through the end of 2008. Earthquake size is defined in terms of the moment magnitude scale (Hanks and Kanamori, 1979), consistent with the magnitude scale used in modern ground motion prediction equations for CEUS earthquakes.

3.1 Goals for the Earthquake Catalog Development

The catalog of past earthquakes that have occurred in a region is an important source of information for the quantification of future seismic hazards. This is particularly true in stable continental regions such as the CEUS where the causative mechanisms and structures for the occurrence of damaging earthquakes are generally poorly understood, and the rates of crustal deformation are low such that surface and near-surface indications of the buildup and release of crustal stresses are difficult to identify. Because the earthquake catalog will be used to characterize the occurrence of future earthquakes in the CEUS, developing an updated earthquake catalog for the study region was an important focus of the CEUS SSC Project. The specific goals for earthquake catalog development are described in the following sections.

3.1.1 Completeness

The goal of compiling an earthquake catalog is to record the occurrence of all known earthquakes in the magnitude range considered important to the characterization of future earthquake hazards. It is recognized that there have been extensive past efforts put forward toward this goal. In the United States, the work performed in the EPRI-SOG project (EPRI, 1988), subsequently revised by Seeber and Armbruster (1991), ultimately led to the catalog used by the U.S. Geological Survey (USGS) for seismic hazard mapping (Mueller et al., 1997; Petersen et al., 2008). Similarly, work by the Geological Survey of Canada (GSC) to develop an earthquake catalog for seismic hazard analysis (Adams and Halchuk, 2003) provides an equally important source catalog for earthquakes in the northern portion of the study region. The CEUS SSC Project relied on the work underlying the USGS and GSC catalogs to form the backbone of the updated project earthquake catalog.

The USGS and GSC catalogs each represent a synthesis of catalog information from many sources into simple one-line catalog entries of date, time, location, and selected estimate(s) of

earthquake size. In that process, some information important to the use of the earthquake catalog for this project may not have been retained. Therefore, an extensive review of original catalog sources was performed as part of the catalog compilation, among them Stover and Coffman (1993); Smith (1962, 1966); the Southeastern United States Network (SUSN) catalog; and the USGS/National Earthquake Information Center (NEIC) Preliminary Determination of Epicenters (PDE) catalog. In addition, numerous special studies of individual earthquakes, earthquake sequences, and specific geographic areas were reviewed and the information compiled as part of the catalog development. The use of these studies is described in subsequent sections of this chapter. A number of these studies included information on important parameters (e.g., moment magnitudes) that is not included in the more regional catalogs.

It is also recognized that the process of catalog compilation from many sources may lead to inclusion of duplicate entries for some earthquakes and inclusion of nontectonic events that have been excluded from other catalogs. To address this issue, catalogs of identified nontectonic events and false entries were also examined and a list of identified nontectonic events was compiled. This list forms one product of the CEUS SSC Project (see Appendix B). The catalog was also reviewed line by line to identify potential duplicate entries not readily identified by automatic means.

3.1.2 Uniformity of Catalog Processing

An important goal of catalog compilation was to use an earthquake size measure that is consistent with the ground motion models that will be used to compute seismic hazards. Most recent ground motion models applicable to the CEUS use the moment magnitude scale, M , as the earthquake size measure, and it is expected that the next generation of ground motion models being developed in the near future will continue to use the moment magnitude scale.

Unfortunately, however, this is not the magnitude scale that has been used for routine earthquake monitoring and catalog compilation. The current practice for many hazard analyses in the CEUS is to estimate earthquake occurrence rates in terms of the catalog magnitude (commonly, body-wave magnitude, or m_b) and then use conversion relationships from this magnitude scale to M as part of the ground motion estimation. This introduces an additional source of uncertainty, particularly since many of the catalog magnitude entries are themselves converted from other size measures, such as shaking intensity for pre-instrumental earthquakes.

The EPRI-SOG project (EPRI, 1988, Vol. 1) developed techniques to produce a catalog with a uniform size measure that is appropriate for unbiased estimation of earthquake occurrence rates for use in seismic hazard assessment. These techniques were used in the EPRI-SOG study to develop a uniform catalog of m_b magnitudes. A goal of the catalog development efforts in this project is to use the same techniques to produce a uniform catalog of moment magnitude values that have properly accounted for the uncertainty in size estimation as part of development of earthquake occurrence rates. This will eliminate the need for magnitude conversion as part of the hazard calculation and avoid propagation of unnecessary uncertainty through the hazard analysis. To achieve this goal, updated conversions were developed from a variety of earthquake size measures to moment magnitude.

An equally important task was to obtain the original size measures for catalog entries in order to use a direct conversion to moment magnitude rather than introduce additional uncertainty by converting previously converted size estimates. One example is that a number of the magnitudes

listed in the GSC catalog are designated local magnitude, M_L . Yet many of these earthquakes occurred in the pre-instrumental period. Examination of the magnitude entries suggests that they were in fact converted from maximum intensity, I_0 , using the Gutenberg and Richter (1956) relationship. Therefore, the original source for the catalog of intensity data was obtained (Smith, 1962, 1966) and the I_0 values for these earthquakes were entered into the catalog in order to make a direct conversion from I_0 to M .

3.1.3 Catalog Review

Development of earthquake catalogs is a complex and a tedious process in which there are many sources of uncertainty and opportunities for either missing important sources of information or adding unwanted or fictitious information. Therefore, an important part of the catalog development process was reviewed by seismologists with extensive knowledge and experience in catalog compilation. The first draft of the catalog was reviewed by Dr. Charles Mueller and Margaret Hopper from the USGS, Dr. John Ebel from Boston College, Dr. Martin Chapman from Virginia Tech, Dr. Pradeep Talwani from the University of South Carolina, Dr. Donald Stevenson from Savannah River Nuclear Solutions, and James Marrone from Bechtel. The following summarizes the main review comments and the actions taken to implement the reviewers' recommendations in the development of the final project catalog.

Use Original Sources

Several reviewers made the comment that original source catalogs should be used as much as possible instead of relying on the compilation catalogs. To address this issue, the entries in the project catalog were traced back to their original sources to the extent possible. For example, the USGS catalog (Mueller et al., 1997; Petersen et al., 2008) considers all earthquake magnitudes as m_b . However, the USGS catalog also lists the source of the magnitude estimate for many earthquakes. These sources were used to identify the proper magnitude type (e.g., m_{bLg} versus M_N). The primary source for the USGS catalog is the NCEER-91 catalog (Seeber and Armbruster, 1991, 1993), which updates the EPRI-SOG (EPRI, 1988) catalog. In the case of instrumentally recorded earthquakes, the preferred magnitude listed in the NCEER-91 catalog is typically the largest among the various magnitude types available in the EPRI-SOG (EPRI, 1988) catalog (e.g., the largest value among magnitude types m_b , m_{bLg} , M_N , M_{CB} , M_D , or M_L). Each of these magnitude types, if present for a particular earthquake, was entered into the project catalog. In addition, to the extent possible, the magnitude entries included the original source of the magnitude estimate (e.g., Weston Observatory; Lamont-Doherty Earth Observatory; the 1983 Nuttli catalog; Dewey and Gordon, 1984).

The NCEER-91 catalog also contained a field in which a flag indicated whether the preferred magnitude was based on instrumental magnitudes (type 1), felt area (type 2), or maximum intensity (type 3). These flags were used to identify those reported magnitudes that were in fact based on shaking intensity measures so that the original size measure, intensity, rather than an estimated magnitude from intensity was used to provide an estimate of moment magnitude. In a similar manner, the Southeastern United States Seismic Network (SEUSSN) catalog (Virginia Tech) provided codes that indicated the source and type of body-wave magnitude reported for each earthquake. These were entered into the project catalog to indicate the type of magnitude and to identify earthquakes whose magnitudes were derived from macroseismic data.

A number of original sources of data suggested by the reviewers were reviewed and added to the project catalog. For example, the Dewey and Gordon (1984) catalog was digitized and included in the project catalog. Felt areas listed in the published paper version of Stover and Coffman (1993) were also digitized and added to the project catalog. The additional catalogs that were reviewed are described in Section 3.2.3.

Examine Individual Magnitude Types

Several reviewers suggested that potential differences in body-wave magnitude types may exist due to differences in the approaches used by various agencies to calculate magnitude. To address this issue, body-wave magnitudes reported by various agencies for the same set of earthquakes were examined for systematic differences. The results of this examination led to inclusion of regional and time-dependent effects in the correlation between various magnitude scales and M , as described in Section 3.3. Examination of M_L magnitudes reported in the catalog obtained from the GSC indicated that many of the reported values were actually based on maximum intensity converted to M_L using the relationship given in Gutenberg and Richter (1956). Moment magnitudes for these catalog entries were estimated using correlations with maximum intensity instead of with instrumental M_L .

Provide Recommendations for Specific Catalog Entries

Individual reviewers provided specific recommendations for a number of catalog entries. For example, Dr. Ebel provided suggestions for the catalog entries in the time period 1500–1700 and the larger earthquakes post-1700 in the northeastern portion of the study region. Dr. Talwani and Dr. Stevenson reviewed the catalog entries in the vicinity of the 1886 Charleston, South Carolina, earthquake. The suggestions made by the reviewers included indications of possible false, duplicate, or erroneous catalog entries, and changes to earthquake locations and times. These suggestions were implemented in the project catalog with indications of the source of the catalog update. Dr. Mueller recommended specific catalog sources and in particular catalog entries from the International Seismological Centre (ISC) for the study region. Review of the project catalog, however, indicated that a number of catalog entries with ISC magnitude values of about 3 were derived from local catalogs that contained either much smaller magnitude entries for the earthquake or no entry at all. Therefore, the ISC catalog was not used as a source in developing the final catalog.

Create a Catalog of Nontectonic Events

A number of reviewers suggested that a separate catalog be created listing nontectonic events identified as part of the catalog compilation. Appendix B contains a listing of the nontectonic events (e.g., explosions, mine collapses, false entries) identified during the course of the catalog development and includes the reference for the event classification.

3.2 Catalog Compilation

The process used for catalog compilation was to provide each entry in a source catalog with a unique ID number specific to that catalog. The catalogs were merged by sorting all records in chronological order based on the calculated Julian date of each earthquake. After merging, each earthquake was assigned a project ID number that is common to multiple entries from different catalogs (duplicates). As an example, the 1897/5/31 Giles County earthquake is reported by eight catalogs: USGS (record number 1065); NCEER (record number 1079); Ohio Geological Survey

(record number 61); SEUSSN (record number 1743); Hopper (record number 97); USHIS (record number 101); EPRI (record number 840); and Reinbold and Johnston (1987; record number 39). Each of these catalog entries receives the same project ID number (TMP02921) indicating that each of the eight records is a duplicate entry for the Giles County earthquake. In the following sections the major sources of catalog data are described.

3.2.1 Continental-Scale Catalogs

The catalogs developed by the USGS and the GSC were the primary sources for earthquake entries. The primary earthquake listing that forms the basis for the USGS catalog was obtained from Dr. Charles Mueller, and the primary earthquake listing that forms the basis for the GSC catalog was obtained from Dr. Steven Halchuk. Figure 3.2-1 shows the areal coverage of these two catalogs. The region outlined by the blue box in the figure indicates the portion of each catalog that was used to develop the project catalog. The USGS catalog was updated through the end of 2008 using the NEIC PDE catalog website, and the GSC catalog was updated through the end of 2008 using data from the National Earthquake Database (NEDB) of Canada.

The USGS catalog is itself a compilation based on a number of other sources including the catalogs of Stover and Coffman (1993); Stover et al. (1984); EPRI (1988) as updated by Seeber and Armbruster (1991) and Armbruster (2002); NEIC PDE; U.S. Advanced National Seismic System (ANSS), and the Centennial Catalog (Engdahl and Villasenor, 2002). The purpose of including all these additional sources in the compilation of the CEUS SSC catalog was to obtain as much information as possible on size measures for the earthquakes. A principal example is obtaining shaking intensity values for pre-instrumental earthquakes that are not given in the primary sources. In some cases, the printed copies of catalogs were used to make hand entries of size measures into the database. For example, the felt area data listed in Stover and Coffman (1993) was entered into the database. As described above in Section 3.1.3, the magnitude type for the entries in the USGS catalog was identified using the source designation provided in the USGS catalog. The source for most of the entries in the USGS catalog was the NCEER-91 catalog (Seeber and Armbruster, 1991), and the NCEER-91 catalog entries were included in the combined earthquake compilation, along with the primary source for the NCEER-91 catalog, the EPRI-SOG catalog (EPRI, 1988). The NCEER-91 catalog contains entries for multiple magnitude types based on the entries in the EPRI-SOG catalog. These entries were used to identify the magnitude type reported in the USGS catalog. For example, if the source of a USGS record is an NCEER record obtained from the EPRI-SOG catalog, and the source used in EPRI-SOG is Dewey and Gordon (1984), all the records (EPRI, NCEER, and USGS) were modified to reflect that the magnitude type is m_{bLg} and the magnitude source is Dewey and Gordon (1984).

The GSC catalog entries consist primarily of two magnitude types, M_L and M_N . The source of the pre-1900 M_L values is most likely intensity. Figure 3.2-2 shows a histogram of M_L magnitudes from the GSC catalog for the time period 1660–1899 for the region east of longitude -105° and south of latitude 53° . The dashed vertical lines indicate magnitudes computed using the Gutenberg and Richter (1956) relationship $M_L = \frac{2}{3}I_0 + 1$. The magnitudes clearly line up on values computed from specific modified Mercalli intensity scale (MMI) I_0 values spaced at $\frac{1}{2}$ intensity units. Figure 3.2-3 shows the data for the period 1900–1930. With the exception of a few entries, the magnitudes again line up with specific I_0 values. Figure 3.2-4 shows the data for the period 1930–1979, and Figure 3.2-5 shows the data for the period 1980–2007. These plots indicate that after 1980, most M_L values are probably instrumental, but during the period 1930–

1980, the GSC catalog likely contains a mixture of intensity-based and instrumental M_L magnitudes.

To sort out intensity-based M_L magnitudes in the GSC catalog, the catalogs of Smith (1962, 1966) were used to identify those earthquakes where instrumental M_L values were reported. In addition, the SUSN and EPRI/NCEER catalogs were used to separate instrumental from I_0 based magnitudes. Where no primary source catalog provided an indication that an instrumental magnitude was recorded, the reported M_L values that are consistent with $M_L = \frac{2}{3}I_0 + 1$ for the I_0 value in the catalog in the time period after 1928 (the earliest reported M_L in the Smith catalogs) were considered to be computed from I_0 . If not, the values were considered to be instrumental M_L magnitudes. Figure 3.2-6 shows the histogram of what are interpreted to be instrumental M_L magnitudes in the GSC catalog for the time period 1928–1979. For the most part, the values appear to indicate an exponential distribution, although some I_0 based magnitudes may remain in the catalog.

An additional source of shaking intensity data for recent earthquakes is the USGS “Did You Feel It?” (DYFI) program (<http://earthquake.usgs.gov/earthquakes/dyfi/>; Wald et al., 1999). Two types of data are available from the DYFI website: (1) the archives, which list date, time, location, magnitude, and intensity of each earthquake; and (2) the reports, which contain the number of responses, average MMI for a specific zip code (not rounded), and distance for each zip code. The epicentral intensity reported in the DYFI data for an earthquake is the maximum intensity observed, independent of the distance and/or the number of observations. For some earthquakes, felt reports are prepared using geocoding, a technique that assigns latitude and longitude to street addresses, but this kind of report is available only for a limited number of earthquakes because observers often do not disclose their address. While reports based on zip code were used in this project, it should be noted that they do not describe how the distance from the epicenter to each observation is determined. If the distance is calculated from the center of the zip code, it may introduce a bias if the zip code covers a very large area.

The DYFI archives were downloaded and compared to the corresponding earthquake records in the CEUS SSC catalog. It was found that all the earthquakes occurred within the study region listed in the DYFI archives were already in the catalog. In more than half of the cases, the I_0 level in the catalog corresponds to the intensity from the DYFI archives. In one-third of the cases, the intensity from the DYFI archive was higher (typically by one level) than the I_0 value in the catalog. In a few cases (2001/6/3 Lake Erie, OH; 2004/7/20 South Carolina; 2005/2/23 Maryland), the difference between the DYFI intensity and the I_0 in the catalog (from NEIC) was as high as three levels. To find an explanation for this difference, the felt reports of these three earthquakes were downloaded and analyzed. In all cases, the intensity assigned by DYFI is reported by few observers (in some cases just one) at great distance from the epicenter (100 km, or 62 mi., or more). The I_0 obtained from NEIC for the same earthquakes approximates the largest intensity observed at short distance.

Approximately 20 earthquakes with $I_0 \geq 4$ MMI in the DYFI archives did not have a corresponding intensity value in the CEUS SSC catalog. Because the same intensity is assigned to the entire zip code, maps of the earthquake effects from DYFI are very different from isoseismal maps, and the appropriate intensity level for the earthquake may not be immediately visible. Therefore, the felt reports for the earthquakes that do not have an intensity measure in the CEUS SSC catalog were carefully analyzed. Intensities obtained from just a few responses at

very great distances were disregarded. In almost all cases, it was found that the estimated maximum intensity needed to be adjusted to reflect the responses at close distance to the epicenter and to take into account the number of responses. This is consistent with the approach followed by Stover and Coffman (1993), who select I_0 as the maximum intensity observed, and it can be argued from their isoseismal maps that it is typically very close to the epicenter.

If there are no observations within 20–30 km (12–18.5 mi.) of the epicenter, I_0 is calculated adding one level to the average observed MMI at the closest distance. This accounts for a decay of about one degree in 30 km, consistent with the Atkinson and Wald (2007) MMI attenuation relation assuming a $M 4 \pm 0.5$, which is an appropriate value for the earthquakes analyzed. In four cases, the responses were too sparse and/or too distant and a value of I_0 was not assigned.

3.2.2 Regional Catalogs

The following regional catalogs were included in the compilation:

- Center for Earthquake Research and Information (CERI) catalog
- Saint Louis University (Nuttli, microearthquake, and moment magnitude catalogs)
- Lamont-Doherty Cooperative Seismographic Network catalog (LDO)
- Weston Observatory catalog (WES)
- Ohio Seismic Network catalog
- Department of Conservation and Natural Resources of Pennsylvania catalog
- Reinbold and Johnston (1987)
- Oklahoma Geological Survey catalog (OKO)
- South Carolina Seismic Network (SCSN) catalog
- Southeastern United States (SUSN) catalog (Virginia Tech)

These catalogs were used to obtain additional information on the size measures for earthquakes and to identify the magnitude types reported for each earthquake. For example, the Nuttli catalog from Saint Louis University indicates when the reported m_b values are instrumental and when they are based on shaking intensity data. The SUSN catalog contains both earthquakes recorded by SEUSSN and data taken from Stover et al. (1984). Included in the SUSN catalog is information on the type and source of individual magnitude values that was incorporated into the project catalog. Based on the recommendation of Dr. John Ebel (e-mail comm., January 13, 2011), magnitudes reported in the Weston Observatory catalog were classified as M_N for years prior to 1995 and as $m_{Lg}(f)$ based on the use of the Ebel (1994) formula for 1995 and later years.

3.2.3 Catalogs from Special Studies

A number of published studies contain information on specific earthquakes in limited geographical areas, often providing seismic moment or moment magnitude values and revised locations and/or depths, or indicating events of nontectonic origin. Information from the following studies was included in the catalog development: Adams and Simmons (1991); Atkinson et al. (2008); Basham et al. (1979); Bent (1992, 1995, 1996a, 1996b, 2009); Bent and

Hasegawa (1992); Bent and Perry (2002); Bent et al. (2002, 2003); Boatwright (1994); Brown and Ebel (1985); Dineva et al. (2004); Du et al. (2003); Ebel (1996, 2000, 2006a); Ebel et al. (1986); Faust et al. (1997); Fujita and Sleep (1991); Kim et al. (2006); Lamontagne and Ranalli (1997); Lamontagne et al. (2004); Larson (2002); Leblanc (1981); Ma and Atkinson (2006); Ma and Eaton (2007); Ma et al. (2008); Macherides (2002); Nabelek and Suarez (1989); Nicholson et al. (1988); Pomeroy et al. (1976); Reagor et al. (1980); Ruff et al. (1994); Scharnberger (1990); Seeber and Armbruster (1993); Seeber et al. (1998); Shedlock (1987); Shumway (2008); Stevenson and McColluh (2001); Street and Turcotte (1977); Street et al. (1975, 2002); and Sykes et al. (2008).

For the most part, the authors of these studies indicate the specific magnitude type reported, and this information was included in the project catalog. For example, Jones et al. (1977) and Street and Turcotte (1977) provide m_{bLg} values. Bollinger (1979) uses Nuttli's (1973) formula to determine m_{bLg} for 17 earthquakes in the southeastern United States, using World-Wide Standardized Seismograph Network (WWSSN) records. His study indicates that Nuttli's (1973) formula is applicable to earthquakes in this region, provided that epicentral distance is less than 2,000 km (1,243 mi.). However, Dr. Ebel (e-mail comm., January 13, 2011) pointed out that Nuttli's formula should only be applied to Lg waves with periods ranging between 0.7 and 1.3 sec. In Table 2 of Bollinger (1979) the period of the Lg wave used in some stations is smaller than the specified range; therefore, these magnitudes are considered in the CEUS catalog as M_N rather than m_{bLg} . The catalog by Basham et al. (1979) is a mix of different magnitudes (mI_0 , mFA , ML , m_b , m_{bLg} , M_N), all assumed to be equal. Since in most cases it was impossible to determine what kind of magnitude was indicated, the CEUS catalog does not specify any kind of magnitude for the events that originate in the Basham et al. (1979) catalog. Instead, the magnitudes were cross-checked against other sources to identify the magnitude type.

In addition to the above, catalogs from three studies addressing historical earthquakes were included in the composite catalog. The first was the catalog of earthquakes in New Brunswick identified from historical records by Burke (2009). The second was the catalog developed by Metzger et al. (2000) covering the region around New Madrid. The third was the catalog developed by Munsey (2006) from newspaper archives for the region of Kentucky and Tennessee and adjoining areas. These studies provide either felt area or maximum intensity measures of earthquake size.

3.2.4 Focal Depth Data

The compiled catalog contains a variety of depth estimates from different agencies and authors. Depths are routinely determined by the software used to locate the earthquakes (e.g., HYPO71, HYPOELLIPSE, etc.) and may have an associated flag that ranks the quality of the solution, and/or a flag that identifies depths fixed or assigned by a geophysicist. Depths of this kind are found in most regional (e.g., CERL, Saint Louis University, SUSN, LDO) and national (e.g., NEIC, NEDB, GSC) catalogs and in studies such as Brown and Ebel (1985); Dineva et al. (2003); Shedlock (1987); and Shumway et al. (2009). In addition, a number of studies (i.e., Atkinson, 2008; Bent, 1992, 1995, 1996a, 1996b; Bent and Hasegawa, 1992; Bent and Perry, 2002; Bent et al., 2002; Du et al., 2003; Ebel, 1986; Ma and Atkinson, 2006; Ma and Eaton, 2007; Ma et al., 2008; Nabelek and Suarez, 1989) calculate earthquake depths from regional depth phases or moment tensor analysis.

Depths were added to the catalog from studies published in the literature. Studies by Chapman and Bollinger (1984); Chapman et al. (1997); Dunn et al. (2010); Johnston et al. (1985); Pulli and Guenette (1981); Rhea (1987); Shoemaker et al. (2009); Talwani (1982); Teague et al. (1986); and Vlahovic et al. (1998) calculate earthquake depth while relocating earthquakes and microearthquakes. However, only the depths obtained by Chapman and Bollinger (1984); Chapman et al. (1997); Johnston et al. (1985); Shoemaker et al. (2009); and Stepp (2008) have been added to the project catalog because the other studies either do not provide tables with data, or focus on microearthquakes that are not included in the project catalog because of their very small magnitude.

The depth flags in the project catalog were standardized as follows: depths assigned to historical events are flagged by the letter H; fixed depths by F; depths obtained from regional depth phases or moment tensor analysis by D; and unreliable or questionable depths by a question mark (?). The latter include all the depths calculated by inversion software with quality of solution D, which according to Johnston et al. (1985) are unreliable.

Histograms of the earthquakes depth distribution for the events that are not flagged as fixed, historical, or unreliable show clear peaks at 5, 10, 18, and 33 km (3, 6, 11, and 20.5 mi.). These depths correspond to the typical fixed depth values adopted by Ohio, Oklahoma, and Pennsylvania catalogs (5 km), NEIC and other U.S. regional catalogs (10 km [6 mi.] for shallow and 33 km [20.5 mi.] for deep events), and Canadian catalogs (18 km, or 11 mi.). This indicates that a number of fixed depths have not been flagged in the original catalogs and consequently in the project catalog. Only a small number of these depths are calculated depths that have been rounded to the nearest integer. For example, Shedlock (1987) calculated a depth of 10.11 km (6.28 mi.) for the 1978/09/07 earthquake at coordinates 33.063°N, -80.209°E. This earthquake is contained in the NCEER catalog but the depth was rounded to a value of 10 km (6 mi.).

3.2.5 Nontectonic Events

Nontectonic and erroneous earthquake entries were identified using lists compiled by ANSS, ISC, NEDB, and the NEIC Mining Catalog (<http://earthquake.usgs.gov/earthquakes/eqarchives/mineblast/>), and using information given in the SEUSSN bulletins and in a number of the studies listed in Section 3.2.3 (e.g., Seeber and Armbruster, 1993, 2002; Fujita and Sleep, 1991; Scharnberger, 1991a, 1991b; Street et al, 2002; Ma et al., 2008; Sykes et al., 2008; Burke, 2009; Ebel, 1996, 2010). In addition, Dr. Charles Mueller at the USGS shared a personal working file containing a list of nontectonic earthquakes; this has been checked against the information already in the catalog. Comments from Dr. John Ebel, Dr. Pradeep Talwani, and Dr. Donald Stevenson were used to identify many false events, particularly in the historical portion of the catalog. Earthquakes of nontectonic origin include mining-related activity (quarry blasts, collapses); reservoir-induced events; explosions; cryoseism; and other disturbances (sonic booms, storms, etc.). If the nontectonic origin of an earthquake is suspected but not confirmed, the classification is considered “probable.” A separate catalog of events of nontectonic (or probable nontectonic) origin is contained in Appendix B.

3.2.6 Identification of Unique Earthquake Entries

The compiled master catalog listing containing all entries from multiple sources is retained in the CEUS SSC Project database. This listing is described in Appendix B. The final stage of catalog

compilation was the identification of duplicate entries for individual earthquakes within the master listing.

Duplicates were first identified by an algorithm that flags all events that occurred within a narrow time window. The time window is specified as difference in Julian date and it is larger for older events and smaller for newer events. The time windows were determined by running tests on different portions of the catalog.

An initial check of the catalog of duplicates identified indicated that many more duplicates still needed to be removed. The main issue appeared to be the difference between local and universal time. In order to identify these events, each line of the catalog was manually checked to confirm or modify the results of the algorithm. Information contained in some of the studies listed in Section 3.2.3 (e.g., Sykes et al., 2008; Fujita and Sleep, 1991; Bent, 2009) and reviewers' comments were used to identify and flag earthquake records with errors in date or time. In all cases, the date and time listed in the original record was retained but the record was considered a duplicate of the correct catalog entry, and a short explanation was added in the "Comment" field of the master catalog listing.

The master listing was then searched for earthquakes identified by only a single source. These earthquake sources were then rechecked to verify the master listing entries. For example, a number of entries have as a single source the SUSN catalog. A list of these events was submitted to Dr. Martin Chapman at Virginia Tech who provided references for all of them. Another source of information that was useful in verifying the correctness of several records was the USGS's online Earthquake History by State (<http://earthquake.usgs.gov/earthquakes/states/>).

Upon completion of these reviews, the master catalog listing was then re-examined line by line to verify the assignment of individual entries to unique earthquake identification numbers. Earthquake entries from different catalogs with similar origin times, locations, and sizes were typically assigned the same identification number unless visual examination indicated multiple earthquakes from one of the source catalogs. Comments were added to the "Comment" field of the master catalog listing to indicate interpretations of duplicate entries.

The next step in catalog processing was to select a preferred entry for each unique earthquake number while retaining the relevant information on various size measures for use in assigning a uniform magnitude and identification of a nontectonic entry. The following order of preference was used for selection of the preferred time and location for each catalog entry. If the earthquake was included in one of the special studies listed in Section 3.2.3, then that entry was used as the preferred entry. Otherwise, if the earthquake was contained in one of the two national catalogs used for seismic hazard mapping, the USGS catalog for earthquakes south of the U.S.-Canada border and the GSC/NEDB catalogs north of the border, then that catalog's entry was selected as the preferred entry. This choice was based on the assumption that these two catalogs have already undergone considerable review within each agency. If the earthquake was not contained in one of these two catalogs, then the local regional catalog entry was selected as the preferred entry (e.g., SUSN, CERL, Weston, Saint Louis University, Lamont-Doherty, the Oklahoma Geological Survey).

Finally, if the earthquake was listed only in other compilations, such as ANSS or Stover and Coffman (1993), then that entry was used as the preferred entry. Entries for earthquakes within the study region that only appear in the ISC catalog were not retained in the final catalog. This

decision was based on the observation that if the ISC reported magnitudes for these entries were of sufficient size (typically magnitude 3 or larger), then the earthquakes should have been contained in one or more regional catalogs. Questions about ISC catalog entries were raised by Dr. Charles Mueller of the USGS during the review of the draft catalog.

The multiple entries of earthquake size were used for assessing the uniform magnitude for each earthquake. Different values reported for the same magnitude scale by different source catalogs were not resolved, as this would require obtaining the original records and reassessing the magnitudes, a task well beyond the scope of the present study. Instead, these different magnitudes were retained and factored into the uncertainty in the assigned uniform magnitude measure for each earthquake.

The final project catalog contains 3,298 individual earthquakes of uniform moment magnitude $E[M]$ 2.9 and larger (the development of the uniform moment magnitude estimate $E[M]$ is described in Section 3.3). Most of these earthquakes (2,642) are also contained in the USGS seismic hazard mapping catalog (Petersen et al., 2008). Table 3.2-1 summarizes the number of additional earthquakes as a function of time period, and Table 3.2-2 summarizes the sources of the added earthquakes. Figure 3.2-7 shows a map of the final CEUS SSC Project. The locations of the earthquakes added to the USGS catalog are denoted by the colored symbols with the catalog source indicated by the color code in the legend. The largest group added to the USGS catalog (319) are smaller-magnitude earthquakes that occurred in the time period 1960–2006 and are contained in multiple other catalog sources. The second largest group of added earthquakes (190) occurred in the period 1800–1899. Many of these earthquakes were identified in the studies of historical documents conducted by Burke (2009), Metzger et al. (2000), and Munsey (2006).

3.3 Development of a Uniform Moment Magnitude Earthquake Catalog

As stated in Section 3.1.2, an important goal is to provide an earthquake catalog that can be used to develop unbiased estimates of the recurrence of earthquakes as a function of magnitude using a magnitude scale that is consistent with modern ground motion prediction equations for the CEUS: the moment magnitude scale defined by Hanks and Kanamori (1979). Because the size measures available for most of the earthquakes in the project catalog are different from this scale, a process for converting from a variety of magnitude and shaking intensity measures to moment magnitude is needed. In addition, it has been shown by Veneziano and Van Dyck (1985) and Tinti and Mulargia (1985) that uncertainty in the magnitudes reported in an earthquake catalog can lead to bias in the estimation of earthquake recurrence rates unless appropriate adjustments are applied. The EPRI-SOG project (EPRI, 1988) developed an approach for assigning a uniform magnitude measure to earthquakes in an earthquake catalog and producing unbiased recurrence parameters from that catalog. The EPRI-SOG approach was updated for application in the CEUS SSC Project.

3.3.1 Approach for Uniform Magnitude and Unbiased Recurrence Estimation

The magnitudes for all earthquakes reported in an earthquake catalog contain some amount of uncertainty. This uncertainty arises from the estimation process as magnitude is typically assigned as a statistical average of measurements obtained by a number of seismograph stations. In addition, the process of conversion from one magnitude scale to another introduces additional

uncertainty. If the reported magnitudes are used to estimate earthquake recurrence parameters using standard techniques, such as the Weichert (1980) maximum likelihood approach using earthquake counts in magnitude bins, then the uncertainty in the magnitudes leads to a bias in the estimated recurrence rate. This bias arises because of the underlying exponential distribution of earthquake magnitudes in a large source region. Considering the number of earthquakes in magnitude bin m_i , the exponential distribution in magnitude means that there are more earthquakes in the next smaller magnitude bin, m_{i-1} and fewer earthquakes in the next larger magnitude bin, m_{i+1} . The unequal numbers of earthquakes in adjacent magnitude bins means that more earthquakes are shifted from magnitude bin m_{i-1} to m_i due to statistical magnitude uncertainty than are shifted from magnitude bin m_i to bin m_{i+1} . A similar and consistent bias in the shifted earthquake counts occurs between magnitude bins m_i and m_{i+1} .

The effect of uncertainty on recurrence parameter estimation is readily illustrated through simulation. The process used is to simulate a catalog of 10,000 earthquakes from a truncated exponential distribution in the magnitude range of \mathbf{M} 3 to \mathbf{M} 7 with a recurrence rate of 100 earthquakes per year of \mathbf{M} 3 and larger and a b -value of 1.0. A catalog of observed magnitudes, $\hat{\mathbf{M}}$, is simulated by adding a normally distributed random error to each earthquake magnitude with a standard deviation of 0.2 magnitude units. The resulting catalogs of \mathbf{M} and $\hat{\mathbf{M}}$ are then used to compute recurrence parameters for magnitudes of \mathbf{M} 4 and larger using the Weichert (1980) method with a magnitude bin width of 0.5 units. The purpose of using magnitudes of 4 and larger is to eliminate the truncation effects at the lower end of the magnitude range that result from starting the magnitude simulation at magnitude 3. The process was repeated for 500 simulations. The following table lists the average earthquake counts in each magnitude bin and the resulting average values of $N(\mathbf{M} \geq 4)$ and b -value. The table also contains results for the adjusted magnitude \mathbf{M}^* that is described below.

Average Results from 500 Simulated Catalogs of True \mathbf{M} , $\hat{\mathbf{M}}$, and \mathbf{M}^*

Parameter	True \mathbf{M}	$\hat{\mathbf{M}}$	\mathbf{M}^*
Number $4.0 \leq \mathbf{M} < 4.5$	685	762	685
Number $4.5 \leq \mathbf{M} < 5.0$	216	241	217
Number $5.0 \leq \mathbf{M} < 5.5$	68	76	69
Number $5.5 \leq \mathbf{M} < 6.0$	21	24	21
Number $6.0 \leq \mathbf{M} < 6.5$	7	7	7
Number $6.5 \leq \mathbf{M} < 7.0$	2	2	2
$N(\mathbf{M} \geq 4)$	10.00	11.13	10.01
b -value	1.004	1.003	1.005

As indicated by these results, the counts of $\hat{\mathbf{M}}$ in each magnitude bin are larger than those for the true magnitudes, and the resulting estimate of $N(\mathbf{M} \geq 4)$ is biased, although the b -value estimate is unbiased.

Tinti and Mulargia (1985) explored this bias, finding that the estimated b -value is unaffected by the magnitude uncertainty (as long as the same uncertainty applies to all magnitudes). They introduced a correction to the recurrence rate estimated from $\hat{\mathbf{M}}$ given by

$$N(\mathbf{M}_{true}) = N(\hat{\mathbf{M}}) \exp\{-\gamma^2\} \quad (3.3.1-1)$$

with

$$\gamma^2 = \frac{\beta^2 \sigma^2[\mathbf{M}|\hat{\mathbf{M}}]}{2} \quad (3.3.1-2)$$

Parameter β is equal to the b -value in natural log units ($\beta = b \ln\{10\}$) and $\sigma[\mathbf{M}|\hat{\mathbf{M}}]$ is the standard deviation of the normally distributed error in the observed magnitudes. Using the fitted b -value of 1.0 and $\sigma[\mathbf{M}|\hat{\mathbf{M}}] = 0.2$ yields γ^2 equal to 0.106. Applying Equation 3.3.1-1 to the value of $N(\mathbf{M} \geq 4)$ estimated from $\hat{\mathbf{M}}$ in the table above yields a value of 10.01, very close to the correct value of 10.00 obtained from the true \mathbf{M} catalog.

The EPRI-SOG project (EPRI, 1988, Vol. 1) developed an alternative approach for obtaining unbiased recurrence parameter estimates.¹ An adjusted magnitude, \mathbf{M}^* , was introduced defined by the expression:

$$\mathbf{M}^* = \hat{\mathbf{M}} - \beta \sigma^2[\mathbf{M}|\hat{\mathbf{M}}] / 2 \quad (3.3.1-3)$$

Recurrence parameters estimated using the adjusted magnitudes were shown to be unbiased. The simulations described above were repeated to include the calculation of \mathbf{M}^* for each earthquake in each simulated catalog using Equation 3.3.1-3. The right-hand column of the above table shows the resulting average counts by magnitude bin and the resulting recurrence parameters. The values are very close to those obtained using the true \mathbf{M} values. These results are to be expected as the adjustment defined by Equations 3.3.1-1 and 3.3.1-2 is equivalent to the adjustment defined by Equation 3.3.1-3 as the value of $\gamma^2 = \beta \times (\hat{\mathbf{M}} - \mathbf{M}^*) = \beta^2 \sigma^2[\mathbf{M}|\hat{\mathbf{M}}] / 2$.

Figure 3.3-1 shows this equivalence graphically.

The EPRI-SOG project (EPRI, 1988, Vol. 1) extended the adjustment defined by Equation 3.3.1-3 to the case where the magnitudes \mathbf{M} are estimated from a vector of other size measures \mathbf{X} , such as other magnitude scales or shaking intensity measures. In this case, the adjusted magnitude \mathbf{M}^* is given by

$$\mathbf{M}^* = E[\mathbf{M}|\mathbf{X}] + \beta \sigma^2[\mathbf{M}|\mathbf{X}] / 2 \quad (3.3.1-4)$$

The change in sign of the adjustment occurs because, as also shown by EPRI (1988), the expected value of the true magnitude, $E[\mathbf{M}]$, given uncertainty $\sigma[\mathbf{M}|\hat{\mathbf{M}}]$ and an underlying exponential distribution in magnitude is given by

$$E[\mathbf{M}] = \hat{\mathbf{M}} - \beta \sigma^2[\mathbf{M}|\hat{\mathbf{M}}] \quad (3.3.1-5)$$

¹ The EPRI-SOG project used m_b as the uniform magnitude scale. However, the relationships developed there for obtaining unbiased recurrence estimates and uniform magnitudes are not dependent on the chosen magnitude scale.

Applying Equation 3.3.1-5 to Equation 3.3.1-3 yields

$$\mathbf{M}^* = E[\mathbf{M}] + \beta\sigma^2[\mathbf{M}|\hat{\mathbf{M}}]/2 \quad (3.3.1-6)$$

Thus, the adjustments from $E[\mathbf{M}]$ to \mathbf{M}^* are the same regardless of whether $E[\mathbf{M}]$ is estimated from other size measures \mathbf{X} or from the observed magnitudes $\hat{\mathbf{M}}$.

The process of using Equation 3.3.1-4 to correct for bias when \mathbf{M} is estimated from \mathbf{X} was also tested using simulation. The simulation steps consisted of the following:

1. Simulate a catalog of true values of \mathbf{M} from a truncated exponential distribution in the magnitude range of 3 to 8 with a b -value of one.
2. Add a normally distributed random error to \mathbf{M} to produce observed magnitudes $\hat{\mathbf{M}}$.
3. Simulate associated values of m_b using the relationship $m_b = \mathbf{M} + 0.3$. Include a normally distributed random error with standard deviation 0.3 to simulate randomness in the relationship between \mathbf{M} and m_b from earthquake to earthquake. (Note that inclusion of measurement error in m_b in effect just adds to the random difference between \mathbf{M} and m_b and it is unimportant to separate this component from the total random difference between the two magnitude scales).
4. Regress $\hat{\mathbf{M}}$ against m_b and obtain the values of $E[\mathbf{M}|m_b]$ and $\sigma[\hat{\mathbf{M}}|m_b]$ for each simulated m_b . This is performed by first trimming the catalog to $m_b \geq 4$ to remove the truncation effect at the low end resulting from the initial limit of \mathbf{M} to ≥ 3 .
5. Use Equation 3.3.1-4 to obtain a catalog of \mathbf{M}^* . Trim off the events below $\mathbf{M}^* 4$ to remove the edge effect and estimate the seismicity parameters $N(\mathbf{M} \geq 4)$ and b -value from the counts of \mathbf{M}^* .
6. Estimate the recurrence parameters for the simulated catalogs using the true \mathbf{M} values, the $E[\mathbf{M}]$ values, and the \mathbf{M}^* values.

The following table presents the results averaged over 500 simulations.

Average Results from 500 Simulated Catalogs of True \mathbf{M} , $\hat{\mathbf{M}}$, m_b , and \mathbf{M}^*

Parameter	True \mathbf{M}	$E[\mathbf{M}]$	\mathbf{M}^*	$\mathbf{M}^*_{adjusted}$
$N(\mathbf{M} \geq 4)$	10.00	8.02	10.68	10.06
b -value	1.000	1.001	1.001	1.001

Use of the catalog of $E[\mathbf{M}]$ values results in an underestimate of the true recurrence rate. Use of the catalog of adjusted magnitudes \mathbf{M}^* produces a close but slight overestimate of the true rate. Examination of Equation 3.3.1-4 indicates that the source of the difference is that the adjusted magnitudes should be based on the value of $\sigma[\mathbf{M}|m_b]$, the variability in true \mathbf{M} given m_b , while the results of the regression between the observed values of the two magnitude scales produces $\sigma[\hat{\mathbf{M}}|m_b]$. The latter value is inflated over $\sigma[\mathbf{M}|m_b]$ due to the random error in the observed

values of $\hat{\mathbf{M}}$ used in the regression. This suggests that a modified value of \mathbf{M}^* be computed using the relationship

$$\mathbf{M}^*_{adjusted} = E[\mathbf{M}|\mathbf{X}] + \beta(\sigma^2[\hat{\mathbf{M}}|\mathbf{X}] - \sigma^2[\mathbf{M}|\hat{\mathbf{M}}])/2 \quad (3.3.1-7)$$

using the assumption that

$$\sigma^2[\mathbf{M}|\mathbf{X}] = \sigma^2[\hat{\mathbf{M}}|\mathbf{X}] - \sigma^2[\mathbf{M}|\hat{\mathbf{M}}] \quad (3.3.1-8)$$

where $\sigma^2[\mathbf{M}|\hat{\mathbf{M}}]$ is the variance in the observed values $\hat{\mathbf{M}}$ used in the regression of \mathbf{X} versus $\hat{\mathbf{M}}$.

The right-hand column of the above table shows that the use of Equation 3.3.1-7 to compute \mathbf{M}^* results in predicted recurrence parameters very close to those obtained using the simulated true \mathbf{M} values.

As part of the simulation testing, the average value of $(\text{true } \mathbf{M} - E[\mathbf{M}|m_b])$ was found to be less than 0.01, indicating that the regression of m_b against $\hat{\mathbf{M}}$ produces $E[\mathbf{M}]$.

The advantage of the \mathbf{M}^* approach is that it allows inclusion of the variability in the values of $\sigma[\mathbf{M}|\hat{\mathbf{M}}]$ and $\sigma[\mathbf{M}|X]$ from earthquake to earthquake. EPRI (1988) provided the following relationships for the case where $E[\mathbf{M}]$ is estimated from a vector $\hat{\mathbf{X}}$ of R observed size measures:

$$E[\mathbf{M}|\hat{\mathbf{X}}] = \left\{ \sum_i \frac{\sigma^2[\mathbf{M}|\hat{\mathbf{X}}]}{\sigma^2[\mathbf{M}|\hat{X}_i]} \cdot E[\mathbf{M}|\hat{X}_i] \right\} + (R-1)\beta\sigma^2[\mathbf{M}|\hat{\mathbf{X}}] \quad (3.3.1-9)$$

and

$$\sigma^2[\mathbf{M}|\hat{\mathbf{X}}] = \left\{ \sum_i \frac{1}{\sigma^2[\mathbf{M}|\hat{X}_i]} \right\}^{-1} \quad (3.3.1-10)$$

where \hat{X}_i is a single member of $\hat{\mathbf{X}}$. The individual values of $\sigma[\mathbf{M}|X_i]$ should include the adjustment given by Equation 3.3.1-8. Use of Equation 3.3.1-9 represents a variance weighted estimate of $E[\mathbf{M}]$. The final term of Equation 3.3.1-9 is needed to adjust for bias introduced by the underlying exponential distribution in magnitude. Simulation testing using multiple size measures showed that Equation 3.3.1-9 produced the correct value of $E[\mathbf{M}]$ and the use of Equation 3.3.1-7 to compute \mathbf{M}^* with the variance given by Equation 3.3.1-10 resulted in unbiased recurrence parameters.

The procedure developed by Tinti and Mulargia (1985) can also be applied to the case of $E[\mathbf{M}]$ estimated from $\hat{\mathbf{X}}$. The parameter γ^2 is computed using the variance defined by Equation 3.3.1-10. However, in this case the adjustment to the computed recurrence rate is given by

$$N(\mathbf{M}_{True}) = N(E[\mathbf{M}]) \exp\{+\gamma^2\} \quad (3.3.1-11)$$

The change in sign is due to the true rate being underestimated from the $E[\mathbf{M}]$ magnitudes and is a direct result of relationship between $\hat{\mathbf{M}}$ and $E[\mathbf{M}]$ defined by Equation 3.3.1-5.

The above results were obtained using earthquake catalogs that had the same level of completeness at all magnitude levels; that is, the catalogs contain all earthquakes that occurred during the time period used for the simulation. The process was repeated using simulation of partially complete catalogs in which the completeness of reporting for smaller magnitudes is less than for the larger magnitude, the typical case encountered in practice. These tests showed that the use of the \mathbf{M}^* correction did not lead to unbiased estimates of the earthquake recurrence parameters; in general, the values of $N(\mathbf{M} \geq 4)$ and b -value were biased low. The source of this bias can be envisioned by comparing the EPRI (1988) and Tinti and Mulargia (1985) bias adjustments. If one considers the magnitude interval m_i (e.g., magnitudes $4.5 \leq \mathbf{M} < 5$), the true rate of earthquakes in that interval, λ_{i_i} , is equal to $n_{i_i}^C / T_{i_i}^C$, where $n_{i_i}^C$ is the count of true \mathbf{M} in the catalog completeness period for that magnitude interval $T_{i_i}^C$.

In the case where the catalog contains the observed magnitudes $\hat{\mathbf{M}}$, the results of Tinti and Mulargia (1985) show that the counts of $\hat{\mathbf{M}}$ are too large by the factor $\exp\{\gamma^2\}$ and the true rate can be obtained by multiplying the observed counts by the factor $\exp\{-\gamma^2\}$. The \mathbf{M}^* approach of EPRI (1988) is to shift the observed magnitudes down by the factor $\gamma^2 / \beta = \beta \sigma^2 [\mathbf{M} | \hat{\mathbf{M}}]$ such that the counts in the interval m_i are effectively reduced by the same factor $\exp\{-\gamma^2\}$. If the catalog instead consists of the expected magnitudes $E[\mathbf{M}]$, then the adjustment is in the opposite direction. The counts of $E[\mathbf{M}]$ are too low by the factor $\exp\{+\gamma^2\}$ and one can either adjust the rate using Equation 3.3.1-11 or shift the magnitudes using Equation 3.3.1-7 to effectively increase the counts by the same factor. Where the problem lies is that when the completeness for earthquakes in the next lowest magnitude interval is less than for magnitudes in the interval in question ($T_{i-1}^C < T_{i_i}^C$), then insufficient earthquakes are shifted from magnitude interval m_{i-1} to m_i using the \mathbf{M} and the true rate remains underestimated.

The solution to this problem is to use the approach of Tinti and Mulargia (1985) to adjust the earthquake counts in each magnitude interval rather than use the EPRI (1996) adjusted magnitudes \mathbf{M}^* . However, to maintain the EPRI (1988) ability to account for differences in magnitude uncertainty for individual earthquakes, the adjustment is applied individually, earthquake by earthquake, rather than globally to the total earthquake counts in a magnitude interval. The earthquake catalog is processed to obtain values of $E[\mathbf{M}]$ and $\sigma[\mathbf{M}]$ for each earthquake as described above. Each earthquake is then assigned an equivalent count N^* defined as

$$N^* = \exp\left\{\beta^2 \sigma^2 [|\mathbf{M}|\hat{\mathbf{M}}]/2\right\}$$

or

$$N^* = \exp\left\{\beta^2 \sigma^2 [|\mathbf{M}|\mathbf{X}]/2\right\} \tag{3.3.1-12}$$

The rate of earthquakes in the magnitude interval m_i is then obtained by summing the values of N^* for earthquakes with values of $E[\mathbf{M}]$ in the magnitude interval and dividing by period of completeness for the magnitude interval. Earthquake recurrence parameters are thus computed using standard approaches, such as maximum likelihood, and the effective counts N^* rather than the observed counts.

The performance of the use of the N^* approach compared to the \mathbf{M}^* approach was tested on simulated catalogs. The simulation steps were as follows:

1. Simulate a catalog of true values of \mathbf{M} from a truncated exponential distribution in the magnitude range $3 \leq \mathbf{M} \leq 8$ with a recurrence rate of $25 \mathbf{M} \geq 3$ earthquakes per year and a 300-year complete catalog.
2. Add random error to each value of \mathbf{M} to produce a catalog of observed magnitudes.
3. Simulate an estimate of size measure \mathbf{X} for each \mathbf{M} with random variability in the relationship between \mathbf{X} and \mathbf{M} .
4. Regress against \mathbf{X} to obtain the values of $E[\mathbf{M}|\mathbf{X}]$ and $\sigma[\mathbf{M}|\mathbf{X}]$.
5. Use Equation 3.3.1-7 to obtain a catalog of \mathbf{M}^* .
6. Use Equation 3.3.1-12 to obtain N^* for each earthquake.
7. Assign to each earthquake a probability of being observed based on its size and specified relative values of equivalent periods of completeness as a function of magnitude.
8. Reduce the simulated catalog to the observed one in the periods of completeness for each magnitude.
9. Trim off the events below $\mathbf{M}^* 4$ to remove the edge effect and estimate the seismicity parameters $N(\mathbf{M} \geq 4)$ and b -value from the counts of \mathbf{M}^* .
10. Trim off the events below $E[\mathbf{M}] = 4$ to remove the edge effect and estimate the seismicity parameters $N(\mathbf{M} \geq 4)$ and b -value from the counts of N^* .
11. Repeat the process for 500 simulations and compute the average difference between the values of $N(\mathbf{M} \geq 4)$ and b -value obtained by steps 9 and 10 from the values computed from the full catalog of simulated true values of \mathbf{M} .

Simulations were performed for three cases: m_b was computed from \mathbf{M} using the expression $m_b = \mathbf{M} + 0.3$; I_0 was computed from \mathbf{M} using the expression $I_0 = 3(\mathbf{M}-1)/2$; and a mixture of the two. Three levels of catalog completeness were used as listed in the table below. The partial completeness cases consist of T^C_i for magnitude 4 being about two-thirds of the catalog length (“Two-thirds” case) and T^C_i for magnitude 4 being half of the catalog length (“Half” case).

Completeness Cases Used in Simulations

Completeness Case	Equivalent Period of Completeness (years) for Magnitude Interval:									
	3–3.5	3.5–4	4–4.5	4.5–5	5–5.5	5.5–6	6–6.5	6.5–7	7–7.5	7.5–8
Full	300	300	300	300	300	300	300	300	300	300
Two-thirds	200	210	220	230	240	250	260	280	300	300
Half	100	125	150	175	200	225	250	275	300	300

The results of the simulations are listed in the following table. Shown for each case are the average percent errors between the values of $N(\mathbf{M} \geq 4)$ and b -value obtained using the \mathbf{M}^* and N^* approaches and the values obtained using the simulated true values of \mathbf{M} . The X cases labeled “Mixture” consist of the use of I_0 for the first 200 years and m_b for the last 100 years, consistent with the general mix of size measures in the CEUS SSC Project catalog. For the case of full completeness, either method works as well as the other. However, as the relative completeness in the lower magnitudes becomes smaller, the bias in the \mathbf{M}^* estimates increases while the results obtained using the N^* approach remain close to those obtained using the true simulated values of \mathbf{M} . These results indicate that the N^* approach performs better than the \mathbf{M}^* approach for earthquake catalogs with variable levels of completeness as a function of magnitude. As this is the case for the CEUS SSC Project catalog, the N^* approach was used to obtain unbiased estimates of earthquake recurrence parameters. Consistent with this approach, the uniform magnitude measure adopted for the CEUS SSC Project catalog is $E[\mathbf{M}]$, the expected value of moment magnitude for each earthquake given the uncertainty in estimating its size.

Results of Simulation Testing of \mathbf{M}^* and N^* Approaches for Partially Complete Catalogs

X Case	Completeness Case	Percent Error In Parameters Obtained by:			
		Estimation Using \mathbf{M}^*		Estimation Using N^*	
		$N(\mathbf{M} \geq 4)$	b -value	$N(\mathbf{M} \geq 4)$	b -value
I_0	Full	2.29%	0.56%	1.79%	-0.14%
I_0	Two-thirds	-25.00%	-2.37%	1.11%	0.96%
I_0	Half	-48.42%	-11.28%	1.19%	0.36%
m_b	Full	0.10%	0.04%	0.14%	0.21%
m_b	Two-thirds	-26.02%	-3.87%	-0.52%	0.09%
m_b	Half	-48.09%	-12.01%	-1.34%	0.00%
Mixture	Full	1.49%	0.48%	1.25%	0.17%
Mixture	Two-thirds	-25.32%	-3.29%	1.05%	0.20%
Mixture	Half	-49.59%	-12.52%	-0.83%	-0.69%

3.3.2 Estimation of $E[M]$ for the CEUS SSC Project Catalog

This section summarizes the relationships used to develop the uniform moment magnitude estimate $E[M]$ for earthquakes in the CEUS SSC Project catalog. Two general types of data are available for the estimation of $E[M]$, either direct observation of moment magnitudes, \hat{M} , or observations of other size measures X that require development of scaling relationships from X to $E[M]$. The majority of earthquakes in the project catalog that occurred after about 1930 have reported values of instrumental magnitude in one or more of the magnitude scales m_b , m_{bLg} , M_N , M_S , M_L , M_C , or M_D . The data in the project catalog were used to develop scaling relationships between these magnitude scales and moment magnitude. The final relationships are listed in Table 3.3-1.

Before presenting these relationships, the issue of the effect of rounding off in reported magnitudes will be addressed.

3.3.2.1 Effect of Magnitude Rounding on Statistical Tests

As part of the development of scaling relationships from various magnitude scales to moment magnitudes, statistical tests were performed to identify potential differences in scaling between different catalog sources. Most of the magnitudes are reported in various catalogs to the first decimal place. The issue of the effect of rounding in reported magnitudes has been examined by Felzer (2008) with regard to the effect on seismicity rates, with emphasis on the effect of rounding to the nearest 0.5 magnitude units. For the CEUS SSC Project, the issue is the potential impact of rounding of data to the first decimal place on results of t -tests for nonzero values of the difference between magnitudes reported by source A and by source B (e.g., the difference between M_N reported by the GSC and that reported by Weston for a set of common earthquakes).

The impact of rounding to the nearest 0.1 magnitude unit was examined by simulating hypothetical data sets for Source A and Source B with specified average differences in magnitude and specified random variability in the magnitude differences. A t -test is performed comparing the mean difference between the magnitudes from Source A and Source B to see if a nonzero difference is statistically significant at the 5 percent level (p -value = 0.05). This corresponds to the absolute value of the mean difference divided by the standard deviation of mean differences being greater than 2.13. The simulated magnitudes from the two sources are then rounded to the nearest 0.1 magnitude units and the t -test is repeated. Differences in the test results for the unrounded and rounded simulated samples would indicate that rounding potentially affects the ability to properly detect differences in reported magnitudes. The selected 5 percent significance level means that even if the true average difference in magnitude reported by the two agencies is zero, one would expect to see a statistically significant difference in 5 percent of random samples.

The following table reports the results of simulation tests performed for magnitude sample sizes of 50 and 100. For each case, a mean difference in magnitude was specified along with the standard deviation for the random variability in magnitudes reported by the two agencies. Then 10,000 simulations of each data set were performed. The percentage of simulated samples that indicated a statistically significant difference is given in the table below. For the cases with specified mean difference of zero, approximately 5 percent of the simulated samples show a statistically significant difference, consistent with expectation. Comparison of the results in the last two columns indicates that nearly the same percentages are obtained for the unrounded and

rounded samples. The results indicate that the rounding to 0.1 magnitude units does not cause a significant disruption in t -test results for identifying mean differences in magnitudes between two magnitude sources, and its effect can be ignored.

Simulation of t -Test Results for Differences in Magnitudes

Sample Size	Specified Mean Difference	Specified Standard Deviation of Difference of Individual Magnitudes	Percentage with p -value ≤ 0.05 for unrounded sample	Percentage with p -value ≤ 0.05 for rounded sample
100	0	0.1	5.1	5.1
100	0	0.2	5.2	5.0
100	0	0.3	5.1	5.1
100	0.1	0.1	100	100
100	0.1	0.2	99.9	99.9
100	0.1	0.3	91.4	91.1
100	0.2	0.3	100	100
100	0.2	0.4	99.8	99.8
50	0	0.1	4.9	5.2
50	0	0.2	5.3	5.2
50	0	0.3	5.0	5.0
50	0.1	0.1	100	100
50	0.1	0.2	93.4	92.9
50	0.1	0.3	63.8	63.6
50	0.2	0.3	99.6	99.6
50	0.2	0.4	93.6	93.4

3.3.2.2 Moment Magnitude Data

Moment magnitude data for earthquakes in the project catalog provide both a direct assessment of $E[\mathbf{M}]$ and the necessary data for the development relationships between moment magnitude and other size measures. Two types of moment magnitude data were used. The first are published moment magnitudes for specific earthquakes that are assumed to be based on a reliable assessment of seismic moment from inversions of either long-period waveforms or surface-wave spectra. Table B-2 in Appendix B lists the 272 earthquakes with reported values of \mathbf{M} that were used for both observed values of \mathbf{M} for specific earthquakes and for developing the magnitude conversions.

As discussed in Section 3.3.1, the reported values of moment magnitude represent $\hat{\mathbf{M}}$, magnitude measured with uncertainty. These magnitude values are adjusted to $E[\mathbf{M}]$ using Equation 3.3.1-5. The values of $\sigma[\mathbf{M}|\hat{\mathbf{M}}]$ are taken from the source of the reported magnitude estimate, if available. If an uncertainty was not reported, then the following average values for

moment magnitude estimation as a function of time were used. The average of the values of uncertainty in moment magnitude estimates presented by Johnston (1996a, Table B2) gives 0.28 for the period prior to 1960, 0.15 for earthquakes in the time period 1960–1974, and 0.13 for the period 1975–1990. The average uncertainty in \mathbf{M} for the seven CEUS earthquakes in the Harvard Centroid Moment Tensor catalog in the period 1978–1984 is 0.12 and for the eight earthquakes in the period 1985–present is 0.10. Using this information, the following nominal uncertainty values were assigned to instrumental moment magnitudes when data for a specific earthquake was not available.

Assigned Values of $\sigma[\mathbf{M}|\hat{\mathbf{M}}]$

Time Period	Nominal $\sigma[\mathbf{M} \hat{\mathbf{M}}]$
1920–1959	0.30
1960–1975	0.15
1975–1984	0.125
1985–2008	0.10

The second type of moment magnitude estimates are those obtained by approximate means in the studies of Atkinson (2004a, 2004b), Boatwright (1994), and Moulis (2002). These approximate moment magnitudes were corrected for minor biases as described below before using them to augment the \mathbf{M} data set.

Atkinson (2004) Study

Atkinson (2004a, 2004b) developed estimates of moment magnitudes for eastern Canada earthquakes based on analysis of Fourier spectra. Figure 3.3-2 compares her estimates of \mathbf{M} with moment magnitudes listed in Table B-2 in Appendix B for earthquakes in common. The moment magnitude values obtained by Atkinson (2004a, 2004b) are close to reported moment magnitudes for values of \mathbf{M} above magnitude 4, but they overestimate \mathbf{M} by about 0.2 units for smaller values. The one exception is the estimate for the 1989 Ungava, Quebec, foreshock. Atkinson (pers. comm., 2011) indicates that her estimate for this event is unreliable given the great distances between the earthquake and the stations she used. Ignoring this one event, a locally weighted least-squares fit to the data shown on Figure 3.3-2 was used to adjust the values of moment magnitudes reported in Atkinson (2004b) to values of \mathbf{M} used in this study.

Boatwright (1994) Study

Boatwright (1994) inverted vertical recordings from the Eastern Canada Telemetered Network (ECTN) to obtain estimates of earthquake source spectra, including seismic moment. Figure 3.3-3 compares Boatwright’s (1994) estimates of moment magnitude with moment magnitudes listed in Table B-2 in Appendix B for earthquakes in common. The moment magnitude values obtained by Boatwright (1994) are close to reported moment magnitudes for values of \mathbf{M} below 3.5 and tend to slightly underestimate the value of \mathbf{M} at larger values. A locally weighted least-squares (Loess) fit to the data shown on Figure 3.3-3 was used to adjust the moment magnitudes reported in Boatwright (1994) to values of \mathbf{M} used in this study.

Moulis (2002) Study

Moulis (2002) developed estimates of moment magnitudes for northeastern United States earthquakes using a coda wave technique. Figure 3.3-4 compares her estimates of moment magnitude with moment magnitudes listed in Table B-2 in Appendix B for earthquakes in common. The moment magnitude values obtained by Moulis (2002) are close to reported moment magnitudes, albeit with more scatter than shown by the Atkinson (2004a, 2004b) and Boatwright (1994) estimates. A least-squares fit to the data shown on Figure 3.3-4 was used to adjust the moment magnitudes reported in Moulis (2002) to values of \mathbf{M} used in this study.

Combined Estimates

The relationships shown on Figures 3.3-2, 3.3-3, and 3.3-4 were used to compute $E[\mathbf{M}]$ for each earthquake with an approximate moment magnitude estimate from the three studies described above. Where multiple estimates are available from two or three of the studies, they were combined using the variance weighing approach defined by Equations 3.3.1-9 and 3.3.1-10. Table B-3 in Appendix B lists the resulting approximate moment magnitudes.

3.3.2.3 Estimation of $E[\mathbf{M}]$ from Body-Wave Magnitudes

Two types of body-wave magnitudes are contained in the catalog data, magnitudes computed from the amplitude of compression waves, and m_{bLg} magnitudes computed from amplitude of Lg waves. The latter are sometimes denoted as M_N or Nuttli magnitudes, referring to Nuttli (1973), who originally proposed the relationship for defining the m_{bLg} scale. The distinction between m_{bLg} and M_N is maintained in the project catalog as not all agencies compute Lg magnitudes in exactly the same way. Herrmann and Kijko (1983) discuss this issue and suggest the magnitude scale $m_{Lg(f)}$ to indicate what frequencies were used to compute the magnitude. This scale is currently being used by the Weston Observatory (see below). Catalog data were examined to assess the potential for regional/time/network differences in the conversion from various body-wave magnitude scales to \mathbf{M} .

Comparison of Body-Wave Magnitudes Reported by Various Agencies

The largest differences found in comparing magnitudes reported by different agencies were in comparison of M_N magnitudes for earthquakes in the northeastern United States and southeastern Canada reported by the GSC and Weston Observatory. Figure 3.3-5 shows the difference in reported magnitudes for the same earthquake as a function of time. John Ebel (pers. comm., 2011) indicates that the history of magnitude calculations reported in the Weston Observatory catalog consists of four periods:

- 1938–1962: M_N computed from the original Weston Observatory Benioff system (Ebel, 1987)
- 1962–1975: M_N computed from the Weston Observatory WWSSN system (Ebel, 1987)
- 1975–1994: M_N computed from the Weston Observatory Develocorder system or early digital system (NEUSSN bulletins and the Weston Observatory earthquake catalog)
- 1994–present: $m_{Lg(f)}$ computed from the evolving seismometer and digital systems at Weston Observatory

The M_N magnitudes reported in the GSC and National Earthquake Database (NEDB) for Canada are computed using Nuttli's formula but with a broader frequency range than originally defined by Nuttli (1973) without making a specific frequency correction (J. Adams, pers. comm., 2011).

The data on Figure 3.3-5 show clearly that there are time periods where the two magnitude scales cannot be considered equivalent: 1938–1975, and after about 1997. The time periods of differences in magnitude reporting generally coincide with changes in magnitude calculation methods used by Weston Observatory, as indicated by the color coding on Figure 3.3-5.

The SUSN catalog also contained a number of earthquakes in the northeastern United States. The catalog indicated that the magnitude data were obtained from the Earth Physics Branch (EPB) of Canada. Tests of these magnitudes against M_N magnitudes reported in the GSC/NEDB catalog indicate that the mean difference is small (~ 0.03 units) and is only statistically significant when using a combination of m_b and m_{bLg} magnitudes reported by EPB. Therefore, the SUSN magnitudes reported with a sited source of EPB were considered equivalent to GSC M_N magnitudes.

The other major seismic network in the northeastern United States is the Lamont-Doherty network. Earthquake magnitudes in the catalog obtained from the Lamont-Doherty catalog have the source designation LDO or PAL (Palisades), or are based on work by Sykes et al. (2008). Testing of the difference between magnitudes reported by Lamont and magnitudes reported by Weston Observatory indicate a small (-0.08 magnitude unit) difference that is statistically significant.

For the remaining portions of the study region, the magnitudes come from a variety of sources. The SUSN catalog lists the following sources for magnitudes in the CEUS:

- B—Bollinger (1975), Southeastern U.S. Catalog 1754–1974
- E—Earth Physics Branch (EPB), Canadian catalog
- G—USGS State Seismicity Maps (Stover et al., 1984)
- I—EPRI-SOG Catalog (EPRI, 1988)
- M—Sibol et al. (1987)
- N—Nielsen (1982)—Stanford Data Base
- O—Nuttli (1974)
- R—Barstow et al. (1981) (Rondout Associates), NUREG/CR-1577
- S—Street and Turcotte (1977)
- T—Reinbold and Johnston (1987)
- U—Earthquake History of the U.S./U.S. Earthquakes (Stover and Coffman, 1993)
- V—SEUSSN Bulletins (Virginia Tech Publication)
- W—Nuttli et al. (1979)

The separation of magnitude source and type was achieved using the following earthquake catalog sources.

- Although all earthquakes in the USGS seismic hazard mapping catalog are considered to be m_b magnitude, the catalog does provide references for the assigned magnitude. These were used to indicate the magnitude type according to the magnitude source. The major source was NCEER and the NCEER magnitude (last column of the NCEER-91 catalog) was used as the assigned magnitude.
- For those events where the magnitude source was “NCEER,” the NCEER-91 catalog was used to determine which of the several magnitude types was used to define the “NCEER Magnitude.” In the case of instrumental magnitudes, this was typically the magnitude type with the largest reported magnitude, which in a number of cases is M_L or M_C . The USGS magnitude type was corrected to correspond to the specified type used in NCEER, and the NCEER source was indicated in the catalog where possible, based on comparisons of the magnitude with those reported by other sources. The SUSN catalog was particularly useful in inferring the source of many of the NCEER/EPRI magnitudes.
- The Nuttli (1983) catalog from Saint Louis University was also reviewed to change those magnitudes with source NUT that were determined from macroseismic data from m_b to m_{10} or m_{FA} , as appropriate.
- The Dewey and Gordon (1984) catalog was reviewed to include those earthquakes for which Dewey and Gordon (1984) calculated the m_{bLg} magnitude and for these the magnitude source was indicated as D&G.

Comparisons of magnitudes among these different sources indicated differences in some cases of 0.1 to 0.2 units (e.g., comparing D&G m_{bLg} with m_b from other sources) or differences of less than 0.1 (e.g., comparing D&G m_{bLg} with m_{bLg} from other sources), although these comparisons were often for small samples.

Analysis of Regional/Network Differences in Body-Wave Magnitude to Moment Magnitude Scaling

The comparisons among body-wave magnitudes reported from various sources indicated that there may be regional/catalog source differences in scaling from body-wave magnitudes to moment magnitude. The next step was to test the scaling from body-wave magnitudes to moment magnitude. The largest differences appeared to be in the northeastern portion of the study region (northeastern United States and southeastern Canada). Therefore, separate investigations were performed for this portion of the study region and for the remaining portion of the study region.

Scaling from m_b to M in the Midcontinent Portion of the Study Region

The first phase was testing for magnitude differences among sources in the main portion of the study region, excluding the northeastern United States and southeastern Canada. Figure 3.3-6 shows the spatial distribution of earthquakes with reported body-wave and M magnitudes (112 earthquakes) color-coded by magnitude source. The primary sources for the M magnitude for these earthquakes were Street et al. (1975) and Dr. Robert Herrmann at Saint Louis University (http://www.eas.slu.edu/eqc/eqc_mt/MECH.NA/).

Figure 3.3-7 shows the m_b - \mathbf{M} data set for these earthquakes, together with three published relationships that have been used in the past for conversion from m_b to \mathbf{M} for hazard calculations. After eliminating the data for $m_b < 3$ to remove truncation effects, a linear relationship was fit to the data, resulting in a slope of 0.96 ± 0.03 . The linear fit included all specified values for body-wave magnitude for each earthquake, with equal weights assigned to each value. Testing of the linear fit versus an offset model, $\mathbf{M} = m_b + C$, indicated that the linear model did not have greater predictive power as measured by the Akaike (1974) information criterion (AIC). The AIC is often used to select between models, in this case between a linear model with two parameters and an offset model with a single parameter. In selecting among models, the one with the lower AIC value is typically preferred. The test results indicate that the slope parameter difference from 1.0 is not statistically significant, and the offset model provides a satisfactory fit to the data. The resulting constant is -0.28 ± 0.02 , and the offset line is shown on Figure 3.3-7. It is recognized that at larger magnitudes, there is a tendency for saturation of the m_b scale with increasing moment magnitude (e.g., Boore and Atkinson, 1987). However, the focus in catalog development is in estimating \mathbf{M} from instrumentally derived m_b magnitudes in the magnitude range of 3 to 6. All the larger earthquakes in the CEUS SSC catalog have been subjected to special studies, and more robust estimates of \mathbf{M} have been developed from these efforts.

Testing of inclusion of the m_b source as a predictor showed no statistical significance for any source differences. Testing of magnitude type indicated no statistical difference between m_b and m_{bLg} and a weak difference for M_n , which is based on only 9 earthquakes. Thus it is concluded that in the midcontinent portion of the study region, the various reported magnitudes m_b , m_{bLg} , and the few M_N values can be considered equivalent for purposes of estimating $E[\mathbf{M}]$.

Figure 3.3-8 shows a plot of the residual for the offset model (Figure 3.3-7) against earthquake year. There is an apparent shift in the residuals after about 1995 such that the average m_b - \mathbf{M} difference becomes about 0.1 magnitude units. There are 26 earthquakes in the post-1995 data set scattered throughout the region, and the difference shown on Figure 3.3-8 appears to be statistically significant, although it does not correspond to a known change in network configuration. Because the difference is small and has not been independently reported, it was not factored into the magnitude scaling used for the CEUS SSC Project catalog.

Scaling from m_b to \mathbf{M} in the Northeastern Portion of the Study Region

The data for the northeastern United States and southeastern Canada come from two principal sources, the GSC and the Weston Observatory. Figure 3.3-9 shows the spatial distribution of earthquakes with both body-wave and \mathbf{M} magnitudes (580 earthquakes), color coded by magnitude source.

Figure 3.3-10 shows the m_b - \mathbf{M} data. There are two types of \mathbf{M} magnitudes for these earthquakes. The points shown as solid circles were determined mostly from waveform modeling by various researchers. The open circles indicate the data where approximate methods were used to estimate the seismic moment. These represent the work of Atkinson (2004a, 2004b), Boatwright (1994), and Moulis (2002). Also shown on the figure are the three scaling relationships shown on Figure 3.3-7 plus the Sonley and Atkinson (2005) relationship between M_N and \mathbf{M} .

To examine the correlation between the magnitude scales, the data were again limited to the magnitude range of primary interest ($m_b \geq 3.5$). The very limited data for $m_b > 6$ were also

removed to eliminate the effects of m_b saturation. Testing again showed that a linear fit has a slope near 1 (0.97 ± 0.02) and an offset model produces a lower AIC value. However, for this data set, there are marginally significant differences among the sources, with the largest difference between the GSC and other sources. A statistically significant difference among the body-wave magnitude types in this data set was found, principally between m_b and other magnitude types.

Figure 3.3-11 shows a plot of the residuals from the fit shown on Figure 3.3-10 versus time. The red points indicate the m_b magnitude types. Time-dependent changes in residuals may be at least partly an effect of magnitude type. Testing of the effect of magnitude type for data prior to 1980 indicates that type becomes much less significant. Exploring further, Figures 3.3-12 and 3.3-13 show the residuals from Figure 3.3-10 versus year for only the GSC and Weston (WES) data, respectively. These two data sets show shifts in scaling that occur at different times: at about 1995 for the GSC data and about 1980 for the WES data. Both offsets appear statistically significant. The difference in M_N to M scaling in the GSC data has been noted previously by Bent (2010). The difference in M_N to M scaling in the WES data corresponds to about the time of a change in magnitude processing and also to the period where the M_N magnitudes are most similar between the GSC and WES data (Figure 3.3-5). These results indicate that time dependent scaling of m_b to M should be included in converting the GSC and WES body-wave magnitudes.

Figure 3.3-14 shows the residuals from the fit shown on Figure 3.3-10 versus year for the other catalog sources. A similar time trend to that shown by the WES data can be seen. The sources for most of the data shown on the figure are EPRI and SRA (Stover et al., 1984). Both of these are compilations of other catalog sources and the data are following the trends seen in the primary regional catalogs. As the EPRI and SRA source catalogs are compilations, the assignment of magnitudes to a specific network was made by assuming that if that network source (e.g., GSC or WES) reports the same magnitude value as in the compilation, then that region catalog is the likely source of the EPRI or SRA magnitude. In this manner, most of the magnitudes listed in these two catalogs could be assigned to either the GSC or WES source.

The other important magnitude source in the region is the Lamont-Doherty Earth Observatory (LDO) catalog. There are only three earthquakes in the catalog with both body-wave magnitudes attributed to LDO and moment magnitudes so the scaling cannot be tested for this catalog source. Comparison of body-wave magnitudes from LDO to those from other sources is also inconclusive. Figure 3.3-15 shows a plot of the difference between body-wave magnitudes attributed to LDO and those from other sources. The results do not suggest any difference as the time period when most of the earthquakes were recorded corresponds to the period when the GSC and WES magnitudes are essentially equivalent (Figure 3.3-5).

Figure 3.3-16 shows the spatial distribution of earthquakes with reported GSC body-wave magnitudes and moment magnitudes. Figure 3.3-17 shows the $M-m_b(M_N)$ difference as a function of time for the data with both reported magnitudes. There is a suggestion that the m_b - M scaling is different in the midcontinent region (southwest of the dashed line on Figure 3.3-16), but this may be due to the GSC reporting magnitudes determined by other sources.

Another source of body-wave magnitudes is the Oklahoma Geological Survey Leonard Geophysical Observatory (OKO) catalog, which reports both m_{bLg} and $m(3Hz)$ magnitudes. Figure 3.3-18 shows the difference between m_{bLg} and $m(3Hz)$ in that catalog as a function of

m_{bLg} . For magnitudes in the range of interest to this study ($m_{bLg} > 3$) there is no statistically significant difference between the two magnitudes and $m(3\text{Hz})$ was considered equivalent to m_{bLg} for purposes of estimating $E[\mathbf{M}]$.

Model for Scaling from m_b to $E[\mathbf{M}]$

Based on the analyses presented above, the a model for scaling body magnitudes to $E[\mathbf{M}]$ was developed as follows. A data set of m_b - \mathbf{M} pairs was created for study region using the following criteria:

- Magnitudes from composite catalogs (e.g., SRA, EPRI, LLL) were assigned a source from one of the primary source catalogs (e.g., WES, GSC) when the reported magnitude was the same.
- Magnitudes with source GSC in the midcontinent area were discarded unless they represent the only reported magnitude for an earthquake.
- Magnitude types m_b , m_{bLg} , M_N , $m_{Lg(f)}$, and $m(3\text{Hz})$ are considered equivalent. However, catalog source designations are retained.

Figure 3.3-19 shows the resulting data set. It was found that if the data below magnitude about m_b 3.5 were removed, then an offset model, $\mathbf{M} = m_b + C$, has a better (lower) AIC value; that is, the difference from a slope of unity is not statistically significant. A change in slope can be seen in the data for lower magnitudes. This change may be due to the effects of data truncation or actual changes in the scaling relationships between the two magnitude scales. However, the lower magnitudes are not of primary interest in developing earthquake recurrence relationships for assessing seismic hazard. At the upper end of the magnitude range there is the issue of saturation of the m_b scale, which has been shown from numerical modeling (e.g., Boore and Atkinson, 1987). Truncation of the data set to remove magnitudes above m_b 6 resulted in little change to the value of C or the statistical significance of a departure from a slope of unity.

The data from the GSC were then analyzed to identify the best year for the transition in scaling, which was found to be 1997. A similar analysis was performed to identify the best year for a transition in scaling in the WES data, which was found to be 1982. Differences in scaling between the earthquakes in the midcontinent region and the GSC catalog and earthquakes in the midcontinent and the WES catalog (post-1982) were both found to be statistically significant with a difference of about 0.1 magnitude units. The difference in scaling between GSC and WES data after 1982 and before 1997 was found to be only 0.02 units and is not statistically different from zero. It is difficult to determine if the difference between scaling in the northeastern United States applies only to the WES catalog or to both WES and LDO, but the limited data that can be attributed to LDO show no clear difference from the WES catalog (Figure 3.3-15), and the LDO magnitudes were assumed to be equivalent to the WES. The resulting form of the scaling relationship is

$$E[\mathbf{M}] = m_b - 0.316 - 0.118Z_{NE} - 0.192Z_{1997GSC} + 0.280Z_{1982NE}$$

$$\sigma_{M|mb} = 0.24$$

where Z_{NE} is 1 for earthquakes located in the northeast (northeast of the dashed line on Figure 3.3-16 including GSC data) and 0 otherwise;

$Z_{1997GSC}$ is 1 for earthquakes occurring after 1997 recorded by the GSC and 0 otherwise;
and

Z_{1982NE} is 1 for earthquakes occurring in the Northeast prior to 1982 recorded by other than the GSC and 0 otherwise.

The value of $\sigma_{M|mb} = 0.24$ reflects the value of 0.29 obtained from regression reduced by the average value of $\sigma[\mathbf{M}|\hat{\mathbf{M}}] = 0.16$ for the earthquakes used in the regression (Equation 3.3.1-8).

A test of the model that accounts for a difference between the long-period spectral estimates of \mathbf{M} and the corrected approximate values of \mathbf{M} found a statistically insignificant difference of 0.02 magnitude units.

Examination of the residuals indicated that there is more scatter (larger variance) for the data prior to 1980 than for the data after 1980. The ratio of the variances, 1.6, is statistically significant using an F-test. However, use of variance weighted regression produces only about 0.01 unit magnitude differences in the scaling relationships and even less in the N^* corrections. Therefore, the variance weighted results were not used.

3.3.2.4 Estimation of $E[\mathbf{M}]$ from M_L Magnitudes

Local magnitudes, M_L , are reported by a number of agencies. These magnitudes were calibrated by the various agencies to correspond to the original local magnitude definition given by Richter (1935). Figure 3.3-20 shows the spatial distribution of earthquakes with reported instrumental M_L magnitude of 3 and larger in the project catalog. There are a number of earthquakes in the region offshore of Canada. These are $M_{L(Sb)}$ magnitudes (J. Adams, pers. comm., 2011) that may need different conversion relationships than the onshore M_L data. However, they occur primarily outside of the CEUS SSC model study region and are not analyzed further. Figure 3.3-21 shows the spatial distribution of earthquakes that have both M_L and \mathbf{M} magnitudes in the project catalog. The spatial distribution of the M_L - \mathbf{M} pairs is limited and is insufficient to examine regional or catalog differences in M_L to \mathbf{M} scaling in the CEUS directly.

Figure 3.3-22 shows the M_L - \mathbf{M} data set. The data for the two offshore Canada earthquakes fall within the distribution of the other data. The data for the two earthquakes in the western part of the study region also lie within the distribution of the other data. Shown on the figure are the relationships developed by Johnston (1996a) and Miao and Langston (2007). The trend of the data on Figure 3.3-22 displays the typical flattening of slope at the lower magnitudes. To minimize the influence of this flattening on the estimation of \mathbf{M} in the range of interest, the data below M_L 3.5 were not used in fitting the model. The presence of a few outlying data points suggests the use of robust regression and the resulting fitted linear model is shown.

The data shown on Figure 3.3-22 suggest that for the larger M_L values, the slope of the M_L - \mathbf{M} relationship may approach 1. Herrmann and Nuttli (1982) report that M_L and m_{bLg} values are nearly equal in the western United States. Kim (1998) found that M_L and m_{bLg} were nearly equal for earthquakes in eastern North America. This suggests that the better defined m_b to \mathbf{M} scaling might be used for the M_L data.

Figure 3.3-23 compares M_N and M_L magnitudes reported by the GSC. For $M_N \geq 3$, the data are well fit by the relationship $M_L = M_N + 0.21$, with a standard error of 0.30. Robust regression was used because the observed scatter suggests possible outliers in the data. However, ordinary least squares produced only a 0.02 magnitude unit difference in the offset factor and a small increase in the standard error to 0.34. Also shown on Figure 3.3-23 is the relationship developed by Kim (1998). The difference between the results shown for the GSC data and the Kim (1998) relationship may be due to the fact that Kim (1998) used PDE m_{bLg} magnitudes and computed M_L , while the data shown on Figure 3.3-23 are based on the reported GSC magnitudes from the project catalog. The data shown on Figure 3.3-23 indicate that the GSC M_L magnitudes can be converted to $E[M]$ by subtracting 0.21 magnitude units and then using the M_N to M conversion, with an increase in standard error to account for the additional step. This would bring the standard error to a value of 0.42, similar to that for the fitted relationship shown on Figure 3.3-22.

The M_L data from the remaining portion of the study region require variable treatment. Figure 3.3-24 shows the data for earthquakes in the northeastern portion of the study region with reported M_L magnitudes and either M_C or M_D magnitudes from catalog sources other than the GSC. There are two M_D values reported by CERI in this region, the largest being for the 1983/10/07 earthquake. Analysis of the data above M_C or M_D values of 2.5 indicates that on the average M_L is equivalent to M_C or M_D , although with considerable scatter. As will be shown in Section 3.3.2.6, there is a large sample with which to estimate the M_C to M scaling. Figure 3.3-25 shows the data for earthquakes in the northeastern portion of the study region with M magnitudes a M_L magnitude from sources other than the GSC. Shown on the figure is the relationship developed in Section 3.3.2.6 for converting M_C to M . Testing of the difference between the observed values of M and those predicted assuming M_L equivalent to M_C showed no statistically significant difference. For $M_L \geq 2.5$, the mean offset (using robust estimation) is 0.11 ± 0.06 and for $M_L \geq 3$ the mean offset is -0.06 ± 0.08 . Therefore, in the northeastern portion of the study region, M_L magnitudes were converted using the M_C conversion relationship, with an increased standard error of 0.46 to account for the larger scatter in the data compared to that for the M_C - M data.

As shown on Figure 3.3-20, only a few earthquakes outside of the northeastern portion of the study region have reported M_L and M magnitudes. Therefore, scaling relationships for M_L magnitudes in this portion of the study region were based on correlation of M_L with other magnitude scales. The two principal examples are as follows:

- The M_L magnitudes reported by SCSN are equivalent to the M_C magnitudes reported by SCSN.
- The M_L magnitudes reported by ANSS in the vicinity of New Madrid are equivalent (with minor exception) to the M_D magnitudes reported by CERI for $M_D \geq 3$.

3.3.2.5 Estimation of $E[M]$ from M_S Magnitudes

Surface wave magnitudes, M_S , are computed from the amplitude of low frequency (< 0.1 Hz) surface waves. Figure 3.3-26 shows the spatial distribution of earthquakes with M_S magnitude of 3 and larger in the project catalog. Figure 3.3-27 shows the M_S - M data set. Also shown on Figure 3.3-27 is the quadratic relationship developed by Johnston (1996a). This relationship was developed using larger magnitudes and does not extrapolate well into the magnitude range of the

CEUS SSC data set. A quadratic polynomial was fit to the data. Figure 3.3-27 shows the fitted model, the 90% confidence interval of the mean, and the 90% prediction interval. At $M_S > 5$, the fitted model is very similar to the Johnston (1996a) global model. The resulting conversion relationship is

$$E[\mathbf{M}] = 2.654 + 0.334M_S + 0.040M_S^2$$

$$\sigma_{\mathbf{M}|M_S} = 0.20$$

The value of $\sigma_{\mathbf{M}|M_S} = 0.20$ reflects the value of 0.24 obtained from regression reduced by the average value of $\sigma[\mathbf{M}|\hat{\mathbf{M}}] = 0.13$ for the earthquakes used in the regression (Equation 3.3.1-8).

3.3.2.6 Estimation of $E[\mathbf{M}]$ from M_C and M_D Magnitudes

The coda magnitude scale, M_C , and the duration magnitude scale, M_D , are based on correlations of the length of the seismic signal and earthquake size measured in other magnitude scales, typically m_b or M_L . They are typically applied to smaller magnitude earthquakes. The spatial distribution of earthquakes with M_C magnitudes ≥ 2.5 in the project catalog is shown on Figure 3.3-28. These include many earthquakes with magnitude type labeled “UNK” in the LDO catalog that appear to be M_C magnitudes based on values reported by other agencies. The major sources of data are the WES, LDO, and Southeastern United States (SEUS) networks. The spatial distribution of earthquakes with M_C magnitudes ≥ 2.5 and \mathbf{M} magnitudes are shown on Figure 3.3-29. The data are only sufficient for estimating the scaling of M_C to \mathbf{M} in the northeastern portion of the study region, predominantly magnitudes reported by WES and LDO.

Figure 3.3-30 shows the spatial distribution of earthquakes with M_D magnitude of 3 and larger in the project catalog. The major sources of data are the CERI, SEUS, OKO, and SNM (Sanford et al., 2002) networks. The spatial distribution of earthquakes with both M_D and \mathbf{M} magnitudes is shown on Figure 3.3-31. These data indicate that direct comparisons between M_D and \mathbf{M} magnitudes are limited primarily to data from CERI in the midcontinent portion of the study region and to data from WES and LDO in the northeastern portion of the study region.

Scaling to $E[\mathbf{M}]$ for the Northeastern Portion of the Study Region

Figure 3.3-32 shows the M_C - \mathbf{M} data set. Testing for differences in scaling between the WES and LDO sources found no statistically significant differences. This was true both assuming that the LDO “UNK” magnitudes are M_C from that source and using only the magnitudes actually labeled M_C . The green symbols indicate the few M_D magnitudes that differ from the reported M_C magnitudes for the same event. These data points fall well within the mass of the data, consistent with assuming that M_C and M_D magnitudes can be considered equivalent in the northeastern portion of the study region. Testing indicated that a linear fit to the data with slope less than 1 provided a better fit than an offset model. Tests for outliers gave conflicting results that suggest that one may be present. However, a robust regression fit to the data produced nearly the same regression coefficients. Therefore, the ordinary least-squares result was used. The resulting model is

$$E[\mathbf{M}] = 0.633 + 0.806M_C$$

$$\sigma_{\mathbf{M}|M_C} = 0.27$$

The value of $\sigma_{M|MC} = 0.27$ reflects the value of 0.31 obtained from regression reduced by the average value of $\sigma[M|\hat{M}] = 0.15$ for the earthquakes used in the regression (Equation 3.3.1-8).

Scaling in Midcontinent East of Longitude 100°W

As indicated on Figures 3.3-29 and 3.3-31, the spatial distribution of M_C - M magnitude pairs and M_D - M magnitude pairs is limited. The possibility of combining the two magnitude measures was examined by comparing M_C and M_D magnitudes across the study region. Figure 3.3-33 shows the spatial distributions of the data sets investigated.

Figures 3.3-34, 3.3-35, 3.3-36, 3.3-37, and 3.3-38 compare the M_C and M_D magnitudes for each data set shown on Figure 3.3-33. Figure 3.3-34 compares M_C and M_D magnitudes for earthquakes with magnitude values coming from either the WES or LDO catalog. The data indicates that these two scales can be considered equivalent in the northeastern portion of the study region.

Figure 3.3-35 shows that the M_C or M_D magnitudes reported in the OKO catalog are essentially equivalent to values of M_C or M_D reported in other catalogs. Figures 3.3-36 and 3.3-37 show similar comparisons for the CERI and SCSN catalogs, respectively. Figure 3.3-38 shows the comparison for other catalog sources. In all cases, M_C and M_D can be considered essentially equivalent for magnitudes above about 2.5. Note that there is only one earthquake west of longitude 100°W that can be used to compare magnitudes.

Figure 3.3-39 shows the data set for M_D and M magnitudes for the midcontinent portion of the study region. Also shown on the figure are the limited data for M_C - M and M_L - M pairs for the same region. These data are generally consistent with the M_D - M data. In addition, the relationship developed by Miao and Langston (2007) between M_L and M is plotted. The Miao and Langston relationship is also consistent with the data. A linear regression was performed of data larger than magnitude 2.9, resulting in the relationship shown by the red curves on Figure 3.3-39. Inclusion of differences between M_C , M_D , and M_L did not produce a statistically significant improvement in the fit. The resulting relationship is

$$E[M] = 0.869 + 0.762 (M_C, M_D, \text{ or } M_L)$$

$$\sigma_{M|MC} = 0.25$$

The value of $\sigma_{M|MD} = 0.25$ reflects the value of 0.28 obtained from regression reduced by the average value of $\sigma[M|\hat{M}] = 0.11$ for the earthquakes used in the regression (Equation 3.3.1-8).

Scaling in the Region Between Longitudes 105°W and 100°W

The portion of the study region between longitudes 105°W and 100°W has very few earthquakes with reported moment magnitudes. Figures 3.3-40, 3.3-41, and 3.3-42 compare the various magnitude scales for earthquakes in this region contained in the CEUS SSC Project catalog. These comparisons indicate that m_b correlates fairly well with the other magnitude scales, except for M_L prior to 1970 (the events on Figure 3.3-41 prior to 1970 occurred after 1960). Therefore, the m_b - M scaling relationship was applied to scale those events in the region of longitude 105°W to 100°W when only M_C , M_D , or M_L magnitudes were available.

3.3.2.7 Estimation of E[**M**] from the Logarithm of Felt Area

Figure 3.3-43 shows the spatial distribution of earthquakes in the project catalog with reported values of $\ln(\text{FA})$, where FA is felt area measured in km^2 . The red symbols denote those earthquakes that also have a reported value of **M**. The point located offshore Newfoundland is the 1929 Grand Banks earthquake.

Figure 3.3-44 shows the $\ln(\text{FA})$ -**M** data from the project catalog. The form of the relationship used to fit the data was that proposed by Frankel (1994) based on theoretical grounds. This form was used by Johnston (1996b) to fit data from a worldwide database of SCR earthquakes. The Johnston (1996b) relationship, shown on Figure 48, is generally consistent with the data from the project catalog.

The data were trimmed below $\ln(\text{FA}) = 8.5$ to limit the effects of sample truncation at low magnitude values. The resulting relationship is shown by the red curves on Figure 3.3-44. Trimming the data at larger values of $\ln(\text{FA})$ produced greater differences between the fitted model and the Johnston (1996b) relationship.

The data set used to develop the model included the $\ln(\text{FA})$ value for the 1929 Grand Banks earthquake. The fact that this earthquake occurred offshore increases the uncertainty in estimation of the felt area. Removal of the earthquake from the data set produced a small reduction in the predicted magnitudes for large felt area of about 0.2 magnitude units, less than one standard deviation in the prediction for a single earthquake. The data from this earthquake were used by Johnston (1996b) and are used to develop the model for used for the CEUS SSC Project. The fitted model is

$$E[\mathbf{M}] = 1.41 + 0.218 \times \ln(\text{FA}) + 0.00087\sqrt{\text{FA}}$$
$$\sigma_{M|\ln(\text{FA})} = 0.22$$

The value of $\sigma_{M|\ln(\text{FA})} = 0.22$ reflects the value of 0.29 obtained from regression reduced by the average value of $\sigma[\mathbf{M}|\hat{\mathbf{M}}] = 0.185$ for the earthquakes used in the regression (Equation 3.3.1-8).

Note that the standard error is comparable to the estimation of **M** from m_b .

A *t*-test of the difference between the project data and the Johnston (1996b) predictions for $\ln(\text{FA}) \geq 10$ (the region where Johnston's data lie) showed a statistically significant difference from zero, indicating that the above relationship provides a better fit to the CEUS project data than the Johnston (1996b) relationship.

3.3.2.8 Estimation of E[**M**] from the Maximum Intensity, I_0

The size measure available for most pre-instrumental earthquakes is maximum shaking intensity, I_0 , predominately reported in the MMI scale. Figure 3.3-45 shows the spatial distribution of earthquakes in the project catalog with reported values of maximum intensity, I_0 , which is assumed to be epicentral intensity. The red symbols denote those earthquakes that also have a reported value of **M**. The blue symbols denote offshore earthquakes where the assessment of I_0 is problematic. The offshore earthquakes were not used in the development of the I_0 to E[**M**] scaling.

Figure 3.3-46 shows the I_0 - M data from the project catalog. The red curves show a locally weighted least-squares (Loess) fit to the CEUS data, treating the I_0 values as numeric quantities. The blue dashed curve shows the relationship derived by Johnston (1996b) from a worldwide data set of SCR earthquakes consisting primarily of values for I_0 of V and larger. The Johnston (1996b) relationship overpredicts the value of M derived from the CEUS data set for intensities values between IV and VII.

The Loess fit to the CEUS data shows a pronounced change in slope at about I_0 equal to V. Similar changes in scaling have been observed previously in developing relationships between I_0 and m_b . Figure 3.3-47 shows the I_0 and m_b data pairs from the NCEER-91 catalog (Seeber and Armbruster, 1991), together with the relationships between I_0 and m_b developed by the EPRI-SOG project (EPRI, 1988) and Sibol et al. (1987). EPRI-SOG (EPRI, 1988) proposed that a linear fit was adequate for the intensity range of interest, although the observed data for I_0 III fall generally above the fitted relationship. Sibol et al. (1987) proposed a variety of fits, including the nonparametric fits to the data for individual intensity classes shown on Figure 3.3-47. The Sibol et al. (1987) nonparametric fits were used by Seeber and Armbruster (1991) to develop the intensity-based magnitude estimates in the NCEER-91 catalog.

The departure from a linear I_0 -magnitude relationship is much less pronounced for the m_b magnitude data shown on Figure 3.3-47 than for the M data shown on Figure 3.3-46, particularly at m_b values of 3 and larger that have been used to develop earthquake occurrence relationships by EPRI-SOG (EPRI, 1988) and by the USGS (e.g., Petersen et al., 2008). Therefore, the nonlinearity likely has had minimal effect on the estimation of seismicity parameters. However, the stronger departure from linear scaling observed for the I_0 - M pairs, coupled with the incorporation of uncertainty in magnitude estimates through the use of M^* or N^* adjustments, produced significant departures from exponential behavior in initial estimates of earthquake recurrence rates as a function of magnitude as well as possible overestimation of magnitudes from small intensities. The change in scaling slope may be due to inherent nonlinearity in the I_0 - M relationship, or it may be affected by truncation in the observed data at the lower magnitude and intensity levels. Truncation of the data is likely on the magnitude axis because of the limited number of small values of M reported in the literature and in various catalogs. Truncation of the data is likely on the intensity axis because of the lack of intensity reporting for recent earthquakes in earthquake catalogs and the limited felt areas of small earthquakes.

In order to investigate the possible effects of magnitude truncation on the scaling, the I_0 - M data were analyzed in reverse order (i.e., I_0 is estimated a function of M). Figure 3.3-48 shows the data from Figure 3.3-46 plotted with M as the independent variable. The value of I_0 as a function of M can be considered as a categorical response, one that falls into discrete categories. For the intensity data, the categories are ordered. One method of modeling ordered categorical responses is the proportional odds model (e.g., Fox, 2002), which provides the probability of a response being in the individual classes as a function of the predictor variables. This is a generalization of the logistic model for dichotomous (0-1) response variables. The result of fitting the model is a relationship between M and the probability of observing a specific category of I_0 . Figure 3.3-49 shows examples of these relationships from fits to the data shown on Figure 3.3-48. The magnitude at which the maximum probability is obtained for each intensity class is shown by the red circles on Figure 3.3-48. These results indicate an approximately linear relationship between the value of M that maximizes the probability of observing a particular intensity class and the nominal intensity class value for M 3 and greater and I_0 IV and greater.

The proportional odds model imposes the requirement that the logistic models for each intensity class differ only by their intercepts; that is, they have the same coefficient applied to magnitude. A less restrictive model is the multinomial logit model, in which the order of the categories is not important. Applying this model produces the values of \mathbf{M} that maximize the probability of observing a particular intensity class shown by the blue diamonds on Figure 3.3-48. These results are more scattered at the edges of the data as the model parameters are less restricted by the functional form. However, the multinomial results also suggest an approximately linear trend over the same range as the proportional odds model. Based on these results it is concluded that a linear relationship between I_0 and \mathbf{M} is appropriate for the CEUS SSC catalog data, at least for I_0 above IV.

Initial analysis of the I_0 - \mathbf{M} data produced scaling relationships that appeared inconsistent with published relationships between I_0 and m_b and the relationships between m_b and \mathbf{M} developed here, suggesting a possible bias in the data sample. Figure 3.3-50 shows the data from the project catalog for earthquakes with reported values of I_0 and m_b (m_b , m_{bLg} , M_N , $m_{Lg(f)}$). The solid circles indicate those earthquakes that also have a value of \mathbf{M} . The blue and red curves show locally weighed least-squares (Loess) fits to the entire data set and only those earthquakes with reported values of \mathbf{M} , respectively. As can be seen, there is an offset in the fit for the subset of earthquakes with reported values of \mathbf{M} compared to the fit of the larger data set. Also shown on Figure 3.3-50 are the relationships between I_0 and m_b developed by EPRI (1988) and Sibol et al. (1987).

As discussed above, linear relationship between I_0 and magnitude is appropriate in the magnitude range of interest for this study. Figure 3.3-51 shows a linear least-squares fit to the data for values of $I_0 \geq V$. Again, the subset with \mathbf{M} shows an offset in the scaling relationship compared to that obtained for the full I_0 - m_b data set. Figures 3.3-52 and 3.3-53 show the effect of repeating the analysis using values of m_b adjusted for differences in m_b to \mathbf{M} scaling found in Section 3.3.2.3. These results show the same effect as the analysis of the reported m_b values without adjustment.

To address the apparent bias in the sample of earthquakes with just I_0 and \mathbf{M} data, the regression data set was augmented with the much larger data set of earthquakes, with I_0 and m_b using \mathbf{M} estimated from m_b for those earthquakes without values of \mathbf{M} . However, the effect of the underlying exponential distribution in earthquake sizes needs to be accounted for in mixing the data from earthquakes with values of \mathbf{M} with data where \mathbf{M} is estimated from m_b . The reported values of moment magnitude are designated $\hat{\mathbf{M}}$ to indicate that they are measured with uncertainty. As described in Section 3.3.1, regression of \mathbf{M} versus m_b produces the estimate $E[\mathbf{M}]$. Equation 3.3.1-5 shows that adjusting the values of $E[\mathbf{M}|m_b]$ to be consistent with $\hat{\mathbf{M}}$ requires addition of the factor $\beta \sigma^2[\mathbf{M}|m_b]$. Using the value of $\sigma^2[\mathbf{M}|m_b]$ of 0.24 found in Section 3.3.2.3 and a b -value of 0.95 (the value typically obtained from analysis of the catalog), the estimated values of $E[\mathbf{M}|m_b]$ were adjusted upward by 0.12 magnitude units before combining with the $\hat{\mathbf{M}}$ data set.

Figure 3.3-54 shows the resulting composite data set used to estimate the I_0 to \mathbf{M} conversion. Plotted on the figure is a locally weighted least-squares (Loess) fit to the data. Also plotted are the relationships of EPRI (1988) and Sibol et al. (1987) shifted by an average m_b to \mathbf{M} factor of

-0.32. The fit to the I_0 - \mathbf{M} data is now consistent with past models for the relationship between I_0 and m_b and the relationship between m_b and \mathbf{M} found in this study.

The Loess model fit indicates a break in slope between I_0 IV and V, consistent with the indication that a linear relationship between I_0 and \mathbf{M} is appropriate for larger intensity values. Therefore, the data set was trimmed to remove $I_0 \leq IV$. Figure 3.3-55 shows a linear fit to the data for $I_0 > IV$. Although there is large scatter, tests of the residuals using the method of Grubbs (1950) did not indicate the presence of outliers in the data set. In addition, a robust regression produces a relatively small reduction in standard error from 0.56 to 0.49. The linear model has a slope of 2/3.

Cavallini and Rebez (1996) propose that a linear model is not appropriate for relating I_0 to magnitude over the entire range because I_0 is bounded; in particular, as magnitude increases, I_0 is limited to a maximum of XII. They propose instead the use of an inverse sigmoid curve, which is represented by the inverse of the error function (Erf) and the function form:

$$M = C_1 + C_2 \sqrt{2} \text{Erf}^{-1} \left[\frac{I_0}{6} - 1 \right] \quad (3.3.2-1)$$

The model represented by Equation 3.3.2-1 was also fit to the data, with the result of a very slight improvement in the fit. However, one issue with the form specified by Cavallini and Rebez (1996) is that it does not allow for I_0 to reach its maximum of XII. There are insufficient data in the project catalog with which to define an appropriate shape at the upper end. In order to allow for I_0 equal to XII, Equation 3.3.2-1 was modified to the following form:

$$M = C_1 + C_2 \sqrt{2} \text{Erf}^{-1} \left[\frac{(I_0 - 6)}{6.5} \right] \quad (3.3.2-2)$$

The fit of Equation 3.3.2-2 to the project data is shown on Figure 3.3-55. The fit is essentially identical to the linear model over most of the range of the data, and is slightly better at the upper end. The inverse sigmoid model has a slightly lower AIC value.

The resulting linear model is

$$\begin{aligned} E[\mathbf{M}] &= 0.017 + 0.666I_0 \\ \sigma_{\mathbf{M}|I_0} &= 0.50 \end{aligned}$$

and the inverse sigmoid model is

$$\begin{aligned} E[\mathbf{M}] &= 4.008 + 3.411 \times \sqrt{2} \text{Erf}^{-1} \left[\frac{(I_0 - 6)}{6.5} \right] \\ \sigma_{\mathbf{M}|I_0} &= 0.50 \end{aligned}$$

The value of $\sigma_{\mathbf{M}|I_0} = 0.50$ reflects the value of 0.56 obtained from regression reduced by the average value of $\sigma[\mathbf{M}|\hat{\mathbf{M}}] = 0.25$ for the earthquakes used in the regression (Equation 3.3.1-8), which includes the estimates of \mathbf{M} from m_b .

F-tests for unequal variances at I_0 values above and below I_0 VI and above and below I_0 VII found no statistically significant differences.

Another issue with the form proposed by Cavallini and Rebez (1996) occurs at the lower end of the intensity scale. An assigned intensity value of $I_0 = I$ means the event was too small to be felt, but this does not require an extremely small negative magnitude. For this project the differences between the linear and inverse sigmoid fit are insignificant over most of the I_0 range of interest. Therefore, the linear fit was used for $I_0 \leq VI$ and the inverse sigmoid fit was used for $I_0 > VI$.

3.3.2.9 Uniform Moment Magnitude Catalog of $E[\mathbf{M}]$ and N^* Values

As described in Section 3.3.1, the uniform magnitude measure used in the CEUS SSC earthquake catalog is $E[\mathbf{M}]$, the expected value of moment magnitude given its uncertainty in estimation. The hierarchy of estimates used to develop this size measure is as follows:

1. If an estimate of moment magnitude from assessment of the long-period amplitude of the source spectrum is available (e.g., a Harvard Centroid Moment Tensor solution), then it is used as the only size measure. The estimate is designated $\hat{\mathbf{M}}$ to indicate that it is measured with uncertainty. This is consistent with the approach used to develop the EPRI-SOG catalog and is based on the assumption that a direct estimate of moment magnitude is greatly preferred over one estimated from other size measures.
2. Special studies of larger pre-instrumental earthquakes have derived estimates of \mathbf{M} from the area of isoseismals (e.g., Johnston et al., 1994; Johnston, 1996b) or from the intensity field and its fall-off with distance (e.g., Bakun and Hopper, 2004b; Bakun et al., 2003). If these are available for an earthquake, then they are preferred over estimates developed from the regressions against intensity measures developed in this study. Moment magnitude estimates based on use of isoseismal areas given in Johnston et al. (1994) and Johnston (1996b) were used, as the Johnston et al. (1994) relationships between felt area and \mathbf{M} are consistent with the project catalog data, and the use of multiple isoseismal areas is considered preferable to the use of just felt area. However, moment magnitudes given in Johnston et al. (1994) based on conversion from I_0 were not used because the conversion relationships developed for the CEUS SSC Project are considered more appropriate for moderate-sized earthquakes in the CEUS than the relationships developed by Johnston et al. (1994) and Johnston (1996b) from worldwide I_0 data.
3. Approximate moment magnitudes from the studies of Atkinson (2004a, 2004b), Boatwright (1994), and Moulis (2002) provide estimates of \mathbf{M} . These are treated as estimates of \mathbf{M} from size measure X with its associated uncertainty and are combined with estimates from other size measures.
4. For the majority of earthquakes, the values of $E[\mathbf{M}]$ are based on other size measures, \mathbf{X} . These include other magnitude scales and the macroseismic values of $\ln(\text{FA})$ or I_0 . The estimates from the available size measures \mathbf{X} are combined using the variance weighted approach of Equations 3.3.1-9 and 3.3.1-10.

The values of $E[\mathbf{M}]$ and $\sigma[\mathbf{M}]$ obtained for each earthquake are given in the project catalog listed in Appendix B, Table B-1. Using the values of $\sigma[\mathbf{M}]$ and a b -value of 0.95 determined from initial analysis of the catalog, values of the equivalent counts N^* are computed using Equation 3.3.1-12. These values are also listed in the project catalog (Table B-1).

3.4 Identification of Independent Earthquakes

The PSHA formulation typically used to model the occurrence of distributed seismicity is based on the Poisson model for the occurrence of independent earthquakes. Therefore, dependent earthquakes (foreshocks and aftershocks) must be identified and not included in the earthquake statistics used to develop estimates of earthquake recurrence rates. This process is referred to as catalog declustering. There are several techniques in use for the identification of dependent earthquakes. One of the first methods to be developed was that proposed by Gardner and Knopoff (1974), in which all smaller earthquakes within a fixed time and distance window around a larger earthquake are classified as dependent earthquakes. Gardner and Knopoff (1974) developed estimates of the size of the time and distance windows as a function of earthquake magnitude from analyses of Southern California earthquakes. Their approach and time and distance windows are widely used and form the basis for the identification of dependent earthquakes in the earthquake catalog used by the USGS for seismic hazard mapping in the CEUS (Petersen et al., 2008). Other applications of this approach have developed alternative criteria for the magnitude-dependent time and distance windows of foreshock and aftershock sequences, such as those developed by Grünthal (1985) for central Europe earthquakes.

Another approach was developed by Reasenber (1985) based on fitting an Omori aftershock decay model to earthquakes in the space-time vicinity of a larger earthquake to define the length of an aftershock sequence. Again, all earthquakes that occur within a fitted aftershock sequence are identified as dependent earthquakes.

EPRI-SOG (EPRI, 1988, Vol. 1) developed a somewhat different approach for identification of dependent earthquakes involving the use of statistical testing to identify clusters of earthquakes. The basic concept is illustrated on Figure 3.4-1. The earthquake catalog is analyzed starting with the largest earthquake and proceeding to the smallest. In the vicinity of an earthquake selected from this ordered sequence, two space-time windows are constructed according to user specified criteria. The first is a local window, W_l , in the immediate vicinity of the selected earthquake with space-time volume V_l . The second is a much larger extended window, W_e , with volume V_e . The local and extended windows contain observed earthquake counts of n_l and n_e , respectively. Assuming that the occurrence of earthquakes in the space-time vicinity of the earthquake being tested is a stationary Poisson process with unknown intensity parameter μ , then the random counts of earthquakes in each window, N_l , and N_e , would have expected values proportional to the volume of each window, μV_l and μV_e , respectively. The null hypothesis that there is no elevated seismicity in the space-time vicinity of the earthquake being tested is given by

$$H_0 : \frac{E[N_l]}{V_l} = \frac{E[N_e]}{V_e} \quad (3.4-1)$$

The alternative hypothesis that the earthquake intensity μ is higher in the local window (i.e., there is local clustering in space and time) is given by

$$H_1 : \frac{E[N_l]}{V_l} > \frac{E[N_e]}{V_e} \quad (3.4-2)$$

Citing Lehmann (1959), EPRI (1988, Vol. 1) indicates that under the null hypothesis H_0 and assuming that the expected value of N_e equals the observed value n_e , the hypothesis can be tested assuming that the number of earthquakes in the local window N_l had a binomial distribution with n_e trials and probability of success $p = V_l/V_e$. The distribution for N_l is given by

$$P(N_l = n_l | N_e = n_e) = \binom{n_e}{n_l} p^{n_l} (1-p)^{n_e - n_l} \quad (3.4-3)$$

The hypothesis H_0 is rejected when n_l exceeds the rejection limit n_l^R given by

$$n_l^R = \min \{ n \text{ for which } P(N_l > n | N_e = n_e) \leq \alpha \} \quad (3.4-4)$$

where α is a suitable low significance level. A value of 0.02 is recommended for α in EPRI (1988, Vol. 3).

Parts (b) and (c) of Figure 3.4.1 illustrate two additional tests performed if the null hypothesis is not rejected. Part (b) applies to the case where a local cluster extends outside the initial local window W_l such that the counts affect the estimated background rate in the extended window. A buffer around the local window is defined, W_b , and the volume and earthquake counts within the buffer are removed. The test of H_0 is then performed comparing the number of earthquakes within the local volume to the rate estimated from the extended window without the buffer region. Part (c) applies to the case where the cluster is too small (in time and/or space) to be observed within the initial local space-time window. A contraction factor is applied to the local window parameters to construct a smaller local window and the test is repeated.

If the null hypothesis is rejected, then the procedure moves to identifying the extent of the local cluster. This is accomplished by testing adjacent space and time windows around the local window for clustering by comparing the counts in these adjacent portions with the counts in the extended window W_e , ignoring those earthquakes already identified as a cluster. The process is continued until no additional space-time segments are identified that reject the null hypothesis.

The final step is illustrated on Figure 3.4-2. The EPRI (1988) procedure does not classify all earthquakes within the identified space-time window of the cluster as secondary (dependent) earthquakes. Instead, it uses a process of thinning the earthquake counts in the cluster region to the point where the intensity matches the background rate in the extended window W_e . This is accomplished by simulating a Poisson process within the cluster region using the background intensity μ . These simulated earthquakes are illustrated by the pluses in the top plot on Figure 3.4-2. The nearest neighbor among the recorded earthquakes to each simulated earthquake is identified as a primary earthquake (i.e., main shock). All the rest are then identified as secondary (dependent) earthquakes. The result is a space-time pattern of earthquakes that is consistent with the background rate, as shown in the bottom plot of Figure 3.4-2.

After the first pass through the earthquake catalog, the process is repeated for a second iteration with the secondary earthquakes identified in the first pass removed. It is suggested in EPRI (1988, Vol. 3) that two iterations are typically all that are needed.

The advantages of the EPRI (1988) approach are that it is insensitive to incompleteness, as a homogeneous Poisson process is only assumed in the general vicinity of the earthquake sequence being tested (the extended window W_e) and it does not assume a priori a shape for the clusters.

Testing during its development on synthetic catalogs generated by a Poisson process showed that it retained nearly all earthquakes as independent occurrences (Van Dyck, 1986).

Figure 3.4-3 shows the results of application of the EPRI (1988) declustering approach to the CEUS SSC catalog. The EPRI-SOG (EPRI, 1988) computer program EQCLUSTER was used for the calculations. The data points represent the length in days of individual clusters and the maximum distance between earthquakes assigned to a cluster and the identified mainshock. The red dashed lines indicate the average values as a function of $E[M]$. The blue dashed lines indicate the starting values for cluster size used in the declustering algorithm. These were taken from EPRI (1988), adjusting for the conversion from m_b to $E[M]$. Shown for comparison are the time and distance windows developed by Gardner and Knopoff (1974) for Southern California earthquakes and by Grünthal (1985) for central Europe earthquakes. The Gardner and Knopoff (1974) time windows shown are their published aftershock time windows multiplied by 1.5 to add a foreshock window based on the difference between the Grünthal (1985) aftershock and foreshock time windows. It should be noted that the time and distance windows developed by Gardner and Knopoff (1974) and Grünthal (1985) represent optimized envelopes to their observations. The average spatial dimension of the clusters identified in the project catalog is less than the published distance window envelopes, and the average time length of a cluster is comparable to the published envelope values. The EPRI (1988) procedure does identify some clusters that have a much longer duration than the published time windows.

In order to provide a comparison of the effect of alternative declustering approaches, the Gardner and Knopoff (1974) method was applied to the CEUS SSC catalog using the computer program CAT3E developed by Dr. Charles Mueller at the USGS for use in earthquake catalog processing for seismic hazard estimation. Table 3.4-1 compares the results of the two methods in terms of the number of independent earthquakes in various magnitude intervals. The two methods produce very similar results, with the overall difference in the number of independent earthquakes being about 1.5 percent. The largest difference is the numbers in the $E[M]$ 2.9 to 3.6 magnitude bin, but this difference is only 4.4 percent. Thus, it is concluded that the use of the alternative Gardner and Knopoff (1974) declustering approach would not have a significant effect on earthquake recurrence rates computed from the declustered catalog.

The dependent earthquakes identified with the EPRI (1988) procedure are indicated in the earthquake catalog listed in Appendix B, Table B-1.

3.5 Catalog Completeness

The assessment of earthquake catalog completeness is necessary in order to prevent underestimation of earthquake recurrence rates. One approach is to evaluate the detection capability of seismic networks as a function of time on the basis of density of stations and type of instrumentation. An example is McLaughlin et al.'s (1997) analysis of the capability of the U.S. National Seismic Network (USNSN). However, the more common approach is the use of the general technique first proposed by Stepp (1972). This approach evaluates the catalog completeness for specific magnitude ranges by starting at the present and moving back in time and counting the total number of earthquakes in the catalog in each magnitude interval. At each point in time when an earthquake in the specified magnitude interval occurred, the rate of earthquakes in the magnitude interval is computed by dividing the sum of the number of earthquakes from that point in time to the end of the catalog by the length in time from that point

to the end of the catalog. Assuming that the rate of earthquakes is constant in time, plotting these values versus date for the complete portion of the catalog will show an approximately horizontal line. As one moves further back in time, eventually the plotted line will start to trend downward, indicating that not all earthquakes are being reported (again assuming stationarity in time of the true rate). The point at which this downward trend begins indicates the beginning of the complete period of catalog reporting for the specific magnitude interval. These plots are sometimes referred to as “Stepp” plots, after their originator.

A common practice is to use this technique to identify the period of complete catalog reporting for each magnitude interval and then use only the data from that portion of the catalog to assess earthquake recurrence parameters. The length of catalog completeness is typically a function of magnitude, with larger magnitudes having longer completeness periods. The data identified in this way would be used to assess recurrence parameters using a procedure such as Weichert’s (1980) maximum likelihood formulation for binned magnitude data.

Using only the complete portion of the catalog may be quite satisfactory where the change in slope on a Stepp plot can be clearly defined and often may correspond to known seismic network changes. However, in regions with a long history of earthquake reporting through felt effects, there may be a long gradual decline in the level of completeness. Ignoring the data from the partially complete period may mean discarding information that is important to the assessment of seismic hazards.

The EPRI-SOG Project (EPRI, 1988, Vol. 1) developed an approach for incorporating the catalog data in the partially complete period into the assessment of earthquake recurrence parameters. Assuming that earthquakes in magnitude interval i occur as a constant Poisson process in time with rate λ_i , then the expected number of earthquakes to have occurred during the period of complete reporting T_i^C for magnitude interval i is equal to $\lambda_i T_i^C$. The maximum likelihood estimator for λ_i is given by

$$\lambda_i = \frac{N_i^C}{T_i^C} \quad (3.5-1)$$

where N_i^C is the number of earthquakes in magnitude interval i observed during the period of complete recording T_i^C . EPRI (1988) extended this concept into the period of incomplete recording. A parameter called the probability of detection, P^D , was defined that represented the probability that an earthquake in any point in time would be recorded and would appear in the seismic record. Again under the assumption of a stationary Poisson process, the expected number of earthquakes that would be observed in any time interval T_j is given by the expression

$$E[N_{ij}] = \lambda_i \times T_j \times P^D(m_i, T_j, X) \quad (3.5-2)$$

where $E[N_{ij}]$ is the expected number of earthquakes and $P^D(m_i, T_j, X)$ is the average probability of detection of earthquakes in magnitude interval m_i during time period T_j and over spatial locations X . Assessment of the rate parameter λ_i requires knowledge of P^D . If one assumes that the larger magnitudes are complete at present, and imposes the constraints that P^D should decrease more or less monotonically with increasing time into the past and should increase monotonically with magnitude at each point in time, then—again invoking stationarity—the parameters λ_i and P^D can be estimated jointly from the earthquake catalog data. Considering only

a single magnitude interval and ignoring the spatial aspect for the moment, the likelihood function for the observed number of earthquakes over the total duration of the catalog is given by

$$L = \prod_j \frac{(\lambda_i P_{ij}^D T_j)^{N_{ij}} \exp(-\lambda_i P_{ij}^D T_j)}{N_{ij}!} \quad (3.5-3)$$

where P_{ij}^D is a shortened notation for $P^D(m_i, T_j)$. The maximum likelihood solution for λ_i becomes

$$\lambda_i = \frac{\sum_j N_{ij}}{\sum_j P_{ij}^D T_j} \quad (3.5-4)$$

If the values of P_{ij}^D are known (or have been estimated previously), then the term in the denominator of Equation 3.5-4 can be replaced by what is called the effective period of completeness, T_{ij}^E , given by the expression

$$T_{ij}^E = \sum_j P_{ij}^D T_j \quad (3.5-5)$$

The maximum likelihood estimator of λ_i becomes equal to the total number of earthquakes in the catalog in magnitude interval i divided by the effective period of completeness for that magnitude interval.

EPRI (1988) developed an approach to jointly estimate the recurrence parameters that define λ_i and its spatial variability along with $P^D(m_i, T_j, X)$. The approach is termed penalized likelihood and is described in detail in Section 5.3.2, along with refinements developed for the CEUS SSC Project. The original formulation assessed earthquake recurrence parameters and $P^D(m_i, T_j, X)$ using a one-degree-longitude-by-one-degree-latitude discretization of the CEUS. While the enhancements of the methodology presented in Section 5.3.2 extend the methodology to smaller cell sizes, the original discretization is sufficient for the estimation of the probability of detection, as it is not expected to vary rapidly spatially across the CEUS. The original formulation as implemented in the EPRI-SOG program EQPARAM (EPRI, 1988, Vol. 3) was used to perform the assessment of $P^D(m_i, T_j, X)$. The program was modified to use the concept of N^* by changing the counting of earthquakes to the summing of the N^* values.

Through analysis of the history of population growth and earthquake recording, EPRI (1988) defined 13 completeness regions covering most of the CEUS. These regions represent portions of the CEUS where catalog completeness as a function of time and magnitude is assessed to be sufficiently similar such that it can be treated as the same. These completeness regions are shown on Figure 3.5-1 along with the independent earthquakes in the EPRI-SOG earthquake catalog. With the exceptions noted below, the information on the history of population growth and seismic network instrumentation has not changed significantly from what was available in the mid 1980's. Therefore, the EPRI (1988) completeness regions were used for the CEUS SSC Project with some modifications. The revised completeness regions together with the CEUS SSC Project catalog are shown on Figure 3.5-2. The modifications address additional sources of historical earthquakes used in the CEUS SSC Project that modify the history of catalog reporting

used in the EPRI-SOG study, and the extension of the completeness regions to cover the entire SSC model.

Two interior boundary modifications were made. First, the analysis of historical records, principally by Metzger et al. (2000), has extended the catalog coverage in the area around New Madrid. Consequently, the western boundary of Completeness Region 4 was extended to the southwest to incorporate the longer period of reporting in that area into the relatively long period of catalog reporting centered on New Madrid. The second significant change was to Completeness Regions 3 and 12. As shown on Figure 3.5-1, Completeness Region 3 covers both the Midwestern states west of New Madrid and the southern states all the way to eastern Tennessee and northern Georgia. The review of historical documents by various investigations, principally Munsey (2006), has greatly extended the completeness in the eastern portion of Completeness Region 3. Based on discussions with Jeffrey Munsey (pers. comm., 2011), Completeness Region 12 was expanded to cover this area, as the history of newspaper publishing in eastern Tennessee and northern Georgia is more similar to that of the western Carolinas than to the Midwestern states west of New Madrid. Other modifications include combining and extending Completeness Region 11 to cover the area north of the U.S.-Canada border, extending Completeness Region 11 into the northeastern Great Plains, and extending Completeness Region 1 to cover Texas. An additional Completeness Region 14 was added to cover the Gulf of Mexico, as offshore earthquakes in that area are important to the assessment of seismic hazards along the Gulf Coast.

EPRI (1988) defined time periods over which catalog completeness was assessed to be relatively constant. These time periods were 1625–1779, 1780–1859, 1860–1909, 1910–1949, 1950–1974, and post-1974. Figure 3.5-3 shows space-time plots of the independent earthquakes in the CEUS SSC catalog. The red lines denote the boundaries of the time periods defined by EPRI (1988). For the most part, these time periods coincide with changes in the density of recorded earthquakes and were retained for use in estimating completeness for the CEUS SSC catalog. An additional time period of 1995–2008 was added to accommodate the potential for recent improvements in earthquake recording.

More detailed examinations of catalog completeness as a function of time can be made on Figure 3.5-4. Shown are “Stepp” plots for each completeness region. These plots show a long history of earthquake recording in many areas of the CEUS with the typical trend of a gradual decay in completeness with increasing time into the past. These results indicate the importance of using a methodology that allows for the incorporation of most of this history into the assessment of earthquake recurrence rates and their spatial variation across the CEUS.

The catalog completeness analysis and subsequent assessment of earthquake recurrence parameters uses earthquakes binned in magnitude intervals. These magnitude intervals were centered on $E[M]$ values obtained from conversion of whole-degree values of I_0 to mimic the grouping of the converted magnitudes. These magnitude intervals are 2.9 to 3.6, 3.6 to 4.3, 4.3 to 5.0, 5.0 to 5.7, 5.7 to 6.4, 6.4 to 7.1, and 7.1 and higher.

Following EPRI (1988), the probabilities of detection were calculated using no spatial smoothing on the rate parameter, and medium smoothing on b , and no prior on b . As discussed in Section 5.3.2, several analysis cases were performed that assign different weights to the lower magnitude intervals to address potential departures from exponential behavior. These are Case A, full weight on all magnitude intervals; Case B with a reduced weight of 0.1 on the lowest

magnitude interval; and Case E with elimination of the first magnitude interval and 0.3 weight on the second interval.

McLaughlin et al. (1997) analyzed the capability of the USNSN and associated regional networks to detect at least four P waves for each earthquake. The analysis shows that for most of the eastern United States, there is 80 percent probability of detecting earthquakes with $m_{blg} = 3.25$. The detection capability decreases toward the Atlantic Ocean to the east and toward the Gulf of Mexico to the south. The probability of detection is less than 80 percent in parts of southern Indiana, Illinois, and western Kentucky due to the scarcity of stations in the upper Midwest. If the Canadian stations are added to the USNSN, the probabilities increase in the northern United States and southern Canada. During 2004–2006, the USNSN was upgraded and expanded to become the current ANSS backbone national network of nearly 100 stations, and many ANSS regional network stations have been added in the CEUS during the past decade. However, the USNSN analysis still serves as a useful baseline for assessing the level of catalog completeness at the end of the twentieth century.

Based on the results presented in McLaughlin et al. (1997), the earthquake catalog for the study region was assumed complete (probability of detection of 1.0) for all magnitude intervals in the time period 1995–2008 in most of the completeness regions. Locally, the probability of detection of the first two magnitude intervals was calculated, and the results are lower than 1.0.

The estimated probabilities of detection for the magnitude and time intervals are given in Tables 3.5-1, 3.5-2, and 3.5-3 for Cases A, B, and E, respectively.

The final step in the catalog analysis was the computation of regional b -values for the CEUS. These values were used as prior values to aid in the penalized-likelihood estimation of earthquake recurrence parameters as described in Section 5.3.2. The regional b -values were computed using the Weichert (1980) formulation, with N given by the sum of the N^* values and T defined as T^E for each magnitude and completeness region. The calculations were made assuming a homogeneous seismicity rate in each completeness region that was allowed to vary from completeness region to completeness region, but a constant b -value over the entire CEUS. The following table lists the computed regional b -values.

Regional b -Values Assessed for the CEUS SSC Project Catalog

Magnitude Weighting Case	Regional b -value
A	1.02
B	0.99
E	1.00

Table 3.2-1
Summary of Earthquakes Added–USGS Earthquake Catalog by Time Period

Time Period	Number of Earthquakes in E[M] Magnitude Range						Total
	2.9–3.6	3.6–4.3	4.3–5.0	5.0–5.7	5.7–6.4	≥6.4	
1558 through 1799	9	6	1	1	0	0	17
1800 through 1899	106	58	23	3	0	0	190
1900 through 1959	40	10	13	5	0	1	69
1960 through 2006	285	27	5	2	0	0	319
2007 and 2008	49	8	3	1	0	0	61

Table 3.2-2
Summary of Earthquakes Added–USGS Earthquake Catalog by Source

Source	Number of Earthquakes in E[M] Magnitude Range						Total
	2.9–3.6	3.6–4.3	4.3–5.0	5.0–5.7	5.7–6.4	≥6.4	
Metzger et al. (2000)	20	21	9	2	0	0	52
Munsey (2006)	44	17	11	0	0	0	72
GSC/NEDB and Burke (2009)	44	6	1	2	0	0	53
SUSN only	54	2	2	1	0	0	59
Single source, such as Lamont-Doherty; Ohio Survey; Oklahoma Survey; Reinbold and Johnston (1987); Seeber and Armbruster (1987); Saint Louis University; Weston Observatory; Adams and Simmons (1991); Bent (2003); CERI; Ma and Atkinson (2006); SCSN; Stover and Coffman (1993); Sykes et al. (2008)	70	16	5	1	0	0	92
Contained in multiple other sources	208	39	14	5	0	1	267

Table 3.3-1
Conversion Relationships Used—Develop Uniform Moment Magnitudes E[M]

Size Measure	Conversion Relationship	$\sigma[M X]$
Body-wave magnitude (m_b , m_{bLg} , $m_{Lg(f)}$, M_N)	$E[M] = m_b - 0.316 - 0.118Z_{NE} - 0.192Z_{1997GSC} + 0.280Z_{1982NE}$ <p>$Z_{NE} = 1$ for earthquakes located in the Northeast (northeast of the dashed line on Figure 3.3-16, including GSC data), and 0 otherwise</p> <p>$Z_{1997GSC} = 1$ for earthquakes occurring after 1997 recorded by GSC, and 0 otherwise</p> <p>$Z_{1982NE} = 1$ for earthquakes occurring in the Northeast before 1982 recorded by other than GSC, and 0 otherwise</p>	0.24
M_L reported by GSC	Compute $m_b = M_L - 0.21$ and use m_b conversion	0.42
M_S	$E[M] = 2.654 + 0.334M_S + 0.040M_S^2$	0.20
M_C , M_D , M_L in northeastern United States (other than GSC)	$E[M] = 0.633 + 0.806(M_C, M_D, \text{ or } M_L)$	0.27
M_C , M_D , M_L in midcontinent United States east of longitude 100°W	$E[M] = 0.869 + 0.762 (M_C, M_D, \text{ or } M_L)$	0.25
M_C , M_D , M_L in midcontinent United States west of longitude 100°W	Use m_b conversion	0.24
$\ln(FA)$ (in km^2)	$E[M] = 1.41 + 0.218 \times \ln(FA) + 0.00087\sqrt{FA}$	0.22
I_0	<p>for $I_0 \leq VI$</p> $E[M] = 0.017 + 0.666I_0$ <p>for $I_0 > VI$</p> $E[M] = 4.008 + 3.411 \times \sqrt{2} \text{Erf}^{-1} \left[\frac{(I_0 - 6)}{6.5} \right]$	0.50

Table 3.4-1
Comparison of CEUS SSC Catalog Declustering Results Obtained Using the
EPRI (1988) Approach with the Gardner Knopoff (1974) Approach

E[M] Magnitude Range	Number of Earthquakes in E[M] Magnitude Range		
	Entire Catalog	Independent Earthquakes Using EPRI (1988) Approach	Independent Earthquakes Using Gardner Knopoff (1974) Approach
2.9–3.6	2333	1787	1865
3.6–4.3	696	554	530
4.3–5.0	204	168	155
5.0–5.7	44	36	33
5.7–6.4	13	13	13
6.4–7.1	4	4	3
7.1–7.8	3	2	0
7.8–8.3	1	1	1

Table 3.5-1
Probability of Detection and Equivalent Periods of Completeness for the CEUS for
Magnitude Weighting Case A

Magnitude Interval	Probability of Detection for Time Period							Equivalent period of Completeness, TE (years)	Beginning of Usable Period
	1625–1780	1780–1860	1860–1910	1910–1950	1950–1975	1975–1995	1995–2009		
Region 1									
2.9–3.6	0	0	0	0.141	0.265	0.595	0.673	33.6	1910
3.6–4.3	0	0	0	0.212	0.531	0.595	1	47.7	1910
4.3–5.0	0	0	0	0.212	0.713	0.751	1	55.3	1910
5.0–5.7	0	0	0	0.961	0.961	1	1	96.5	1860
5.7–6.4	0	0	1	1	1	1	1	149.0	1860
6.4–8.3	0	0	1	1	1	1	1	149.0	1860
Region 2									
2.9–3.6	0	0	0.111	0.239	0.391	1	1	58.9	1860
3.6–4.3	0	0	0.181	0.672	1	1	1	94.9	1860
4.3–5.0	0	0	0.261	0.672	1	1	1	98.9	1860
5.0–5.7	0	0	0.261	1	1	1	1	112.1	1860
5.7–6.4	0	0	0.261	1	1	1	1	112.1	1860
6.4–8.3	0	0	0.261	1	1	1	1	112.1	1860
Region 3									
2.9–3.6	0	0	0.08	0.199	0.243	0.859	1	49.2	1860
3.6–4.3	0	0.056	0.381	0.529	0.743	0.859	1	94.4	1780
4.3–5.0	0	0.056	0.977	0.977	0.977	0.977	1	150.4	1780
5.0–5.7	0	0.428	1	1	1	1	1	183.2	1780
5.7–6.4	0	0.428	1	1	1	1	1	183.2	1780
6.4–8.3	0	0.428	1	1	1	1	1	183.2	1780
Region 4									
2.9–3.6	0	0	0.242	0.431	0.449	1	1	74.6	1860
3.6–4.3	0	0.239	0.756	0.756	0.756	1	1	140.1	1780
4.3–5.0	0	0.288	1	1	1	1	1	172.0	1780
5.0–5.7	0	0.56	1	1	1	1	1	193.8	1780
5.7–6.4	0	0.621	1	1	1	1	1	198.7	1780
6.4–8.3	0	0.621	1	1	1	1	1	198.7	1780
Region 5									
2.9–3.6	0	0.072	0.444	0.636	0.839	1	1	108.4	1780
3.6–4.3	0	0.5	0.567	0.788	0.839	1	1	154.8	1780
4.3–5.0	0.345	0.5	1	1	1	1	1	242.5	1625
5.0–5.7	0.345	0.5	1	1	1	1	1	242.5	1625
5.7–6.4	1	1	1	1	1	1	1	384.0	1625
6.4–8.3	1	1	1	1	1	1	1	384.0	1625

Magnitude Interval	Probability of Detection for Time Period							Equivalent period of Completeness, TE (years)	Beginning of Usable Period
	1625–1780	1780–1860	1860–1910	1910–1950	1950–1975	1975–1995	1995–2009		
Region 6									
2.9–3.6	0	0.164	0.735	0.735	1	1	1	138.3	1780
3.6–4.3	0	0.981	0.981	0.981	1	1	1	225.8	1780
4.3–5.0	0.434	1	1	1	1	1	1	296.3	1625
5.0–5.7	0.434	1	1	1	1	1	1	296.3	1625
5.7–6.4	0.434	1	1	1	1	1	1	296.3	1625
6.4–8.3	0.434	1	1	1	1	1	1	296.3	1625
Region 7									
2.9–3.6	0	0	0.185	0.185	0.446	0.635	0.635	49.4	1860
3.6–4.3	0	0	1	1	1	1	1	149.0	1860
4.3–5.0	0	0	1	1	1	1	1	149.0	1860
5.0–5.7	0	0	1	1	1	1	1	149.0	1780
5.7–6.4	0	0.746	1	1	1	1	1	208.7	1780
6.4–8.3	0	0.948	1	1	1	1	1	224.8	1780
Region 8									
2.9–3.6	0	0	0	0	0.38	1	1	43.5	1950
3.6–4.3	0	0	0	0	0.499	1	1	46.5	1950
4.3–5.0	0	0	0	0	1	1	1	59.0	1950
5.0–5.7	0	0	0	0	1	1	1	59.0	1910
5.7–6.4	0	0	0	0	1	1	1	59.0	1910
6.4–8.3	0	0	0	1	1	1	1	99.0	1910
Region 9									
2.9–3.6	0	0	0	0.257	0.543	0.652	0.652	46.0	1910
3.6–4.3	0	0	0.146	0.332	0.932	0.932	1	76.5	1860
4.3–5.0	0	0	0.244	1	1	1	1	111.2	1860
5.0–5.7	0	0	0.244	1	1	1	1	111.2	1860
5.7–6.4	0	0	0.244	1	1	1	1	111.2	1860
6.4–8.3	0	0	0.424	1	1	1	1	120.2	1860
Region 10									
2.9–3.6	0	0	0.107	0.451	0.774	1	1	76.7	1860
3.6–4.3	0	0.045	0.295	1	1	1	1	117.3	1780
4.3–5.0	0	0.49	0.49	1	1	1	1	162.7	1625
5.0–5.7	0	1	1	1	1	1	1	229.0	1625
5.7–6.4	0	1	1	1	1	1	1	229.0	1625
6.4–8.3	0	1	1	1	1	1	1	229.0	1625

Magnitude Interval	Probability of Detection for Time Period							Equivalent period of Completeness, TE (years)	Beginning of Usable Period
	1625–1780	1780–1860	1860–1910	1910–1950	1950–1975	1975–1995	1995–2009		
Region 11									
2.9–3.6	0	0	0	0	0.192	0.371	0.371	17.4	1950
3.6–4.3	0	0	0	0	0.59	0.59	1	40.5	1950
4.3–5.0	0	0	0	0	1	1	1	59.0	1910
5.0–5.7	0	0	0	0	1	1	1	59.0	1910
5.7–6.4	0	0	0	0	1	1	1	59.0	1910
6.4–8.3	0	0	0	0.673	1	1	1	85.9	1910
Region 12									
2.9–3.6	0	0.033	0.224	0.243	0.419	1	1	68.0	1780
3.6–4.3	0	0.109	0.373	0.373	0.926	1	1	99.4	1780
4.3–5.0	0	0.597	1	1	1	1	1	196.8	1625
5.0–5.7	0	1	1	1	1	1	1	229.0	1625
5.7–6.4	0	1	1	1	1	1	1	229.0	1625
6.4–8.3	0	1	1	1	1	1	1	229.0	1625
Region 13									
2.9–3.6	0	0	0.419	0.834	0.834	0.834	1	105.8	1860
3.6–4.3	0	0	0.995	1	1	1	1	148.7	1860
4.3–5.0	0	0	0.995	1	1	1	1	148.7	1860
5.0–5.7	0	0	0.995	1	1	1	1	148.7	1860
5.7–6.4	0	0	0.995	1	1	1	1	148.7	1860
6.4–8.3	0	0	0.995	1	1	1	1	148.7	1860
Region 14									
2.9–3.6	0	0	0	0	0	0	0.505	7.1	1995
3.6–4.3	0	0	0	0	0	0.364	0.505	14.3	1975
4.3–5.0	0	0	0	0	0.901	0.901	1	54.5	1950
5.0–5.7	0	0	0	0	0.901	0.901	1	54.5	1950
5.7–6.4	0	0	0	0	0.901	0.901	1	54.5	1950
6.4–8.3	0	0	0	0	1	1	1	59.0	1950

Table 3.5-2
Probability of Detection and Equivalent Periods of Completeness for the CEUS for
Magnitude Weighting Case B

Magnitude Interval	Probability of Detection for Time Period							Equivalent Period of Completeness, TE (years)	Beginning of Usable Period
	1625–1780	1780–1860	1860–1910	1910–1950	1950–1975	1975–1995	1995–2009		
Region 1									
2.9–3.6	0	0	0	0.156	0.292	0.587	0.746	35.7	1910
3.6–4.3	0	0	0	0.218	0.553	0.587	1	48.3	1910
4.3–5.0	0	0	0	0.218	0.697	0.735	1	54.8	1910
5.0–5.7	0	0	0	0.885	0.885	1	1	91.5	1860
5.7–6.4	0	0	1	1	1	1	1	149.0	1860
6.4–8.3	0	0	1	1	1	1	1	149.0	1860
Region 2									
2.9–3.6	0	0	0.109	0.235	0.386	1	1	58.5	1860
3.6–4.3	0	0	0.175	0.651	1	1	1	93.8	1860
4.3–5.0	0	0	0.252	0.651	1	1	1	97.6	1860
5.0–5.7	0	0	0.252	1	1	1	1	111.6	1860
5.7–6.4	0	0	0.252	1	1	1	1	111.6	1860
6.4–8.3	0	0	0.265	1	1	1	1	112.2	1860
Region 3									
2.9–3.6	0	0	0.072	0.178	0.217	0.697	1	44.1	1860
3.6–4.3	0	0.053	0.358	0.496	0.697	0.697	1	87.3	1780
4.3–5.0	0	0.053	0.964	0.964	0.964	0.964	1	148.4	1780
5.0–5.7	0	0.45	1	1	1	1	1	185.0	1780
5.7–6.4	0	0.45	1	1	1	1	1	185.0	1780
6.4–8.3	0	0.45	1	1	1	1	1	185.0	1780
Region 4									
2.9–3.6	0	0	0.201	0.356	0.372	0.735	1	62.3	1860
3.6–4.3	0	0.21	0.663	0.663	0.663	0.735	1	121.7	1780
4.3–5.0	0	0.267	1	1	1	1	1	170.4	1780
5.0–5.7	0	0.547	1	1	1	1	1	192.8	1780
5.7–6.4	0	0.644	1	1	1	1	1	200.5	1780
6.4–8.3	0	0.644	1	1	1	1	1	200.5	1780
Region 5									
2.9–3.6	0	0.078	0.482	0.69	0.958	0.958	1	115.1	1780
3.6–4.3	0	0.525	0.598	0.831	0.958	0.958	1	162.2	1780
4.3–5.0	0.352	0.525	1	1	1	1	1	245.6	1625
5.0–5.7	0.352	0.525	1	1	1	1	1	245.6	1625
5.7–6.4	1	1	1	1	1	1	1	384.0	1625
6.4–8.3	1	1	1	1	1	1	1	384.0	1625

Magnitude Interval	Probability of Detection for Time Period							Equivalent Period of Completeness, TE (years)	Beginning of Usable Period
	1625–1780	1780–1860	1860–1910	1910–1950	1950–1975	1975–1995	1995–2009		
Region 6									
2.9–3.6	0	0.175	0.782	0.782	1	1	1	143.4	1780
3.6–4.3	0	1	1	1	1	1	1	229.0	1780
4.3–5.0	0.438	1	1	1	1	1	1	296.9	1625
5.0–5.7	0.438	1	1	1	1	1	1	296.9	1625
5.7–6.4	0.438	1	1	1	1	1	1	296.9	1625
6.4–8.3	0.438	1	1	1	1	1	1	296.9	1625
Region 7									
2.9–3.6	0	0	0.187	0.187	0.466	0.646	0.646	50.4	1860
3.6–4.3	0	0	1	1	1	1	1	149.0	1860
4.3–5.0	0	0	1	1	1	1	1	149.0	1860
5.0–5.7	0	0	1	1	1	1	1	149.0	1780
5.7–6.4	0	0.72	1	1	1	1	1	206.6	1780
6.4–8.3	0	0.943	1	1	1	1	1	224.4	1780
Region 8									
2.9–3.6	0	0	0	0	0.537	1	1	47.4	1950
3.6–4.3	0	0	0	0	0.61	1	1	49.2	1950
4.3–5.0	0	0	0	0	1	1	1	59.0	1950
5.0–5.7	0	0	0	0	1	1	1	59.0	1910
5.7–6.4	0	0	0	0	1	1	1	59.0	1910
6.4–8.3	0	0	0	1	1	1	1	99.0	1910
Region 9									
2.9–3.6	0	0	0	0.329	0.696	0.834	0.834	58.9	1910
3.6–4.3	0	0	0.165	0.376	1	1	1	82.3	1860
4.3–5.0	0	0	0.24	1	1	1	1	111.0	1860
5.0–5.7	0	0	0.24	1	1	1	1	111.0	1860
5.7–6.4	0	0	0.24	1	1	1	1	111.0	1860
6.4–8.3	0	0	0.24	1	1	1	1	111.0	1860
Region 10									
2.9–3.6	0	0	0.131	0.554	0.949	1	1	86.4	1860
3.6–4.3	0	0.049	0.324	1	1	1	1	119.1	1780
4.3–5.0	0	0.479	0.479	1	1	1	1	161.3	1625
5.0–5.7	0	1	1	1	1	1	1	229.0	1625
5.7–6.4	0	1	1	1	1	1	1	229.0	1625
6.4–8.3	0	1	1	1	1	1	1	229.0	1625

Magnitude Interval	Probability of Detection for Time Period							Equivalent Period of Completeness, TE (years)	Beginning of Usable Period
	1625–1780	1780–1860	1860–1910	1910–1950	1950–1975	1975–1995	1995–2009		
Region 11									
2.9–3.6	0	0	0	0	0.229	0.442	0.442	20.8	1950
3.6–4.3	0	0	0	0	0.673	0.673	1	44.3	1950
4.3–5.0	0	0	0	0	1	1	1	59.0	1910
5.0–5.7	0	0	0	0	1	1	1	59.0	1910
5.7–6.4	0	0	0	0	1	1	1	59.0	1910
6.4–8.3	0	0	0	0.671	1	1	1	85.8	1910
Region 12									
2.9–3.6	0	0.04	0.27	0.293	0.506	1	1	75.1	1780
3.6–4.3	0	0.121	0.415	0.415	1	1	1	106.0	1780
4.3–5.0	0	0.619	1	1	1	1	1	198.5	1625
5.0–5.7	0	1	1	1	1	1	1	229.0	1625
5.7–6.4	0	1	1	1	1	1	1	229.0	1625
6.4–8.3	0	1	1	1	1	1	1	229.0	1625
Region 13									
2.9–3.6	0	0	0.277	0.469	0.552	0.552	1	71.4	1860
3.6–4.3	0	0	0.707	0.707	1	1	1	122.6	1860
4.3–5.0	0	0	0.707	0.707	1	1	1	122.6	1860
5.0–5.7	0	0	0.707	0.707	1	1	1	122.6	1860
5.7–6.4	0	0	0.707	0.86	1	1	1	128.7	1860
6.4–8.3	0	0	0.841	0.961	1	1	1	139.5	1860
Region 14									
2.9–3.6	0	0	0	0	0	0	0.209	2.9	1995
3.6–4.3	0	0	0	0	0	0.209	0.209	7.1	1975
4.3–5.0	0	0	0	0	0.633	0.633	1	42.5	1950
5.0–5.7	0	0	0	0	0.633	0.633	1	42.5	1950
5.7–6.4	0	0	0	0	0.633	0.633	1	42.5	1950
6.4–8.3	0	0	0	0	1	1	1	59.0	1950

Table 3.5-3
Probability of Detection and Equivalent Periods of Completeness for the CEUS for
Magnitude Weighting Case E

Magnitude Interval	Probability of Detection for Time Period							Equivalent Period of Completeness, TE (years)	Beginning of Usable Period
	1625–1780	1780–1860	1860–1910	1910–1950	1950–1975	1975–1995	1995–2009		
Region 1									
3.6–4.3	0	0	0	0.168	0.595	0.595	1	47.5	1910
4.3–5.0	0	0	0	0.168	0.743	0.784	1	55.0	1910
5.0–5.7	0	0	0	0.921	0.921	1	1	93.9	1860
5.7–6.4	0	0	1	1	1	1	1	149.0	1860
6.4–8.3	0	0	1	1	1	1	1	149.0	1860
Region 2									
3.6–4.3	0	0	0.177	0.584	1	1	1	91.2	1860
4.3–5.0	0	0	0.255	0.584	1	1	1	95.1	1860
5.0–5.7	0	0	0.255	1	1	1	1	111.7	1860
5.7–6.4	0	0	0.255	1	1	1	1	111.7	1860
6.4–8.3	0	0	0.255	1	1	1	1	111.7	1860
Region 3									
3.6–4.3	0	0.038	0.325	0.451	0.634	0.634	1	79.9	1780
4.3–5.0	0	0.038	0.939	0.939	0.939	0.939	1	143.8	1780
5.0–5.7	0	0.475	1	1	1	1	1	187.0	1780
5.7–6.4	0	0.475	1	1	1	1	1	187.0	1780
6.4–8.3	0	0.475	1	1	1	1	1	187.0	1780
Region 4									
3.6–4.3	0	0.15	0.473	0.473	0.473	0.473	1	89.9	1780
4.3–5.0	0	0.229	1	1	1	1	1	167.3	1780
5.0–5.7	0	0.568	1	1	1	1	1	194.4	1780
5.7–6.4	0	0.845	1	1	1	1	1	216.6	1780
6.4–8.3	0	0.845	1	1	1	1	1	216.6	1780
Region 5									
3.6–4.3	0	0.434	0.562	0.781	0.793	0.793	1	143.7	1780
4.3–5.0	0.324	0.434	1	1	1	1	1	233.9	1625
5.0–5.7	0.324	0.434	1	1	1	1	1	233.9	1625
5.7–6.4	1	1	1	1	1	1	1	384.0	1625
6.4–8.3	1	1	1	1	1	1	1	384.0	1625
Region 6									
3.6–4.3	0	1	1	1	1	1	1	229.0	1780
4.3–5.0	0.432	1	1	1	1	1	1	296.0	1625
5.0–5.7	0.432	1	1	1	1	1	1	296.0	1625
5.7–6.4	0.432	1	1	1	1	1	1	296.0	1625
6.4–8.3	0.432	1	1	1	1	1	1	296.0	1625

Magnitude Interval	Probability of Detection for Time Period							Equivalent Period of Completeness, TE (years)	Beginning of Usable Period
	1625–1780	1780–1860	1860–1910	1910–1950	1950–1975	1975–1995	1995–2009		
Region 7									
3.6–4.3	0	0	1	1	1	1	1	149.0	1860
4.3–5.0	0	0	1	1	1	1	1	149.0	1860
5.0–5.7	0	0	1	1	1	1	1	149.0	1780
5.7–6.4	0	0.681	1	1	1	1	1	203.5	1780
6.4–8.3	0	0.931	1	1	1	1	1	223.5	1780
Region 8									
3.6–4.3	0	0	0	0	0.53	0.628	0.628	34.6	1950
4.3–5.0	0	0	0	0	1	1	1	59.0	1950
5.0–5.7	0	0	0	0	1	1	1	59.0	1910
5.7–6.4	0	0	0	0	1	1	1	59.0	1910
6.4–8.3	0	0	0	1	1	1	1	99.0	1910
Region 9									
3.6–4.3	0	0	0.161	0.365	1	1	1	81.7	1860
4.3–5.0	0	0	0.218	1	1	1	1	109.9	1860
5.0–5.7	0	0	0.218	1	1	1	1	109.9	1860
5.7–6.4	0	0	0.218	1	1	1	1	109.9	1860
6.4–8.3	0	0	0.218	1	1	1	1	109.9	1860
Region 10									
3.6–4.3	0	0.055	0.362	1	1	1	1	121.5	1780
4.3–5.0	0	0.499	0.499	1	1	1	1	163.9	1625
5.0–5.7	0	0.991	1	1	1	1	1	228.3	1625
5.7–6.4	0	0.991	1	1	1	1	1	228.3	1625
6.4–8.3	0	0.991	1	1	1	1	1	228.3	1625
Region 11									
3.6–4.3	0	0	0	0	0.75	0.75	1	47.7	1950
4.3–5.0	0	0	0	0	1	1	1	59.0	1910
5.0–5.7	0	0	0	0	1	1	1	59.0	1910
5.7–6.4	0	0	0	0	1	1	1	59.0	1910
6.4–8.3	0	0	0	0.661	1	1	1	85.4	1910
Region 12									
3.6–4.3	0	0.123	0.422	0.422	1	1	1	106.8	1780
4.3–5.0	0	0.627	1	1	1	1	1	199.2	1625
5.0–5.7	0	1	1	1	1	1	1	229.0	1625
5.7–6.4	0	1	1	1	1	1	1	229.0	1625
6.4–8.3	0	1	1	1	1	1	1	229.0	1625

Magnitude Interval	Probability of Detection for Time Period							Equivalent Period of Completeness, TE (years)	Beginning of Usable Period
	1625–1780	1780–1860	1860–1910	1910–1950	1950–1975	1975–1995	1995–2009		
Region 13									
3.6–4.3	0	0	0.393	0.393	0.779	0.779	1	84.4	1860
4.3–5.0	0	0	0.393	0.393	0.779	0.779	1	84.4	1860
5.0–5.7	0	0	0.393	0.393	0.779	0.779	1	84.4	1860
5.7–6.4	0	0	0.535	0.798	1	1	1	117.7	1860
6.4–8.3	0	0	0.779	0.954	1	1	1	136.1	1860
Region 14									
3.6–4.3	0	0	0	0	0	0.155	0.155	5.3	1975
4.3–5.0	0	0	0	0	0.535	0.535	1	38.1	1950
5.0–5.7	0	0	0	0	0.535	0.535	1	38.1	1950
5.7–6.4	0	0	0	0	0.535	0.535	1	38.1	1950
6.4–8.3	0	0	0	0	1	1	1	59.0	1950

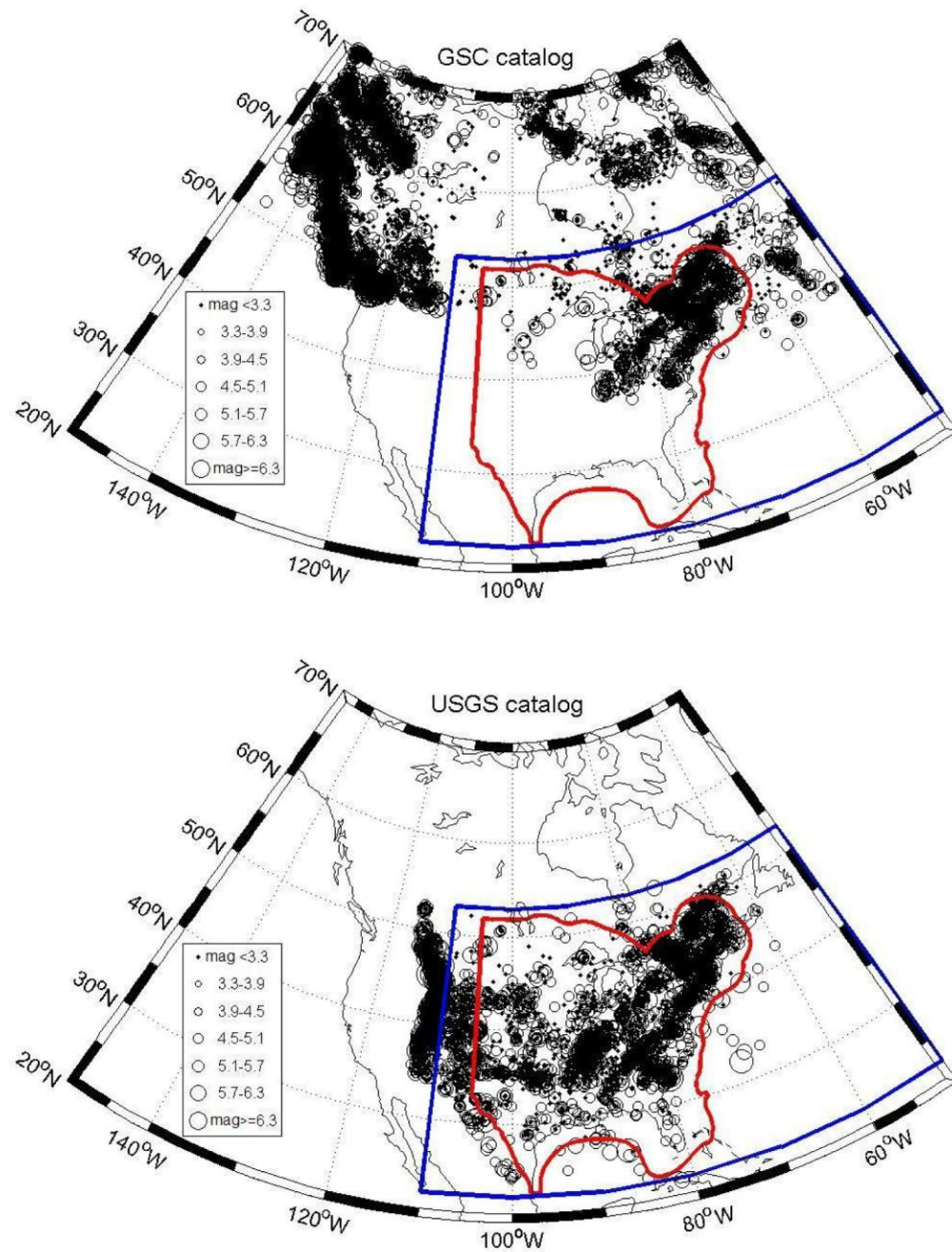


Figure 3.2-1
Areal coverage of the primary earthquake catalog sources. Top: GSC catalog (Halchuk, 2009); bottom: USGS seismic hazard mapping catalog (Petersen et al., 2008). Red line denotes boundary of study region. Blue line denotes portion of each catalog used for development of project catalog.

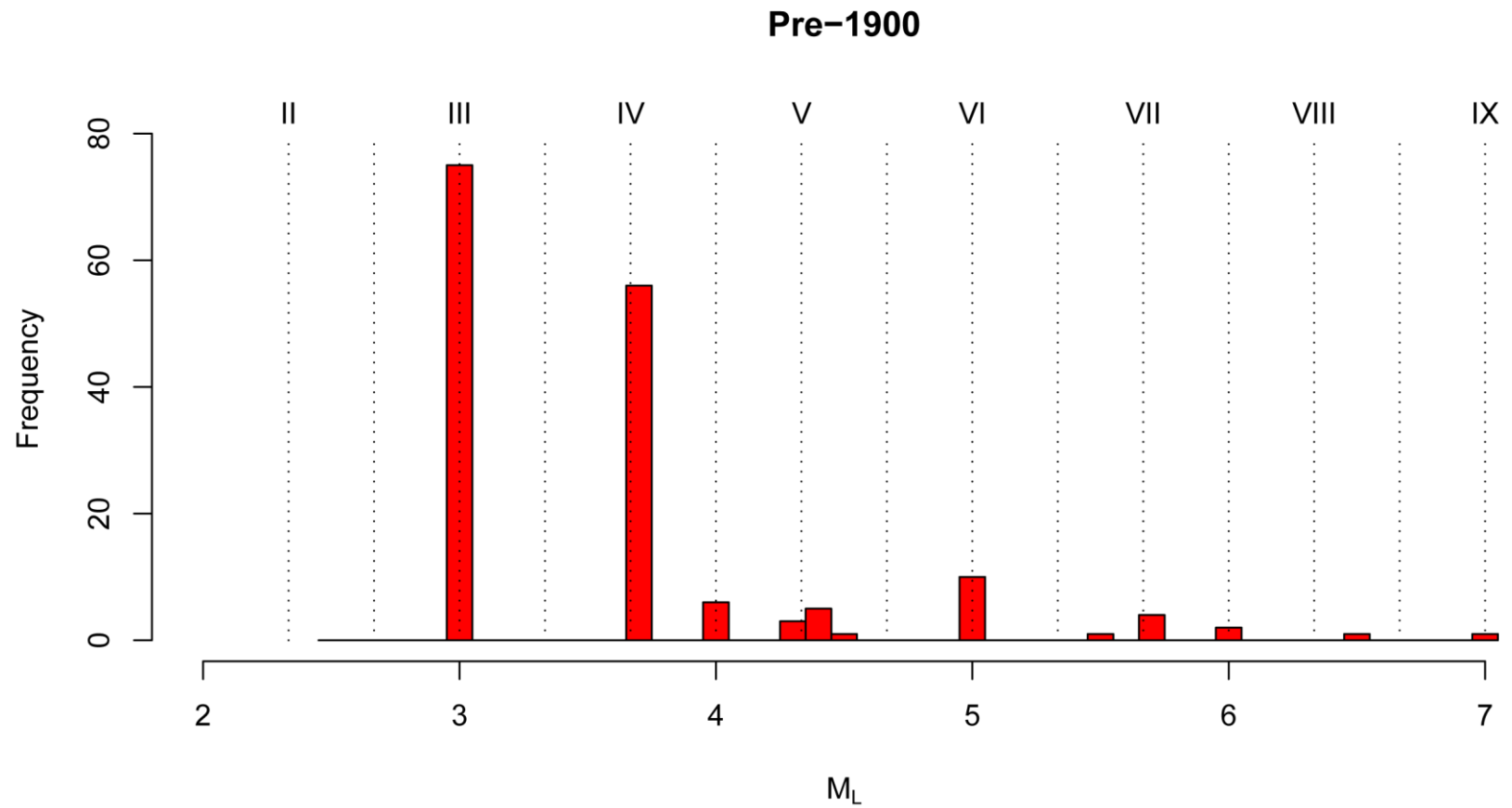


Figure 3.2-2
Histogram of M_L magnitudes from the GSC SHEEF catalog for the time period 1600-1899 and the region east of longitude -105° and south of latitude 53°

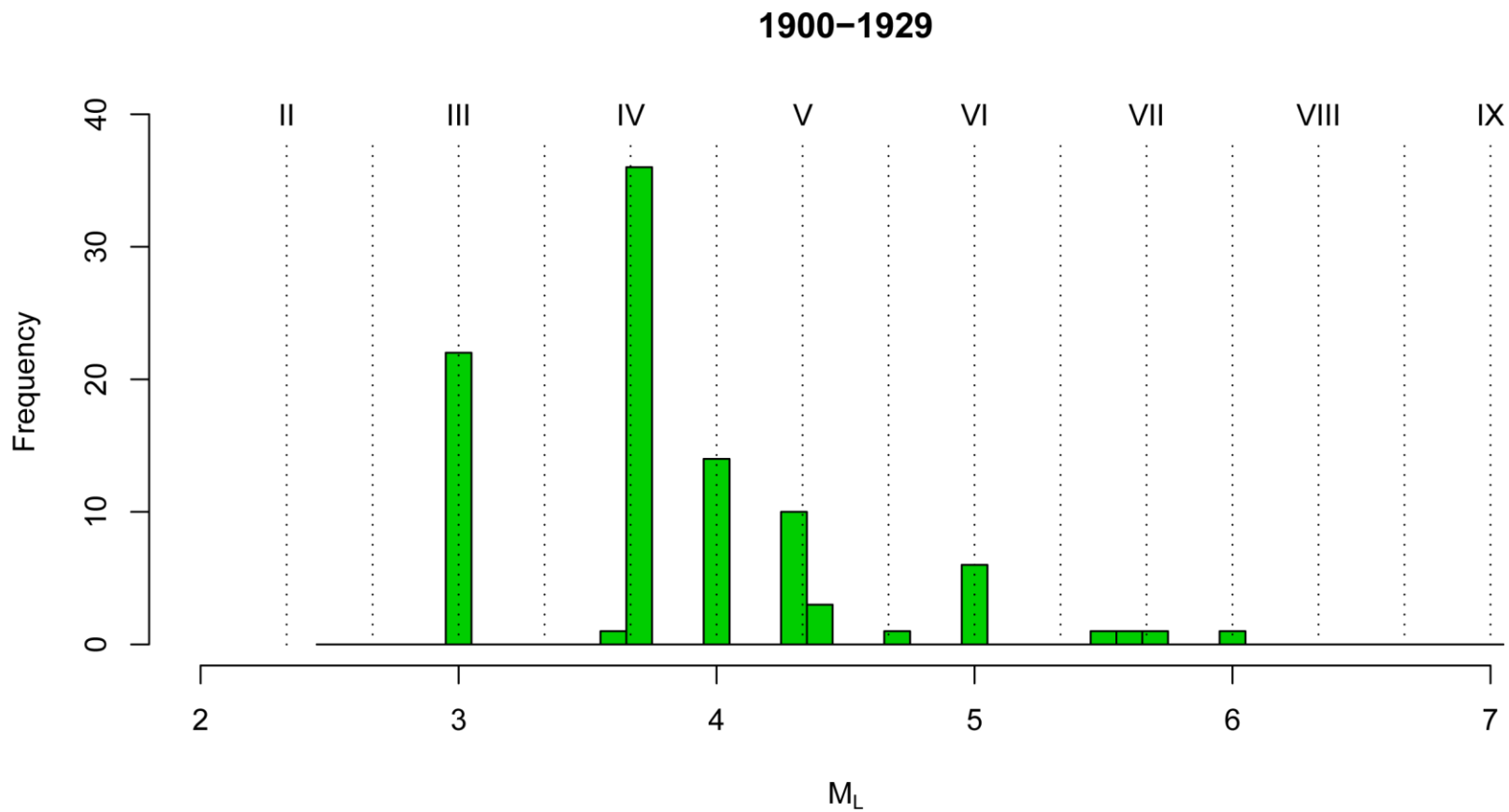


Figure 3.2-3
Histogram of M_L magnitudes from the GSC SHEEF catalog for the time period 1900-1929 and the region east of longitude -105° and south of latitude 53°

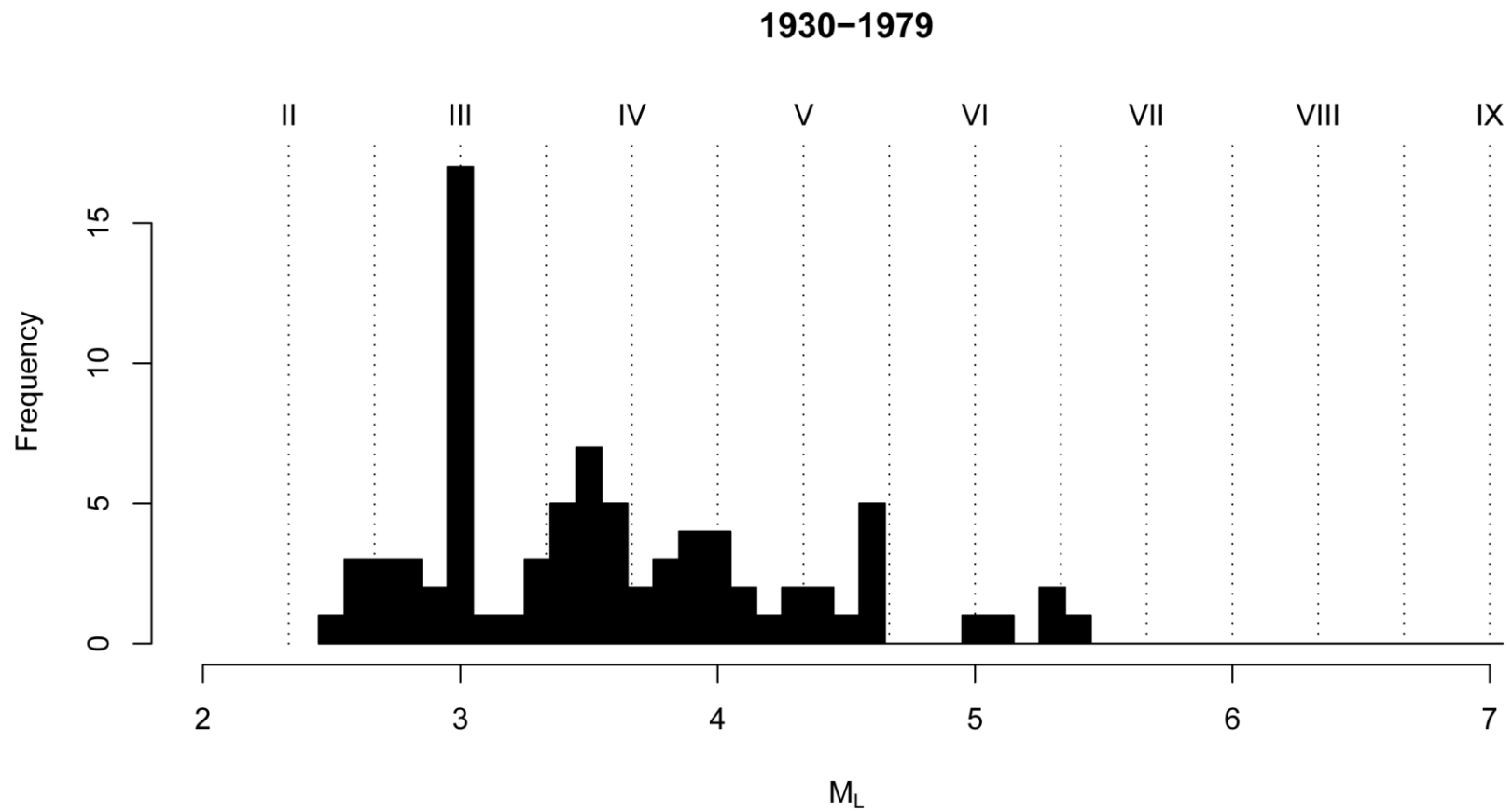


Figure 3.2-4
Histogram of M_L magnitudes from the GSC SHEEF catalog for the time period 1930-1979 and the region east of longitude -105° and south of latitude 53°

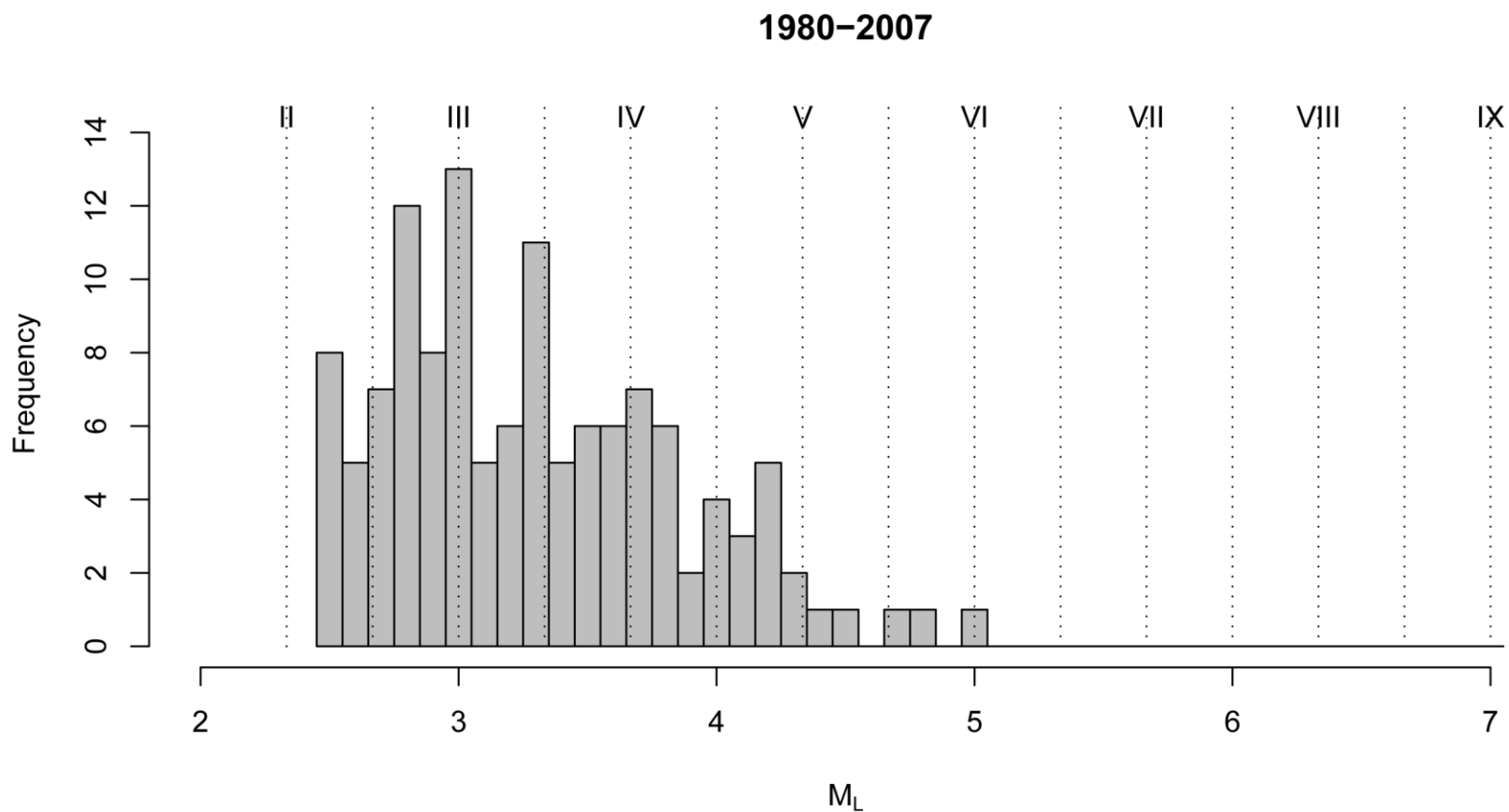


Figure 3.2-5
Histogram of M_L magnitudes from the GSC SHEEF catalog for the time period 1980-2007 and the region east of longitude -105° and south of latitude 53°

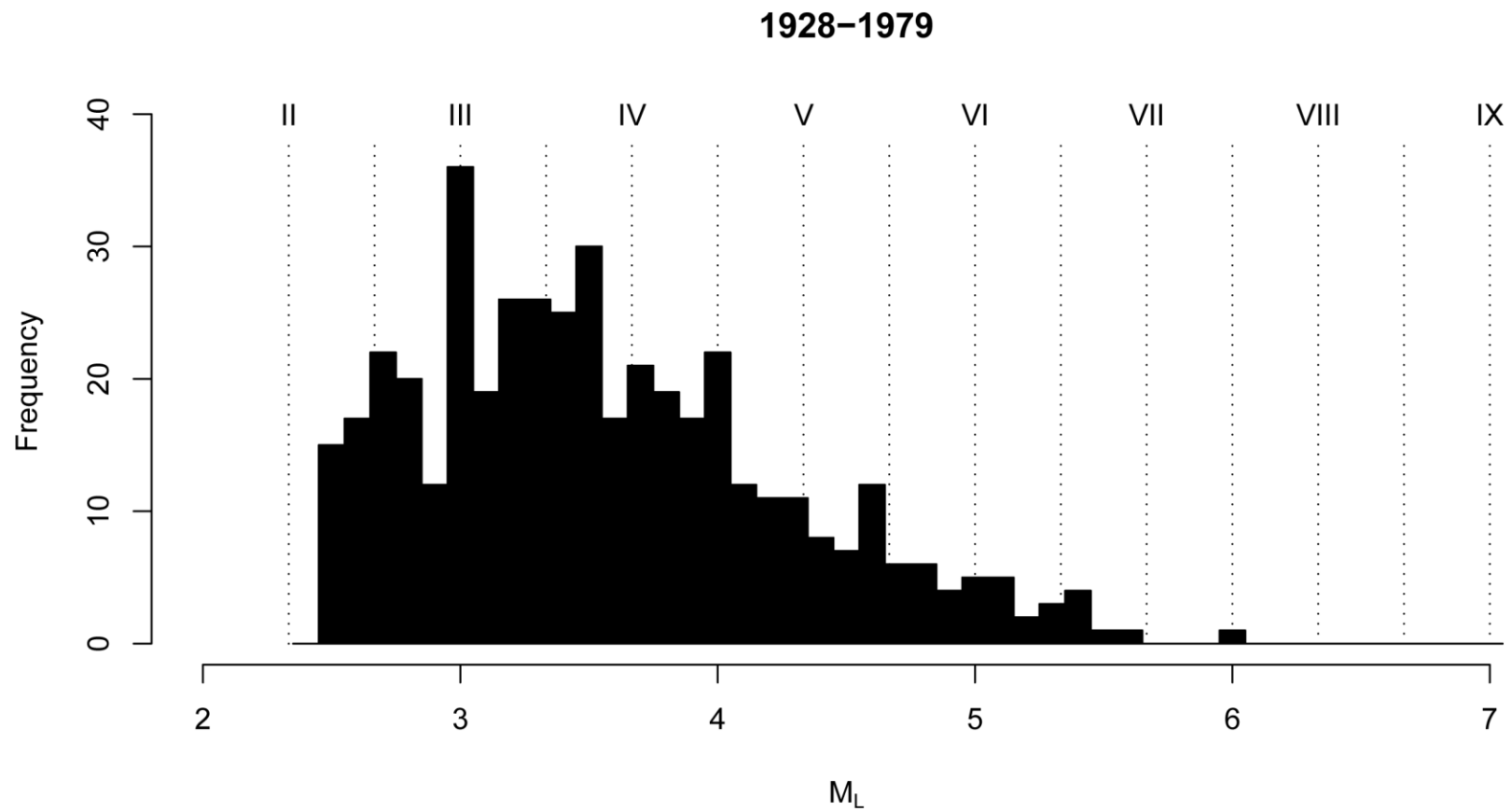


Figure 3.2-6
Histogram of M_L magnitudes from the revised catalog with GSC as the source for the time period 1928-1979

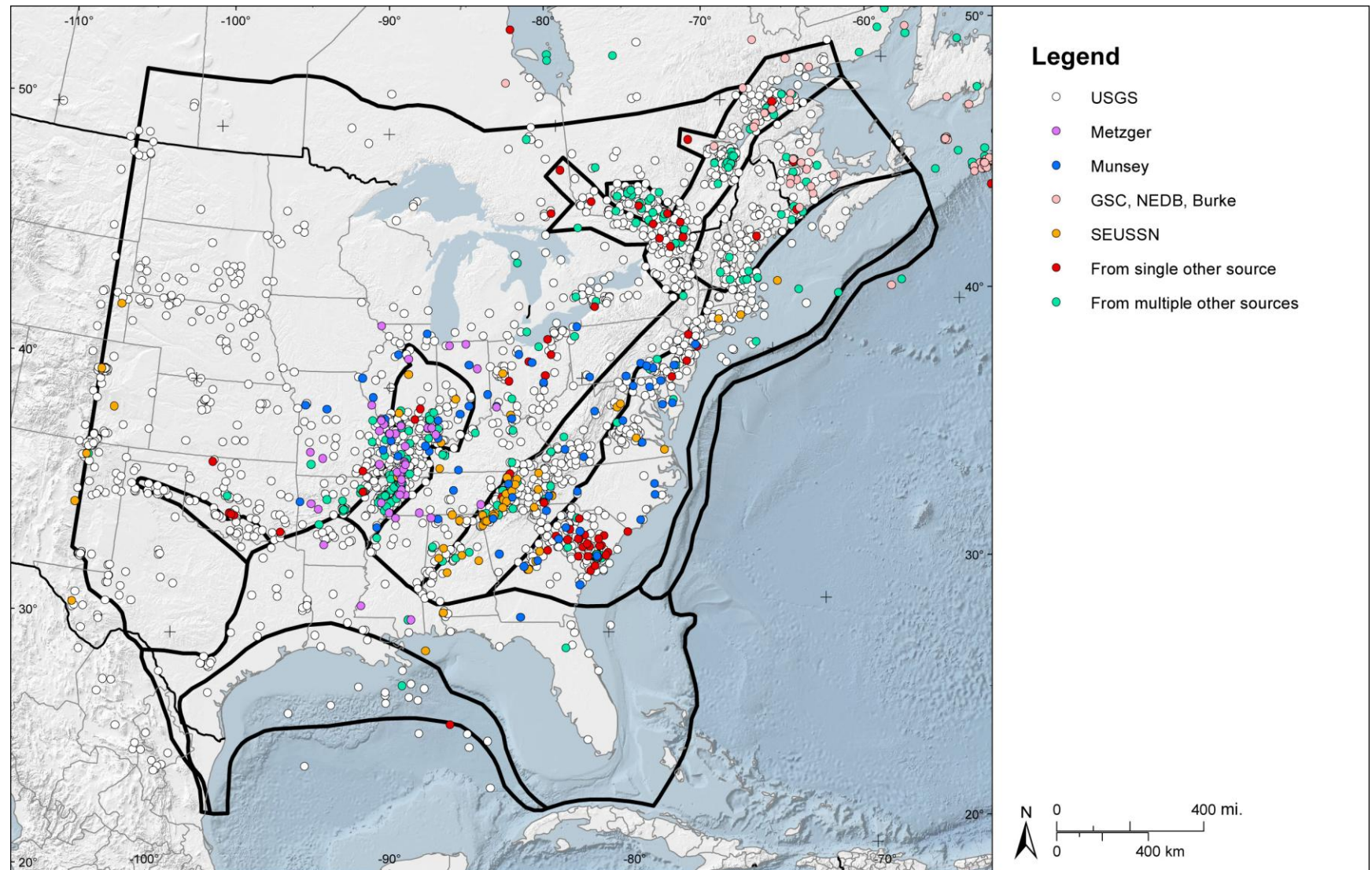


Figure 3.2-7
Map of the CEUS SSC Project catalog showing earthquakes of uniform moment magnitude $E[M]$ 2.9 and larger. Colored symbols denote earthquakes not contained in the USGS seismic hazard mapping catalog.

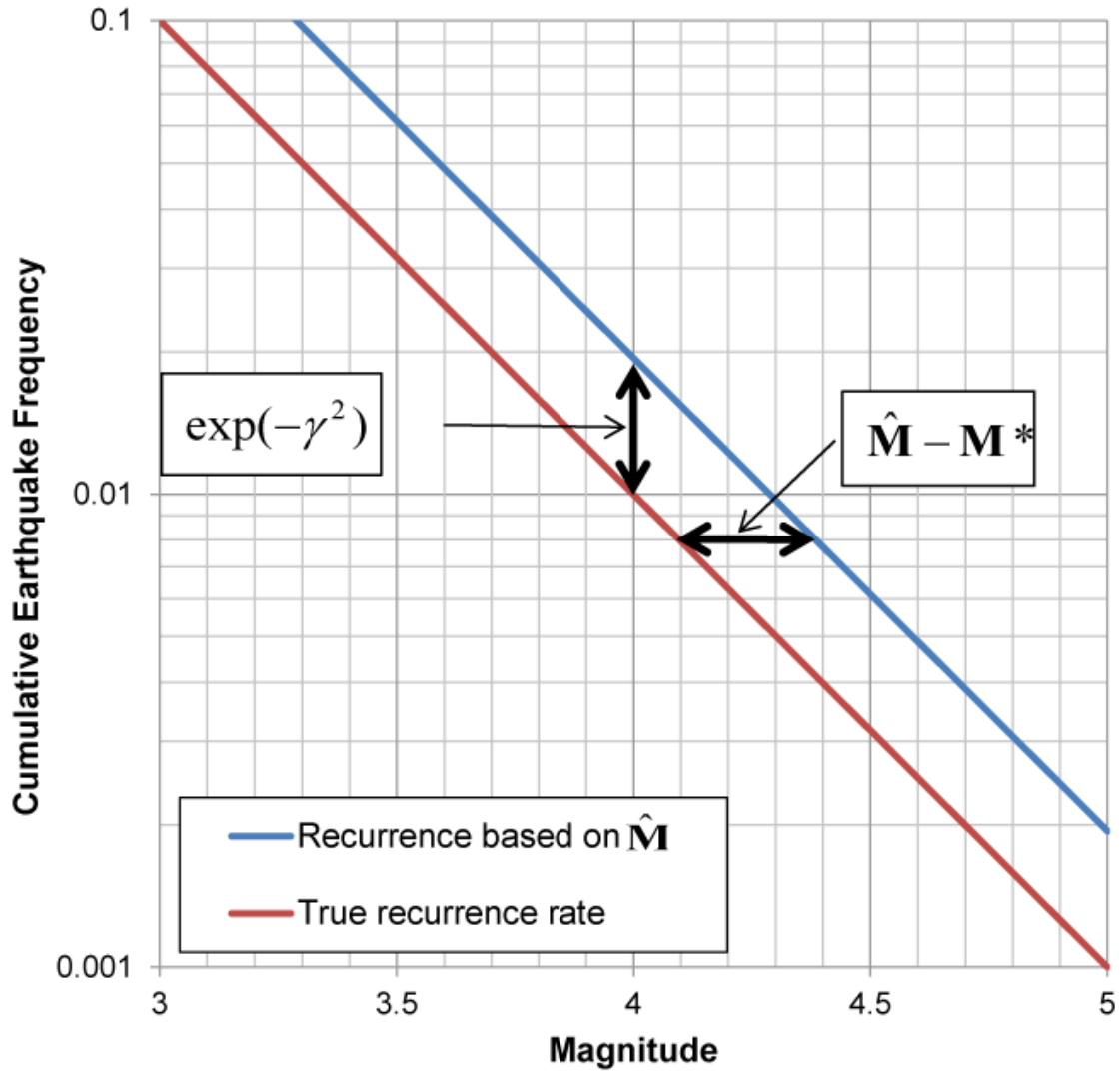


Figure 3.3-1
Illustration of equivalence of the M^* and γ^2 corrections to remove bias in earthquake recurrence relationships estimated from magnitudes with uncertainty, \hat{M}

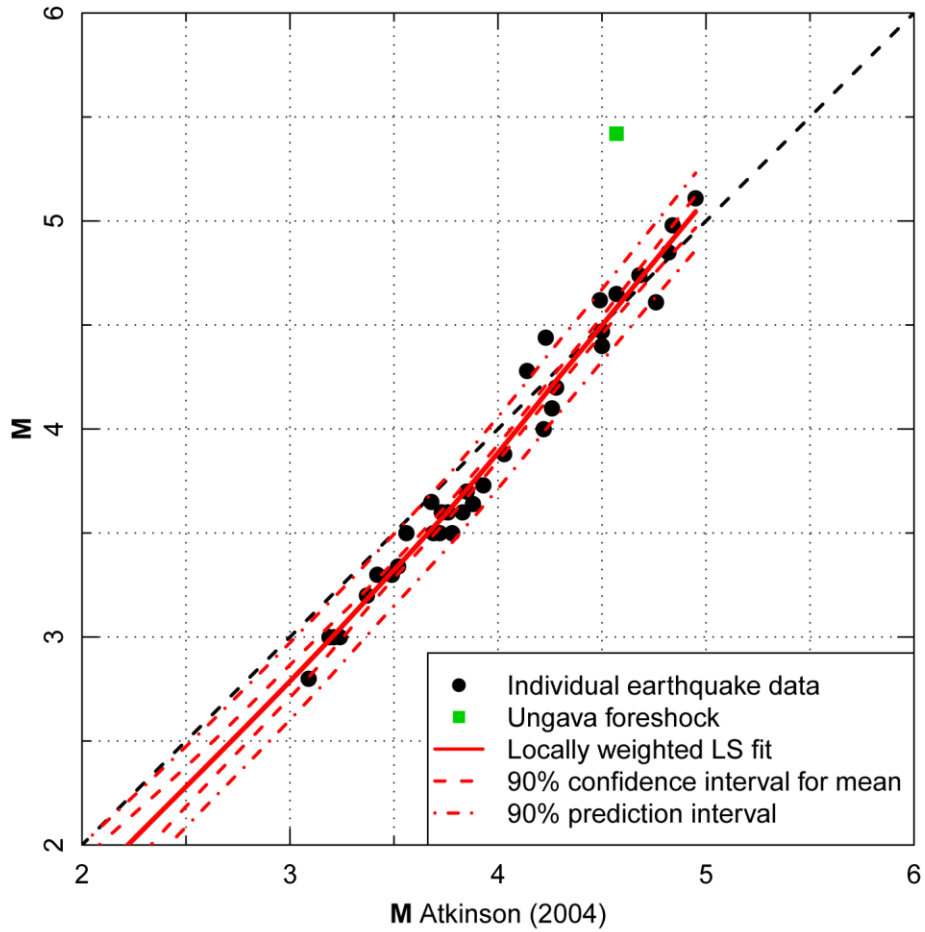


Figure 3.3-2
Approximate moment magnitudes from Atkinson (2004b) compared to values of M given in Table B-2 in Appendix B for earthquakes in common

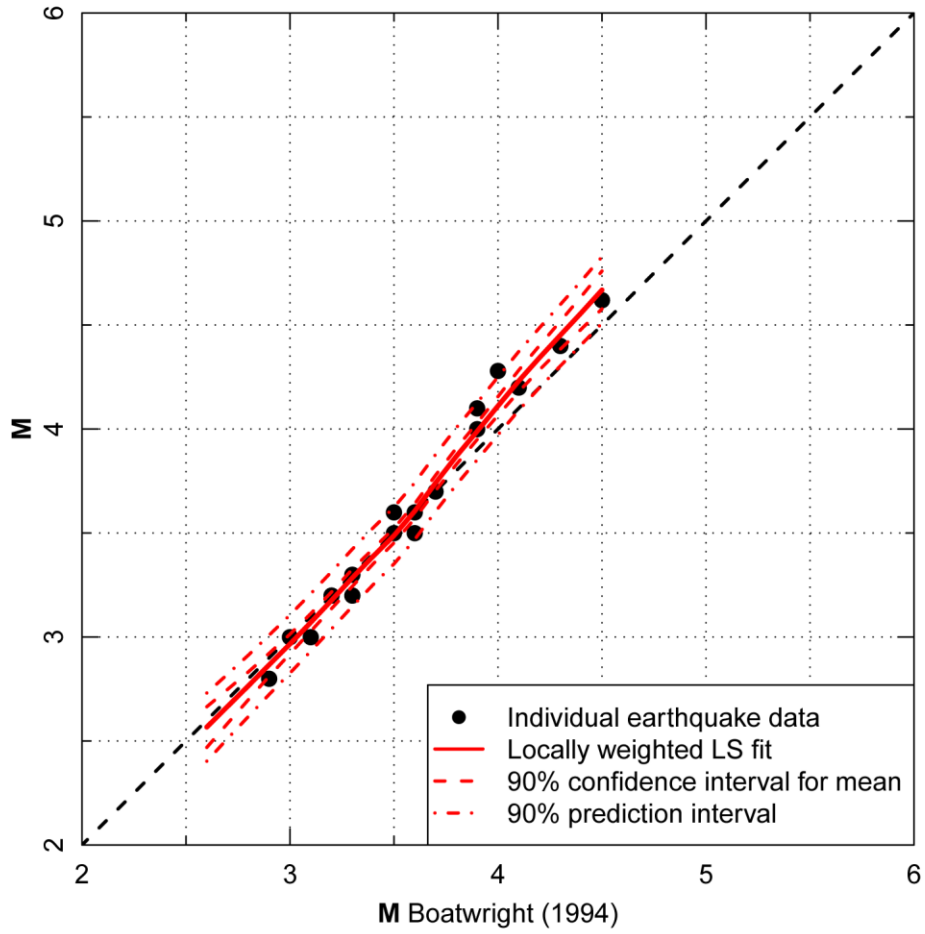


Figure 3.3-3
Approximate moment magnitudes from Boatwright (1994) compared to values of M given in Table B-2 in Appendix B for earthquakes in common

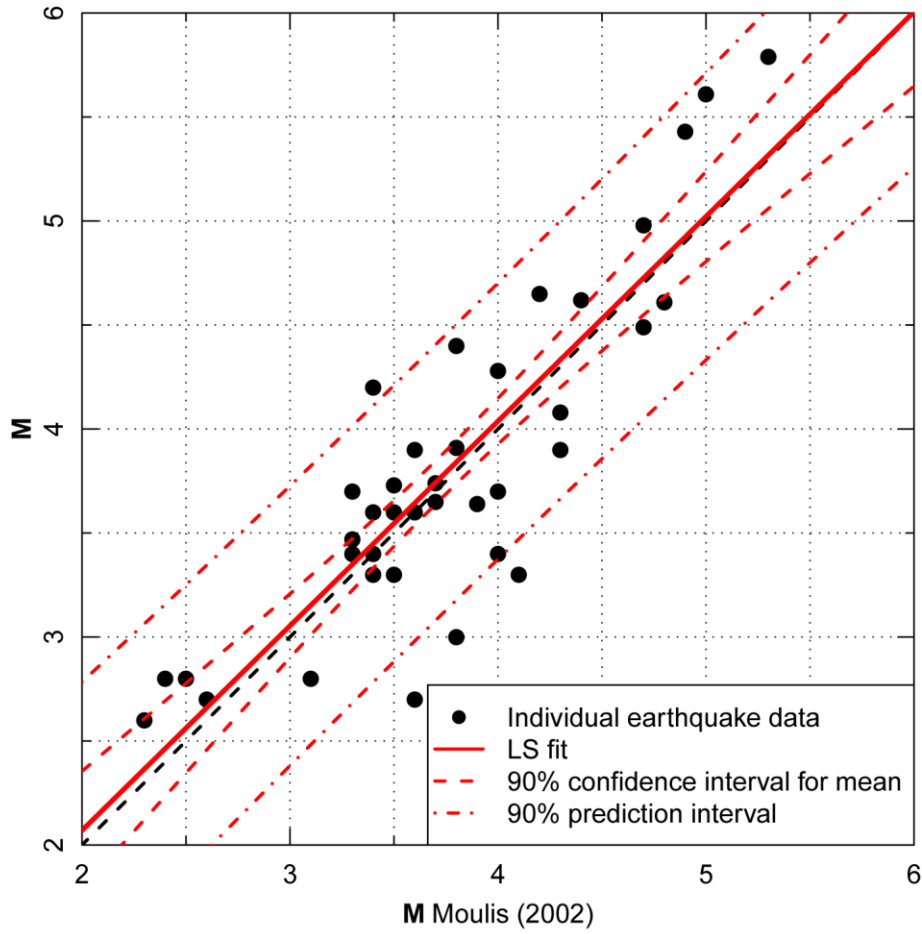


Figure 3.3-4
Approximate moment magnitudes from Moulis (2002) compared to values of M given in Table B-2 in Appendix B for earthquakes in common

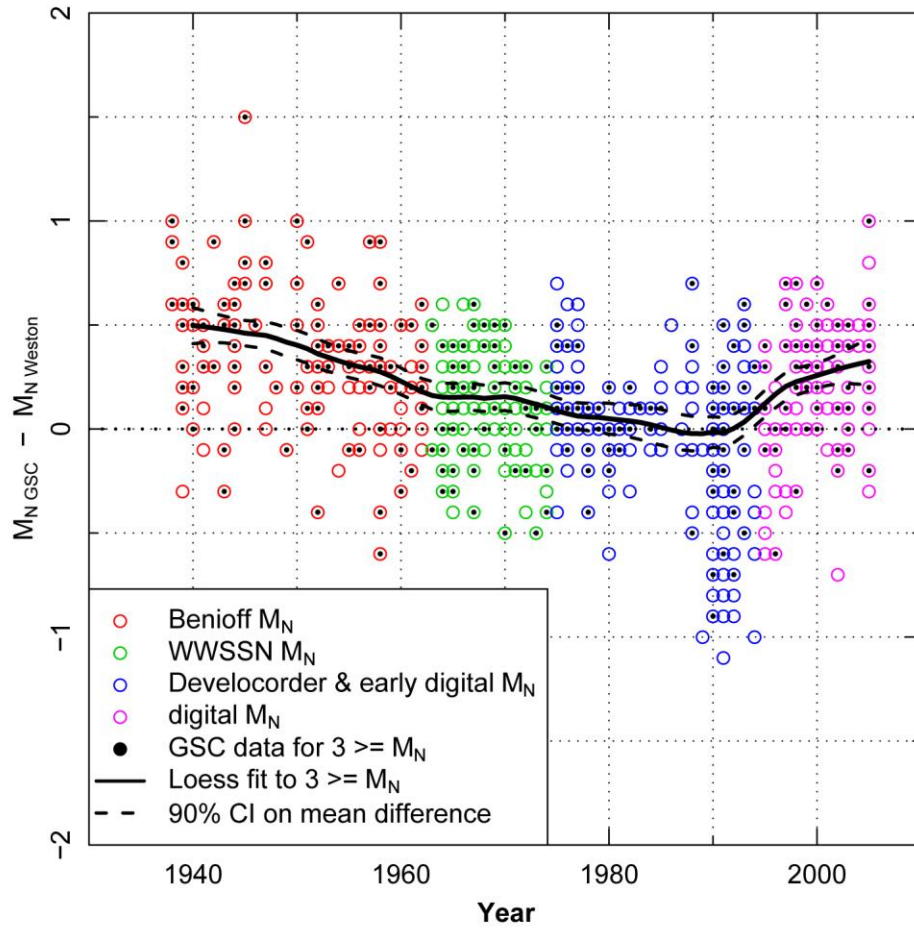


Figure 3.3-5
Difference between M_N reported by the GSC and M_N or $m_{Lg(f)}$ reported by the Weston Observatory catalog as a function of time

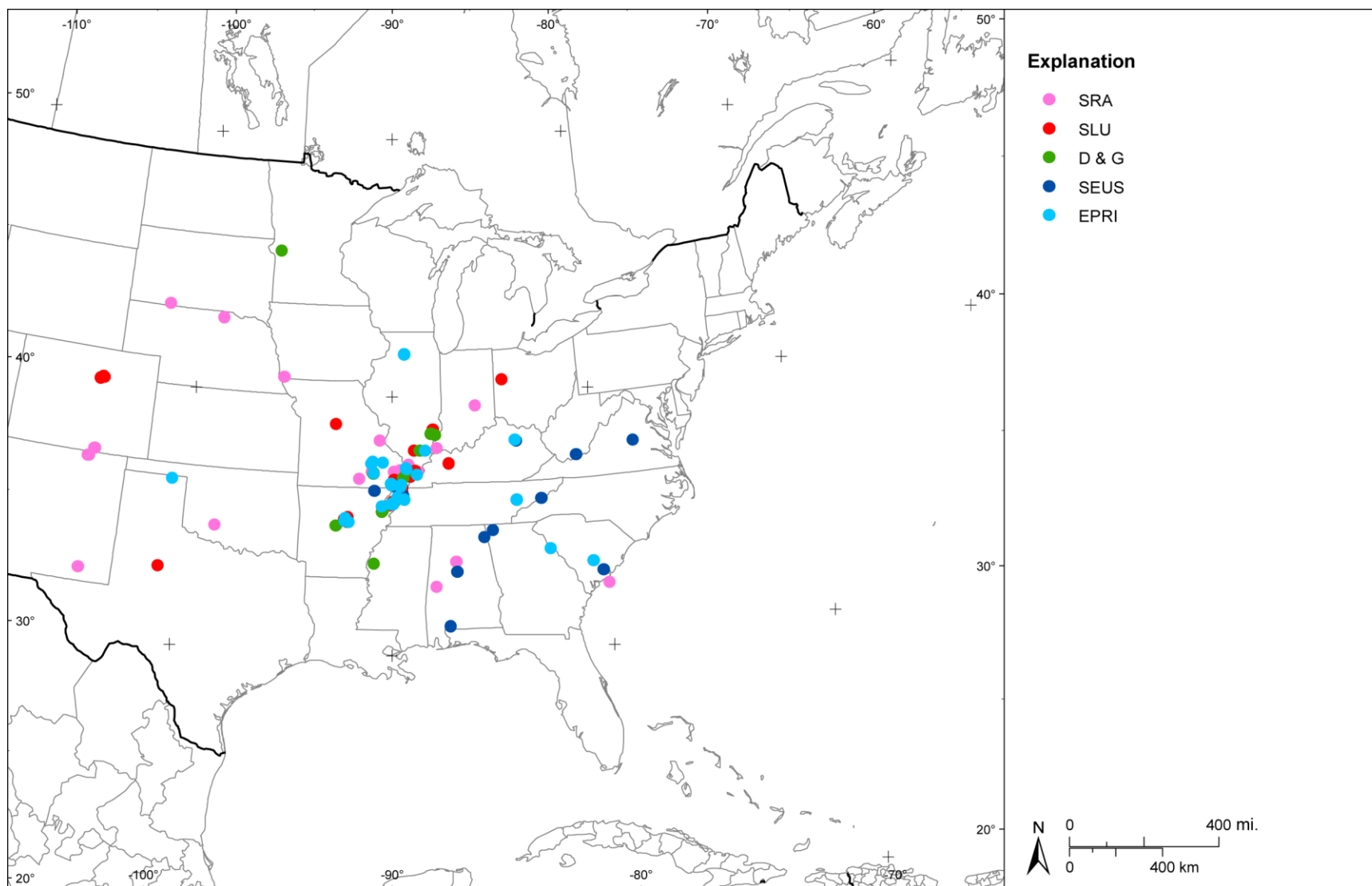


Figure 3.3-6
Spatial distribution of earthquakes with body-wave (m_b , m_{bLG} , M_N) and M magnitudes in the CEUS SSC Project catalog for the Midcontinent region. Color codes indicate the source of the body-wave magnitudes.

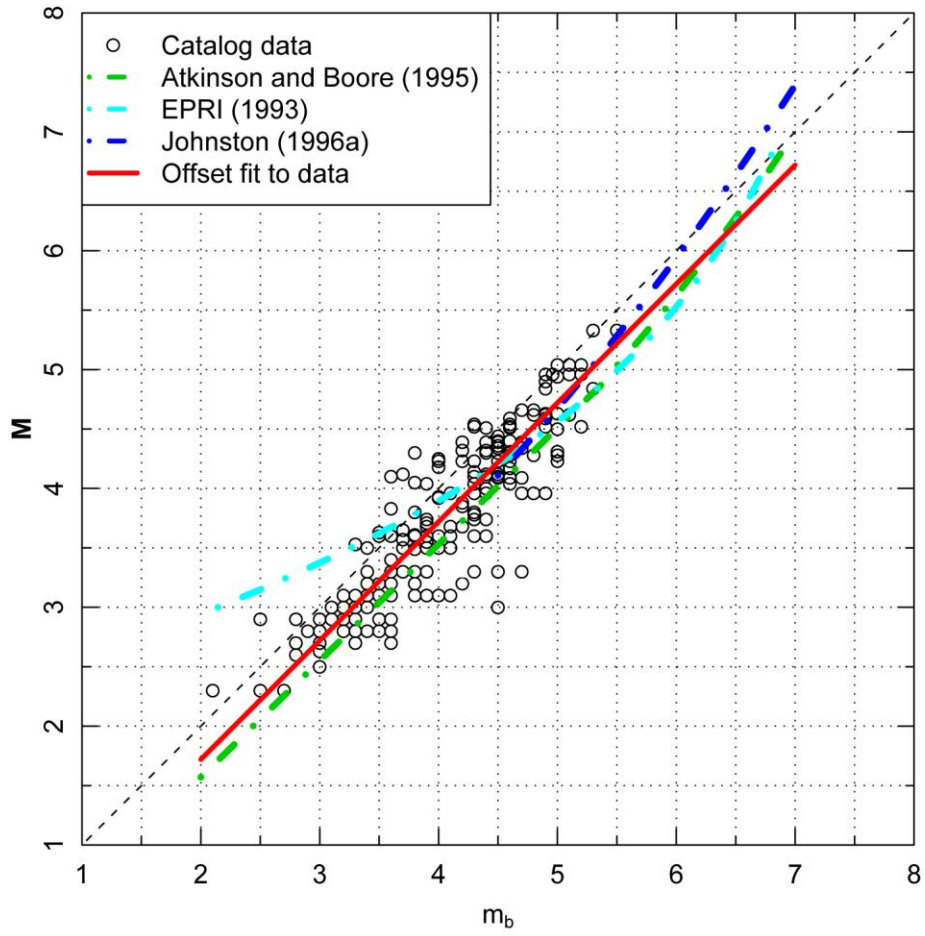


Figure 3.3-7
 m_b - M data for the earthquakes shown on Figure 3.3-6. Red curve shows the preferred offset fit $M = m_b - 0.28$.

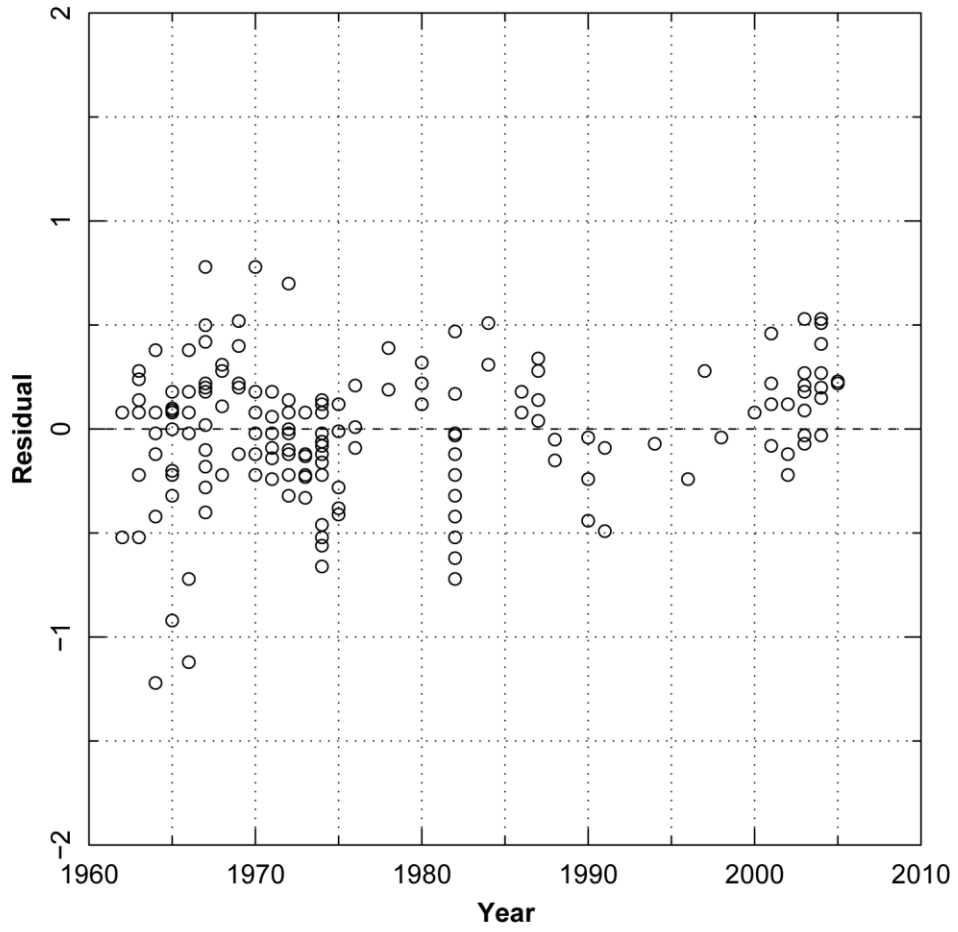


Figure 3.3-8
Residuals from offset fit shown on Figure 3.3-7 plotted against earthquake year

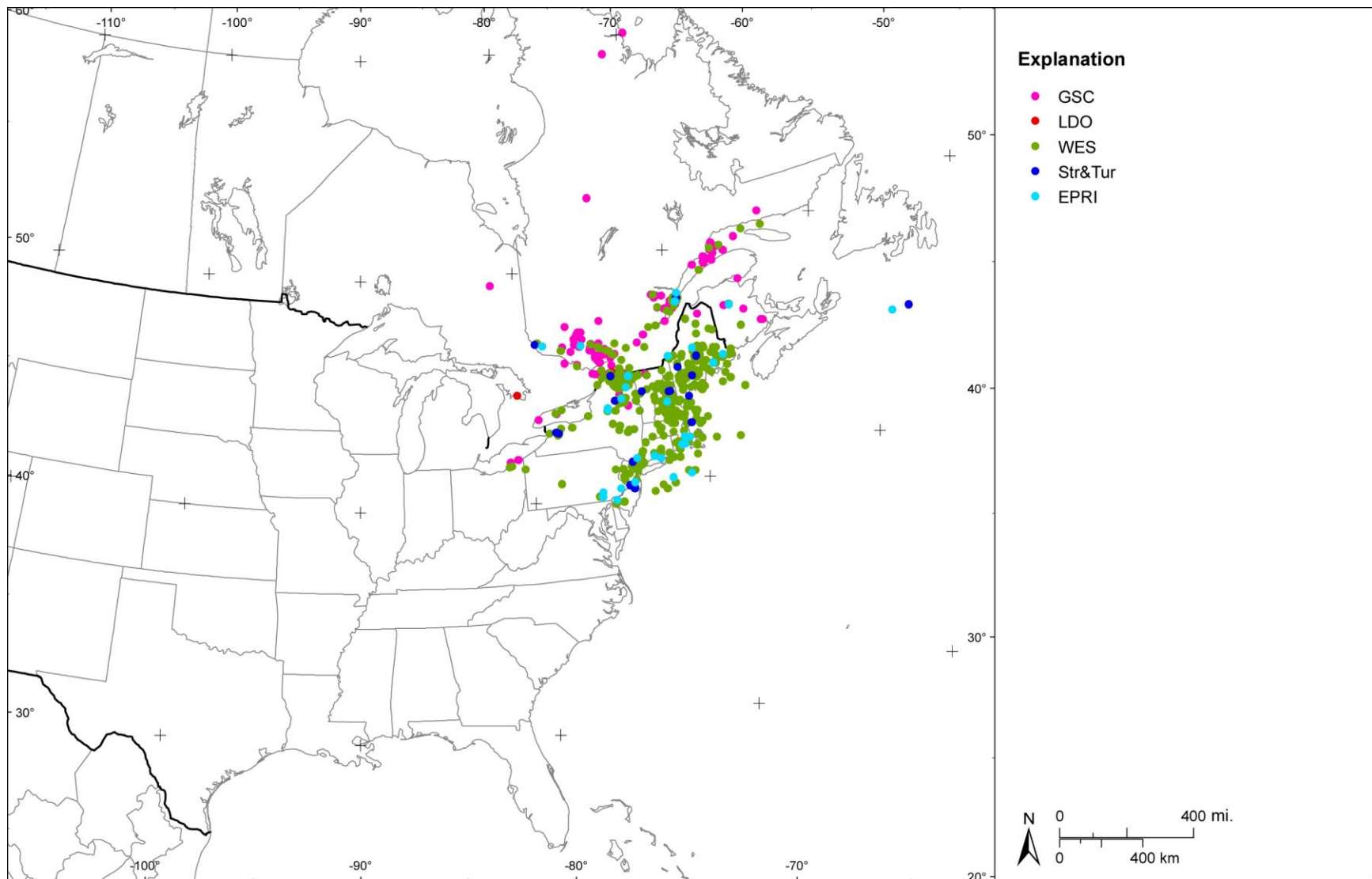


Figure 3.3-9
Spatial distribution of earthquakes with body wave (m_b , m_{bLG} , M_N) and M magnitudes in the CEUS SSC Project catalog for the northeastern portion of the study region. Color codes indicate the source of the body-wave magnitudes.

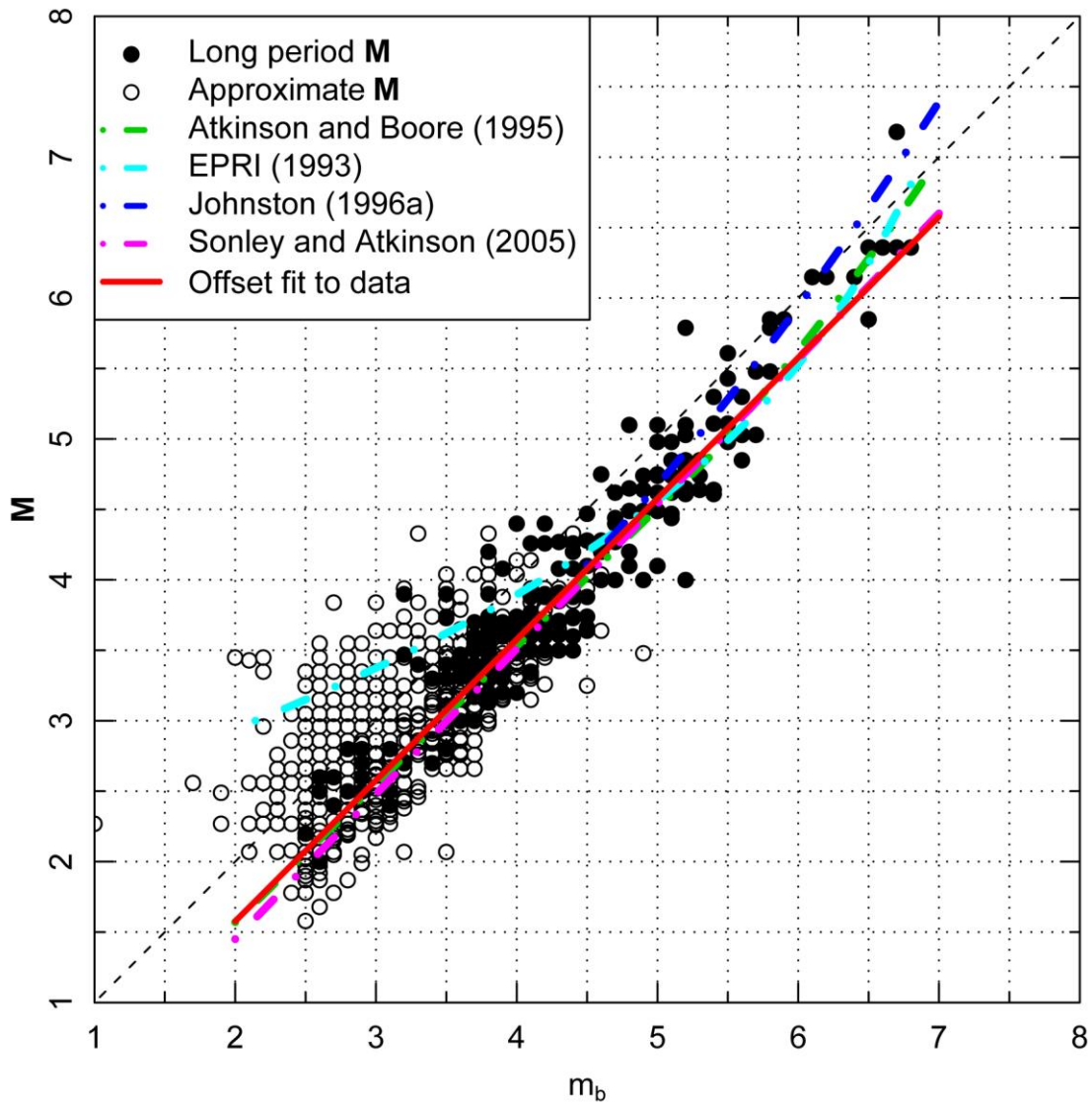


Figure 3.3-10
 m_b - M data for the earthquakes shown on Figure 3.3-9. Red curve shows the preferred offset fit $M = m_b - 0.42$.

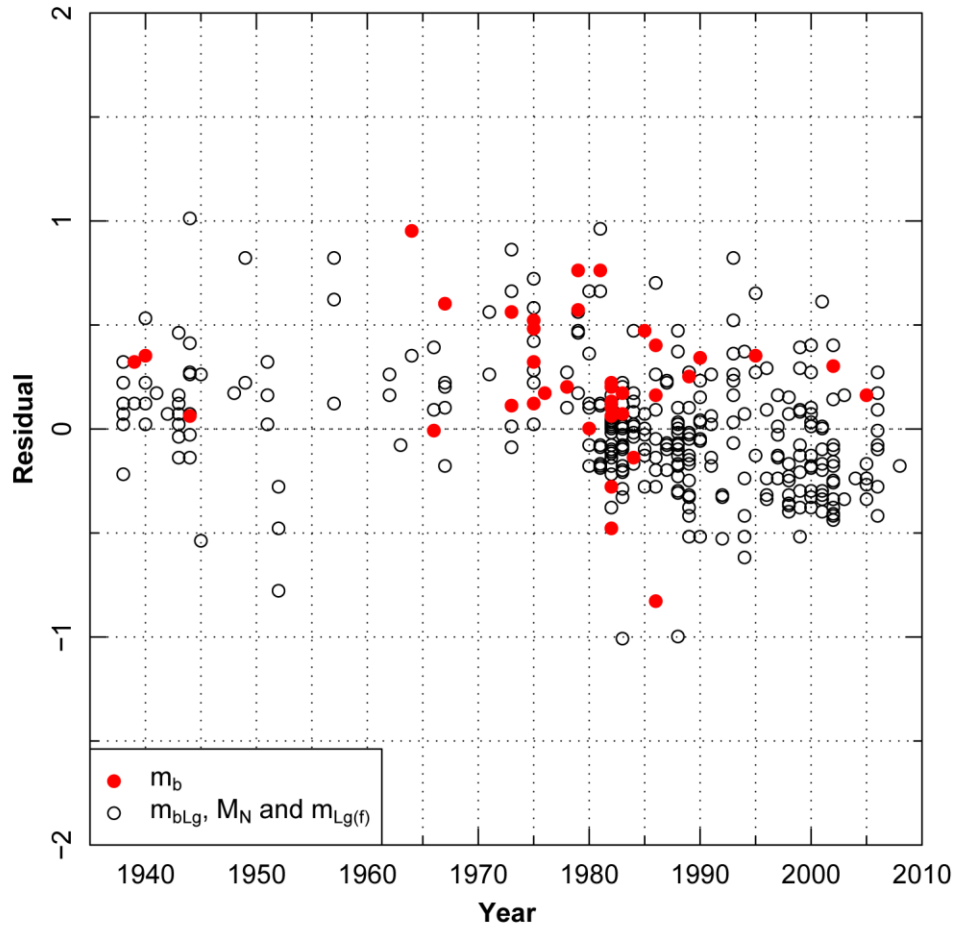


Figure 3.3-11
Residuals from offset fit shown on Figure 3.3-10 plotted against earthquake year

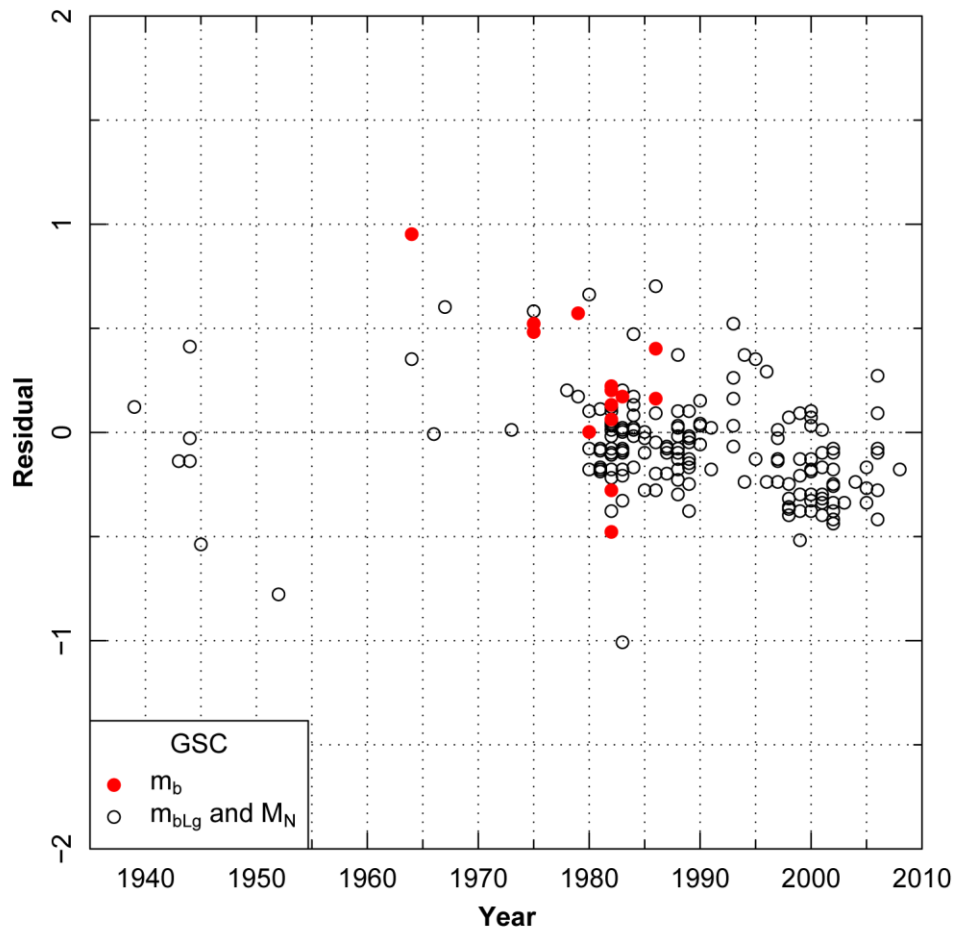


Figure 3.3-12
Residuals for GSC data from offset fit shown on Figure 3.3-10 plotted against earthquake year

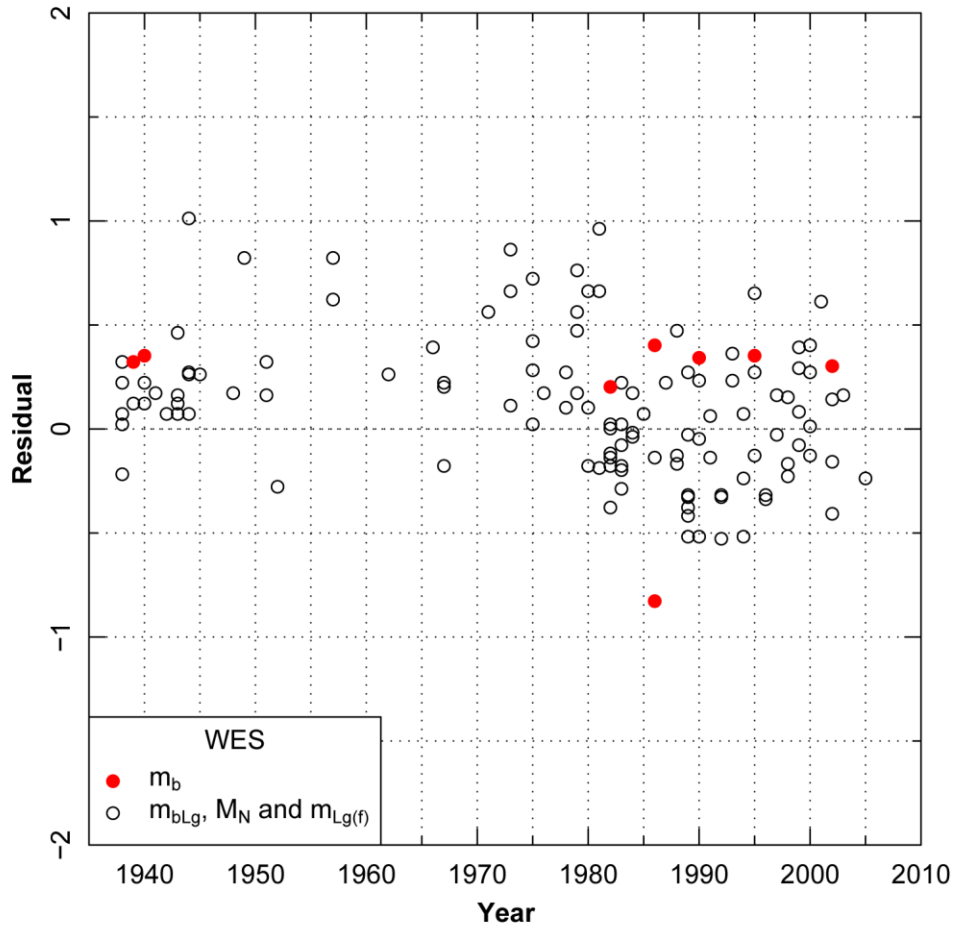


Figure 3.3-13
Residuals for WES data from offset fit shown on Figure 3.3-10 plotted against earthquake year

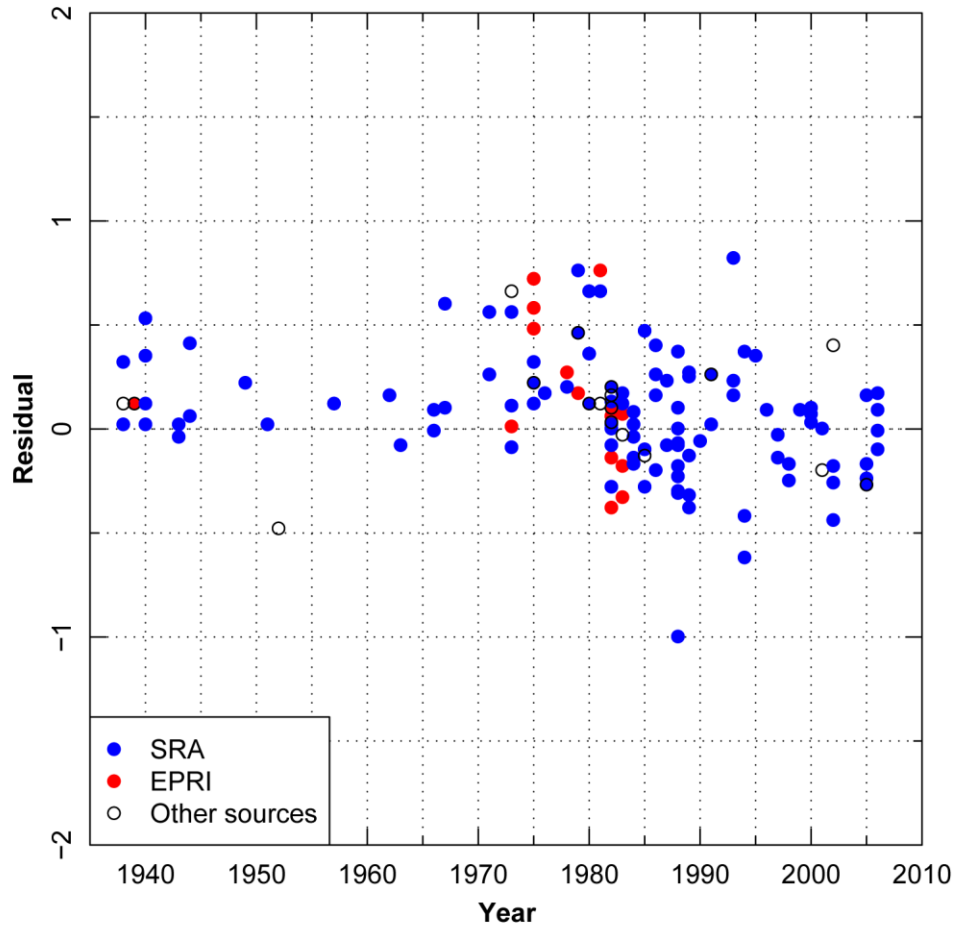


Figure 3.3-14
Residuals for data from sources other than GSC or WES from offset fit shown on Figure 3.3-10 plotted against earthquake year

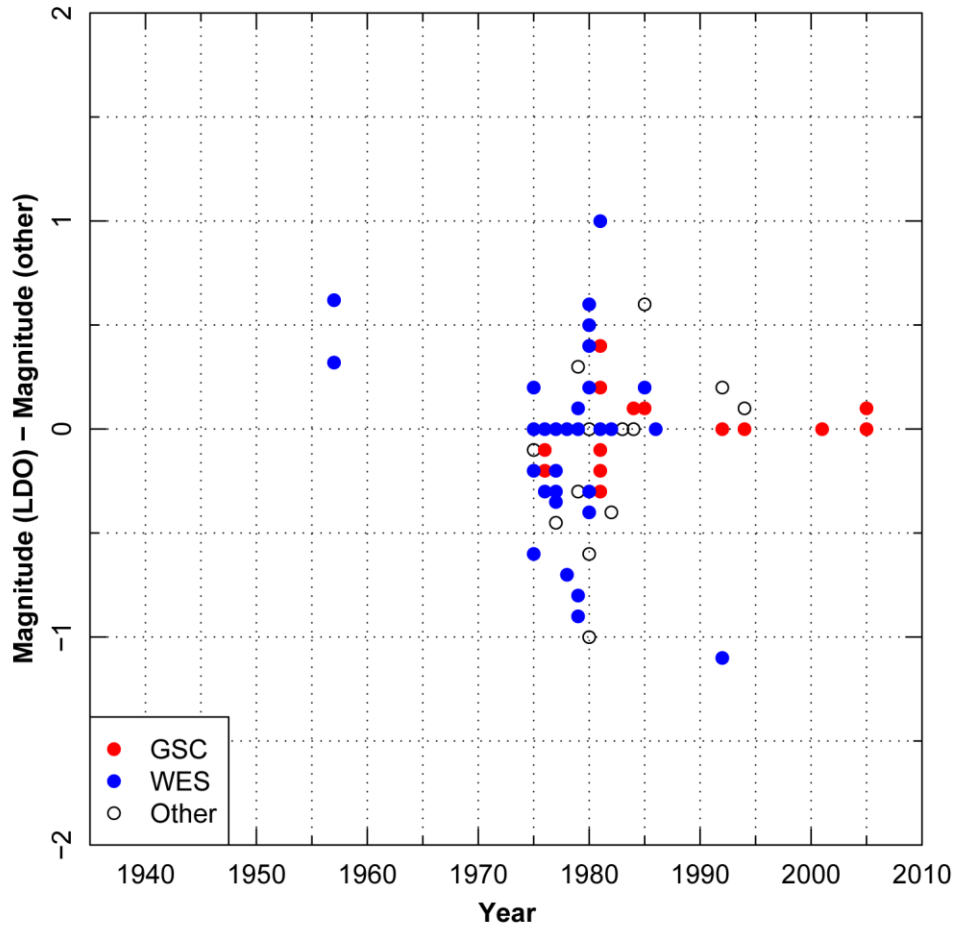


Figure 3.3-15
Difference between body-wave magnitudes reported by LDO and those by other sources as a function of year

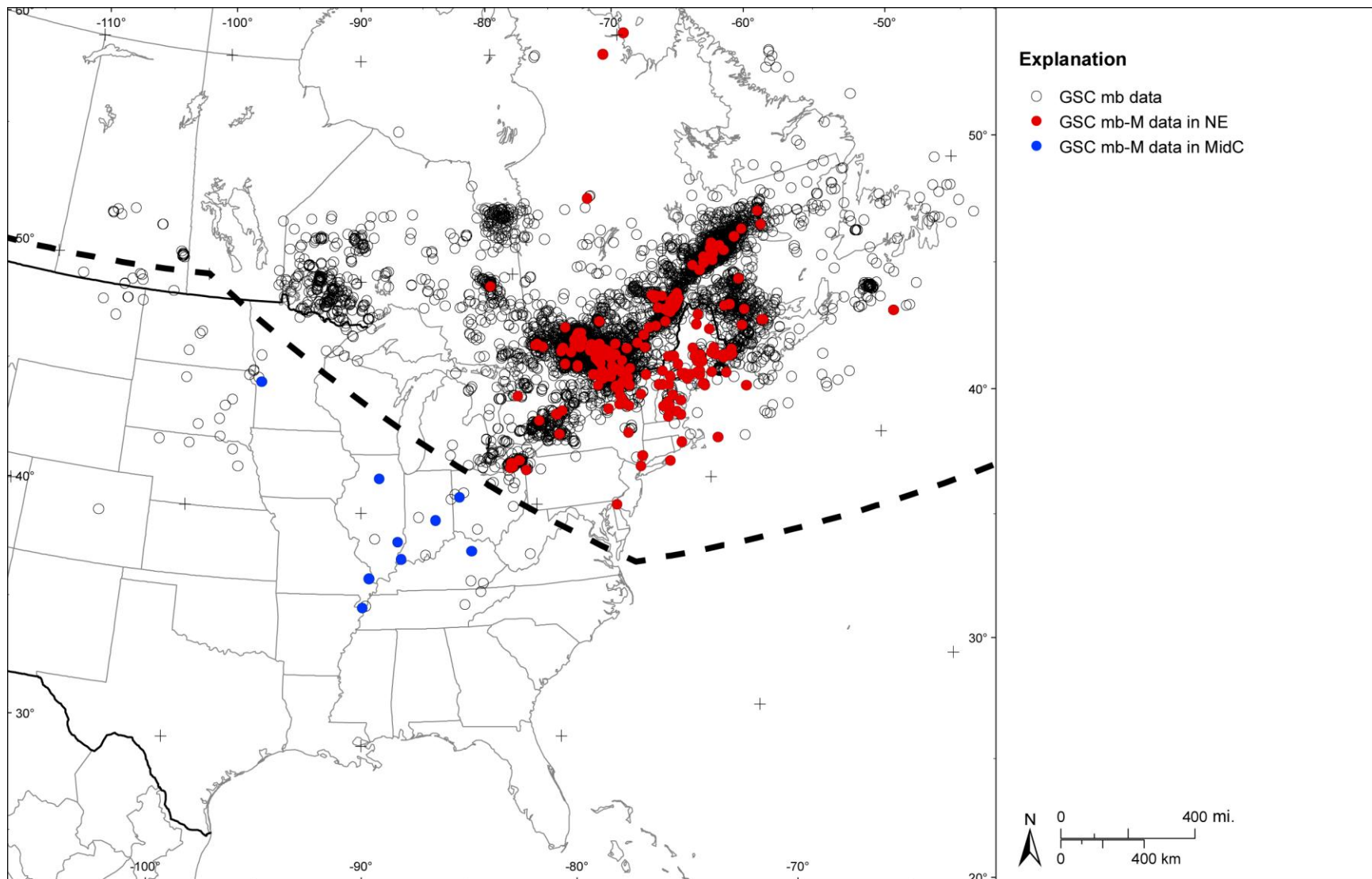


Figure 3.3-16
Spatial distribution of earthquakes with reported GSC body-wave magnitudes. Red and blue symbols indicate earthquakes with both m_b and M magnitudes for $m_b \geq 3.5$. Dashed line indicates the portion of the study region considered the "Northeast" for purposes of magnitude scaling.

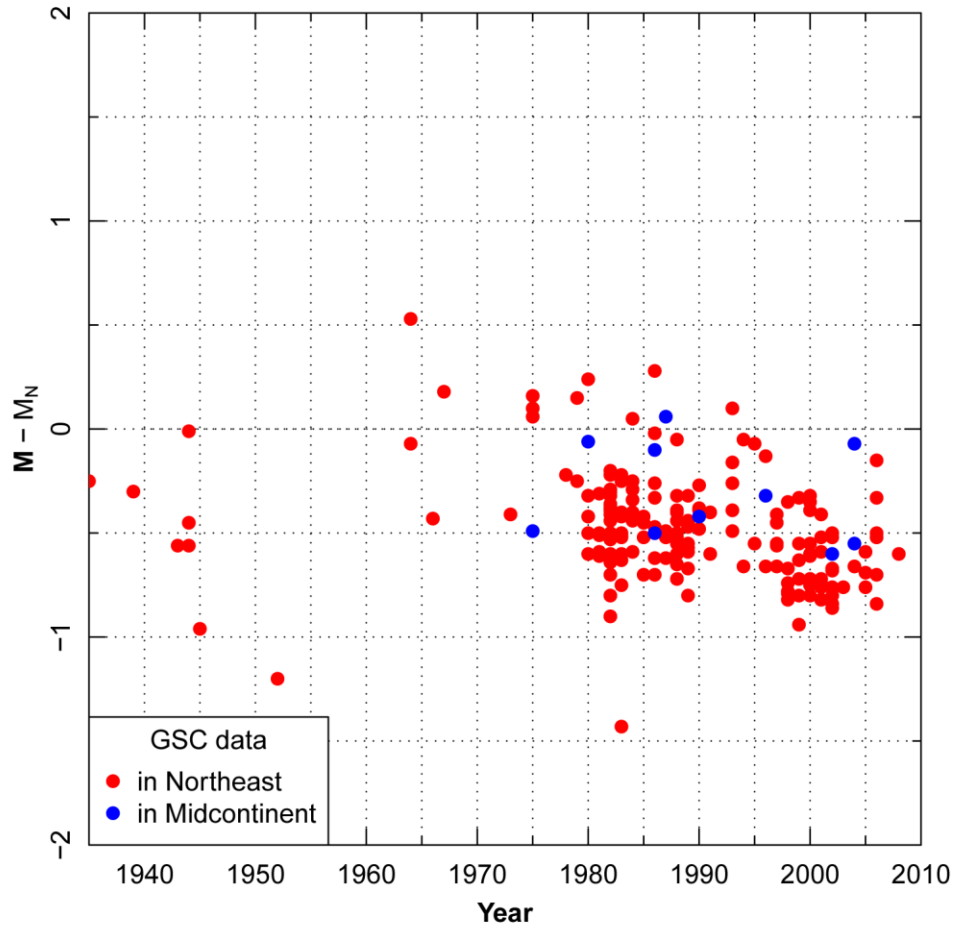


Figure 3.3-17
M-m_b as a function of time for m_b data from the GSC shown on Figure 3.3-16

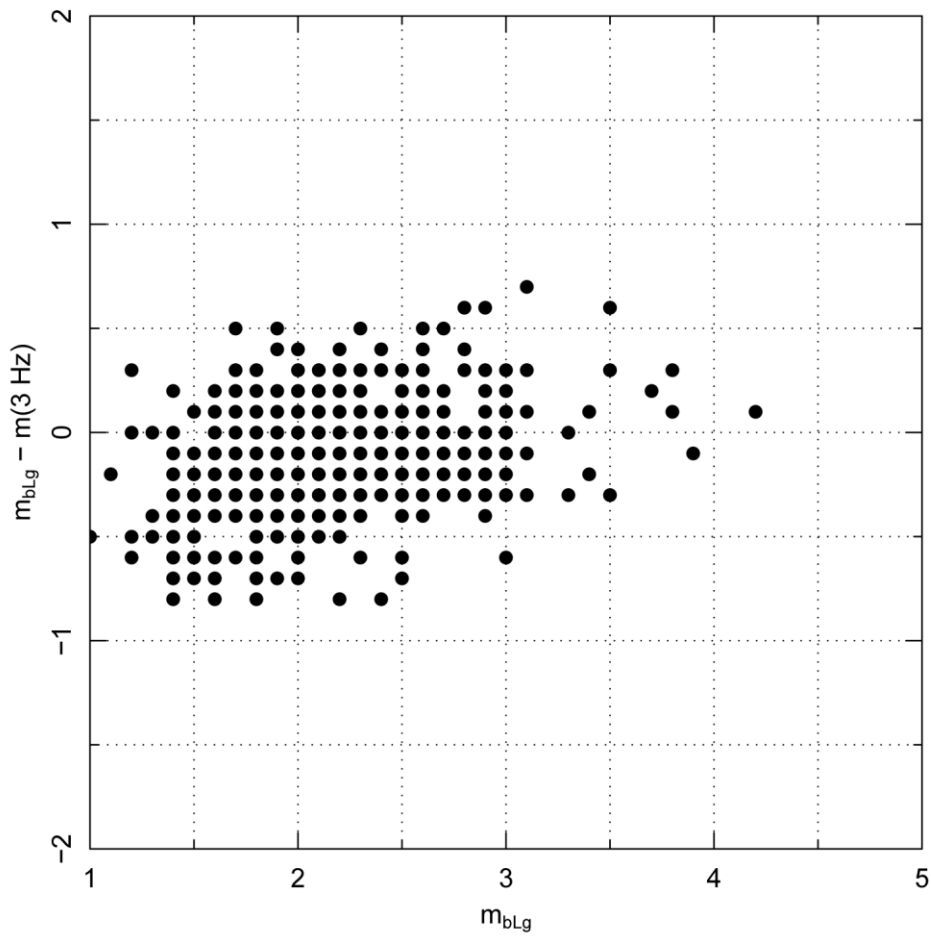


Figure 3.3-18
Plot of magnitude differences $m_{bLg} - m(3 \text{ Hz})$ for the OKO catalog

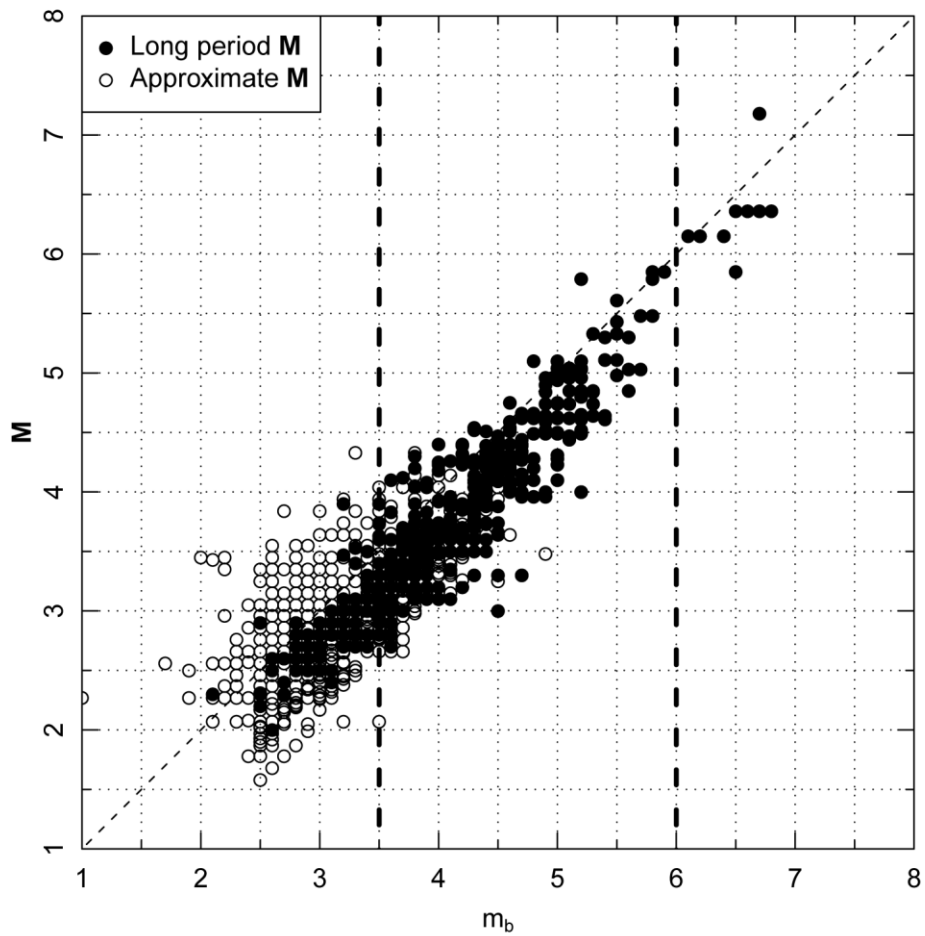


Figure 3.3-19
Final m_b -M data set. Vertical dashed lines indicate the magnitude range used to develop the scaling relationship. Diagonal line indicates a one-to-one correlation.

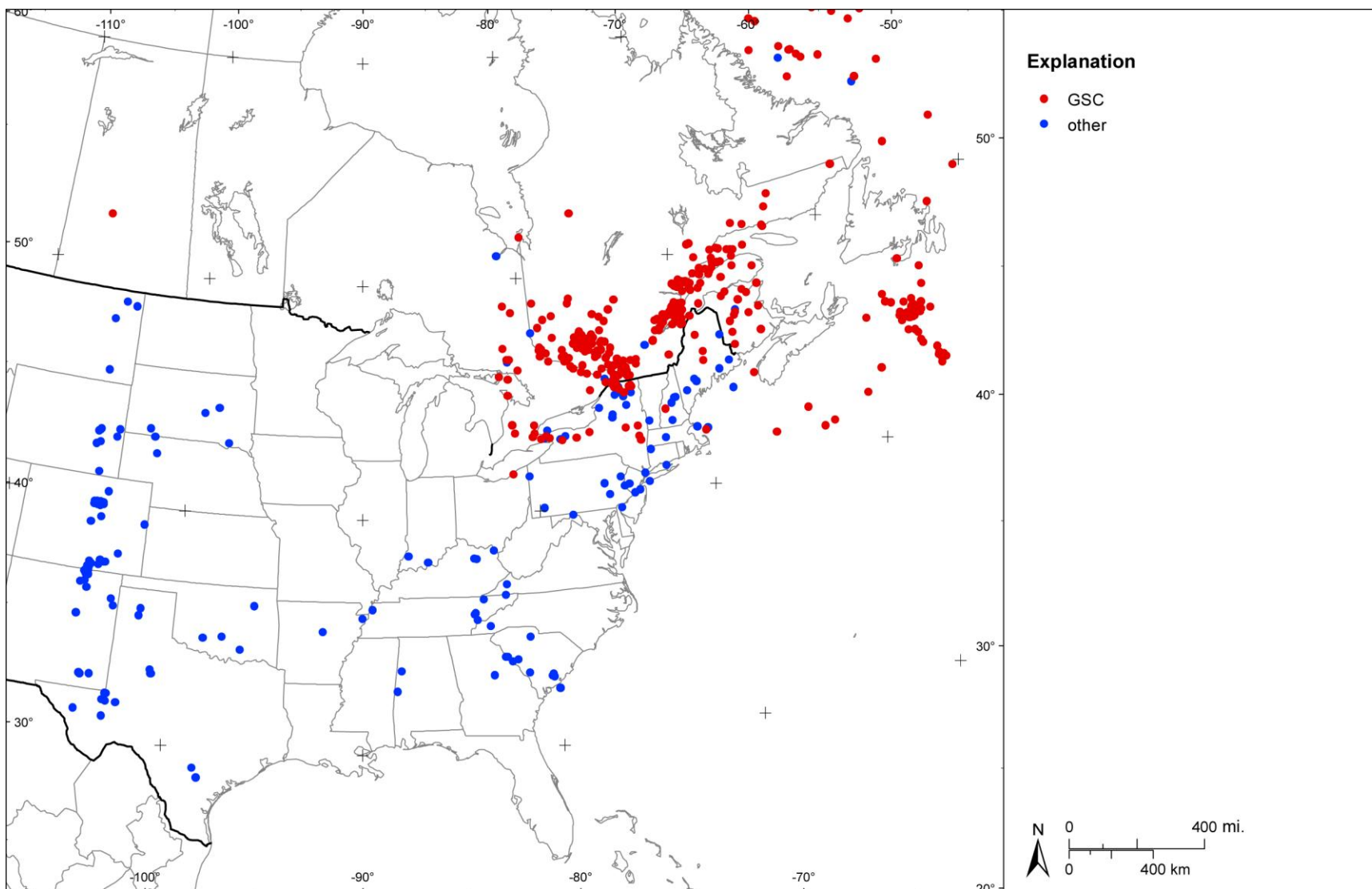


Figure 3.3-20
Spatial distribution of earthquakes in the CEUS SSC Project catalog with instrumental M_L magnitudes

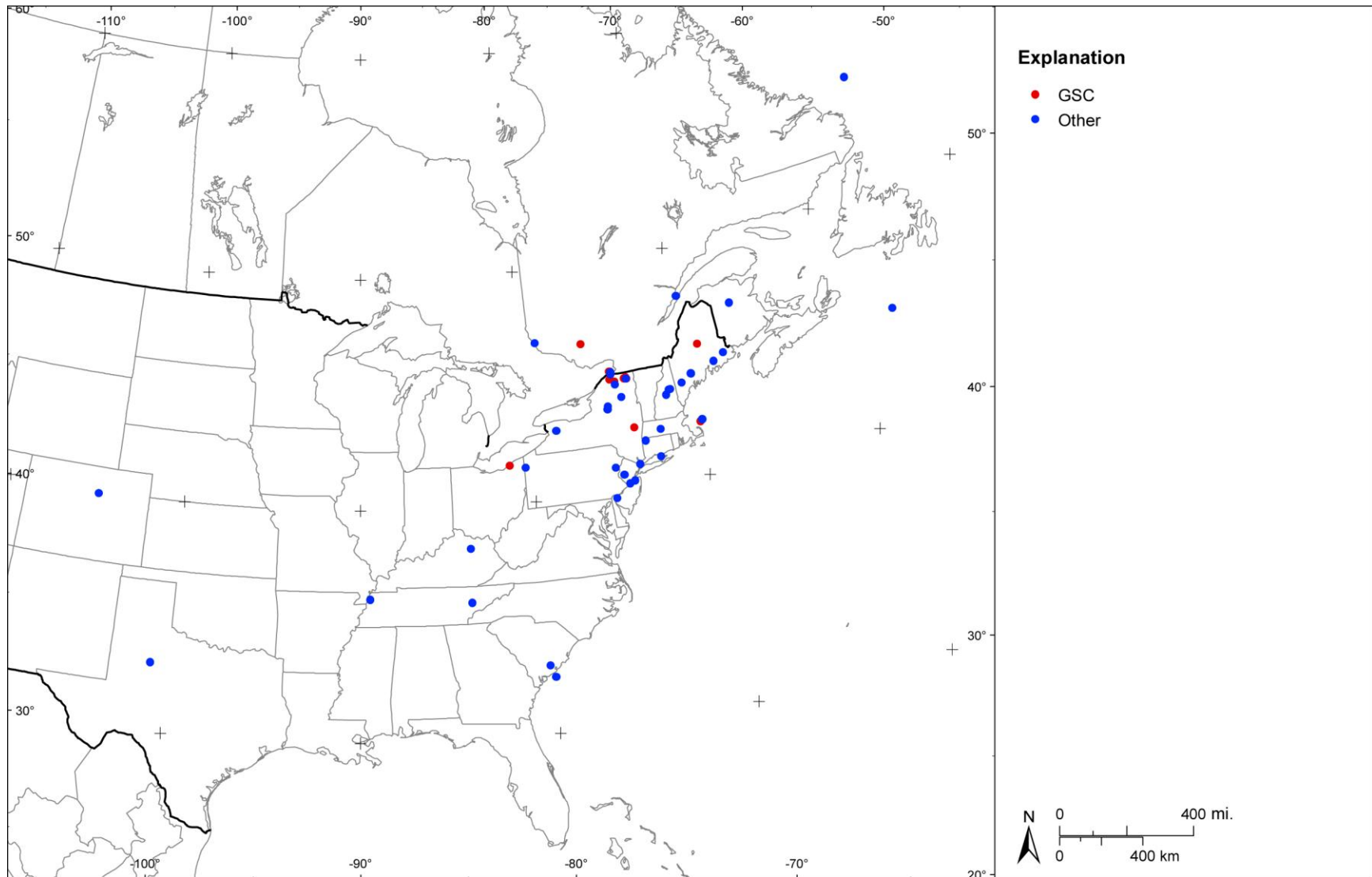


Figure 3.3-21
Spatial distribution of earthquakes in the CEUS SSC Project catalog with instrumental M_L magnitudes and M magnitudes

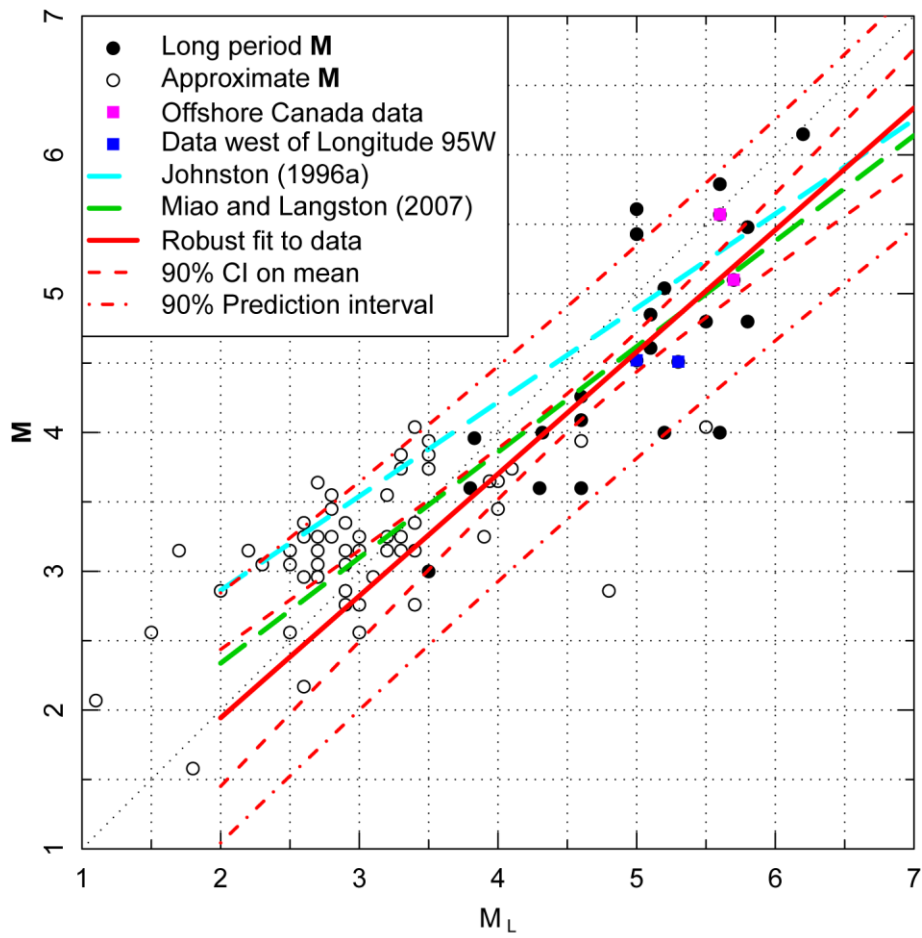


Figure 3.3-22
 M_L - M data from the CEUS SSC Project catalog and robust regression fit to the data

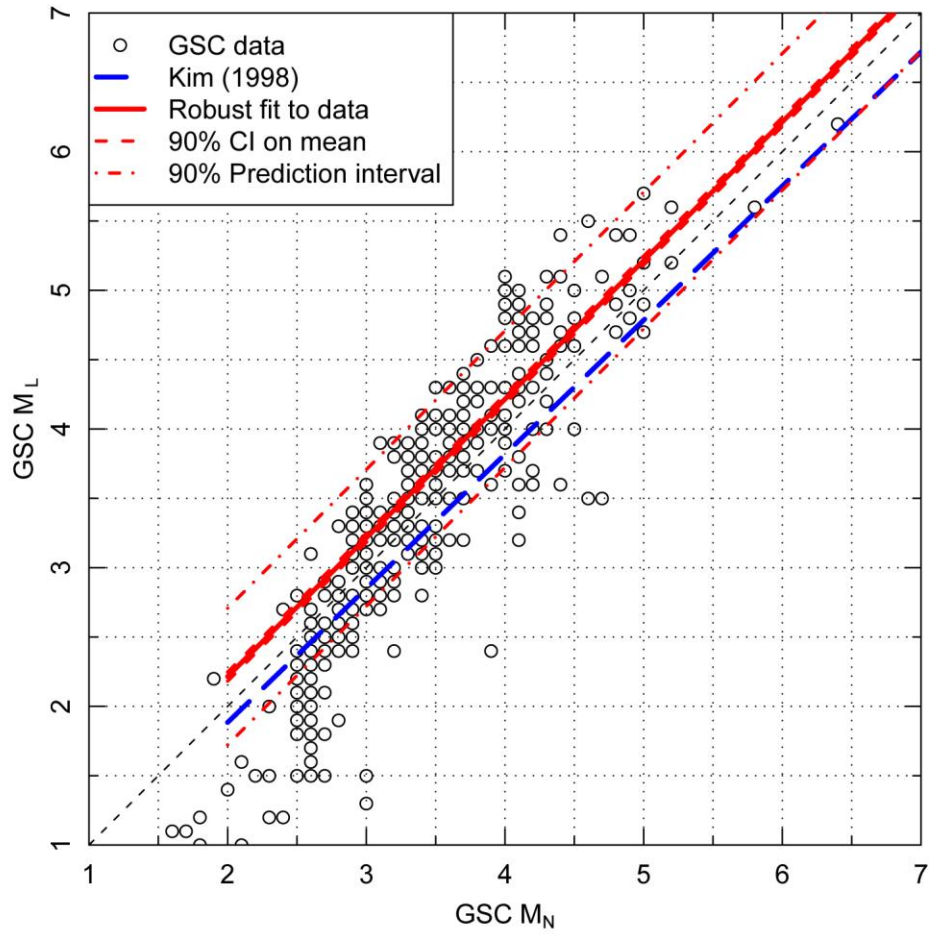


Figure 3.3-23
Relationship between M_N and M_L for the GSC data

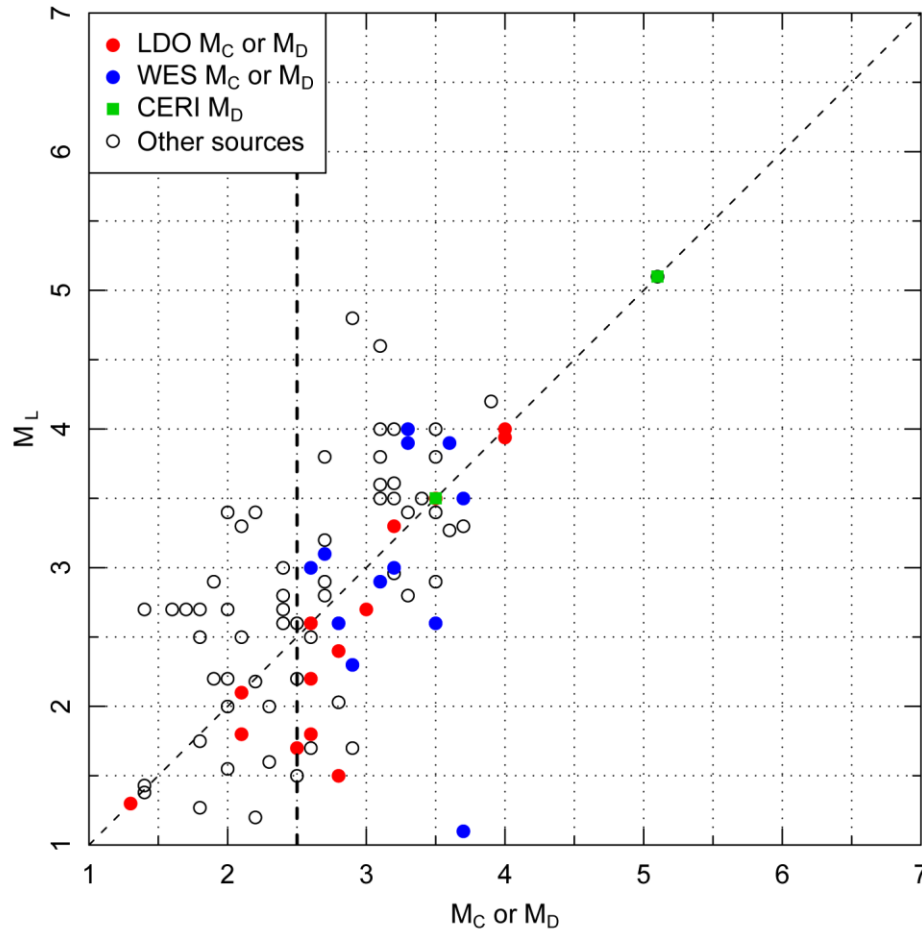


Figure 3.3-24
Data from the northeastern portion of the study region with M_L and M_C or M_D magnitude from catalog sources other than the GSC

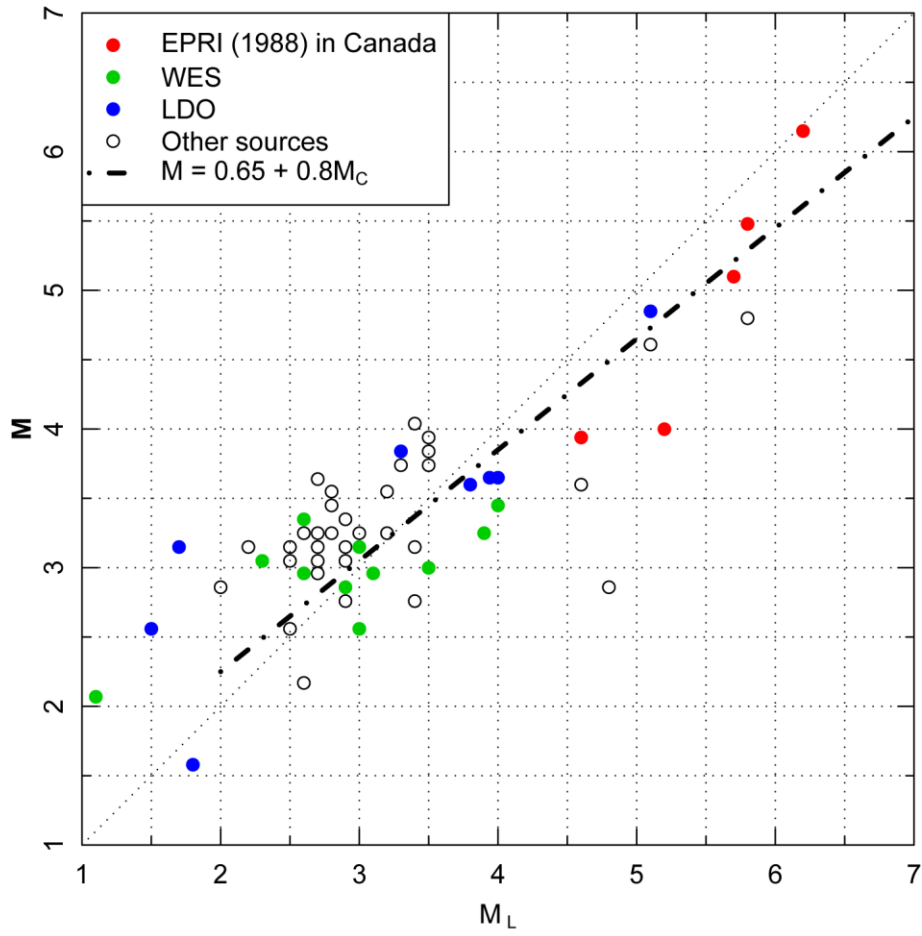


Figure 3.3-25
Data from the northeastern portion of the study region with M_L and M magnitudes from sources other than the GSC

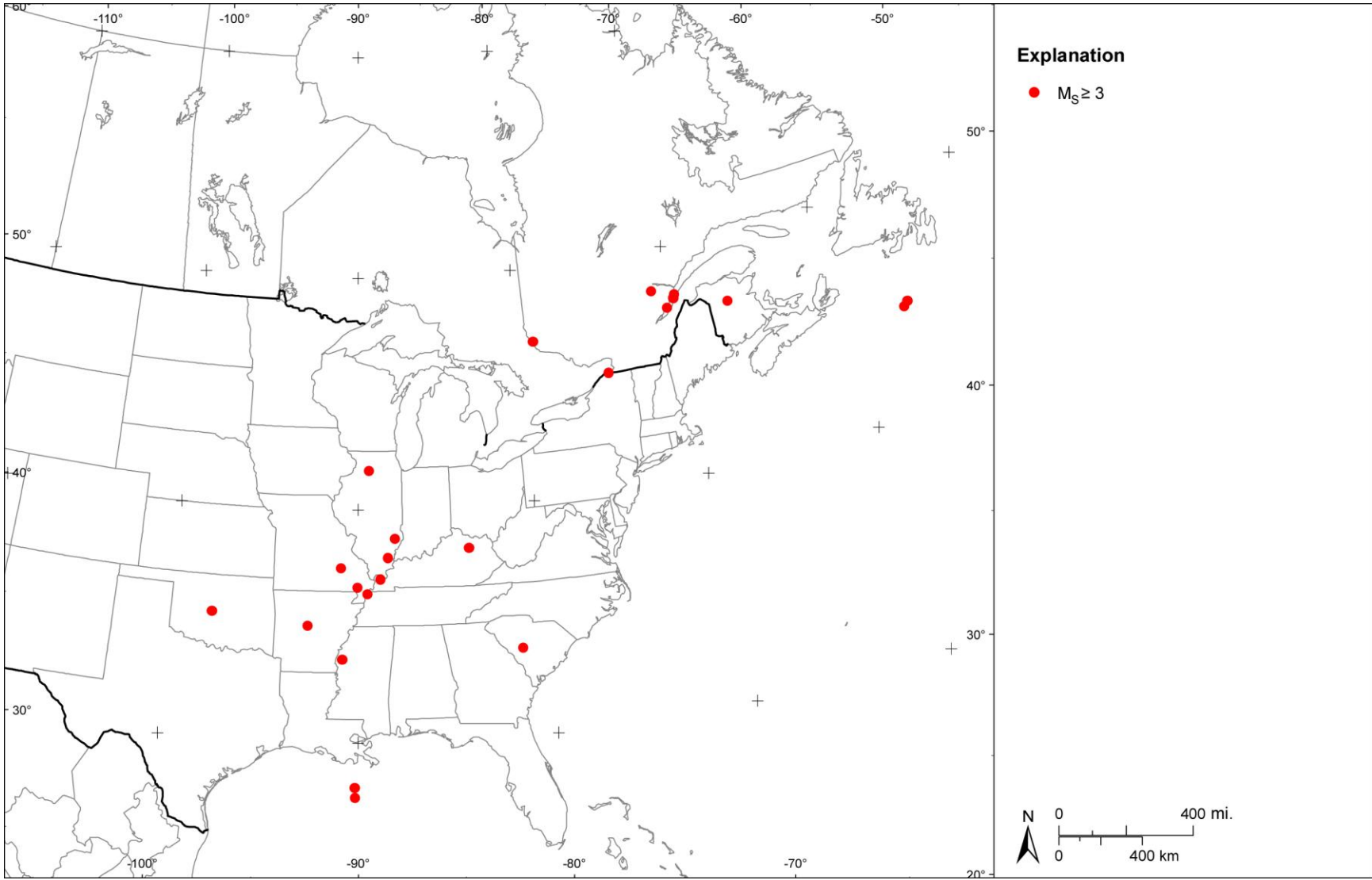


Figure 3.3-26
Spatial distribution of earthquakes in the CEUS SSC Project catalog with $M_S \geq 3$ magnitudes

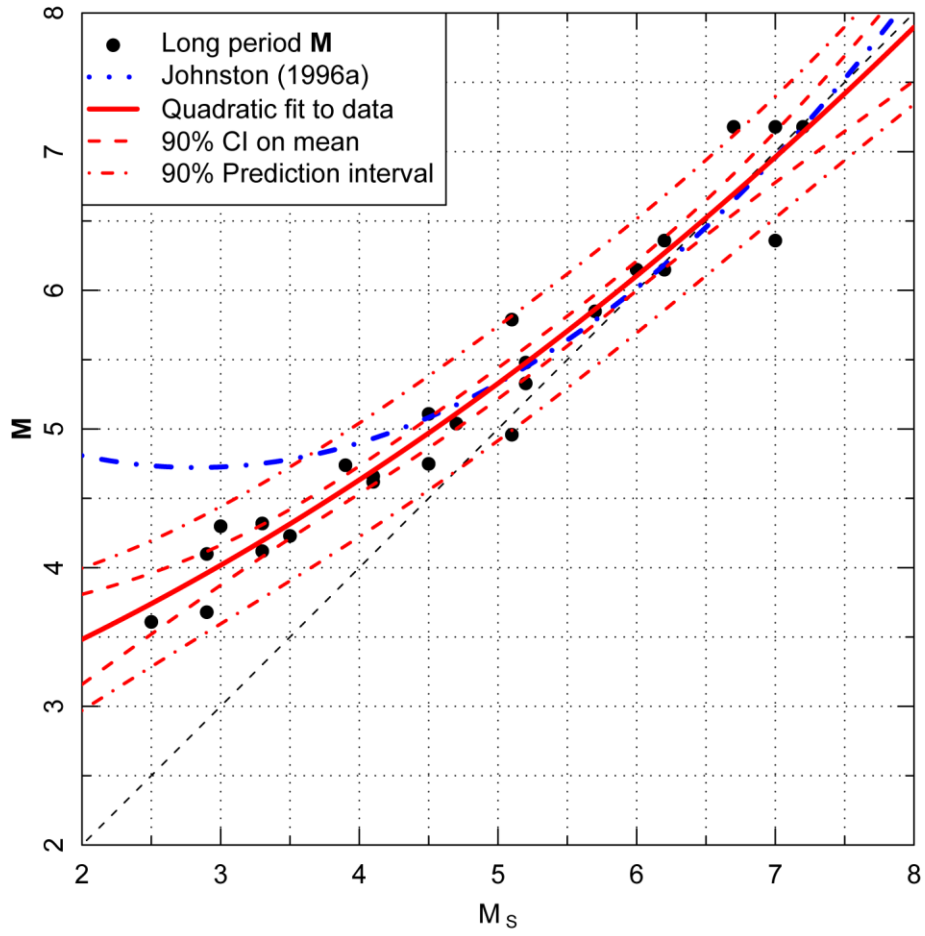


Figure 3.3-27
 M_s - M data from the CEUS SSC Project catalog and quadratic polynomial fit to the data

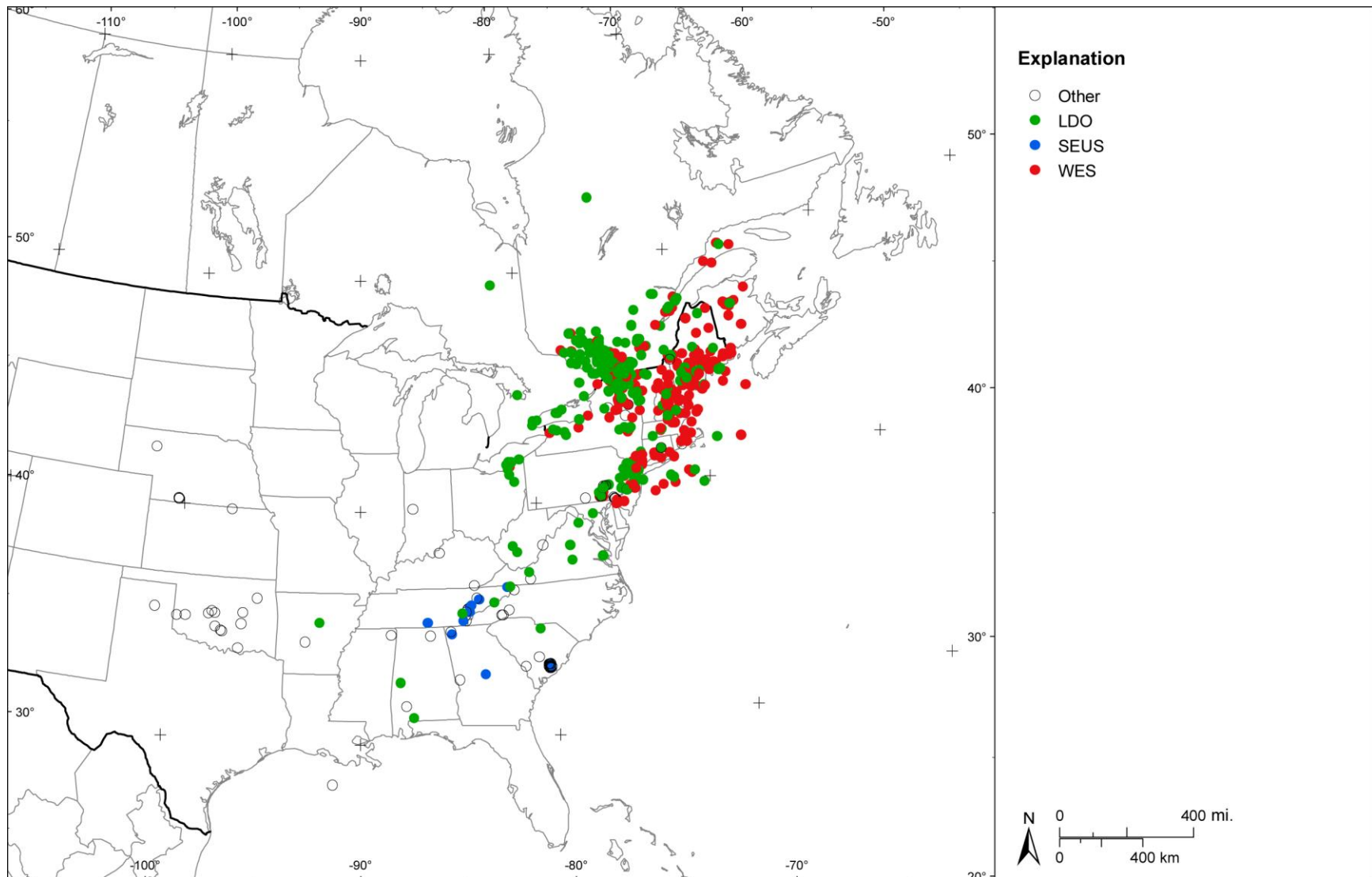


Figure 3.3-28
Spatial distribution of earthquakes in the CEUS SSC Project catalog with $M_C \geq 2.5$ magnitudes

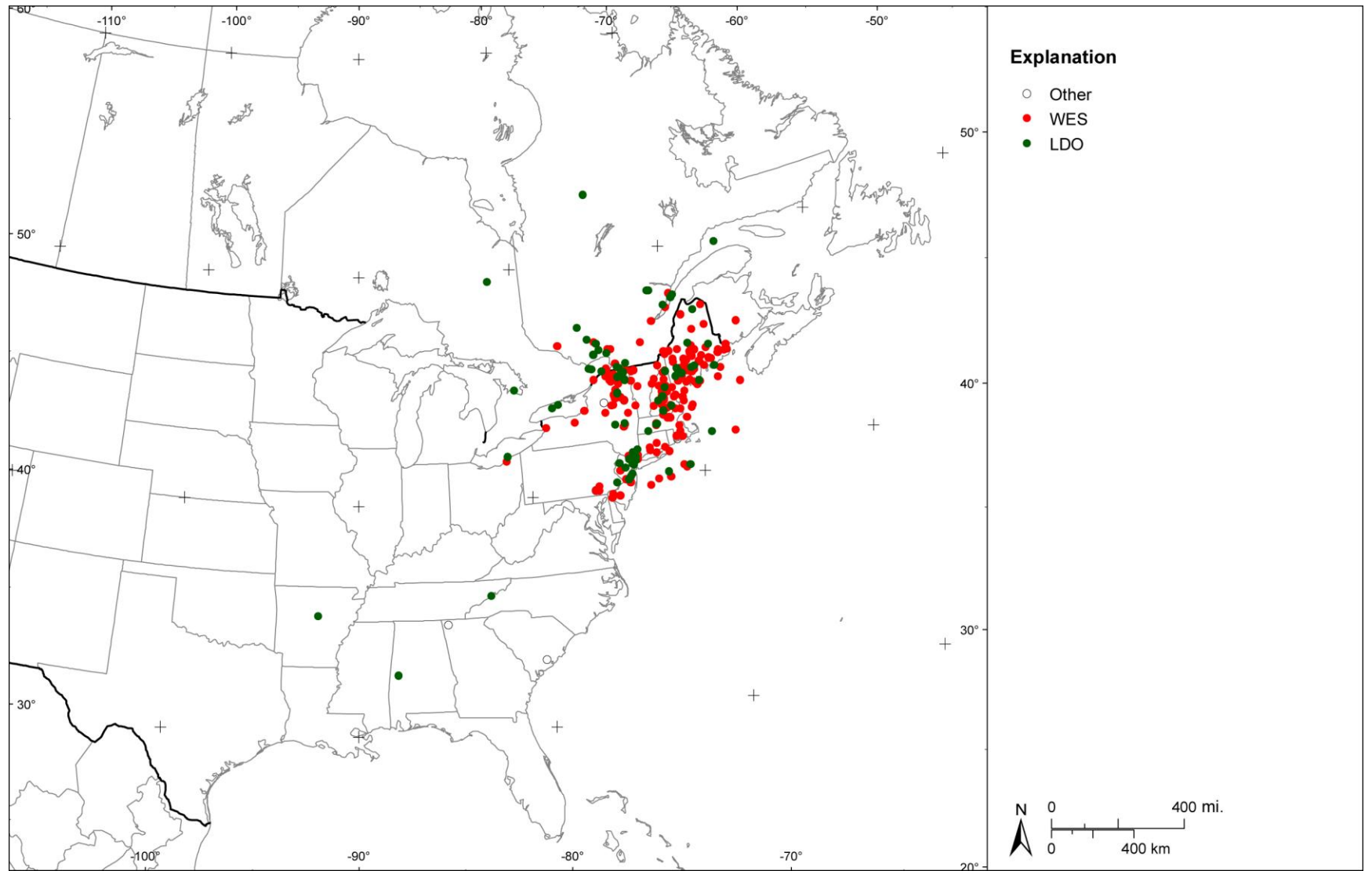


Figure 3.3-29
Spatial distribution of earthquakes in the CEUS SSC Project catalog with $M_C \geq 2.5$ and M magnitudes

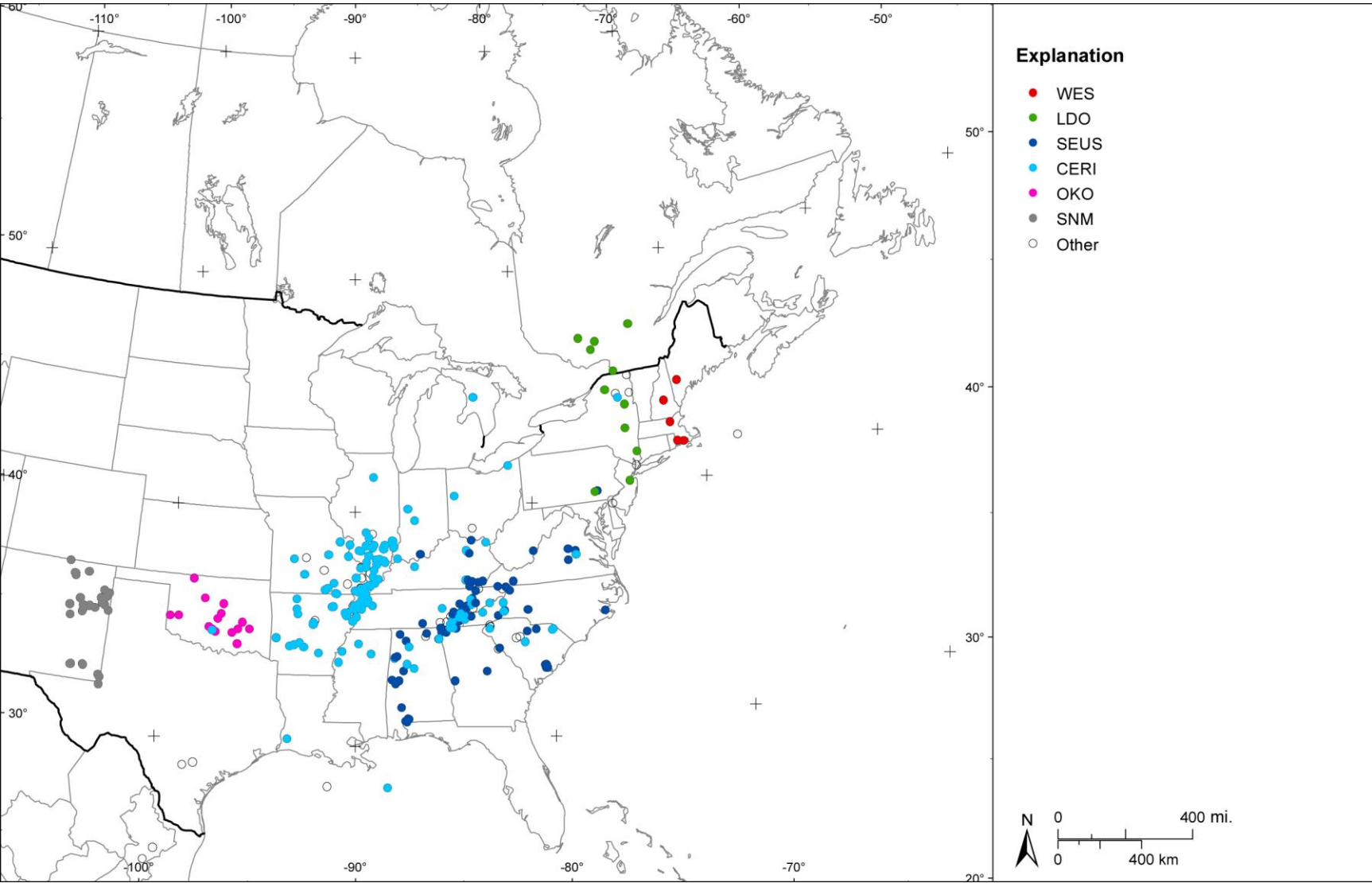


Figure 3.3-30
Spatial distribution of earthquakes in the CEUS SSC Project catalog with $M_D \geq 3$ magnitudes

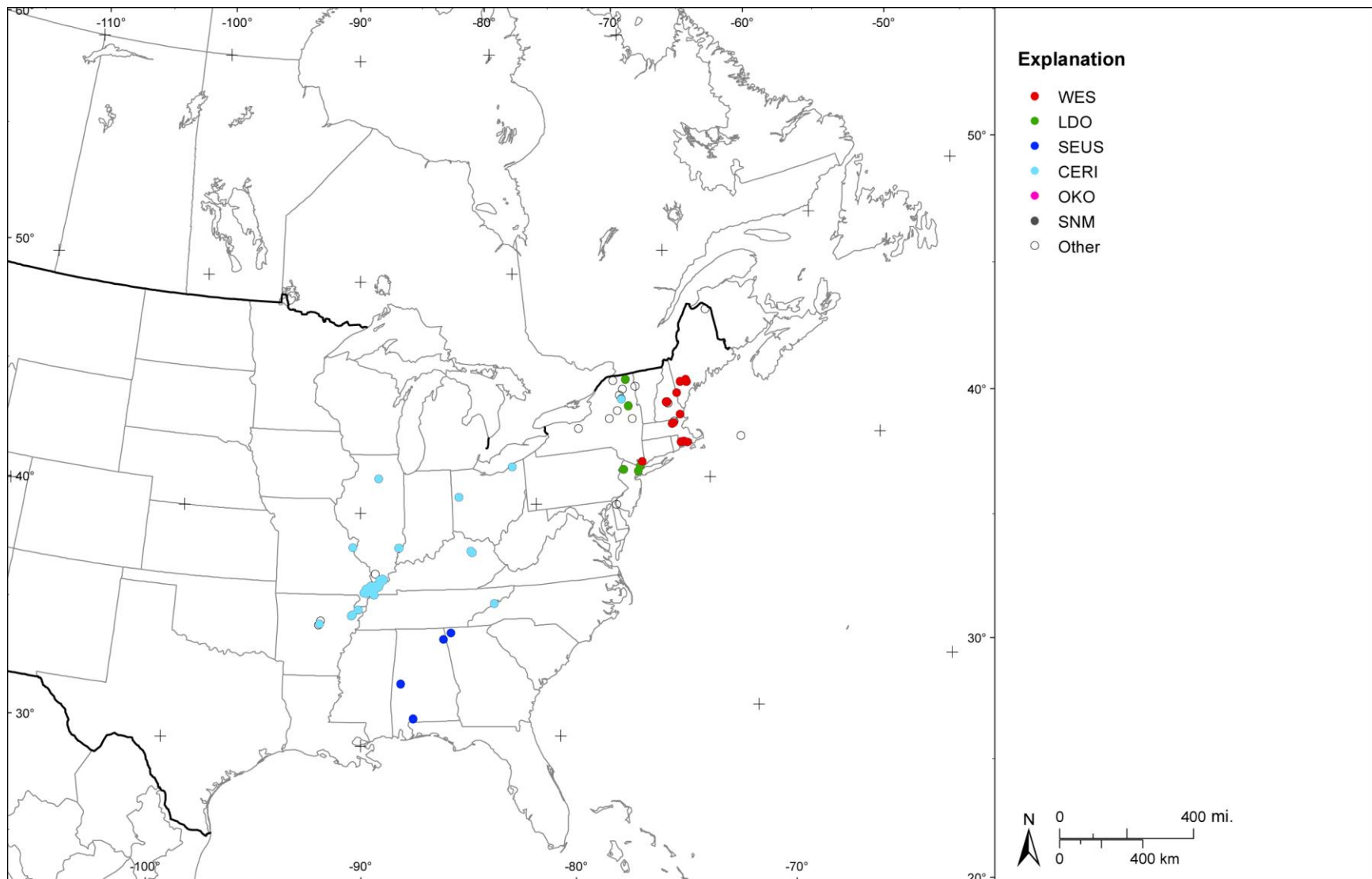


Figure 3.3-31
Spatial distribution of earthquakes in the CEUS SSC Project catalog with both M_D and M magnitudes

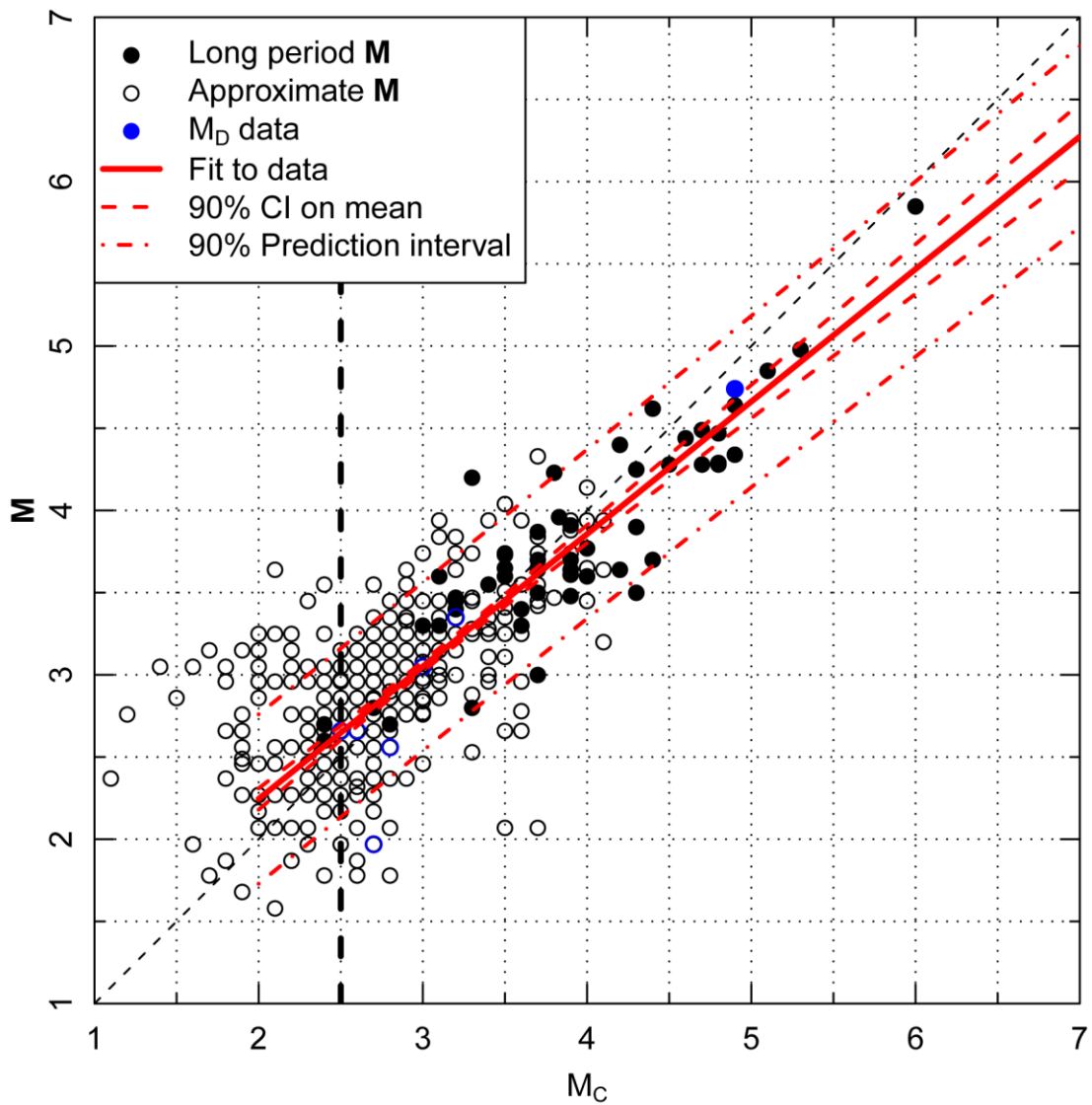


Figure 3.3-32
 M_C - M data from the CEUS SSC Project catalog and linear regression fit to the data

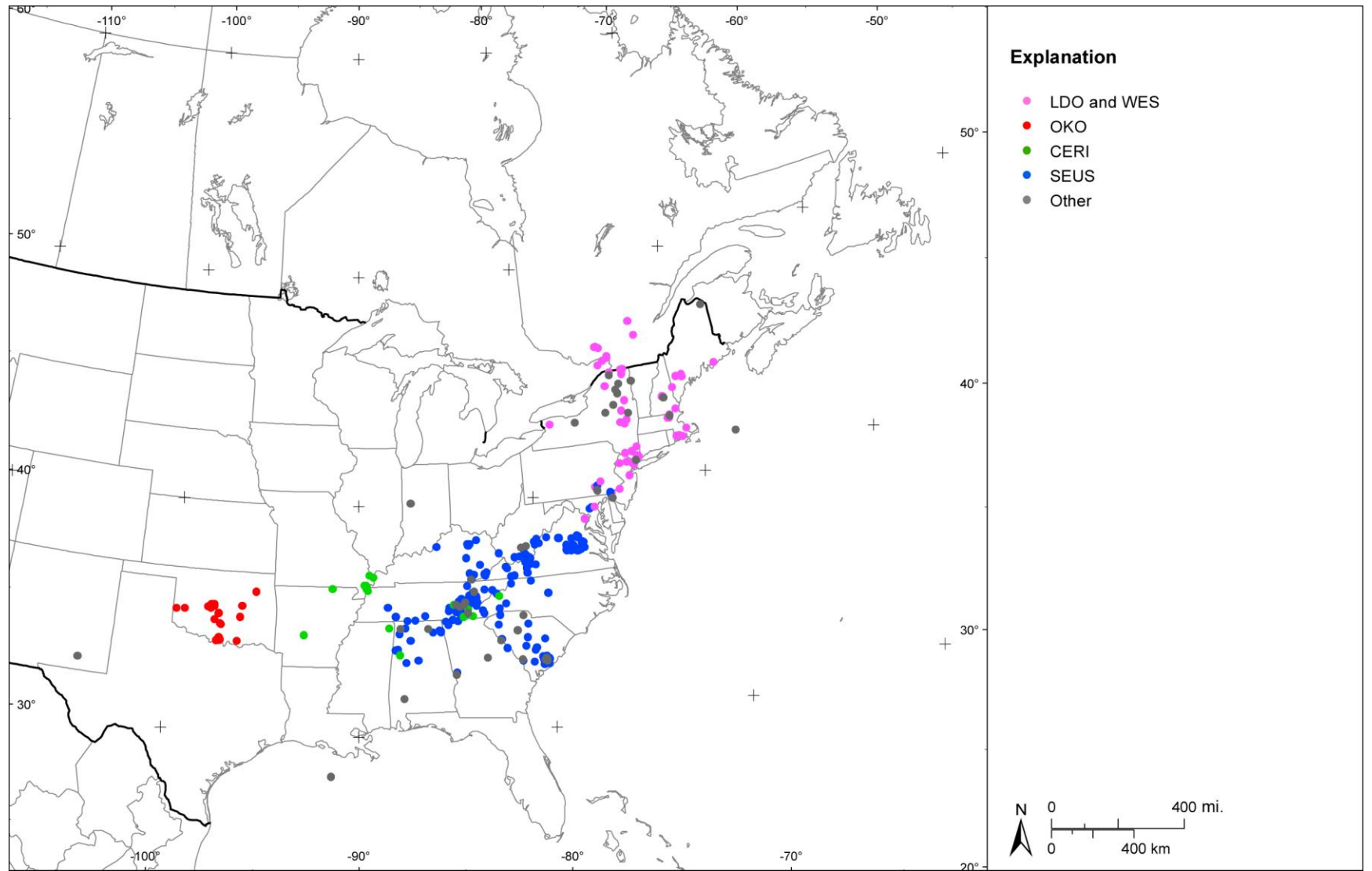


Figure 3.3-33
Spatial distribution of earthquakes with reported M_C and M_D magnitudes

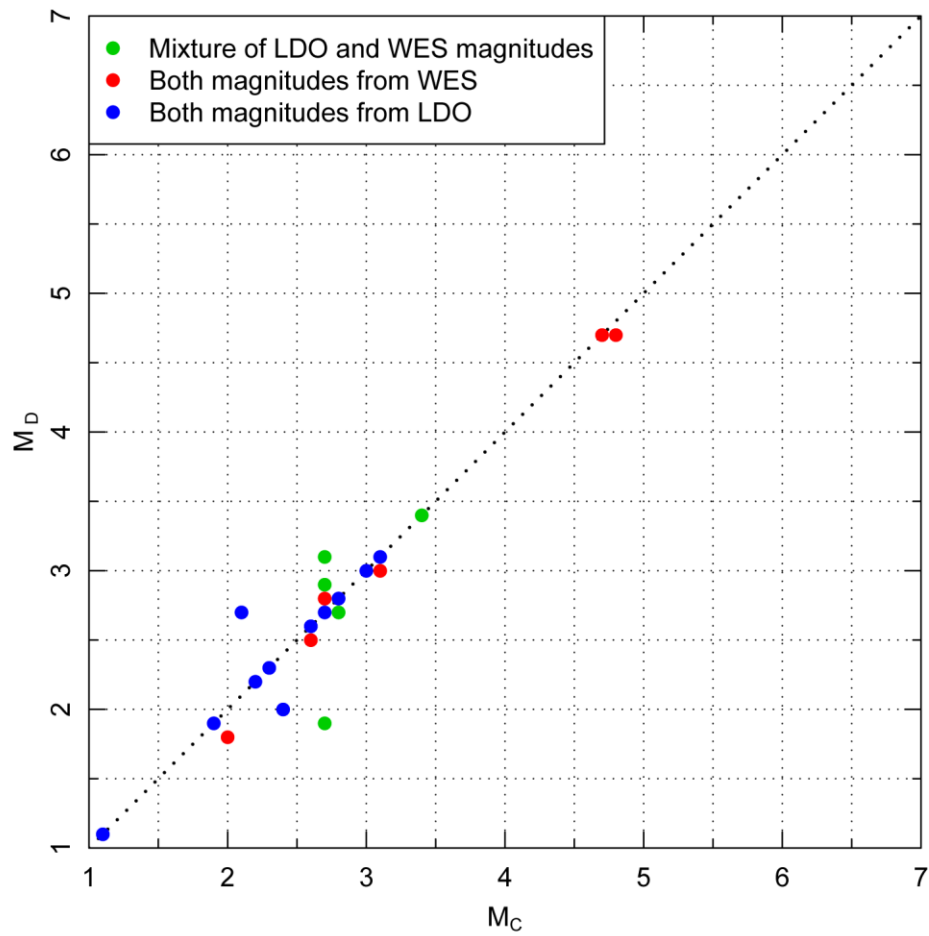


Figure 3.3-34
Comparison of M_C and M_D magnitudes for the LDO and WES catalogs

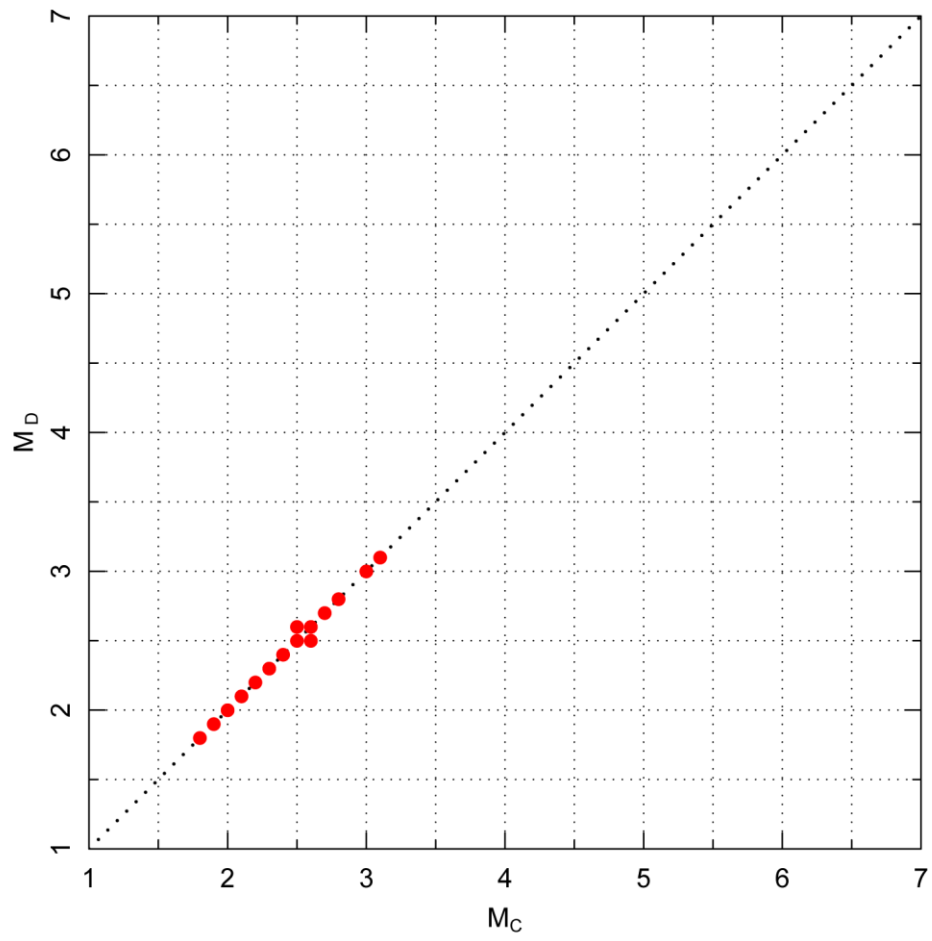


Figure 3.3-35
Comparison of M_C with M_D for at least one of the two magnitude types reported in the OKO catalog

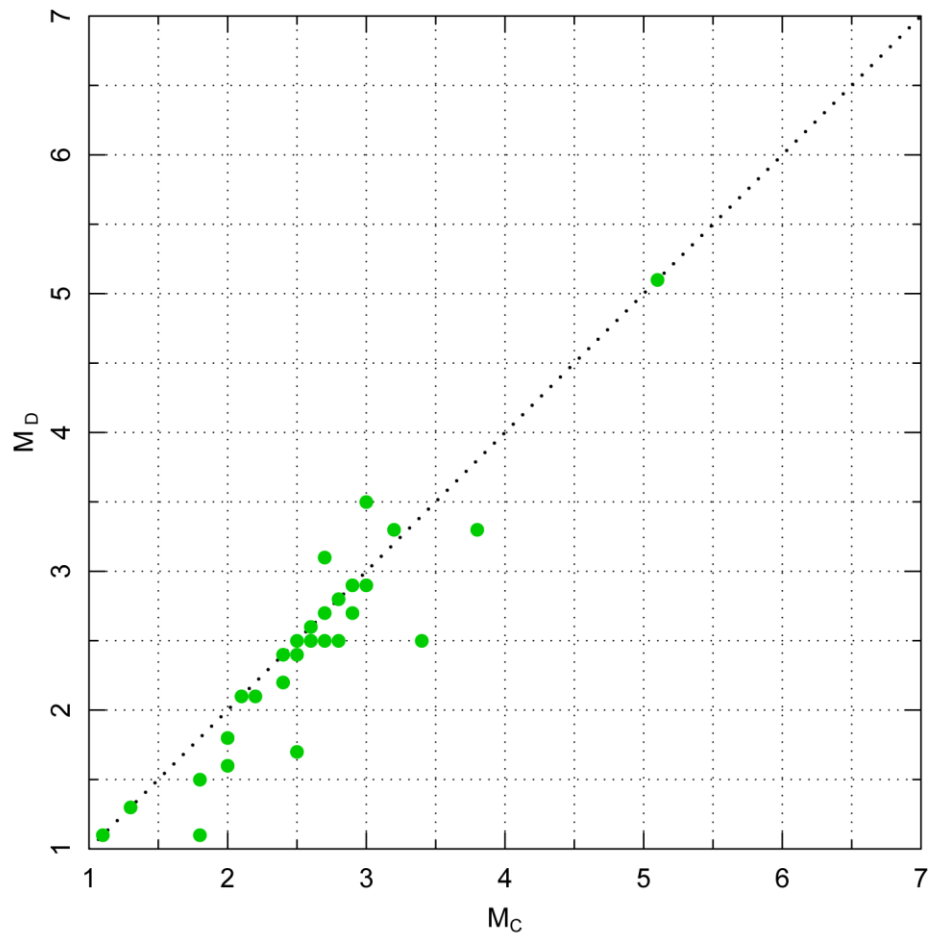


Figure 3.3-36
Comparison of M_C with M_D for at least one of the two magnitude types reported in the CERI catalog

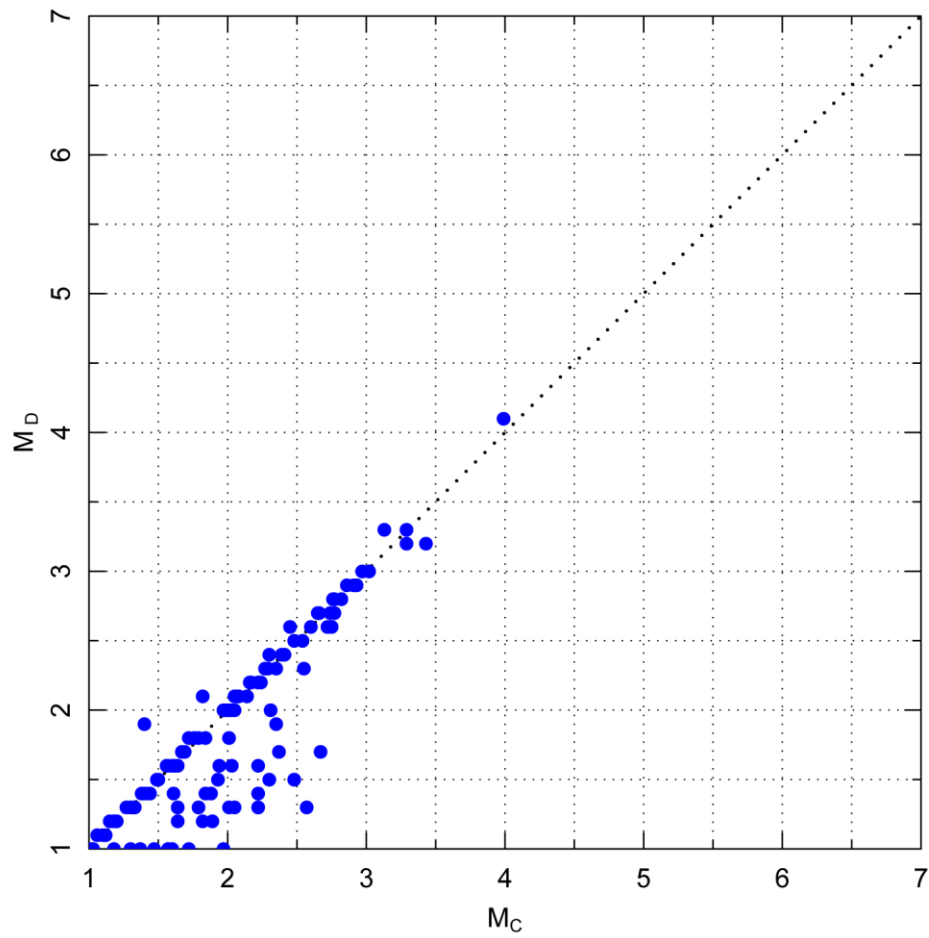


Figure 3.3-37
Comparison of M_C with M_D for at least one of the two magnitude types reported in the SCSN catalog

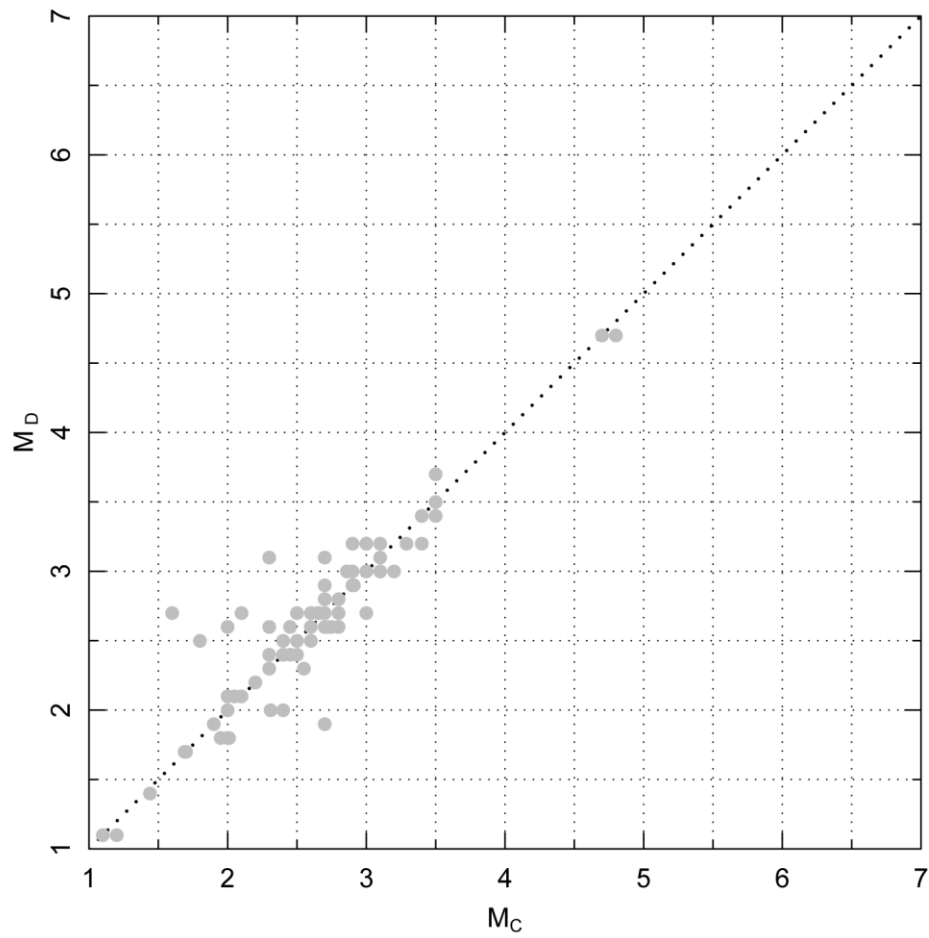


Figure 3.3-38
Comparison of M_C with M_D for at least one of the two magnitude types reported in other catalogs for earthquakes in the Midcontinent portion of the study region

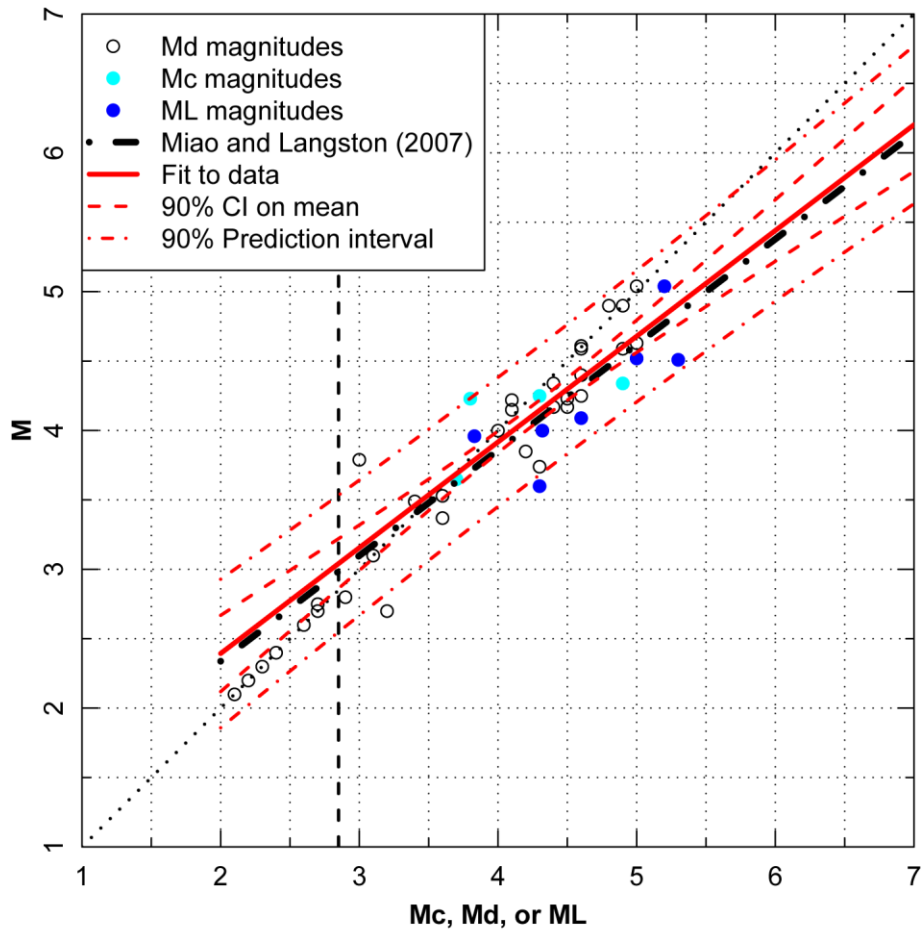


Figure 3.3-39
Relationship between M and M_C , M_D , or M_L for the Midcontinent portion of the study region

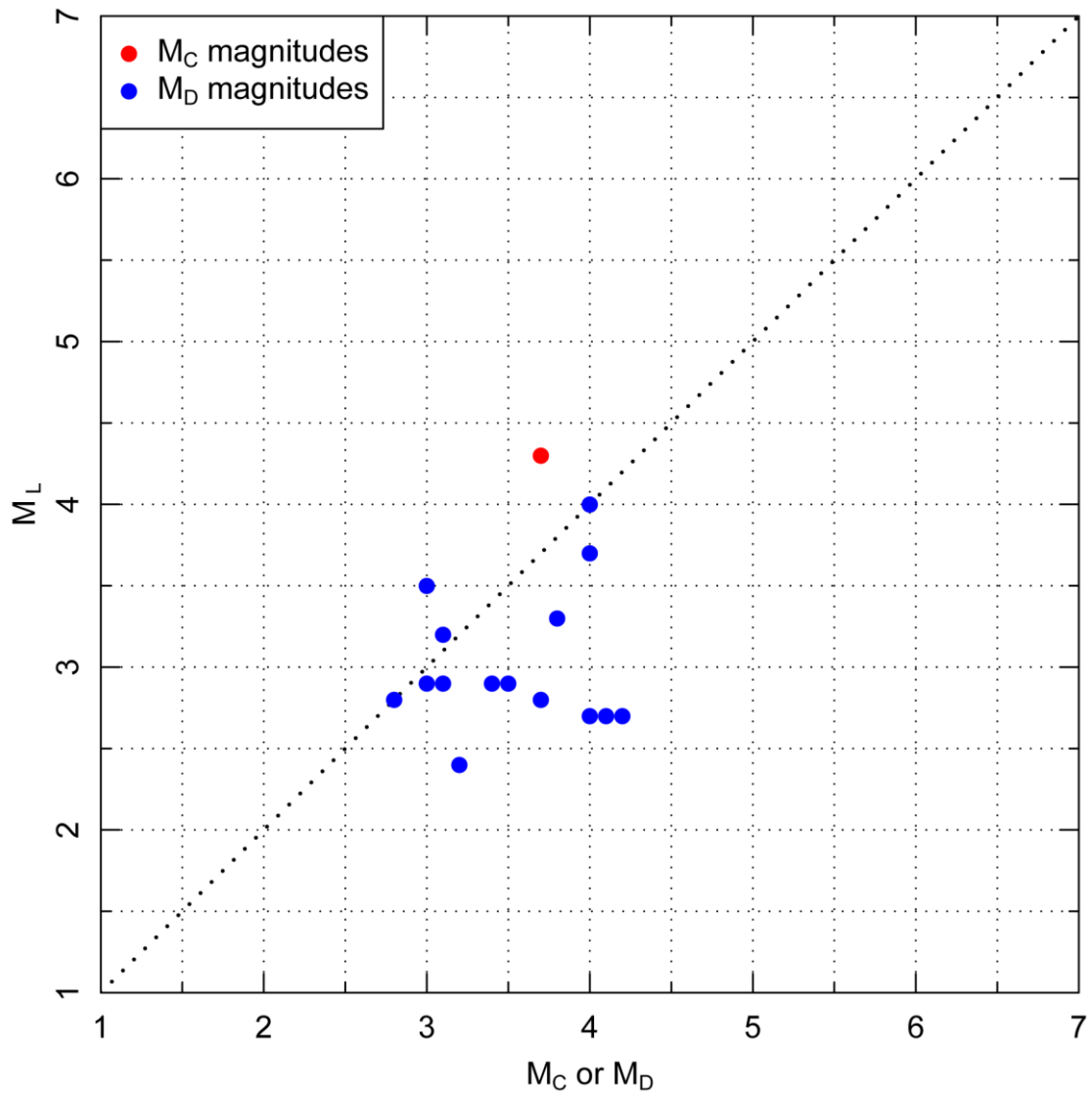


Figure 3.3-40
Comparison of M_C and M_D magnitudes with M_L magnitudes for the region between longitudes 105°W and 100°W

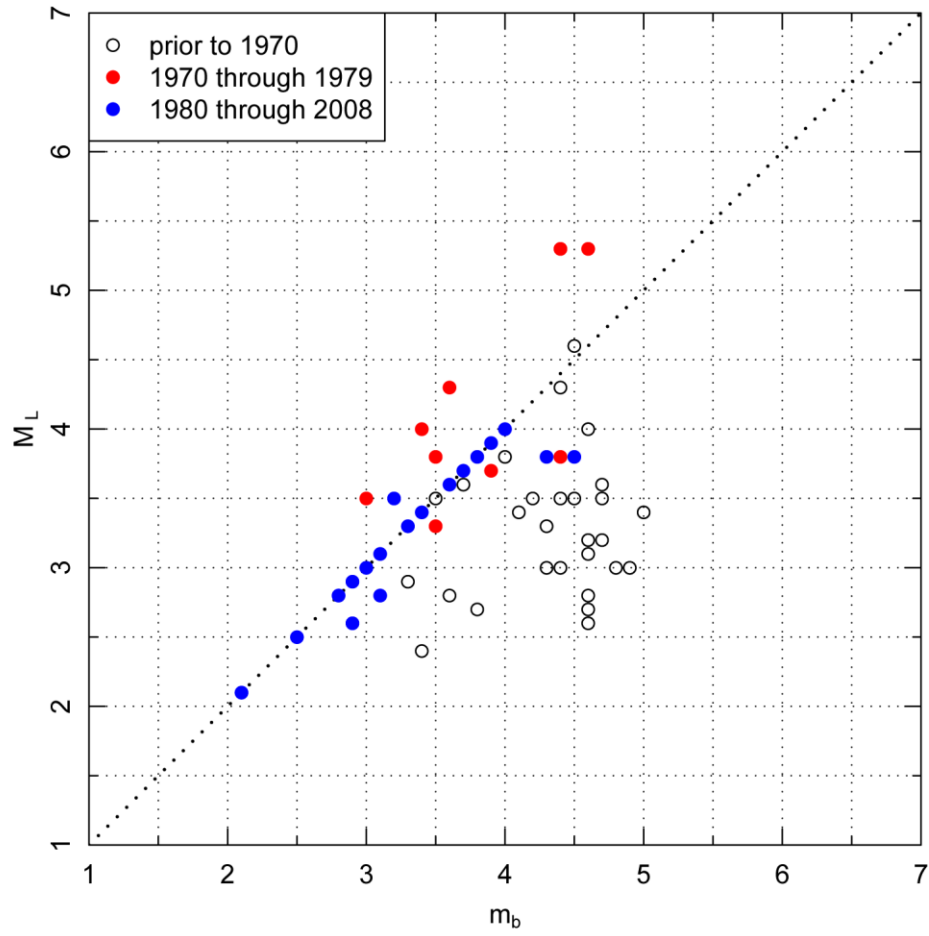


Figure 3.3-41
Comparison of m_b magnitudes with M_L magnitudes for the region between longitudes 105°W and 100°W

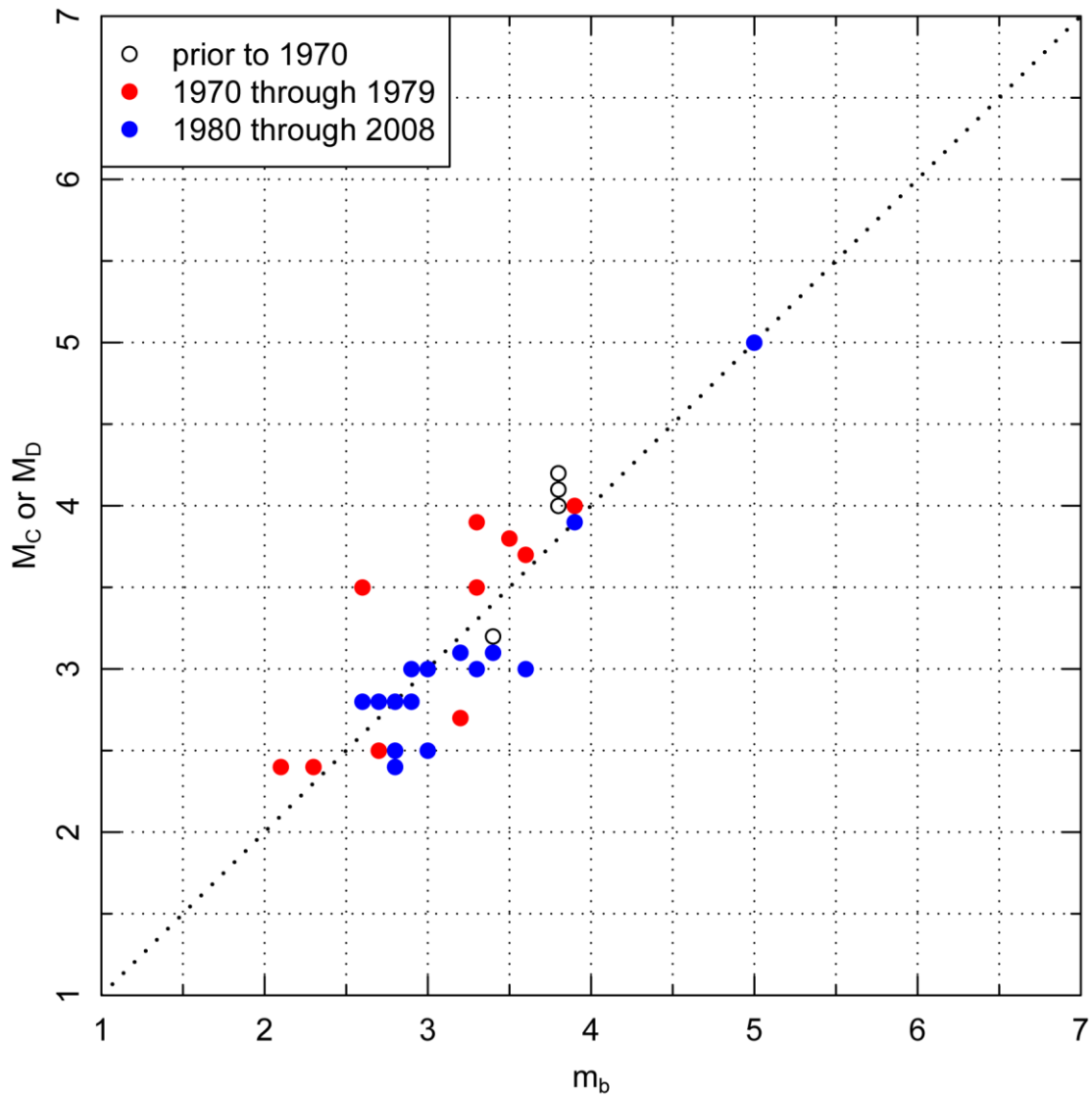


Figure 3.3-42
Comparison of m_b magnitudes with M_c and M_D magnitudes for the region between longitudes 105°W and 100°W

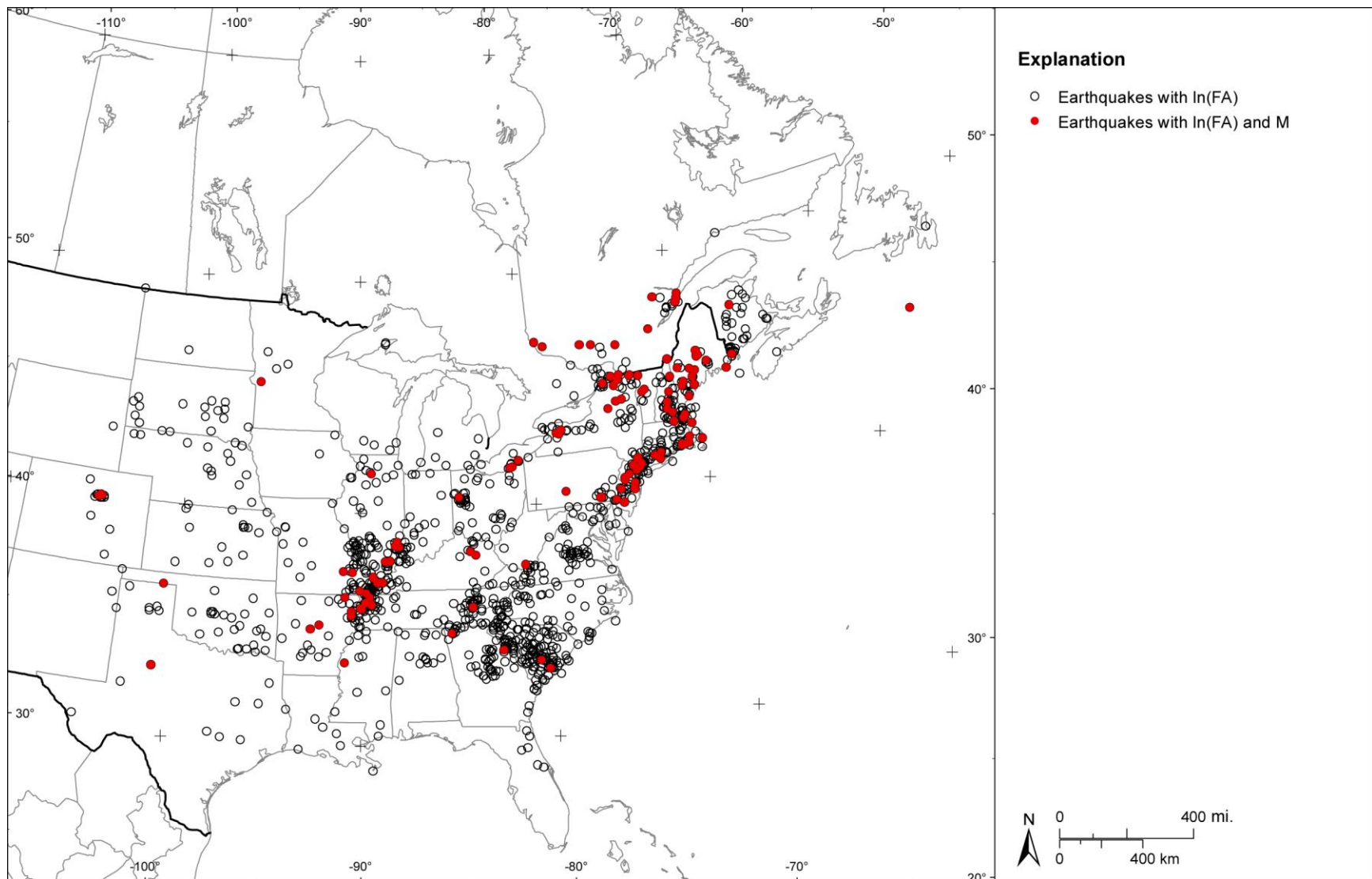


Figure 3.3-43
Spatial distribution of earthquake with In(FA) in the CEUS SSC Project catalog

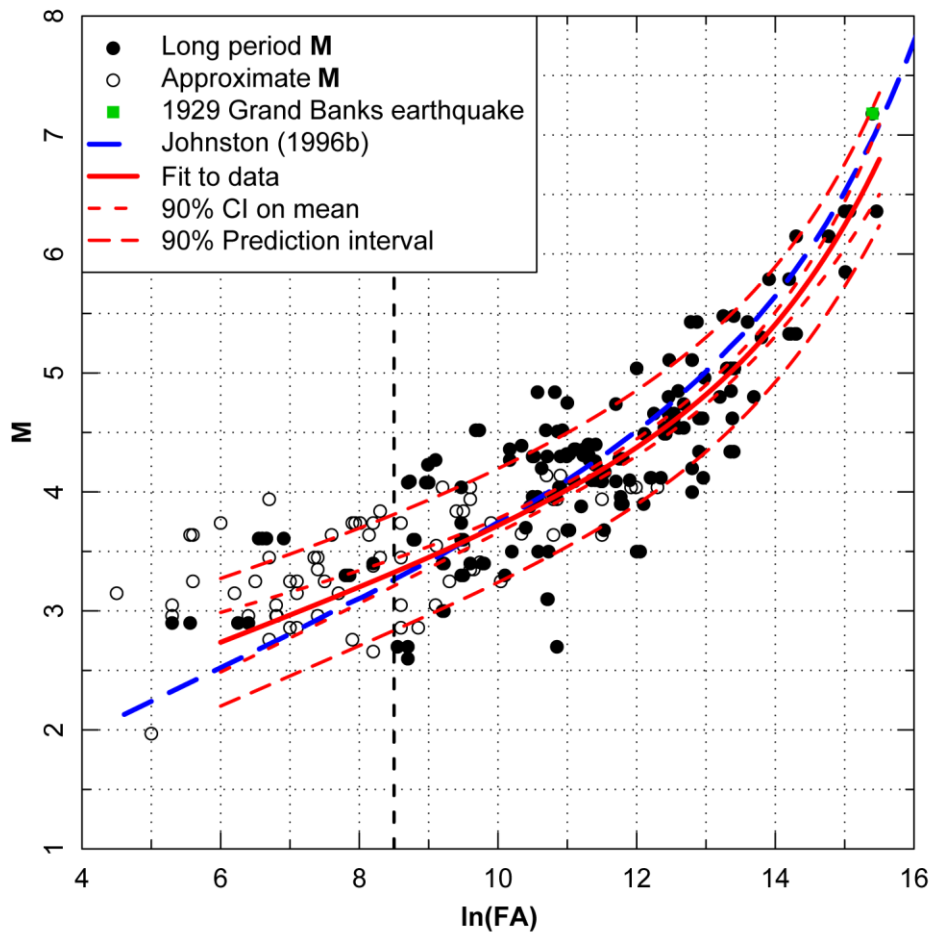


Figure 3.3-44
Catalog ln(FA)–M data and fitted model

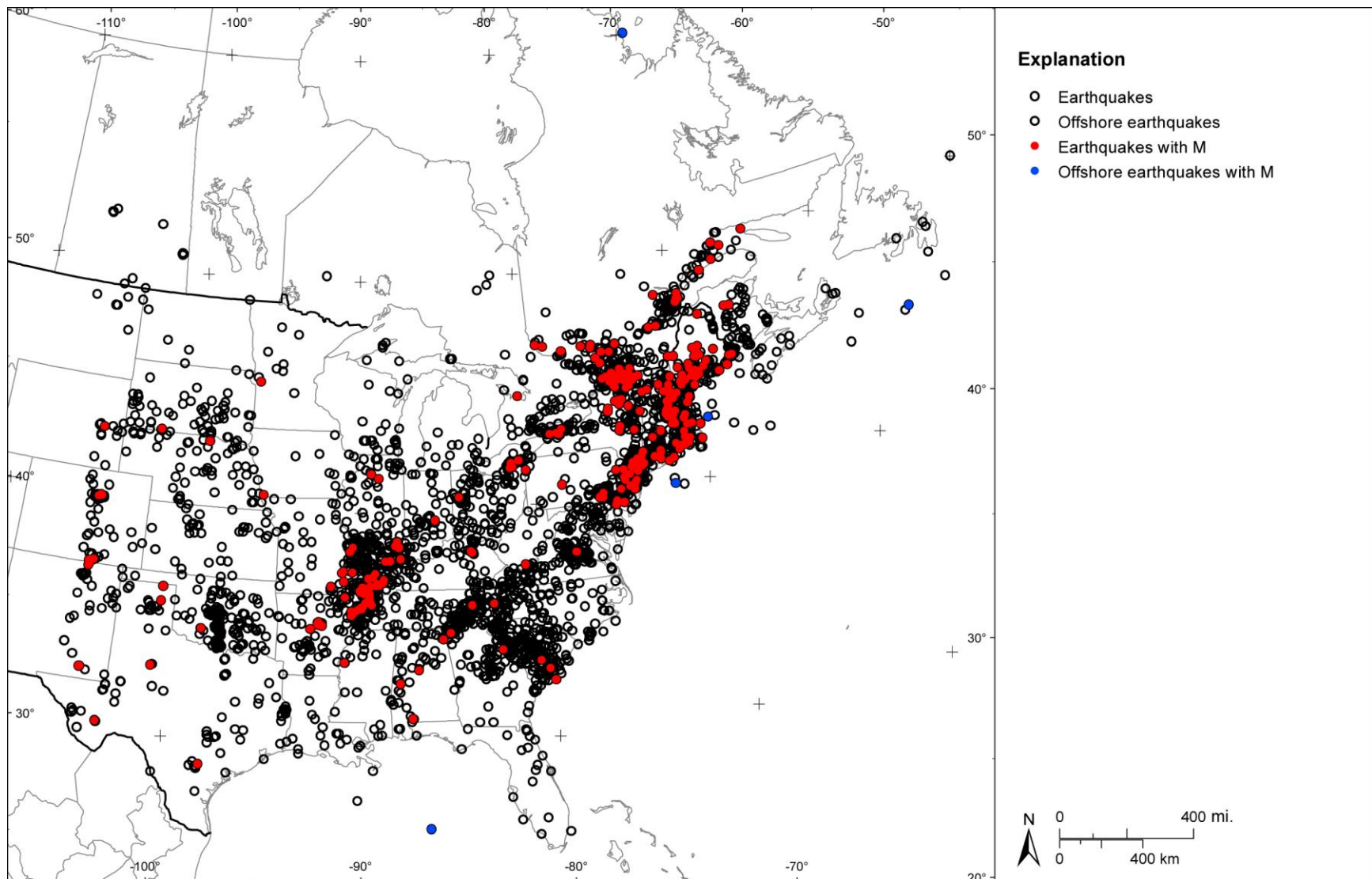


Figure 3.3-45
Spatial distribution of earthquakes in the CEUS SSC Project catalog with reported values of I_0

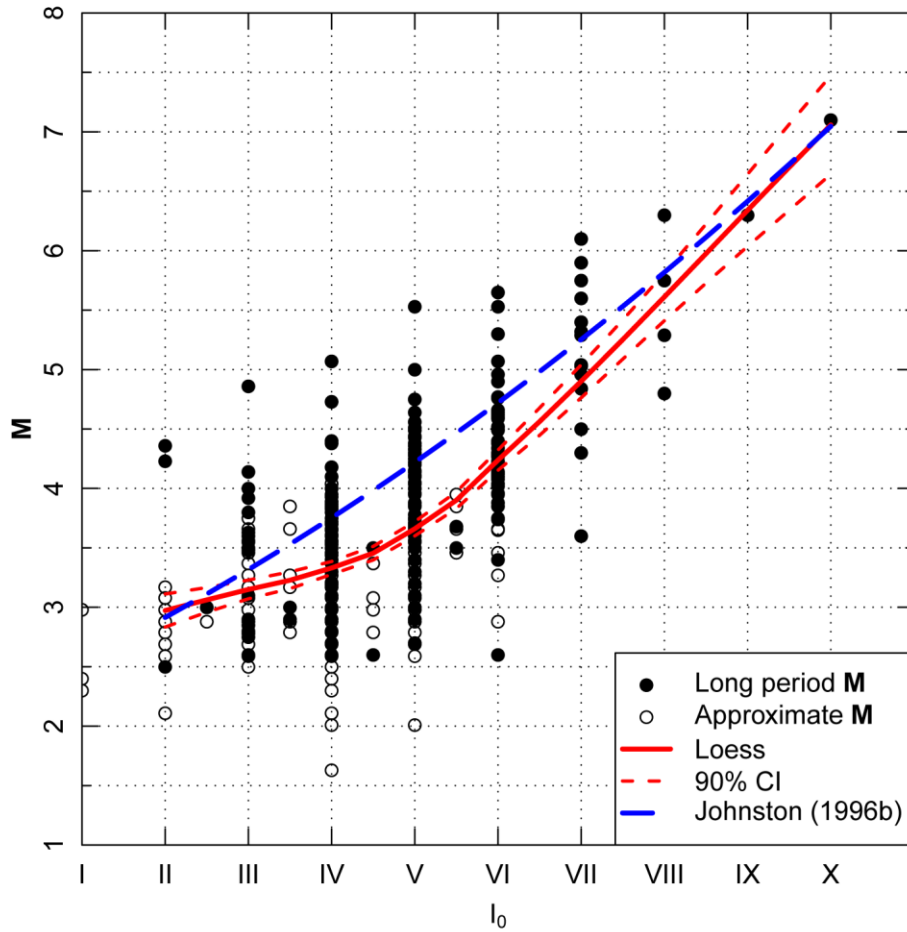


Figure 3.3-46
 I_0 and M data for earthquakes in the CEUS SSC Project catalog. Curves show locally weighted least-squares fit (Loess) to the data and the relationship published by Johnston (1996b).

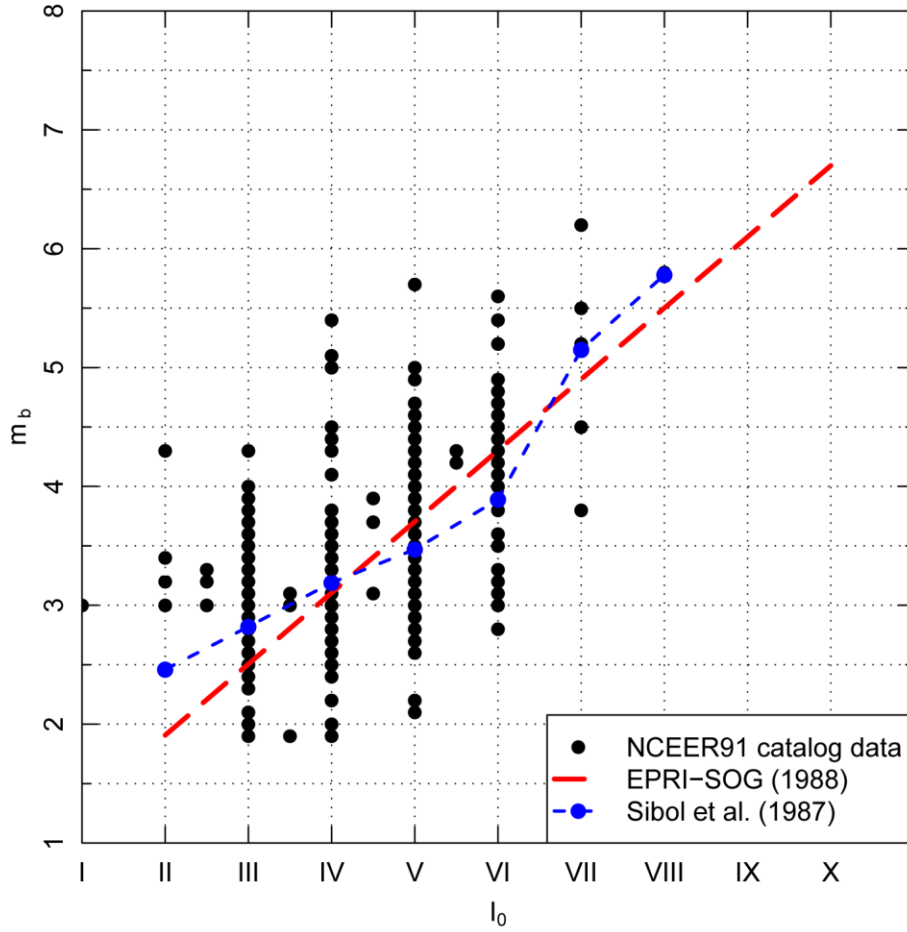


Figure 3.3-47
 I_0 and m_b data from the NCEER91 catalog. Plotted are the relationships between I_0 and m_b developed by EPRI (1988) (EPRI-SOG) and Sibol et al. (1987).

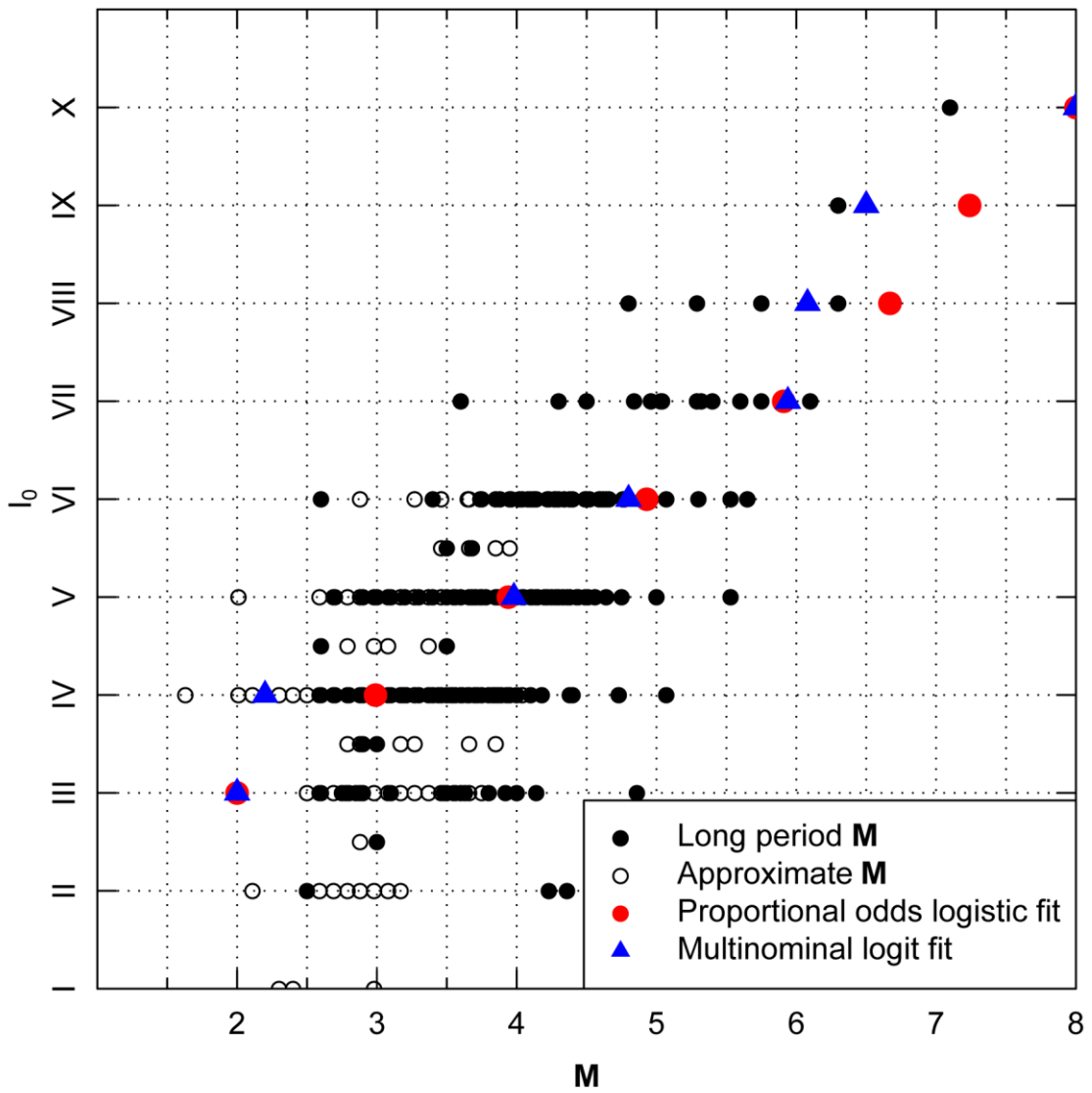


Figure 3.3-48
Categorical model fits of I_0 as a function and M for earthquakes in the CEUS SSC Project catalog

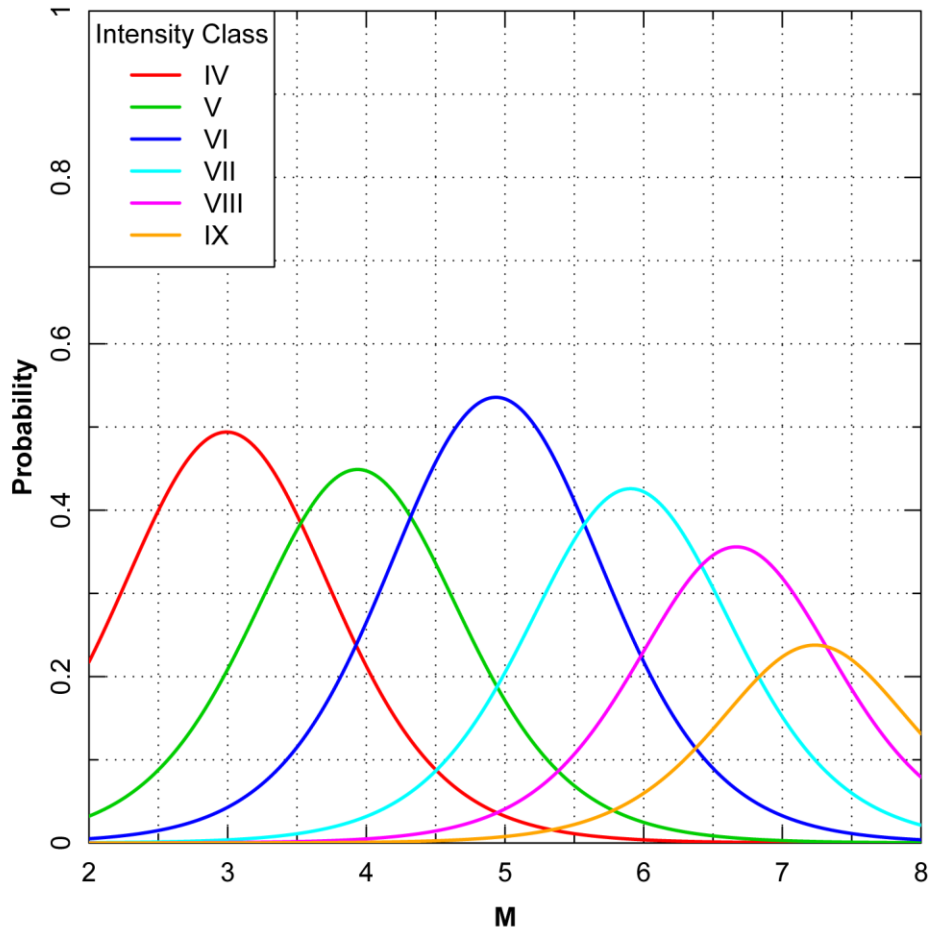


Figure 3.3-49
Results from proportional odds logistic model showing the probability of individual intensity classes as a function of M

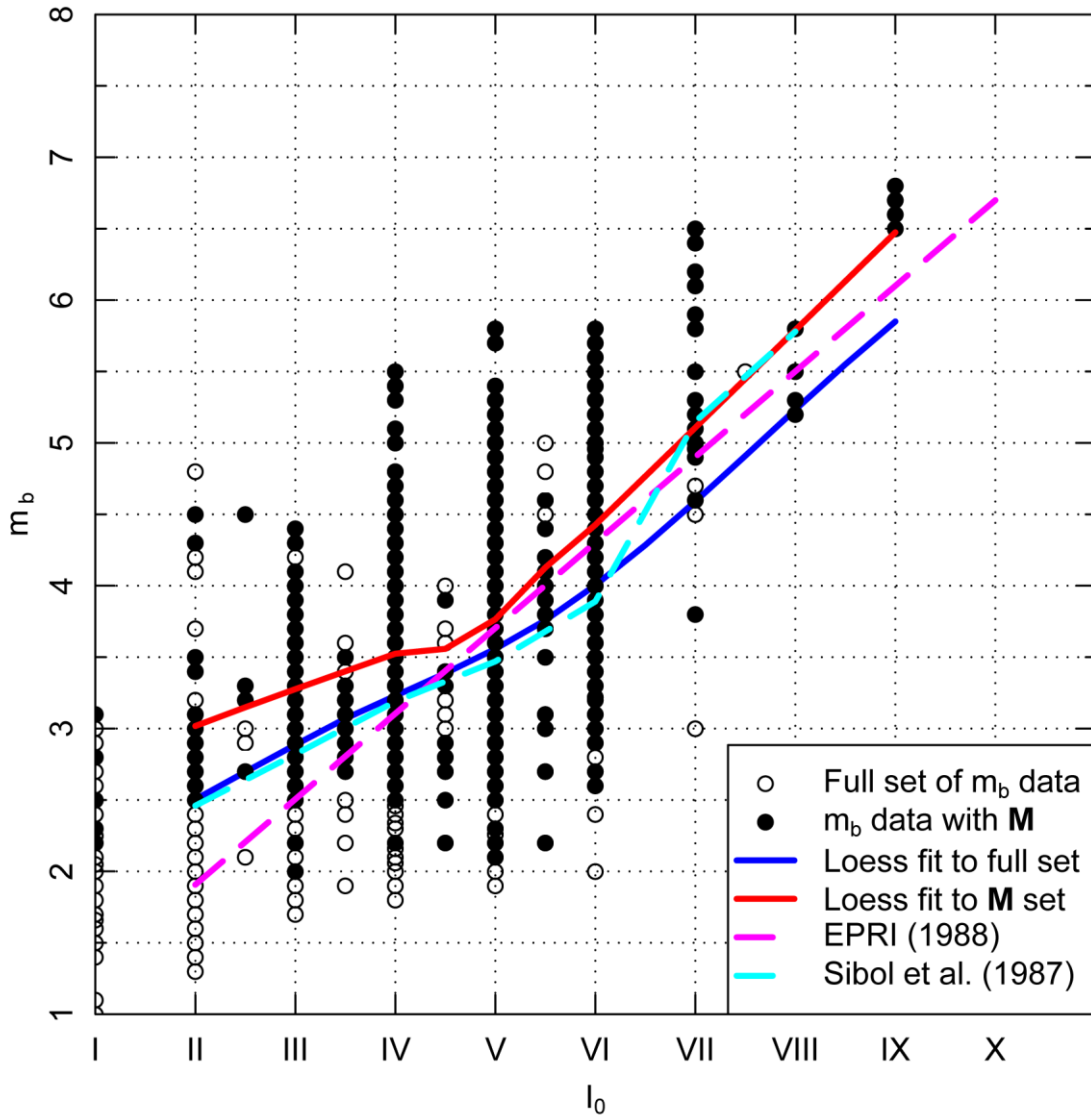


Figure 3.3-50
Comparison of I_0 and m_b data from the CEUS SSC Project catalog for those earthquakes with reported values of M (M set) and the full catalog (full set). Locally weighted least-squares fits to the two data sets are shown along with the relationship used to develop the EPRI (1988) catalog and the Sibol et al. (1987) relationship used in the NCEER91 catalog.

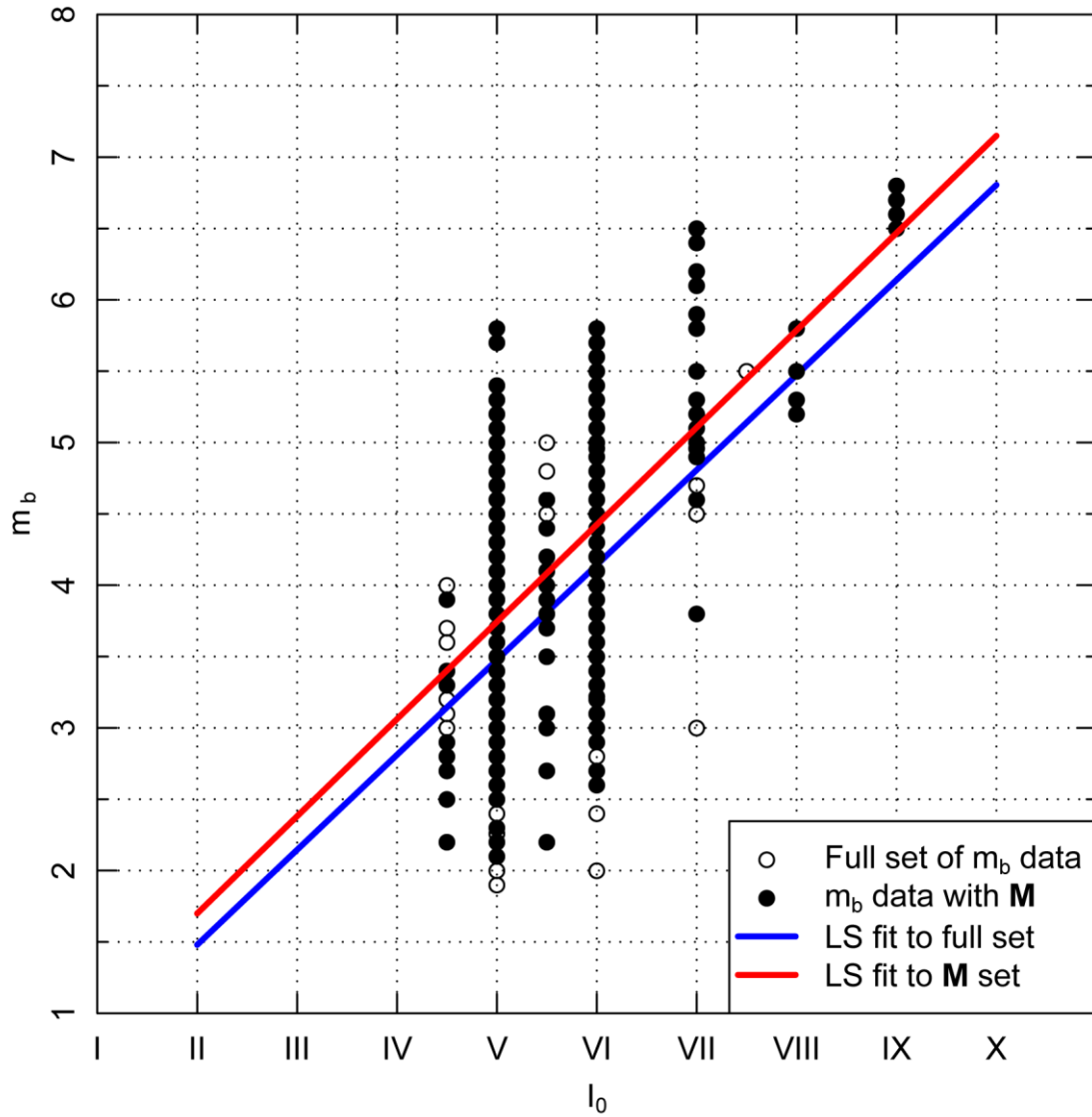


Figure 3.3-51
Linear fits to the data from Figure 3.3-50 for $I_0 \geq V$

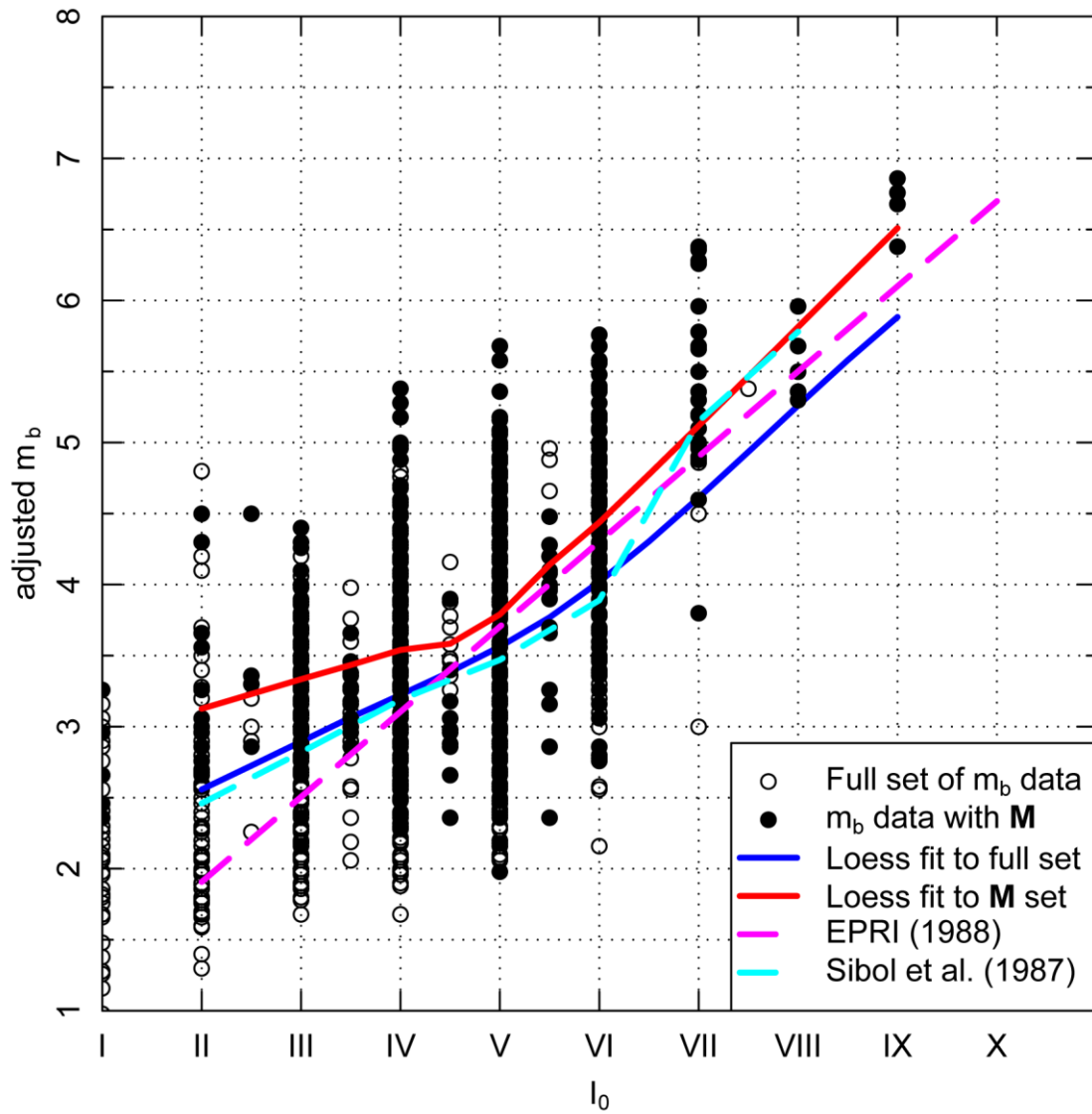


Figure 3.3-52
Comparison of I_0 and m_b data from the project, with m_b adjusted for the difference in m_b to M scaling

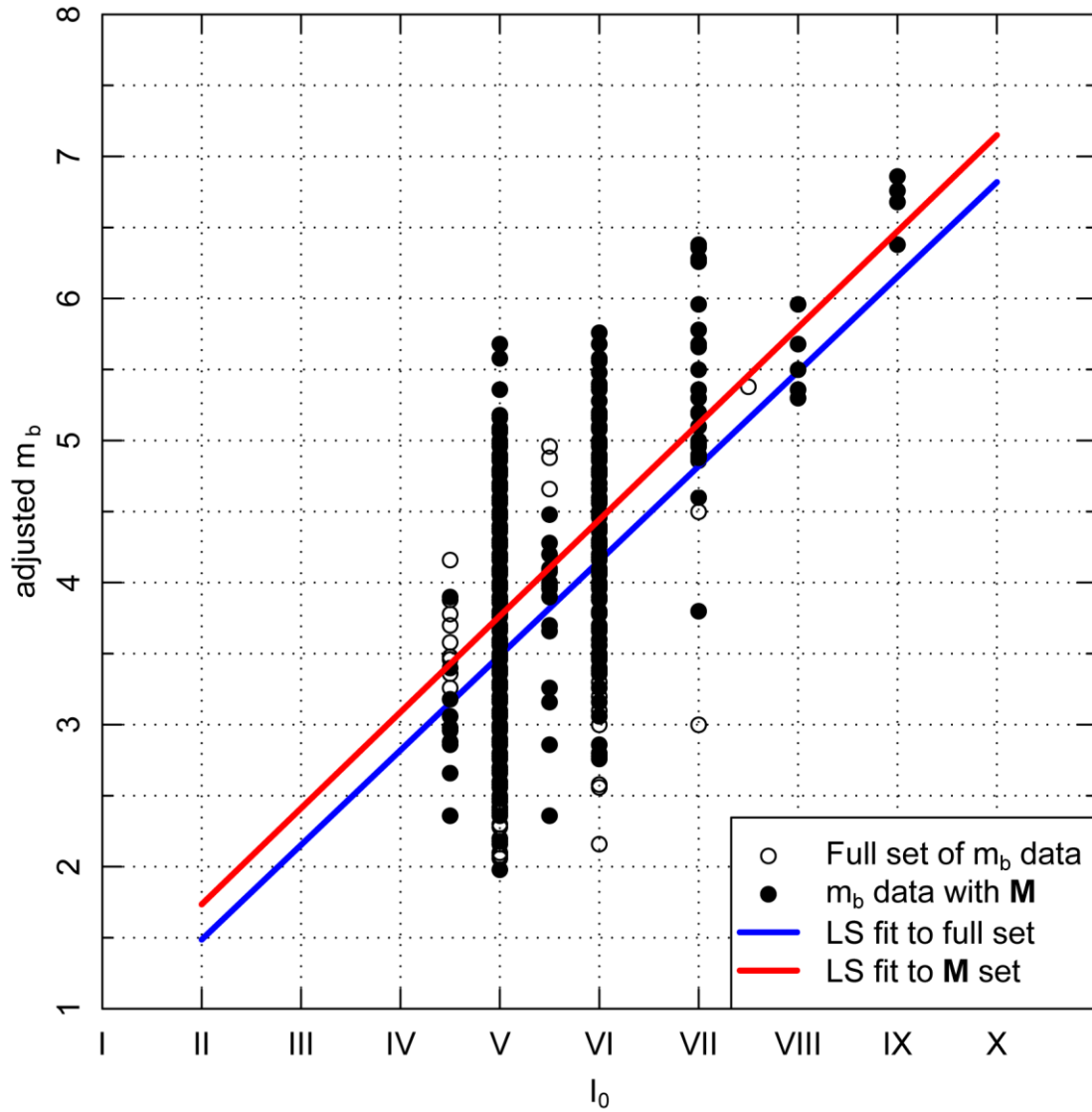


Figure 3.3-53
Linear fits to the data from Figure 3.3-52 for $I_0 \geq V$

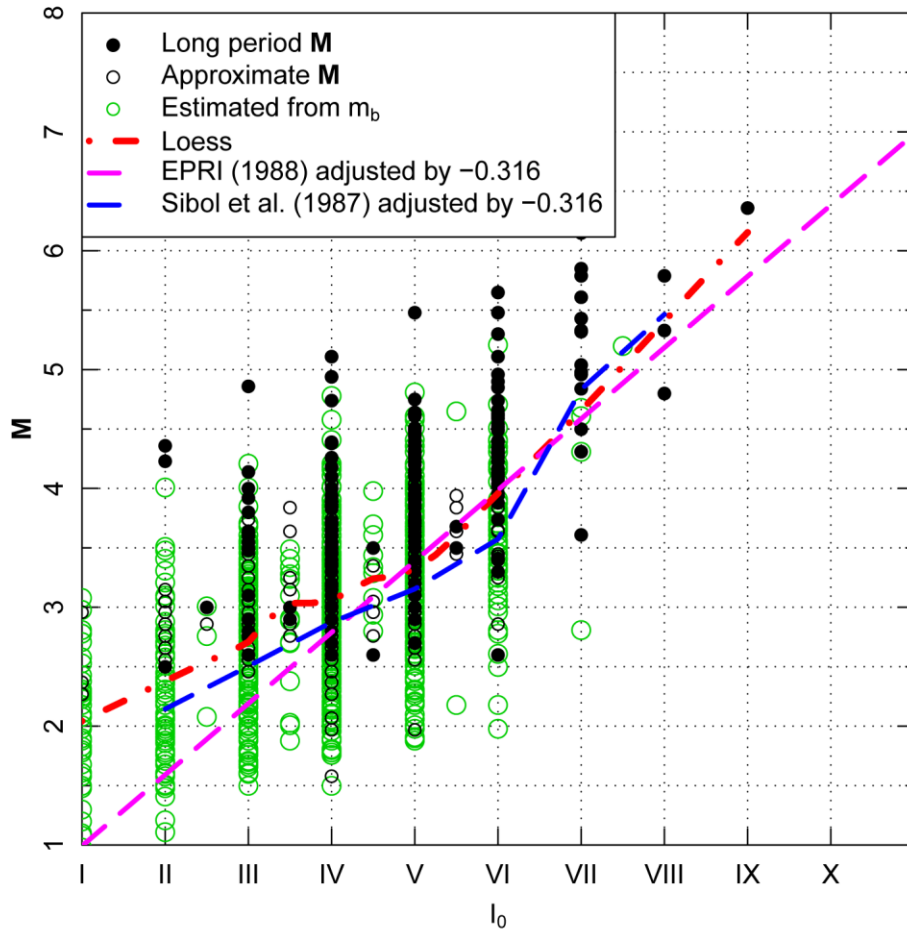


Figure 3.3-54
Composite I₀-M data set used for assessment of I₀ scaling relationship

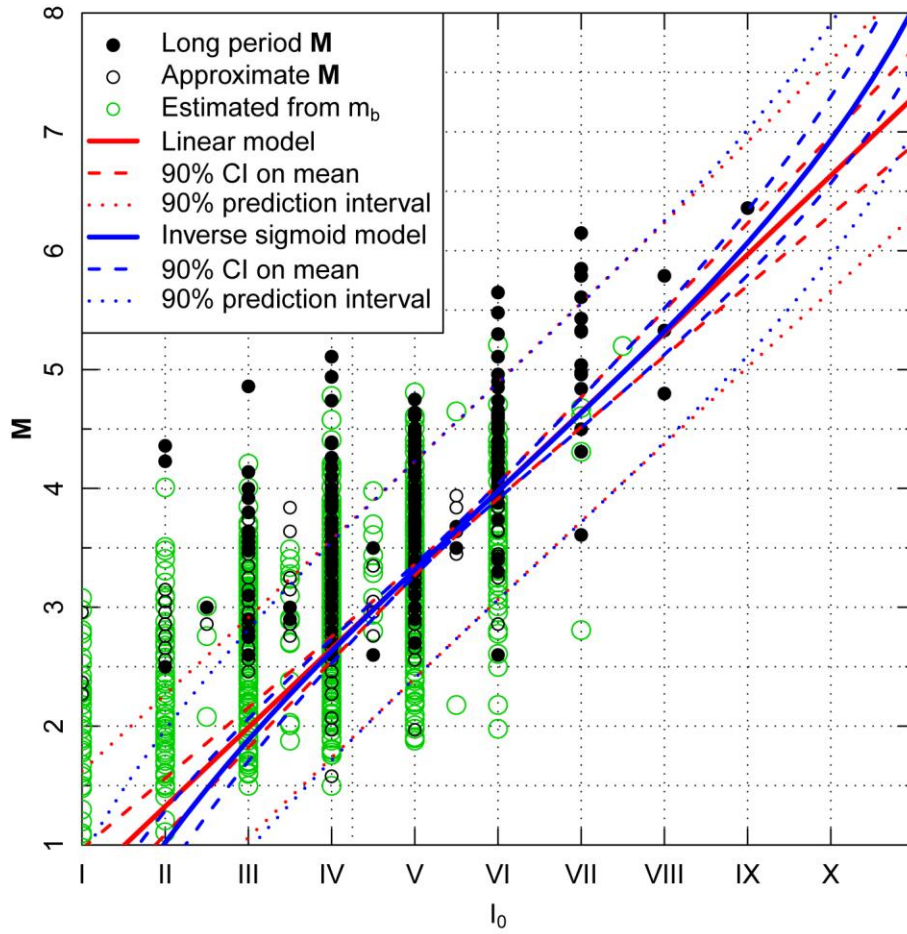


Figure 3.3-55
Linear and inverse sigmoid models fit to the project data for $I_0 > IV$

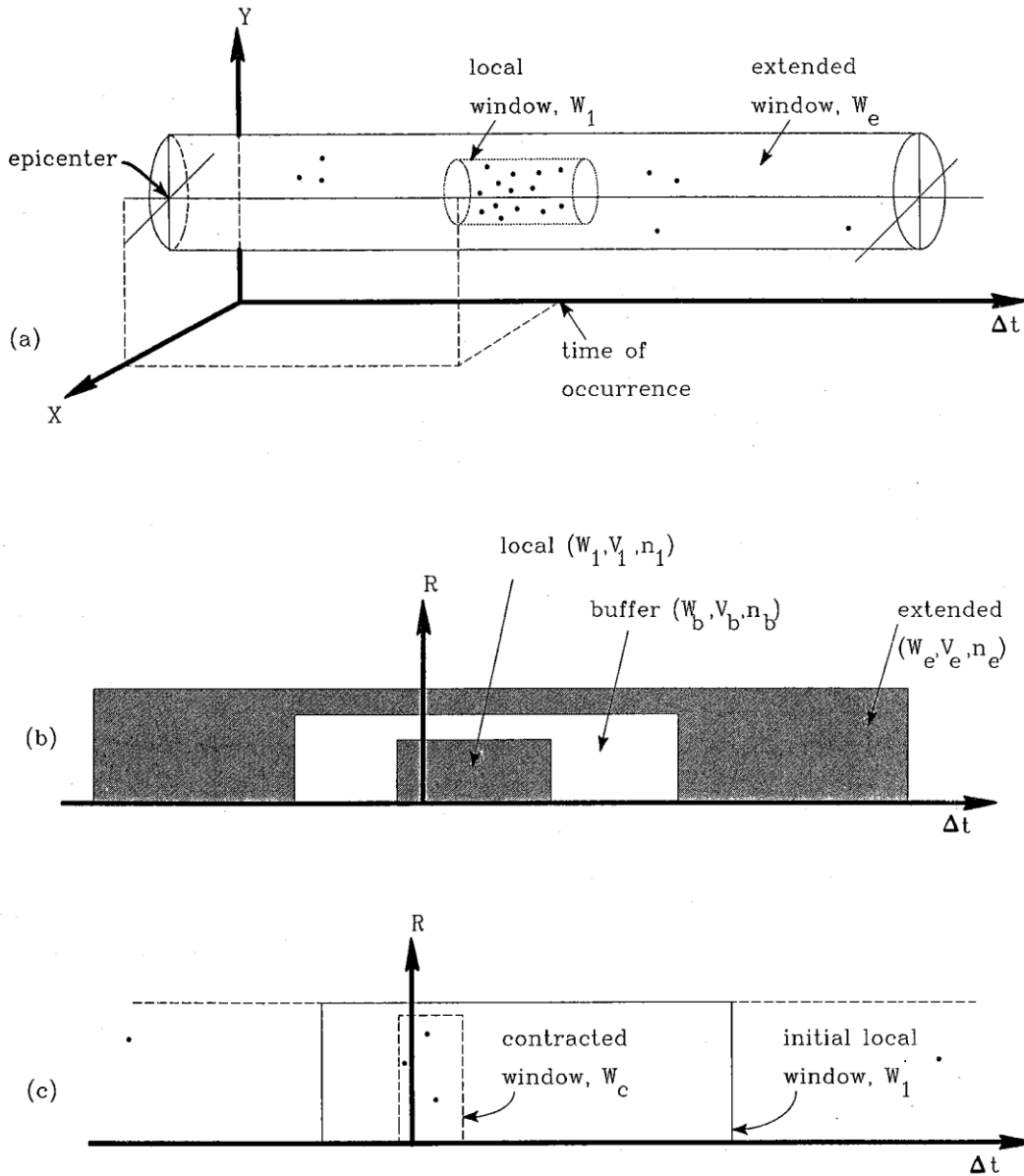


Figure 3.4-1
Illustration of process used to identify clusters of earthquakes (from EPRI, 1988, Vol. 1):
(a) local and extended time and distance windows, (b) buffer window, and (c) contracted window

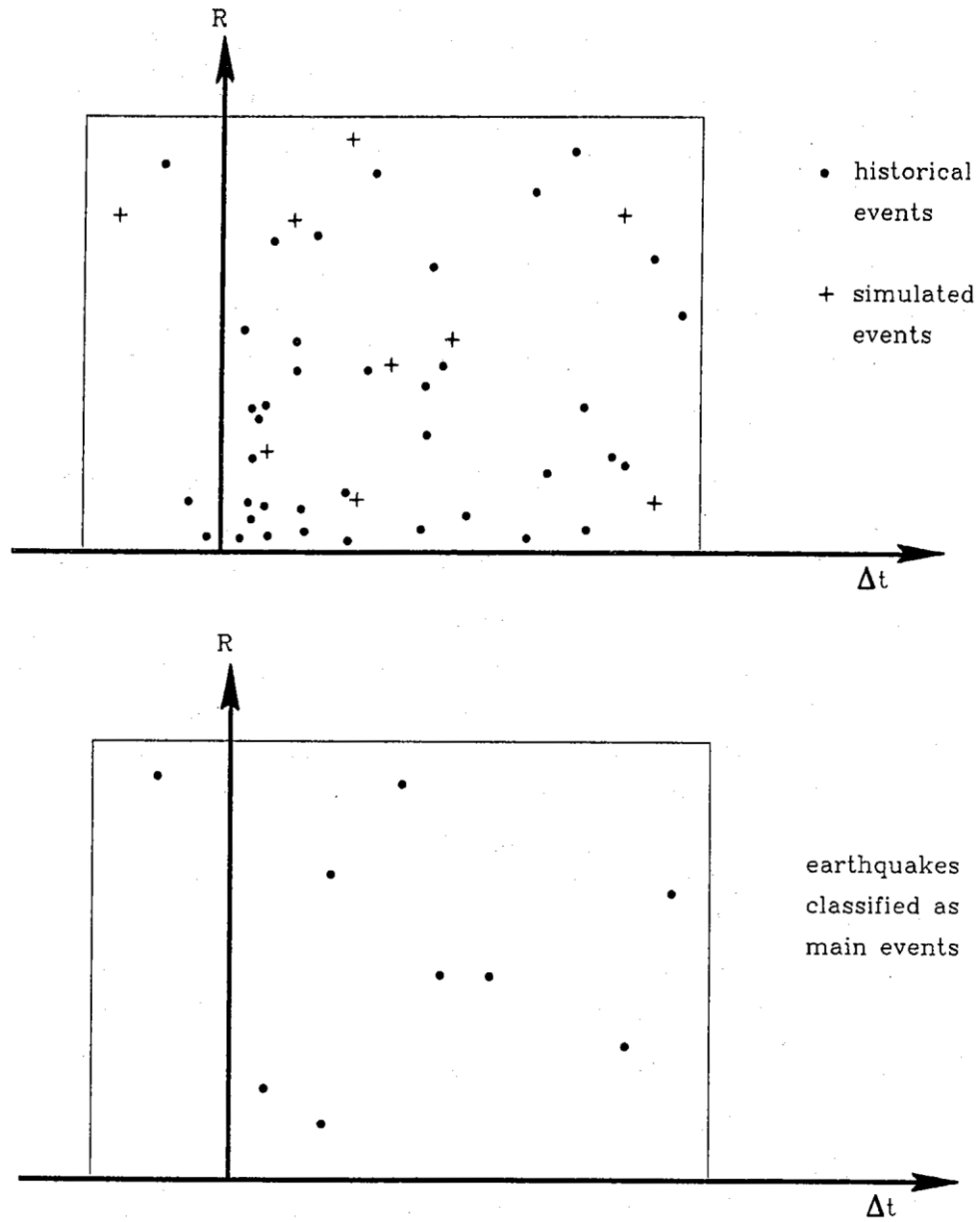


Figure 3.4-2
Identification of secondary (dependent) earthquakes inside the cluster region through Poisson thinning (from EPRI, 1988, Vol. 1)

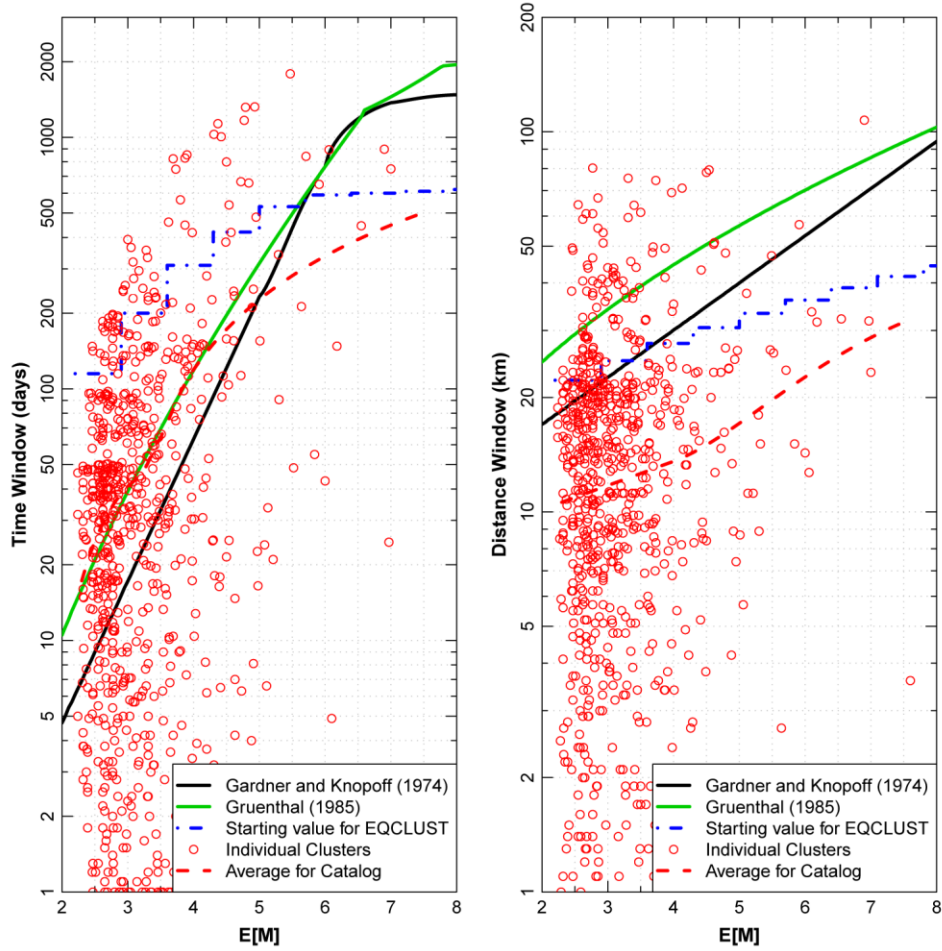


Figure 3.4-3
Comparison of dependent event time and distance windows with results for individual clusters in the project catalog

Note: Time windows represent the sum of the foreshock and aftershock windows for Grünthal (1985) and 1.5 times the aftershock window for Gardner and Knopoff (1974).

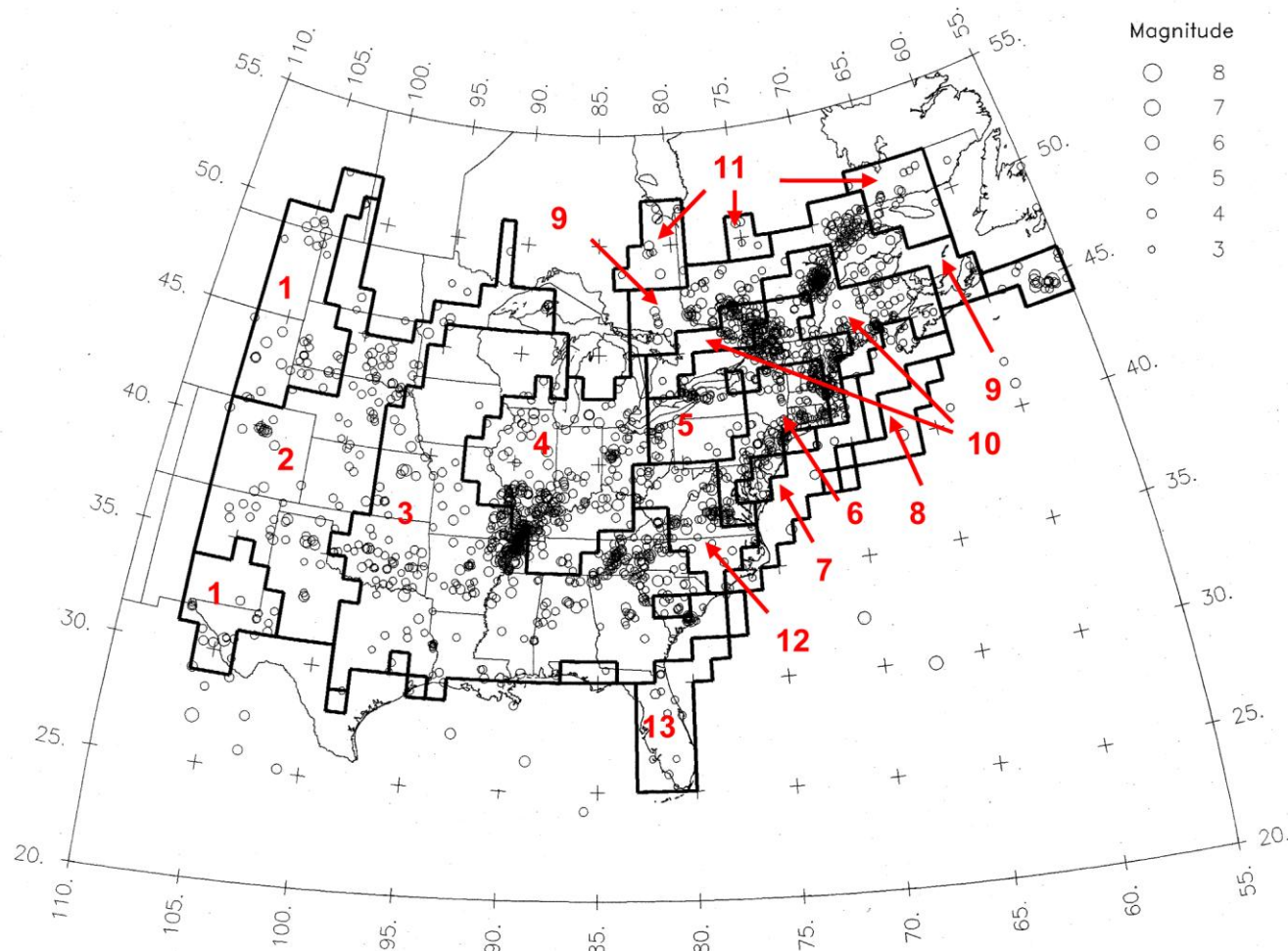


Figure 3.5-1
Earthquake catalog and catalog completeness regions used in EPRI-SOG (EPRI, 1988)

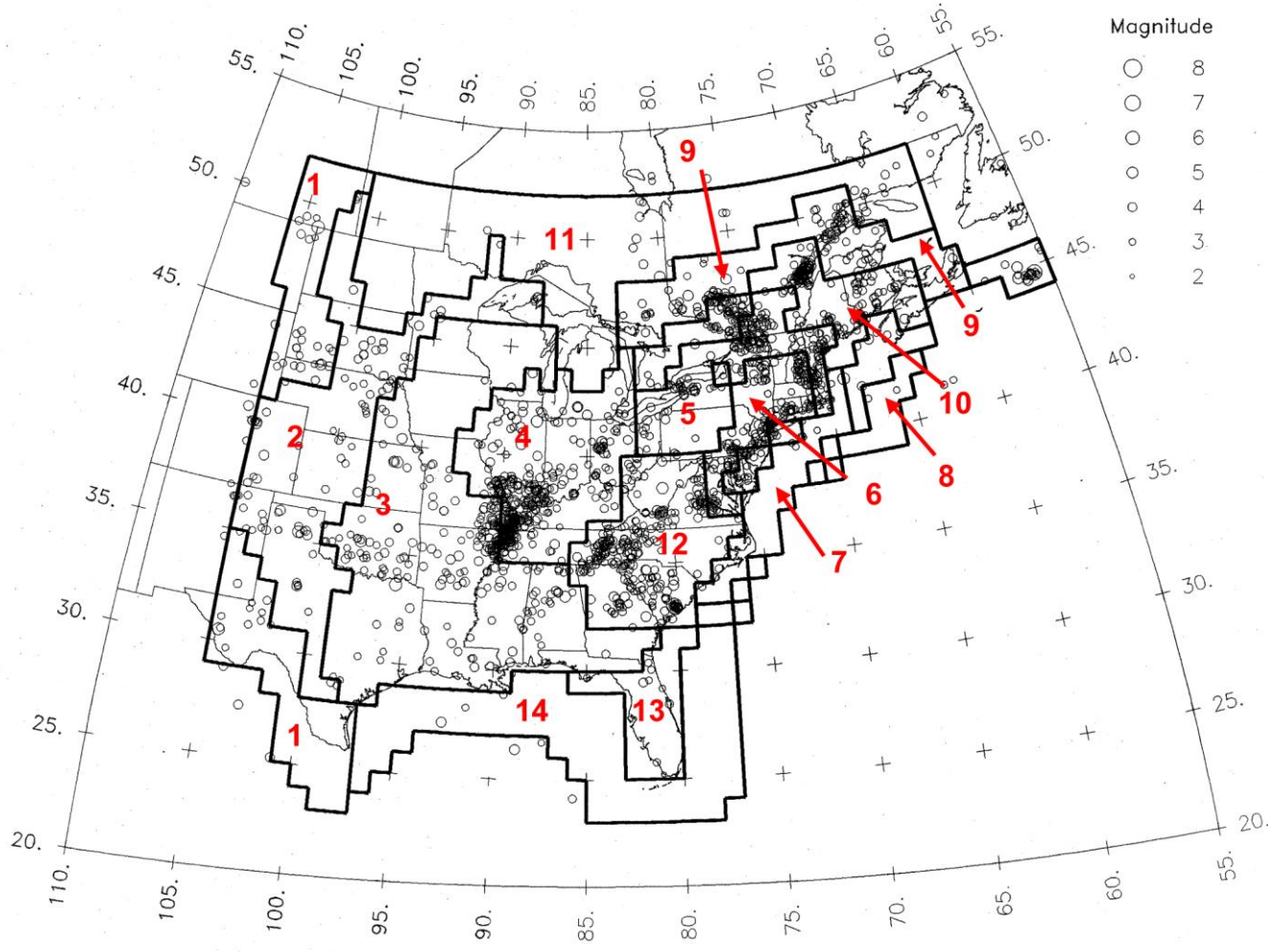


Figure 3.5-2
CEUS SSC Project earthquake catalog and modified catalog completeness regions

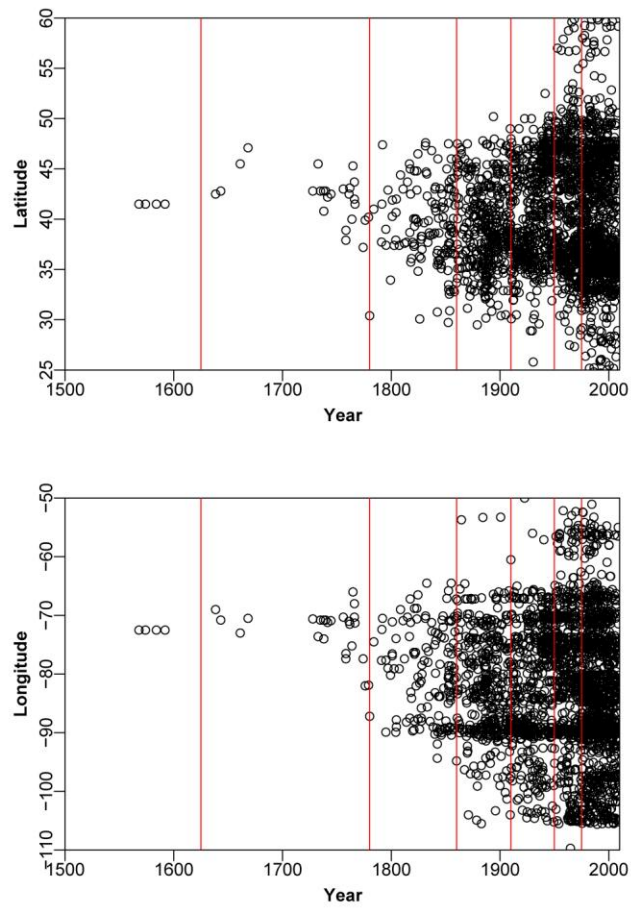


Figure 3.5-3
Plot of year versus location for the CEUS SSC Project earthquake catalog. Red lines indicate the boundaries of the catalog completeness time periods.

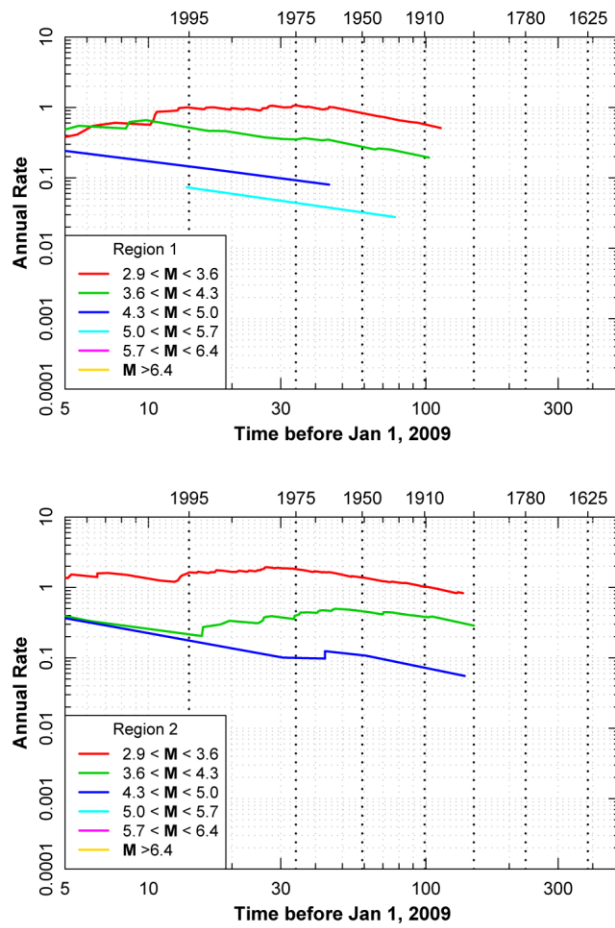


Figure 3.5-4 (1 of 7)
“Stepp” plots of earthquake recurrence rate as a function of time for the individual catalog completeness regions shown on Figure 3.5-2

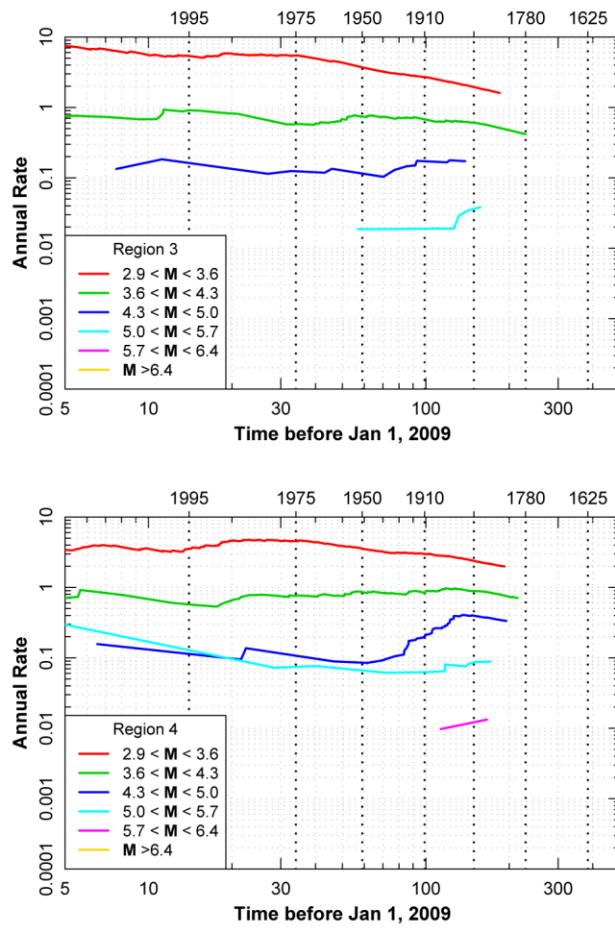


Figure 3.5-4 (2 of 7)
“Stepp” plots of earthquake recurrence rate as a function of time for the individual catalog completeness regions shown on Figure 3.5-2

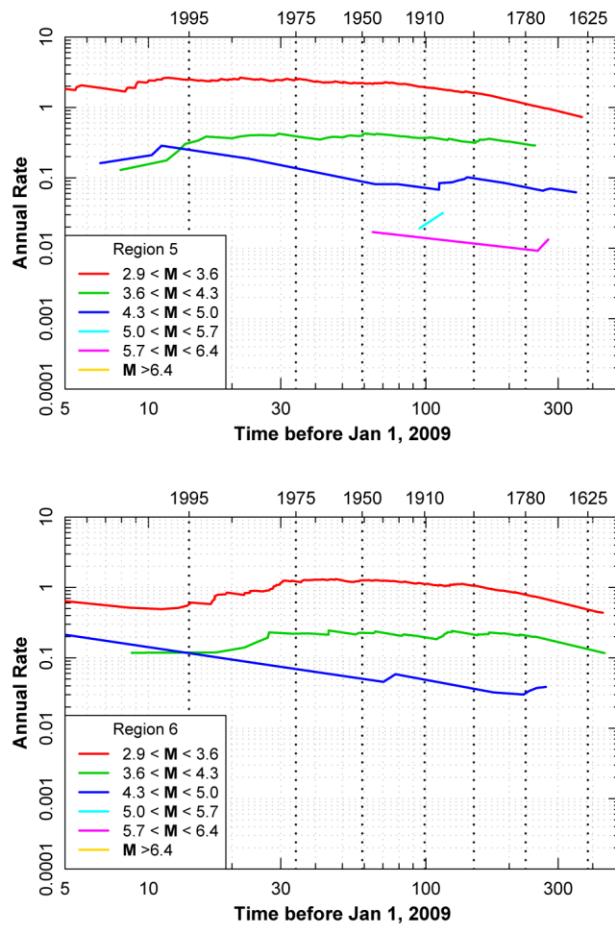


Figure 3.5-4 (3 of 7)
“Stepp” plots of earthquake recurrence rate as a function of time for the individual catalog completeness regions shown on Figure 3.5-2

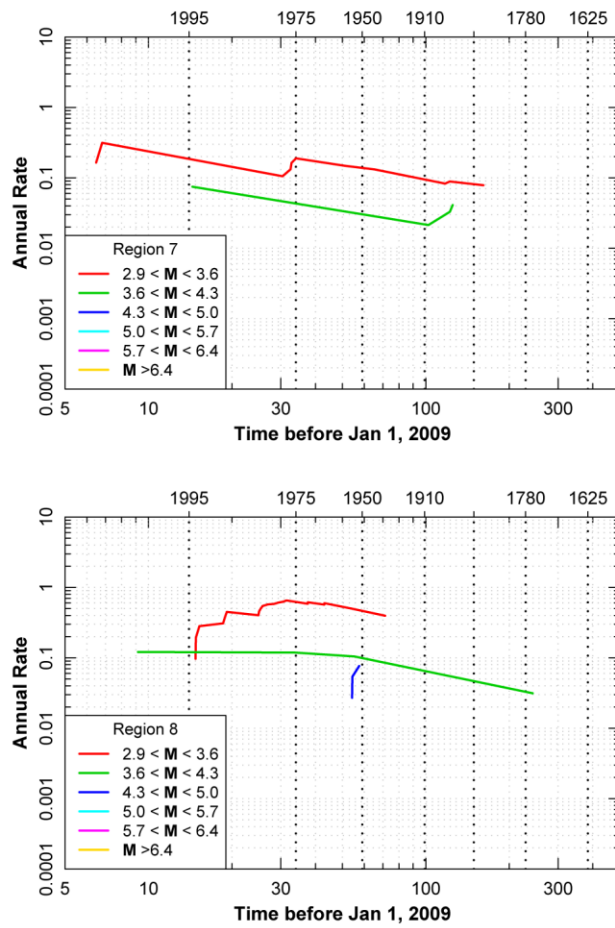


Figure 3.5-4 (4 of 7)
“Stepp” plots of earthquake recurrence rate as a function of time for the individual catalog completeness regions shown on Figure 3.5-2

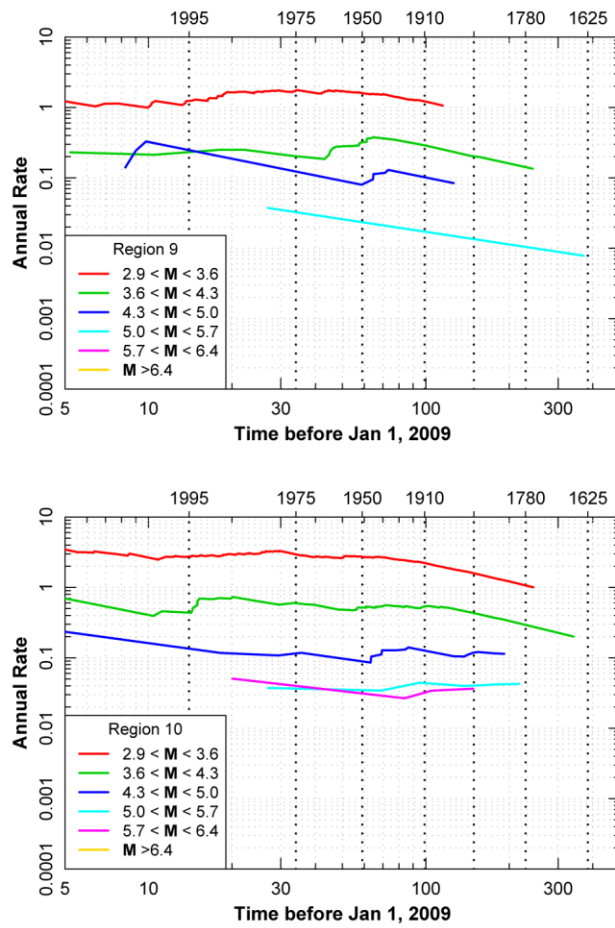


Figure 3.5-4 (5 of 7)
“Stepp” plots of earthquake recurrence rate as a function of time for the individual catalog completeness regions shown on Figure 3.5-2

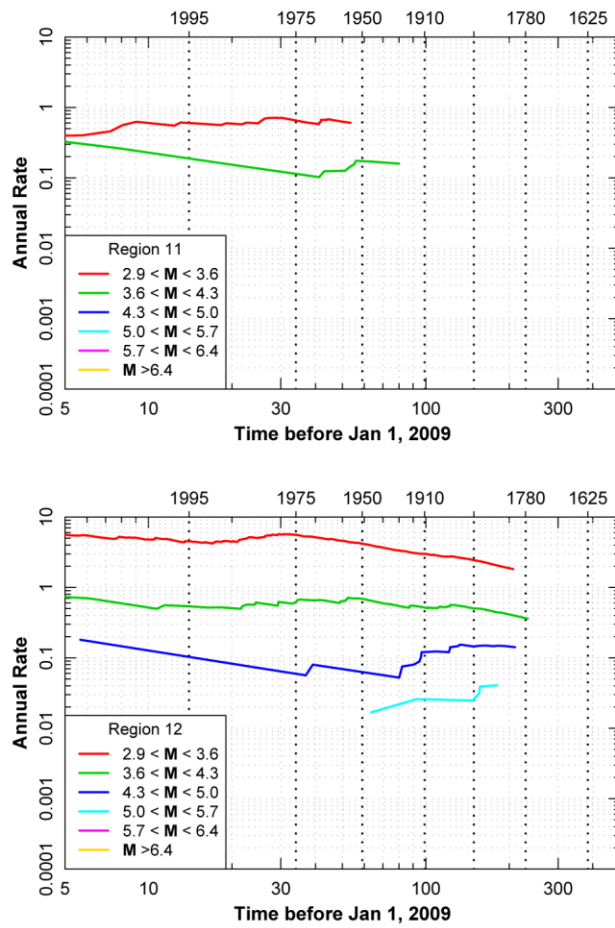


Figure 3.5-4 (6 of 7)
“Stepp” plots of earthquake recurrence rate as a function of time for the individual catalog completeness regions shown on Figure 3.5-2

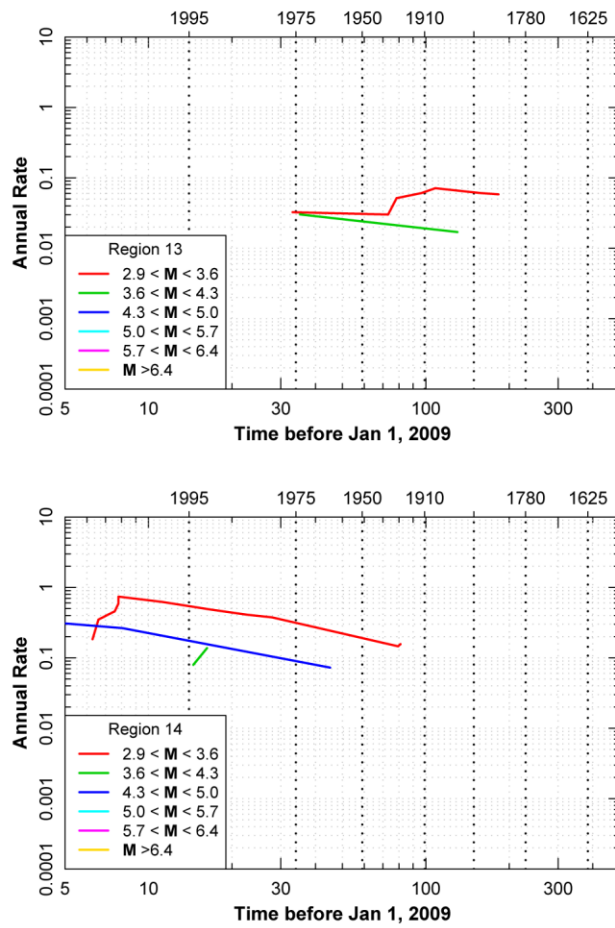


Figure 3.5-4 (7 of 7)
“Stepp” plots of earthquake recurrence rate as a function of time for the individual catalog completeness regions shown on Figure 3.5-2

4

CHAPTER 4 CONCEPTUAL SEISMIC SOURCE CHARACTERIZATION FRAMEWORK

The conceptual SSC framework described in this section was developed early in the project to provide the entire TI Team with a consistent approach and philosophy to the identification and characterization of seismic sources for use in future PSHAs. The description of the conceptual SSC framework is included in the project report to help the reader understand the basic underpinnings of the SSC model developed for the project, and to show how the framework led to the basic structure and elements of the master logic tree for the SSC model.

The TI Team, which consists of expert evaluators who are responsible for all the technical assessments, includes individuals and organizations with extensive experience in characterizing seismic sources in the CEUS for purposes of PSHA. The TI Team members have experience in PSHAs for nuclear facilities and a variety of other facilities throughout the region. This is a significant benefit to the project in that the team started with a high level of knowledge of the applicable databases for the evaluations, and of the various tools available to assist with the source characterization. Because of this knowledge and experience level, the TI Team was already familiar with the basic tools associated with SSC and uncertainty quantification (e.g., logic trees and probability distributions). So the conceptual SSC framework provided the TI team with the following guidance:

- Reminders of the advanced tools in the “SSC toolbox” for characterizing sources and quantifying uncertainties.
- A systematic approach to use in identifying and documenting applicable data and evaluations of the data relative to its use in SSC.
- Systematic identification and application of various tectonic and seismologic criteria for defining seismic sources that exist within the larger technical community.

The goal was to outline a logical, systematic, and complete framework for characterizing seismic sources within the context of a SSHAC process. To ensure consistency between this framework and the actual SSC effort, the framework was tied directly to the master logic tree of the SSC model.

Organized in this section are the concepts developed over the years for assessing seismic sources within stable continental regions (SCRs), including the CEUS. An early version of this section provided a useful tool to the team members during the course of their evaluations and to the peer reviewers, who sought to understand the framework within which the team worked. After the

actual SSC effort was completed, this section was refined to reflect the actual project implementation and it became a part of the project report documentation.

4.1 Needs for a Conceptual SSC Framework

In consideration of the purpose of the CEUS SSC Project, the TI Team identified three attributes that are needed for a conceptual SSC framework:

1. A systematic and documented approach to treating alternatives using logic trees, including alternative conceptual models for future spatial distributions of seismicity (e.g., stationarity), alternative methods for expressing the future temporal distribution of seismicity (e.g., renewal models, Poisson models), and alternative data sets for characterizing seismic sources (e.g., paleoseismic data, historical seismicity data).
2. A systematic and documented approach to identifying applicable data for the source characterization, evaluating the usefulness of the data, and documenting the consideration given to the data by the TI Team.
3. A methodology for identifying seismic sources that is based on defensible criteria for defining a seismic source, incorporates the lessons learned in SSC over the past two decades, and identifies the range of approaches and models that can be shown to be significant to hazard.

The need for an SSC framework that would fulfill these needs was encouraged by the PPRP early in the project, and the PPRP provided valuable feedback during the course of developing the framework. Each of these needs has been addressed in the development of the framework for the project, as discussed in Sections 4.1.1 through 4.1.3 below.

4.1.1 Logic Tree Approach to Representing Alternatives and Assessing Uncertainties

Over the past 25 years, it has become clear that a significant contribution to epistemic uncertainties in SSC comes from uncertainty in alternative conceptual models. Logic trees provide an effective means of clearly representing the credible alternative models and assigning weights to the alternatives. Logic trees were originally defined in a probabilistic framework for use in PSHA (e.g., Kulkarni et al., 1984) with a specification that the values on the branches of the tree be mutually exclusive and that all branches at a node of the tree be collectively exhaustive. Some have called this assumption into question in common applications, because it is often not possible to prove that *all* branches have been included or that they are *completely* mutually exclusive (Bommer and Scherbaum, 2008). Nevertheless, with these cautions in mind, logic trees provide a practical means of representing alternative hypotheses, expressing the relative weight for each hypothesis given the available data, and combining the hypotheses for use in the hazard analysis.

Logic trees have become common tools for application in SSC and specifically for the model-building or *integration* phase of a SSHAC project (Section 2.1), and the TI Team used them for expressing the epistemic uncertainties in alternative methods and approaches to characterizing

sources. For example, the first elements of the master logic tree (discussed in Section 4.2) define the basic alternative approaches to defining seismic sources as a function of the criteria used. Once these approaches are defined and the relative weight for each is assigned, the subsequent characterization will follow the approach defined for that branch. Thus the “logic” that comes into play in a logic tree is defining the dependencies among the assessments on the branches, and the outcomes that derive from each branch. Therefore, logic trees typically begin with general assessments (e.g., alternative conceptual models) and proceed to more specific assessments that are conditional on the general assessments. The assessments found to the right on the logic tree are commonly the specific elements and parameter values that are associated with a particular conceptual model. For example, an assessment of alternative temporal models (e.g., Poisson versus renewal) would be to the left on the logic tree, and each model would then be defined by nodes to the right that define the required parameters for each model (e.g., mean recurrence, elapsed time, coefficient of variation of recurrence intervals).

4.1.1.1 Examples of Logic Trees

Examples of logic trees used in actual projects are shown on Figures 4.1.1-1 and 4.1.1-2. The first figure comes from the PEGASOS project in Switzerland (NAGRA, 2004). The SSC team evaluated the potential that Permo-Carboniferous troughs within the Molasse basin of Switzerland might be seismogenic and localizers of moderate to large earthquakes. The first node of the logic tree identifies this evaluation and the relative probabilities assigned to the alternative hypotheses (reactivated or inactive). A second example logic tree is given on Figure 4.1.1-2, which comes from the probabilistic volcanic hazard analysis for Yucca Mountain (SNL, 2008). This tree begins with the assessment of the relevant volcanic events to be considered for the analysis, then proceeds to the alternative spatial and temporal models identified to define the future distribution of volcanic events. In this case, the weights assigned to the alternative branches are expressed as percentages, with the branches at a particular node summing to 100 percent. Regardless of the form—probabilities or percentages—the values on the branches are weights that represent an assessment of the relative credibility of the alternatives given on each branch.

4.1.1.2 Assigning Weights to Logic Tree Branches

In some cases, continuous parameter distributions can be accurately defined by a discrete set of logic tree branches and associated weights. However, in most cases in the CEUS SSC Project, the weights assigned to the branches are subjective and based on the TI Team’s assessment of the relative support for the alternative branches, given the available data. Although the final assignments of weights to logic tree branches are subjective, the weights represent assessments informed by the totality of the SSHAC evaluation process. Before weights were assigned, the TI Team heard from a properly wide range of resource and proponent experts, reviewed extensive technical information, created the Data Summary and Data Evaluation tables, and evaluated a wide range of issues with members of the knowledgeable broader technical community. In this way, the subjective weights are informed by the consideration of data, models, and methods in the *evaluation* phase of the SSHAC process.

Across all assessments in the SSC model, the total set of logic tree branches and weights represent the team's assessment of the center, body, and range of technically defensible interpretations (see Section 2.1 for a discussion of this concept). Those assessed alternatives that are judged not to be credible should not be included in a logic tree. In some cases, it was deemed helpful in the project documentation to identify those alternatives that have not been included, and the basis for not including them, but there is no requirement to include the global set of noncredible alternatives. An example of a noncredible alternative might be a model that has been proposed in the literature but whose application to a particular seismic source would violate the available data. A recurrence model that would overpredict the observed seismicity by orders of magnitude after accounting for uncertainties in catalog completeness is an example of an alternative that can be assigned zero weight and not be included in the logic tree. A discussion in the report that such a model was considered and rejected assists the reader in understanding the full range of considerations made by the evaluation team.

The weights applied to the branches of the logic trees reflect the TI Team's assessment that the particular branch is the *correct* branch. It is important to note that the TI Team spent considerable effort identifying alternative logic tree branches to be included that are significantly different from one another—from a hazard point of view. For example, at an early point in the project, alternative source geometries were postulated for the Charlevoix zone. However, the differences between the alternatives were minor for use in a regional seismic hazard model and so did not warrant incorporation into the source logic tree as two separate branches. Commonly, for purposes of PSHA, the branches are used to represent data, models, and methods that have some level of credibility as the correct parameter value, model, or method. It is the available data and information that provide the basis for the TI Team's assessment of the relative weights. If there is no basis in the available data for a preference from among the alternative branches, then the weights will be the same for all alternatives. For example, if the available data give equal support to two alternative positions of a seismotectonic zone boundary, then the alternatives are assessed equal weight.

For purposes of illustration, assuming there are two alternative branches in a logic tree, a higher weight is assessed for one of the alternatives if there is a technical basis in the available data to do so. Moving from weights of 0.6/0.4 (slight preference) to 0.9/0.1 (strong preference), the relative preference for the alternatives is becoming more pronounced, reflecting the stronger technical support for one of the alternatives. Although numbers (weights) are being used, these are treated as subjective probabilities and there is rarely a quantitative basis for assigning these weights. Exceptions on the CEUS SSC Project are the five-point distributions to represent quantified continuous distributions of selected parameters (for example, see the description of recurrence parameters for RLME sources in Section 5.3.3.1.3). The TI Team evaluated the alternatives using available data and information and made its best attempt to represent the present uncertainty. The Team reviewed the positions of various proponents of the alternatives, if those positions have been taken, and considered the degree of support the alternatives would have if members of the technical community were aware of all the project databases and had gone through the interactive SSHAC process of evaluating the alternatives. Ultimately, the key to the use of logic trees is clear documentation of the models/parameters that are given on the branches of the tree and justification for the weights assessed for the various branches. For

example, the seismic source characteristics for the seismotectonic zones are given in Section 7, along with a discussion of the technical bases for all assessments and weights on the logic tree.

4.1.2 Data Identification and Evaluation

Documentation of SSC requires that the data be identified that were considered and used in the analyses. The term “data” is used in a general sense to indicate all types of information that have potential use in defining and characterizing seismic sources for PSHA. By identifying the data, the reader will understand the technical bases for the assessments and, if some time has passed since the project was conducted, will have information about the data and references that were available and considered at the time of the project. Also, the documentation should preferably include an assessment of the quality of the data and the degree of reliance that was placed on various data sets.

Data identification and evaluation occur at the earliest part of a PSHA project and continue until the model-building or integration process is complete. A distinction is made between data *identification*, which is the process of becoming aware of and compiling available information having relevance to SSC, and data *evaluation*, which is the process of assessing the quality and applicability of the information to SSC. The process by which the data were identified and evaluated for the CEUS SSC Project is discussed in Sections 4.1.2.1 and 4.1.2.2.

4.1.2.1 “Generic” Data Identification to Address Indicators of a Seismic Source

For purposes of the CEUS SSC Project, the data identification process was informed by available guidance issued for this purpose, as well as by the experience of members of the TI Team in conducting SSC projects. Existing guidance documents provide recommendations as to the types of data that can be useful in defining seismic sources. For example, Table 4.1.2-1 is taken from the standard ANSI/ANS-2.27-2008, *Criteria for Investigations of Nuclear Facility Sites for Seismic Hazard Assessments*, and indicates the types of data that can be used to identify and characterize fault sources and areal source zones (American Nuclear Society, 2008a). Table 4.1.2-2 provides another example taken from the SSHAC guidance (Budnitz et al., 1997). It includes a further specification of data that can be used for various source types, as well as an evaluation of the relative usefulness of various types of data for identifying and characterizing seismic sources. These types of summaries are useful at the outset of an SSC project in focusing the database identification and compilation efforts toward the data that are likely to be useful in characterizing seismic sources for PSHA.

For the CEUS SSC Project, the data identification process is “generic” in the sense that it applies to the entire CEUS study region and not to any particular seismic source or subregion. Rather than tie the data to particular types of sources (e.g., faults, source zones), the types of data are identified that can be used to address a variety of “indicators” of a unique seismic source (Table 4.1.2-3). Table 4.1.2-3 documents the evaluation of the indicators of seismic sources and the relative usefulness of various types of data that can be used to address the indicators. This assessment is similar to that given in the examples in Tables 4.1.2-1 and 4.1.2-2, but provides

further evaluation of possible indicators of seismic sources and of the relative usefulness of various data in addressing those indicators.

The assessment of possible indicators of seismic sources and their relative value is necessarily subjective and reflects the TI Team's consideration of the current views of the SSC community. Also, the indicators are particularly pertinent to the CEUS, which is an SCR (Johnston et al., 1994) in which the causative faults giving rise to seismicity are generally not known. Therefore, unlike an assessment of indicators of seismic sources in an active plate boundary region, the indicators within the CEUS are more uncertain and vary from evidence of geologically young deformation, to observed zones of earthquakes, to other types of geologic and geophysical evidence. The types of data that are potentially useful in addressing these indicators also vary. The generic data identification in Table 4.1.2-3 is intended to associate the types of data that may be useful for SSC with potential indicators of seismic sources. In this way, as the knowledge of the technical community evolves regarding the most important indicators of seismic sources in the CEUS, the table can be updated to reflect that evolution. Also, if particular data types emerge in the technical community as being more diagnostic in defining seismic sources, those data types can be assigned higher weight in the table.

The various columns of Table 4.1.2-3 are defined and discussed below.

- The first column is a listing of possible indicators of a unique seismic source. If we assume that we start with a map of the entire CEUS, these are the indicators that could cause one to consider subdividing the region spatially to indicate a unique potential seismic source. Further, it is assumed for purposes of this table, which is a generic evaluation, that the indicator is known with certainty. In application to any particular region, there may be uncertainty as to whether the indicator exists.
- The second column is an evaluation by the TI Team of the relative usefulness of each of the indicators in identifying seismic sources. Note that the indicators and evaluation of their usefulness are snapshots of the knowledge at the time this table was made. It is expected that future scientific studies will provide additional insights into the causative factors related to CEUS seismicity. Accordingly, the relative usefulness of various indicators can be expected to change with time.
- The third column is a listing of the types of data that can be used to address the indicators. This list builds on previous efforts to identify the types of data that are potentially useful for characterizing seismic sources, including those shown in Tables 4.1.2-1 and 4.1.2-2.
- The fourth column provides an evaluation of the relative usefulness of each data type in addressing the indicators. Because the evaluation of usefulness is a function of both data type and quality of the data, it is assumed for this assessment that high-quality data are available. For example, consider the indicator "high strain rates." This indicator is assigned a relatively high level of usefulness (a score of 4) for identifying a seismic source. Two types of data are identified for addressing this indicator: (1) tectonic geodetic strain data and (2) geologic indicators of recent strain. In evaluating the relative usefulness of the two data types, it should be assumed that good-quality geodetic data as well as geologic data are available. Given this assumption, the geodetic data are assigned a moderately high usefulness (score of 4), and the recent geologic data are assigned a higher usefulness (score of 5) in addressing

the high-strain-rate indicator. This is because the geologic data would span a longer period than the geodetic strain indicators.

- The fifth column is an identification of the part of the SSC model that would be affected by the indicator. The aspects of the model are the spatial component, which describes the location and geometry of seismic sources, or the temporal component, which describes the recurrence rate and magnitude distribution. One or the other or both components may be affected.

The assessments given in Table 4.1.2-3 provided a basis for the TI Team to identify the applicable data that should be compiled for purposes of SSC. The weights assigned to potential indicators of seismic sources and to the usefulness of various data types were not used in a quantitative way in the project. Rather, they provide a basis for documenting the current thinking regarding the relative importance of potential indicators and the relative usefulness of various types of data to address the indicators. They also provided a means of prioritizing the data compilation efforts toward those data that have the highest potential usefulness in the SSC process. For example, paleoseismic indicators of $M > 5$ earthquakes are judged to be highly diagnostic indicators of seismic sources, whereas zones of weakness in the crust or mantle are given a relatively low weight as an indicator. Spatially concentrated earthquakes are given a high weight. Consistent with these assessments, the TI Team turned the focus of the project database toward the development of a new earthquake catalog and devoted a major effort to compiling paleoliquefaction data.

4.1.2.2 Data Evaluation for Particular Seismic Sources: Data Evaluation and Data Summary Tables

The second part of the data identification and evaluation process is the identification of specific data that were considered and used to characterize particular seismic sources, including RLME sources or seismotectonic zones. The purpose of this evaluation is to identify the data used, evaluate the quality of the data, and specify the degree of reliance on each data set in characterizing seismic sources. Data Evaluation tables were developed for this purpose (Table 4.1.2-4 is an example), and the tables for each source are included in Appendix C. The process also provides an opportunity to identify data sets that were considered in the evaluation even if they were not ultimately used to characterize seismic sources. Data Summary tables were developed for this purpose (Table 4.1.2-5 is an example), and those tables are included in Appendix D.

The Data Evaluation tables include the following attributes (see Table 4.1.2-4):

- The first column is a listing of the data, by data type, used in the evaluation for a particular RLME or seismotectonic source.
- The second column is an assessment of the quality of the data by the TI Team. This assessment is qualitative and takes into account the resolution, completeness, and distribution of the data relative to the best data of that type currently available. In some cases the assessment of the quality of a particular data set differs somewhat for different seismic

sources. This is a reflection of the perceived value of the particular data set toward addressing the SSC characteristics of each seismic source.

- The third column is used for notes about the data quality. This usually includes comments about whether the data have been published in abstract form or full papers and other issues regarding the defensibility of the data.
- The fourth column identifies the particular seismic source to which the data have been applied in the evaluation.
- The fifth and sixth columns provide an assessment of the degree of reliance on the data set for purposes of SSC, and a short description of how the data were relied on. The intent is to assist the reader in understanding how the data set was used and what the evaluation of the degree of reliance was based on.
- The seventh column indicates whether the data exists in GIS format within the project database. If the data are not in GIS format, they will be found in the database in other formats such as a PDF file.

Data Summary tables (example in Table 4.1.2-5) provide information on the various data that were considered during the course of the characterization of various seismic sources. The tables provide the citations to the data and a description of the key conclusions and their potential relevance to SSC. The goal is to provide the reader with the TI Team's view of the data set and how it might pertain to SSC. This can be particularly useful to other researchers—perhaps some years from now—in understanding what data sources were considered at the time of the CEUS SSC and how their relevance was assessed.

The Data Evaluation and Data Summary tables are not intended to replace the documentation of an SSC effort, but rather to supplement it. The discussions in a project report of the data used in the evaluation are not always comprehensive and it can be difficult to gain a clear understanding of exactly which data sets were considered, which were actually used in the evaluation, and the degree of reliance that was placed on them. Therefore, these tables were designed to make the data evaluation process more transparent and reasonably complete. It should be noted that these tables in particular—and the documentation in general—are a snapshot of a particular point in time. That is, the types of data available and their quality and utility are a function of our present understanding of SSC for PSHA. It is likely that in the future, additional data will become available that will prove useful for identifying or characterizing seismic sources.

Also, it is likely that the degree of reliance on any given data set will change in the future. For example, at the present time, GPS geodetic data are available for only a relatively limited part of the CEUS, and the period of observation is relatively short, such that errors in the data may exceed the signal. Moreover, it is not clear, given our present understanding of earthquake strain accumulation processes, exactly how geodetic strain rates provide direct constraints on seismic source characteristics. For example, the Independent Expert Panel on New Madrid Seismic Zone Earthquake Hazards (NEPEC, 2011) concluded that the observations of a lack of deformation based on the geodetic evidence were not sufficient to rule out the potential for future large earthquakes. Yet it is likely that uncertainties in the use of geodetic data will decrease with time and that this data set will become more valuable in the future for SSC. It is also possible that

entirely new types of data will become available in the future on which the SSC community will become increasingly reliant.

Although the CEUS SSC Project placed a premium on compiling a wide variety of databases and placing many of the databases on a common GIS platform to facilitate their use, not all of the data were used directly in the characterization of seismic sources. This is simply because some data and references have been superseded by later studies or some types of data are viewed as having only a limited usefulness in meeting the criteria for defining seismic sources.

Nevertheless, the documentation process followed in the data tables will allow the reader to understand which data were considered in the course of the evaluation process, as well as which data were relied on in the seismic source model.

4.1.3 Methodology for Identifying Seismic Sources

The methodology used in the CEUS SSC Project to identify seismic sources takes advantage of the experience gained over the past three decades in assessing SSCs for PSHAs. It incorporates the range of views in the scientific community regarding spatial stationarity of seismicity, and it is appropriate for a *regional* SSC assessment that can be applied on a consistent basis throughout the CEUS. A regional PSHA requires that the assessment include elements that are of sufficient specificity to include new thinking and contemporary data on seismic sources, yet is not reliant on site-specific information that cannot be applied systematically throughout the entire CEUS. Further, over time, new data are likely to be developed on a site-specific basis, thus calling for a stable regional model that can be refined for future new findings. For example, in recent years, paleoliquefaction data have been gathered and interpreted at particular locations, such as the New Madrid, Charleston, and Charlevoix seismic zones. For the vast majority of the CEUS, however, such features may not be present or data may not have been systematically gathered and evaluated; thus they are not available for incorporation into a hazard analysis. Accordingly, the SSC methodology advanced in this project can allow for the incorporation of such data in those cases where it is available, but given the incomplete distribution of the data across the region, the methodology should not assume or require that such data be available throughout the regional SSC model.

Workshop #2 on Alternative Interpretations provided an opportunity for the TI Team to discuss with members of the technical community several important issues with potential relevance to the identification of seismic sources. For example, paleoseismic indicators of possible RLME sources were discussed, including locations with strong evidence and those with equivocal evidence. In particular, considerable discussion in the workshop centered on the evidence for the location, size, and timing of earthquakes based on paleoliquefaction evidence. Given the potentially high significance of these types of data and their increasing credibility within the technical community as indicators of seismic sources, the project and the TI Team were encouraged by the PPRP to place high priority on the identification and evaluation of paleoliquefaction data and to complete the paleoliquefaction database that culminated in Appendix E to this report. Another issue discussed was the degree to which the spatial patterns of observed earthquakes provide an indication of future patterns. Proponents dealt with the issue of observed geodetic strain rates and their consistency with the presence or absence of sources of

large earthquakes identified by other means. Likewise, alternative possible tectonic explanations were proposed to explain concentrations of observed seismicity, with the potential implications of using those explanations to define seismic sources. All of these issues have potential implications for defining the criteria for source identification in a meaningful way. That is, the criteria must take into account the technical community's views of the important indicators of seismic sources and they must also be implementable across the study region given the available data.

It is assumed that the methodology outlined in this section will provide the *regional* component of the SSC, which is subject to refinement with the consideration of *site-specific* data and information. For example, the output from this project will be a reasonably complete specification of the knowledge and uncertainty regarding the spatial and temporal aspects of seismic sources on a consistent basis throughout the CEUS study region. It can therefore be exercised in a PSHA (which will include ground motion characterization) at any location in the study region. If the results are to be used for purposes of licensing at a particular nuclear facility location, regulatory guidance (e.g., NRC Regulatory Guide 1.208) requires that a site-specific database be developed. Similar guidance for other nuclear facilities requires the consideration of local and site-specific information (e.g., ANSI/ANS-2.27-2008, ANSI/ANS-2.29-2008). Once it is developed, the applicant will need to evaluate whether the site-specific database includes information pertinent to SSC and, if it does, then the site-specific information will need to be incorporated into the CEUS SSC source model. Alternatively, the applicant might consider the hazard significance of the site-specific information and determine that it would not require a refinement to the CEUS SSC model (see Section 9.4.3 for a discussion of hazard significance).

The concept of a “regional” SSC model is easily understood, as is the type of “site-specific” information that is commonly developed to support a regulatory license application under current regulatory guidance. However, the TI Team has considered whether further specification can be made of what is considered “regional” and what is considered “site-specific.” In other words, is there a “scale cutoff” below which one would consider the data too local to be systematically characterized throughout the entire study region? Clearly, local tectonic features that lie entirely within the 8 km (5 mi.) radius site area, and likely the 40 km (25 mi.) radius site vicinity, as defined in NRC Regulatory Guide 1.208, would be too site-specific to be included on a systematic basis in the CEUS SSC source model. Unless special studies have been carried out that demonstrate the existence of tectonic features having a significant seismogenic potential, the consideration and potential incorporation of specific tectonic features would be part of the refinement of the CEUS SSC model for site-specific application. Thus the TI team is unable to specify a quantitative cutoff dividing regional from site-specific.

A more reasonable criterion that was applied in the CEUS SSC Project is the following: the CEUS SSC model provides the regional characterization of sources on a consistent basis throughout the study region, including those special areas that have been the subject of considerable scrutiny in the past. Consideration of site-specific refinement of the CEUS SSC model would be required by current regulatory guidance and would occur only if such refinement would lead to significant differences in hazard.

4.1.3.1 Hazard-Informed Approach

Numerous PSHAs have been conducted within the CEUS and other SCRs over the past three decades. The experience gained over that time was used in defining the framework for identifying and characterizing seismic sources. The knowledge gained on the important SSC issues will likely contribute to the hazard results at annual frequencies of exceedance important to nuclear facilities. Likewise, the most important contributors to uncertainty can be anticipated. It is also possible to anticipate those technical issues that will have lesser or no significance to the hazard results.

For example, SSC studies conducted in the 1980s, such as the EPRI-SOG project, focused on the issue of evaluating the probability for particular tectonic features to localize moderate to large ($M \geq 5$) earthquakes within the contemporary tectonic regime. The evaluation of this probability of activity, P_a , was viewed as a fundamental part of the SSC process. Included in the evaluation were hypotheses related to the causative mechanisms of CEUS seismicity, the nature of the contemporary stress regime, and various data indicators that would provide insights into whether a tectonic feature—or class of features—might be seismogenic. These 1980s assessments provided valuable insights into the then-current state of knowledge and uncertainty about the causes of CEUS earthquakes. We can take advantage of these insights in outlining our SSC approach some 25 years later.

One of the insights gained from experience on several PSHAs is that observed seismicity is perceived by the larger technical community as providing a fundamental constraint on estimates of the future spatial and temporal distribution of moderate to large earthquakes. This is despite the heavy emphasis placed on studies like the EPRI-SOG project on tectonic features and their potential to be seismogenic. Examples of the reliance on observed seismicity in these studies can be found in several source types. Within the more active zones, such as New Madrid, the seismicity data were used to define the spatial location of the seismic sources as well as the recurrence rates for the sources. Away from the more active zones, background zones were identified whose probability of activity was typically 1.0 and whose recurrence rate was defined by the diffuse seismicity within the zone. Seismicity within large background seismic source zones was also used to “smooth” recurrence parameters (a - and b -values), providing for spatial variations based on seismicity.

The assessment of maximum earthquake magnitudes for seismic sources within the CEUS is typically not constrained by physical characteristics of the source itself (e.g., fault rupture length); instead, it is estimated considering the largest earthquakes within the seismic source as well as analogues to other sources that are tectonically similar. Even in those cases where tectonic features were identified as candidates for localizing future $M \geq 5$ earthquakes, the most diagnostic criterion for evaluating seismogenic potential was the spatial association of the feature with observed seismicity. Those tectonic features that were assessed to have a low probability of being spatially associated with seismicity (often due to low numbers of observed earthquakes) were assigned a low probability of being seismogenic, P_a , regardless of any existing evidence. In nearly all cases, conclusive geologic evidence for recent fault displacement—which would be a diagnostic criterion if it did exist—simply was not identified in the available data. As a result, in

nearly all cases, the hazard significance of individual tectonic features was assessed to be very low to negligible.

We conclude from this experience that the characteristics of the observed seismicity record—both the spatial and temporal distribution of earthquakes—are important constraints and have high hazard significance. Therefore, the SSC methodology advanced in the CEUS SSC Project appropriately places heavy emphasis on the systematic and consistent development of seismicity databases and on approaches to their use in defining and characterizing seismic sources.

Conversely, less emphasis is placed on identifying and evaluating tectonic features that are not clearly associated with observed seismicity or that do not show geologic evidence of recent activity within the present tectonic regime.

This should not be interpreted as suggesting that the earthquake community has discarded the search for associations between earthquakes and tectonic features within SCRs, or that observed seismicity provides an unequivocal description of future earthquakes. Earthquake research within SCRs continues to hypothesize a variety of possible mechanisms for the observed seismicity; spatial associations with deep crustal or mantle anomalies are such candidates. Rather, it reminds us that the purpose of the CEUS SSC Project is to develop a seismic source model to be used in a seismic hazard analysis, and not to answer research questions about SCR earthquake causative mechanisms. Postulated spatially and/or temporally clustered/episodic behavior of large-magnitude earthquakes at New Madrid is an example of a hypothesis that has potentially significant hazard implications and that is addressed directly in the seismic source model.

An additional insight gained during the past 20 years, due largely to a number of geologic studies conducted over that period, is that paleoseismicity is important and its potential for hazard assessment is very significant. Beyond the observed historical and instrumental seismicity record, no single data set has had a more profound influence on matters of maximum size of SCR earthquakes, their spatial distribution over periods much longer than the historical record, and the rates and behavior of currently active seismic sources. With very few notable exceptions, such as the Meers fault, the paleoseismicity evidence has been based entirely on shaking effects rather than observed displacements along the causative fault. For this reason, the causative structures giving rise to the paleoearthquakes remain elusive in most cases. Likewise, significant uncertainties exist regarding the locations, magnitudes, and recurrence of the earthquakes based on the geologic record. Nevertheless, the existence of the paleoearthquakes is in most cases undeniable and, because of their potentially high hazard significance and the technical community's general support, they must be incorporated explicitly into the seismic source model. Because the causative faults for these earthquakes are not known, the paleoearthquakes can be viewed as simply an extension of the observed seismicity catalog back in time. Of course, in doing so, care must be taken to properly evaluate the interpretation of paleoseismic evidence and assess the uncertainties in the size and timing of the earthquakes.

To further identify and understand the issues of most hazard significance, seismic hazard calculations were conducted using the SSC sensitivity model prior to Workshop #3 for a series of sensitivity cases. The issues identified as having the most hazard significance were as follows:

- Large-magnitude sources (e.g., New Madrid, Charleston, Charlevoix)

- Magnitude of the “characteristic” (repeated large-magnitude) earthquake
- Recurrence rate
- Location of the source
- Moderate-magnitude sources (e.g., Eastern Tennessee seismic zone, Central Virginia seismic zone, Wabash Valley)
 - Source geometries
 - Maximum earthquake magnitude
 - Recurrence rate
 - Smoothing (i.e., whether seismicity is distributed uniformly within the zone or smoothed locally)
- Background zones
 - Maximum earthquake magnitude
 - Smoothing
 - Probability of activity (i.e., whether the zone has a P_a less than 1.0)

These findings reinforce the importance of focusing on the locales that have hosted moderate- to large-magnitude earthquakes in the observed seismic record, and of using that record, along with other indicators such as paleoseismic information, to define the location/geometry, maximum size, and recurrence rates. Away from those locales, issues related to the seismogenic potential of the background regions were found to be important if the P_a was judged to be less than 1.0; that is, if there was some finite probability that the region was not capable of generating a $M \geq 5$ earthquake. However, with time and continued study of SCRs around the world, there is increasing consensus that *any* region within an SCR is capable of generating earthquakes of those magnitudes. Further, the uncertainties in this assessment can be readily addressed in the assessment of M_{max} for the zones. Therefore, the P_a issue for background zones has much less hazard significance.

4.1.3.2 Conclusions Regarding the Hazard Significance of Various SSC Issues

Based on the experience of multiple PSHAs in the CEUS since the time that major studies were conducted in the 1980s, as well as sensitivity studies conducted for the CEUS SSC Project, the following conclusions can be drawn regarding the most important SSC issues and their implications in developing an SSC methodology.

- Despite continued study, the causative structures (faults) for the observed moderate- to large-magnitude earthquakes in the CEUS remain unknown, with very few exceptions. Thus a seismic source model comparable to those developed in the WUS (e.g., faults with background zones) is not possible.
- The observed record of seismicity, despite uncertainties in the locations and magnitudes of earthquakes, and the completeness of the record, is the fundamental means of assessing the future locations, sizes, and rates of earthquakes needed for a PSHA. Our tools for quantifying

the uncertainties in the record have become better developed, as have our tools for using the record (e.g., spatial smoothing).

- Evaluations of potential causative tectonic features, which include hypotheses about crustal loading mechanisms due to deeper mantle processes, remain an active area of seismologic research. But experience has shown that only those tectonic features/hypotheses having a significant probability of being seismogenic (P_a greater than about 0.5) will have hazard significance. Therefore, the evaluation of tectonic features/hypotheses with low P_a can only be represented in the regional characterization of seismotectonic source zones. Any consideration of local tectonic features would be part of a site-specific refinement to the regional SSC model.
- Geologic observations of paleoearthquakes are now largely accepted within the technical community and can be viewed as an extension of the observed seismicity record back in time. Further, these earthquakes have been shown to have a profound effect on hazard estimates for many sites within the CEUS. Therefore, they must be included explicitly in the seismic source model for the CEUS. However, the uncertainties in the location, magnitude, and recurrence of these earthquakes are evaluated differently from those of the historical and instrumental seismicity record. As a result, the CEUS SSC model should provide for paleoseismic earthquakes explicitly, but should also provide for addressing their uncertainties in a manner different from the rest of the observed seismicity catalog.
- The logic structure for the SSC model, represented by a master logic tree, should provide alternative approaches and conceptual models for our current understanding of the constraints on the location, size, and recurrence of future earthquakes. For clarity and efficiency, the logic tree should start with the most basic descriptions of seismic sources and should gain complexity only as needed to represent specific hypotheses and data sets that have hazard significance. In this way, unnecessarily complex source models will be avoided, such as those that depict a large number of tectonic features, none of which have a significant probability of being seismogenic.

4.1.3.3 Criteria for Defining Seismic Sources

Embarking on the development of a new SSC for the CEUS demanded that attention be given to the experience gained from similar efforts over the past few decades, in terms of both the development of new data and tools and the experience with issues of most significance to hazard at annual frequencies of interest for nuclear power plants. On the one hand, geologic and geophysical studies of the crust since the 1980s have provided little new information about tectonic features and the geologic history of the region that may have a bearing on evaluation of seismic hazards; a possible exception, however, is the improved understanding of the Illinois Basin Extended Basement and its features. On the other hand, paleoliquefaction studies have been useful in defining and characterizing seismic source zones.

The methodology needed to be consistent with the seismotectonic setting of the CEUS and our current knowledge base for assessing the locations, sizes, and rates of *future* earthquakes. For example, we currently lack a clear definition of the causative faults giving rise to the observed seismicity, so applying a methodology that relies on knowledge of fault location and behavior

would not be appropriate. Similarly, geodynamic data on contemporary crustal strain are currently limited in their duration and spatial extent; in addition, available physical models are unable to make a unique association between geodetic strain and earthquake processes (NEPEC, 2011). Therefore, although such data may be useful in assisting with the evaluation of seismic source characteristics, the methodology should not rely on knowledge of the relationship between short-term crustal strain data and future earthquake characteristics.

Various authors over time have defined seismic sources for purposes of PSHA in different ways. For example:

- “Sources are explicitly defined as being of uniform earthquake potential; that is, the chance of an earthquake of a given size is the same throughout the source.” (Reiter, 1990)
- “[A seismic source is] a region of the earth’s crust that is assumed for PSHA to have relatively uniform seismic source characteristics.” (Budnitz et al., 1997)
- “A seismic source is a volume of the earth’s crust that has the same earthquake potential as defined by the size of events that may be generated.” (BC Hydro, 2008)

A common theme in these definitions is a degree of “uniform” earthquake potential or characteristics, although exactly what this means is not clear or varies with the application. Early in the history of PSHA, the M_{max} (and associated uncertainty) and recurrence rates (expressed as a - and b -values) within identified seismic sources were assumed to be “uniform.” “Uniform” in this case meant the same throughout the source without spatial variation. Since then, a number of approaches have been developed to express the spatial variation of recurrence parameters. For example, the EPRI-SOG project provided for spatial variation of a - and b -values at the scale of one-degree cells (~100 km [~62 mi.] dimensions), and the USGS national hazard maps utilize a Gaussian smoothing kernel to express spatial variations in a -values. Thus far, the spatial variation in M_{max} has only been expressed by the identification of separate sources (including fault sources within areal source zones), and a strong technical basis for spatial variations of M_{max} within source zones has not been established.

Given the evolution of approaches to identifying seismic sources, it is appropriate to provide a set of criteria and the logic for their application in the CEUS SSC Project. In the project, unique seismic sources are defined to account for distinct differences in the following criteria:

- Earthquake recurrence rate
- Maximum earthquake magnitude (M_{max})
- Expected future earthquake characteristics (e.g., style of faulting, rupture orientation, depth distribution)
- Probability of activity of tectonic feature(s)

Rather than treat these criteria as operating simultaneously or without priority, the CEUS SSC methodology works through them sequentially. Their sequence represents their relative significance to seismic hazard results, with earthquake recurrence rate being most important and the probability of activity having lesser impact on calculated hazard results. Further, because each criterion adds complexity to the seismic source model, it is applied only if its application

would lead to hazard-significant changes in the model. In this way, the model becomes only as complex as required by the available data and information.

Examples will assist in illustrating the notion of progressively applying the seismic source criteria. To begin, consider the entire CEUS study region and the first criterion of differences in earthquake recurrence rate. In general, the record of past earthquakes is obtained from the historical/instrumental catalog and from the paleoseismic record of prehistoric earthquakes. For the CEUS SSC Project, RLME sources are the locations of repeated (more than one) large-magnitude ($M \geq 6.5$) earthquakes, and paleoseismic evidence is used to define the source's recurrence rate (see Section 4.4.1.1 for further discussion of RLME sources). This is an example of identifying distinct seismic sources based on differences in recurrence.

Spatial smoothing of the recurrence rate (a - and b -values) based on observed seismicity accounts for the spatial variation in rate. The approach used in the CEUS SSC is a refinement of that used in the EPRI-SOG project. Conceptually, the smoothed seismicity model is the least complex seismic source representation. Embedded within the concept of spatial smoothing is the notion of spatial stationarity; that is, the pattern of past earthquakes is a predictor of the pattern of future earthquakes. Studies of seismicity in the CEUS have concluded that this is a reasonable interpretation (Kafka, 2007, 2009). Further, because the historical record of observed earthquakes is relatively short (about 200 years in most of the CEUS) relative to the recurrence intervals for large-magnitude earthquakes, there is an assumption that the spatial distribution of observed smaller-magnitude earthquakes constrains the spatial distribution of larger-magnitude earthquakes. The use of spatial smoothing to represent earthquake recurrence, together with RLME sources, means that there may not be a need to identify seismic source boundaries within a region due to recurrence differences.

After spatial variations in rate have been established using smoothing, then the CEUS can be subdivided to account for differences in M_{max} . Current approaches to assessing M_{max} within SCRs such as the CEUS are based on analogies to domains having similar tectonic characteristics. The EPRI M_{max} project (Johnston et al., 1994) presented a Bayesian approach to assessing M_{max} that establishes *prior* distributions of M_{max} for two domains: extended crust (defined as having undergone major extension in Paleozoic and younger time) and non-extended crust. These prior distributions are modified by a likelihood function that reflects the earthquake counts within a seismic source and is truncated at the low-magnitude end by the largest observed earthquake within the source of interest. The SCR database and analysis of the data given in Johnston et al. (1994) were updated as part of the CEUS SSC Project (see the discussion in Section 5.2.1.1).

The results of the data reanalysis suggest that there is only a weak statistical basis for separation of the SCR data to establish a prior distribution on M_{max} . As a result, the CEUS SSC model invokes either a single prior distribution that is applicable to the entire CEUS SSC study region, or two prior distributions: one that is based on Mesozoic-and-younger extension and one that is based on non-extended regions or older extended regions. In the latter case, a seismic source boundary is drawn (including uncertainty) to separate the regions of Mesozoic-and-younger extension from the remainder of the study area. This is an example of a seismic source being defined on the basis of M_{max} differences.

From variations in recurrence and M_{max} , the next criterion for subdividing the CEUS is expected significant differences in future earthquake characteristics, such as their depth distribution, style of faulting, and expected orientation of earthquake ruptures (strike and dip). In seismic hazard models, future earthquakes are modeled as having finite dimension, magnitude-dependent rupture dimensions, orientations, and depth extent. This is because these characteristics are important to modern ground-motion prediction equations, including those that will be developed for the CEUS region as part of the ongoing Next Generation Attenuation East (NGA-East) project (PEER, 2010). To accommodate these assessments, the CEUS study region was subdivided into seismotectonic zones having comparable characteristics. These subdivisions may also have implications for M_{max} assessments in that the likelihood function varies with the size of the largest observed earthquake for the source of interest. Within these subdivisions, spatial smoothing of seismicity is carried out to express the variation of recurrence rate spatially.

A final assessment that can be considered is the identification of particular tectonic features that have significant potential to localize seismicity; that is, they are assessed to have a P_a that is greater than about 0.5. These might be associated with a paleoearthquake, smaller-magnitude earthquakes, or they might have geologic indicators of activity. In the cases where potentially seismogenic tectonic features are identified, it is necessary to consider the relationship between the feature and the local background within which the feature lies. For example, if the feature has a P_a less than 1.0, then there is a finite probability ($1-P_a$) that the feature is not seismogenic and does not localize seismicity. In that case, the background zone would need to be identified. Likewise, in the case where the feature is judged to be seismogenic, the earthquakes that should be assumed to be associated with the feature need to be identified so that recurrence rate for the feature and the background zone can be calculated. The CEUS SSC Project identified very few local tectonic features with clear and compelling reported evidence of activity and these are the RLME fault sources (e.g., the Meers fault and Cheraw fault). However, because the CEUS SSC model is a regional model, any site-specific use of the model will need to consider whether any local evidence for tectonic feature activity might exist and, if so, refine the model locally.

The basis for the assessment of the recency of fault displacement and the potential for Quaternary activity is the comprehensive study conducted by Crone and Wheeler (2000), who place each feature into Classes A through D depending on what is known about the feature's geologic evidence for Quaternary activity. The inclusion of faults that only have a high probability of activity in the CEUS SSC model does not preclude, however, the need to consider local site-specific data and evidence for the potential activity of tectonic features on a local scale. It is anticipated that the required site-specific data collection studies for a nuclear facility will provide the basis for identifying potential local seismic sources and, if necessary, local refinements to the CEUS SSC model.

The application of the criteria for identifying seismic sources results in the suite of seismic sources given in the CEUS SSC model. A summary of the criteria that resulted in the identification of each of the seismic sources is given in Table 4.1.3-1. A detailed description of the application of the criteria to each source is given in the "Basis for Defining Seismotectonic Zone" sections in Chapter 7 (e.g., Sections 7.3.6.2 and 7.3.7.2). In addition, the bases for defining the RLME sources and the M_{max} zones are given in applicable sections of Chapter 6 (e.g., Section 6.2.1). In those cases where alternative source geometries are included in the SSC

model, a discussion of the alternatives and the basis for the weights assigned to each alternative are also given in the applicable sections of Chapters 6 and 7.

To represent the uncertainties in the seismic source identification process, both a master logic tree and individual seismic source logic trees were constructed. These are discussed below.

4.2 Master Logic Tree

The master logic tree establishes the framework for the entire seismic source model. It identifies the alternative approaches and conceptual models that will be used and establishes the relative weights assigned to the main alternatives. By laying out the alternatives at the start, the subsequent detailed source evaluations will each be conducted within a framework that ensures consistency across all sources. Likewise, the sum total of the source evaluations will be logically combined in such a way as to avoid double-counting and provide for meaningful weighted combinations. In this section, the discussion of the master logic tree is followed by a description of the major elements of the logic trees that describe the various seismic sources. The detailed discussions of the individual seismic sources and the characterizations in their logic trees are given in Sections 6 and 7 of this report.

4.2.1 Description of Logic Tree Elements

Using the criteria given in Section 4.1.3.3 and the associated conceptual basis, a master logic tree was developed that provides a framework for all of the seismic source evaluations in the CEUS SSC (Figure 4.2.1-1). The basic structure of the logic tree has been developed to include the simplest representation of seismic sources (smoothing of observed seismicity with subdivisions of the CEUS related to recurrence and Mmax) as well as more complex subdivisions to account for differences in the characteristics of future earthquakes. Accordingly, the first-order branches of the tree address the basic conceptual models related to the approaches; these are followed by branches that represent the uncertainties in the implementation of each approach.

The first assessment on the master logic tree (Figure 4.2.1-1), represented by the first node, is the choice between two conceptual models used to assess the spatial and temporal distribution of future seismicity. The application of the seismic source criteria given in Section 4.1.3.3 leads to the identification of RLME sources based on differences in earthquake recurrence (from paleoseismic evidence) from the “background” zones within which they lie. RLME sources are identified based on well-defined evidence for Late Quaternary or Holocene RLMEs. Thus the RLME sources are present for all seismic source interpretations.

The “Mmax zones” model involves identifying alternative configurations based on differences in the prior distribution of Mmax using the Bayesian Mmax approach (see Section 5.2.1.1). Accordingly, the CEUS SSC study region is either subdivided according to evidence of Mesozoic and younger extension (with associated uncertainties in the location of the boundary) or not subdivided. In this model, the spatial variation of recurrence parameters is based on spatial smoothing of observed earthquakes. The “seismotectonic zones” model also includes the concept of subdividing the region according to differences in the prior Mmax distributions, and identifies

seismic sources based on spatial variations in the characteristics of future earthquakes (the third criterion identified in Section 4.1.3.3).

In addition to the RLME sources, the region is divided into seismotectonic zones that provide for differences in expected future earthquake characteristics. For example, differences in the style of faulting, strike of ruptures, and depth distribution of future earthquakes can be accommodated in the “seismotectonic zones” model. The model also accommodates any differences in M_{max} among the seismotectonic zones due to differences in the size of the largest observed earthquakes; Sections 5.2.1.1 and 5.2.1.2 describe the influence of the largest observed earthquakes on the M_{max} estimates.

The weights assigned to the “ M_{max} zones” and “seismotectonic zones” branches reflect the relative preference for the alternative approaches for characterizing the future spatial and temporal distribution of earthquakes and their characteristics, given the available data for the CEUS. The two models are quite similar in many respects. They both include RLME sources as independent sources defined by paleoseismic evidence for the size and recurrence rate for the RLME earthquakes. Moreover, both allow spatial variation of recurrence parameters by smoothing within seismic source zones (see Section 5.3.2 for a discussion of spatial smoothing). The key difference between the two models is in their ability to include and represent information related to the characteristics of future earthquakes. The “ M_{max} zones” model is based on average or “default” characteristics that are representative of the the entire study region (Table 5.4-1), whereas the “seismotectonic zones” model can include information that allows for an assessment of spatial variations of future earthquake characteristics at a scale that is appropriate to a regional SSC model (see Table 5.4-2 for the characteristics of each seismotectonic zone). A higher weight (0.6) is assigned to the seismotectonic zones branch than to the M_{max} zones branch (0.4) because the seismotectonic zones approach allows for more relevant information on the characteristics of future earthquakes to be included in the model. While many of the characteristics of the seismotectonic zones are uncertain, such as the locations of the source boundaries and the characteristics of future earthquake ruptures, they are still judged to provide a better description of the applicable source characteristics.

Early in the project, as part of the SSC sensitivity model, a third conceptual model was considered that would be even simpler conceptually than the M_{max} zones model. This model was called the “zoneless” model and it postulated that *all* earthquakes—both those defined from the historical record and those defined from paleoseismic evidence—would be subject to spatial smoothing. As such, the model would not need to invoke any source zone boundaries, including those that identify RLME sources. With further consideration, however, it was found that the model cannot be applied with confidence given our present knowledge. This is because the spatial smoothing approach is actually smoothing the recurrence parameters a and b , which require that the record be complete over a given time interval. Completeness adjustments can readily be made for the historical record, but there is not sufficient information in the paleoseismic record to make the same type of completeness adjustments. The current spatial distribution of paleoseismic investigations is decidedly non-uniform. Some areas have been investigated in detail, and estimates of the completeness of the record locally are possible, but other areas have not been subject to searches for paleoseismic evidence at all. Until systematic searches for paleoseismic evidence are conducted such that the completeness of the record can be

assessed and corrected for, it is not possible to exercise the “zoneless” model, and it has been dropped from the CEUS SSC model. It is mentioned here, however, in anticipation that future work will allow its incorporation into SSC models.

Given either the Mmax zones or seismotectonic zones branches of the master logic tree, certain source characteristics are defined in the subsequent parts of the logic tree. A detailed discussion is given in Section 5 of the various approaches used in the CEUS SSC Project to characterize the Mmax (Section 5.2), earthquake recurrence (Section 5.3), and future earthquake characteristics (Section 5.4). Here we present the major elements of the master logic tree and discuss why they are included. The discussion in this section also includes the relative weights assigned to assessments that are not source-specific. The source-specific assessments for RLME sources are given in Section 6.1, for Mmax zones in Section 6.2, and for seismotectonic zones in Section 7.3.

4.2.2 RLME Source Logic Tree

RLME sources are identified and characterized in either the Mmax zones or the seismotectonic zones branches. The logic tree that describes the RLME source characteristics is given on Figure 4.2.2-1, which shows an example tree for the Marianna RLME source. Figure 4.2.2-2 identifies the RLME sources, which are listed in Table 4.2.2-1. In this section of the report, the characteristics are described generically without reference to any particular RLME source. Individual RLME source characteristics are described in Section 6.1.

The first node of the logic tree for RLME sources (Figure 4.2.2-1) deals with the issue of temporal clustering of large-magnitude earthquakes. Many seismic sources, especially those within SCRs, display evidence of clustering through time such that the recurrence rates may be elevated for several seismic cycles during a cluster, followed by much longer time intervals. This behavior can be modeled by identifying two rates: the within-cluster rate and the out-of-cluster rate. The SSC model resulting from the CEUS SSC Project will be useful for engineering applications that will entail up to approximately the next 50 years;¹ for this reason, it is important to assess whether the source is currently (i.e., over approximately the next 50 years) within or out of a cluster such that the within-cluster or out-of-cluster rate is applicable. This is the first assessment in the RLME source logic tree.

The second node of the logic tree is the assessment of the nature of the localizing tectonic feature for the RLMEs. In some cases the source will be modeled as a fault source; in other cases the existing data will not allow for a clear definition of causative faults, and some type of areal source zone will be used. Alternative geometries are then defined at the third node of the tree for the localizing tectonic feature(s).

The fourth and fifth nodes of the tree provide information regarding the rupture characteristics for future earthquakes within the RLME source. As discussed in Section 5.4 and shown in Table 5.4-1, a “default” set of characteristics were developed for the entire study region, and the

¹ Note that 50 years is the approximate lifetime of nuclear facilities and is used in this context as the time period of interest for assessing within-cluster or out-of-cluster rates. There is no implication that the lifetime of the CEUS SSC model is 50 years.

assessments made by the TI Team for individual seismic sources could either adopt the default characteristics or, if sufficient data were available to do so, specify source-specific characteristics. Source-specific characteristics are included on the logic tree and are shown in Table 5.4-2. Shown are seismogenic crustal thickness, rupture orientation, and source boundary characteristics. Seismogenic crustal thickness can be important in the assessment of distance from ruptures for ground-motion prediction equations, as well as in calculations of seismic moment rate from geologic slip rates. Also, the dimensions of rupture are magnitude dependent (Section 5.4), and finite ruptures, using the assessed rupture orientations and downdip dimensions, are modeled for purposes of the hazard calculations. The hazard model assumes that the epicenters of all earthquakes will occur within the seismic source, although the seismic source boundary characteristics are assessed for whether the rupture can cross the source boundary (termed a “leaky” boundary) or must remain within the boundary (“strict” boundary). Not shown on the tree is the assessment of the style of faulting for the source.

The sixth node of the logic tree expresses the estimates of the RLME magnitudes. Because most of the evidence for the RLMEs in the CEUS comes from paleoseismic data, there can be significant uncertainty in the size of the earthquakes. There are two components to this assessment: an aleatory component that expresses the variations in the size of the RLME event-to-event, and an epistemic component that expresses the uncertainty in the average size of the RLME. The epistemic component is given in the logic tree, and the aleatory component is assumed to be plus or minus 0.25 magnitude units about the mean unless there is source-specific information that suggests otherwise. The value of 0.25 magnitude is judged to be appropriate based on observations of the repeated sizes of paleoearthquakes in well-studied areas.

The seventh node of the logic tree is the recurrence method and differs depending on whether the “in-cluster” or “out-of-cluster” branch is being followed. Given the “in-cluster” branch, approaches to estimating recurrence include either interevent times (recurrence intervals) or slip rates. In either case, the data should be those that are applicable to the present cluster and that would apply for the future period of interest of about 50 years. Given the “out-of-cluster” branch, the assessments of recurrence should again focus on the applicable recurrence information that would apply to the future period of interest.

The eighth “events/data” node of the logic tree expresses the data that are used in the recurrence assessment for the RLME source. In most cases, this is an assessment of the dates of past earthquakes, which includes the uncertainty in the timing of earthquakes given the available paleoseismic data. In other cases, an assessment is made of the number of events that have occurred over a particular time interval. The approaches taken in the estimation of RLME recurrence are described in Section 5.3.3.

The earthquake occurrence model in the ninth node of the logic tree expresses the approach that is used to model the temporal occurrence of earthquakes. Two alternative models are considered, depending on the availability of data for the RLME source of interest. A Poisson model assumes that earthquakes occur in a temporally random way that is defined simply by a mean recurrence rate without regard to the time elapsed since the last earthquake. The Poisson model is the most commonly used in PSHA because of the minimal number of parameters that must be constrained. An alternative model is the renewal model (strictly, a Brownian passage time, or

BPT, model is used [see Section 5.3.3.2]), which requires information not only on the mean recurrence rate, but also on the aperiodicity factor (α) and the time elapsed since the most recent earthquake. The model is based on a strain accumulation and release physical model that is most applicable to a fault source. To be compatible with common PSHA models, the resulting recurrence rates for both the Poisson and renewal models are expressed as equivalent annual frequencies, as shown in the last node of the RLME source logic tree.

4.2.3 Mmax Zones Logic Tree

As implied by the name, the Mmax zones model considers possible subdivisions of the CEUS based on considerations of Mmax. As discussed in Section 5.2, two approaches to estimating Mmax are used in the CEUS SSC Project:

- The Bayesian approach (Johnston et al., 1994), in which prior distributions are based on statistical analyses of tectonically analogous domains to the CEUS worldwide, and likelihood functions are derived from the number and size of earthquakes that occur within the seismic source of interest.
- The Kijko (2004) approach, in which the statistics of observed earthquakes within the source of interest are used to estimate Mmax.

The two approaches are similar in the use of observed seismicity data within the source of interest, but they differ in the use of a prior distribution in the Bayesian approach. For the CEUS SSC Project, the global database of tectonically analogous earthquakes was updated from the Johnston et al. (1994) study and the prior distributions from that study were reassessed. As discussed in Section 5.2, the statistics do not strongly define the prior distributions. This means that there are no unique tectonic characteristics that strongly correlate with maximum earthquake size. Past studies using the database have suggested that a difference exists between sources having Paleozoic and younger extension and those that do not. However, the analysis conducted for this project does not support that view, but suggests that the only potentially significant difference is between sources having Mesozoic and younger extension and those that do not.

Based on the analyses conducted for Mmax, two alternative models define the first branch of the Mmax zones logic tree (Figure 4.2.3-1): a branch that represents the entire CEUS SSC study region by a single prior distribution, and a branch that calls for the separation of Mesozoic and younger extended regions from those that do not display such evidence. The available evidence and statistical analyses of the global SCR database (Section 5.2) carried out as part of the CEUS SSC Project suggests that the separation into Mesozoic and younger sources is significant, but only marginally so. Therefore, the approach that uses the separation is preferred (0.6) over the approach that does not recognize a separation (0.4), although the preference is not large, given the marginal statistical significance.

The second node of the Mmax zones logic tree, which applies only to the Mesozoic and younger separation branch, considers the uncertainty in the location of the boundary between Mesozoic and younger regions and those that do not show evidence of such extension. As discussed in Section 6.2, there is stronger technical support for the “narrow” interpretation in the available

data than the “wide” interpretation. Two alternative locations are considered, with higher weight (0.8) given to the narrow interpretation than the wide interpretation (0.2). These two alternative locations of the boundary are shown on Figures 4.2.3-2 and 4.2.3-3.

The third node addresses the issue of the weight assigned to various magnitudes in the estimation of seismicity parameters for the seismic source zones. The three alternatives, Cases A, B, and E are discussed in Section 5.3.2.2.1, along with the bases for the weights assigned to the alternatives.

The remaining assessments of the logic tree are a function of the region that is being characterized, which is either the entire study region, the Mesozoic extended-wide, the Mesozoic extended-narrow, or the non-Mesozoic extended regions.

Similar to the RLME sources, the next assessments in the logic tree are related to the characteristics of future earthquake ruptures. The first assessment is seismogenic crustal thickness, which controls the downdip extent of ruptures, and the second is rupture orientation and boundary characteristics. Given the large extent of the regions of interest in the Mmax zones model, the characteristics of future ruptures are those given in the “default” set of characteristics for the entire study region (see Section 5.4).

The next level of the logic tree addresses the approach used for assessing seismicity rates and their spatial distribution. Allowing both the *a*-value and the *b*-value to vary spatially is the selected approach. Seismicity parameters are estimated for $\frac{1}{4}^{\circ} \times \frac{1}{4}^{\circ}$ cells using an update of the approach developed in EPRI-SOG.

The “degree of smoothing” level of the logic tree addresses the degree of smoothing applied in the seismicity parameter estimation in each source region. An “objective” approach is used to select the degree of smoothing, as discussed in Section 5.3.2.4.

The next level of the logic tree addresses the seismicity parameter epistemic uncertainty. The seismicity parameter distributions for the “variable a and b” approach are represented by eight alternative spatial distributions developed by simulation from the fitted parameter distributions (Section 5.3.2.5).

The final level of the logic tree addresses the uncertainty in the maximum magnitude for each region. This assessment includes uncertainty in the basic approach to estimating Mmax as well as uncertainties with a given approach. The two alternative approaches estimating Mmax are the Bayesian approach developed in Johnston et al. (1994) with updated prior distributions developed in this project, and the Kijko (2004) approach that uses the numbers and magnitudes of observed earthquakes directly without a prior distribution. As discussed in Section 5.2.1.3, the relative weights applied to the two approaches are source-specific and region-specific and are related directly to the *p*-value derived from the Kijko approach. Given the Bayesian approach, two prior distributions are considered, depending on the assessment in the first node of the logic tree. If the region is not subdivided (the “no” branch on the first node), then a single composite prior distribution is used. If a separation is made between Mesozoic and younger extension and

non-Mesozoic extension, then the appropriate prior distributions for those regions are used for the Mmax estimates.

4.2.4 Seismotectonic Zones Branch

The seismotectonic zones identified for the CEUS SSC model are listed in Table 4.2.4-1. The logic tree for the seismotectonic zones branch of the master logic tree is shown on Figure 4.2.4-1, and the maps of the seismotectonic zones are shown on Figures 4.2.4-2 through 4.2.4-5. Following the “seismotectonic zones” branch of the master logic tree, the first assessment is the uncertainty in the western boundary of the Paleozoic Extended Crust seismotectonic zone. The two alternatives are the narrow interpretation (0.8) and the wide interpretation (0.2). As discussed in Section 7.3.4, there is significantly more technical support for the location of the boundary in the narrow case.

The second node of the logic tree addresses the uncertainty in the eastern extent of the Reelfoot Rift zone—whether or not it includes the Rough Creek Graben. These two logic tree branches lead to the four alternative seismotectonic zonation configurations shown on Figures 4.2.4-2 through 4.2.4-5. The discussion of this assessment and the associated weights is given in Section 7.3.6.3.

The third node of the logic tree represents the uncertainty in the issue of the weight assigned to various magnitudes in estimating seismicity parameters for the seismotectonic zones. The assessment is the same as that given in the Mmax zones branch and is discussed in Section 5.3.2.2.1

The next element of the tree (which is not a node but a listing) identifies the various seismotectonic zones included in the CEUS SSC model, which are given in Table 4.1.3-1.

Similar to the RLME sources, the next assessments in the logic tree are related to the characteristics of future earthquake ruptures. The first assessment is seismogenic crustal thickness, which controls the downdip extent of ruptures, and the second is rupture orientation and boundary characteristics. The characteristics of future ruptures are discussed in the “default” set of characteristics for the entire study region (see Section 5.4); each seismotectonic zone is assigned a set of characteristics based on the applicable data specific to that zone.

The next level of the logic tree addresses the approach used for assessing seismicity rates and their spatial distribution. Allowing both the *a*-value and the *b*-value to vary spatially is the selected approach. Seismicity parameters are estimated for $\frac{1}{4}^{\circ} \times \frac{1}{4}^{\circ}$ cells using an update of the approach developed in EPRI-SOG.

The “degree of smoothing” level of the logic tree addresses the degree of smoothing applied in the seismicity parameter estimation in each seismotectonic zone. An “objective” approach is used to select the degree of smoothing, as discussed in Section 5.3.2.4.

The next level of the logic tree addresses the seismicity parameter epistemic uncertainty. The seismicity parameter distributions for the “variable a and b” approach are represented by eight alternative spatial distributions developed by simulation from the fitted parameter distributions (Section 5.3.2.5).

The final level of the logic tree addresses the uncertainty in the maximum magnitude for each seismotectonic zone. This assessment includes uncertainty in the basic approach to estimating M_{max} as well as uncertainties for a given approach. The two alternative approaches estimating M_{max} are the Bayesian approach developed by Johnston et al. (1994) with updated prior distributions developed in this project, and the Kijko (2004) approach that uses the numbers and magnitudes of observed earthquakes directly without a prior distribution. As discussed in Section 5.2, the relative weights applied to the two approaches are source-specific and region-specific and are related directly to the p -value derived from the Kijko approach. Given the Bayesian approach, two options are available regarding prior distributions: a “composite” prior that is based on the entire SCR data set, or two priors that are based on Mesozoic or younger extension and non-Mesozoic or younger extension. As discussed in Section 5.2, the relative weight assigned to the composite distribution is 0.4 and the relative weight of the two-prior option is 0.6. These relative weights are assigned to each seismotectonic source, but given the two-prior option, a source-specific assessment must be made as to whether the zone lies within a Mesozoic or younger extended region.

Table 4.1.2-1
 Sample table indicating particular types of data that can be considered in the identification and characterization of seismic sources (Table 2, ANSI/ANS-2.27-2008)

DATA TYPE	SEISMIC SOURCE							
	INDIVIDUAL FAULTS						AREA/VOLUME SOURCES	
	Location	Activity	Length	Dip	Depth	Style	Area	Depth
Geological/Remote Sensing								
Detailed mapping	X	X	X	X		X		
Geomorphic data	X	X	X			X	X	
Quaternary surface rupture	X	X	X			X		
Fault trenching data	X	X		X		X		
Paleoliquefaction data	X	X					X	
Borehole data	X	X		X		X		
Aerial photography	X	X	X					
Low sun-angle photography	X	X	X					
Satellite imagery	X		X				X	
Regional structure	X			X		X	X	
Balanced Cross Section	X			X	X		X	
Geophysical/Geodetic								
Regional potential field data	X		X				X	X
Local potential field data	X		X	X	X	X		
High resolution reflection data	X	X		X		X		
Standard reflection data	X			X		X		
Deep crustal reflection data	X			X	X		X	X
Tectonic geodetic/strain data	X	X		X	X	X	X	X
Regional stress data						X	X	
Seismological								
Reflected crustal phase data								X
Pre-instrumental earthquake data	X	X			X	X	X	
Teleseismic earthquake data							X	
Regional network seismicity data	X	X	X	X	X		X	X
Local network seismicity data	X	X	X	X	X			X
Focal mechanism data				X		X		

Footnote: * Length includes both total fault length and information on segmentation.

Table 4.1.2-2
Sample table identifying the types of data that can be considered for characterizing different types of seismic sources, and an evaluation of the relative usefulness or credibility of the various data types (Budnitz et al., 1997)

Data Used to Assess Seismic Source Locations and Geometries and Their Relative Usefulness		
TYPE OF SOURCE	DATA/BASIS FOR SOURCE	RELATIVE USEFULNESS/ CREDIBILITY
		(1: high, 3: low)
Type 1: Faults	Mapped fault with historical rupture	1
	Mapped Quaternary fault at surface	1
	Mapped localized Quaternary deformation, inferred fault at depth	2
	Borehole evidence for fault, especially in young units	2
	Geophysical evidence (e.g. seismic reflection) of fault at depth	2
	Map of pre-Quaternary faults	3
Type 2: Concentrated Zone	Concentrated zone of well-located instrumental seismicity	1
	Mapped fault(s) at surface or subsurface in proximity to seismicity	1
	Zone of historical/poorly located seismicity	2
	Structural features/trends parallel to seismicity zone	2
	Focal mechanisms/stress orientation	3
	Rapid lateral changes in structures/tectonic features	3
Type 3: Regional Zone	Changes in spatial distribution/concentration/density of seismicity	1
	Regions of genetically-related tectonic history	1
	Regions of similar structural styles	2
	Changes in crustal thickness or crustal composition	2
	Regions of different geophysical signature	3
	Changes in regional stresses	3
Type 4: Background Zones	Changes in regional physiography	3
	Regional differences in structural styles/tectonic history	1
	Major physiographic/geologic provinces	1
	Changes in character of seismicity	3

Table 4.1.2-3
 Table showing the “generic” (not source-specific) evaluation of data to address indicators of a unique seismic source. The table indicates the TI Team’s assessment of the types of data that can be used to address the indicators and their relative usefulness.

Indicators of a Potential Seismic Source	Usefulness of Indicator in Defining Seismic Sources 5 = High 1 = Low	Data to Address Indicator	Relative Usefulness of Data in Addressing Indicator 5 = High 1 = Low	Notes: Source Aspect (Temporal, Spatial)
Paleoseismic indicators of M > 5 earthquakes	5	Paleoliquefaction evidence	4	Temporal, spatial
		Quaternary faulting	5	
		Quaternary deformation	3	
High strain rates in contemporary tectonic setting	4	Tectonic geodetic strain data	4	Temporal, perhaps spatial
		Geologic indicators of recent strain (e.g., Quaternary)	5	
Variations in stress/strain orientations	3	Tectonic geodetic strain data	3	Spatial
Zones of weakness, including both crustal and mantle (including hotspot tracks and lithospheric upwelling)	1	Tectonic geodetic strain data/modeling	1	Spatial
		Geophysical evidence of mantle anomalies (e.g., tomography, heat flow, concentration of heat-producing elements)	3	
		Consideration of rheology based on rock types/petrology	2	
		Geologic mapping	3	
Evidence for recent and/or repeated reactivation of preexisting structures (Note: General types of structures should be identified with a focus on those that may contain faults of sufficient dimension)	(see below)	(see below)	(see below)	(see below)

Indicators of a Potential Seismic Source	Usefulness of Indicator in Defining Seismic Sources 5 = High 1 = Low	Data to Address Indicator	Relative Usefulness of Data in Addressing Indicator 5 = High 1 = Low	Notes: Source Aspect (Temporal, Spatial)
to cause M > 5 earthquakes.)				
(1) Cratons	1	Geologic mapping	2	Spatial
		Potential field geophysics (magnetic, gravity)	2	
		Historical and instrumental seismicity	2	
		Deep crustal seismic profiles	3	
		Compilations of historical analogues	2	
(2) Extended Margins—and age (Mesozoic and younger)	1	Geologic mapping	2	Spatial
		Potential field geophysics (magnetic, gravity)	2	
		Historical and instrumental seismicity	2	
		Deep crustal seismic profiles	3	
		Compilations of historical analogues	2	
(3) Rifted Margins—and age (Mesozoic and younger)	2	Geologic mapping	2	Spatial
		Potential field geophysics (magnetic, gravity)	2	
		Historical and instrumental seismicity	2	
		Deep crustal seismic profiles	3	
		Compilations of historical analogues	2	
(4) Rift Basins	2	Geologic mapping	2	Spatial
		Potential field geophysics (magnetic, gravity)	2	

Indicators of a Potential Seismic Source	Usefulness of Indicator in Defining Seismic Sources 5 = High 1 = Low	Data to Address Indicator	Relative Usefulness of Data in Addressing Indicator 5 = High 1 = Low	Notes: Source Aspect (Temporal, Spatial)
		Historical and instrumental seismicity	2	
		Deep crustal seismic profiles	3	
		Compilations of historical analogues	2	
(5) Failed Rift (Paleozoic and younger)	1	Geologic mapping	2	Spatial
		Potential field geophysics (magnetic, gravity)	2	
		Historical and instrumental seismicity	2	
		Deep crustal seismic profiles	3	
		Compilations of historical analogues	2	
Cold strong crust	1	Heat flow	2	Spatial
		Geophysical modeling of mantle processes (e.g., tomography)	3	
Geologic evidence for potential zones of stress concentration/amplification	2–3	Analysis of instrumental seismicity data (depths, focal mechanisms)	2	Spatial
		Consideration of rheological contrasts based on geologic mapping and modeling (mafic plutons, intersecting faults)	2	
Orientation of structures relative to underlying stress field (either favorable or unfavorable)	2	Analysis of instrumental seismicity data (depths, focal mechanisms)	2	Spatial
		Geologic mapping and geophysical interpretations of structures at depth	2	

Indicators of a Potential Seismic Source	Usefulness of Indicator in Defining Seismic Sources 5 = High 1 = Low	Data to Address Indicator	Relative Usefulness of Data in Addressing Indicator 5 = High 1 = Low	Notes: Source Aspect (Temporal, Spatial)
Local loading mechanisms (as stress concentrators)	1	Geologic mapping	2	Spatial
		Detailed topographic analysis	2	
		Isostatic analyses (sediment load/denudation, glacial forebulge, or rebound)	3	
Evidence of geologically recent fault displacement	5	Mapped fault with historical rupture	5	Spatial, temporal
		Mapped Quaternary fault at surface	5	
		Mapped localized Quaternary deformation, inferred fault at depth	4	
		High-resolution seismic reflection or borehole evidence for fault, especially in young units	3	
Fault having significant dimensions	1	Geophysical evidence (e.g., seismic reflection) of fault at depth	3	Spatial
		Map of pre-Quaternary faults	3	
Concentrated zone of observed seismicity	4	Well-located instrumental seismicity	5	Spatial, Temporal
		Fault(s) mapped at surface or subsurface in proximity to seismicity; alignments parallel to structure	3	
		Historical seismicity	3	
		Focal mechanisms/stress orientation	2	
Rapid lateral changes in structures/tectonic features/observed seismicity	3–4	Historical and instrumental seismicity showing changes in spatial distribution/concentration/density of seismicity	3	Spatial

Indicators of a Potential Seismic Source	Usefulness of Indicator in Defining Seismic Sources 5 = High 1 = Low	Data to Address Indicator	Relative Usefulness of Data in Addressing Indicator 5 = High 1 = Low	Notes: Source Aspect (Temporal, Spatial)
		Geologic/tectonic maps showing regions of genetically related tectonic history; similar structural styles	3	
		Geophysical maps showing changes in crustal thickness or crustal composition	3	
		Regions of different geophysical signature	3	
		Stress indicators showing changes in regional stresses (e.g., compressional to tensional; orientation of horizontal stress directions)	2	
		Changes in regional physiography (e.g., fall line)	2	
Regional or local strain energy buildup following larger ($M > 7$) earthquakes (e.g., New Madrid earthquakes trigger earthquakes to the north)		Note: The occurrence of the $M > 7$ earthquake would define the unique seismic source; current temporal methods do not account for triggering of adjacent earthquakes.		Temporal
Stress shadows following large earthquakes		Note: Occurrence of large earthquakes would be considered in defining seismic source; real-time model would be needed to account for time-dependent temporal behavior; this indicator has more applicability for modeling of stress interactions among faults in WUS.		Spatial, temporal
Regional variations in expected M_{max} or recurrence (background zones)		Note: These are applicable criteria, but they are based on a derivative product (M_{max} or recurrence) and not data per se.		Spatial, temporal

1. Each indicator is assumed to be known with certainty.

2. It is assumed that high-quality data exist of the type identified.
3. Could be accounted for using spatial smoothing, thus not requiring a source boundary.

Table 4.1.2-4
Example of Data Evaluation Table for the Illinois Basin–Extended Basement Zone (IBEB)

Data/References	Quality (1=low, 5=high)	Notes on Quality of Data	Source Considered	Used in SSC and Reliance Level (0=no, 5=high)	Discussion of Data Use	In GIS Database
Instrumental Seismicity						
CEUS SSC earthquake catalog	5	Comprehensive catalog; includes magnitude conversions and uncertainty assessments.	IBEB	5	Used to evaluate recurrence parameters.	Y
Hamburger et al. (2008)	3	Abstract	IBEB	4	Style of faulting and future earthquake characteristics—Reactivation of structures in contemporary stress regime in Illinois basin region—04:30 CDT, April 18, 2008, M 5.4 earthquake, located near New Harmony fault at depth of ~14 km (~9 mi.).	Y
Withers et al. (2009)	3	Abstract—citing preliminary analysis.	IBEB	4	Style of faulting and future earthquake characteristics—Reactivation of structures in contemporary stress regime in Illinois basin region—April 18, 2008, M _w 5.2 (M _w 5.4 GCMT [http://www.globalcmt.org]) Mt. Carmel, Illinois, earthquake. Largest event in 20 years in Wabash Valley seismic zone.	Y

Note: Only a portion of the table is shown as an example.

Table 4.1.2-5
Example of Data Summary Table for the Extended Continental Crust–Atlantic Margin (ECC-AM) and Atlantic Highly Extended Crust (AHEX) Zones

Citation	Title	Description and Relevance to SSC
General for Region		
Austin et al. (1990)	Crustal Structure of the Southeast Georgia Embayment-Carolina Trough: Preliminary Results of a Composite Seismic Image of a Continental Suture(?) and a Volcanic Passive Margin	The authors use multichannel seismic-reflection data to image the Carolina platform and conclude that observed magnetic anomaly in this region is the product of Mesozoic rifting processes, not Paleozoic collision.
Bird et al. (2005)	Gulf of Mexico Tectonic History: Hotspot Tracks, Crustal Boundaries, and Early Salt Distribution	The authors interpret deep basement structural highs in Gulf of Mexico as hotspot tracks. In this interpretation, the basin began to form as the Yucatan experienced continental crustal extension and 22 degrees of counterclockwise rotation (160–150 Ma). This was followed by a further 20 degrees of counterclockwise rotation and seafloor spreading in the gulf.
Cook (1984)	Geophysical Anomalies Along Strike of the Southern Appalachian Piedmont	Documents trends in both Bouguer gravity and magnetic anomalies associated with the Appalachians in Georgia and Virginia.
Crough (1981)	Mesozoic Hotspot Epeirogeny in Eastern North America	Attributes a 600 km (373 mi.) wide zone of epeirogeny in SE Canada and New England during the Cretaceous and early Tertiary to the Great Meteor hotspot, as evidenced by apatite fission-track dating.
Daniels et al. (1983)	Distribution of Subsurface Lower Mesozoic Rocks in the Southeastern United States, as Interpreted from Regional Aeromagnetic and Gravity Maps	<p>Concludes that Brunswick magnetic anomaly must be older than the Mesozoic features that it can be traced over, and is therefore not sourced by South Georgia rift.</p> <p>The authors performed a paleostress analysis of the New England–Quebec igneous province, which provides an alternative interpretation for the distribution of Cretaceous plutons. Dikes display ESE-WNW and ENE-WSW trends and are spatially distributed in three E-W-striking dike swarms 75 by 300 km (47 by 186 mi.) in area. Leucocratic dikes occur closer to plutons and disappear within 3–4 km (2–2.5 mi.), likely recording local stress effects due to pluton emplacement. Lamprophyre dikes occur independently of plutons and strike parallel to regional dike swarms, recording regional far-field stresses. Normal faults in the regions display two orientations:</p>

Citation	Title	Description and Relevance to SSC
		<p>1. E-W-striking normal faults found predominantly in Montreal area are parallel to graben boundaries and axis of the Monteregian Hills, with vertical offsets ranging between 100 and 430 m (328 and 1,411 ft.).</p> <p>2. NW-SE to WNW-ESE-striking normal faults are oblique to graben boundaries, with less than 100 m (328 ft.) of vertical offset.</p> <p>NW-SE to WNW-ESE faults are older than E-W-striking faults but exhibit crosscutting relationships, suggesting that some were reactivated during formation of the E-W-striking faults. Some E-W-striking brittle faults and joints are observed in several Cretaceous plutons with similar orientations to dikes that are locally crosscut by these normal faults, suggesting that dike emplacement and faulting are contemporaneous. Conjugate sets of NE-WS dextral and ESE-WNW sinistral strike-slip faults and WNW-SSW reverse faults provide evidence for a compressional stress regime postdating emplacement of the Cretaceous plutons.</p>

Note: Only a portion of the table is shown as an example.

Table 4.1.3-1
Criteria Used to Define the Seismotectonic Zones and Mmax Zones

Zone	Criteria Used for Defining Source Zone ²				
	Earthquake Recurrence Rate	Mmax	Future Earthquake Characteristics		
			Style of Faulting	Rupture Orientation	Seismogenic Depth
Seismotectonic Zones					
Atlantic Highly Extended Crust (AHEX)				X	X
Extended Continental Crust–Atlantic Margin (ECC-AM)		X		X	
Extended Continental Crust–Gulf Coast (ECC-GC)		X		X	X
Gulf Coast Highly Extended Crust (GHEX)					X
Great Meteor Hotspot (GMH)	X	X	X	X	X
Illinois Basin Extended Basement (IBEB)	X	X			X
Midcontinent-Craton (MidC-A, B, C, D)		X		X	
Northern Appalachian (NAP)		X	X		X
Oklahoma Aulacogen (OKA)			X	X	
Paleozoic Extended Crust (PEZ-N, PEZ-W)		X			
Reelfoot Rift (RR, RR-RCG)		X	X	X	X
St. Lawrence Rift (SLR)	X	X	X		X
Mmax Zones					
Mesozoic-and-Younger Extension (MESE)		X			
Non-Mesozoic-and-Younger Extension (NMESE)		X			

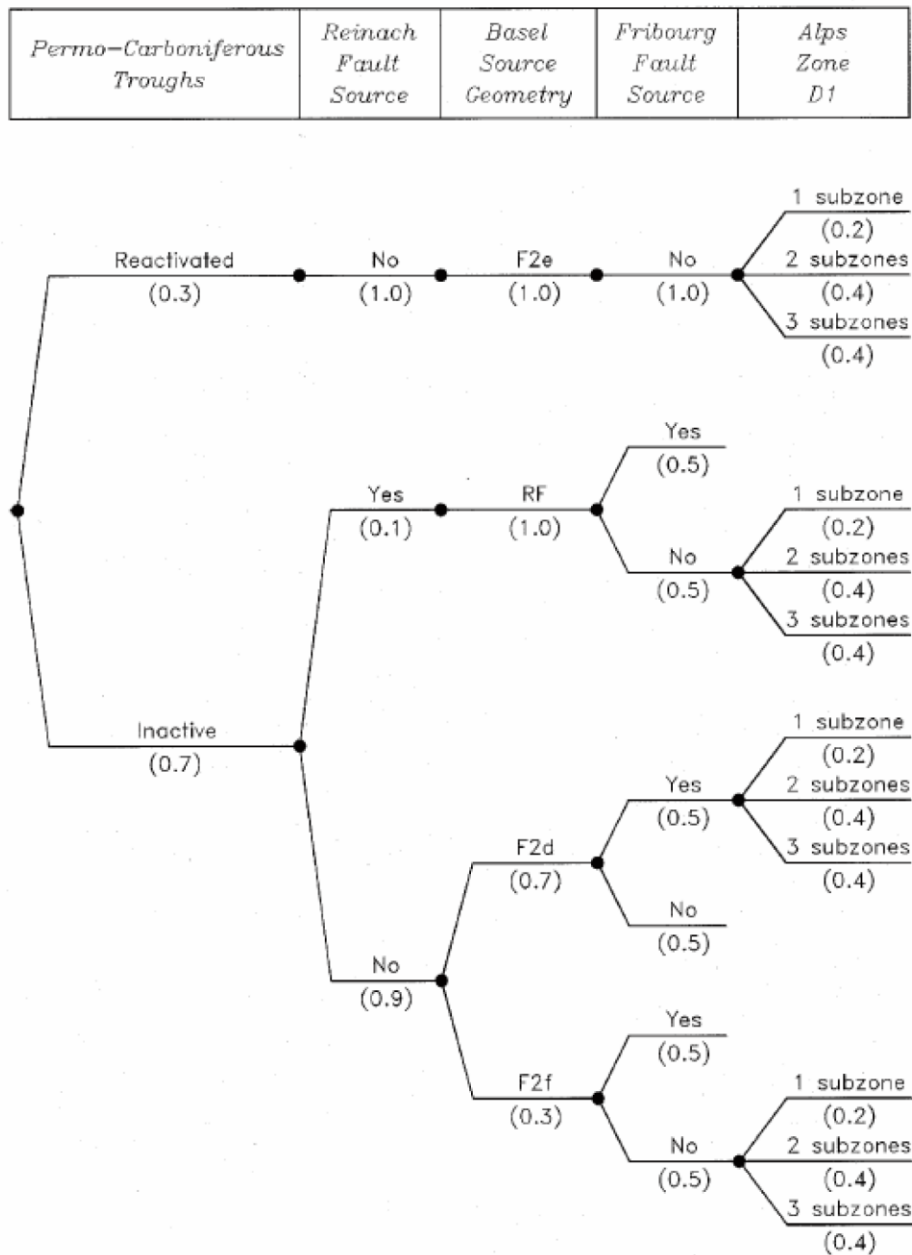
² The criteria that have been used to define the seismic source zones are indicated with an “X.” Note that none of the seismic source zones are defined based on the criterion of the probability of activity. However, this criterion was used to define the RLME fault sources.

**Table 4.2.2-1
 RLME Sources**

Source	Alternatives	Report Section
Charlevoix	Charlevoix	6.1.1
Charleston	Charleston—local	6.1.2
	Charleston—narrow	
	Charleston—regional	
Cheraw Fault	Cheraw fault	6.1.3
	Cheraw fault—extended	
Meers Fault	Meers fault—Quaternary	6.1.4
	Meers fault—extended	
	Oklahoma Aulacogen	
Reelfoot Rift Central Fault System—New Madrid North	New Madrid North—short New Madrid North—extended	6.1.5
Reelfoot Rift Central Fault System—New Madrid South	New Madrid South: Blytheville fault zone New Madrid South: Bootheel lineament	
Reelfoot Rift Central Fault System—Reelfoot Thrust	Reelfoot thrust—short Reelfoot thrust—extended	
Reelfoot Rift—Eastern Rift Margin	Eastern rift margin—north	6.1.6
	Eastern rift margin—south/Crittenden County	
	Eastern rift margin—south/river (fault) picks	
Reelfoot Rift—Marianna	Marianna	6.1.7
Reelfoot Rift—Commerce Fault Zone	Commerce fault zone	6.1.8
Wabash Valley	Wabash Valley	6.1.9

Table 4.2.4-1
Seismotectonic Zones

Zone Acronym	Seismotectonic Source Zone
AHEX	Atlantic Highly Extended Crust
ECC-AM	Extended Continental Crust—Atlantic Margin
ECC-GC	Extended Continental Crust—Gulf Coast
GHEX	Gulf Coast Highly Extended Crust
GMH	Great Meteor Hotspot
IBEB	Illinois Basin Extended Basement
MidC-A, B, C, D	Midcontinent-Craton (various geometries depending on PEZ and RR geometries)
NAP	Northern Appalachian
OKA	Oklahoma Aulacogen
PEZ-N and PEZ-W	Paleozoic Extended Crust narrow and Paleozoic Extended Crust wide
RR and RR-RCG	Reelfoot Rift, Reelfoot Rift with Rough Creek Graben
SLR	St. Lawrence Rift, including the Ottawa and Saguenay grabens



Logic tree for EG1a seismic source zonation

Figure 4.1.1-1
 Example logic tree from the PEGASOS project (NAGRA, 2004) showing the assessment of alternative conceptual models on the logic tree. Each node of the logic tree represents an assessment that is uncertain. Alternative branches represent the alternative models or parameter values, and the weights associated with each branch reflect the TI Team's relative degree of belief that each branch is the correct model or parameter value.

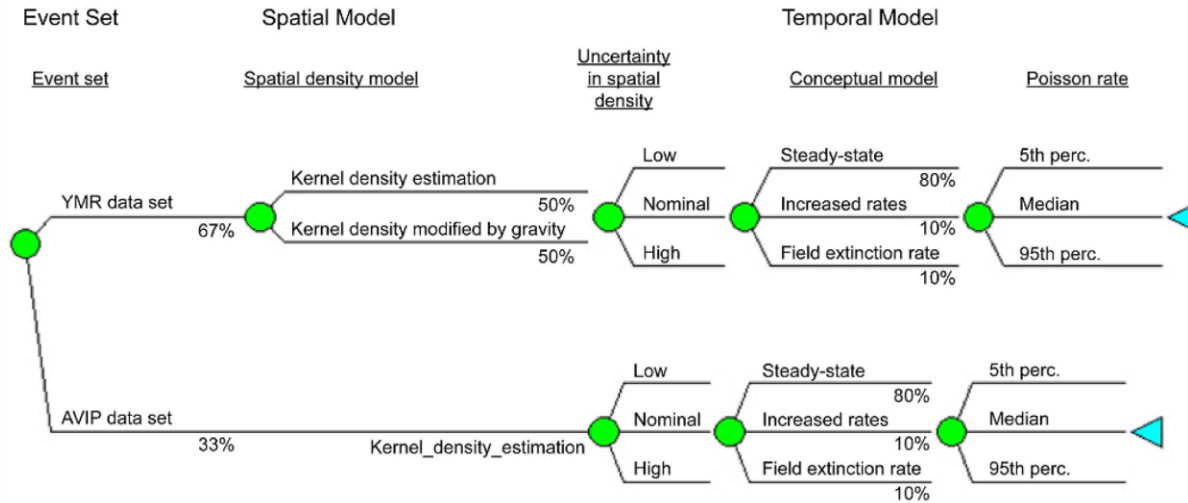


Figure 4.1.1-2
 Example logic tree from the PVHA-U (SNL, 2008) project showing the treatment of alternative conceptual models in the logic tree

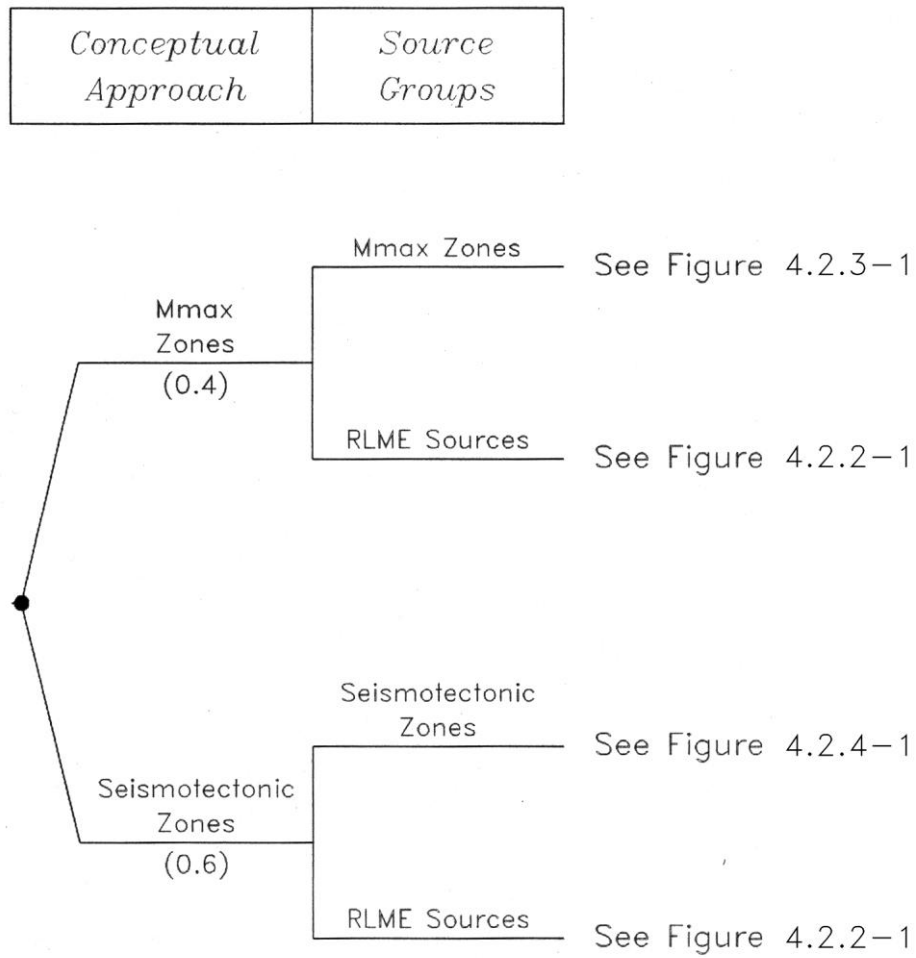
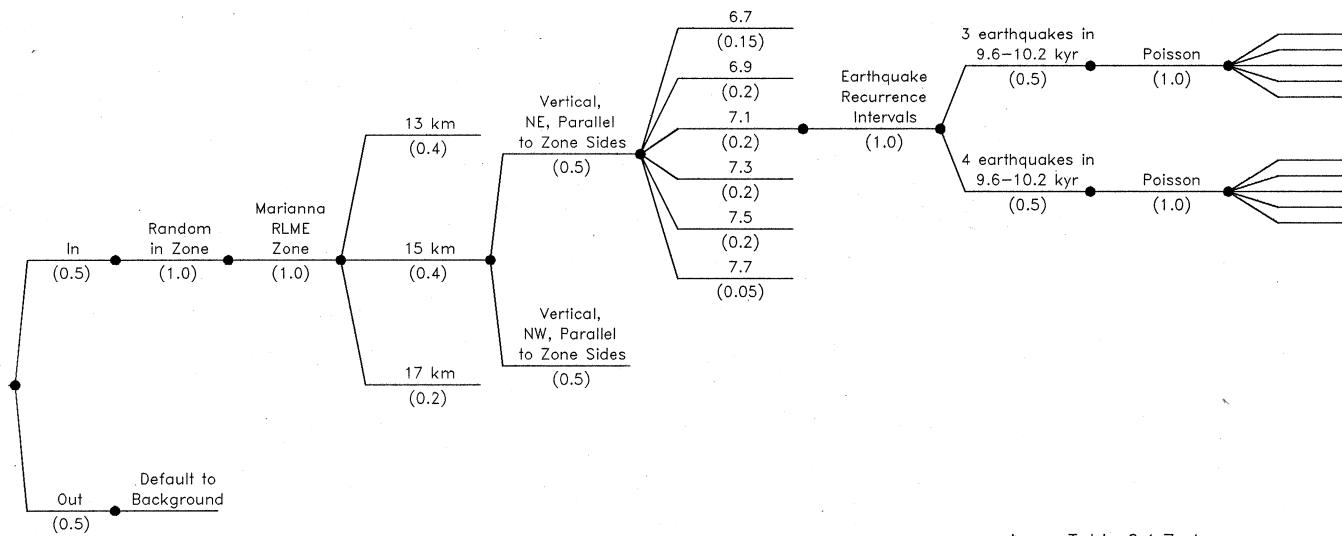


Figure 4.2.1-1
 Master logic tree showing the Mmax zones and seismotectonic zones alternative conceptual models for assessing the spatial and temporal characteristics of future earthquake sources in the CEUS

<i>In or Out of Cluster</i>	<i>Localizing Tectonic Feature</i>	<i>Source Geometry</i>	<i>Seismogenic Crustal Thickness</i>	<i>Rupture Geometry</i>	<i>RLME Magnitude</i>	<i>Recurrence Method</i>	<i>Recurrence Data</i>	<i>Earthquake Recurrence Model</i>	<i>RLME Annual Frequency *</i>
-----------------------------	------------------------------------	------------------------	--------------------------------------	-------------------------	-----------------------	--------------------------	------------------------	------------------------------------	--------------------------------



* see Table 6.1.7-1

Figure 4.2.2-1
Example of a logic tree for RLME sources. Shown is the tree for the Marianna RLME source.

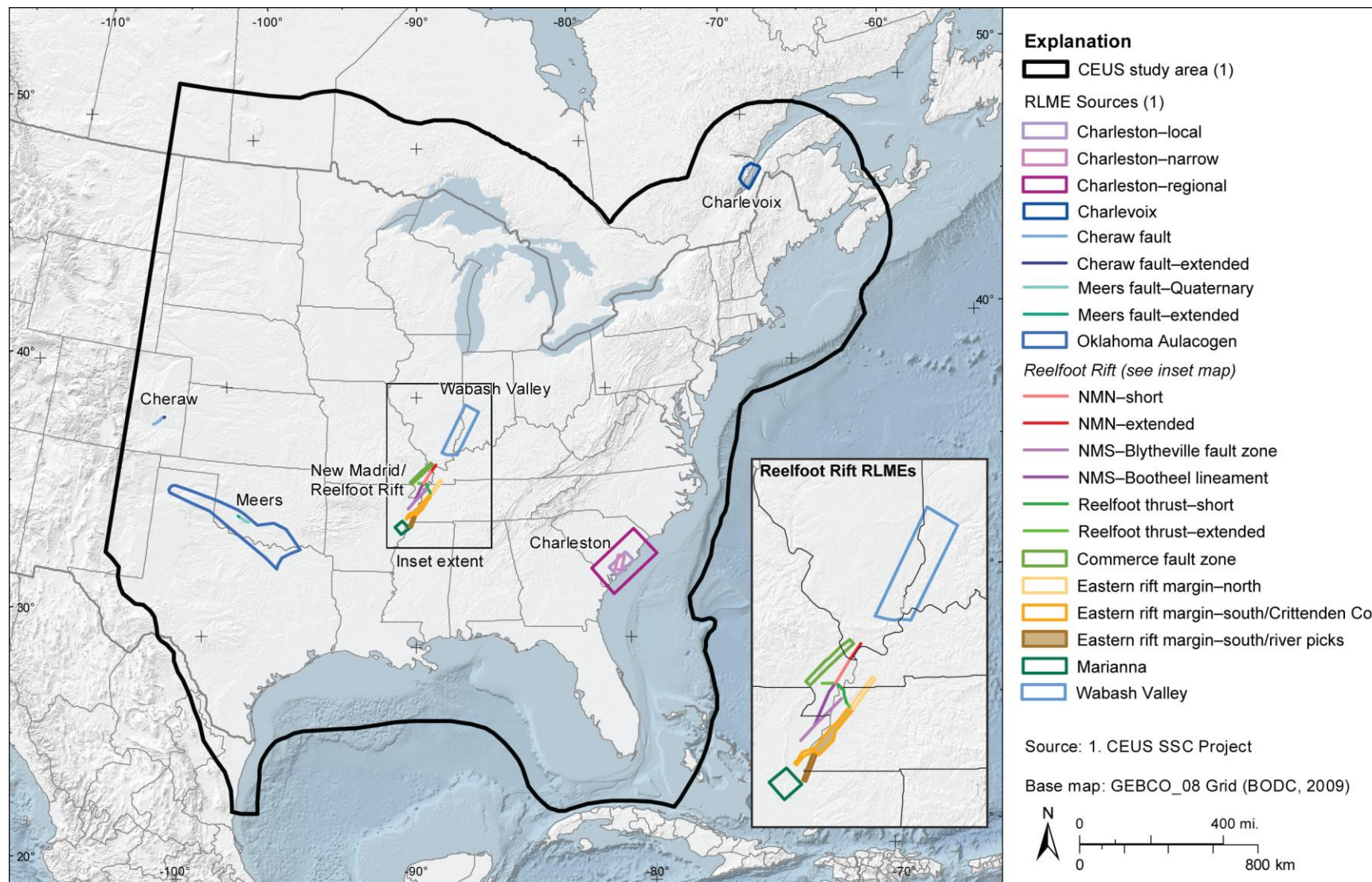


Figure 4.2.2-2
 Map showing RLME sources, some with alternative source geometries (discussed in Section 6.1).

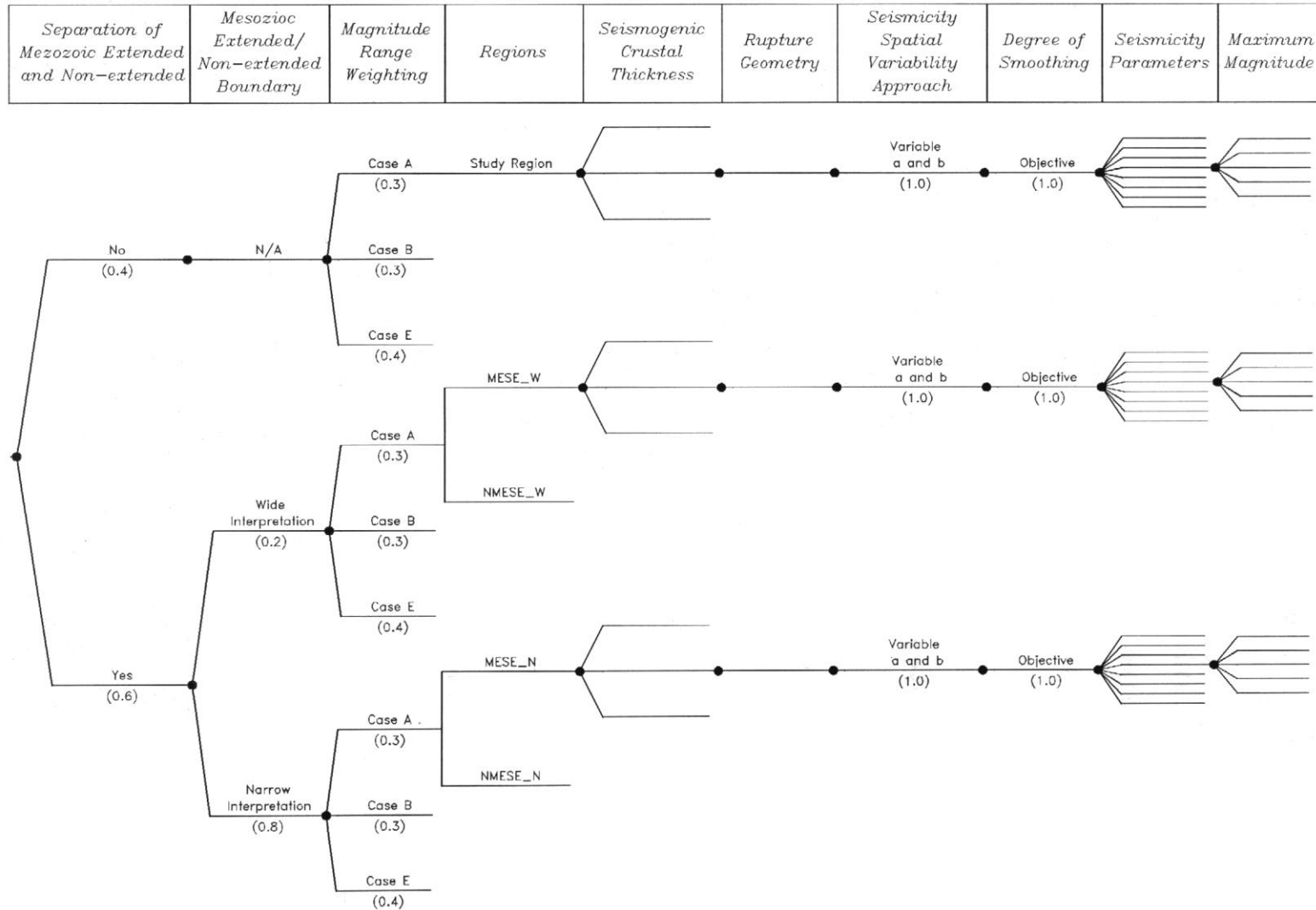


Figure 4.2.3-1
Logic tree for the Mmax zones branch of the master logic tree

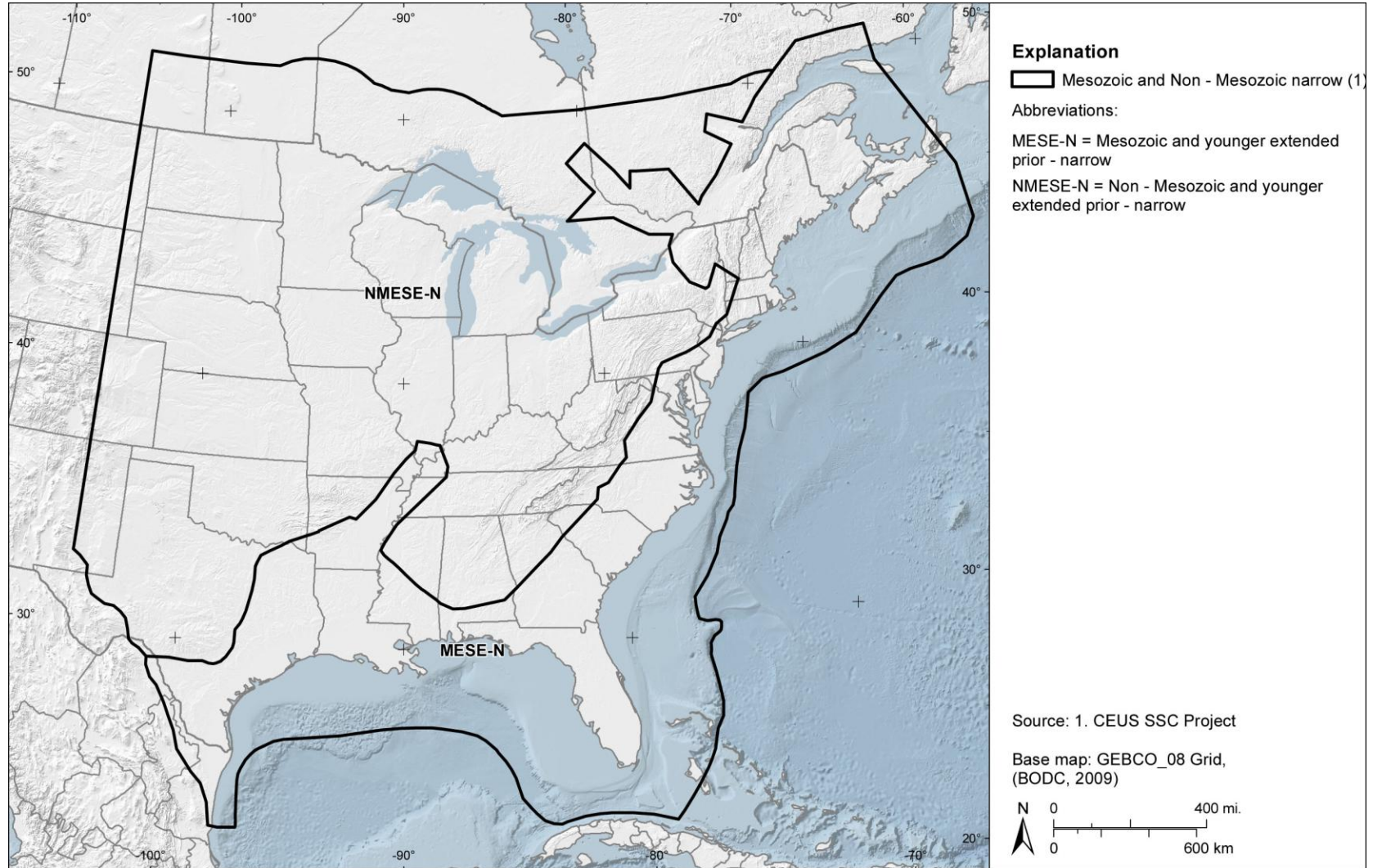


Figure 4.2.3-2
Subdivision used in the Mmax zones branch of the master logic tree. Either the region is considered one zone for purposes of Mmax or the region is divided into two zones as shown: a Mesozoic-and-younger extension (MESE) zone and a non-Mesozoic-and-younger zone (NMESE). In this figure the “narrow” MESE zone is shown.

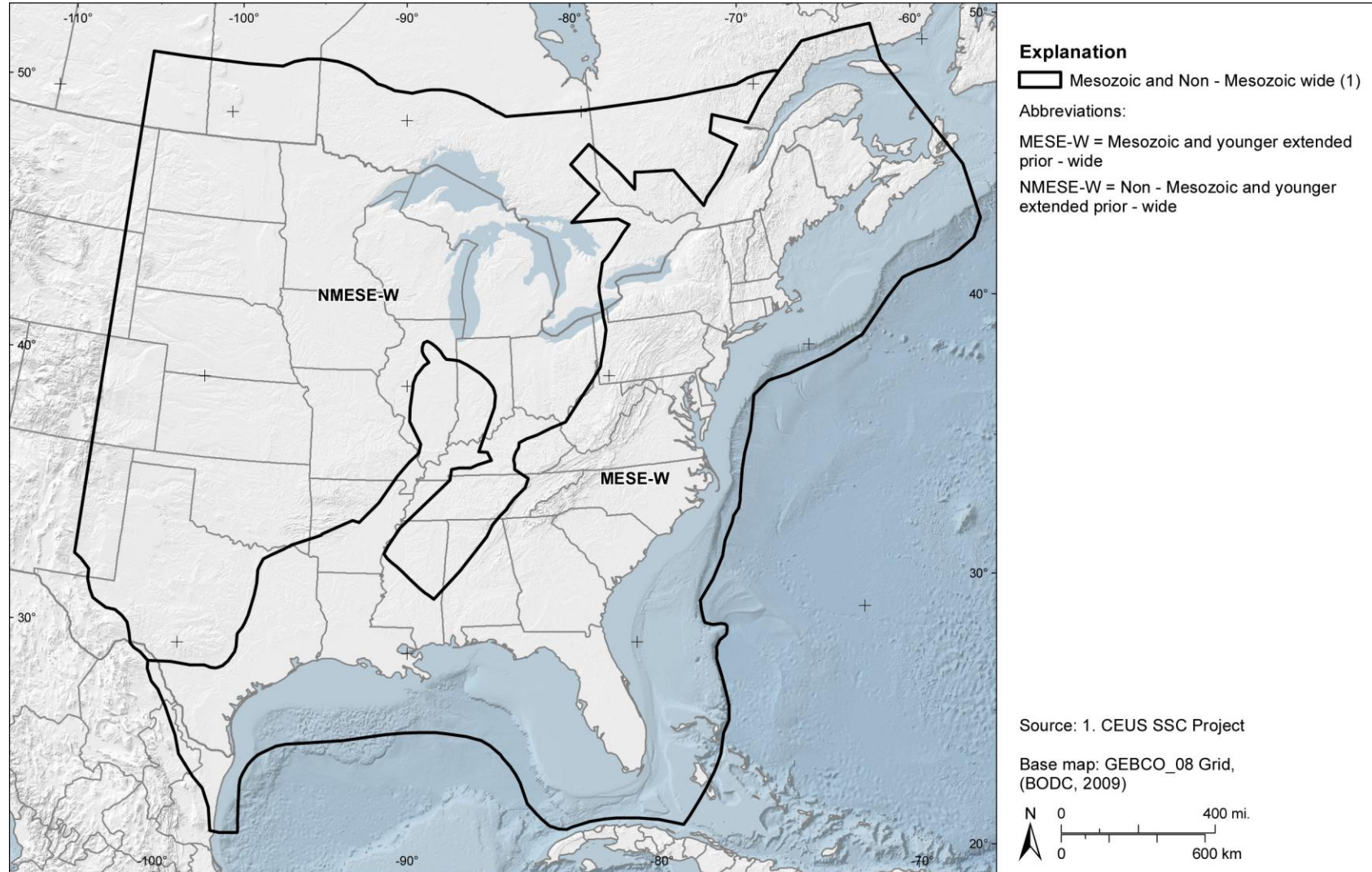


Figure 4.2.3-3
Subdivision used in the Mmax zones branch of the master logic tree. Either the region is considered one zone for purposes of Mmax or the region is divided into two zones as shown: a Mesozoic-and-younger extension (MESE) zone and a non-Mesozoic-and-younger zone (NMESE). In this figure the “wide” MESE zone is shown.

Chapter 4
 Conceptual Seismic Source Characterization Framework

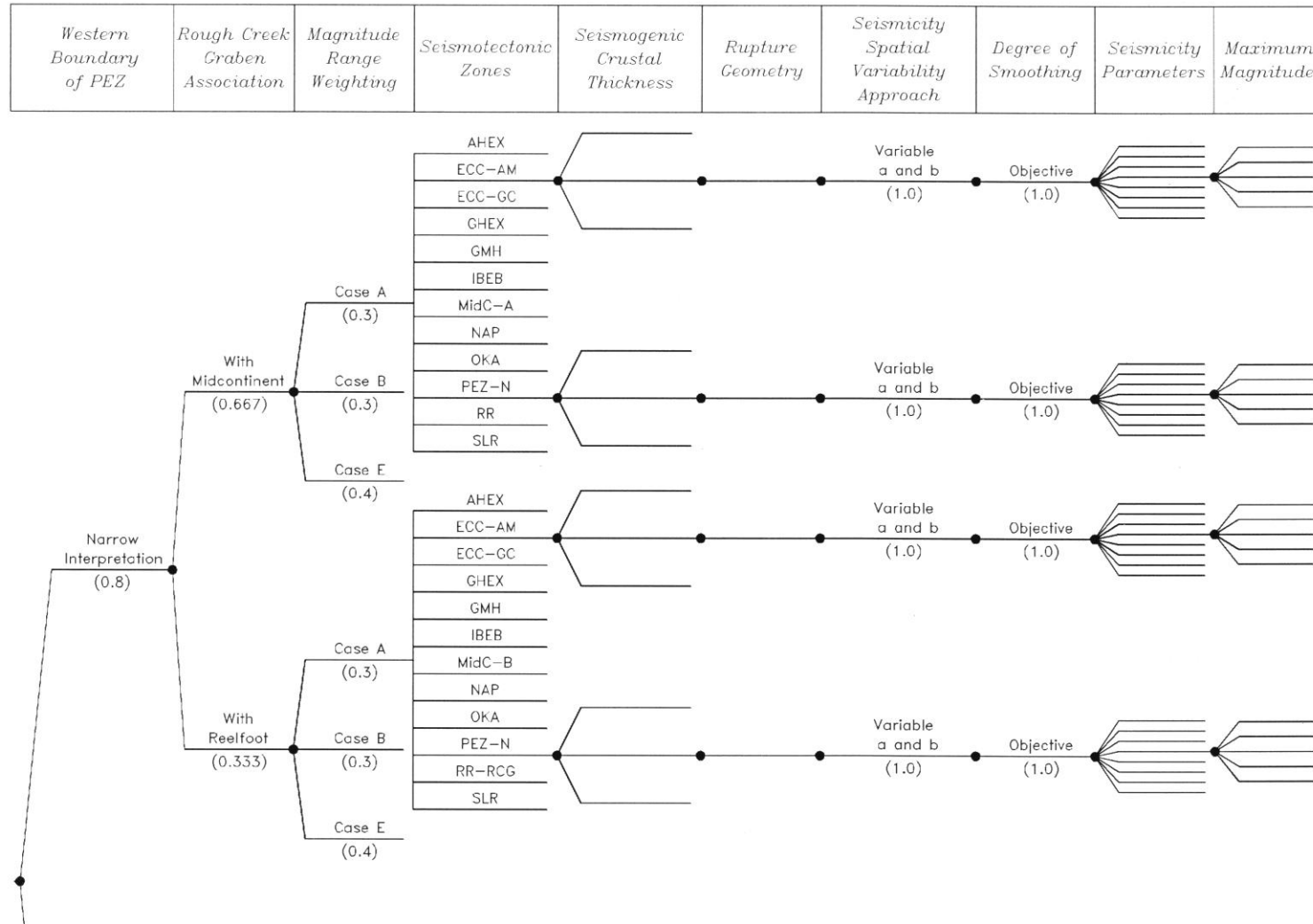


Figure 4.2.4-1(a)
 Logic tree for the seismotectonic zones branch of the master logic tree

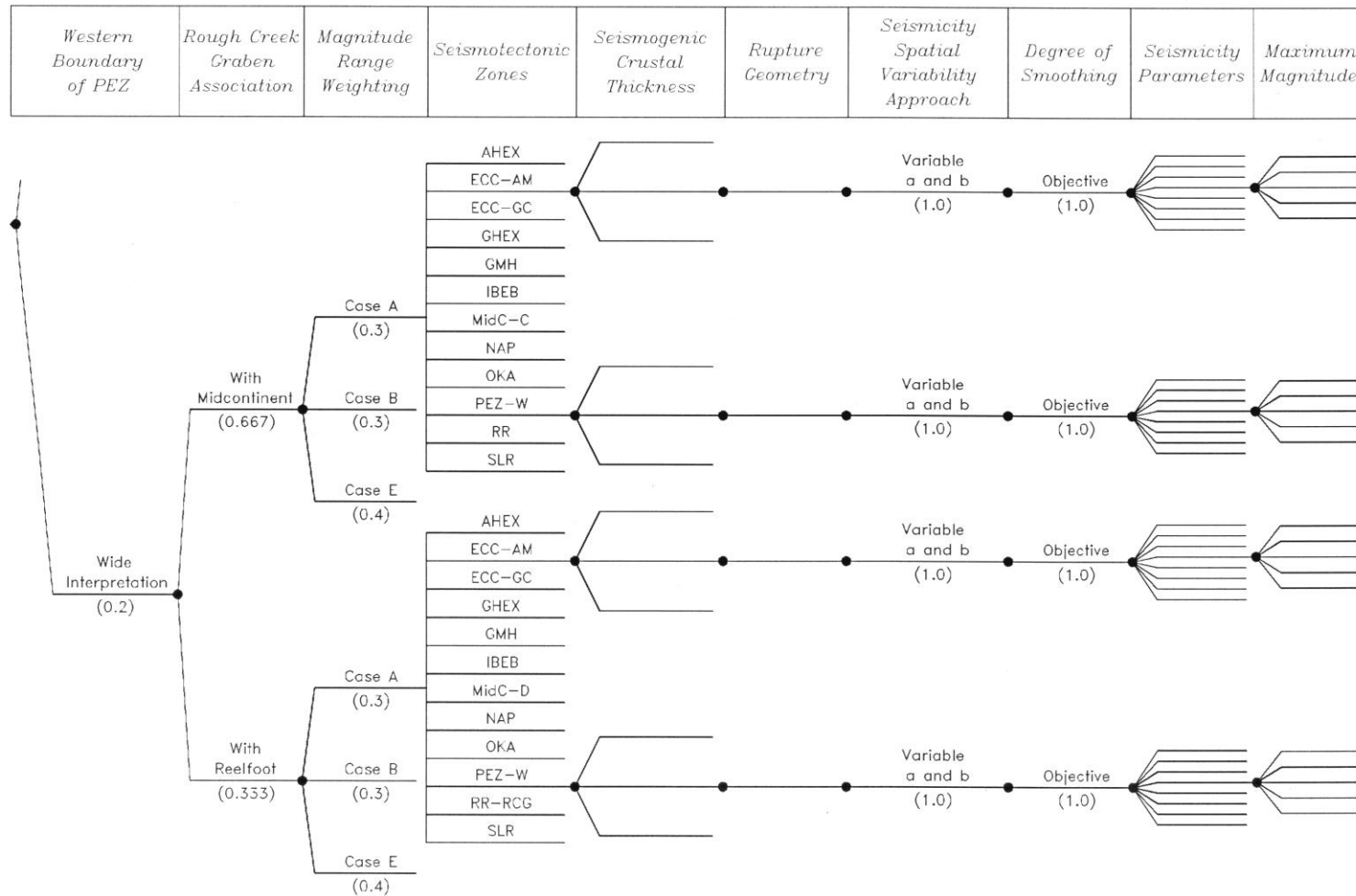


Figure 4.2.4-1(b)
Logic tree for the seismotectonic zones branch of the master logic tree

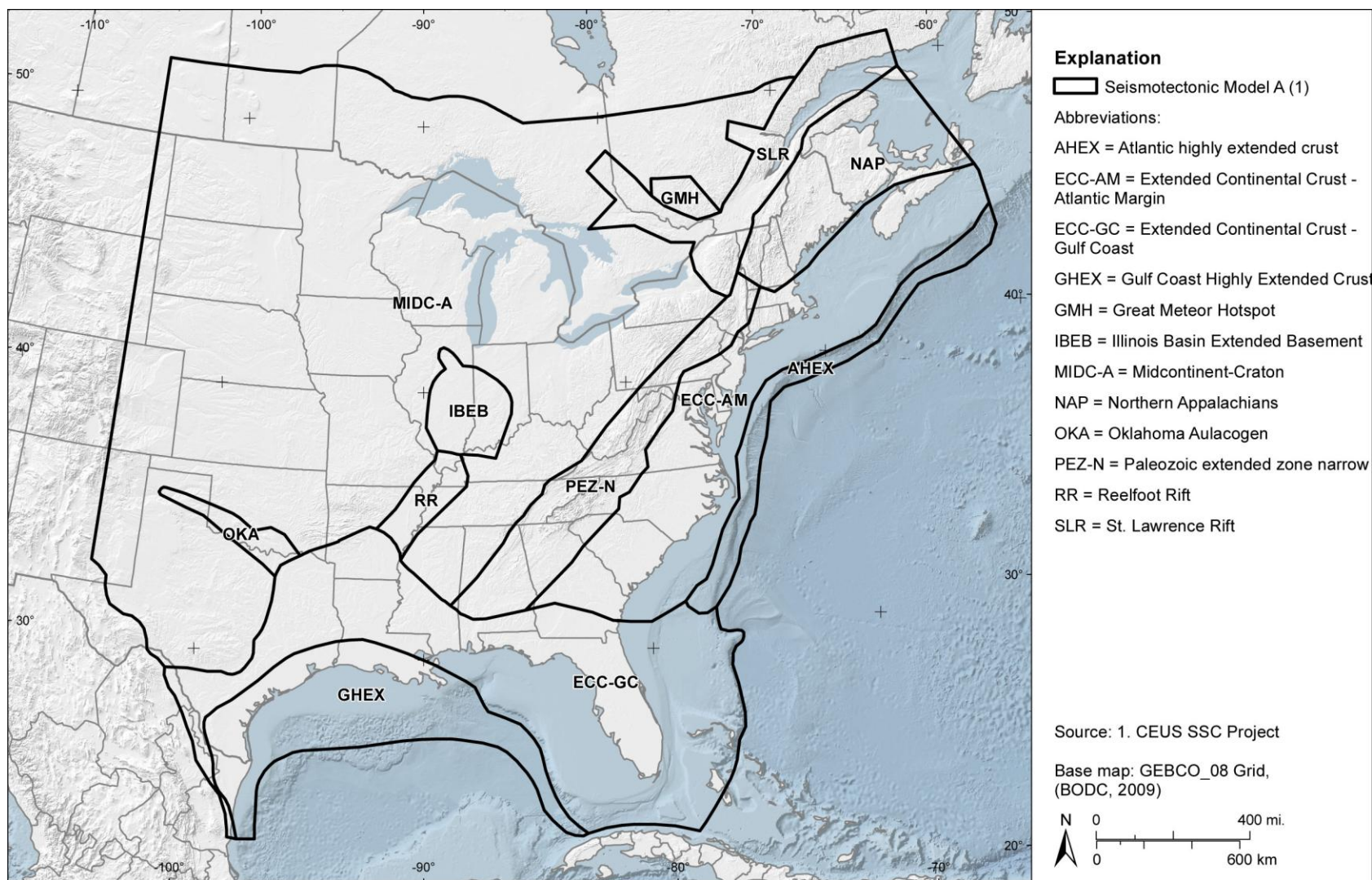


Figure 4.2.4-2
 Seismotectonic zones shown in the case where the Rough Creek Graben is not part of the Reelfoot Rift (RR), and the Paleozoic Extended Zone is narrow (PEZ-N)

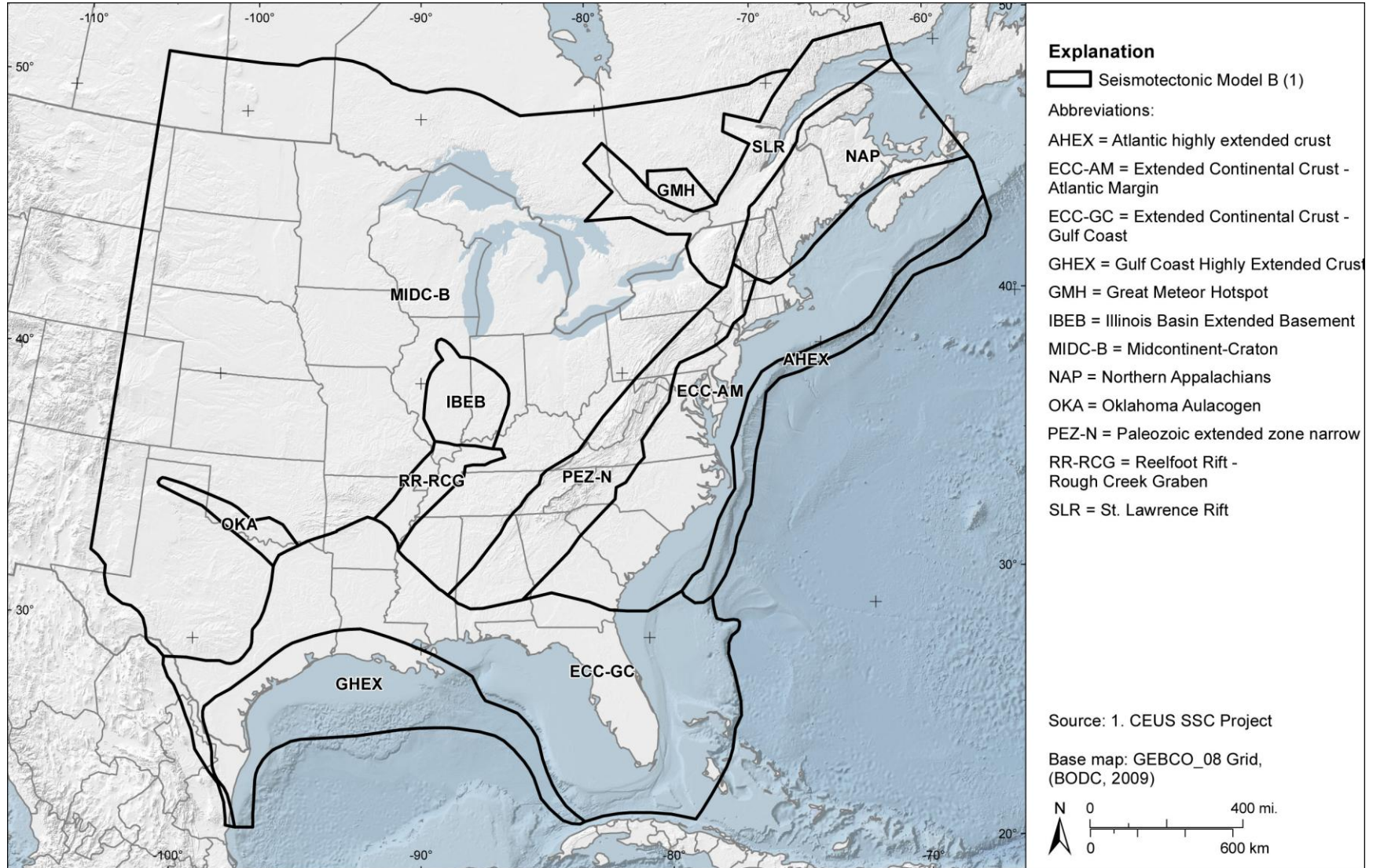


Figure 4.2.4-3
Seismotectonic zones shown in the case where the Rough Creek Graben is part of the Reelfoot Rift (RR-RCG), and the Paleozoic Extended Zone is narrow (PEZ-N)

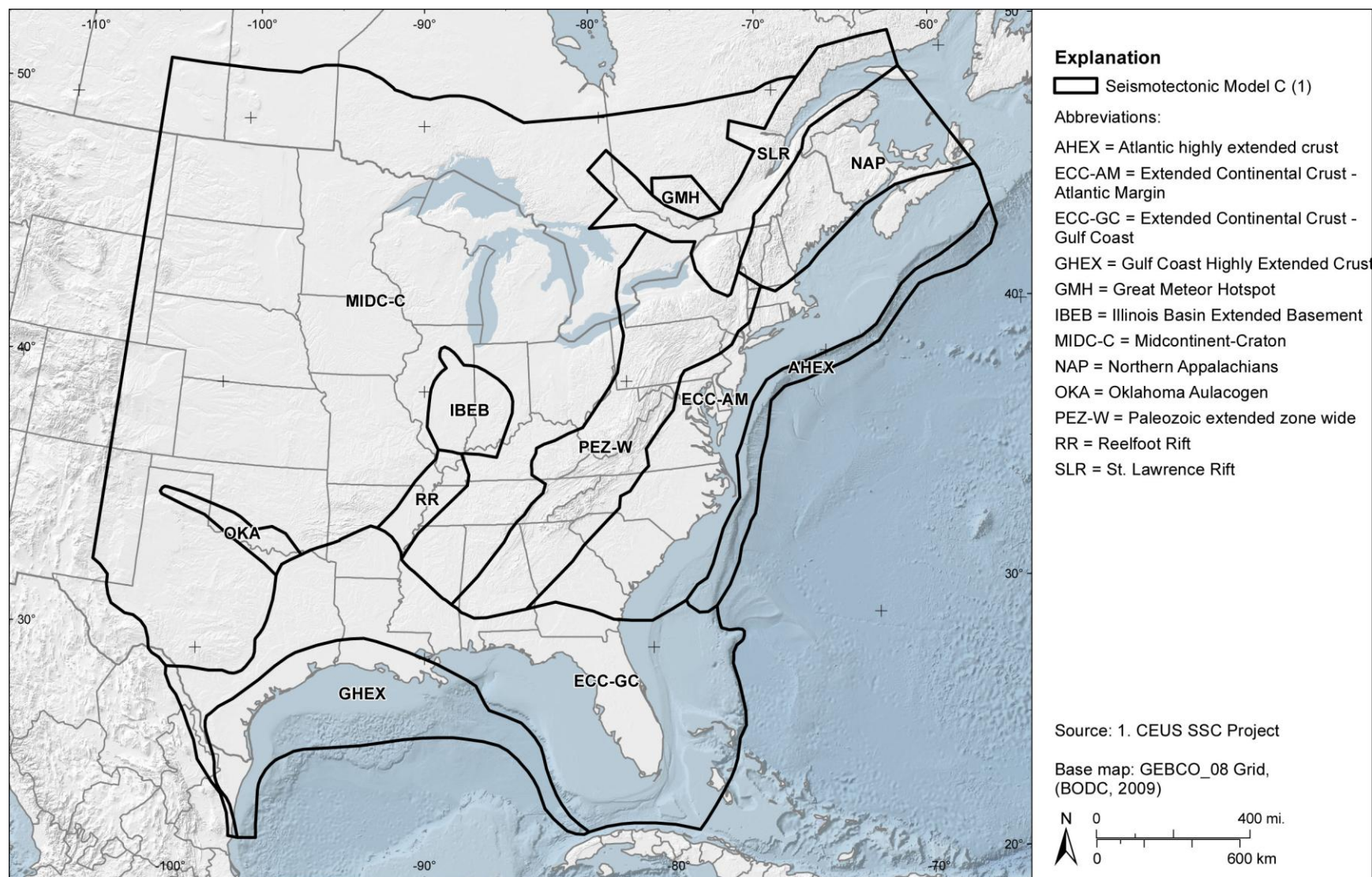


Figure 4.2.4-4
 Seismotectonic zones shown in the case where the Rough Creek Graben is not part of the Reelfoot Rift (RR), and the Paleozoic Extended Crust is wide (PEZ-W)

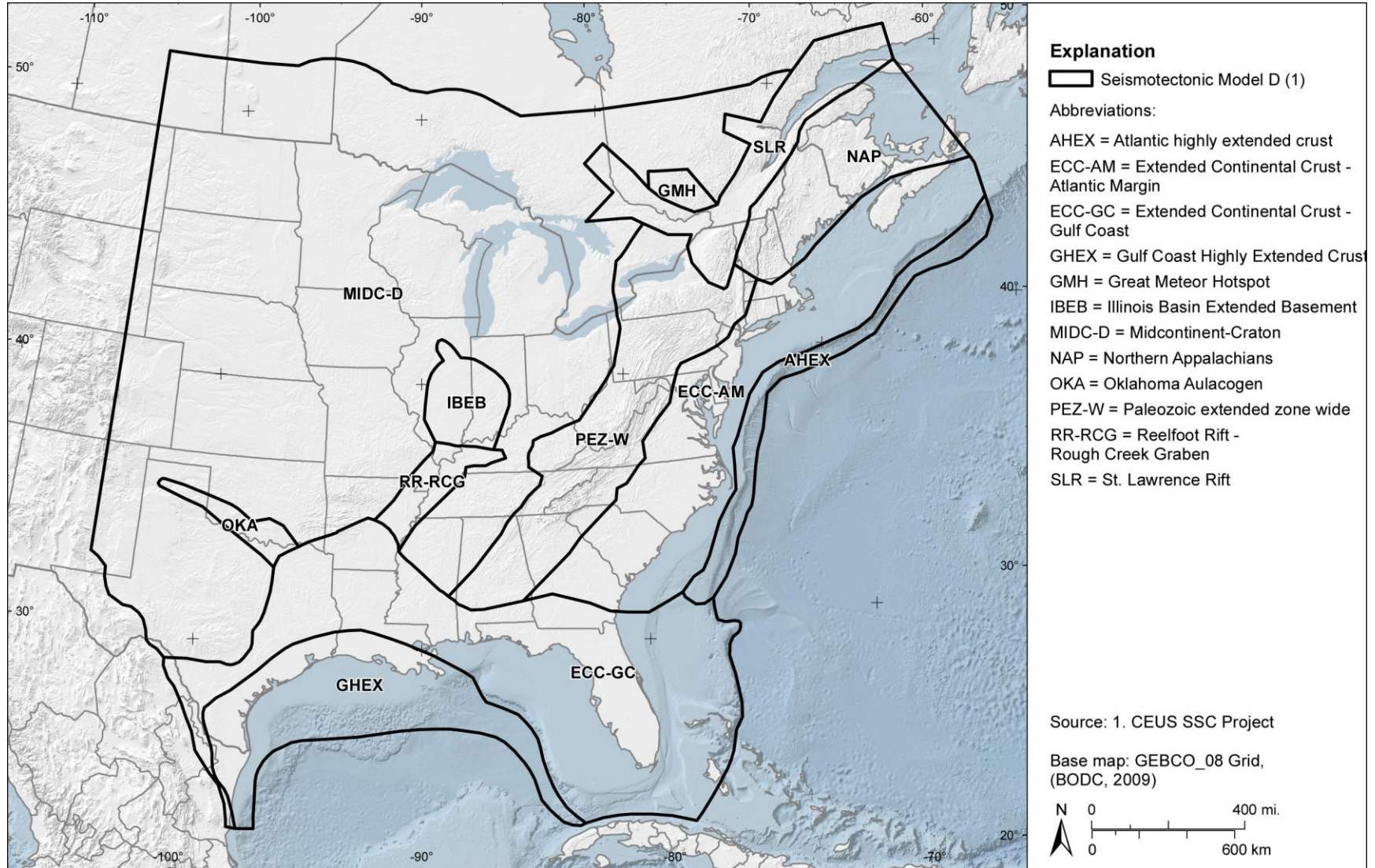


Figure 4.2.4-5
Seismotectonic zones shown in the case where the Rough Creek Graben is part of the Reelfoot Rift (RR-RCG), and the Paleozoic Extended Crust is wide (PEZ-W)

BIBLIOGRAPHIC DATA SHEET

(See instructions on the reverse)

NUREG-2115
Vol. 1

2. TITLE AND SUBTITLE

Central and Eastern United States Seismic Source Characterization for Nuclear Facilities

Volume 1: Chapters 1 to 4

3. DATE REPORT PUBLISHED

MONTH	YEAR
January	2012

4. FIN OR GRANT NUMBER

K6877

5. AUTHOR(S)

G. Stirewalt (NRC), L. Salomone (Savannah River Nuclear Solutions, LLC), S. McDuffie (DOE), K. Coppersmith (Coppersmith Consulting, Inc), Fugro William Lettis & Associates, Inc.: C. Fuller, R. Hartleb, W. Lettis, S. Lindvall, R. McGuire, G. Toro, D. Slayter, R. Cumbest, A. Shumway, F. Syms, AMEC Geomatrix, Inc: L. Glaser, K. Hanson, R. Youngs, S. Bozkurt, V. Montaldo Falero, R. Perman, R. McGuire (Risk Engineering), M. Tuttle (M. Tuttle & Associates)

6. TYPE OF REPORT

Technical

7. PERIOD COVERED (Inclusive Dates)

8. PERFORMING ORGANIZATION - NAME AND ADDRESS (If NRC, provide Division, Office or Region, U.S. Nuclear Regulatory Commission, and mailing address; if contractor, provide name and mailing address.)

U.S. Nuclear Regulatory Commission, Office of Nuclear Regulatory Research, Washington DC 20555
U.S. Department of Energy, 1000 Independence Avenue SW, Washington DC 20585
Electric Power Research Institute, 3420 Hillview Avenue, Palo Alto, CA 94304

9. SPONSORING ORGANIZATION - NAME AND ADDRESS (If NRC, type "Same as above"; if contractor, provide NRC Division, Office or Region, U.S. Nuclear Regulatory Commission, and mailing address.)

U.S. Nuclear Regulatory Commission, Office of Nuclear Regulatory Research, Washington DC 20555
U.S. Department of Energy, 1000 Independence Avenue SW, Washington DC 20585
Electric Power Research Institute, 3420 Hillview Avenue, Palo Alto, CA 94304

10. SUPPLEMENTARY NOTES

11. ABSTRACT (200 words or less)

This report describes a new seismic source characterization (SSC) model for the Central and Eastern United States (CEUS). It will replace the Seismic Hazard Methodology for the Central and Eastern United States, EPRI Report NP-4726 (July 1986) and the Seismic Hazard Characterization of 69 Nuclear Plant Sites East of the Rocky Mountains, Lawrence Livermore National Laboratory Model, (Bernreuter et al., 1989). The objective of the CEUS SSC Project is to develop a new seismic source model for the CEUS using a Senior Seismic Hazard Analysis Committee (SSHAC) Level 3 assessment process. The goal of the SSHAC process is to represent the center, body, and range of technically defensible interpretations of the available data, models, and methods. Input to a probabilistic seismic hazard analysis (PSHA) consists of both seismic source characterization and ground motion characterization. These two components are used to calculate probabilistic hazard results (or seismic hazard curves) at a particular site. This report provides a new seismic source model.

12. KEY WORDS/DESCRIPTORS (List words or phrases that will assist researchers in locating the report.)

Probabilistic seismic hazard analysis (PSHA)
Seismic source characterization (SSC)
Seismic source characterization model
Central and Eastern United States (CEUS)

13. AVAILABILITY STATEMENT

unlimited

14. SECURITY CLASSIFICATION

(This Page)

unclassified

(This Report)

unclassified

15. NUMBER OF PAGES

16. PRICE

